

Biochemical Characterization and Ligand Identification of *Pseudomonas aeruginosa* Lectins and their Orthologs in other Pathogenic Bacteria

DISSERTATION

zur Erlangung des Grades

des Doktors der Naturwissenschaften

der Naturwissenschaftlich-Technischen Fakultäten

der Universität des Saarlandes

von

Ghamdan Beshr, M.Sc.

Saarbrücken

2018

Day of Colloquium: 31.08.2018

Dean: Prof. Dr. Guido Kickelbick

Chairman: Prof. Dr. Anna K. H. Hirsch

Commission: Dr. Alexander Titz
Prof. Dr. Rolf W. Hartmann

Acad. Colleague: Dr. Martin Frotscher

Die vorliegende Arbeit wurde von September 2014 bis Januar 2018 unter Anleitung von Herrn Dr. Alexander Titz in der Fachrichtung Pharmazie der Naturwissenschaftlich-Technischen Fakultät der Universität des Saarlandes sowie am Helmholtz-Institut für Pharmazeutische Forschung Saarland (HIPS) – NWG. Chemische Biologie der Kohlenhydrate angefertigt.

In memory of Musaab Sadeq Khaleel Al-Tuwaitari

”من أنا لأقول لكم ما أقول لكم“

محمود درويش

TABLE OF CONTENTS

Summary	vi
Zusammenfassung	vii
Papers included in the thesis	viii
Contributions Report	ix
Abbreviations	xi
1. Introduction	1
1.1. Glycobiology	1
1.2. Glycosylation and its role in human biology	2
1.3. Glycomics	5
1.4. Lectins and their role in microbial pathogenicity	6
1.5. <i>Pseudomonas aeruginosa</i> lectins	9
1.5.1. LecA (PA-IL)	9
1.5.2. LecA orthologs in other pathogenic bacteria	10
1.5.3. LecB (PA-IIL)	11
1.5.4. LecB orthologs in other pathogenic bacteria	12
2. Aim of the thesis	14
3. Results	15
3.1. Identification of <i>Pseudomonas aeruginosa</i> LecB inhibitors using a fluorescence polarization-based high-throughput assay	15
3.2. Photoswitchable Janus glycodendrimer micelles as multivalent inhibitors of LecA and LecB from <i>Pseudomonas aeruginosa</i>	39
3.3. Development of a competitive binding assay for the <i>Burkholderia cenocepacia</i> lectin BC2L-A and the structure activity relationship of natural and synthetic inhibitors	48
3.4. <i>Photorhabdus luminescens</i> lectin A (PIIA) - a new probe for detecting α -galactoside-terminating glycoconjugates	61
3.5. Structure-guided engineering of PIIA carbohydrate binding specificity	79
4. Conclusion and outlook	90
5. Supporting information	98
5.1. Supporting information for subchapter 3.1	98
5.2. Supporting information for subchapter 3.2	115
5.3. Supporting information for subchapter 3.3	195
5.4. Supporting information for subchapter 3.4	213
Conference Contributions	xiii
Curriculum vitae	xiv
Acknowledgement	xv

SUMMARY

Carbohydrates and their binding proteins (Lectins) play important role in all living organisms and the development of new analytical technologies in the past few years allowed us to partially decipher the significance of carbohydrates in biology. Moreover, the role of lectins in pathogenicity was pointed out in the last decade, revealing that lectins play a crucial role in bacterial infection through, for example, virulence and adherence to the host as well as in biofilm formation. In this work, various biophysical and structural techniques were employed to identify anti-biofilm agents for human-opportunistic, Gram-negative bacterium pathogens, such as *Pseudomonas aeruginosa* and *Burkholderia cenocepacia*, by targeting their lectins and studying the binding properties of lectin blockers upon binding on their desired target. Furthermore, a new lectin (PIIA) from the entomopathogenic bacterium *Photorhabdus luminescens* was characterized; this resulted in a new tool for lectinology and biomedical research, as a probe for detecting α -galactoside-terminating glycoconjugates.

ZUSAMMENFASSUNG

Kohlenhydrate und dessen Bindepoteine (Lektine) spielen eine wichtige Rolle in allen Lebewesen. Durch die Entwicklung von neuen analytischen Verfahren wird die Bedeutsamkeit von Kohlenhydraten in der Biologie ersichtlich. Es zeigt sich, dass Lektine bei der Pathogenität durch Bakterien in Bezug auf die Virulenz, Haftfestigkeit und deren Eigenschaft zur Biofilmbildung eine wesentliche Rolle spielen. In dieser Arbeit wurden verschiedene biophysikalische und strukturelle Techniken angewendet, um Biofilm verhindernde Wirkstoffe gegen opportunistische Erreger, wie den Gram-negativen Bakterien *Pseudomonas aeruginosa* und *Burkholderia cenocepacia*, zu erforschen. Dazu wurden die Bindepoteigenschaften der Lektinblocker an entsprechenden Zielen untersucht.

Außerdem wurde ein neues Lektin (PIIA) vom entomopathogenen Bakterium *Photorhabdus luminescens* charakterisiert. Es bindet an α -Galactoside und kann zur Erkennung von Glykokonjugaten in der Lektinologie und in der biomedizinischen Forschung eingesetzt werden.

PAPERS INCLUDED IN THE THESIS

This thesis is divided into five chapters, three of which have been published as separate papers.

Identification of *Pseudomonas aeruginosa* LecB Inhibitors using a fluorescence polarization–based high-throughput assay

Ghamdan Beshr, Matthew Calvert, Ronald Garcia, Jennifer Herrmann, Dirk Hauck, Rolf Müller and Alexander Titz

Photoswitchable Janus glycodendrimer micelles as multivalent inhibitors of LecA and LecB from *Pseudomonas aeruginosa*

Yingxue Hu, Ghamdan Beshr, Christopher Garvey, Rico Tabor, Alexander Titz and Brendan Wilkinson.

Colloids and Surfaces B: Biointerfaces, **2017** (159), 605-612 -
DOI: 10.1016/j.colsurfb.2017.08.016

Development of a competitive binding assay for the *Burkholderia cenocepacia* lectin BC2L-A and structure activity relationship of natural and synthetic inhibitors

Ghamdan Beshr, Roman Sommer, Dirk Hauck, David Chan Bodin Siebert, Anna Hofmann, Anne Imberty and Alexander Titz

Medicinal Chemistry Communications, **2016**; 7 (3), 519-530 - DOI: 10.1039/C5MD00557D

***Photorhabdus luminescens* lectin A (PIIA) - a new probe for detecting α -galactoside-terminating glycoconjugates**

Ghamdan Beshr, Asfandiyar Sikandar, Eva-Maria Jemiller, Nikolai Klymiuk, Dirk Hauck, Stefanie Wagner, Eckhard Wolf, Jesko Koehnke, and Alexander Titz

Journal of Biological Chemistry, **2017**; 292 (48), 19935-19951 - DOI: 10.1074/jbc.M117.812792

Structure-guided engineering of PIIA carbohydrate binding specificity

Ghamdan Beshr, Anika Liu, and Alexander Titz

CONTRIBUTIONS REPORT

GB would like to clarify his contributions to the papers/manuscripts included in this thesis.

Identification of *Pseudomonas aeruginosa* LecB Inhibitors using a fluorescence polarization–based high-throughput assay

Ghamdan Beshr, Matthew Calvert, Ronald Garcia, Jennifer Herrmann, Dirk Hauck, Rolf Müller, and Alexander Titz

GB and AT designed and analyzed the experiments. GB developed the fluorescence polarization screening assays and performed all the screening studies. In addition, he developed the large-scale fractionation method for myxobacterial extract using preparative HPLC with the assistance of MC. RG, and JH did the cultivation and extraction of *Myxobacteria* strains with the assistance of GB. GB did the docking and molecular dynamics experiments and wrote this subchapter.

Photoswitchable Janus glycodendrimer micelles as multivalent inhibitors of LecA and LecB from *Pseudomonas aeruginosa*

Yingxue Hu, Ghamdan Beshr, Christopher Garvey, Rico Tabor, Alexander Titz and Brendan Wilkinson.

Colloids and Surfaces B: Biointerfaces, **2017** (159), 605-612 -
DOI: 10.1016/j.colsurfb.2017.08.016

GB and AT designed and performed the biological evaluation of glycoamphiphiles with *Pseudomonas aeruginosa* LecA and LecB including protein production and purification as well as fluorescence polarization measurements. In addition, GB was involved in the writing of the manuscript.

Development of a competitive binding assay for the *Burkholderia cenocepacia* lectin BC2L-A and structure activity relationship of natural and synthetic inhibitors

Ghamdan Beshr, Roman Sommer, Dirk Hauck, David Chan Bodin Siebert, Anna Hofmann, Anne Imberty and Alexander Titz

Medicinal Chemistry Communications, **2016**; 7 (3), 519-530 - DOI: 10.1039/C5MD00557D

GB, RS, and AT designed and analyzed all experiments. GB performed all *in-vitro* evaluation and performed docking studies. GB, RS and AT wrote the manuscript.

***Photorhabdus luminescens* lectin A (PIIA) - a new probe for detecting α -galactoside-terminating glycoconjugates**

Ghamdan Beshr, Asfandiyar Sikandar, Eva-Maria Jemiller, Nikolai Klymiuk, Dirk Hauck, Stefanie Wagner, Eckhard Wolf, Jesko Koehnke, and Alexander Titz

Journal of Biological Chemistry, **2017**; 292 (48), 19935-19951 - DOI: 10.1074/jbc.M117.812792

GB, JK and AT wrote the manuscript. GB and AT designed, performed and analyzed the experiments shown in Figures 1-4, Tables 1-2. GB performed the docking experiments. SW designed and performed the cloning of the PIIA expression vector with the assistance of GB. AS and JK designed, performed and analyzed the experiments shown in Figures 5-8, Table 3, with the assistance of GB.

Structure-guided engineering of PIIA carbohydrate binding specificity

Ghamdan Beshr, Anika Liu, and Alexander Titz

GB and AT designed the experiments. AL and GB performed and analyzed the experiments and wrote this subchapter.

ABBREVIATIONS

GTKO	α -1,3-galactosyltransferase knockout
ACN	Acetonitrile
N _{agg}	Aggregation number
<i>B. cenocepacia</i>	<i>Burkholderia cenocepacia</i>
CRD	Carbohydrate-recognition domain
Cat no	Catalogue number
CFG	Consortium for Functional Glycomics
CAC	Critical aggregation concentration
CF	Cystic fibrosis
K_d	Dissociation constant
DLS	Dynamic light scattering
ER	Endoplasmic reticulum
EBA-175	Erythrocyte-binding antigen-175
eDNA	Extracellular DNA
FITC	Fluoresceine isothiocyanate
FI	Fluorescence intensity
FP	Fluorescence polarization
FA	Formic acid
Fuc	Fucose
Gal	Galactose
GalCer	Galactosylceramide
DZIF	German Center for Infection Research
Gb3	Globotriaosylceramide
Glc	Glucose
GlcCer	Glucosylceramide
GlcA	Glucuronic acid
HA	Hemagglutinin
HPLC	High-pressure liquid chromatography

HTS	High-throughput screening
IdA	Iduronic acid
LacCer	Lactosylceramide
Man	Mannose
MS	Mass spectrometry
MOE	Molecular operating environment software
GalNAc	N-Acetylgalactosamine
GalNAcT	N-Acetylgalactosamine transferase
GlcNAc	N-Acetylglucosamine
OD	Optical density
<i>P. luminescens</i>	<i>Photorhabdus luminescens</i>
pRBC	Pig red blood cells
PDB	Protein data bank
<i>P. aeruginosa</i>	<i>Pseudomonas aeruginosa</i>
RBC	Red blood cells
r.t.	Room temperature
rpm	Rotations per minute
Sia	Sialic acid
SEC	Size-exclusion chromatography
SANS	Small angle neutron scattering
Sp	Spacer
Spp.	Species
SD	Standard deviation
SAR	Structure activity relationship
IC ₅₀	The concentration of an inhibitor where the response (or binding) is reduced by half
TLC	Thin layer chromatography
UV	Ultra violet
Xyl	Xylose

1. INTRODUCTION

1.1. GLYCOBIOLOGY

Glycobiology is the study of the structure, biosynthesis, and function of carbohydrates (glycans) in living organisms. Complex glycans are widely distributed in nature and play key roles in many biological processes (e.g. cell differentiation, cell–cell recognition, cell signaling, host–pathogen interaction during infection, host immune response, and membrane rigidity) (Figure 1).¹

Compared to genome and proteome, the investigation accomplished was less in the carbohydrate biology due to the complexity of carbohydrates and to the fact they are not encoded in the genome.² The development of new technologies over the last few years has drawn attention to glycobiology and many recent studies have focused on the role of glycans in human health and in diseases, particularly cancer and infections.

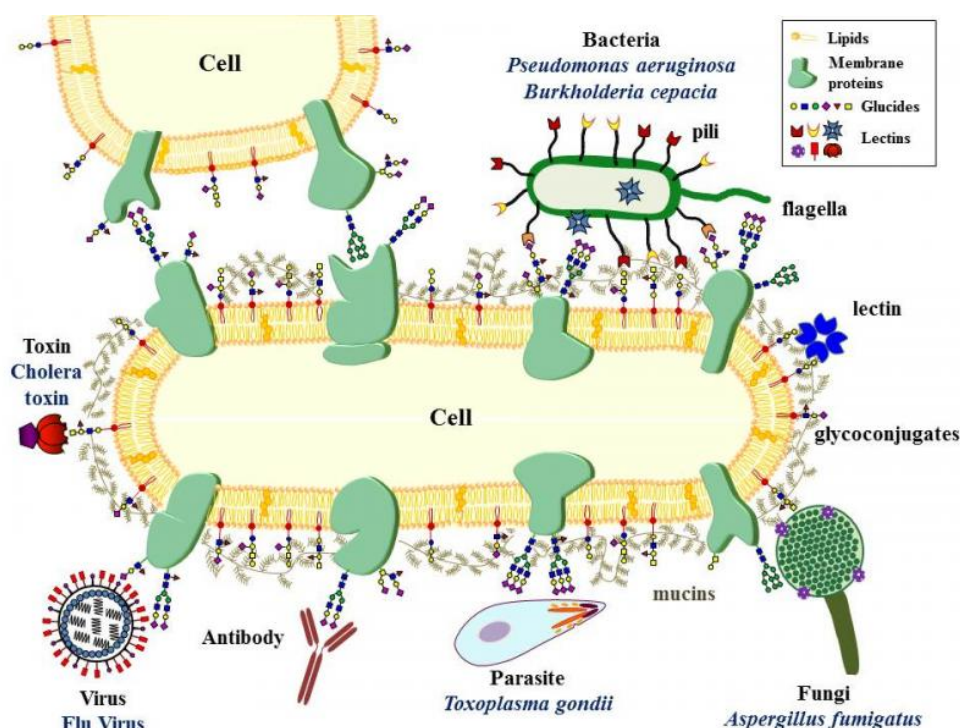


Figure 1. The roles of carbohydrates in biological processes. Carbohydrates are involved in cell recognition, adhesion, and signalling as well as in immune triggering. This figure was taken from <http://www.cermav.cnrs.fr/sites/default/files/u1394/infectionen.jpg> (28.04.2015).

1.2. GLYCOSYLATION AND ITS ROLE IN HUMAN BIOLOGY

Glycosylation refers to the process by which sugar moieties are attached to proteins, lipids, and all substances resulting in structures called glycoconjugates. 10 monosaccharide units are the building blocks for complex oligosaccharide polymers in mammals (Figure 2). Glycan monosaccharides are connected through their anomeric centre to many hydroxyl groups, resulting in numerous linkages with linear or branched structures. Furthermore, the anomerization at the anomeric centre of each monomer ends with a high number of possible glycan epitopes.³ Glycosylation is a critical biological process in many living organisms, especially in the folding and stabilization of proteins. In eukaryotes, more than 70 % of the proteins are glycosylated, whereas in prokaryotes it is still too early to predict the full extent of its protein glycosylation.⁴ Protein N-linked (Asn), O-linked (Ser/Thr), and lipid glycosylation are the most common glycosylation mechanisms.

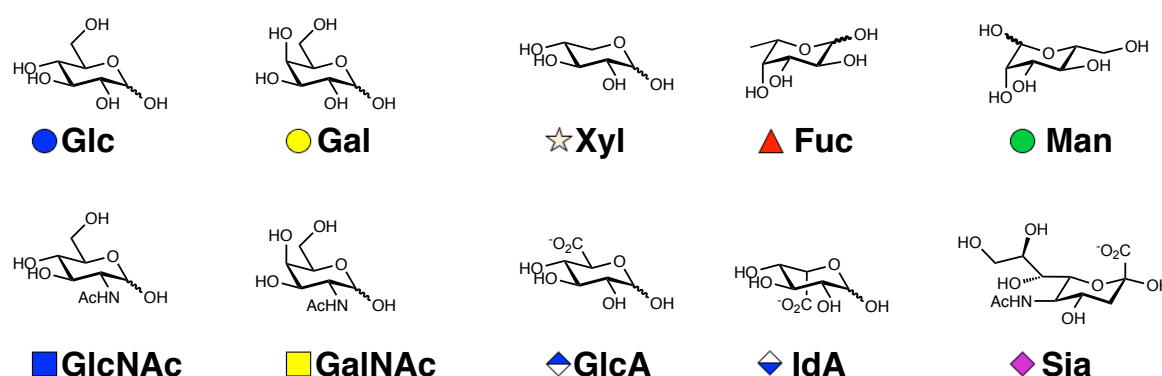


Figure 2. The monosaccharide building units of mammalian glycans. Glucose (Glc), galactose (Gal), mannose (Man), fucose (Fuc), N-acetylglucosamine (GlcNAc), N-acetylgalactosamine (GalNAc), xylose (Xyl), glucuronic acid (GlcA), iduronic acid (IdA) and sialic acid (Sia). The more commonly used three-letter codes and the symbolic notations used by the consortium for functional glycomics are shown here. This figure has been adapted from reference³.

N-linked glycosylation is a very prevalent form of glycosylation and dolichol-linked oligosaccharide precursor is required to transfer the sugar chain to the nascent protein using a multisubunit protein complex in the endoplasmic reticulum (ER) membrane of eukaryotes, called

oligosaccharyltransferase. In this process, a 14 carbohydrate-long common oligosaccharide precursor (2 N-acetylglucosamine, 9 mannose, and 3 glucose) is attached to the amide side chain of asparagine of the target peptide chain. Upon protein folding in ER, three glucose moieties split from the glycan part and then protein transfers to the Golgi apparatus. In the Golgi apparatus, further modification may occur through remodelling of sugar moieties with other sugars, such as N-acetylglucosamine (GlcNAc), N-acetylgalactosamine (GalNAc), galactose (Gal), fucose (Fuc) and sialic acid.^{2,1}

O-linked glycosylation is simpler since the dolichol-linked oligosaccharide precursor is not required. By O-linked glycosylation, GalNAc makes a covalent bond to the hydroxyl of serine or threonine of the target peptide chain in the Golgi apparatus via a GalNAc transferase (GalNAcT) enzyme. Afterwards, several sugars such as Fuc, Gal, GlcNAc and sialic acid are added to the GalNAc and elongate the sugar chain.¹

Lipid glycosylation is carried out by the addition of either glucose or galactose to 1-hydroxy group of C-18 ceramide, producing a simple glucosylceramide (GlcCer) or galactosylceramide (GalCer). From these building blocks several complex structures can be generated, such as lactosylceramide (LacCer), and globotriaosylceramide (Gb3).^{5,6}

Human A, B, and O blood-group antigens represent the essential role of glycosylation among human beings. The O antigen (also called the H antigen) consists of three sugar moieties that are attached to a ceramide lipid or serine/threonine residue of proteins on the surface of the erythrocytes. A and B antigens differ from the O antigen by having an additional α -linked GalNAc or Gal on the terminal Gal residue, respectively (Figure 3). All people have enzymes that synthesise the O antigen, whereas some with types A, B and AB have, in addition, GalNAc transferase or Gal transferase or both transferases, respectively.⁷

Another example of a glycosylation difference among mammals is the so-called α -Gal epitope (Gal- α -1,3-Gal- β -1,4-GlcNAc). α -Gal is a ubiquitous antigen in non-primate mammals and new-world monkeys. This epitope is absent in humans and old-world monkeys due to the evolutionary loss of the galactosyltransferase gene that is responsible for α -Gal synthesis. The human body

has additionally developed antibodies against the α -Gal epitope, which causes a severe immune rejection upon xenotransplantation.^{8,9}

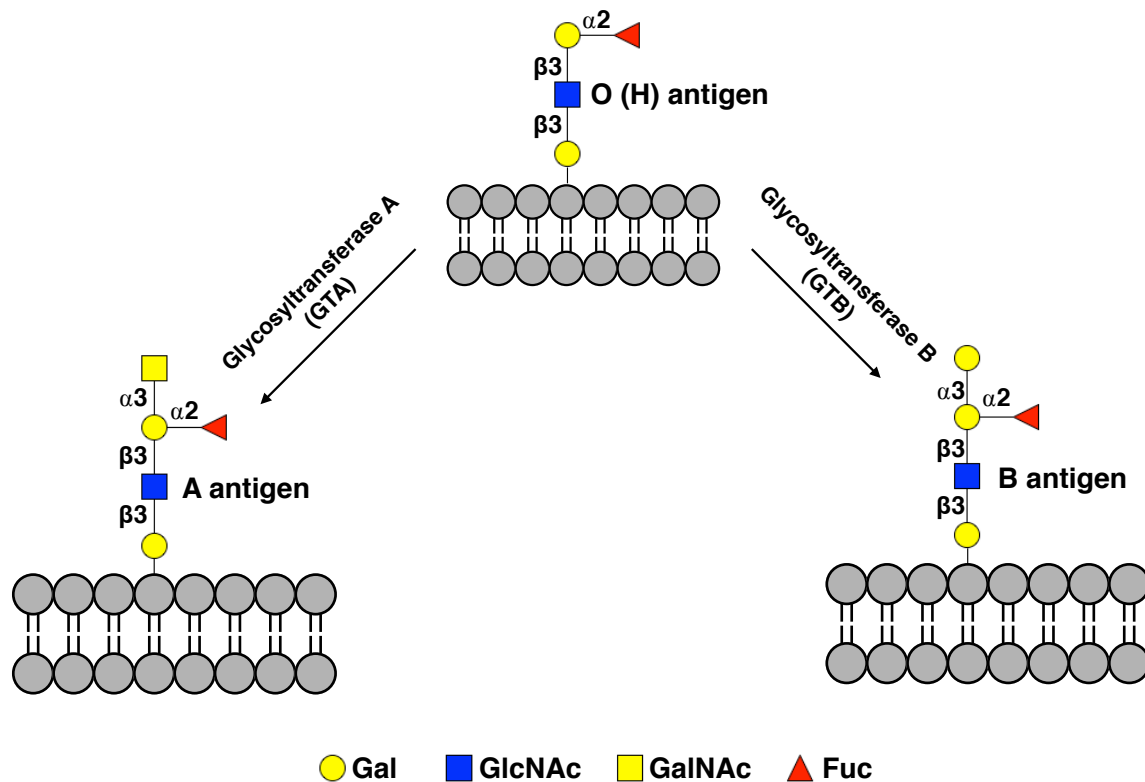


Figure 3. The human ABO blood-group antigens. The presence or absence of certain glycosyltransferase leads to a different glycosylation pattern for human erythrocytes, resulting in different antigen structures and blood groups.

What is the impact of glycosylation on human diseases?

A complex mechanism controls the biosynthesis of N-linked and O-linked glycosylation in ER and in the Golgi apparatus through several manifestations of glycosyltransferase and glycosidase, resulting in numerous carbohydrate structures, varying in different species, cell types, and tissue types. The regulation of this biosynthesis depends on several parameters, such as the level of gene expression, enzyme protein activity and localization, and through substrate and co-factor concentrations at the synthesis site.¹⁰

Diseases are thus accompanied by a change in the glycosylation pattern where the relative proportions of carbohydrate structures are often characteristically different from healthy ones.

These changes can also enable us to assess the stage of the disease and to give a diagnosis. In liver cirrhosis and hepatitis, transferrin and α -1-acid glycoprotein show a change in their glycosylation repertoire, manifested by increased branching or fucosylation.^{10,11} Contrary to this, a reduction in serum IgG galactose content has been reported in rheumatoid arthritis patients due to a decrease in Gal transferase activity in the antibody-producing B cell.¹² In tumorigenesis, glycan is excessively expressed in different forms but they still have the complete or incomplete sequence of sugars. In addition to this, some over-expressed glycans may contain a truncated form of oligosaccharide. For example, there can be a high level of Tn antigen and Lewis^{x&y} expression in breast and lung cancer cells, respectively. By contrast, reduced glycan expression has been reported in bladder cancer where the activity of the ABO transferases decreases leading to less presentation of the ABO antigens.¹³

Some of the mechanisms underlying glycoprotein alterations in disease have recently been elucidated and glycans are therefore now regarded as biomarkers for many diseases.¹⁴ Hence, there is a current need to improve the analytic tools for glycan, which will in turn lead to a more accurate diagnosis.

1.3. Glycomics

Glycomics describes the complete repertoire of the glycans that are produced under specified conditions of time, location, and environment.⁸ The complexity of glycans which has a bearing on glycoconjugates makes their analysis a challenge. Mass spectrometry (MS), high-pressure liquid chromatography (HPLC), and lectins are the common tools that are currently used in glycomics. Mass spectrometry is the most widely used technique in glycomics to analyze complex glycans. The drawback of this technique, however, is the requirement for glycans to be liberated from their glycoconjugates, and this slows down the analytical process. Moreover, diverse glycan isomers cannot be analyzed by MS. HPLC is another common method for glycan analysis. Here, the separation depends on carbohydrate chemistry. The reducing end after N-linked glycan release is tagged with different tracers to assess the visualization and to enable a comparison between two samples.³ A more specific technique that assigns carbohydrates according to their

isomerizations is a lectin microarray. Lectins are carbohydrate-binding proteins that are neither enzymes nor antibodies.¹⁵ They are ubiquitous in nature and highly specific for sugar moieties. In lectin microarrays, the well-defined lectins, mostly plant-derived with different carbohydrate specificities, are immobilized onto a solid support and used for profiling complex glycan features without the need for the liberation of glycans. This method has been intensely used in medical fields for the analysis of disease-related biomarkers, such as when drastic glycosylation changes occur along with tumorigenesis and metastasis.^{16–18} Despite the success of lectin microarrays, several issues must still be resolved to make this technology even more useful in glycomics. First, most of the characterized lectins are of plant origin with unreliable availability. Second, many lectins often have a broader carbohydrate specificity which complicates the interpretation of the data by these lectins. Third, less common glycans, such as sulphated glycans, are still lacking a lectin probe. There is therefore an urgent need to characterize new lectins, which can be recombinantly produced in bacterial cells, or to engineer the existing lectins to improve their specificity and affinity to solve the above obstacles.¹⁹

1.4. Lectins and their role in microbial pathogenicity

Lectins play numerous biological roles, for example, cell adhesion and recognition (see figure 1). They contain a carbohydrate-recognition domain (CRD) that recognizes and binds their specific carbohydrate ligand.

Lectins are also expressed by microbes, such as viruses, bacteria, fungi, and protozoa, and were initially detected based on their tendency to aggregate or to induce the hemagglutination of erythrocytes.²⁰ In the 1970's, Nathan Sharon and colleagues described for the first time how lectins facilitate the attachment or adherence of bacteria to host cells, which is a prerequisite for bacterial colonization and infection. The trimeric influenza viral hemagglutinin (HA) is an example of a viral lectin which binds specifically to the sialic acid on the host cells and mediates endocytosis and the pH-dependent fusion of the viral envelope with the endosomal membrane, leading to the eventual release of the viral RNA into the cytosol. Parasite invasion to their host

cells is also mediated by lectins, such as the erythrocyte-binding antigen-175 (EBA-175) in *Plasmodium falciparum* (malaria). EBA-175-glycan binding triggers the invasion of merozoites into red blood cells, where they develop and subsequently release newly formed merozoites into the bloodstream. Similar to viral and parasite lectins, bacterial lectins are involved first in cell adhesion and then in invasion of host cells (Table.1). In addition to this, some bacterial lectins are toxins such as the cholera and Shiga toxins in *Vibrio cholera* and *Shigella dysenteriae*, respectively. They contain both a CRD and a catalytic domain, where the CRD binds to the terminal glycan of the glycolipid which mediates the endocytosis into the host cells and the catalytic domain inactivates a crucial function inside the cells, leading to cell death.²⁰

Moreover, bacterial lectins contribute to bacterial pathogenicity through biofilm formation. LecA (also called PA-IL) and LecB (also called PA-IIL) from *Pseudomonas aeruginosa* (*P. aeruginosa*) and BC2IA,B,C from *Burkholderia cenocepacia* (*B. cenocepacia*) play a crucial role in biofilm formation, leading to an increase in bacterial resistance to conventional antibiotics.^{21–23} Thus, the targeting of these bacterial lectins constitutes a new strategy to fight bacterial resistance, especially in *P. aeruginosa*.²⁴

Table 1. Examples of bacterial lectins and their carbohydrate specificities and sites of infection. This table was adapted from reference ²⁰.

Microorganism	Lectin	Glycan-receptor specificity	Site of infection
<i>Actinomyces naeslundii</i>	fimbriae	Gal- β -1,3-GalNAc- β -	oral
<i>Bordetella pertussis</i>	filamentous hemagglutinin (FHA)	sulfated glycolipids, heparin	ciliated epithelium in the respiratory tract
<i>Borrelia burgdorferi</i>	ErpG protein	heparan sulfate	endothelium, epithelium, and extracellular matrix
<i>Campylobacter jejuni</i>	flagella, LPS	Fuc- α -1,2-Gal- β -1,4-GlcNAc- β - (H-antigen)	intestinal cells
<i>Escherichia coli</i>	P fimbriae	Gal- α -1,4-Gal- β -	urinary tract
	S fimbriae	gangliosides GM3, GM2	neural
	type-1 fimbriae	Man- α -1,3(Man- α -6-Man- α -1,6) Man	urinary tract
	K99 fimbriae	gangliosides GM3, Neu5Gc- α -2,3-Gal- β 1,4-Glc	intestinal cells
<i>Haemophilus influenzae</i>	HMW1 adhesin	Neu5Ac- α -2,3-Gal- β 1,4 GlcNAc- β -, heparan sulfate	respiratory epithelium
<i>Helicobacter pylori</i>	BabA	sialyl Lewis ^x	stomach
	SabA	Lewis ^b	stomach and stomach duodenum
<i>Mycobacterium tuberculosis</i>	heparin-binding hemagglutinin adhesin (HBHA)	heparan sulfate	respiratory epithelium
<i>Neisseria gonorrhoeae</i>	Opa proteins protein	LacCer; Neu5Ac- α -2,3-Gal- β -1,4-GlcNAc- β -, syndecans, heparan sulfate	genital tract
<i>Pseudomonas aeruginosa</i>	type IV pili	asialo GM1 and GM2	respiratory tract
	LecA	Gal- α -1,4-Gal- β -1,4-glucosyl ceramide (Gb3)	respiratory tract
	LecB	Fucose and Lewis ^a	respiratory tract
<i>Staphylococcus aureus</i>	signal peptide of panton valentine leukocidin	heparan sulfate	connective tissues and endothelial cells

1.5. *Pseudomonas aeruginosa* lectins

P. aeruginosa is a Gram-negative bacterium and one of the ESKAPE pathogens (*Enterococcus faecium*, *Staphylococcus aureus*, *Klebsiella pneumoniae*, *Acinetobacter baumannii*, *Pseudomonas aeruginosa*, and *Enterobacter species*), which are the leading cause of nosocomial infections throughout the world, and most of them are multi-drug resistant.²⁵ *P. aeruginosa* causes serious infections in patients who are immunocompromised or suffer from cystic fibrosis (CF). It protects itself from the host immune system and antibiotics by building up a biofilm which is a matrix of extracellular polymeric substances (i.e. rhamnolipids, exopolysaccharides, extracellular DNA, and several proteins).²⁶ Among the extracellular proteins are two soluble lectins, called LecA and LecB, which were briefly mentioned in the previous section.

1.5.1. LECA (PA-IL)

LecA is one of the *P. aeruginosa* lectins that are found on bacterial surfaces as well as extracellularly. Its crystal structure reveals that LecA contains one calcium ion in each binding pocket, mediating the recognition to the carbohydrate ligand, and a hydrophobic region close to the carbohydrate recognition domain, which is formed by the amino acids H50 and P51 (Figure 4 A,B).^{21,24} The 12.8 kDa LecA specifically binds to D-galactose or its glycoconjugates and it has recently been reported that LecA binds to Gb3 sphingolipid, which mediates the bacterial engulfment into host cells.²⁷ Like other lectins, LecA shows a low binding affinity to its natural ligand D-galactose (**1**, figure 4C) with K_d of 87.5 μ M.²⁸ Several LecA inhibitors have been developed, and the most potent monovalent inhibitors are the β -linked galactosides with aromatic aglycon, such as naphthyl β -thio-D-galactoside (**2**, figure 4C) with a K_d value of 6.3 μ M.²⁹ This improvement in binding affinity is due to the additional CH- π interaction between the aromatic ring of the binding ligand and H50 at the binding pocket (Figure 4B).²⁹ In contrast to monovalent inhibitors, the multivalent LecA inhibitors show a potent inhibitory effect with K_d values in the nano-molar range.²⁴ To date, the most potent divalent LecA inhibitor is compounds **3** which has

been designed by Pieters and co-workers where they bridged the space between two binding galactose residues by using a rigid spacer, resulting in a high-affinity binder with a K_d of 28 nM (Figure 4A,C).³⁰

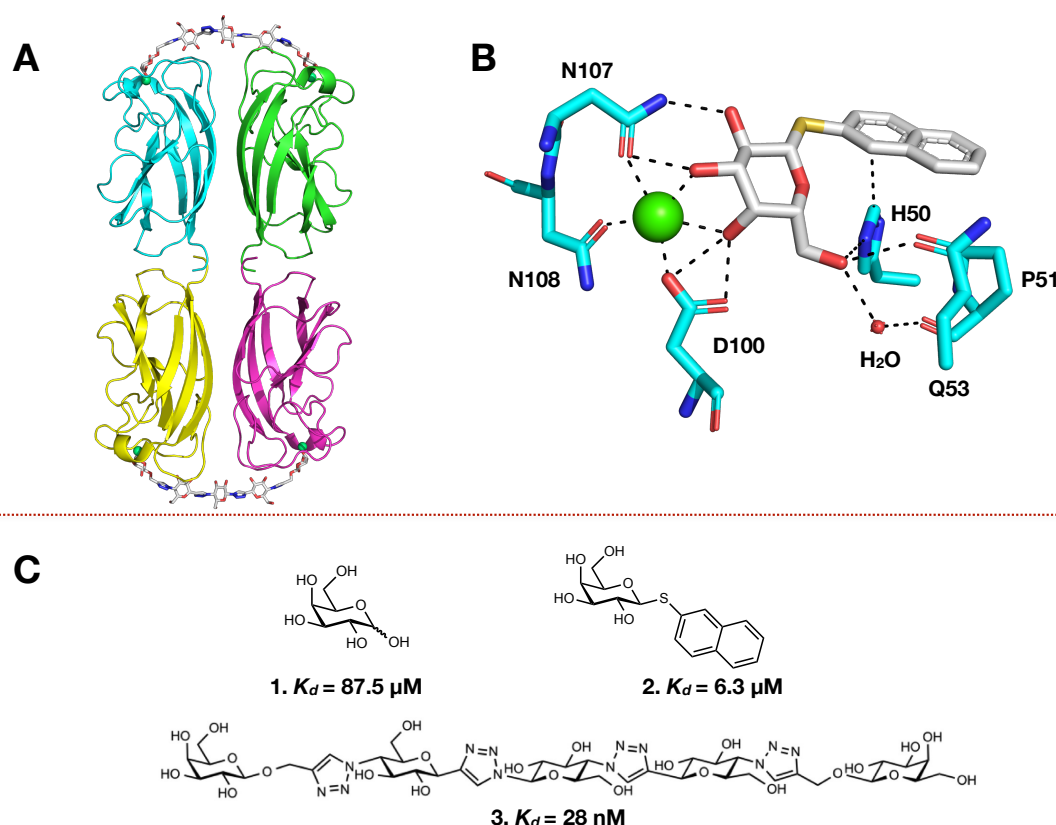


Figure 4. **A)** Homotetramer of LecA (cartoon coloured by chain, PDB code 4YWA) co-crystallized with compound **3** and one Ca^{2+} ion per binding site (green spheres). **B)** LecA binding pocket with naphthyl β -thio-D-galactoside (**2**, PDB code 4A6S). **C)** Mono- and multivalent- carbohydrate-based inhibitors of the lectin LecA. The K_d values and structure of compound **3** were taken from reference ²⁴. Compound **2** and **3** are depicted as sticks coloured by the elements (N: blue, O: red, S: yellow, C: grey); LecA amino acids (N: blue, O: red, C: marine).

1.5.2. LEC A ORTHOLOGS IN OTHER PATHOGENIC BACTERIA

Only one gene (i.e. plu2096) has been reported as a potential gene that encodes LecA homolog protein in the insect pathogen bacterium *Photobacterium luminescens* and was later confirmed to be a galactose-binding lectin.^{31,32}

1.5.3. *LEC*B (*PA-III*)

LecB (*PA-III*) is a 11.8 kDa lectin shows a preference for L-fucose over D-mannose and other sugars (Figure 5C). The crystal structure of LecB shows that it is a homotetrameric lectin with two calcium ions in each CRD (Figure 5A). These ions help the carbohydrate ligand to accommodate in the binding pocket by establishing interactions with 2OH, 3OH and 4OH of L-fucose and D-mannose (Figure 5B).³³ Most of LecB present in the cytosol and it was also found extracellularly in the biofilm.²² The secretion mechanism of LecB is still unknown and transient N-glycosylation of LecB is hypothesized as a key player in the secretion process.³⁴ As mentioned before, LecB is involved in biofilm formation: the proof of this concept was demonstrated in 2005 where the LecB knock-out *P. aeruginosa* strain was not able to grow the biofilm.²² Through a sequence analysis of more than 200 *P. aeruginosa* strains originating from natural or clinical isolates, LecB gene was found in two main clusters which were assigned as PAO1-like and PA14-like. The sequence variation between PAO1 and PA14 was 14 %, whereas the fucose binding pocket is conserved in all strains.³⁵ Thus, the targeting of the conserved fucose binding pocket of LecB is currently being promoted as a new strategy to inhibit biofilm formation.^{24,36} Up until now, the natural Lewis^a (**6**, figure 5C) is the most potent monovalent LecB inhibitor with a K_d value of 212 nM. More improvement in its potency was achieved by designing divalent, oligovalent, and dendrimer-based inhibitors.²⁴ For instance, tetravalent glycopeptide (**7**, figure 5C) showed a 10-fold increase (IC_{50} 140 nM) in potency per L-fucose compared to its monovalent epitope.³⁷ However, the multivalent inhibitors have some drawbacks when using them as a drug since they may mediate the aggregation and cross-linking of bacteria and their physicochemical properties also need further optimization.³⁸ Then, several monovalent LecB inhibitors were designed, based on L-fucose or Lewis^a disaccharide core (α -Fuc-1,4-GlcNAc), but they failed to reach methyl α -L-fucoside or Lewis^a potency.^{39,40} Therefore, since 2013 our research group has been focusing on designing monovalent drug-like inhibitors for LecB, based on low-affinity D-mannoside. The introduction of sulfonamides at C6 of methyl α -D-mannoside (**8**, figure 5C) showed a remarkable

improvement in the K_d value from 71 to 3.3 μM , respectively.⁴¹ Then, the hybrid structure (**9**, figure 5C) was synthesized with the important features of L-fucose and D-mannose for LecB binding and the K_d value was 16 μM .⁴² A further extension of the hybrid structure was done by adding sulfonamides at C6, which led to a further improvement in the K_d value, reaching the nanomolar range (e.g. compound **10**).⁴³

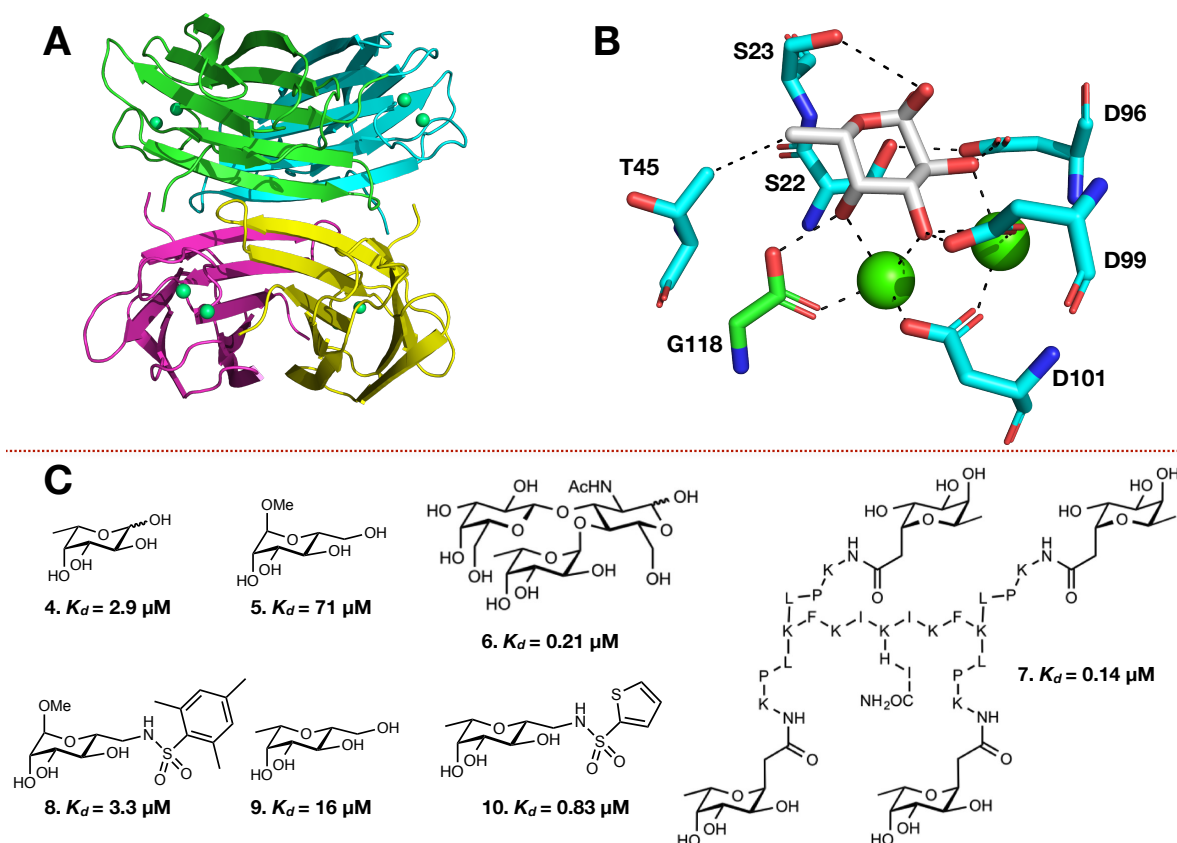


Figure 5. **A**) Homotetramer of LecB (cartoon coloured by chain, ligand not shown, PDB code 1OXC) with two Ca^{2+} ions per binding site (green spheres). **B**) LecB binding pocket with L-fucose (**4**, PDB code 1OXC). **C**) Mono- and multivalent- carbohydrate-based inhibitors of the lectin LecB. The K_d values and the structure of **6** and **7** were taken from reference ²⁴. Compound **4** is depicted as sticks coloured by the elements (N: blue, O: red, C: grey); LecB amino acids of chain A (N: blue, O: red, C: marine); LecB amino acids of chain B (N: blue, O: red, C: green).

1.5.4. LECB ORTHOLOGS IN OTHER PATHOGENIC BACTERIA

LecB-like sequences have been identified in the genomes of some opportunistic bacteria, such as *Ralstonia solanacearum* (*R. solanacearum*), *Chromobacterium violaceum*, (*C. violaceum*) and

Burkholderia cenocepacia (*B. cenocepacia*).⁴⁴⁻⁴⁷ Like LecB, RS-IIL from *R. solanacearum* and CV-IIL from *C. violaceum* share the same tetrameric arrangement of subunits with the presence of two calcium ions in the CRD. They show a binding affinity to their ligands in the micromolar range and recognize both L-fucose and D-mannose.^{44,47} In contrast to LecB, BC2L-A from *B. cenocepacia* is a dimeric lectin with two calcium ions in the binding site and shows a high affinity to D-mannose over L-fucose.⁴⁵ As mentioned in subchapter 1.4, BC2L-A is involved in biofilm formation; inhibiting this lectin is a current ongoing work to develop potent mono- and multivalent-inhibitors.⁴⁸⁻⁵⁰ Another well-characterized *B. cenocepacia* lectin is the fucose-binding BC2L-C. It is a hexameric superlectin with an additional TNF domain binding fucose in addition to the mannose-binding LecB domain at the C-terminal. BC2L-B is also a *B. cenocepacia* lectin with an additional N-terminal domain, but without homology to known domains; this lectin has not been characterized yet.^{46,51}

2. AIM OF THE THESIS

2.1. To find new antibacterial agents for human pathogenic bacteria by targeting their lectins

25,000 deaths and extra costs of €900 million in the European Union in 2007 were caused by antibiotic-resistant strains in health care units and nosocomial infections.⁵² Furthermore, the number of newly approved antibiotics decreased in the last decades, leading to a huge gap between the number of existing antibiotics and the number of antibiotic-resistant strains. There is thus an urgent need to speed up the development of new anti-infectives as well as to develop new strategies to fight bacterial resistance. The targeting of extracellular lectins is one of the new strategies to control infections by Gram-negative bacteria through inhibiting biofilm formation; there is here no necessity to overcome the bacterial membrane and resist its efflux pumps. The aim of this work is to find more potent or new classes of inhibitors for some Gram-negative human pathogen bacterium lectins by screening several natural, semi-synthetic and synthetic libraries.

2.2. To characterize new lectins from pathogenic bacteria

The need for the characterization of new lectins with a sharp specificity has already been highlighted in subchapter 1.3, which described the improvement of glycome analysis using lectin microarrays. Together with the absence of characterized *P. aeruginosa* LecA homologs, the identification, expression and analysis of LecA homologs from other pathogenic bacteria is the second aim of this work.

3. RESULTS

3.1. IDENTIFICATION OF *PSEUDOMONAS AERUGINOSA* LecB INHIBITORS USING A FLUORESCENCE POLARIZATION-BASED HIGH-THROUGHPUT ASSAY

Ghamdan Beshr, Matthew Calvert, Ronald Gracia, Jennifer Herrmann, Dirk Hauck, Rolf Müller, and Alexander Titz

Introduction

Besides the existing approaches for LecB inhibition (see subchapter 1.5.3), we decided to pursue another strategy, namely, to explore new classes of LecB inhibitors by screening natural product and semisynthetic as well as non-carbohydrate libraries. Natural products are considered by many pharmaceutical companies to be a major source of antibiotics and anti-tumour drugs, where the diversity of these compounds makes them an attractive source for potential new drugs.^{1,2} Myxobacteria is one of the best known natural product producers for it has a broad spectrum of secondary metabolites that show many bioactivities (e.g. anti-bacterial, anti-fungal, anti-tumour, anti-biofilm and other bioactivities).³ 29 % of myxobacterial metabolites demonstrate anti-bacterial activity through targeting different biological processes in other bacteria. For instance, etnangien and orallopyronin target DNA and RNA polymerase, respectively, althiomycin inhibits protein synthesis, and myxovalargin damages cell membrane. Carolacton is the only myxobacterial metabolite that shows an anti-biofilm activity, which was reported in a Gram-positive *Streptococcus mutans*.⁴

In this study, we present our strategy for the discovery of LecB inhibitors. The first step in such a screening study is the establishment of an appropriate system which allows the identification and characterization of hit compounds. We therefore developed a simple but robust fluorescence polarization-based binding assay, using a tracer with a red-shifted fluorophore for LecB, and demonstrated its utility for testing several libraries, including concentrated natural product extracts. Polarization-based high-throughput assays have been used in many studies and have shown a feasibility for high-throughput screening.⁵⁻⁷ Using this assay, a set of ~1944 compounds (including myxobacterial pure metabolites and semi/full-synthetic compounds) were screened. In addition to this, 2200 crude extracts from myxobacteria strains underwent the screening process and then one of the active extracts was investigated to find the active compound.

Experimental details

Chemicals

L-fucose and methyl α -L-fucoside (**2**) were purchased from Dextra Laboratories (UK); **SPECS-308**, **-432**, **-387**, **-605**, and **-836** from SPECS, Netherlands; OTAVA glycomimetic focused library from OTAVA Ltd. (Canada).

LecB and LecA expression and purification

LecB_{PAO1} and LecA_{PAO1} were produced according to the previously published protocols.^{8,9} In short, *E. coli* BL21 (DE3) carrying the plasmid of either LecB or LecA were grown in 1 L of LB medium (supplemented with 100 $\mu\text{g mL}^{-1}$ ampicillin) to an OD₆₀₀ = 0.5-0.6 at 37 °C and 180 rpm. The expression was induced with the addition of IPTG to a final concentration of 0.5 mM (LecB) or 0.25 mM (LecA) and the bacteria were then further cultured for 4 h at 37 °C (LecB) or 30 °C (LecA) and 180 rpm. The cells were harvested by centrifugation (9000 x g, 10 min) and the pellet was washed with TBS/Ca (20 mM Tris, 137 mM NaCl, 2.6 mM KCl at pH 7.4, supplemented with 100 μM CaCl₂). The cells were resuspended in 60 mL TBS/Ca with PMSF (1 mM) and lysozyme (0.4 mg mL⁻¹) and subsequently disrupted by 5 cycles in a microfluidic homogenizer (Microfluidics Corp., USA). Cell debris was removed by centrifugation (19'000 x g, 60 min) and the supernatant was loaded on mannosylated or galactosylated sepharose CL-6B for LecB and LecA, respectively.¹⁰ The column was washed with TBS/Ca and either LecB or LecA was eluted by 100 mM D-mannose or D-galactose, respectively. The eluted fractions were extensively dialyzed against distilled water and then TBS/Ca buffer. The concentration was determined by UV absorbance at 280 nm using a calculated molar extinction coefficient of 6990 or 27960 M⁻¹ cm⁻¹ for LecB and LecA, respectively.

Direct binding of the tracer 1 to LecB

10 μL of tracer **1** (20 nM) in TBS/Ca was mixed with 10 μL serial dilutions (234 - 0.014 μM , i.e., a final concentration of 117 μM to 0.007 μM) of LecB in TBS/Ca in triplicates in black 384-well microtiter plates (Greiner Bio-One, Germany, cat no 781900). After incubation for 4 h at r.t., the blank corrected fluorescence intensity was recorded, using a PheraStar FS microplate reader (BMG Labtech GmbH, Germany) with excitation filters at 590 nm and emission filters at 675 nm, and fluorescence polarization was calculated. The data were analyzed using a four-parameter fit of the MARS Data Analysis Software (BMG Labtech GmbH, Germany). A minimum of two independent measurements on two plates was performed.

Testing of LecB stability at different concentration of DMSO

Four serial dilutions (666 - 0.085 μM) of methyl α -L-fucoside (**2**) were prepared in different DMSO concentrations (i.e. 0, 2, 4, and 10 %). Thereafter, 10 μL of each serial dilution was added in triplicates to a 384-well plate (Greiner Bio-One, Germany, cat no 781900). Then, 10 μL of LecB and **1** were added to each well at final concentrations of 150 nM and 10 nM, respectively. After incubation for 4 h at r.t., the fluorescence polarization was determined using a microplate reader, as described above. The data were analyzed using a four-parameter fit of the MARS Data Analysis Software.

Screening libraries using polarization-based high-throughput assays

Each analyte was diluted in a TBS/Ca buffer, as shown in table 1. Pre-and fractionated myxobacterial extracts were additionally centrifuged for 1 h at 4000 rpm (Hettich® UNIVERSAL 320 R; Hettich 2 X 500 g rotor, cat no. 1460, Hettich GmbH & Co. KG, Tuttlingen, Germany) to remove the insoluble components. 10 μL of diluted samples were added in duplicates or triplicates to a 384-well plate (Greiner Bio-One, Germany, cat no 781900). Afterwards, 10 μL of either LecB or LecA with Cy5-conjugated α -L-fucoside (**1**) for LecB or FITC-conjugated α -D-galactose (**9**)⁹ for LecA was added to each well at final concentration of 150 nM (LecB) or 20 μM (LecA) and 10 nM of tracer. The final concentration of each library is listed in table 1. After incubation for 4 h or 1 h for LecB or LecA, respectively, at r.t., the blank corrected fluorescence intensity was recorded, using a PheraStar FS microplate reader with excitation filters at 590 or 485 nm (for LecB and LecA tracer, respectively) and emission filters at 675 nm or 535 nm (for LecB and LecA tracer, respectively), and the fluorescence polarization was calculated. The data were analyzed using a four-parameter fit of the MARS Data Analysis.

The percentage of inhibition for the FP assays was calculated according to equation 1.

$$\% \text{ of inhibition} = \frac{\text{mean of negative control} - \text{mean of sample}}{\text{mean of negative control} - \text{mean of positive control}} \times 100$$

Equation 1. Calculation of the percentage of inhibition of the tested compound.

Generally, compounds enhancing or quenching the total fluorescence intensity in a dose-dependent manner (deviating value of fluorescence intensity > 20 % from the controls) were excluded from further investigation.⁵

Calculation of the Z factor

The Z factor is a dimensionless value used to evaluate the quality of the HTS assay, using equation 2: a good assay should have a Z factor of between 0.5 and 1.¹¹

$$Z = 1 - \frac{3SD \text{ of sample} + 3SD \text{ of control}}{|\text{mean of sample} - \text{mean of control}|}$$

Equation 2. Z factor calculation. SD refers to the standard deviation.

Table 1. All screened libraries with their stock, diluted concentrations and the final concentration in the screening assay.

Library	Number of analytes	Concentration of stocks	Dilution ratio in TBS/Ca buffer	Final concentration in assay	Provider/supplier
Test plate	48	100 X (see table S2)	1:50	1 X	Prof. Bilitewski (HZI)
Pure myxobacterial compounds	259	10 mM (DMSO) 1 mM (DMSO)	1:10 1:50	500 µM 10 µM	Prof. Müller (HIPS)
Myxobacterial extracts	2200	100 % of methanolic crude extract	1:20	2.5 % of methanolic crude extract	Prof. Müller (HIPS)
Fractionated myxobacterial extracts	863	100 % of each fraction	1:20	2.5 % of each fraction	Prof. Müller (HIPS)
Hydrophilic SPECS library	1120	10 mM (DMSO)	1:10	500 µM	Prof. Bilitewski (HZI)
ExNCL 1-4	340	1 mM (DMSO)	1:25	20 µM	Prof. Müller (HIPS)
OTAVA (LecB)	134	10 mM (DMSO)	1:100	50 µM	OTAVA Ltd
OTAVA (LecA)	134	10 mM (DMSO)	1:50	100 µM	OTAVA Ltd

Cultivation and extraction of secondary metabolites of *Cystobacter violaceus* Cbvi28

50 mL of pre-culture of *Cystobacter violaceus* Cbvi28 strain (*C. violaceus* Cbvi28) was prepared by inoculating 50 mL of the media (Table S3) with a piece of agar that contained *C. violaceus* Cbvi28 cells. The pre-culture was incubated for 3 days at 30 °C and 180 rpm. Thereafter, the main-culture with 2 % of XAD-16 resin was inoculated by 5 % of its volume with the pre-culture and then incubated for 10 days at 30 °C and 180 rpm. Cells were harvested afterwards by centrifugation at 4000 rpm for 40 min and resuspended in 37.5 % of the main-culture volume with acetone and stirred for 3 h at r.t. Then, the whole extract was filtered (3 hw filter paper, Sartorius AG, Germany), and rotatory evaporated at 40 °C and 300 mbar. The sample was finally dissolved in 1.1 % of the main-culture volume with methanol and stored at - 20 °C for further use.

Small-scale LC-MS fractionation of extract

All fractionation was performed on a Dionex Ultimate 3000 RSLC system using a Waters BEH (C18, 100 x 2.1 mm, 1.7 µm) column by the injection of five µL of the methanolic sample. Separation was achieved by a linear gradient with (A) H₂O + 0.1 % FA to (B) ACN + 0.1 % FA at a flow rate of 550 µL/min and 45 °C. The gradient was initiated by a 0.27 min isocratic step at 5 % B, followed by an increase to 95 % B in 18 min to end up with a 1.5 min flush step at 95 % B before equilibration under the initial conditions. Coupling the HPLC to the MS was supported by an Advion Triversa Nanomate nano-ESI system attached to a Thermo Scientific Orbitrap. Mass spectra were acquired in a centroid mode ranging from 200 – 2000 m/z at a resolution of R = 30000. The flow was split to 500 nL/min before entering the ion source. The Nanomate transfers the remaining LC flow into a 96 well plate within a time range from 0.6 to 20.6 min. Each well is filled for 10 µL yielding 93 wells in total. The well plate is dried using a Genevac centrifugal evaporator (Genevac Ltd., Suffolk, UK) and used for bioactivity assay afterwards.

Large-scale HPLC fractionation of extract

The fractionation was performed on a Dionex Ultimate 3000 RSLC system using NUCLEODUR® C18 Gravity-SB (C18, 250 X 10 mm, 5 µm) by injection of 1.3 mL of 1:2.6 (H₂O:ACN) contains ~ 50 mg of dry extract. The separation was achieved by a linear gradient with (A) H₂O +0.1% FA to (B) ACN + 0.1% FA at flow rate 8 mL/min. The gradient was initiated by 1 min of isocratic step at 5 % of B, followed by an increase to 95 % of B in 20 min and remains at 95 % of B for 4 min to end up with a 5 min flush step to reach 5 % of B. During this separation, more than 100 fractions in 1.5 - 2 mL were collected. The volume of fractions was not equal at the beginning since the collection was manually performed but we could then automate this collection process. Afterwards, the fractionated samples were dried using a Thermo Savant SpeedVac SPD111V Centrifugal Evaporator (ThermoFisher, Germany) and subsequently dissolved in 10 µL of DMSO and transferred into 96 well plates. The plates were stored at - 20 °C for bioactivity assay afterwards.

Molecular Docking

SPECS-836 was docked into the binding site of LecB using PLANTS v1.1 software.¹² The calculation of charge and energy minimization of the protein and tested compounds was done using Molecular Operating Environment (MOE), 2014.09. Thereafter, the standard docking procedure (PLANTS Manual, available at <http://www.tcd.uni-konstanz.de/plants/download/download/manual1.1.pdf>) was validated by removing the D-mannose ligand and redocking it inside the active site of LecB (PDB code: 1OUR, RMSD: 0.165 Å). The docking site was limited inside a 13.3 Å radius sphere centred in the mass centre (coordination: X = 45.806, Y = 29.194 and Z = 5.333) of the crystallized ligand. Ser22, Ser23, Asp96, and Asp99 were set as flexible residues in the input file.

Polarimetry

Optical rotations of **SPECS-836** (3 mg mL⁻¹ DMSO) were determined on a P-2000 polarimeter (JASCO, Gross- Umstadt, Germany) at 22.5 °C and 589 nm using equation 3.

$$[\alpha]_{\lambda}^T = \frac{\alpha}{l * C} \longrightarrow [\alpha]_{289}^{22.5} = \frac{0.021}{0.5 * 0.003} = + 14$$

Equation 3. Calculation of optical rotation. α for measured rotation in degrees; T for temperature in degrees Celsius; λ for wavelength in nanometers; l for path length in decimeters; C in concentration in g/mL.

Molecular dynamics

The molecular dynamics was done using Molecular Operating Environment (MOE), 2014.09. Afterwards, the molecular dynamics ran for cis and trans configuration at the tetrahydrothiophene ring of **SPECS-836** and the dihedral angles were collected each 0.5 sec for 50 sec. Thereafter, the calculation of ³J values was done using the average of collected dihedral angles according to equation 4.¹³

$$\text{Calculated } ^3J = 7 - \cos(\theta) + 5\cos(2\theta)$$

Equation 4. Calculation of ³J from dihedral angles which were recorded from molecular dynamics simulation.

Results and discussion

Development of a screening assay based on fluorescence polarization technique

The competitive binding assay, based on fluorescence polarization, has been used before for lectins to assign the binding affinity of several inhibitors.^{8,9,14,15} Instead of using fluorescein-labeled sugar as a tracer, we used here Cy5-labeled α -L-fucoside (**1**). Cy5 is a red-shifted dye, the signal of which shows minimal interference with natural products compared to fluorescein in fluorescence based-assays.⁵ Cy5-conjugated α -L-fucoside (**1**) was synthesized by Dirk Hauck and then evaluated by direct titration of a constant amount of **1** with different concentrations of LecB (Figure 1). Compound **1** showed a K_d value of 235 nM, which is in good agreement with the reported K_d of methyl α -L-fucoside.¹⁶

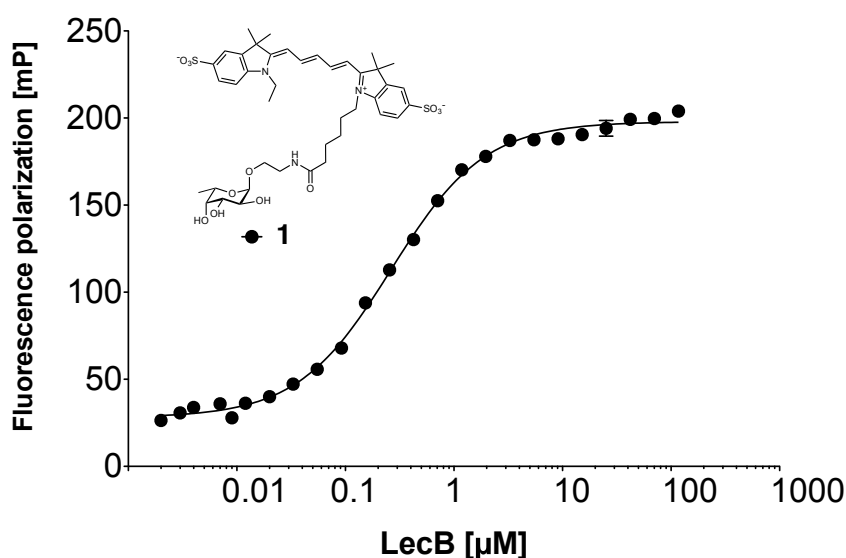


Figure 1. Determination of the dissociation constant for Cy5-conjugated α -L-fucoside (**1**) with LecB. Dissociation constant was obtained from a four-parameter fitting procedure to the concentration-dependent increase in fluorescence polarization ($K_d = 235 \pm 41$ nM). Dissociation constant and standard deviations were determined from two independent measurements of triplicates each.

Thereafter, compound **1** was displaced by methyl α -L-fucoside (**2**) in the presence of different quantities of DMSO (0 - 5 %) to check the assay tolerance for DMSO. The IC_{50} values of compound **2** corresponded to the reported one without significant effect from DMSO up to 5 % (Table S1).¹⁶

A test plate that contains several antibiotics and synthetic peptides, were subsequently tested at 1 % of DMSO stock (see table S2) as the first run. Our screening assay showed a high Z factor value (> 0.8), which is considered to be good quality for an HTP screening assay. Moreover, we monitored the fluorescence intensity of each compound to eliminate fluorescence enhancer or quencher compounds (Figure 2). Here, three hits, namely, Quercetin, WTE: A-A-W-R-A-A-C peptide and PD98059, were identified with more than 20 % of inhibition and two of them (Quercetin and WTE: A-A-W-R-A-A-C peptide) were out of the acceptable range of fluorescence intensity. Then, the concentration-dependent inhibition was analyzed; unfortunately, all of these compounds could not bind to LecB up to 500 μM for Quercetin and PD98059, and 175 μM for WTE: A-A-W-R-A-A-C peptide.

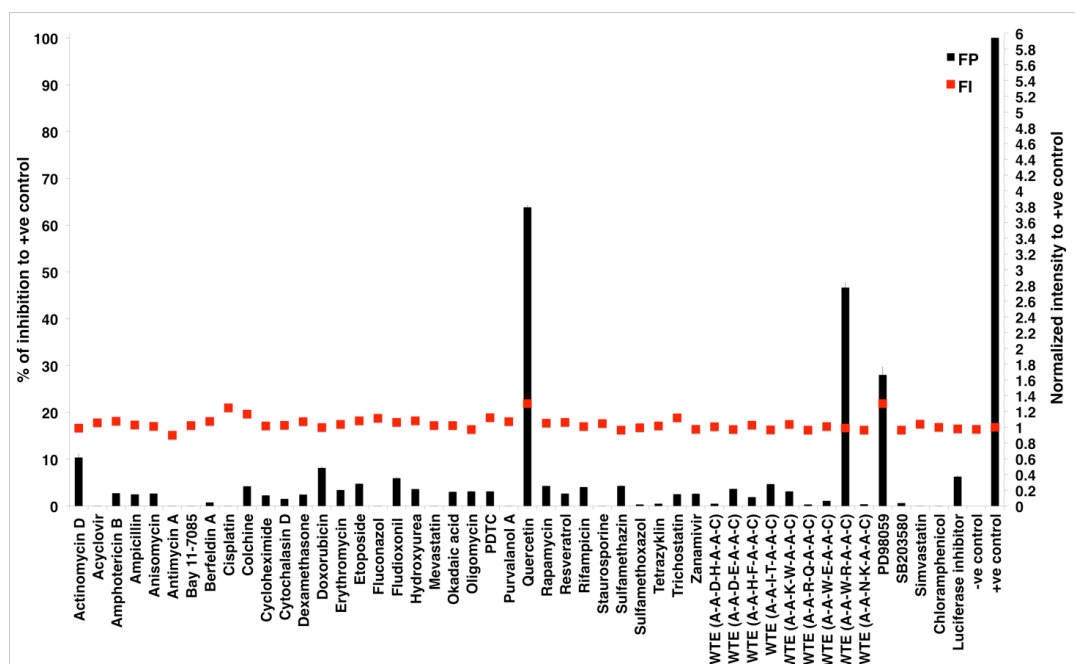


Figure 2. Screening of test plate which contains several antibiotics and synthetic peptides against LecB at 1% of stocks (see table 2) using a competitive binding assay based on fluorescence polarization. Black columns represent the calculated percentage of inhibition; red squares represent the normalized fluorescence intensity signals to the signal of positive control. The acceptable fluorescence intensity data should have $0.8 < \text{fluorescence intensity} < 1.2$. Each column and square represent the average of results from three different wells. +ve control is L-fucose; -ve control is LecB with tracer 1 and without inhibitors.

Screening of the myxobacterial natural product library

Myxobacteria are a group of Gram-negative soil bacteria that hold a large genome (e.g. ≈ 13 million nucleotides in the *Myxobacterium sorangium cellulosum* strain) and is sub-divided into 7500 strains (up to year 2010). At least 100 distinct core structures have been discovered in myxobacterial strains, exhibiting various bio-activities.³ Here, 259 myxobacterial secondary metabolites, derived from a DZIF natural compound library (Class IV), were screened in duplicate at 500 μM . The results showed outlier fluorescence intensity signals, which cannot be considered in our screening assay (Figure S1). The inconsistency of fluorescence intensity signals might have come from the poor solubility of the tested compounds; the screening was therefore performed again at a lower concentration (10 μM) to overcome precipitation of the tested compounds (Figure 3). As a result, none of the myxobacterial pure compounds was able to block LecB at 10 μM .

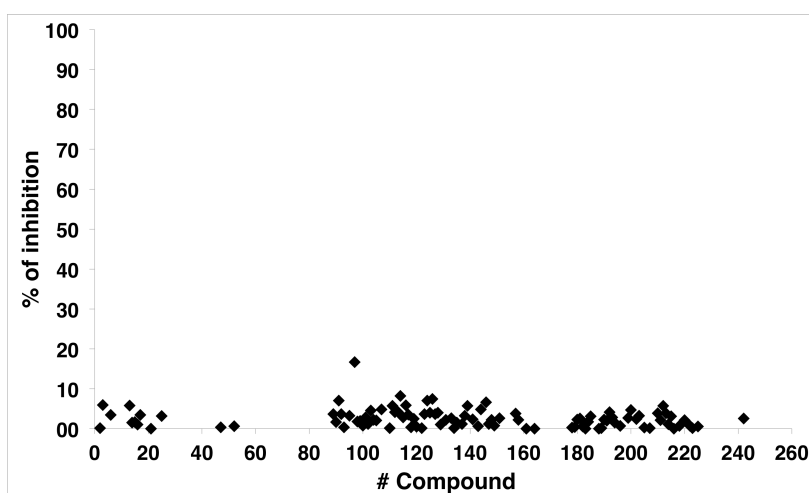


Figure 3. Screening of 259 myxobacterial secondary metabolites against LecB at 10 μM . Compounds with % of inhibition < zero (with fluorescence polarization > than negative control) are not shown. The dots of the scatter plot represent the averaged data of at least two measurements for each compound.

Since myxobacteria are producing plenty of secondary metabolites, most of which have not been characterized yet, we decided next to explore extracts of myxobacterial strain cultures to find LecB inhibitors.³

2200 myxobacteria extracts were tested at 2.5 % of their methanolic crude extract and interestingly a large number of hits were identified (Figure 4).

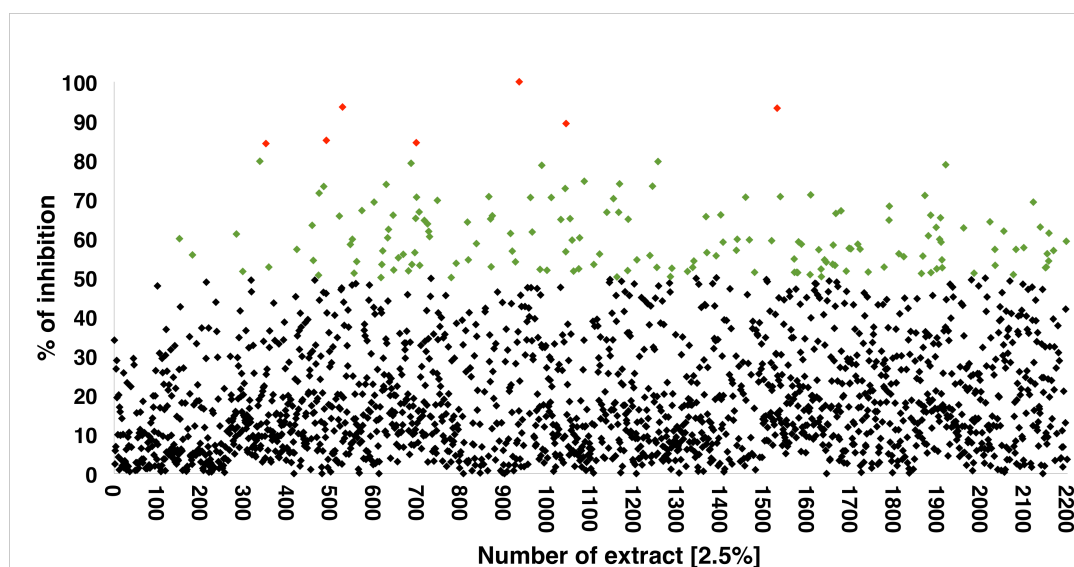


Figure 4. Screening of the myxobacterial extract library against LecB at 2.5 % of methanolic crude extract. The dots of the scatter plot represent averaged data from at least duplicates for each extract. Black dots for % of inhibition < 60; Green dots for $60 \leq$ % of inhibition < 80; Red dots for % of inhibition ≥ 80 .

7 extracts showed ≥ 80 % of LecB inhibition and then, to reduce the complexity, we minimized the size of the investigated extracts to the top three (Table 2). The extracts of strain **A**, **B**, and **C** were chosen according to their result reproducibility and fluorescence intensity, as well as the percentage of inhibition of each.

Table 2. The best 7 hits with more than 80% LecB inhibition from the myxobacterial strains' extract screen and their fluorescence intensity deviation from the positive control. SD: standard error and represents three independent measurements of at least duplicates each; FI: fluorescence intensity.

Strain	<i>Myxobacteria</i> strain	% of inhibition to +ve control \pm SD	% of FI deviation from +ve control \pm SD
A	"unclassified bacterium" NOSO3 (DSM 53667)	82 ± 5	102 ± 4
B	<i>Cystobacter violaceus</i> Cbvi28	82 ± 3	105 ± 6
C	<i>Stigmatella erecta</i> Pde45	83 ± 6	119 ± 8
D	<i>Cystobacter fuscus</i> Cbf33	90 ± 9	137 ± 5
E	<i>Myxococcus virescens</i> Mxv214	65 ± 11	147 ± 9
F	<i>Stigmatella erecta</i> Pde30	82 ± 10	149 ± 7
G	<i>Nannocystis exedens</i> 9237	115 ± 13	221 ± 10

They were then fractionated into 93 fractions, using a 96-well plate automated LC-MS fractionation procedure, by Rolf Müller's group and were subsequently evaluated for their binding to LecB. As illustrated in figure 5, the binding signals in the investigated fractions mostly came from fraction one (Fr.1) in all extracts, whereas extract of strain **B** showed additional moderate to high active fractions at Fr.72 and Fr.73. Thereafter, the concentration-dependent inhibition of all active fractions was analyzed (except Fr.72 from strain's extract **B**) (Figure S2).

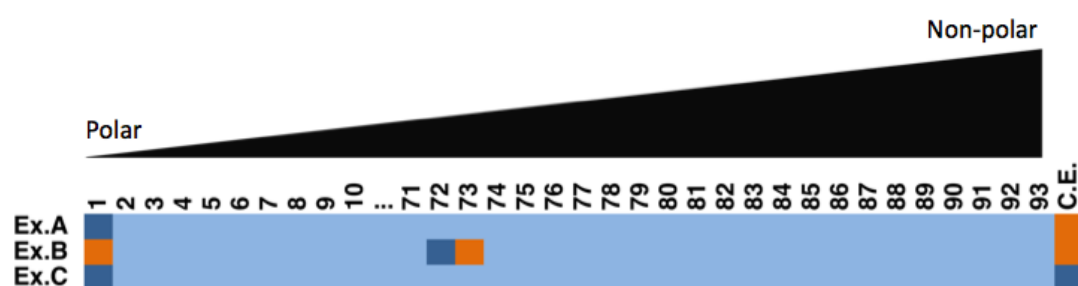


Figure 5. Screening of fractionated extracts from three myxobacterial strains that showed activity to LecB in the initial screen. Fractions with % of inhibition < 40 represented by the sky-blue colour; 40 ≤ % of inhibition < 60 by dark blue colour; % of inhibition ≥ 60 by orange colour. C.E. refers to the pre-fractionated crude extract.

As a result, Fr.1 and Fr.73 from extract of strain **B** are the only ones showing 69 % of inhibition at 3 % of Fr.1 and an IC_{50} of 0.05 % of Fr.73. Here, the search for active compounds was narrowed within extract of strain **B** and even more so within Fr.73 since the hydrophilic Fr.1 seems to be sugars from the growth medium (see below). The LC-MS spectrum at Fr.73 showed a low MS signal with two major peaks, $m/z = 371.0994$ and 403.1258 , which do not match any characterized class in the myxobacterial database (Figure S3). The production of compounds in Fr.73 was therefore optimized by cultivating the strain **B** in five different media (Table S3). Besides, cell-free media underwent the same cultivation and extraction procedure to be used as a control in further assays. The IC_{50} values of the bacterial extract and of the control were generated and showed the highest binding signals at CLF medium either with or without bacterial cells ($IC_{50} = 0.111$ and 0.087 % of their methanolic extract, respectively) (Figure 6).

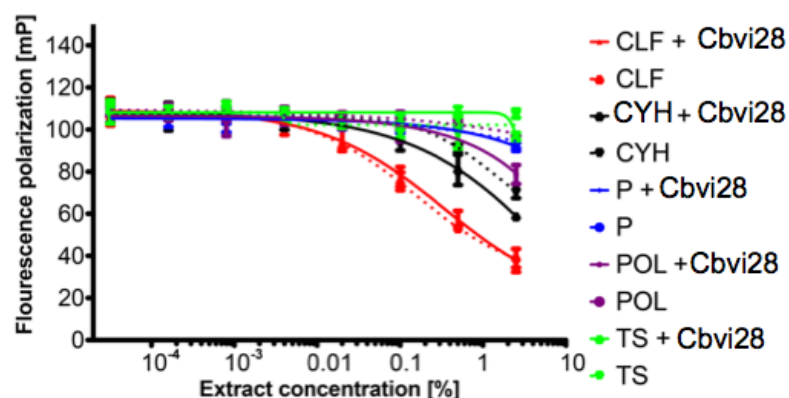


Figure 6. Optimization of active fractions' production in extract of strain **B** by the cultivation strain **B** in different media. The extracts of cultivated cells in each medium and cell-free media were analyzed with LecB by generating their concentration-dependent inhibition curves. The solid line refers to extracts of cultivated cell in each media; the dash line is for cell-free media extracts. The different colours represent different media.

The CLF medium was used in the cultivation of strain **B** in the previous experiments. Furthermore, the extract of the cell-free CLF medium showed an equivalent effect to the cells' extract, which could be due to the skimmed milk that was uniquely present in the CLF medium constituents (Table S3). It has been reported that human milk oligosaccharides block *P. aeruginosa* LecB, but whether skimmed milk blocks LecB remains to be investigated.^{17,18}

At that time, we speculated that the strong signal in the extract of strain **B** could be acquired from polar sugar components inside the medium, in addition to other less polar active metabolites, which were identified at Fr.73. We scaled up the cultivation of the strain **B** in the CLF medium from 200 mL to 2 L to improve the amount of the active compounds within Fr.73. Furthermore, a large-scale fractionation procedure using a preparative HPLC system was established. Three independent batches of strain **B** extract (2 X 200 mL and 1 X 2 L batches) in addition to the extract of cell-free CLF medium were fractionated by preparative HPLC and subsequently examined their inhibitory effect to LecB at 2.5% of each fraction (Figure 7).

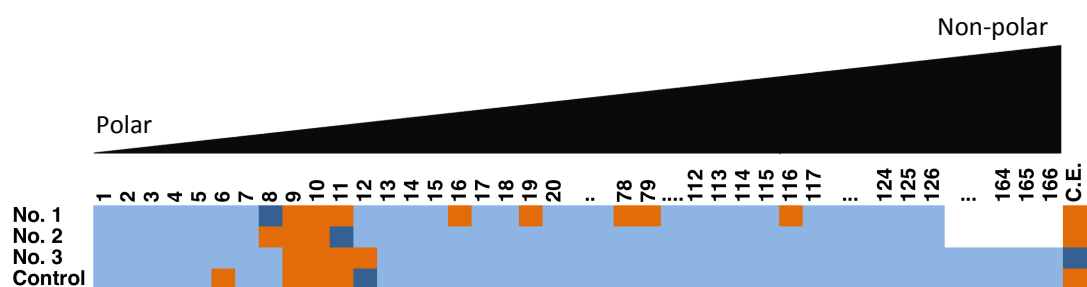


Figure 7. Screening of the fractionated stain **B** extract from different batches in addition to the control (extract from cell-free CLF medium). Fractions with % of inhibition < 40 represented by the sky-blue colour; 40 ≥ % of inhibition < 60 by the dark blue colour; % of inhibition ≥ 60 by the orange colour. White colour: no sample. No.1 and 2 the extracts from different 200 mL batches; No. 3 extracts from a different 2 L batch; Control from a 200 mL batch; C.E. refers to the unfractionated crude extract.

As shown in figure 7, there is a lack of reproducibility of the results from the active fractions with non-polar property, i.e Fr.78, 79, and 116 in batch No.1. In contrast to this, the high polar active (i.e. Fr.9 - 11) fractions were present in all fractionated batches, including the extract of the cell-free medium. We therefore stopped working with the myxobacterial extracts as the outcome was not reproducible and the culture medium contained LecB blockers.

Screening of the natural products library (NxCL)

The NxCL library is part of the DZIF screening library and contains 340 compounds. These compounds are mostly antibiotics, mainly originating from *Streptomyces*, fungi, plants, *Cyanobacteria*, etc. The NxCL library was screened at 20 µM and unfortunately none of tested compounds showed significant interactions with the LecB at 20 µM (Figure 8).

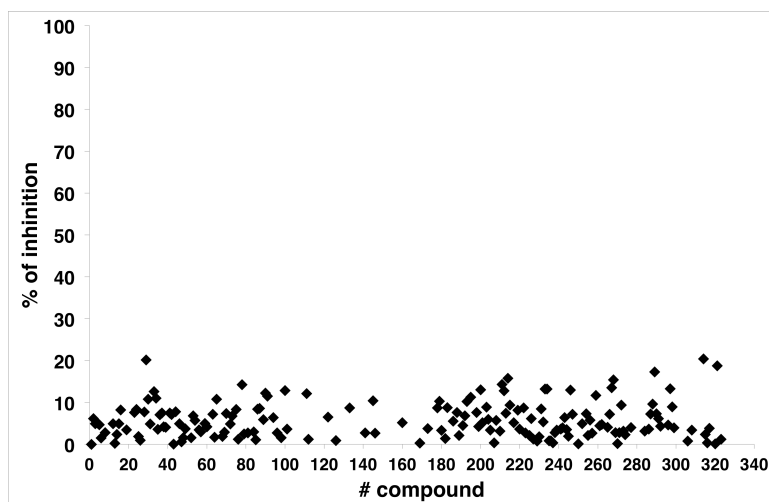


Figure 8. Screening of the NxCL library against LecB at 20 μ M. The dots of the scatter plot represent averaged data of at least two measurements for each tested compound.

Screening of the SPECS library

The SPECS library contains chemically diverse compounds, which have been synthesized and brought from more than 2,000 academic sources worldwide. In this study, 1120 hydrophilic compounds, which were selected at DZIF, were tested to target the hydrophilic binding pocket in LecB. The SPECS compounds were tested at 500 μ M and five hits showed more than 20 % of inhibition (Figure 9, S4).

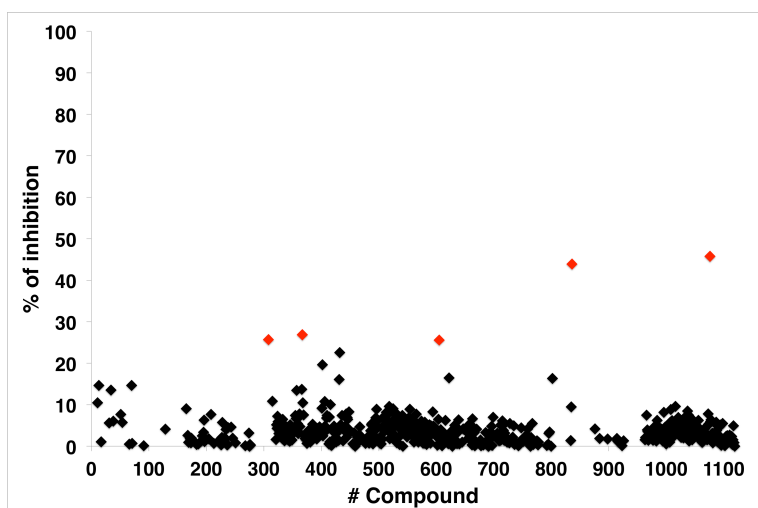


Figure 9. Screening of SPECS library with LecB at 500 μ M. The dots in the scatter plot represent the averaged data from screening compounds. The red dots represent hits with more than 20 % of LecB inhibition.

All compounds that were identified as hits in the initial screen were then purchased from commercial vendors, freshly prepared in DMSO and validated by analysing their concentration-dependent inhibitory effect (Figure S5). Only one of the five hits, **SPECS-836**, showed binding with 60% inhibition at 1 mM. To confirm **SPECS-836** binding to LecB, we tried to co-crystallize the LecB in a complex with **SPECS-836** in Anne Imberty's lab but the compound could not be found in the binding pocket. Hence, a molecular docking was carried out afterwards by docking **SPECS-836** (in cis/trans configuration) into the LecB binding pocket. The best pose showed that the 3-OH at the tetrahydrothiophene ring and the carbonyl group in the compound are in the cis configuration and coordinate to Ca^{2+} ions in the same manner as 3-OH and 4-OH in D-mannose (Figure 10B).

Unfortunately, the structural flexibility at the tetrahydrothiophene ring of **SPECS-836** was not given by the supplier and a detailed structural characterization for **SPECS-836** was therefore carried out using NMR spectroscopy, optical polarimetry, and computational methods. The stereochemistry at the tetrahydrothiophene ring could not be addressed by NMR and the specific rotation (+14) indicates a non-racemic compound (Figure S6). Furthermore, a molecular dynamics study was performed to calculate the 3J coupling constant values at the tetrahydrothiophene ring of modelled **SPECS-836** in cis/trans configurations and then compared to the measured 3J values by ^1H NMR (Figure 10C and S7). The calculated 3J values at the tetrahydrothiophene ring of cis configuration were marginally closer to the experimental data, which supports the binding behavior of **SPECS-836** in the previous docking study. Nevertheless, further investigations should be performed to confirm the binding of **SPECS-836** to LecB.

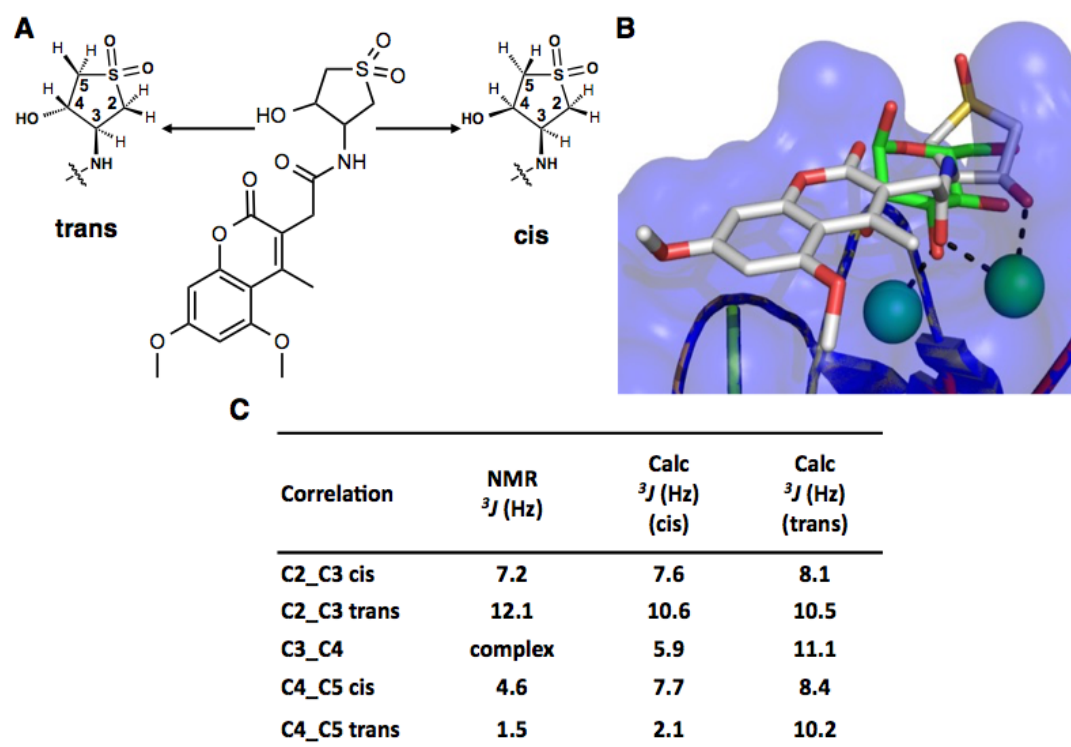


Figure 10. A) Chemical structure of **SPECS-836** with possible stereochemistry at the tetrahydrothiophene. B) Superposition of LecB in a complex with D-mannose (PDB:1OUR) and docked **SPECS-836** into the LecB binding pocket, using PDB:1OUR. D-mannose and **SPECS-836** are depicted as sticks coloured by the elements (O: red, C: green) and (N: blue, O: red, S: yellow, C: grey), respectively. Two Ca^{2+} ions in the binding site are shown as green spheres. C) Comparison of *in-silico* calculated and measured 3J values at the tetrahydrothiophene ring of **SPECS-836**.

Screening of a glycomimetic-focused library (OTAVA)

After screening of many synthetic and natural compound libraries, we concluded that finding non-carbohydrate inhibitors for LecB is challenge. Thus, we decided to focus on libraries which contain glycomimetics or carbohydrate-based compounds. 135 compounds that are mimicking glycans or based on non-acetylated carbohydrates was purchased from OTAVA glycomimetic focused library (Table S6). The OTAVA library was tested at 50 and 100 μM with LecB and LecA, respectively. Five hits ($\geq 20\%$ of inhibition) were identified for LecB, whereas there were 21 hits for LecA (Table S4 & S5). All these hits are based on carbohydrates except compound **OTAVA-51** (LecA hit). A concentration-dependent inhibitory analysis was performed and all LecB hits have IC_{50} values in a range of 6 to 11 μM . Three of them (i.e. **OTAVA-91**, **-122**, and **-134**) are based on L-arabinose, which

is known to be a LecB inhibitor¹⁹, whereas two of them (i.e. **OTAVA-112** and **-116**) are surprisingly based on D-xylose, which is usually not recognized by LecB. Therefore, one of two xylose-based hits (**OTAVA-116**) was characterized, using LC-MS and NMR. The LC-MS spectrum showed a major peak with $m/z = 345.06$ that matches the exact mass of the investigated compound, whereas the NMR spectrum showed differences in the glycone part of the compound where 4-OH at the pyranose ring is axial-oriented instead of being equatorial (Figure S8 and 9). Here, the correct structure of **OTAVA-116** is based on L-arabinose and we supposed the same for **OTAVA-112**.

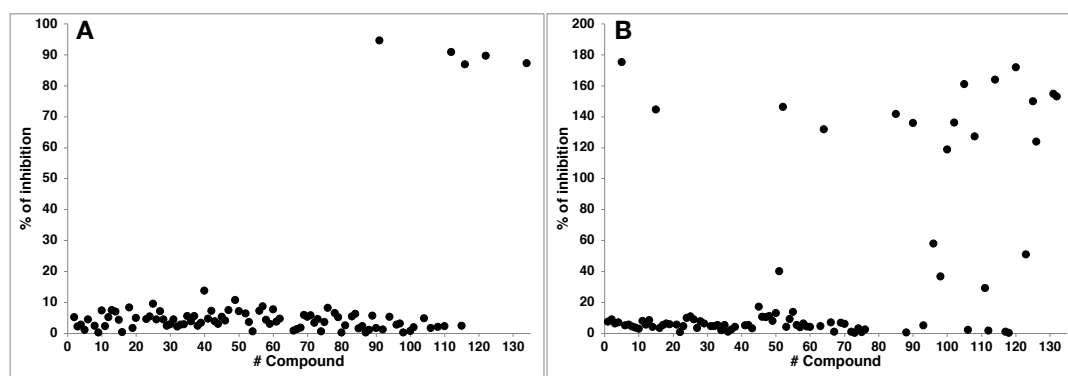


Figure 12. Screening of the glycomimetic-focused library (OTAVA) with LecB (**A**) and LecA (**B**) at 100 and 50 μM , respectively. The dots in the scatter plot represent the averaged data of at least duplicates for each screened compound.

Many of LecA hits showed more than 100 % of inhibition which indicates a higher potency compared to the used positive control (Methyl α -D-galactose) (Figure 12B, table S5). 15 of the LecA hits are based on β -D-galactoside acquiring different substitutes in the aglycon part and they show the IC_{50} values in a two-digit micromolar range (Table S5A). In addition to this, some of the LecA hits are based on structures with unknown stereochemistry at the pyranose ring, from which we speculated that they are D-galactoside-based compounds (Table S5B). This speculation was built on the IC_{50} values of the assayed compounds which are similar to IC_{50} values of β -D-galactoside-based hits and to well-characterized carbohydrates binding to LecA.²⁷ **OTAVA-51** showed the only non-carbohydrate hits for LecA in the initial screen, but it failed to show concentration-dependent binding to LecA up to 500 μM (Table S5B). Generally, most of LecA hits have IC_{50} in the range of 20 - 42 μM except for three weaker binders (**OTAVA-96**, **-123** and **-111**) and the best inhibitor in this set of

compounds was **OTAVA-123** with an IC_{50} value of 20.3 μ M and 5.2 for its relative potency to methyl α -D-galactoside.

Summary

In this study, we developed a high throughput screening assay, using fluorescence polarization measurement. A tracer bearing a Cy5 fluorophore was synthesized and evaluated afterwards with LecB. Our established screening assay showed good quality where we could avoid the interfering signal from the auto-fluorescence compounds by using a tracer containing red-shifted dye. In addition to this, it showed a high throughput property with a Z score of 0.8 - 0.9, which is considered a good screening assay.

Various natural, synthetic and semi-synthetic compound libraries were investigated to find potent LecB inhibitors or new inhibitor classes that we could use as lead structures in the future. None of the tested characterized myxobacteria metabolites could inhibit LecB at 10 μ M, and here the availability and solubility of these compounds required this low tested concentration. A search of myxobacterial extracts was carried out afterwards and thousands of hits were identified, however the evaluation if these hits are bacterial secondary metabolite or sugar constituents in the growth media, was the bottleneck in this study.

After validation of the binding of the most potent 7 hits to LecB, our search was narrowed into one myxobacterial extract, extract of strain **B**. We then established a large-scale fractionation, using the preparative HPLC in our lab, where we could scale up the fractionation of bacterial extract up to ~ 50 mg in more than 100 fractions. It was found that the hit signals originated from the cultivating medium rather than from the bacterial secondary metabolites. The inordinate length of time involved and the complexity of finding a LecB inhibitor among the bacterial extracts as well as false positive signals from the media were sufficient reasons to stop working with myxobacterial extracts.

Thereafter, other natural products and hydrophilic compound libraries, such as NxCL and SPECS, were investigated. Among these libraries, only **SPECS-836** showed a weak binding affinity at 1 mM with incomplete characterization of its chemical structure. More validation and characterization should therefore be done with this compound to address its binding to LecB and it may indeed become a lead structure for new LecB inhibitors. The glycomimetic library was an interesting library

to investigate, since it focuses on carbohydrate-based compounds and compounds mimicking carbohydrates. Some hits were identified for LecB and LecA, but all of them were based on known inhibitors and better or equivalent inhibitors for both lectins were achieved using a rational structure-based design strategy.^{8,9,19,20}

References

- (1) Cragg, G. Natural Products in Drug Discovery and Development. *J. Nat. Prod.* **1997**, *60* (1), 52–60.
- (2) Shu, Y.-Z. Recent Natural Products Based Drug Development: A Pharmaceutical Industry Perspective. *J. Nat. Prod.* **1998**, *61* (8), 1053–1071.
- (3) Weissman, K. J.; Müller, R. Myxobacterial Secondary Metabolites: Bioactivities and Modes-of-Action. *Nat. Prod. Rep.* **2010**, *27* (9), 1276–1295.
- (4) Jansen, R.; Irschik, H.; Huch, V.; Schummer, D.; Steinmetz, H.; Bock, M.; Schmidt, T.; Kirschning, A.; Müller, R. Carolacton--A Macrolide Ketocarboxylic Acid That Reduces Biofilm Formation by the Caries-and Endocarditis-Associated Bacterium *Streptococcus Mutans*. *European J. Org. Chem.* **2010**, *2010* (7), 1284–1289.
- (5) Turek-Etienne, T. C.; Lei, M.; Terracciano, J. S.; Langsdorf, E. F.; Bryant, R. W.; Hart, R. F.; Horan, A. C. Use of Red-Shifted Dyes in a Fluorescence Polarization AKT Kinase Assay for Detection of Biological Activity in Natural Product Extracts. *J. Biomol. Screen.* **2004**, *9* (1), 52–61.
- (6) Maurer, C. K.; Fruth, M.; Empting, M.; Avrutina, O.; Hoßmann, J.; Nadmid, S.; Gorges, J.; Herrmann, J.; Kazmaier, U.; Dersch, P.; et al. Discovery of the First Small-Molecule CsrA--RNA Interaction Inhibitors Using Biophysical Screening Technologies. *Future Med. Chem.* **2016**, *8* (9), 931–947.
- (7) Cho, E. J.; Xia, S.; Ma, L.-C.; Robertus, J.; Krug, R. M.; Anslyn, E. V.; Montelione, G. T.; Ellington, A. D. Identification of Influenza Virus Inhibitors Targeting NS1A Utilizing Fluorescence Polarization--Based High-Throughput Assay. *J. Biomol. Screen.* **2012**, *17* (4), 448–459.
- (8) Hauck, D.; Joachim, I.; Frommeyer, B.; Varrot, A.; Philipp, B.; Möller, H. M.; Imberty, A.; Exner, T. E.; Titz, A. Discovery of Two Classes of Potent Glycomimetic Inhibitors of *Pseudomonas aeruginosa* LecB with Distinct Binding Modes. *ACS Chem Biol* **2013**, *8* (8), 1775–1784.
- (9) Joachim, I.; Rikker, S.; Hauck, D.; Ponader, D.; Boden, S.; Sommer, R.; Hartmann, L.; Titz, A. Development and Optimization of a Competitive Binding Assay for the Galactophilic Low Affinity Lectin LecA from *Pseudomonas aeruginosa*. *Org Biomol Chem* **2016**, *14* (33), 7933–7948.
- (10) Fornstedt, N.; Porath, J. Characterization Studies on a New Lectin Found in Seeds of *Vicia ervilia*. *FEBS Lett.* **1975**, *57* (2), 187–191.
- (11) Zhang, J.-H.; Chung, T. D. Y.; Oldenburg, K. R. A Simple Statistical Parameter for Use in Evaluation and Validation of High Throughput Screening Assays. *J. Biomol. Screen.* **1999**, *4* (2), 67–73.
- (12) Korb, O.; Stützle, T.; Exner, T. E. PLANTS: Application of Ant Colony Optimization to Structure-Based Drug Design. In *International Workshop on Ant Colony Optimization and Swarm Intelligence*; 2006; pp 247–258.
- (13) Becker, E. D. *High Resolution NMR: Theory and Chemical Applications*; Elsevier, 1999.
- (14) Beshr, G.; Sommer, R.; Hauck, D.; Siebert, D. C. B.; Hofmann, A.; Imberty, A.; Titz, A. Development of a Competitive Binding Assay for the *Burkholderia cenocepacia* Lectin BC2L-A and Structure Activity Relationship of Natural and Synthetic Inhibitors. *Medchemcomm* **2016**, *7* (3), 519–530.

-
- (15) Beshr, G.; Sikandar, A.; Jemiller, E.-M.; Klymiuk, N.; Hauck, D.; Wagner, S.; Wolf, E.; Koehnke, J.; Titz, A. Photorhabdus luminescens Lectin A (PIIA): A New Probe for Detecting α -Galactoside--Terminating Glycoconjugates. *J. Biol. Chem.* **2017**, 292 (48), 19935–19951.
- (16) Wagner, S.; Sommer, R.; Hinsberger, S.; Lu, C.; Hartmann, R. W.; Empting, M.; Titz, A. Novel Strategies for the Treatment of Pseudomonas aeruginosa Infections. *J. Med. Chem.* **2016**, 59 (13), 5929–5969.
- (17) Perret, S.; Sabin, C.; Dumon, C.; Pokorná, M.; Gautier, C.; Galanina, O.; Ilia, S.; Bovin, N.; Nicaise, M.; Desmadril, M.; et al. Structural Basis for the Interaction between Human Milk Oligosaccharides and the Bacterial Lectin PA-III of Pseudomonas aeruginosa. *Biochem. J.* **2005**, 389 (2), 325–332.
- (18) Lesman-Movshovich, E.; Lerrer, B.; Gilboa-Garber, N. Blocking of Pseudomonas aeruginosa Lectins by Human Milk Glycans. *Can. J. Microbiol.* **2003**, 49 (3), 230–235.
- (19) Sommer, R.; Exner, T. E.; Titz, A. A Biophysical Study with Carbohydrate Derivatives Explains the Molecular Basis of Monosaccharide Selectivity of the Pseudomonas aeruginosa Lectin LecB. *PLoS One* **2014**, 9 (11), e112822.
- (20) Sommer, R.; Wagner, S.; Rox, K.; Varrot, A.; Hauck, D.; Wamhoff, E.-C.; Schreiber, J.; Ryckmans, T.; Brunner, T.; Rademacher, C.; et al. Glycomimetic, Orally Bioavailable LecB Inhibitors Block Biofilm Formation of Pseudomonas aeruginosa. *J. Am. Chem. Soc.* **2017**.

3.2. PHOTOSWITCHABLE JANUS GLYCODENDRIMER MICELLES AS MULTIVALENT INHIBITORS OF LEC_A AND LEC_B FROM *PSEUDOMONAS AERUGINOSA*

Yingxue Hu, Ghamdan Beshr, Christopher Garvey, Rico Tabor, Alexander Titz and
Brendan Wilkinson.

Colloids and Surfaces B: Biointerfaces, **2017** (159), 605-612 -
DOI: 10.1016/j.colsurfb.2017.08.016



Contents lists available at ScienceDirect

Colloids and Surfaces B: Biointerfaces

journal homepage: www.elsevier.com/locate/colsurfb

Protocols

Photoswitchable Janus glycodendrimer micelles as multivalent inhibitors of LecA and LecB from *Pseudomonas aeruginosa*Yingxue Hu^a, Ghamdan Beshr^{b,c}, Christopher J. Garvey^d, Rico F. Tabor^a, Alexander Titz^{b,c}, Brendan L. Wilkinson^{e,*}^a School of Chemistry, Monash University, Victoria 3800, Australia^b Chemical Biology of Carbohydrates, Helmholtz Institute for Pharmaceutical Research Saarland (HIPS), D-66123 Saarbrücken, Germany^c Deutsches Zentrum für Infektionsforschung, Standort Hannover, Braunschweig, Germany^d Australian Centre for Neutron scattering, ANSTO, Lucas Heights, New South Wales 2234, Australia^e School of Science and Technology, the University of New England, New South Wales 2351, Australia

ARTICLE INFO

Article history:

Received 6 June 2017

Received in revised form 31 July 2017

Accepted 10 August 2017

Available online 16 August 2017

Keywords:

Janus glycodendrimer

Lectin inhibitors

Photoswitchable amphiphiles

ABSTRACT

The first example of the self-assembly and lectin binding properties of photoswitchable glycodendrimer micelles is reported. Light-addressable micelles were assembled from a library of 12 amphiphilic Janus glycodendrimers composed of variable carbohydrate head groups and hydrophobic tail groups linked to an azobenzene core. Spontaneous association in water gave cylindrical micelles with uniform size distribution as determined by dynamic light scattering (DLS) and small angle neutron scattering (SANS). *Trans-cis* photoisomerization of the azobenzene dendrimer core was used to probe the self-assembly behaviour and lectin binding properties of cylindrical micelles, revealing moderate-to-potent inhibition of lectins LecA and LecB from *Pseudomonas aeruginosa*.

Crown Copyright © 2017 Published by Elsevier B.V. All rights reserved.

1. Introduction

Non-covalent carbohydrate-protein binding interactions mediate myriad biological processes, yet the binding affinity of individual interactions are often very weak in highly competitive aqueous environments (disassociation constants ranging from 10^{-3} to 10^{-4} M) [1]. Nature overcomes this intrinsic limitation through the simultaneous binding of clustered, multivalent glycans expressed on cellular surfaces to their cognate receptors, or lectins. The so-called 'multivalent' or 'glycoside cluster' effect results in several-fold enhancement in binding avidity, with energies that are greater than the sum of individual interactions [2]. The development of multivalent mimics of natural glycans has been actively pursued as inhibitors of carbohydrate-protein binding events, which function as structural probes for understanding cellular signaling and physiology or as therapeutic agents with potential anti-microbial, anti-inflammatory and anti-tumour activity [3]. Conventional approaches toward this goal involve the elaboration of multivalent scaffolds with carbohydrate epitopes to yield nanoscale structures including glycodendrimers [4], glycopeptides [5], glycopolymers [6], glycodynamers [7], fullerenes

[8] and calixerenes, etc [9]. In some cases, potent binding affinity and selectivity has been achieved using these structures as a result of favourable ligand preorganization, however such molecular systems offer limited modes of spatial presentation due to the underlying rigid scaffold and suffer drawbacks associated with complex multistep synthesis and purification [10]. An alternative and promising approach towards multivalent glycan presentation involves the spontaneous association of glycoamphiphiles in water to provide self-assembled, soft materials including liposomes and micelles that are capable of mimicking biological membranes [10–12]. Self-assembled systems offer several advantages over rigid molecular assemblies, including ease of molecular synthesis of the monomer and the ability to program ligand density and valency through appropriate molecular design. With this in mind, we were interested in exploring multivalent self-assembled structures possessing light addressable properties in order to tune ligand topology and therefore lectin-carbohydrate binding. In particular, we were interested in utilizing these responsive systems for interrogating pathological lectin-carbohydrate interactions in a spatially and temporally resolved manner, although such systems may also find applications as targeted delivery vehicles with phototriggered release properties.

Reversible *trans-cis* photoisomerization of the well-characterised azobenzene chromophore has been widely exploited for controlling the conformational dynamics of biomolecules [13],

* Corresponding author.

E-mail address: brendan.wilkinson@une.edu.au (B.L. Wilkinson).

including the three-dimensional arrangement of multivalent carbohydrates on cluster glycosides [14], cyclodextrin bilayer vesicles [15], polymers [16] and self-assembled monolayers [17]. Our group has recently reported the photomodulation of bacterial biofilm formation using a library of carbohydrate-based surfactants [18]. Optical control over bacterial growth and biofilm formation in drug-resistant Gram-positive and Gram-negative bacteria was shown to be highly sensitive to the carbohydrate head group and isomeric state of the azobenzene tail group. Based on these observations, we decided to explore the application of amphiphilic, azobenzene functionalized glycodendrimers that undergo self-assembly to derive responsive, multivalent soft materials for probing lectin binding. Herein we report the modular synthesis of a library of 12 amphiphilic 'Janus' glycodendrimers as photoswitchable inhibitors of soluble lectins LecA and LecB from *Pseudomonas aeruginosa*, an opportunistic pathogen known to cause serious biofilm-related illnesses [19]. Glycodendrimers underwent spontaneous association in water to give light-responsive cylindrical micelles with narrow polydispersity, as revealed from dynamic light scattering (DLS) and small angle neutron scattering (SANS), respectively. Micelle structures could be tuned through UV light irradiation, thus underscoring their potential application as addressable antimicrobial agents and tools for studying carbohydrate–protein interactions.

2. Materials and methods

2.1. General methods

Analytical thin layer chromatography (TLC) was performed on commercially prepared silica plates (Merck Kieselgel 60 0.25 mm F254). Flash column chromatography was performed using 230–400 mesh Kieselgel 60 silica eluting with distilled solvents as described. Solvents and reagents were purchased from Sigma-Aldrich and Merck and used without further purification. ^1H NMR and ^{13}C NMR spectra were recorded on a Bruker Avance 400 NMR spectrometer at frequencies of 400 MHz and 100 MHz respectively. Chemical shift is reported as parts per million (ppm) downfield shift to the TMS internal standard. The data are reported as chemical shift (δ), multiplicity, relative integral, coupling constant (J =Hz) and assignment where possible. IR spectra were recorded on a Bruker ATR spectrometer. Optical rotation was measured on an Optical Activity Polaer 2001 (546 nm) polarimeter using a 1 mL cell volume and a 10 cm path length. LCMS was performed on an Agilent Infinity 1260 HPLC coupled to an Agilent 6120 B mass spectrometer. Separations were performed on an Agilent Poroshel 120 high resolution column.

Preparative HPLC was performed on an Agilent Zorbax 300SB C3 column (20 mm ID \times 150 mm) using a linear gradient of 8:1:1 water/AcN/*i*-PrOH (Solvent A) and 1:1 AcN/*i*-PrOH (Solvent B) as the mobile phase. Separations were performed using a linear gradient of 10% solvent B to 100% solvent B over 30 min, operating at a flow rate of 10 mL/min.

2.2. UV–vis spectroscopy

The native *trans* isomers of carbohydrate surfactants were converted into *cis* states by illumination of their aqueous solutions under ambient conditions using a UV lamp with λ_{max} at 361 nm in a time-dependant manner (1–30 min). Five minutes of photoexcitation was found sufficient to convert *trans* isomers into *cis* state. All the studies involving *cis* isomers were obtained after 10 min of illumination with $\lambda_{361\text{nm}}$. Since many biological processes occur at 37 °C, the thermal stability of both the native *trans* isomer as well as the photoinduced *cis* isomer was studied at ambient temperature

(20 °C) and 37 °C using UV–vis spectroscopy. Azobenzene *trans-cis* photoisomerisation was found to be complete within 5 min of UV irradiation. The native *trans* isomers remained stable under ambient lighting conditions at least up to 24 h, as evident from insignificant changes in their UV–vis absorbance spectra over this period. The thermal relaxation studies were performed at ambient temperature and 37 °C for 24 h in Milli-Q water. The half-lives of the *cis* isomers in Milli-Q water at different temperatures were estimated from thermal relaxation studies by plotting the ratios of peak area under 325 nm peak and that under 440 nm peak over a period of 24 h (Figs. S1 and S2). These peaks were chosen as *cis-trans* relaxation results in increase in peak intensity at ~ 325 nm, with a corresponding decrease in peak intensity at 440 nm.

2.3. Determination of CAC

The critical aggregation concentration was determined using Nile red encapsulation assay [20]. A 1 mg mL $^{-1}$ Nile Red stock solution was prepared in chloroform. A glycodendrimer stock solution was made up in Milli-Q water at various concentrations depending on the starting concentration for the assay. Encapsulation samples were made by adding 10 μL Nile red into 4 mL glycodendrimer solution. The fluorescence emission was measured on an Agilent Technology Cary Eclipse fluorescence spectrophotometer using an excitation wavelength of 550 nm. Signals were recorded between 570 and 700 nm with 5 nm excitation/emission slit. To investigate the relationship between conformational exchanges and the concentration of glycodendrimers, the UV–vis spectra of representative glycodendrimer 1–4 were measured at concentrations related to their CAC values (Fig. S8).

2.4. Dynamic light scattering (DLS)

DLS was performed with a Brookhaven NanoBrook Omni instrument. Instrument parameters were determined automatically along with the measurement times. Experiments were performed five times independently. The glycodendrimer was dissolved in Milli-Q water at 0.1 mM concentration and DLS experiments were measured at 20 °C. Samples were irradiated with UV light at 361 nm for 10 min before measuring DLS for compounds at *cis*-dominated PSS.

2.5. Small angle neutron scattering (SANS)

SANS measurements were made on the Quokka instrument at the Bragg Institute, ANSTO, Lucas Heights NSW, Australia. For all samples, raw scattering counts were collected on a 128 \times 128 element area detector, where the sample–detector distances used were 2 m and 14 m, with no detector offset. An incident neutron wavelength of 5 Å was used with a typical spread of 10%, thus giving an effective q range of 0.004–0.4 Å $^{-1}$. Samples were prepared in circular 12.5 mm Hellma quartz cells with a path length of 2 mm, and a thermostatically-controlled automatic sample changer ensured that a temperature of 25 \pm 0.05 °C was maintained. Data were converted from raw counts at the detector into 1D scattering spectra by first subtracting the scattering from an empty cell and then radially averaging the resulting spectrum, normalising for the measured sample transmission. A D $_2$ O background was then subtracted from the final 1D sample data to ensure that the scattering signals seen are from the surfactant only. Model fitting was performed using SasView software, using standard equations for cylindrical form factors. Cylinders were modelled using the Guinier equation [21] for the form factor $P(q,a)$:

$$P(q, a) = 2(\Delta\rho)V\sin(qL\cos\alpha/2) / (qL\cos\alpha/2) \frac{J_1(qrs\sin\alpha)}{(qrs\sin\alpha)}$$

where $\Delta\rho$ is the scattering length density difference between the scatter and the D₂O solvent, V is the volume of the cylinder, L is the length of the cylinder, α is the angle between the axis of the cylinder and the q -vector, J_1 is the first order Bessel function, r is the radius of the cylinder.

Aggregation number (N_{agg}) was calculated from the volume of the formed micelle divided by the volume of monomer obtained by calculating the molecular volume of the structural components of the monomer from their bulk densities. The volumes (\AA^3) used were: triazole 96.2, triethylglycol 221.9, azobenzene 251.5, galactose 173.8, mannose 194.4, fucose 175.2, 2-bromoethanol 117.7, succinic anhydride 135.1, pae 161.5, 3,5-dihydrobenzoic acid 159.9, gallic acid 166.2, 1-bromooctane 286.8, 1-bromododecane 398.7, 2-ethylhexyl bromide 295.3.

2.6. Competitive binding assays to LecA or LecB

LecA or LecB were recombinantly produced in *E. coli* and purified by affinity chromatography as described.^{5b,22} Measurements for competitive binding with LecA and LecB were performed according to previously reported protocols.^{5b,22} A serial dilution of each tested compounds in TBS/Ca (1000 – 0.013 μM) was prepared twice in two different 96-well plates (Carl Roth GmbH, Germany, Item no. 9292.1). One of these plates was irradiated (with the plate put on an ice tray to prevent heating) for 30 min using a UV light source which was comprised of three 9 W halogen tubes, delivering a total power of 27 W at λ_{max} of 361 nm at the source (Nail gel curing lamp). After 30 min of irradiation, 10 μL of a serial dilution of each tested compounds from each plate were added in triplicates to one 384-well plate (Greiner Bio-One, Germany, cat no 781900). Afterward, 10 μL of either LecA or LecB and fluorescent galactose-based compound **9** from reference 5b or fucose-based compound **6** from reference 22 were added to each well at final concentrations of 20 μM for LecA and 150 nM for LecB and 10 nM for both fluorescent ligands. After incubation for 1 h (LecA) or 4 h (LecB) at r.t., blank corrected fluorescence intensity was recorded using a PheraStar FS microplate reader (BMG Labtech GmbH, Germany) with excitation filters at 485 nm and emission filters at 535 nm and fluorescence polarization was calculated. The data were analyzed using a four parameter fit of the MARS Data Analysis Software (BMG Labtech GmbH, Germany). A minimum of two independent measurements on two separate plates was performed for each compound before and after irradiation by UV lamp.

2.7. Synthesis

See supplementary information for NMR spectra and analytical data for new compounds.

2.7.1. General procedure 1 (Synthesis of **18–21**; **27–30**) [10,11a]

Alcohol (1 equiv.), carboxylic acid (1 equiv.), DPTS (1 equiv.) and DCC (2.6 equiv.) were dissolved in dry DCM and stirred under N₂ for 12 h. Then the reaction mixture was diluted with diethyl ether, filtered off the urea and washed with diethyl ether. The filtrate was concentrated and purified by flash chromatography.

2.7.2. General procedure 2 (Synthesis of **22–25**)

Aldehyde **18–21** (1 equiv.), pentaerythritol (1 equiv.) and *p*-toluenesulfonic acid (PTSA, 0.2 equiv.) were dissolved in DMF and stirred at 50 °C under N₂ until TLC showed fully consumption of the starting materials. The crude mixture was concentrated under reduced pressure and purified by flash chromatography.

2.7.3. General procedure 3 (Synthesis of **1–12**) [10,11a]

Into a solution of **27–30** (1 equiv.) in THF was added **31–33** (2.5 equiv.) in water, CuSO₄·5H₂O (0.61 equiv.) in water and sodium ascorbate (0.61 equiv.) in water successively under N₂. The reaction mixture was allowed to stir at room temperature for 36 h. Then dilute with THF, filtered, concentrated and purified by flash chromatography (10–20% MeOH in DCM).

2.7.4. General procedure 4 (Synthesis of **13–16**) [23,11a],[23]

A mixture of methyl benzoate (1 equiv.), bromoalkane (2–3 equiv.) and potassium carbonate (1.2 equiv.) in DMF (15 mL) was heated at reflux with vigorous stirring for 4 h. The reaction mixture was cooled and poured into ice-water, and the precipitate collected and dried, and the crude product purified by flash silica chromatography or recrystallization. The purified methyl benzoate (1 equiv.), KOH (5 equiv.) and water-ethanol (1:6 v/v) were heated at 60 °C for 2 h. Then the reaction mixture was cooled to room temperature and concentrated HCl was added carefully until pH=1. Then the acidic solution was diluted with water, extracted with DCM and the combined organic phase was dried over Na₂SO₄, concentrated under reduced pressure to afford the final compound.

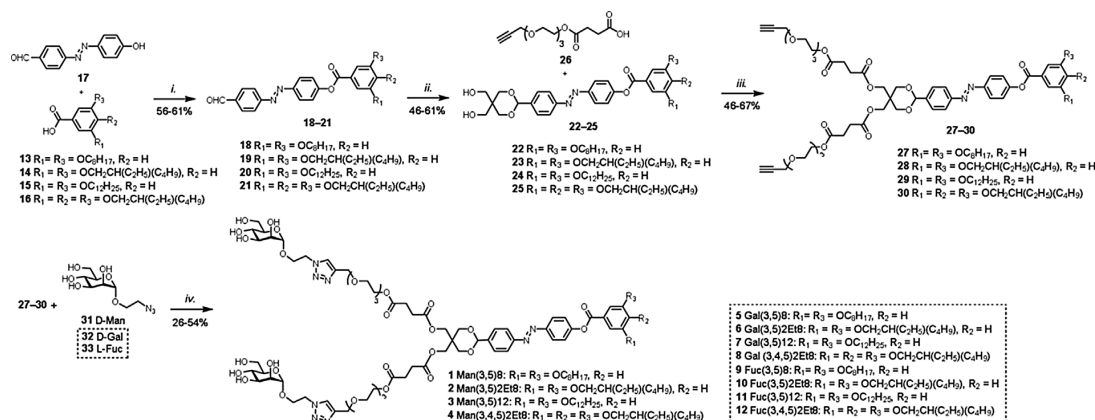
2.7.5. General procedure 5 (Synthesis of **31–33**) [24–27]

To a cooled solution of acetylated sugar (1 equiv.) and 2-bromoethanol (1.2 equiv.) in anhydrous DCM was added dropwise BF₃·Et₂O (4 equiv.). The ice-bath was removed after 1 h and the reaction was continued at room temperature until the starting material had been consumed (monitored by TLC). The reaction mixture was poured onto ice-water and extracted with DCM. The organic phase was washed with water, saturated NaHCO₃, brine, dried over Na₂SO₄ and concentrated under reduced pressure. The synthesized intermediate compound (1 equiv.) and sodium azide (10 equiv.) were dissolved in anhydrous DMF and stirred at 70 °C for 2 h. The reaction mixture was cooled to room temperature, extracted with EtOAc, washed with water, dried over Na₂SO₄ and filtered. The filtrate was concentrated under reduced pressure and purified by flash chromatography (2:3 EtOAc/petroleum spirit). The purified intermediate was deacetylated under Zemplén conditions using catalytic sodium methoxide in methanol, followed by neutralization with Amberlite IR120 acidic ion exchange resin.

3. Results and discussion

The synthesis of Janus glycodendrimers **1–12** is presented in Scheme 1. Glycodendrimers **1–12** were composed of variable monosaccharide head groups as recognition motifs for LecA and LecB, which show binding specificities to D-galactose and L-fucose or D-mannose, respectively [28]. To facilitate self-assembly in water, hydrophobic tail fragments bearing linear and branched alkyl tail groups (**13–16**) were introduced by modified Steglich esterification of the azobenzene core **17** using catalytic 4-(dimethylamino) *p*-toluenesulfonate (DPTS) to give hydrophobic precursors **18–21** [29]. Divergent elaboration of core fragments **18–21** was then carried out, firstly by acetalization of the aldehyde with pentaerythritol to give diols **22–25**, followed by esterification with carboxylic acid **26** to furnish the key alkyne scaffolds **27–30**. Finally, glycoconjugation of **27–30** was performed using the well-described copper(I)-catalysed azide-alkyne conjugation reaction (CuAAC) of the corresponding deprotected azidoethyl glycosides **31–33** to furnish glycodendrimers **1–12** (See supplementary information for details) [30].

Having obtained glycodendrimers **1–12**, we then investigated their photocontrollable aggregation properties. Azobenzene *trans-cis* photoisomerization has been extensively studied by our group for controlling the self-assembly and interfacial activity of



Scheme 1. Synthesis of photoswitchable Janus glycodendrimers **1–12**. Reaction conditions: i) DPTS, DCC, DCM, 56–61% ii) pentaerythritol, PTSA, DMF, 50 °C, 46–61% iii) DPTS, DCC, DCM, 46–67% iv) CuSO₄, sodium ascorbate, THF/water (2:1 v/v), 40 °C, 31–54% DCC = *N,N'*-dicyclohexylcarbodiimide, DCM = dichloromethane, DMF = *N,N*-dimethylformamide, DPTS = 4-(dimethylamino)pyridinium *p*-toluenesulfonate, THF = tetrahydrofuran, PTSA = *p*-toluene sulfonic acid.

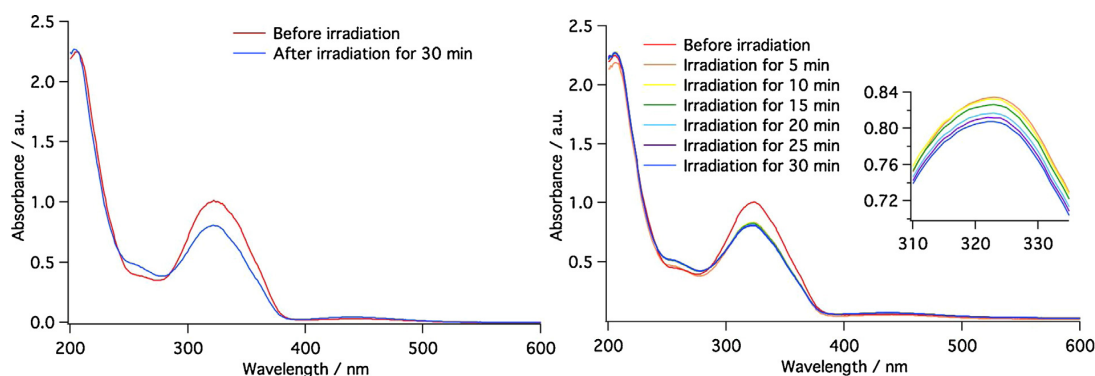


Fig. 1. UV–vis spectroscopy of Man(3,5)12 **3** at 0.05 mM concentration in ultra-pure water, before and after UV irradiation with an UV LED at 325 nm (left), and a UV lamp at 361 nm and 36W radiant power (right).

amphiphilic carbohydrates, and was shown to give clean conversion to the *cis*-dominated photostationary state (PSS) with efficient conversion to the *cis* isomer (up to 75%) [18,31]. Preliminary measurements involved the use of Man(3,5)12 (**3**) as the representative compound. The UV–vis spectra of **3** were recorded in the (assumptively) *trans*-dominated photostationary state, which indicated an intense band at around 325 nm corresponding to the azobenzene $\pi \rightarrow \pi^*$ transition, accompanied by a much weaker band at around 425 nm corresponding to the $n \rightarrow \pi^*$ transition (Fig. 1). In order to induce *trans*–*cis* photoisomerization, compound **3** was irradiated in water at either 325 nm or 361 nm for 30 min and the UV–vis spectrum recorded at 5 min intervals. After this time, a small decrease in peak intensity at 325 nm was observed, which was accompanied by a slight increase in intensity of the peak at 425 nm along with a slight blue shift of approximately 5 nm for the λ_{max} [32]. The thermal half-lives of the *cis* isomer of glycodendrimers **1–4** was then determined by measuring the relaxation rate of the dark adapted *cis*-PSS to the more stable *trans* isomer at 20 °C and 37 °C, respectively (ESI, Figs. S1 and S2). Even at physiologically relevant temperatures, relatively long lived *cis*-states were observed (10–14 h, Fig. S3), which would provide ample opportunity to elicit a change in the lectin binding response. The ratio of *trans* and *cis* isomers at either PSS could be estimated by integrating selected signals in the ¹H NMR spectrum, before and after UV irradiation (Fig. S4–S7). In the resting, *trans*-dominated PSS, 7–9% of molecules existed in *cis*-form, while after UV irradiation

19–30% of molecules were found in the *cis*-form. Whilst the *cis*–*trans* ratio in the *cis*-PSS ratio is low compared to those observed in previously described azobenzene derivatives [31], these findings are consistent with derivatives incorporating bulky substituents, particularly amphiphilic azobenzene analogues leading to densely packed aggregate geometries that may impede light penetration and/or inhibit photoswitching due to steric congestion in the micelle core [32].

Having examined the photoswitching properties of glycodendrimers, our attention focused on the aggregation behaviour of the assembled micelles in water. Interestingly, amphiphilic glycodendrimers did not reduce the surface tension at the air–water interface, and so it was not possible to determine the critical micelle concentration of these compounds by tensiometry. Instead, the critical aggregation concentration (CAC) was evaluated using a Nile Red encapsulation assay [20]. The CAC was calculated by monitoring the wavelength at the maximum intensity for the Nile red probe as a function of the glycodendrimer concentration, whereby the inflection point is indicative of the CAC (Fig. 2). Low molecular CAC values were obtained for dendrimers **1–12** in water, which suggests a strong thermodynamic driving force for aggregation as a result of the favourable hydrophobic interactions between azobenzene and alkyl tail groups within the aggregate core [33]. Furthermore, no clear photomodulation of the CAC was evident for **1–12**, which was most likely a result of the low photoisomerization yields for these molecules. Because of their unusual aggregation

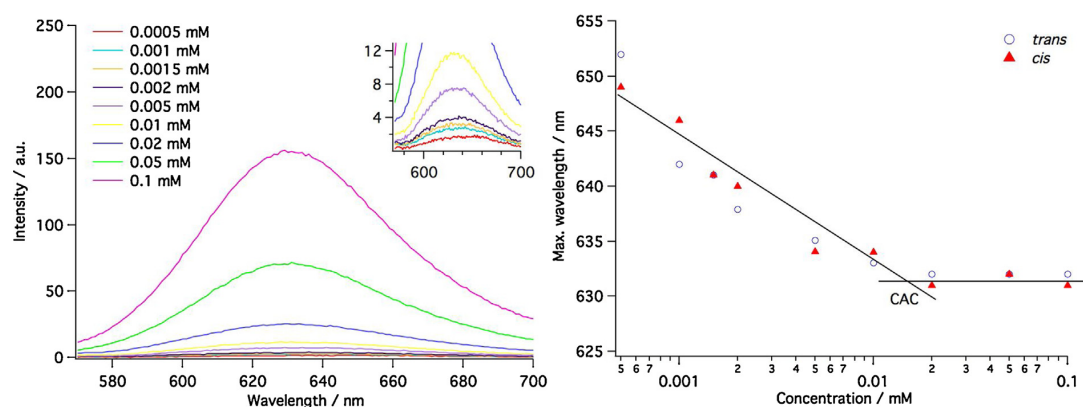


Fig. 2. Fluorescence spectra of Nile Red in the presence of Man(3,5)8 **1** at different concentrations (Left). CAC of Man(3,5)8 **1** in ultra pure water before (open symbols) and after (closed symbols) UV irradiation at 361 nm for 10 min (Right). (For interpretation of the references to colour in this figure legend, the reader is referred to the web version of this article.)

behaviour, we then examined the relationship between conformational exchanges and the concentrations of glycodendrimers. Glycodendrimers **1–4** were dissolved separately in water at 20 °C at several different concentrations: above the CAC (0.05 mM), at the CAC, and below the CAC (0.001 mM). UV–vis spectroscopy was recorded for all these samples, and the absorbance at 325 nm was recorded (ESI, Fig. S8). By plotting the absorbance against concentration, linear trends ($R^2 > 0.999$ for all compounds) were observed, indicating that the glycodendrimers undergo unimolecular conformational exchanges upon self-assembly, which are not affected by changes in concentration [31,34].

The aggregation properties of the glycodendrimers **1–12** in their respective *trans* and *cis* states was further investigated using DLS to determine the hydrodynamic diameter and polydispersity of the assembled structures (ESI, Table S1). Glycodendrimers **1–12** were dissolved in water at a fixed concentration (0.1 mM) and DLS measurements were obtained before and after UV irradiation. Aggregates were shown to be of limited polydispersity in water, with effective diameters of around 100 nm and polydispersity indices (PDIs) of approximately 0.2, with the exception of Fuc(3,5)2Et8 **10** which had a larger diameter of 183 nm. In most cases, any apparent change in diameter between the *trans* and *cis* states was modest, however the hydrodynamic volume of these structures generally increased slightly following UV irradiation (361 nm for 10 min), with the largest difference observed for Man(3,5)8 **1**.

In order to determine the precise geometry and size of these aggregates, along with any changes following *trans-cis* photoisomerization of the azobenzene core, SANS measurements were performed at fixed concentrations above the CAC in D₂O (0.1 mM). Under these conditions, cylindrical geometries of different sizes were observed in the *trans* state as shown in the SANS spectra, with smaller aggregates generally observed for glycodendrimers incorporating *n*-octyl and branched 2-ethylhexyl tail groups (Fig. 3, and ESI, Table S1). The SANS spectra revealed cylindrical geometries of various length (104–915 Å) and radii (32–41 Å). Cylindrical geometries are preferred when amphiphiles try to reduce their interfacial curvature, and the aggregation size can be modulated by adjusting the relative volume occupied by the head and tail group [35]. The diameter of these cylinders is approximately equal to the length of two glycodendrimers that construct the single layered cylindrical micelle structure, and this is commensurate with a typical surfactant aggregate. The sharp increase in scattered intensity at lowest q values likely indicated fractal-type critical scattering from attractive interactions between micelles. This has been seen previously

Table 1

Evaluation of photoswitchable compounds **5–8** with LecA using a competitive binding assay based on fluorescence polarization.^{a,b,c}

^aAverages and standard deviations were obtained from two independent experiments.

^cRelative potency (rp) = IC_{50} (monovalent reference) / IC_{50} (glycodendrimer). The monovalent reference was methyl α -D-galactoside (α -D-GalOMe) for **5–8**.

Compound	n^a	IC_{50} (μ M) ^b	IC_{50} [μ M] (UV _{361nm}) ^b	rp (rp _{UV}) ^c
α -GalOMe		92.1 \pm 23.2		
5	324	22.6 \pm 0.9	24.9 \pm 5.6	4.1 (4.0)
6	296	20.3 \pm 5.2	21.0 \pm 5.3	4.5 (4.7)
7	2846	22.9 \pm 5.5	23.0 \pm 4.4	4.0 (4.3)
8	1072	24.6 \pm 2.1	23.1 \pm 1.0	3.7 (4.3)

^aNumber of sugars per micelle derived from the N_{agg} values in the SANS spectra.

^bAverages and standard deviations were obtained from two independent experiments.

^cRelative potency (rp) = IC_{50} (monovalent reference) / IC_{50} (glycodendrimer). The monovalent reference was methyl α -D-galactoside (α -D-GalOMe) for **5–8**.

for azobenzene surfactant systems [31,36], and thus we anticipate that the same effect occurs here. We model this contribution using a mass fractal model for the aggregation of micelles into larger 'clusters' [37]. From the fitted SANS spectra, the aggregation number (N_{agg}) and area per head group (A_{hg}) of these micelles could be determined, thus providing useful insight into the valency and density of carbohydrates exposed on the micelle surface (ESI, Fig. S9 and Table S1). In order to evaluate changes in self-assembly properties following *trans-cis* photoisomerization, the SANS spectra were also recorded following UV irradiation of representative compounds **1–4** (Fig. S10). Although no notable change in the geometry and size of these micelles was detected in the *cis*-PSS, this was in good agreement with the CAC values and can be attributed to the low photoisomerization yields of the dendrimers and the non-standard aggregation pathway.

The soluble lectins LecA and LecB were chosen as the targets in this study owing to their strong potential for therapeutic intervention and the important roles they play as virulence factors and in biofilm formation [19,38]. Furthermore, both lectins were shown to be present among a large set of strain isolates from clinical sources [39]. Since these soluble bacterial lectins show good affinity and specificity for D-galactose and L-fucose/D-mannose residues, respectively, we measured the binding inhibition of LecA/B against photoswitchable micelles incorporating these head groups (Tables 1 and 2). The affinity of glycodendrimer micelles were measured using a recently described, competitive fluorescence polarization-based assay for LecA and LecB, both in the

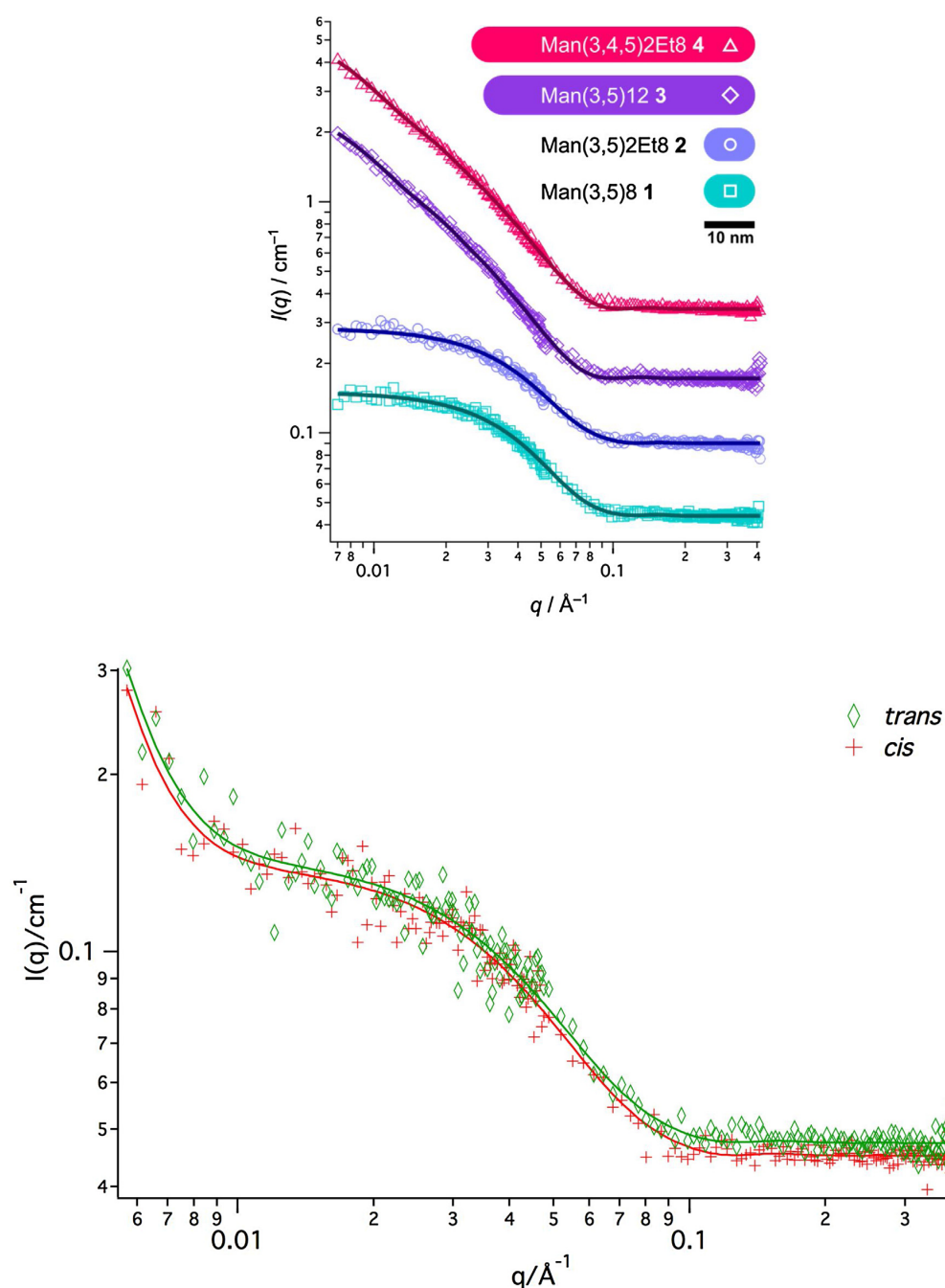


Fig. 3. Representative SANS data (symbols) and model fits (lines) for glycodendrimers 1–4 in the *trans*-dominated PSS at 0.1 mM concentration in D_2O (top), and glycodendrimer Man(3,5)8 1 in both the *trans*- and *cis*-dominated PSS at 0.1 mM concentration in D_2O (bottom). The legend inset shows cross-sectional profiles of corresponding fitted micelle geometries. The legend inset shows the cross-sectional profiles of corresponding fitted micelle geometries, where the scale bar defines the length-scale.

trans- and *cis*-PSS (See ESI for details) [5b,22]. All compounds were tested over a concentration range from a concentration of inhibitor above the CAC value at $300\text{ }\mu\text{M}$, serially diluted down to single digit nanomolar concentrations. Methyl α -D-galactoside (αGalOMe), methyl α -L-fucopyranoside (αFucOMe) or methyl α -D-mannopyranoside (αManOMe) were used as the monovalent references in the same assay for LecA and LecB, respectively [5b,22].

In the case of LecA, glycodendrimers 5–8 bearing a β -galactoside head group showed a modest enhancement (approximately four-fold) in inhibition potency relative to the monovalent compound. Whilst this may suggest a multivalent effect, no clear correlation between particle size and inhibitory potency could be drawn as the relatively small micelles bearing two *n*-octyl and 2-ethyl hexyl side chains of 5 and 6, respectively, were shown to be equally

Table 2

Evaluation of photoswitchable compounds **1–4** and **9–12** with LecB using a competitive binding assay based on fluorescence polarization.^{a,b,c}

^bAverages and standard deviations were obtained from two independent experiments.

^cRelative potency (rp) = IC₅₀ (monovalent reference)/IC₅₀ (glycodendrimer). The monovalent reference was methyl α -L-fucoside (α -L-FucOMe) for **9–12**, and methyl α -D-mannoside (α -D-ManOMe) for **1–4**.

Compound	n ^a	IC ₅₀ [μ M] ^b	IC ₅₀ [μ M] (UV _{361nm}) ^b	rp (rp _{UV}) ^c
α FucOMe		0.35 \pm 0.05		
9	182	0.29 \pm 0.07	0.32 \pm 0.01	1.2 (1.0)
10	1603	0.20 \pm 0.00	0.20 \pm 0.03	1.7 (1.7)
11	799	0.29 \pm 0.04	0.27 \pm 0.02	1.2 (1.2)
12	996	0.25 \pm 0.06	0.24 \pm 0.11	1.4 (1.4)
α ManOMe		87.7 \pm 61.2	76.5 \pm 38.1	
1	138	2.7 \pm 0.5	3.5 \pm 0.3	32.8 (21.5)
2	128	3.3 \pm 0.2	3.8 \pm 0.4	26.2 (20.2)
3	918	3.0 \pm 0.2	2.6 \pm 0.2	29.4 (29.4)
4	795	1.0 \pm 0.2	1.2 \pm 0.4	85.7 (62.6)

^aNumber of sugars per micelle derived from the N_{agg} values in the SANS spectra.

^bAverages and standard deviations were obtained from two independent experiments.

^cRelative potency (rp) = IC₅₀ (monovalent reference)/IC₅₀ (glycodendrimer). The monovalent reference was methyl α -L-fucoside (α -L-FucOMe) for **9–12**, and methyl α -D-mannoside (α -D-ManOMe) for **1–4**.

potent as the larger micelles derived from glycodendrimers **7** and **8** incorporating three alkyl side chains. LecA is a tetrameric protein that binds preferentially to α -galactosides, although high valency ligands presenting β -galactosides, as well as monovalent phenyl β -galactosides have been shown to be potent inhibitors of this lectin. In our case, the weaker binding affinity for these glycodendrimers may be a result of inappropriate ligand spacing due to the flexible linker, which may disfavour a chelate binding mode between adjacent binding sites on the LecA tetramer [3a,40]. Furthermore, no significant change in binding potency was observed for the *galacto*-configured dendrimers following *trans*-*cis* photoisomerization, with the exception of **8** which showed a slight enhancement in inhibition. The negligible photomodulation of binding affinity is in good agreement with the CAC and SANS data, and is most likely a result of the low conversion to the *cis* isomer following UV irradiation.

In contrast to the inhibition of LecA with D-galactoside functionalized dendrimers, glycodendrimers **9–12** incorporating α -fucoside head groups showed good potency against LecB, with sub micromolar IC₅₀ values obtained in the *trans* and *cis* isomeric states. However, these compounds showed no enhancement in potency relative to the monovalent reference compound α FucOMe (IC₅₀ 0.35 μ M). Many studies have revealed the importance of multivalency for generating potent ligands for LecB [41]. However, similar to the observations of the inhibition of micelles of **5–8** against LecA, the binding potency of **9–12** to LecB was insensitive to particle size. Furthermore, no clear photomodulation of inhibition could be detected following UV irradiation, as the *trans* isomer was as equally potent inhibitor as the *cis*-enriched state and is in good agreement with the self-assembly data.

Mannosides are usually weaker inhibitors of LecB when compared to fucosides, but through chemical modification, mannose-derived compounds were also shown to achieve potent LecB inhibition [42]. Micelles assembled from mannosides **1–4** were also tested for inhibition of LecB and low micromolar IC₅₀ values were obtained. In contrast to all other compounds tested for LecA and LecB, the relative potencies of mannosides **1–4** (IC₅₀ values of 1.0–3.4 μ M) with respect to α ManOMe (IC₅₀ 87.7 μ M) were significantly increased up to >80-fold for **4**. Due to the identical aglycons for fucosides **9–12** and mannosides **1–4**, this significant effect observed for mannosides is likely to be a result of an optimal multivalent presentation of the carbohydrate in the manno-series

that matches the spatial requirements of two LecB binding sites in the lectin tetramer.

4. Conclusions

In summary, we report the modular synthesis of a library of photoswitchable Janus glycodendrimers bearing variable alkyl tail groups and carbohydrate head groups. The assembled structures were characterised using DLS and SANS, and revealed uniform cylindrical micelles of various size. Glycodendrimer micelles were assessed as phototunable inhibitors of LecA and LecB from *P. aeruginosa* using a competitive, fluorescence polarization-based assay and revealed moderate-to-potent inhibition of these bacterial lectins with a significant increase potency for mannose derived glycodendrimers. Unfortunately, no clear modulation in the self-assembly and binding potency of these micelles could be observed following UV light irradiation, owing to the low photoisomerization yields for these dendrimers, most likely due to impaired light penetration and steric congestion within the aggregate core. Lectin binding potencies also appeared insensitive to the length and radii of micelles, as smaller structures generally at least as potent binders as the larger, worm-like micelles. The efficient synthesis of these constructs facilitates a rapid entry point to responsive structures with tailored activity against a variety of lectin targets. Future work will be aimed at developing photocontrollable liposomal systems, as well as improving linker and ligand design in order to enhance binding potency and photoswitching efficiency.

Acknowledgements

B. W. acknowledges funding from the Australian Research Council (DE130101673). A.T. acknowledges support from the Helmholtz-Association (grant no. VH-NG-934) and the Deutsche Forschungsgemeinschaft (grant no. Ti 756/2-1).

We acknowledge the support of the Australian Centre for Neutron Scattering, Australian Nuclear Science and Technology Organisation, in providing the neutron research facilities used in this work. This work benefited from SasView software, originally developed by the DANSE project under NSF award DMR-0520547.

Appendix A. Supplementary data

Supplementary data associated with this article can be found, in the online version, at <http://dx.doi.org/10.1016/j.colsurfb.2017.08.016>.

References

- [1] D.K. Mandal, N. Kishore, C.F. Brewer, *Biochemistry* 33 (1994) 1149.
- [2] (a) M. Mammen, S.K. Choi, G.M. Whitesides, *Angew. Chem. Int. Ed.* 37 (1998) 2745;
(b) T.K. Dam, R. Roy, S.K. Das, S. Oscarson, C.F. Brewer, *J. Biol. Chem.* 275 (1998) 14223.
- [3] (a) A. Bernardi, J. Jiménez-Barbero, A. Casnati, C. De Castro, T. Darbre, F. Fieschi, J. Finne, H. Funken, K. Jaeger, M. Lahmann, T.K. Lindhorst, M. Marradi, P. Messner, A. Molinaro, P.V. Murphy, C. Nativi, S. Oscarson, S. Penadés, F. Peri, R.J. Pieters, O. Renaudet, J.L. Reymond, B. Richichi, J. Rojo, F. Sansone, C. Schäffer, W.B. Turnbull, T. Velasco-Torrijos, S. Vidal, S. Vincent, T. Wennekes, H. Zuilhof, Anne Imberty, *Chem. Soc. Rev.* 42 (2013) 4709;
(b) G. Ragupathi, F. Koide, P.O. Livingstone, Y.S. Cho, A. Endo, Q. Wan, M.K. Spassova, S.J. Keding, J. Allen, O. Ouerfelli, R.M. Wilson, S.J. Danishefsky, *J. Am. Chem. Soc.* 128 (2006) 2715;
(c) S. Bhatia, M. Dimde, R. Haag, *Med. Chem. Commun.* 5 (2014) 862;
(d) R. Roy, P.V. Murphy, H.J. Gabius, *Molecules* 21 (2016) 629;
(e) S. Grigalevicius, S. Chierici, O. Renaudet, R. Lo-Man, E. Dériaud, C. Leclerc, P. Dumy, *Bioconj. Chem.* 16 (2005) 1149;
(f) C. Müller, G. Despras, T.K. Lindhorst, *Chem. Soc. Rev.* 45 (2016) 3275.
- [4] (a) S. Andre, R.J. Pieters, I. Vrasidas, H. Kaltner, I. Kuwabara, F.T. Liu, R.M. Liskamp, H.J. Gabius, *ChemBioChem* 2 (2001) 822;
(b) E. Kolomiets, E.M.V. Johansson, O. Renaudet, T. Darbre, J.L. Reymond, *Org. Lett.* 9 (2007) 1465.

- [5] (a) R.U. Kadam, M. Bergmann, M. Hurley, D. Garg, M. Cacciarini, M.S. Swiderska, C. Nativi, M. Sattler, A.R. Smyth, P. Williams, M. Cámara, A. Stocker, T. Dabre, J.L. Reymond, *Angew. Chem. Int. Ed.* 50 (2011) 10631; (b) I. Joachim, S. Rikker, D. Hauck, D. Ponader, S. Boden, R. Sommer, L. Hartmann, A. Titz, *Org. Biomol. Chem.* 14 (2016) 7933; (c) O. Renaudet, L. BenMohamed, G. Dasgupta, I. Bettahi, P. Dumy, *ChemMedChem* 3 (2008) 737; (d) B.L. Wilkinson, S. Day, R. Chapman, S. Perrier, V. Apostolopoulos, R.J. Payne, *Chem. Eur. J.* 18 (2012) 16540.
- [6] J. Rieger, F. Stoffelbach, D. Cui, A. Imberty, E. Lameignere, J.L. Putaux, R. Jérôme, C. Jérôme, R. Auzély-Velty, *Biomacromolecules* 8 (2007) 2717.
- [7] Y. Ruff, E. Buhler, S.J. Candau, E. Kesselman, Y. Talmon, Jean-Marie Lehn, *J. Am. Chem. Soc.* 132 (2010) 2573.
- [8] J.F. Nierengarten, J. Lehl, V. Oerthel, M. Holler, B.M. Illescas, A. Munoz, N. Martin, J. Rojo, M. SanchezNavarro, S. Cecioni, S. Vidal, K. Buffet, M. Durka, S.P. Vincent, *Chem. Commun.* 46 (2010) 3860.
- [9] S. Andre, C. Grandjean, F.M. Gautier, S. Bernardi, F. Sansone, H.J. Gabius, R. Ungaro, *Chem. Commun.* 47 (2011) 6126.
- [10] A. Barnard, D.K. Smith, *Angew. Chem. Int. Ed.* 51 (2012) 6572.
- [11] (a) V. Percec, P. Leowanat, H.J. Sun, O. Kulikov, C.D. Nusbaum, T.M. Tran, A. Bertin, D.A. Wilson, M. Peterca, S. Zhang, N.P. Kamat, K. Vargo, D. Moock, E.D. Johnston, D.A. Hammer, D.J. Pochan, Y. Chen, Y.M. Chabre, T.C. Shiao, M. Bergeron-Briek, S. André, R. Roy, H.J. Gabius, P.A. Heiney, *J. Am. Chem. Soc.* 135 (2013) 9055; (b) S. Zhang, R.O. Moussodia, S. Vértessy, S. Andre, M.L. Klein, H.J. Gabius, V. Percec, *Proc. Natl. Acad. Sci. U. S. A.* 112 (2015) 5585; (c) S. Zhang, R.O. Moussodia, H.J. Sun, P. Leowanawat, A. Muncan, C.D. Nusbaum, K.M. Chelling, P.A. Heiney, M.L. Klein, S. André, R. Roy, H.J. Gabius, V. Percec, *Angew. Chem. Int. Ed.* 53 (2014) 10899.
- [12] (a) E.L. Dane, A.E. Ballok, G.A. O'Toole, M.W. Grinstaff, *Chem. Sci.* 5 (2014) 551; (b) Y. Ogawa, C. Yoshiyama, T. Kitaoka, *Langmuir* 28 (2012) 4404; (c) B.S. Kim, W.Y. Yang, J.H. Ryu, Y.S. Yoo, M. Lee, *Chem. Commun.* 15 (2005) 2035; (d) B.S. Kim, D.J. Hong, J. Bae, M. Lee, *J. Am. Chem. Soc.* 127 (2005) 16333; (e) J.H. Ryu, E. Lee, Y.B. Lim, M. Lee, *J. Am. Chem. Soc.* 129 (2007) 4808.
- [13] A.A. Beharry, G.A. Woolley, *Chem. Soc. Rev.* 40 (2011) 4422.
- [14] (a) N.M. Oruganti Srinivas, A. Suriola, N. J. Am. Chem. Soc. 124 (2002) 2124; (b) T.K. Lindhorst, Jayaraman Beilstein, *J. Org. Chem.* 9 (2013) 223.
- [15] A. Samanta, M.C. Stuart, B.J. Ravoo, *J. Am. Chem. Soc.* 134 (2012) 19909.
- [16] D. Ponader, S. Igde, M. Wehle, K. Märker, M. Santer, D. Bléger, L. Hartmann, Beilstein *J. Org. Chem.* 10 (2014) 1603.
- [17] H. Chandrasekaran, F. Jacob, K. Peterson, F. Kathirvel, Tuzcek, T.K. Lindhorst, *Chem. Eur. J.* 20 (2014) 8744.
- [18] Y. Hu, W. Zou, V. Julita, R. Ramanathan, R.F. Tabor, R. Nixon-Luke, G. Bryant, V. Bansal, B.L. Wilkinson, *Chem. Sci.* 7 (2016) 6628.
- [19] (a) G.G. Anderson, T.F. Kenney, D.L. Macleod, N.R. Henig, G.A. O'Toole, *Pathog. Dis.* 67 (2013) 39.
- [20] (a) C. Tanford, *The Hydrophobic Effect: Formation of Micelles and Biological Membranes*, 2nd ed., J. Wiley, 1980; (b) A. Barnard, P. Posocco, S. Priel, M. Calderon, R. Haag, M.E. Hwang, V.W. Shum, D.W. Pack, D.K. Smith, *J. Am. Chem. Soc.* 133 (2011) 20288.
- [21] A. Guimer, G. Fournet, *Small-angle Scattering of X-rays*, J. Wiley & Sons, New York, 1955.
- [22] D. Hauck, I. Joachim, B. Frommeyer, A. Varrot, B. Philipp, H.M. Möller, A. Imberty, T.E. Exner, A. Titz, *ACS Chem. Biol.* 8 (2013) 1775.
- [23] S. Kuvshinova, A. Zav'yalov, O. Koifman, V. Aleksandriiskii, V. Burmistrov, *Russ. J. Org. Chem.* 40 (2004) 1113.
- [24] J. Dahmén, T. Frejd, G. Grönberg, T. Lave, G. Magnusson, G. Noori, *Carbohydr. Res.* 116 (1983) 303.
- [25] C. Wilcox, J. Jin, H. Charville, S. Swift, T. To, P.A. Kilmartin, C.W. Evans, R. Cooney, M. Brimble, *Aust. J. Chem.* 67 (2014) 562.
- [26] J.R. Hwu, C.I. Hsu, M.H. Hsu, Y.C. Liang, R.C.C. Huang, Y.C. Lee, *Bioorg. Med. Chem. Lett.* 21 (2011) 380.
- [27] H. Tamiaki, A. Shinkai, Y. Kataoka, *J. Photochem. Photobiol. A Chem.* 207 (2009) 115.
- [28] N. Gilboa-Garber, *Methods Enzymol.* 83 (1982) 378.
- [29] (a) E. Fedeli, A. Lancelot, J.L. Serrano, P. Calvot, T. Sierra, *New. J. Chem.* 39 (2015) 1960; (b) B. Neises, W. Steglich, *Org. Synth.* 7 (1990) 93.
- [30] (a) H.C. Kolb, M.G. Finn, K.B. Sharpless, *Angew. Chem. Int. Ed.* 40 (2001) 2004; (b) L. Bornaghi, S.A. Poulsen, T.A. Houston, *Tetrahedron* 62 (2005) 8115.
- [31] R.F. Tabor, D.D. Tan, S.S. Han, S.A. Young, Z.L.E. Zeeger, M.J. Pottage, C.J. Garvey, B.L. Wilkinson, *Chem. Eur. J.* 20 (2014) 13881.
- [32] (a) C. Kordel, C.S. Popeney, R. Haag, *Chem. Commun.* 47 (2011) 6584; (b) M. Uda, A. Momotake, T. Arai, *Photochem. Photobiol. Sci.* 2 (2003) 845; (c) A. Momotake, T. Arai, *Tetrahedron Lett.* 45 (2004) 4131; (d) W.R. Brode, J.H. Gould, G.M. Wyman, *J. Am. Chem. Soc.* 75 (1953) 1856.
- [33] (a) Y. Liu, A.H. Flood, J.F. Stoddart, *J. Am. Chem. Soc.* 126 (2004) 9150–9151.
- [34] J.S. Pedersen, *Soft Matter Characterization*, Springer, 2008, pp. 191–233.
- [35] (a) A. Valiakhmetova, M.J. Pottage, T.M. McCoy, J. Garvey, L. de Campo, C. Rehm, D.A. Kuryashov, R.F. Tabor, *Langmuir* 32 (2016) 12423; (b) J.N. Israelachvili, D.J. Mitchell, B.W. Ninham, *J. Chem. Soc. Faraday Trans. 2* (72) (1976) 1525.
- [36] C.T. Lee Jr., K.A. Smith, T.A. Hatton, *Langmuir* 25 (2009) 13784.
- [37] D. Mildner, P. Hall, *J. Phys. D: Appl. Phys.* 19 (1986) 1535.
- [38] (a) D. Tielker, S. Hacker, R. Loris, M. Strathmann, J. Wingender, S. Wilhelm, F. Rosenau, K.E. Jaeger, *Microbiology* 151 (2005) 1313; (b) N. Gilboa-Garber, *Methods Enzymol.* 83 (1982) 378; (c) S.P. Diggle, R.E. Stacey, C. Dodd, M. Camara, P. Williams, K. Winzer, *Environ. Microbiol.* 8 (2006) 1095.
- [39] (a) R. Sommer, S. Wagner, A. Varrot, C. Nycholat, A. Khaledi, S. Häussler, J. Paulson, A. Imerty, *Chem. Sci.* 7 (2016) 4990; (b) A.M. Boukerb, A. Décor, S. Ribun, R. Tabaroni, A. Rousset, L. Commin, S. Buff, A. Doléans-Jordheim, S. Vidal, A. Varrot, A. Imberty, B. Cournoyer Titz, *Front. Microbiol.* 7 (2016) 811.
- [40] (a) D. Sicard, S. Cecioni, M. Iazykov, Y. Chevolot, S.E. Matthews, J.P. Praly, E. Souteyrand, A. Imberty, S. Vidal, M. Phaner-Goutorbe, *Chem. Commun.* 47 (2011) 9483; (b) F. Pertici, R.J. Pieters, *Chem. Commun* 48 (2012) 4008; (c) S. Cecioni, R. Lalor, B. Blanchard, J.P. Praly, A. Imberty, S.E. Matthews, S. Vidal, *Chem. Eur. J.* 15 (2009) 13232; (d) A.V. Pukin, A.J. Brouwer, L. Koomer, H.C. Quarles van Ufford, J. Kemmink, N.J. de Mol, R.J. Pieters, *Org. Biomol. Chem.* 13 (2015) 10923.
- [41] (a) N. Berthet, B. Thomas, I. Bossu, E. Dufour, E. Gillon, J. Garcia, N. Spinelli, A. Imberty, P. Dumy, O. Renaudet, *Bioconjugate Chem.* 24 (2013) 1598; (b) Y.M. Chabre, D. Giguère, B. Blanchard, J. Rodrigue, S. Rocheleau, M. Neault, S. Rauthu, A. Papadopoulos, A.A. Arnold, A. Imberty, *Chem. Eur. J.* 17 (2011) 6545.
- [42] (a) R. Sommer, T.E. Exner, A. Titz, *PLoS One* 9 (2014) e112822; (b) A. Hofmann, R. Sommer, D. Hauck, J. Stifel, I. Gottker-Schnetmann, A. Titz, *Carbohydr. Res.* 412 (2015) 34; (c) R. Sommer, D. Hauck, A. Varrot, S. Wagner, A. Prestel, H.M. Möller, A. Imberty, A. Titz, *Chemistry Open* 4 (2015) 756; (d) G. Beshr, R. Sommer, D. Hauck, D.C.B. Siebert, A. Hofmann, A. Imberty, A. Titz, *Med. Chem. Commun.* 7 (2016) 519.

3.3. DEVELOPMENT OF A COMPETITIVE BINDING ASSAY FOR THE *BURKHOLDERIA CENOCEPACIA* LECTIN BC2L-A AND THE STRUCTURE ACTIVITY RELATIONSHIP OF NATURAL AND SYNTHETIC INHIBITORS

Ghamdan Beshr, Roman Sommer, Dirk Hauck, David Chan Bodin Siebert, Anna Hofmann, Anne Imberty and Alexander Titz

Medicinal Chemistry Communications, **2016**; 7(3), 519-530 - DOI:
10.1039/C5MD00557D



RESEARCH ARTICLE

View Article Online
View Journal | View IssueCite this: *Med. Chem. Commun.*,
2016, 7, 519Development of a competitive binding assay for the *Burkholderia cenocepacia* lectin BC2L-A and structure activity relationship of natural and synthetic inhibitors^{†‡}Ghamdan Beshr,^{§ab} Roman Sommer,^{§abc} Dirk Hauck,^{abc} David Chan Bodin Siebert,^{¶abc} Anna Hofmann,^{||c} Anne Imberty^d and Alexander Titz^{*abc}

Burkholderia cenocepacia is an opportunistic Gram-negative pathogen and especially hazardous for cystic fibrosis patients. In analogy to its relative *Pseudomonas aeruginosa*, *B. cenocepacia* possess numerous lectins with roles in adhesion and biofilm formation. The LecB homolog BC2L-A is important for biofilm structure and morphology. Inhibitors of this D-mannose specific C-type lectin could be useful as tools in *B. cenocepacia* biofilm research and potentially as anti-biofilm compounds against chronic infections. Here, we report the development of a fluorescence polarization-based competitive binding assay and its application in an extensive structure-activity relationship study of inhibitors of BC2L-A. In contrast to its homolog LecB, BC2L-A is highly selective for D-mannose-based ligands with an absolute requirement of its hydroxyl group at C6. A strict diastereoselectivity was observed for (6S)-mannoheptose-derived ligands. Intriguingly, bioisosteric substitution or methylation of hydroxyl groups directly involved in the calcium-coordination resulted in loss of inhibition for the two homologous lectins BC2L-A and LecB.

Received 4th December 2015,
Accepted 12th January 2016

DOI: 10.1039/c5md00557d

www.rsc.org/medchemcomm

Introduction

Burkholderia cenocepacia is a Gram-negative bacterium and belongs to the *B. cepacia* complex (BCC). BCC currently contains at least 18 genetically different but phenotypically similar species, which could be isolated from different environments.¹ *B. cenocepacia* has been recognized as a problematic opportunistic pathogen, particularly to immunosuppressed patients and patients suffering from cystic fibrosis (CF).

Compared to its relative *Pseudomonas aeruginosa*, mortality of patients infected with *B. cenocepacia* increased and conditions like the cepacia syndrome often lead to pulmonary dysfunction.^{2,3} Treatment of such infections is difficult due to antibiotic resistance of *B. cenocepacia*,⁴ which is increased by its ability to form biofilms. In these social colonies the bacteria are protected by a self-formed extracellular matrix and show up to fifteen-fold higher resistance against antibiotics than *B. cenocepacia* grown in planktonic culture.⁵ Like for *P. aeruginosa*,⁶ the inhibition of bacterial biofilm formation could be a promising approach to overcome antibiotic resistance.

Interestingly, *B. cenocepacia* was shown to form mixed species biofilms with CF isolates of *P. aeruginosa* and both pathogens often infect patients simultaneously.⁷ In *P. aeruginosa* the lectins LecA and LecB are necessary for biofilm formation.^{8,9} *lecB*-like genes were also identified in several other Gram-negative bacteria such as *Chromobacterium violaceum*, *Ralstonia solanacearum*, as well as in *B. cenocepacia*.^{10–12} *B. cenocepacia* has three lectins homologous to *P. aeruginosa* LecB: BclA (BCAM0186), BclB (BCAM0184) or BclC (BCAM0185), also called BC2L-A, BC2L-B and BC2L-C. BC2L-A contains only a LecB domain, whereas BC2L-B and BC2L-C have additional N-terminal domains. This additional domain is without homology to known domains in BC2L-B, and in BC2L-C it contains a tumor necrosis factor-fold domain. The latter has been characterized and reported as super lectin

^a Chemical Biology of Carbohydrates, Helmholtz Institute for Pharmaceutical Research Saarland (HIPS), D-66123 Saarbrücken, Germany.
E-mail: alexander.titz@helmholtz-hzi.de

^b Deutsches Zentrum für Infektionsforschung (DZIF), Standort Hannover-Braunschweig, Germany

^c Department of Chemistry and Graduate School Chemical Biology, University of Konstanz, D-78457 Konstanz, Germany

^d Centre de Recherches sur les Macromolécules Végétales (CERMAV)-CNRS and Université Grenoble Alpes, F-38041 Grenoble, France

[†] The authors declare no competing interests.

[‡] Electronic supplementary information (ESI) available: Supplementary data (¹H-NMR, ¹³C-NMR, ¹⁹F-NMR traces of all synthesized compounds and NOESY spectra for compounds 27 and 29). See DOI: 10.1039/c5md00557d

[§] Both authors contributed equally.

[¶] Current address: Institute for Applied Synthetic Chemistry, TU Wien, Getreidemarkt 9, A-1060 Vienna, Austria.

^{||} Current address: Institute of Pharmacy and Food Chemistry, University of Würzburg, D-97074 Würzburg, Germany.

where the additional TNF domain binds fucose in addition to the mannose-binding LecB domain.^{13,14}

The expression of BC2L-A is positively regulated through activation of *Burkholderia* CepR, a protein homologous to LuxR which is a member of the acyl homoserine lactone quorum sensing system.^{15,16} Later, the *Burkholderia* lectin cluster *bclACB* was shown to be mainly regulated by the *Burkholderia* diffusible signal factor (BDSF) system with *cis*-2-dodecenoic acid as signal molecule and that maximal expression of the lectins is dependent on both signaling systems.¹⁷ Surprisingly, deletion of the *bclACB* gene cluster in the CF isolate *B. cenocepacia* H111 had no effect on biofilm formation in a static microtitre plate biofilm assay.¹⁸ However, under identical conditions the lectin cluster *bclACB* showed an effect on biofilm formation in absence of the major adhesin gene *bapA*. Expression of BapA was therefore suggested to compensate the effect of the lectins BclACB under static biofilm conditions. When analyzed under flow conditions, however, the absence of the lectins BclACB had a profound effect on the biofilm structure also in the presence of *bapA* and large hollow structures were formed. Based on complementation experiments with individual lectins and combinations, Eberl and coworkers suggested that all three lectins cooperate in the structural development of biofilms. Therefore, inhibitors targeting these lectins could serve as tools to study *Burkholderia* biofilm formation.

BC2L-A has been extensively structurally characterized.^{10,19,20} In contrast to the tetramer forming LecB, BC2L-A forms a dimeric assembly of its 13.8 kDa monomers.¹⁰ The carbohydrate specificity of BC2L-A was determined by glycan array analysis, which revealed a high specificity of this lectin for mannose-containing ligands. In contrast to the high affinity of LecB to L-fucose, BC2L-A shows a low affinity to L-fucose ($IC_{50} = 2.3$ mM). Methyl α -D-mannoside is a high affinity ligand with a K_d of 2.7 μ M and co-operative effects upon binding were observed in microcalorimetry experiments. The crystal structure was solved and the carbohydrate specificity was explained on a structural basis: His112 stacks to lipophilic areas in mannosides but would clash with O-1 of fucose and its conjugates. Marchetti *et al.* later showed, that BC2L-A binds also to L-glycero-D-manno-heptose which is a major constituent of bacterial lipopolysaccharide.²⁰ The stereochemistry of the glycol side chain was important for

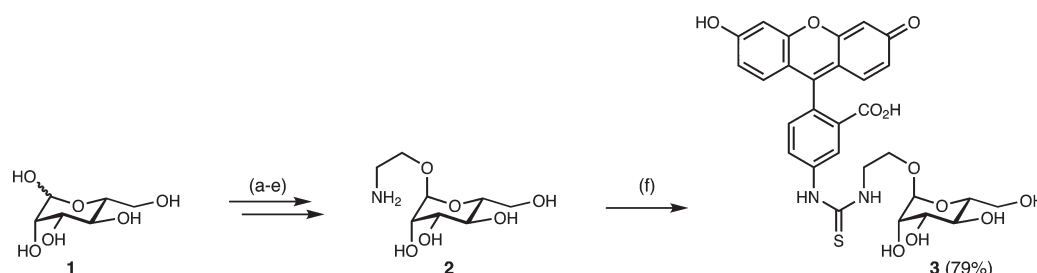
binding and methyl α -L,D-mannoheptoside bound with a K_d of 54 μ M, while its C6 epimer did not bind.

Here, we report the development of a competitive binding assay for BC2L-A based on fluorescence polarization and its application in a detailed structure-activity relationship study with more than 30 potential ligands based on the monosaccharides fucose and mannose.

Results and discussion

Fluorescence polarization-based competitive binding assays have been developed for various lectins.^{21–23} This assay format allows small scale volumes and convenient *in situ* quantification of the inhibitory potencies of given inhibitors. Because BC2L-A binds D-mannosides with high affinity and L-fucosides with low affinity, we designed the D-mannose-based fluorescent tracer 3 (Scheme 1) as assay probe. Its synthesis started from D-mannose (1) and an ethyl linker was introduced by borontrifluoride-catalyzed glycosylation of peracetylated mannose with 2-bromoethanol as published by Dahmen *et al.*²⁴ After subsequent nucleophilic displacement of the bromide with NaN_3 ,²⁵ Zemplén deacetylation yielded intermediate azide, which was reduced to the fully unprotected amine 2.²⁶ The fluorescent tracer 3 was then obtained in 79% yield after coupling with fluorescein isothiocyanate (FITC). Then, mannose-based 3 and fucose-based 4 (ref. 22) were titrated with BC2L-A and fluorescence polarization was determined (Fig. 1A). Mannose derivative 3 showed strong binding to BC2L-A (K_d 3.1 ± 1.7 μ M), whereas fucose derivative 4 only showed binding at protein concentrations greater than 100 μ M. These results are consistent with the known dissociation constant of methyl α -D-mannoside and BC2L-A of $K_d = 2.7$ μ M and the poor binding of L-fucose.¹⁰ The assay was then evaluated by titration of BC2L-A (1.5 μ M) in presence of the reporter ligand 3 (10 nM) with a dilution series of D-mannose (1, Fig. 1B) and an IC_{50} value of 10.8 ± 0.7 μ M was obtained. This data is in good agreement with published data for D-mannose (1, K_d 5.15 μ M) obtained by isothermal microcalorimetry.¹⁰

After establishing the assay, we tested various derivatives of L-fucose and D-mannose for inhibition of BC2L-A (Table 1). The common structural motif contained the 6-membered tetrahydropyran ring structure and all three calcium-



Scheme 1 Synthesis of fluorescently labeled mannose tracer 3. Reagents and conditions: (a) Ac_2O , pyridine, r.t.; (b) $BF_3 \cdot OEt_2$, 2-bromoethanol; (c) NaN_3 , DMF, 70 $^{\circ}C$; (d) $NaOMe$, $MeOH$, r.t.; (e) H_2 , Pd/C , $EtOH$, r.t.; (f) FITC, $NaHCO_3$, DMF, r.t.

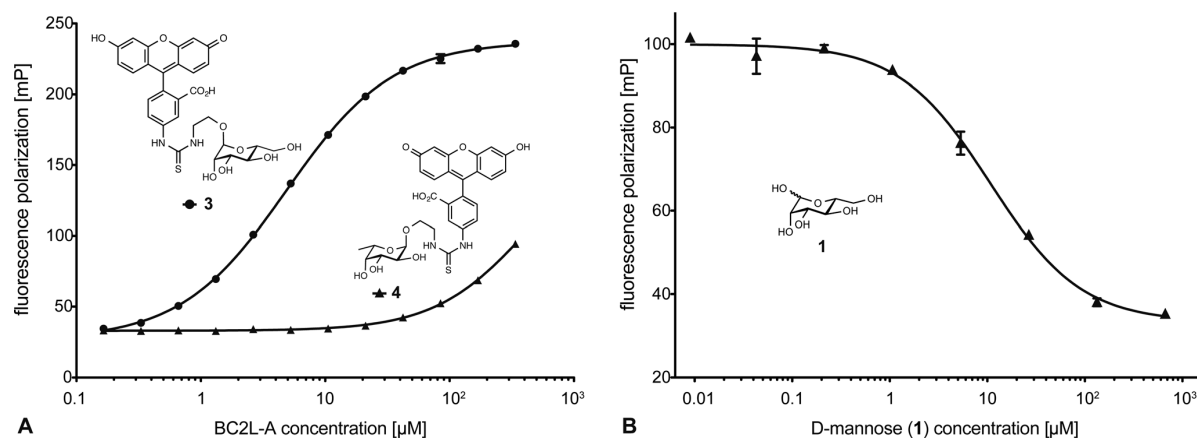


Fig. 1 (A) Titration of mannose-based reporter ligand **3** and fucose-based reporter ligand **4** with BC2L-A and determination of the fluorescence polarization. Binding of **3** ($K_d = 3.1 \pm 1.7 \mu\text{M}$) compared to the low affinity fucose-based ligand **4** indicate the carbohydrate specificity of BC2L-A. (B) Competitive inhibition of the binding of **3** to BC2L-A with D-mannose (**1**, $\text{IC}_{50} = 10.8 \pm 0.7 \mu\text{M}$). One representative titration of independent triplicates (three plates) is shown here and error bars represent standard deviation of triplicates on one plate, standard deviations given for K_d and IC_{50} represent data from three independent experiments (three plates of triplicates each).

coordinating secondary hydroxy groups were present. In a first set of compounds (**1**, **5**–**12**), fucose, mannose and derivatives thereof were tested. This series was previously generated to explain monosaccharide selectivity of the structurally related lectin LecB and dissect individual functional group contributions to the binding affinity.²⁷ For BC2L-A, only a weak affinity of L-fucose (**5**, IC_{50} 498 μM) was detected and no inhibition by the methyl fucosides α -**6** or β -**7** was observed up to 666 μM . Removal of the glycosidic linkage of fucose in **8** or introduction of a C-methyl substituent in **9** also resulted in inactive compounds. The observation that fucose-containing conjugates are poor BC2L-A inhibitors was further supported by the lack of inhibition of BC2L-A by various blood group antigens, e.g., Lewis-type structures Le^x , Le^y , Le^a , Le^b or antigens of the ABO-system blood group A-, B- and H-antigens (data not shown). In contrast, mannose-derived inhibitors **1**, **10**–**12** were potent inhibitors with IC_{50} values ranging from 2.9–13 μM . These potent binders all contain the 6-OH group of D-mannose but possess variations at the anomeric center of mannose as C-glycoside **10**, 1-deoxy mannose **11**, free mannose **1** or the methyl glycoside **12**. A hydroxy group in position 6 of mannose was required for efficient binding to BC2L-A as observed by the comparison of inactive 6-deoxy-**9** and potent inhibition of 6-hydroxy-**10**. This data also reinforces the conclusion made by Marchetti *et al.*, that a lack of an STD effect of D-rhamnose (*i.e.*, 6-deoxy D-mannose) with BC2L-A by NMR spectroscopy resulted from the loss in affinity of such 6-deoxygenated mannose-derivatives.²⁰ Variation of the aglycon in mannosides **12**–**15** had only a minor effect (7.0–14.5 μM), and methyl glycoside α -**12** was as potent as the bulky β -**15** ($\text{IC}_{50} = 7.0 \mu\text{M}$ for **12** and 7.4 μM for **15**).

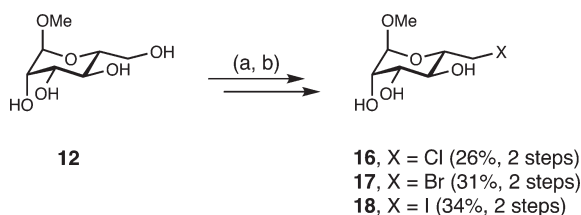
Deoxygenation in position-6 of mannosides resulted in complete loss in binding. Therefore, we isosterically replaced this hydroxy group with other small substituents which could

establish attractive interactions with amino acids of the protein, *i.e.* halogens^{28,29} in **16**–**18** or an amino group in **19**. Halogenated mannosides **16**–**18** were synthesized by selective activation of the 6-hydroxy group in methyl mannoside **12** as tosylate²² and its nucleophilic substitution with the corresponding halogenide salts in DMF at elevated temperatures (Scheme 2). Remarkably, none of the halogenated mannosides nor the amine substituted derivative were able to inhibit the lectin (Table 1), confirming that the presence of a free 6-OH group is essential for binding.

Marchetti *et al.* previously reported the binding of BC2L-A to L,D-mannoheptose with a K_d of 54 μM for its α -methyl glycoside.²⁰ This heptose is a constituent of bacterial surface lipopolysaccharide (LPS) and may play a role in BC2L-A mediated bacterial adhesion. In a previous study, we synthesized a set of mannoheptose derivatives as inhibitors for the homologous lectin *P. aeruginosa* LecB.³⁰ These compounds differ in their stereochemical configuration at position 6 and bear amido- and sulfonamido-substituents in position 7. All compounds were tested for their inhibition of BC2L-A (Table 2). In agreement with the selectivity reported by Marchetti *et al.*, we observed a preferential binding of BC2L-A to the (6*S*)-diastereomers **20**–**22** in the amide series with IC_{50} values of 116, 104 and 64.0 μM , respectively, whereas the corresponding (6*R*)-diastereomers D,D-mannosides **23** and **24** did not show any inhibition. The (6*S*)-configured sulfonamides **25** and **26** both inhibited BC2L-A function and were the most potent inhibitors in the mannoheptose series with IC_{50} s of 14–19 μM . This inhibitory potency is superior to the unsubstituted heptoside previously reported by Marchetti *et al.* The mannohexose analogs bearing these amide and sulfonamide substituents in position 6 were previously reported as potent inhibitors of LecB.^{22,31} However, since these compounds lack a free hydroxy group in position 6, the observed

Table 1 Biochemical evaluation of selected L-fucose and D-mannose derivatives for BC2L-A binding. IC₅₀ values were determined and are averages of at least three independent experiments, standard deviations are given. n.i.: no inhibition observed up to 666 μM

Compound	BC2L-A IC ₅₀ [μM]	Compound	BC2L-A IC ₅₀ [μM]	Compound	BC2L-A IC ₅₀ [μM]
	10.8 ± 0.7		13.0 ± 3.2		7.4 ± 1.6
	498 ± 18.0		2.9 ± 0.5		n.i.
	n.i.		7.0 ± 0.3		n.i.
	n.i.		13.6 ± 4.1		n.i.
	n.i.		14.5 ± 1.7		n.i.
	n.i.				



Scheme 2 Synthesis of 6-deoxy-6-halo mannosides **16**, **17** and **18**. Reagents and conditions: (a) TsCl, pyridine, DMF, 0 °C – r.t.; (b) (CH₃)₄NCl for **16**, KBr for **17** or KI for **18**, DMF, 65 °C.

lack of inhibition of BC2L-A (data not shown) was consistent with the observations for the relative behavior of *e.g.*, compound **9** and **10** (Table 1).

The crystal structure of methyl α -L,D-mannoheptoside in complex with BC2L-A was solved by Marchetti *et al.*²⁰ In this

structure, the 6-OH of the glycol side chain establishes a hydrogen bonding network with the side chain of Asp110 and the main chain nitrogen of Glu31, an interaction pattern similar to 6-OH of mannose¹⁰ in complex with BC2L-A. Both, (6*S*)-**22** and (6*R*)-**24** were docked into the ligand-free form of the mannoheptose-BC2L-A crystal structure previously published by Marchetti *et al.* (Fig. 2). The docking pose of mannoheptose amide (6*S*)-**22** corresponds to the crystal structure of methyl α -L,D-mannoheptoside and the 6-OH group forms the previously mentioned hydrogen bonding interactions since both heptoses have the same stereochemistry at position 6. The diastereomeric analog (6*R*)-**24** could also be docked with its pyranose ring in the same position as the one observed for methyl α -L,D-mannoheptoside, but the OH group at C6 cannot take the same position since it would generate steric hindrance between the rest of the side chain and the protein surface. Thus, the side chain is rotated in its docking pose and the 6-OH group in this (6*R*)-diastereomer

Table 2 Biochemical evaluation of mannoheptose derivatives for BC2L-A binding. IC₅₀ values were determined using competitive binding assay and are averages of at least three independent experiments, standard deviations are given. n.i.: no inhibition observed up to 666 μ M

Compound	BC2L-A IC ₅₀ [μ M]	Compound	BC2L-A IC ₅₀ [μ M]
 20	116 \pm 22	 23	n.i.
 21	104 \pm 18	 24	n.i.
 22	64.0 \pm 3.5	 25	19.1 \pm 1.2
		 26	13.8 \pm 0.9

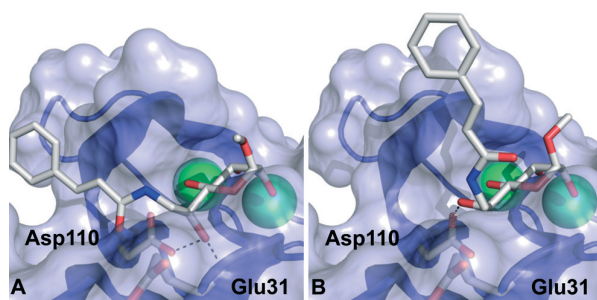
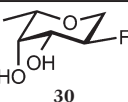
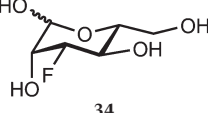
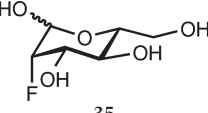
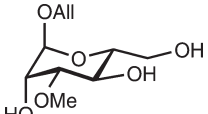
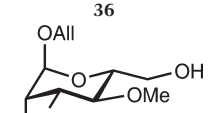


Fig. 2 Molecular docking of cinnamide modified mannoheptose C-6 (S) isomer 22 (A) and C-6 (R) isomer 24 (B) with BC2L-A. The two C-6 diastereomers show same orientation of the carbohydrate ring but differ in orientation of 6-OH and the cinnamide moiety. Carbohydrate recognition domain of BC2L-A is presented as cartoon with transparent surface. Ligands and amino acids forming interaction with 6-OH are depicted as sticks colored by elements (N: blue, O: red, C: grey). Two Ca^{2+} -ions in the binding site are shown as green spheres.

cannot be optimally accommodated in the binding site. In (6S)-22, the cinnamide substituent extends along the cleft and interacts with BC2L-A, whereas in (6R)-24, the same substituent is oriented towards the solvent as a result of the altered stereochemistry at C6. Both properties, the hydrogen-bonding network of 6-OH as well as the van der Waals interaction of the amide substituents as in (6S)-22 could explain the strong selectivity of BC2L-A for (6S)-heptose derivatives over their (6R)-diastereomers.

Table 3 Biochemical evaluation of derivatives substituted in one of the three Ca^{2+} -chelating hydroxyl groups for binding to BC2L-A and its homolog from *P. aeruginosa* LecB. n.i.: no inhibition observed up to 666 μM

Compound	BC2L-A IC_{50} [μM]	LecB IC_{50} [μM]
	n.i.	n.i.
	n.i.	n.i.
	n.i.	n.i.
	56% inhib. (666 μM)	n.i.
	n.i.	n.i.

We were further interested in the importance of the ring hydroxy groups for binding, which are directly coordinating to the two Ca^{2+} ions in BC2L-A or in the related *P. aeruginosa* LecB. Is it possible to replace or to modify one or more of these hydroxy groups and retain or improve affinity to LecB-like proteins? In 2004, Plenio described attractive Ca^{2+} -F interaction in organofluorine compounds.³² In addition, due to similar size, fluorine became an established bioisoster for hydrogens and hydroxyl groups in medicinal chemistry.³³ The introduction of fluorine can have profound effects on a diverse set of properties of drugs, e.g., changes in acidity, lipophilicity or metabolic stability. On the other hand, some lectins are known to preferentially bind to O-methylated carbohydrates, for example *Laccaria bicolor* tectonin³⁴ or *Bos taurus* galectin-1.³⁵ Both lectins, however, do not belong to the C-type lectin family. Galectin-1 was also probed with fluorine-substituted galactose derivatives and binding was completely lost for the 4- and the 6-fluorine analog, whereas a 3-fluoro substitution was well tolerated by galectin-1.³⁵ Fluorinated saccharides as ligands for other carbohydrate binding proteins have been described, e.g. glycogen phosphorylase,³⁶ *Toxoplasma* adhesin TgMIC1,³⁷ calnexin and calreticulin,^{38,39} as well as NMR-active probes for cyanovirin.⁴⁰ However, none of these carbohydrate-binding proteins are C-type lectins. One example of C-type lectins binding fluorinated glycan ligands has been reported by Hoechst AG for fluorinated sialyl Lewis^x and E-selectin.⁴¹ It is important to note, that in this study fluorine was introduced at the galactose moiety of the tetrasaccharide, which is not involved in direct coordination to the protein-bound calcium ion.

Two commercially available fluorinated mannose derivatives (34 and 35, Table 3) were used to study the effect of the substitution of 2-OH and 3-OH with a fluorine atom. A fluorine derivative corresponding to the substitution of mannose 4-OH was not commercially accessible. Therefore, we synthesized 1,2-dideoxy-2-fluoro-L-fucose (30) bearing the fluorine at position C-2 of fucose which corresponds to position C-4 in mannose (Scheme 3). An inversion of the free hydroxy group, its activation as leaving group and fluorination *via* $\text{S}_{\text{N}}2$ -type substitution are the key steps in the synthesis of such fluorinated carbohydrates. However, all attempts to invert the equatorial hydroxyl group at position 2 in selectively protected 27 into its axial epimer 28 failed (Scheme 3), although various conditions were tested. After activation of the hydroxyl group as mesylate, tosylate or triflate leaving groups, the subsequent inversion using various nucleophiles (NaOH, KOH, BzOH or cesium benzoate) was unsuccessful. An attempt to invert the stereochemistry under Mitsunobu conditions was also unsuccessful. Finally, Lattrel-Dax conditions using nitrite ions as nucleophile reagent was tested on the triflate due to previous success in epimerisation of carbohydrate triflates.⁴² Also under these conditions access to 28 remained unsuccessful. In contrast, a direct fluorination of the free hydroxy group in 27 using the reagent Deoxo-Fluor yielded the fluorinated compound 29 with the desired stereochemistry, however, this was only successful in a small scale

test reaction. Finally, 29 could be smoothly obtained in good yields using *N,N*-diethylamino-*S,S*-difluorosulfonium tetrafluoroborate (XtalFluor-E), a new generation fluorination reagent⁴³ with enhanced stability and selectivity. The stereochemistry of 29 and hydrogenolytically deprotected 30 was confirmed using ¹H-NMR (for 29, 30) and ¹H,¹H-NOESY NMR (for 29) spectroscopy. The proton NMR spectrum and observed NOE cross peaks (see ESI† for spectra) between the benzylidene aliphatic proton and H2 in 29 unambiguously confirmed the presence of only one diastereomer, *i.e.*, *exo*-29. The question whether exclusively the *exo*-isomer of 27 reacted to *exo*-29 or the *endo/exo*-mixture of 27 anomerized during the acidic reaction conditions was not further analyzed.

For the selective methylation of calcium-coordinating hydroxy groups, we used the previously reported³⁴ 3-*O*-methyl mannoside 36 (Table 3) and designed the synthesis of its 4-methoxy analogon 33. Fischer glycosylation of *D*-mannose (1) in allylic alcohol, isopropylidene masking of the *cis*-diol OH-2/3 and subsequent tritylation of the primary hydroxyl group yielded the selectively protected mannoside 31 in 23% over 3 steps (Scheme 3). Methylation of 31 using methyl iodide and subsequent simultaneous deprotection of the trityl and isopropylidene protecting groups yielded 4-*O*-methyl mannoside 33 in good yield.

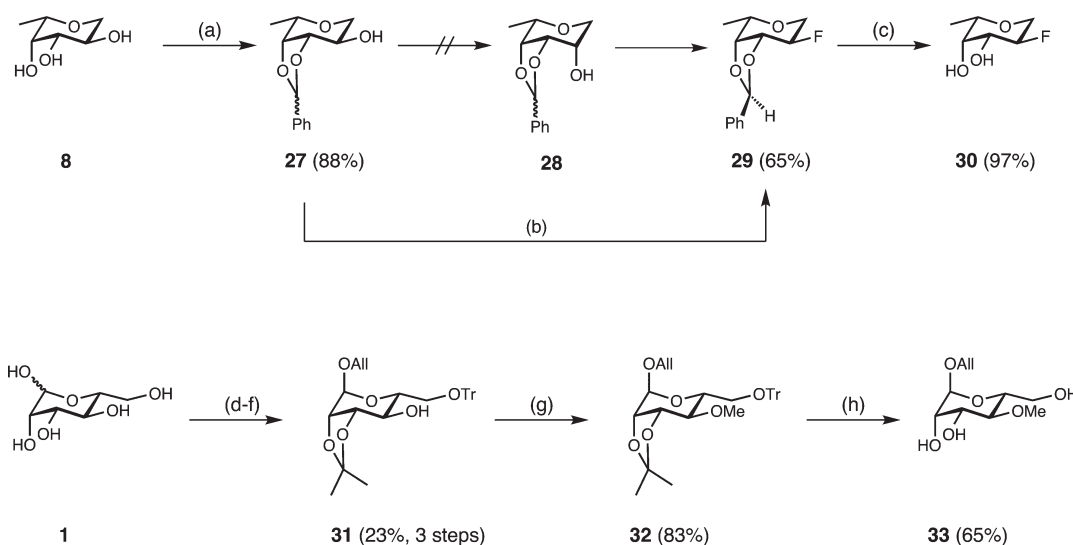
All fluorinated (30, 34, 35) and methylated (33, 36) potential ligands were evaluated in the corresponding competitive binding assays for both C-type lectins, *B. cenocepacia* BC2L-A and its homolog LecB from *P. aeruginosa*. Surprisingly, no competitive binding was observed for any of these derivatives up to concentrations of more than 650 μ M, a concentration more than 10–100-fold above the affinities of the corresponding derivatives with unmodified hydroxy groups. Only compound 36 showed a weak inhibition of BC2L-A. Based on our

previous observations, 2-fluoro fucose 30 was not expected to bind to BC2L-A due to the lack of the primary hydroxy group (see Table 1 for the parent compound 8). However, 8 is a potent inhibitor of LecB²⁷ and no inhibition of LecB function with its fluoro-analog 30 was observed even at concentrations of more than 400-fold higher than the reported IC₅₀ of 8. These observations indicate the crucial importance of free hydroxy groups in all calcium-coordinating positions for binding to LecB and its homolog BC2L-A.

The fluorinated mannose analogs 34 and 35 are hemiacetals and their conformation is not fixed as glycoside in a pyranose ring. Introduction of a strongly electronegative fluorine substituent in positions 2 or 3 could therefore influence the reactivity of the adjacent aldehyde and hydroxyl groups. The influence of these substitutions on the equilibrium of the various cyclic forms in aqueous solution was therefore analyzed by NMR spectroscopy and J-coupling analysis (Table 4). When comparing the proton NMR spectra of *D*-mannose (1) and its fluorinated analogs 34 and 35 under identical conditions, in all three cases both pyranose forms were observed with comparable α/β -ratios. In addition, comparable ³J-coupling constants between H2 and H3 (2.2–3.5 Hz) and between H3 and H4 (9.4–9.8 Hz) indicate comparable conformations for *D*-mannose (1) and its fluorinated analogs 34 and 35 in aqueous solution. Thus, an influence of the fluorine substituents on the conformational equilibrium of mannose could not account for the loss in lectin binding activity.

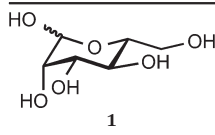
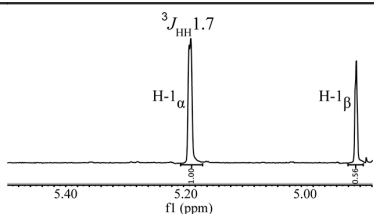
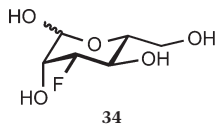
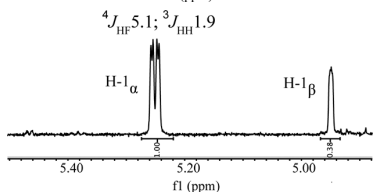
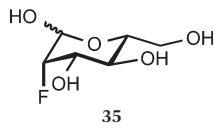
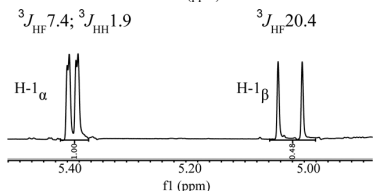
Summary

In summary, we have developed a fluorescence polarization-based competitive binding assay to quantify inhibitory



Scheme 3 Synthesis of 1,2-dideoxy-2-fluoro L-fucose (30) and allyl 4-*O*-methyl α -mannopyranoside (33). Reagents and conditions: (a) benzaldehyde dimethyl acetal, camphorsulfonic acid, DMF, r.t.; (b) XtalFluor-E, Et₃N-3HF, CH₂Cl₂, r.t., 2 h; (c) Pd/C, H₂, EtOH, r.t.; (d) all OH, Amberlite/H⁺, 70 °C; (e) acetone/H₂O = 40:1, pTsOH, 40 °C; (f) triphenylmethyl chloride, pyridine, 50 °C; (g) NaH, MeI, DMF, 0 °C-r.t.; (h) acetone, conc. HCl, 50 °C.

Table 4 Conformational analysis of D-mannose (**1**), 2-deoxy-2-fluoro-D-mannose (**35**) and 3-deoxy-3-fluoro-D-mannose (**34**) by ^1H -NMR in D_2O . The depicted ^1H -NMR spectra show the anomeric protons and quantification of anomeric ratios. Anomeric ratios ($\alpha:\beta$) of the pyranose ring forms were comparable in **1**, **34**, **35**. ^3J -coupling analysis of between H2/H3 and H3/H4 indicate comparable coupling constants, and thus comparable conformations in all three compounds analyzed

	^1H -NMR	α/β	J H3-H2	J H3-H4
 1		2:1	α 3.2 β 2.2	α 9.7 β 9.7
 34		2.6:1	α 3.5 β 3.5	α 9.4 β 9.4
 35		2:1	α 2.7 β 2.7	α 9.8 β 9.7

potencies of different inhibitors of BC2L-A, a potential target for anti-infectives against infections with *B. cenocepacia*. With the help of this assay, we extensively studied the structure-activity relationship of its glycan ligands based on thirty natural carbohydrates and synthetically derived inhibitors. The previously proposed role of the 6-OH group of D-mannosides for the binding to BC2L-A was found to be fundamental for activity, based on a set of approximately 10 compounds including this hydroxyl group, potential bioisosters thereof or with compounds lacking this hydroxyl group. In addition, we tested a set of diastereomeric mannoheptose derivatives, quantified the diastereoselectivity of BC2L-A and proposed the binding mode of the potent derivative which could assist the design of novel heptose-based inhibitors. The diastereoselectivity of BC2L-A is very tight compared to the previously reported data for its homolog LecB.³⁰ This stringent selectivity is likely to originate from its high requirement for optimal coordination of the hydroxyl group at mannose C6, whereas for LecB²⁷ this hydroxyl group does not contribute to the overall binding affinity. Surprisingly, bioisosteric substitution or methylation of hydroxyl groups directly involved in the calcium-coordination resulted in complete loss of inhibition for the two homologous lectins BC2L-A and LecB. Thus, the assay developed here and the detailed information gained from this study will guide future development of lectin-directed inhibitors and anti-virulence drugs against *B. cenocepacia* and *P. aeruginosa*.

Experimental

Chemical synthesis

Thin layer chromatography (TLC) was performed using silica gel 60 coated aluminum sheets containing fluorescence indicator (Merck KGaA, Darmstadt, Germany) using UV light (254 nm) and by charring either in anisaldehyde solution (1% v/v 4-methoxybenzaldehyde, 2% v/v concentrated H_2SO_4 in EtOH), in aqueous KMnO_4 solution or in a molybdate solution (a 0.02 M solution of ammonium cerium sulfate dihydrate and ammonium molybdate tetrahydrate in aqueous 10% H_2SO_4) with heating. Medium pressure liquid chromatography (MPLC) was performed on a Teledyne Isco Combiflash Rf200 system using pre-packed silica gel 60 columns from Teledyne Isco, SiliCycle or Macherey-Nagel. Commercial chemicals and solvents were used without further purification. Deuterated solvents were purchased from Eurisotop (Saarbrücken, Germany). Nuclear magnetic resonance (NMR) spectroscopy was performed on a Bruker Avance III 400 or 500 UltraShield spectrometer at 400/500 MHz (^1H) or 101/126 MHz (^{13}C), respectively. Chemical shifts are given in ppm and were calibrated on residual solvent peaks as internal standard.⁴⁴ Multiplicities were specified as s (singlet), d (doublet), t (triplet) or m (multiplet). The signals were assigned with the help of ^1H , ^1H -COSY, DEPT-135-edited ^1H , ^{13}C -HSQC, ^1H , ^{13}C -HMBC and ^1H , ^1H -NOESY experiments. Mass spectra were obtained on a Bruker amaZon SL spectrometer, high resolution mass

spectra on a Bruker microTOF II ESI spectrometer and the data were analyzed using DataAnalysis from Bruker.

1-Fucose (5), D-mannose (1), umbelliferyl α -D-mannoside (14) and umbelliferyl β -D-mannoside (15) were from Dextra Laboratories (Reading, UK), methyl α -L-fucoside (6), methyl β -L-fucoside (7) and fluoromannoses 34 and 35 from Carbosynth Ltd. (UK). Methyl α -D-mannoside (12) was purchased from Sigma Aldrich (Germany). Fluorescein isothiocyanate isomer I was from Serva Biochemicals (Heidelberg, Germany).

N-(Fluorescein-5-yl)-N'-(α -D-mannopyranosyloxyethyl)-thiocarbamide (3). 2-Aminoethyl α -D-mannopyranoside (2) (53 mg, 0.24 mmol) was dissolved in DMF (3 mL) and FITC (93 mg, 0.24 mmol, 1.0 equiv.) was added. The reaction mixture was stirred at r.t. for 17 h, concentrated *in vacuo* and the residue was purified by MPLC (SiO₂; solvent A: CH₂Cl₂ with 1% HOAc, solvent B: EtOH with 2% HOAc; gradient of 0–57% B) to give the title compound as orange solid (115 mg, 0.19 mmol, 79%). ¹H NMR (500 MHz, MeOH-*d*₄) δ 8.17 (d, *J* = 1.8 Hz, 1H, ArH), 7.79 (dd, *J* = 8.3, 2.0 Hz, 1H, ArH), 7.17 (d, *J* = 8.3 Hz, 1H, ArH), 6.75–6.65 (m, 4H, ArH), 6.55 (dd, *J* = 8.7, 2.4 Hz, 2H, ArH), 4.83 (d, *J* = 1.7 Hz, 1H, H-1), 3.99–3.80 (m, 5H), 3.77–3.68 (m, 3H), 3.65–3.55 (m, 2H); ¹³C NMR (126 MHz, MeOH-*d*₄) δ 183.1 (C=S), 171.3 (C=O), 154.4 (ArC), 142.4 (ArC), 131.6 (ArCH), 130.4 (ArCH), 129.5 (ArC), 125.9 (ArCH), 120.1 (ArCH), 114.0 (ArC), 111.7 (ArCH), 103.5 (ArCH), 101.8 (C-1), 74.8, 72.6, 72.1, 68.6 (C-2, -3, -4, -5), 67.0 (CH₂), 62.9 (CH₂), 45.4 (CH₂); HR-MS calcd. for C₂₉H₂₇N₂O₁₁S: calcd: 611.1341 found: 611.1320.

Methyl 6-chloro-6-deoxy- α -D-mannopyranoside (16). Methyl mannoside 12 was tosylated according to Wang *et al.*,⁴⁵ crude methyl 6-O-tosyl- α -D-mannopyranoside (200 mg, 0.57 mmol, 1 equiv.) was then stirred in DMF (5.7 mL) in presence of (CH₃)₄NCl (314 mg, 2.87 mmol, 5 equiv.) at 65 °C for 2 d. The solvent was removed *in vacuo* and the residue was purified by MPLC (SiO₂; gradient of CH₂Cl₂ to CH₂Cl₂/MeOH = 10:1) to give 16 as colorless solid (32 mg, 26%, 2 steps). ¹H NMR (500 MHz, MeOH-*d*₄) δ 4.64 (d, *J* = 1.7 Hz, 1H, H-1), 3.92–3.88 (m, 1H, H-6a), 3.79 (dd, *J* = 3.3, 1.7 Hz, 1H, H-2), 3.69–3.61 (m, 3H, H-3, -4, -6b), 3.60–3.54 (m, 1H, H-5), 3.39 (s, 3H, OCH₃); ¹³C NMR (126 MHz, MeOH-*d*₄) δ 102.8 (C-1), 74.2 (C-3 or -4), 72.5 (C-3 or -4), 71.9 (C-2), 69.8 (C-5), 55.2 (OCH₃), 45.7 (C-6); ESI-MS calcd. C₇H₁₃ClNaO₅⁺: 235.0; found: 234.8. 16 was first reported by Jennings and Jones⁴⁶ and the proton NMR data corresponded to the data disclosed in the literature.⁴⁷

Methyl 6-bromo-6-deoxy- α -D-mannopyranoside (17). Methyl mannoside 12 was tosylated according to Wang *et al.*,⁴⁵ crude methyl 6-O-tosyl- α -D-mannopyranoside (300 mg, 0.86 mmol, 1 equiv.) was stirred in DMF (8.6 mL) in presence of KBr (512 mg, 4.31 mmol, 5 equiv.) at 65 °C for 3 d. The solvent was removed *in vacuo* and the residue was purified by MPLC (SiO₂; gradient of CH₂Cl₂ to CH₂Cl₂/MeOH = 10:1) to give 17 as colorless solid (60.7 mg, 31%, 2 steps). ¹H NMR (500 MHz, MeOH-*d*₄) δ 4.64 (d, *J* = 1.6 Hz, 1H, H-1), 3.81–3.77 (m, 2H, H-2, -6a), 3.66–3.60 (m, 2H, H-3, -4), 3.56–3.48 (m, 2H, H-5, -6b), 3.41 (s, 3H, OCH₃). ¹³C NMR (126 MHz, MeOH-*d*₄) δ 102.8 (C-1), 74.0 (C-3 or -4), 72.5 (C-3 or -4), 71.9 (C-2),

70.9 (C-5), 55.3 (OCH₃), 33.9 (C-6); ESI-MS calcd. C₇H₁₃BrNaO₅⁺: 279.0; found: 278.8. 17 was first reported by Valentin⁴⁸ and the carbon NMR data corresponded to disclosed data in the literature.⁴⁹

Methyl 6-deoxy-6-iodo- α -D-mannopyranoside (18). Methyl mannoside 12 was tosylated according to Wang *et al.*,⁴⁵ crude methyl 6-O-tosyl- α -D-mannopyranoside (300 mg, 0.86 mmol, 1 equiv.) was stirred in DMF (8.6 mL) in presence of KI (715 mg, 4.31 mmol, 5 equiv.) at 65 °C for 3 d. The solvent was removed *in vacuo* and the residue was purified by MPLC (SiO₂; gradient of CH₂Cl₂ to CH₂Cl₂/MeOH = 10:1) to give 18 as colorless solid (88.1 mg, 34%, 2 steps). ¹H NMR (500 MHz, MeOH-*d*₄) δ 4.62 (d, *J* = 1.7 Hz, 1H, H-1), 3.78 (dd, *J* = 3.4, 1.7 Hz, 1H, H-2), 3.68–3.60 (m, 2H, H-3, -6a), 3.47–3.41 (m, 5H, H-4, -5, OCH₃), 3.27–3.19 (m, 1H, H-6b). ¹³C NMR (126 MHz, MeOH-*d*₄) δ 102.9 (C-1), 74.2 (C-5), 72.5 (C-4), 72.3 (C-3), 72.1 (C-2), 55.5 (OCH₃), 6.4 (C-6); ESI-MS calcd. C₇H₁₃INaO₅⁺: 327.0; found: 326.8. 18 was first reported by Lehmann and Benson⁵⁰ and the NMR data corresponded to disclosed data in DMSO-*d*₆ in the literature.⁵¹

3,4-O-Benzylidene-1-deoxy-L-fucose (27). 1-Deoxy-L-fucose²⁷ (8) (315 mg, 2.13 mmol) was dissolved in DMF (14 mL) and to the solution were added camphorsulfonic acid (50 mg, 0.21 mmol, 0.1 equiv.) and benzaldehyde dimethyl acetal (1 mL, 6.38 mmol, 3 equiv.). The mixture was stirred at r.t. for 19 h. Then, triethylamine (30 μ L) was added, the volatiles were removed *in vacuo* and the residue was purified by MPLC (gradient petrol ether to petrol ether/EtOAc = 2:1) to give 27 as diastereomeric mixture (442 mg, 1.87 mmol, 88%) as colorless solids (ratio *S/R* = 1/1.5). ¹H NMR (400 MHz, MeOH-*d*₄) *S*-isomer: δ 7.59–7.29 (m, 5H, ArCH), 5.91 (s, 1H, PhCH(OR)₂), 4.15 (dd, *J* = 6.1, 2.3 Hz, 1H, H-4), 4.08 (t, *J* = 6.5 Hz, 1H, H-3), 3.94–3.68 (m, 3H, H-2, -5, -1^{eq}), 3.23–3.10 (m, 1H, H-1^{ax}), 1.36 (d, *J* = 6.6 Hz, 3H, H-6); *R*-isomer: δ 7.59–7.29 (m, 5H, ArCH), 6.10 (s, 1H, PhCH(OR)₂), 4.24 (dd, *J* = 6.9, 5.2 Hz, 1H, H-3), 4.05 (dd, *J* = 5.4, 2.0 Hz, 1H, H-4), 3.94–3.68 (m, 3H, H-2, H-5, H-1^{eq}), 3.23–3.10 (m, 1H, H-1^{ax}), 1.32 (d, *J* = 6.6 Hz, 3H, H-6). ¹³C NMR (101 MHz, MeOH-*d*₄) δ 140.9 (ArC), 139.4 (ArC), 130.2 (ArCH), 129.9 (ArCH), 129.3 (2C, ArCH), 129.2 (2C, ArCH), 127.8 (2C, ArCH), 127.3 (2C, ArCH), 105.3 (PhCH(OR)₂, *S*-isomer), 104.2 (PhCH(OR)₂, *R*-isomer), 81.8 (C-3, *R*-isomer), 80.0 (C-4, *S*-isomer), 80.0, 77.6 (C-4, *R*-isomer), 73.9, 73.2, 70.4, 69.6 (C-1, *R*-isomer), 69.5 (C-1, *S*-isomer), 67.2, 17.3 (C-6, *R*-isomer), 17.1 (C-6, *S*-isomer). HR-MS calcd. for C₁₃H₁₆NaO₄⁺: 259.0941; found: 259.0933.

(*R*)-3,4-O-Benzylidene-1,2-dideoxy-2-fluoro-L-fucose (29). To a solution of selectively protected (*R/S*)-27 (100 mg, 423 μ mol) in CH₂Cl₂ (1.3 mL) was added XtalFluor-E (145 mg, 635 μ mol, 1.5 equiv.) and Et₃N·3HF (173 μ L, 0.85 mmol, 2 equiv.) at r.t. and the mixture was stirred for 4 h. The mixture was poured into saturated NaHCO₃ solution (0.5 mL), the organic layer was separated and the aqueous layer was extracted with CH₂Cl₂ (2 \times 2 mL). The combined organic layers were dried over Na₂SO₄ and filtered. The solvent was removed *in vacuo* and the residue was purified by MPLC (petrol ether to petrol ether/EtOAc = 6:1) to give only the (*R*)-3,4-O-benzylidene-1,2-

dideoxy-2-fluoro-L-fucose (29) (65 mg, 272 μ mol, 65%) as colorless solid. ^1H NMR (400 MHz, MeOH- d_4) δ 7.52–7.30 (m, 5H, ArCH), 6.15 (s, 1H, PhCH(OR) $_2$), 4.75 (dddd, J = 49.7, 9.6, 9.6, 6.2 Hz, 1H, H-2), 4.52 (dt, J = 18.9, 6.1 Hz, 1H, H-3), 4.14 (dt, J = 5.8, 1.7 Hz, 1H, H-4), 4.08 (ddd, J = 11.5, 7.2, 5.8 Hz, 1H, H-1^{eq}), 3.82 (qd, J = 6.6, 1.8 Hz, 1H, H-5), 3.42 (ddd, J = 11.6, 9.4, 6.6 Hz, 1H, H-1^{ax}), 1.32 (d, J = 6.6 Hz, 3H, H-6). ^{13}C NMR (101 MHz, MeOH- d_4) δ 140.5 (ArC), 130.1 (ArCH), 129.3 (2C, ArCH), 127.3 (2C, ArCH), 104.8 (PhCH(OR) $_2$), 88.2 (d, J_{CF} = 177.3 Hz, C-2), 78.5 (d, J_{CF} = 23.8 Hz, C-3), 78.0 (d, J_{CF} = 7.0 Hz, C-4), 73.5 (C-5), 66.6 (d, J_{CF} = 26.8 Hz, C-1), 17.0 (C-6). ^{19}F NMR (376 MHz, MeOH- d_4) δ -197.0. HR-MS calcd. for $\text{C}_{13}\text{H}_{15}\text{FNaO}_3^+$: 261.0897; found: 261.0778.

1,2-Dideoxy-2-fluoro-L-fucose (30). Protected 2-fluoro-fucose 29 (35 mg, 0.147 mmol) was stirred in MeOH (10 mL) under hydrogen atmosphere (1 atm) with 10% Pd-C (10 mol%) at r.t. over night. The mixture was filtered through celite and the solvent was removed *in vacuo*. The residue was purified by MPLC (CH_2Cl_2 to $\text{CH}_2\text{Cl}_2/\text{MeOH}$ = 8:1) to give 1,2-dideoxy-2-fluoro-L-fucose (30) (21 mg, 0.142 mmol, 97%) as colorless solid. ^1H NMR (400 MHz, MeOH- d_4) δ 4.60 (dddd, J = 51.3, 10.4, 9.0, 5.8 Hz, 1H, H-2), 4.01 (dd, J = 10.9, 5.7 Hz, 1H, H-1^{eq}), 3.72–3.60 (m, 2H, H-3, H-4), 3.55 (qd, J = 6.5, 1.2 Hz, 1H, H-5), 3.27 (td, J = 10.7, 4.2 Hz, H-1^{ax}), 1.22 (d, J = 6.4 Hz, 3H, H-6). ^{13}C NMR (101 MHz, MeOH- d_4) δ 89.7 (d, J_{CF} = 176.1 Hz, C-2), 76.5 (C-5), 74.7 (d, J_{CF} = 16.6 Hz, C-3), 73.9 (d, J_{CF} = 9.4 Hz, C-4), 68.1 (d, J_{CF} = 28.2 Hz, C-1), 16.8 (C-6). ^{19}F NMR (376 MHz, MeOH- d_4) δ -208.4; ESI-MS calcd. $\text{C}_6\text{H}_{11}\text{FNaO}_3^+$: 173.1; found: 172.8.

Allyl 2,3-O-isopropylidene-6-O-trityl- α -D-mannopyranoside (31). Allyl α -D-mannopyranoside³⁴ (13) was converted to allyl 2,3-O-isopropylidene- α -D-mannopyranoside as described by Kochetkov *et al.*⁵² ^1H NMR (500 MHz, DMSO- d_6) δ 5.88 (dddd, J = 17.2, 10.4, 6.0, 5.2 Hz, 1H, CHCH $_2$ -allyl), 5.24 (dq, J = 17.2, 1.7 Hz, 1H, CHCH $_2$ -allyl), 5.16–5.08 (m, 2H, CHCH $_2$ -allyl, OH-5), 4.92 (br s, 1H, H-1), 4.54 (t, J = 6.0 Hz, 1H, OH-6), 4.12 (ddt, J = 13.1, 5.2, 1.6 Hz, 1H, OCH $_2$ -allyl), 4.02 (dd, J = 5.8, 0.9 Hz, 1H, H-2), 3.93 (ddt, J = 13.1, 6.0, 1.4 Hz, 1H, OCH $_2$ -allyl), 3.88 (t, J = 6.2 Hz, 1H, H-3), 3.62 (ddd, J = 11.9, 6.0, 1.8 Hz, 1H, H-6a), 3.41 (dt, J = 11.8, 5.8 Hz, 1H, H-6b), 3.30–3.25 (m, 2H, H-4, H-5), 1.35 (s, 3H, OCH $_3$), 1.23 (s, 3H, OC(CH $_3$) $_2$); ^{13}C NMR (126 MHz, DMSO- d_6) δ 134.4 (CHCH $_2$ -allyl), 117.1 (CHCH $_2$ -allyl), 108.2 (OC(CH $_3$) $_2$), 95.5 (C-1), 78.5 (C-3), 75.2 (C-2), 71.3 (C-4/C-5), 68.2 (C-4/C-5), 66.8 (OCH $_2$ -allyl), 60.6 (C-6), 28.0 (OC(CH $_3$) $_2$), 26.2 (OC(CH $_3$) $_2$). ESI-MS calcd. $\text{C}_{12}\text{H}_{20}\text{NaO}_6^+$: 283.1; found: 283.1. Allyl 2,3-O-isopropylidene- α -D-mannopyranoside was transformed to allyl 2,3-O-isopropylidene-6-O-trityl α -D-mannopyranoside (31) following the protocol from Gigg *et al.*⁵³ ^1H NMR (500 MHz, DMSO- d_6) δ 7.45–7.36 (m, 6H, ArCH), 7.37–7.29 (m, 6H, ArCH), 7.29–7.21 (m, 3H, ArCH), 6.03 (dddd, J = 17.3, 10.4, 5.9, 5.2 Hz, 1H, CHCH $_2$ -allyl), 5.33 (dq, J = 17.3, 1.7 Hz, 1H, CHCH $_2$ -allyl), 5.27–5.21 (m, 1H, CHCH $_2$ -allyl), 5.13 (d, J = 6.9 Hz, 1H, OH-4), 5.08 (s, 1H, H-1), 4.41 (ddt, J = 13.0, 5.3, 1.6 Hz, 1H, OCH $_2$ -allyl), 4.15 (ddt, J = 12.9, 6.0, 1.4 Hz, 1H, OCH $_2$ -allyl), 4.10 (dd, J = 5.7, 0.8 Hz, 1H, H-2), 3.93 (dd, J = 7.3, 5.8 Hz, 1H, H-3), 3.67 (ddd, J = 9.7, 7.6, 1.7 Hz, 1H, H-5), 3.35–3.28

(m, 1H, H-6a), 3.21 (dt, J = 10.5, 7.1 Hz, 1H, H-4), 3.03 (dd, J = 9.9, 7.6 Hz, 1H, H-6b), 1.38 (s, 3H, OC(CH $_3$) $_2$), 1.27 (s, 3H, OC(CH $_3$) $_2$); ^{13}C NMR (126 MHz, DMSO- d_6) δ 143.9 (3C, ArC), 134.4 (CHCH $_2$ -allyl), 128.3 (6C, ArCH), 127.9 (6C, ArCH), 127.0 (3C, ArCH), 117.1 (CHCH $_2$ -allyl), 108.3 (OC(CH $_3$) $_2$), 95.5 (C-1), 85.8 (C-Tr), 78.5 (C-3), 75.2 (C-2), 69.8 (C-5), 68.5 (C-4), 66.9 (OCH $_2$ -allyl), 63.5 (C-6), 27.9 (OC(CH $_3$) $_2$), 26.2 (OC(CH $_3$) $_2$); ESI-MS calcd. $\text{C}_{31}\text{H}_{34}\text{NaO}_6^+$: 525.2; found: 525.2.

Allyl 2,3-O-isopropylidene-4-O-methyl-6-O-trityl- α -D-mannopyranoside (32). Allyl 2,3-O-isopropylidene-6-O-trityl- α -D-mannopyranoside (31) (310 mg, 0.62 mmol, 1 equiv.) was dissolved in dry DMF (1.5 mL) and NaH (60%, 74 mg, 1.85 mmol, 5 equiv.) was added at 0 $^\circ\text{C}$ under nitrogen atmosphere. After 10 min, MeI (116 μL , 1.85 mmol, 5 equiv.) was added dropwise and the reaction was stirred for 1 h at 0 $^\circ\text{C}$. The reaction mixture was quenched with EtOH (1 mL), sat. NaHCO $_3$ solution (2 mL) was added and the reaction mixture was extracted with EtOAc (3 \times 10 mL). The combined organic layers were dried over Na $_2$ SO $_4$ and the solvent was removed *in vacuo*. The title compound 32 (262 mg, 0.51 mmol, 83%) was obtained after purification by MPLC (petrol ether/EtOAc = 9:1). ^1H NMR (500 MHz, DMSO- d_6) δ 7.45–7.38 (m, 6H, ArCH), 7.38–7.30 (m, 6H, ArCH), 7.29–7.23 (m, 3H, ArCH), 5.97 (dddd, J = 17.3, 10.4, 5.9, 5.2 Hz, 1H, CHCH $_2$ -allyl), 5.30 (dq, J = 17.3, 1.7 Hz, 1H, CHCH $_2$ -allyl), 5.24–5.17 (m, 1H, CHCH $_2$ -allyl), 5.11 (s, 1H, H-1), 4.29 (ddt, J = 13.0, 5.2, 1.5 Hz, 1H, OCH $_2$ -allyl), 4.13 (dd, J = 5.7, 0.8 Hz, 1H, H-2), 4.12–4.04 (m, 2H, OCH $_2$ -allyl, H-3), 3.60 (ddd, J = 10.2, 5.7, 1.9 Hz, 1H, H-5), 3.29 (dd, J = 10.2, 6.9 Hz, 1H, H-4), 3.25 (dd, J = 9.9, 1.9 Hz, 1H, H-6a), 3.21 (s, 3H, OCH $_3$), 3.08 (dd, J = 9.9, 5.7 Hz, 1H, H-6b), 1.48 (s, 3H, OC(CH $_3$) $_2$), 1.30 (s, 3H, OC(CH $_3$) $_2$); ^{13}C NMR (126 MHz, DMSO- d_6) δ 143.7 (3C, ArC), 134.2 (CHCH $_2$ -allyl), 128.2 (6C, ArCH), 127.8 (6C, ArCH), 127.0 (3C, ArCH), 117.2 (CHCH $_2$ -allyl), 108.6 (OC(CH $_3$) $_2$), 95.5 (C-1), 85.7 (Ph $_3$ -CO-), 77.8 (C-3), 77.4 (C-4), 75.1 (C-2), 68.0 (C-5), 67.1 (OCH $_2$ -allyl), 62.5 (C-6), 58.3 (OCH $_3$), 27.7 (OC(CH $_3$) $_2$), 26.1 (OC(CH $_3$) $_2$); ESI-MS calcd. $\text{C}_{32}\text{H}_{36}\text{NaO}_6^+$: 539.2; found: 539.2.

Allyl 4-O-methyl- α -D-mannopyranoside (33). Allyl 2,3-O-isopropylidene-4-O-methyl-6-O-trityl- α -D-mannopyranoside (32) (131 mg, 0.254 mmol) was stirred in acetone (1.6 mL) in presence of aqueous acetic acid (80%, 0.8 mL) for 21 h at r.t. The reaction mixture was neutralized with NaOH, the volatiles were removed *in vacuo* and the residue was purified by MPLC ($\text{CH}_2\text{Cl}_2/\text{EtOH}$ = 95:5) to give 33 as solid (16.2 mg, 0.07 mmol, 27%). ^1H NMR (500 MHz, MeOH- d_4) δ 5.92 (dddd, J = 17.2, 10.5, 5.9, 5.1 Hz, 1H, CHCH $_2$ -allyl), 5.28 (dq, J = 17.3, 1.7 Hz, 1H, CHCH $_2$ -allyl), 5.21–5.13 (m, 1H, CHCH $_2$ -allyl), 4.77 (d, J = 1.3 Hz, 1H, H-1), 4.18 (ddt, J = 13.1, 5.1, 1.6 Hz, 1H, OCH $_2$ -allyl), 3.99 (ddt, J = 13.1, 5.9, 1.4 Hz, 1H, OCH $_2$ -allyl), 3.81–3.74 (m, 3H, H-2, -3, -6a), 3.69 (dd, J = 11.8, 5.1 Hz, 1H, H-6b), 3.54 (s, 3H, OCH $_3$), 3.48 (dddd, J = 9.9, 5.2, 2.3, 0.6 Hz, 1H, H-5), 3.41–3.32 (m, 1H, H-4); ^{13}C NMR (126 MHz, MeOH- d_4) δ 135.4 (CHCH $_2$ -allyl), 117.3 (CHCH $_2$ -allyl), 100.6 (C-1), 78.4 (C-4), 73.8 (C-5), 72.7 (C-2/3), 72.5 (C-2/3), 68.8 (OCH $_2$ -allyl), 62.5 (C-6), 60.9 (OCH $_3$); ESI-MS calcd. $\text{C}_{10}\text{H}_{18}\text{NaO}_6^+$: 257.1; found: 256.9.

Expression of recombinant BC2L-A and LecB and Competitive binding assays

BC2L-A¹⁰ and LecB²² were produced according to the previously published protocols. The competitive binding assay for BC2L-A based on fluorescence polarization was performed in analogy to the published protocol²² for LecB. For titration of 3 and 4 with BC2L-A, 10 μ L of fluorescent reporter ligand *N*-(fluorescein-5-yl)-*N'*-(α -D-mannopyranosyloxyethyl)-thiocarbamide 3 (30 nM) or *N*-(fluorescein-5-yl)-*N'*-(α -L-fucopyranosyl-O-ethyl)-thiocarbamide 4 (30 nM) in TBS/Ca (20 mM Tris, 137 mM NaCl, 2.6 mM KCl at pH 7.4 supplemented with 100 μ M CaCl₂) were mixed with 20 μ L serial dilutions (507 μ M to 0.247 μ M, *i.e.*, a final concentration of 338 μ M to 0.165 μ M) of BC2L-A in TBS/Ca in triplicates. For compound inhibition assay, 20 μ L of a stock solution of BC2L-A (2.25 μ M) and fluorescent reporter ligand 3 (15 nM) in TBS/Ca were mixed with 10 μ L serial dilutions (2 mM to 25.6 nM) of testing compounds in TBS/Ca in triplicates in black 384-well microtiter plates (Greiner Bio-One, Germany, cat no. 781900). In all experiments, the microtiter plates were centrifuged at 800 rpm for 1 min at 23 °C and incubated for 3–4 h at r.t. Fluorescence emission parallel and perpendicular to the excitation plane was measured on a PheraStar FS (BMG Labtech, Germany) plate reader with excitation filters at 485 nm and emission filters at 535 nm. The measured intensities were reduced by buffer values and fluorescence polarization was calculated. The data were analyzed using BMG Labtech MARS software and/or with Graphpad Prism and fitted according to the four parameter variable slope model. A minimum of three independent measurements of triplicates each was performed for every ligand. To assure reliability of the read signal and exclude any influence of the test compounds on the total intensity of the fluorescence of the tracer molecule 3, total fluorescence intensities of each well were monitored. Concentrations of test compounds yielding deviations in fluorescence intensity of >20% of tracer 3 in absence of test compound are generally not taken for determination of IC₅₀ values. Here, none of the tested compounds showed any influence on the total fluorescence intensity of tracer 3, yielding reliable fluorescence polarization data.

Measurements with LecB were performed according to previously reported protocol using the fucose based fluorescent reporter ligand 4.²²

Molecular Docking

The docking study was performed using PLANTS v1.1.⁵⁴ The calculation of charge and energy minimization of the protein and tested compounds was done using Molecular Operating Environment (MOE), 2014.09 (Chemical Computing Group Inc., 1010 Sherbooke St. West, Suite #910, Montreal, QC, Canada, H3A 2R7, 2015). Thereafter, the standard docking procedure (PLANTS Manual, available at http://www.tcd.uni-konstanz.de/plants_download/download/manual1.1.pdf) was validated by removing the mannoheptose ligand and redocking it inside the active site of BC2L-A (PDB code:

4AOC). The docking site was limited inside a 13.3 Å radius sphere centered in the mass center (coordination: $X = -27.73$, $Y = 53.64$ and $Z = -12.64$) of the crystallized ligand. Glu31, Asp110, Gly111 and His112 were set as flexible residues in the input file. After docking the original mannoheptose ligand for validation of the process, a good agreement was observed between the localization of the docked ligand and in the crystal structure (rmsd = 2.0 Å). This validated docking protocol was then used for docking the derivatives 22 and 24 into the crystal structure of the protein.

Acknowledgements

We are grateful to Benjamin Frommeyer and Leandra Hahn for assistance with the synthesis of compound 3 and Emilie Gillon for assistance in producing BC2L-A. Thomas Exner is kindly acknowledged for providing the PLANTS software and supporting the docking experiments. The authors thank Holger Bußkamp for HR-MS and Josef Zapp for NMR measurements. We are grateful to the Helmholtz Association [VH-NG-934], the Konstanz Research School Chemical Biology, and the Deutsche Forschungsgemeinschaft [Ti756/2-1] for financial support.

References

- 1 E. Mahenthiralingam, A. Baldwin and C. G. Dowson, *J. Appl. Microbiol.*, 2008, **104**(6), 1539–1551.
- 2 A. Isles, I. Maclusky, M. Corey, R. Gold, C. Prober, P. Fleming and H. Levison, *J. Pediatr.*, 1984, **104**(2), 206–210.
- 3 A. M. Jones, M. E. Dodd, J. R. W. Govan, V. Barcus, C. J. Doherty, J. Morris and A. K. Webb, *Thorax*, 2004, **59**(11), 948–951.
- 4 S. D. Aaron, W. Ferris, D. A. Henry, D. P. Speert and N. E. Macdonald, *Am. J. Respir. Crit. Care Med.*, 2000, **161**(4 Pt 1), 1206–1212.
- 5 M. Desai, T. Bühler, P. H. Weller and M. R. Brown, *J. Antimicrob. Chemother.*, 1998, **42**(2), 153–160.
- 6 R. Sommer, I. Joachim, S. Wagner and A. Titz, *Chimia*, 2013, **67**(4), 286–290.
- 7 K. L. Tomlin, O. P. Coll and H. Ceri, *Can. J. Microbiol.*, 2001, **47**(10), 949–954.
- 8 S. P. Diggle, R. E. Stacey, C. Dodd, M. Cámara, P. Williams and K. Winzer, *Environ. Microbiol.*, 2006, **8**(6), 1095–1104.
- 9 D. Tielker, S. Hacker, R. Loris, M. Strathmann, J. Wingender, S. Wilhelm, F. Rosenau and K.-E. Jaeger, *Microbiology*, 2005, **151**(Pt 5), 1313–1323.
- 10 E. Lameignere, L. Malinová, M. Sláviková, E. Duchaud, E. P. Mitchell, A. Varrot, O. Sedo, A. Imberty and M. Wimmerová, *Biochem. J.*, 2008, **411**(2), 307–318.
- 11 K. Zinger-Yosovich, D. Sudakevitz, A. Imberty, N. C. Garber and N. Gilboa-Garber, *Microbiology*, 2006, **152**(Pt 2), 457–463.
- 12 D. Sudakevitz, N. Kostlánová, G. Blatman-Jan, E. P. Mitchell, B. Lerrer, M. Wimmerová, D. J. Katcoff, A. Imberty and N. Gilboa-Garber, *Mol. Microbiol.*, 2004, **52**(3), 691–700.

- 13 O. Sulák, G. Cioci, E. Lameignère, V. Balloy, A. Round, I. Gutsche, L. Malinovská, M. Chignard, P. Kosma, D. F. Aubert, C. L. Marolda, M. A. Valvano, M. Wimmerová and A. Imberty, *PLoS Pathog.*, 2011, 7(9), e1002238.
- 14 O. Sulák, G. Cioci, M. Delia, M. Lahmann, A. Varrot, A. Imberty and M. Wimmerová, *Structure*, 2010, 18(1), 59–72.
- 15 R. J. Malott, E. P. O'Grady, J. Toller, S. Inhülsen, L. Eberl and P. A. Sokol, *J. Bacteriol.*, 2009, 191(8), 2447–2460.
- 16 A. Suppiger, N. Schmid, C. Aguilar, G. Pessi and L. Eberl, *Virulence*, 2013, 4(5), 400–409.
- 17 N. Schmid, G. Pessi, Y. Deng, C. Aguilar, A. L. Carlier, A. Grunau, U. Omasits, L.-H. Zhang, C. H. Ahrens and L. Eberl, *PLoS One*, 2012, 7(11), e49966.
- 18 S. Inhülsen, C. Aguilar, N. Schmid, A. Suppiger, K. Riedel and L. Eberl, *MicrobiologyOpen*, 2012, 1(2), 225–242.
- 19 E. Lameignere, T. C. Shiao, R. Roy, M. Wimmerova, F. Dubreuil, A. Varrot and A. Imberty, *Glycobiology*, 2010, 20(1), 87–98.
- 20 R. Marchetti, L. Malinowska, E. Lameignère, L. Adamova, C. de Castro, G. Cioci, C. Stanetty, P. Kosma, A. Molinaro, M. Wimmerova, A. Imberty and A. Silipo, *Glycobiology*, 2012, 22(10), 1387–1398.
- 21 Z. Han, J. S. Pinkner, B. Ford, R. Obermann, W. Nolan, S. A. Wildman, D. Hobbs, T. Ellenberger, C. K. Cusumano, S. J. Hultgren and J. W. Janetka, *J. Med. Chem.*, 2010, 53(12), 4779–4792.
- 22 D. Hauck, I. Joachim, B. Frommeyer, A. Varrot, B. Philipp, H. M. Möller, A. Imberty, T. E. Exner and A. Titz, *ACS Chem. Biol.*, 2013, 8(8), 1775–1784.
- 23 P. Sörme, B. Kahl-Knutsson, M. Huflejt, U. J. Nilsson and H. Leffler, *Anal. Biochem.*, 2004, 334(1), 36–47.
- 24 J. Dahmen, T. Frejd, G. Gronberg, T. Lave, G. Magnusson and G. Noori, *Carbohydr. Res.*, 1983, 116(2), 303–307.
- 25 W. Hayes, H. M. I. Osborn, S. D. Osborne, R. A. Rastall and B. Romagnoli, *Tetrahedron*, 2003, 59(40), 7983–7996.
- 26 M. Kleinert, N. Rockendorf and T. Lindhorst, *Eur. J. Org. Chem.*, 2004, 3931–3940.
- 27 R. Sommer, T. E. Exner and A. Titz, *PLoS One*, 2014, 9(11), e112822.
- 28 L. C. Gilday, S. W. Robinson, T. A. Barendt, M. J. Langton, B. R. Mullaney and P. D. Beer, *Chem. Rev.*, 2015, 115(15), 7118–7195.
- 29 R. Wilcken, M. O. Zimmermann, A. Lange, A. C. Joerger and F. M. Boeckler, *J. Med. Chem.*, 2013, 56(4), 1363–1388.
- 30 A. Hofmann, R. Sommer, D. Hauck, J. Stifel, I. Göttker-Schnetmann and A. Titz, *Carbohydr. Res.*, 2015, 412, 34–42.
- 31 R. Sommer, D. Hauck, A. Varrot, S. Wagner, A. Audfray, A. Prestel, H. M. Möller, A. Imberty and A. Titz, *ChemistryOpen*, 2015, 4(6), 756–767.
- 32 H. Plenio, *ChemBioChem*, 2004, 5(5), 650–655.
- 33 S. Purser, P. R. Moore, S. Swallow and V. Gouverneur, *Chem. Soc. Rev.*, 2008, 37(2), 320–330.
- 34 T. Wohlschlager, A. Buttschi, P. Grassi, G. Sutov, R. Gauss, D. Hauck, S. S. Schmieder, M. Knobel, A. Titz, A. Dell, S. M. Haslam, M. O. Hengartner, M. Aebi and M. Künzler, *Proc. Natl. Acad. Sci. U. S. A.*, 2014, 111(27), E2787–E2796.
- 35 D. Solís, J. Jiménez-Barbero, M. Martín-Lomas and T. Díaz-Mauriño, *Eur. J. Biochem.*, 1994, 223(1), 107–114.
- 36 I. P. Street, C. R. Armstrong and S. G. Withers, *Biochemistry*, 1986, 25(20), 6021–6027.
- 37 S. A. Allman, H. H. Jensen, B. Vijayakrishnan, J. A. Garnett, E. Leon, Y. Liu, D. C. Anthony, N. R. Sibson, T. Feizi, S. Matthews and B. G. Davis, *ChemBioChem*, 2009, 10(15), 2522–2529.
- 38 Y. Ito, S. Hagihara, M. A. Arai, I. Matsuo and M. Takatani, *Glycoconjugate J.*, 2004, 21(5), 257–266.
- 39 A. Tatami, Y.-S. Hon, I. Matsuo, M. Takatani, H. Koshino and Y. Ito, *Biochem. Biophys. Res. Commun.*, 2007, 364(2), 332–337.
- 40 E. Matei, S. André, A. Glinschert, A. S. Infantino, S. Oscarson, H.-J. Gabius and A. M. Gronenborn, *Chem. – Eur. J.*, 2013, 19(17), 5364–5374.
- 41 W. Stahl, U. Sprengard, G. Kretzschmar and H. Kunz, *Angew. Chem., Int. Ed. Engl.*, 1994, 33(20), 2096–2098.
- 42 R. Albert, K. Dax, R. W. Link and A. E. Stütz, *Carbohydr. Res.*, 1983, 118, C5–C6.
- 43 A. L'heureux, F. Beaulieu, C. Bennett, D. R. Bill, S. Clayton, F. Laflamme, M. Mirmehrabi, S. Tadayan, D. Tovell and M. Couturier, *J. Org. Chem.*, 2010, 75(10), 3401–3411.
- 44 H. E. Gottlieb, V. Kotlyar and A. Nudelman, *J. Org. Chem.*, 1997, 62(21), 7512–7515.
- 45 P. Wang, G. Shen, Y. Wang, Y. Ichikawa and C. Wong, *J. Org. Chem.*, 1993, 58(15), 3985–3990.
- 46 H. J. Jennings and J. K. N. Jones, *Can. J. Chem.*, 1965, 43(8), 2372–2386.
- 47 C. W. Holzapfel, J. M. Koekemoer and C. F. Marais, *S. Afr. J. Chem.*, 1984, 37(1), 19–26.
- 48 F. Valentin, *Collect. Czech. Chem. Commun.*, 1934, 6, 354–370.
- 49 D. Cicero, O. Varela and R. M. De Lederkremer, *Carbohydr. Res.*, 1991, 211(2), 295–308.
- 50 J. Lehmann and A. A. Benson, *J. Am. Chem. Soc.*, 1964, 86(20), 4469–4472.
- 51 P. Leon-Ruau and D. Plusquellec, *Tetrahedron*, 1991, 47(28), 5185–5192.
- 52 N. K. Kochetkov, B. A. Dmitriev, A. Y. Chernyak and A. B. Levinsky, *Carbohydr. Res.*, 1982, 110(2), C16–C20.
- 53 J. Gigg, R. Gigg, S. Payne and R. Conant, *Carbohydr. Res.*, 1985, 141(1), 91–97.
- 54 O. Korb, T. Stützle and T. E. Exner, *Lecture Notes in Computer Science*, 2006, 4150, 247–258.

3.4. *PHOTORHABDUS LUMINESCENS* LECTIN A (PLLA) - A NEW PROBE FOR DETECTING α -GALACTOSIDE-TERMINATING GLYCOCONJUGATES

Ghamdan Beshr, Asfandiyar Sikandar, Eva-Maria Jemiller, Nikolai Klymiuk, Dirk Hauck, Stefanie Wagner, Eckhard Wolf, Jesko Koehnke, and Alexander Titz.

Journal of Biological Chemistry, **2017**; 292 (48), 19935-19951 - DOI:
10.1074/jbc.M117.812792

Reprinted with permission from the American Society for Biochemistry and Molecular
Biology



Photorhabdus luminescens lectin A (PILa): A new probe for detecting α -galactoside-terminating glycoconjugates

Received for publication, August 17, 2017, and in revised form, September 25, 2017. Published, Papers in Press, September 28, 2017, DOI 10.1074/jbc.M117.812792

Ghamdan Beshr^{†§¶}, Asfandiyar Sikandar^{¶||}, Eva-Maria Jemiller^{**}, Nikolai Klymiuk^{**}, Dirk Hauck^{‡§}, Stefanie Wagner^{‡§}, Eckhard Wolf^{**}, Jesko Koehnke^{¶||1}, and Alexander Titz^{‡§¶12}

From the [†]Divisions of Chemical Biology of Carbohydrates and ^{||}Structural Biology of Biosynthetic Enzymes, Helmholtz Institute for Pharmaceutical Research Saarland (HIPS), D-66123 Saarbrücken, the [§]Deutsches Zentrum für Infektionsforschung (DZIF), Standort Hannover-Braunschweig, the [¶]Department of Pharmacy, Saarland University, 66123 Saarbrücken, and the ^{**}Chair for Molecular Animal Breeding and Biotechnology, Gene Center and Department of Veterinary Sciences, Ludwig Maximilian University of Munich, 81377 Munich, Germany

Edited by Gerald W. Hart

Lectins play important roles in infections by pathogenic bacteria, for example, in host colonization, persistence, and biofilm formation. The Gram-negative entomopathogenic bacterium *Photorhabdus luminescens* symbiotically lives in insect-infecting *Heterorhabditis* nematodes and kills the insect host upon invasion by the nematode. The *P. luminescens* genome harbors the gene *plu2096*, coding for a novel lectin that we named PILa. We analyzed the binding properties of purified PILa with a glycan array and a binding assay in solution. Both assays revealed a strict specificity of PILa for α -galactoside-terminating glycoconjugates. The crystal structures of apo PILa and complexes with three different ligands revealed the molecular basis for the strict specificity of this lectin. Furthermore, we found that a 90° twist in subunit orientation leads to a peculiar quaternary structure compared with that of its ortholog LecA from *Pseudomonas aeruginosa*. We also investigated the utility of PILa as a probe for detecting α -galactosides. The α -Gal epitope is present on wild-type pig cells and is the main reason for hyperacute organ rejection in pig to primate xenotransplantation. We noted that PILa specifically recognizes this epitope on the glycan array and demonstrated that PILa can be used as a fluorescent probe to detect this epitope on primary porcine cells *in vitro*. In summary, our biochemical and structural analyses of the *P. luminescens* lectin PILa have disclosed the structural basis for PILa's high specificity for α -galactoside-containing ligands, and we show that PILa can be used to visualize the α -Gal epitope on porcine tissues.

Photorhabdus luminescens is a Gram-negative γ -proteobacterium belonging to the Enterobacteriaceae family. In its complex life cycle it lives symbiotically in the intestine of *Heterorhabditis*

abditidae entomopathogenic nematodes and pathogenically in insect larvae upon nematode invasion. *P. luminescens* was first isolated in 1977 as a symbiont bacterium of *Heterorhabditidae* nematodes and classified initially as *Xenorhabdus luminescens* (1, 2) and later renamed *P. luminescens* (3). The genus *Photorhabdus* consists of the four species *P. luminescens*, *P. temperata*, *P. heterorhabditis*, and *P. asymbiotica* (4–6), with the latter species being pathogenic to humans (7). Both *Xenorhabdus* and *Photorhabdus* species enter a wide range of insect larvae via Steinernematidae and *Heterorhabditidae* nematodes, respectively (4, 8). Once the nematodes enter into the insect at their infective juvenile developmental stage, their bacterial symbionts are released into the insect's blood, and both bacteria and nematode are able to kill the larvae within 48 h (9).

The complete genome of *P. luminescens* subsp. *laumondii* TTO1 was published in 2003 by Duchaud *et al.* (10). Compared with other bacteria, it shows a high number of genes predicted as toxins, and some of them, such as *Tca* and *Tcd*, have been extensively studied (10–12). Often, bacterial carbohydrate-binding proteins, *i.e.* lectins, also act as toxins in addition to their function as adhesins to enable host colonization. A number of predicted lectins are present in the genome of *P. luminescens*, but only one example, the fucose-binding protein PLL (13), has been experimentally characterized. In *Pseudomonas aeruginosa*, a ubiquitous opportunistic pathogen with a high current medical need for new therapeutics (14), the two lectins LecA and LecB are both toxins and adhesins with roles in biofilm formation and persistent infection (15–17). LecB (18, 19)-type proteins are relatively common, and several LecB homologs have also been previously characterized in other bacterial species such as *Ralstonia solanaceum* (20), *Burkholderia cenocepacia* (21–23), and *Chromobacterium violaceum* (24). The *P. luminescens* genome harbors several genes of predicted lectins that are homologs of LecB (25). In contrast, homologs of LecA are comparably rare and are not present in the genomes of the former species. In *P. luminescens*, a single gene encoding for a LecA homolog (*plu2096*) was predicted by Duchaud *et al.* (10).

Here, we report the biochemical and structural characterization of the *P. luminescens* lectin PILa. We demonstrate that PILa is highly specific for α -galactoside-containing ligands. By determining several crystal structures of PILa in

The authors declare that they have no conflicts of interest with the contents of this article. The content is solely the responsibility of the authors and does not necessarily represent the official views of the National Institutes of Health.

This article contains supplemental Figs. S1–S11, Tables S1–S2 and Scheme S1. The atomic coordinates and structure factors (codes 5OFZ, 5ODU, 5OFX, and 5OFI) have been deposited in the Protein Data Bank (<http://www.pdb.org/>).

¹ Recipient of Emmy Noether Fellowship KO4116/3-1 from Deutsche Forschungsgemeinschaft. To whom correspondence may be addressed. E-mail: jesko.koehnke@helmholtz-hzi.de.

² Recipient of Helmholtz Association Grant VH-NG-934 and Deutsche Forschungsgemeinschaft Grant Ti 756/2-1. To whom correspondence may be addressed. E-mail: alexander.titz@helmholtz-hzi.de.

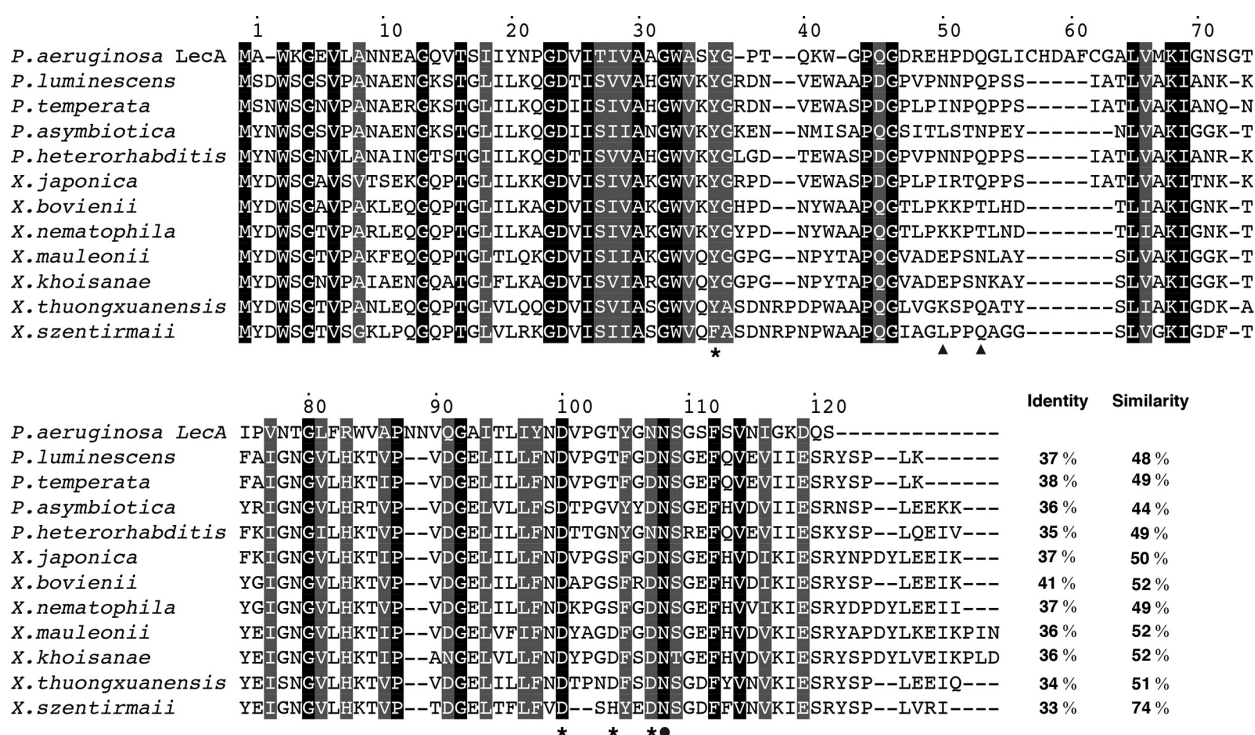
Photorhabdus lectin A — PIIA

Figure 1. Sequence alignment of LecA from *P. aeruginosa* with hypothetical LecA-like proteins from *Photobhabdus* and *Xenorhabdus* species (one single ortholog per organism selected based on highest identity to LecA). Strictly conserved amino acids are shaded black, and similarly conserved amino acids are shaded gray. Black dot, amino acid of LecA involved in Ca^{2+} binding; black triangles, amino acids of LecA involved in sugar binding; asterisks, amino acids of LecA involved in both Ca^{2+} and sugar binding. Amino acid numbering follows the LecA crystal structure where the N-terminal methionine is lacking. The depicted protein sequence of *P. luminescens* (PIIA) is encoded by the *plu2096* gene.

complex with ligands, we were able to rationalize PIIA's strong preference for α -galactosides. We further demonstrate that PIIA can serve as a detection tool for the specific visualization of the α -Gal epitope present on porcine tissue. This epitope is responsible for hyperacute rejection of pig to primate organ xenotransplants.

Results and discussion

Identification and production of PIIA

Although *P. aeruginosa* LecB orthologs have been widely studied, orthologs of LecA have not been characterized in detail. We searched the publicly accessible NCBI database using protein blast and the protein sequence of LecA from strain PAO1 as a template. A moderate number of orthologs was retrieved from only a few different genera of Gram-negative bacteria. These were mainly entomopathogenic *Photobhabdus* and *Xenorhabdus* species, as well as human opportunistic pathogens from the *Enterobacter* spp. and a few other pathogenic bacterial species (see supplemental Fig. S1).

In *P. luminescens*, the gene *plu2096* was previously proposed as the coding gene for a LecA-like protein (10) and later confirmed (26) to be a galactose-binding lectin. An alignment of the retrieved orthologs of LecA in each *Photobhabdus* and *Xenorhabdus* species shows a high degree of similarity within these entomopathogenic species (Fig. 1). Although the residues involved in metal and ligand binding in LecA are relatively conserved, distinct differences to *P. aeruginosa* LecA were

observed; LecA contains an insert flanked by two cysteines that are absent in PIIA, and the *Photobhabdus* and *Xenorhabdus* homologs contain an additional C-terminal tail of 5–13 amino acids, which is partially conserved (Fig. 1).

PIIA has 37% sequence identity to LecA, and all amino acids whose side chains are involved in calcium ion binding are conserved except for one Asn (LecA) to Asp (PIIA) variation. Amino acids involved in carbohydrate recognition are only partially conserved.

Recombinant production and purification of PIIA

The *plu2096* gene was amplified from genomic DNA of *P. luminescens* subsp. *laumondii* TTO1 and cloned into the pET22b(+) vector. Recombinant expression in *Escherichia coli* BL21(DE3) yielded a protein product at a 13-kDa apparent molecular mass by SDS-PAGE (Fig. 2A), which corresponds to its predicted size of 12.95 kDa. Because of the sequence homology to galactose-binding LecA, we subjected the cell lysate to galactosylated Sepharose (27), and PIIA was retained on this affinity resin. Subsequent elution was achieved using galactose in the elution buffer. Purification yielded ~6 mg of PIIA/liter of bacterial culture, which was later improved to 19 mg/liter by purification on melibiose-coupled Sepharose (see below).

Because lectins often oligomerize and LecA forms a tetramer (28), we analyzed PIIA's multimeric state using

Photorhabdus lectin A — PIIA

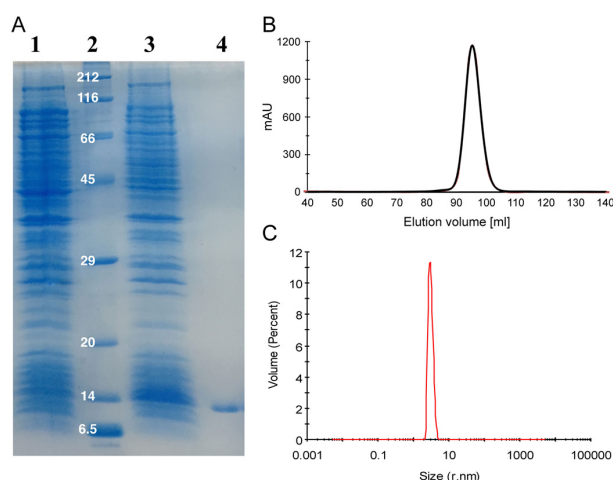


Figure 2. A, recombinant expression and affinity purification of PIIA analyzed by SDS-PAGE (15%). *E. coli* whole-cell extracts of uninduced (lane 1) and IPTG-induced cultures (lane 3), and purified PIIA (lane 4), molecular mass marker in kDa (lane 2) are shown. B, Sepharose size-exclusion chromatogram of PIIA; C, DLS analysis of PIIA.

size-exclusion chromatography (SEC).³ The protein's observed apparent molecular mass was 27 kDa, which suggested a PIIA dimer (Figs. 2B and supplemental Fig. S2). When we used the more robust technique of dynamic light scattering (DLS), we observed a homogeneous sample with an apparent molecular mass of 52.1 kDa (Fig. 2C). The tetramer LecA was also studied by DLS under identical conditions, and its apparent molecular mass of 52.4 kDa (supplemental Fig. S3) matched the value for PIIA and thus suggests the tetramerization of PIIA in solution. The observed differences for PIIA in SEC and DLS could result from weak interactions between PIIA and the glycan-based Sepharose resin, altering the observed molecular mass to a smaller size.

Carbohydrate-binding specificity of PIIA using the CFG glycan array

To assess the carbohydrate-binding specificity of PIIA, the protein was fluorescently labeled using fluorescein isothiocyanate (FITC), and binding to a glycan array containing over 600 carbohydrate epitopes was performed at the Consortium for Functional Genomics (Fig. 3A). The LecA homolog PIIA showed a strict specificity toward glycans with terminal α -galactosides, whereas β -galactosides and other carbohydrates only showed very weak or no binding. The highest apparent binding affinity was detected for the bivalent α -Gal-terminating *N*-glycan (Gal- α -1,3-Gal- β -1,4-GlcNAc)₂Man₃GlcNAc₂ (glycan nos. 360 and 550) or its difucosylated derivative glycan no. 368 bearing blood group B antigens at the non-reducing end and the two monovalent disaccharides Gal- α -1,3-GalNAc (glycan no. 112) and Gal- α -1,4-GlcNAc (glycan no. 123).

The highest apparent binding was observed for bivalent Gal- α -1,3-Gal- β -1,4-GlcNAc terminating glycans (glycans no. 360, 368, and 550). This glycan structure, called the α -Gal epitope (29), is a ubiquitous constituent of glycans in non-primate mammals and new world monkeys. The nematode *Parelaphostrongylus tenuis* also contains *N*-glycans decorated with this epitope (30). This epitope is mainly responsible for hyperacute rejection of porcine organ transplants in humans during xenotransplantation (29, 31). Interestingly, the corresponding monovalent glycans (no. 105 and 115) showed a 4–5-fold lower binding signal (Table 1), indicating that PIIA binds carbohydrates multivalently as known for its ortholog LecA. Interestingly, when the same monovalent epitopes were presented on a shorter spacer (Sp0) with one mannose between spacer and epitope (no. 516 and 517), binding was reduced further.

Apart from the divalent ligands, only the two disaccharides, Gal- α -1,3-GalNAc and Gal- α -1,4-GlcNAc, showed a high binding signal among the monovalent series (Fig. 3A). These two ligands are monovalently displayed and may reveal the intrinsic specificity of PIIA, because other monovalent ligands showed only weak or no binding to PIIA on this glycan array. Interestingly, these two ligands displayed much stronger binding than analogous Gal- α -1,3-Gal and Gal- α -1,2-Gal, suggesting an important role of the acetamide moiety in the penultimate residue for binding to PIIA (Table 1). Among the monovalent ligands on the array, the observed linkage specificity of PIIA was broad for glycans containing terminal Gal- α -1,3 and Gal- α -1,4 linkages. The single present Gal- α -1,6-linked ligand (Gal- α -1,6-Glc) was moderately bound, whereas the single Gal- α -1,2-linked ligand (Gal- α -1,2-Gal) was not recognized by PIIA (Table 1).

To compare the carbohydrate specificity of PIIA with its previously characterized ortholog LecA (32), glycan array binding data of monovalent glycan ligands for both lectins was normalized and plotted (Fig. 3B). Notably, LecA showed the best binding to Gal- α -1,4-Gal- β -1,4-GlcNAc, which is only weakly recognized by PIIA. This glycan is part of the glycosphingolipid Gb3, which when bound by LecA triggers membrane bending, a process that was proposed as an entry pathway for *P. aeruginosa* invasion into the host cell (33). In contrast, PIIA showed high apparent binding to the epitopes Gal- α -1,3-GalNAc and Gal- α -1,4-GlcNAc, whereas LecA only shows moderate apparent binding as observed for a number of other α -galactosides on the glycan array (Fig. 3B). In summary, LecA is a rather promiscuous receptor for a variety of monovalent galactosides. In addition to PIIA's binding to the bivalent *N*-glycan structures described above, PIIA was rather specific for Gal- α -1,3-GalNAc and Gal- α -1,4-GlcNAc, one or both of which may be the natural ligand of PIIA.

Development of a competitive binding assay for PIIA

To rapidly assess and quantify the binding specificity of PIIA, we developed a competitive binding assay for PIIA by utilizing fluorescence polarization, which is based on our previous work (19, 21, 27, 34) for four different lectins. Four different FITC-labeled *D*-galactosides (27) were titrated with increasing amounts of PIIA (Fig. 4, A–C). All three β -linked galactosides

³ The abbreviations used are: SEC, size-exclusion chromatography; PDB, Protein Data Bank; r.m.s.d., root mean square deviation; BisTris, 2-bis(2-hydroxyethyl)amino-2-(hydroxymethyl)propane-1,3-diol; DLS, dynamic light scattering; GTKO, α -1,3-galactosyltransferase knock-out; SCNT, somatic cell nuclear transfer; IPTG, isopropyl 1-thio- β -D-galactopyranoside; BAC, bacterial artificial chromosome.

A

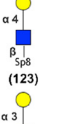
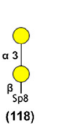
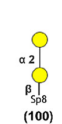
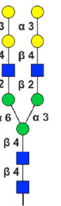

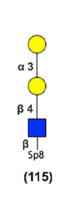
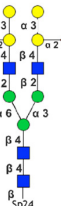

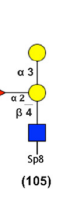
Figure 2A displays MS/MS spectra for various glycan structures. The x-axis represents the mass-to-charge ratio (m/z) from 0 to 600, and the y-axis represents the average relative fluorescence unit (RFU) from 0 to 6000. The legend indicates the following components: Gal (yellow circle), Fuc (red triangle), Man (green circle), GalNAc (yellow square), and GlcNAc (blue square). The spectra are labeled with the number of ions (n) and the glycan structure (e.g., (112) Gal α 3-Sp8, (123) Gal α 4-Sp8, (360) Gal α 3-Gal β 4-GlcNAc β -Sp20, (368) Gal α 3-Gal β 4-GlcNAc β -Sp2, (550) Gal α 3-Gal β 4-GlcNAc β -Sp). The spectra show characteristic fragmentation patterns, with the most intense peak (base peak) typically corresponding to the precursor ion. The legend also indicates the fragmentation type: terminal α -Gal (black bar), terminal β -Gal (red bar), and other (blue bar).

B

Figure 2B shows the relative intensities of PI and PI-1A for the same glycan structures. The x-axis lists the glycan structures, and the y-axis represents the normalized RFU from 0 to 1.2. The legend indicates the following components: PI (black bar) and PI-1A (gray bar). The structures are labeled with the number of ions (n) and the glycan structure (e.g., (31) Gal α -1,4-Gal β -1,4-GlcNAc β -Sp1, (123) Gal α -1,3-Gal β -1,4-GlcNAc β -Sp2, (167) Gal α -1,3-Gal β -1,4-Fuc α -1,3-GlcNAc β -Sp1, (18) Gal α -1,4-GlcNAc-Sp2, (213) Gal α -1,6-Glc-Sp4 BT, (168) Gal α -1,3-Fuc α -1,2-Gal β -1,4-GlcNAc β -Sp2, (105) Gal α -1,3-Gal β -1,4-Glc β -Sp1, (183) Gal α -1,3-Gal β -1,4-Glc β -Sp1, (64) Gal α -1,3-Gal β -Sp2, (112) Gal α -1,3-GalNAc β -Sp2, (68) Gal α -1,3-GalNAc β -Sp2, (118) Gal α -1,3-GalNAc β -Sp2, (138) Gal α -1,3-GalNAc β -Sp2, (119) Gal α -1,3-GalNAc β -Sp2, (134) Gal α -1,2-Gal β -Sp2, (100) Gal α -1,2-Gal β -Sp2, (123) Gal α -1,3-Fuc α -1,2-Gal β -Sp2, (107) Gal α -1,3-Fuc α -1,2-Gal β -Sp2, (123) Gal α -1,3-Fuc α -1,2-Gal β -Sp2).

The latter system was then used for a competitive binding assay, where fluorescent α -galactoside **1** was competitively displaced from PIIA using methyl α -D-galactoside (**12**), and a set of available D-galactose derivatives (Fig. 4D and Table 2). Interest-

Note: Spacers vary on the glycan array.

Glycan sample (Chart ID)	Average RFU	Glycan sample (Chart ID)	Average RFU	Glycan sample (Chart ID)	Average RFU
 <p>α 4 β₁ Sp8 (123) α 3 β₁ Sp8 (112)</p>	<p>3370 ± 323</p> <p>3366 ± 925</p>	 <p>α 3 β₁ Sp8 (118)</p>	<p>180 ± 22</p>	 <p>α 2 β₁ Sp8 (100)</p>	<p>7 ± 2</p>
 <p>α 3 β 4 β 2 α 6 β 4 β 4 Sp24 (550)</p>	<p>4154 ± 619</p>	 <p>α 3 β 4 β 2 Sp0 (516)</p>	<p>182 ± 25</p>	 <p>α 3 β 4 β₁ Sp8 (115)</p>	<p>747 ± 233</p>
 <p>α 3 β 4 β 2 α 6 β 4 β 4 Sp24 (368)</p>	<p>1996 ± 185</p>	 <p>α 3 β 2 β 2 Sp0 (517)</p>	<p>84 ± 5</p>	 <p>α 3 β 4 β₁ Sp8 (105)</p>	<p>500 ± 75</p>

● Gal
▲ Fuc
● Man
■ GalNAc
■ GlcNAc

ingly, the obtained IC₅₀ for **12** was 0.52 mM, which is ~10-fold weaker than the determined affinity of the fluorescent analog **1**. Among the monosaccharides tested, free D-galactose (**9**), showed inhibition of PIIa with a reduced affinity (IC₅₀ = 1.57 mM) compared with glycoside **12**, probably due to the partial presence of the non-binding β-anomer. Methyl α-glycosides of D-glucose (**5**), L-fucose (**6**), D-mannose (**7**), or methyl β-D-arabinoside (**8**) did not show detectable binding to PIIa. Replacement of the 2-hydroxy group of galactose with a free amine in D-galactosamine (**10**) led to a 2-fold increase in the binding affinity (IC₅₀ = 0.86 mM). Acetamide substitution in the same position, *i.e.* N-acetylgalactosamine (**11**), resulted in a complete loss of binding. Next, we tested α-galactosides with different aglycons of varying size, *e.g.* methyl, allyl, 4-nitrophenyl, 4-methylumbelliferyl, and X-Gal (**12–14**, **16–18**). These modifications only showed a small effect on the binding affinity. O-Alkylation of ring hydroxyl groups is a requirement for ligand binding of some lectins like the tectonins (35, 36). For PIIa, O-methylation of the 3-hydroxyl group resulted in a complete loss of affinity (**14** → **15**). A similar loss of affinity was observed for O-methylation of the *P. aeruginosa* LecB or *B. cenocepacia* BC2L-A ligands fucose and mannose (21).

Photorhabdus lectin A — PIIA

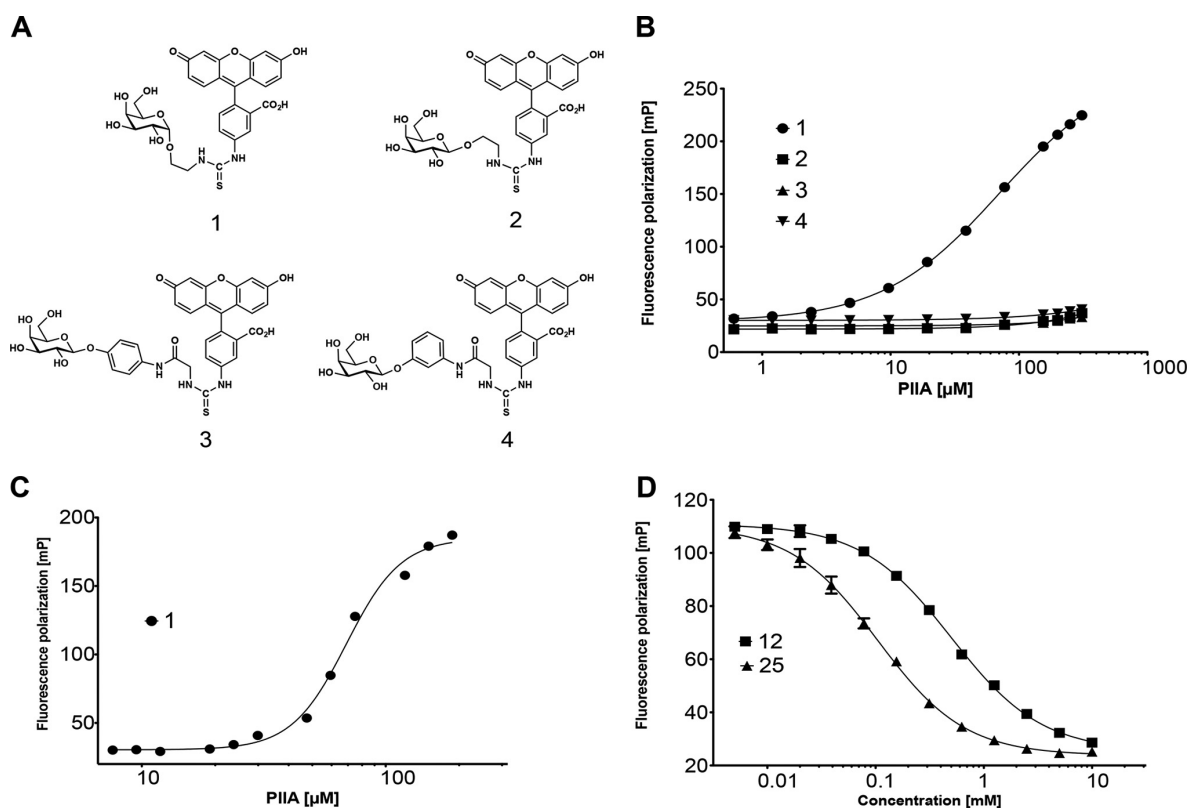


Figure 4. Establishing a carbohydrate-binding assay for PIIA in solution. A, structure of fluorescent ligands 1–4 based on D-galactose. B, titration of fluorescent ligands 1–4 with PIIA. C, dissociation constant for 1 was obtained from a four-parameter fitting procedure to the dose-dependent increase in fluorescence polarization (K_d , $62.7 \pm 3.8 \mu\text{M}$). D, competitive inhibition of the binding of 1 to PIIA with methyl α-D-galactoside (12, $\text{IC}_{50} = 0.52 \pm 0.07 \text{ mM}$) and raffinose (25, $\text{IC}_{50} = 0.11 \pm 0.01 \text{ mM}$). One representative titration experiment of triplicates on one plate is shown. Dissociation constant and standard deviations given were obtained from at least three independent replicates of triplicates on three plates each.

We also tested a set of oligosaccharides containing α-galactosyl residues for competitive binding to PIIA. Gal-α-1,3-Gal (20, $\text{IC}_{50} = 0.90 \text{ mM}$) and Gal-α-1,4-Gal (21, $\text{IC}_{50} = 1.08 \text{ mM}$) showed a 2-fold lower binding affinity to PIIA than melibiose (Gal-α-1,6-Glc, 22, $\text{IC}_{50} = 0.39 \text{ mM}$), whereas Gal-α-1,2-Gal (19) was only weakly active and resulted in ~50% inhibition at 10 mM. A comparable binding specificity for Gal-α-1,6-Glc has been reported for LecA from *P. aeruginosa* (37). The plant trisaccharide raffinose (25) contains a terminal melibiose motif and showed the highest binding to PIIA among all tested compounds with an IC_{50} of 0.11 mM. This ubiquitous plant galactoside has also shown an inhibitory effect on *P. aeruginosa* biofilms and inhibits LecA in a similar affinity range ($K_d = 32 \mu\text{M}$) (37, 38). The tetrasaccharide stachyose (26) is another plant derivative of raffinose with an additional 1,6-linked α-galactoside moiety. For PIIA an IC_{50} of 0.34 mM was observed, indicating that longer oligosaccharides do not improve the binding affinity to PIIA, which is different for LecA. Bivalent oligosaccharides containing the α-Gal antigen Gal-α-1,3-Gal-β-1,4-GlcNAc were identified as the apparent best ligands of the glycan array (Fig. 3A). The corresponding monovalent trisaccharide 27 was tested in our competitive binding assay and showed only ~70% inhibition of PIIA at 10 mM. This weak binding is in good agreement with the glycan array data where the

monovalent α-Gal epitope had reduced binding to PIIA compared with its bivalent structure (see Table 1).

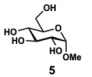
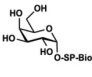
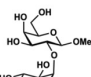
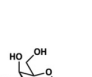
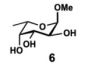
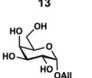
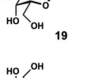
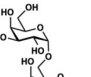
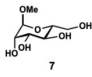
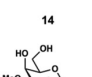
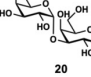
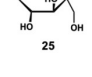
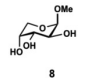
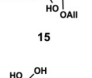
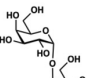
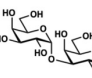
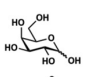
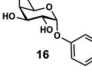
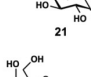
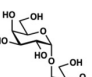
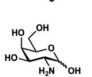
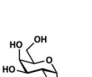
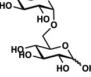
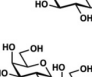
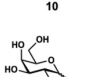
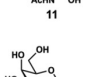
Because Gal-α-1,3-GalNAc and Gal-α-1,4-GlcNAc were identified as the monovalent ligands with the highest apparent affinity on the glycan array, we tested the corresponding biotinylated disaccharides 23 and 24, respectively. Both soluble glycans differ only in spacer identity and for 23 also in the anomeric configuration from those glycans used for the production of the glycan array. Surprisingly, they were as active as the comparably biotinylated α-galactosyl monosaccharide 13, displaying IC_{50} values from 0.59 to 0.66 mM.

The human blood group antigen P₁ (28) (39) was also moderately recognized by PIIA on the glycan array (ligand 121, supplemental Table S1) and in the competitive binding assay soluble monovalent 28 showed a moderate binding affinity ($\text{IC}_{50} = 1.80 \text{ mM}$) to this lectin. Because PIIA was shown to bind to α-Gal residues but not to GalNAc residues (see above) and it recognized the blood group B-terminating ligand 368 on the glycan array (Fig. 3A), we also tested soluble blood group B antigens 29 and 30. These oligosaccharides were inhibitors of PIIA with moderate potency (IC_{50} of 1.18 and 1.35 mM, respectively). This specificity of PIIA is in contrast to LecA, which binds to B and A antigens (27). Thus, PIIA could be used as a new reagent for rapid identification of blood group B sero-

Photorhabdus lectin A — PIIA

Table 2
Evaluation of natural and synthetic inhibitors of PIIA using the competitive binding assay

Averages and standard deviations were obtained from three independent experiments. n.i.: no inhibition observed up to 10 mM. SP: spacer $-(CH_2)_3NH-CO(CH_2)_5NH-$.

Compound	IC ₅₀ [mM]	Compound	IC ₅₀ [mM]	Compound	IC ₅₀ [mM]	Compound	IC ₅₀ [mM]
	n.i.		0.59 ± 0.05		47.8 ± 0.8% inhibition @ 10 mM		0.11 ± 0.01
	n.i.		0.93 ± 0.129		0.90 ± 0.05		0.34 ± 0.05
	n.i.		n.i.		1.08 ± 0.004		68.5 ± 0.04% inhibition @ 10 mM
	n.i.		1.32 ± 0.262		0.39 ± 0.02		1.80 ± 0.06
	1.57 ± 0.08		1.15 ± 0.434		0.65 ± 0.004		1.18 ± 0.05
	0.86 ± 0.22		0.47 ± 0.138		0.66 ± 0.02		1.35 ± 0.26
	n.i.						
	0.52 ± 0.07						

types such as the currently used GS-IB4 isolectin from *Griffonia simplicifolia* (40).

PIIA, a lectin with a unique tetrameric structure

Apo-PIIA crystallizes in space group $P3_121$ and crystals diffracted to 1.7 Å. Data collection and refinement statistics for all presented PIIA structures can be found in Table 3. The core of PIIA consists of two four-stranded anti-parallel β -sheets (Fig. 5). We did not observe the canonical Ca^{2+} ion found in other C-type lectins at the sugar-binding site, which may be a result of the crystallization buffer that contained a high concentration of citrate known to chelate calcium ions.

The asymmetric unit contained two PIIA dimers, which form tetramers with symmetry mates in accordance with DLS data. The C-terminal five-residue extension (Fig. 1) of the four protomers are engaged in well-defined interactions leading to a 90° twist in the tetramer (Fig. 6A). Of the tail residues (YSPLK), Tyr-118 packs hydrophobically against Pro-120, and Ser-119 forms two hydrogen bonds with the tetramer partner (Ser-119 side-chain hydroxyl with side-chain amino group of Lys-82, Ser-119 carbonyl with the main chain of Thr-83). Residue Leu-121 is inserted into a tailored hydrophobic pocket of the tetramer partner, which is composed of residues Leu-22, Ile-28, Ala-60, Ile-68, Phe-73, Ile-75, Val-79, Val-84, and Leu-90 (Fig. 6B). When we compared the structure of PIIA with the struc-

ture of the well-studied protein LecA, we found the structures to be very similar ($C\alpha$ r.m.s.d. of 0.67 over 78 atoms, [supplemental Fig. S11](#)). The main differences are found in the region between $\beta 3$ and $\beta 7$ (Fig. 5C), which has a profound impact on carbohydrate binding (see below).

The sequence alignment of PIIA with LecA from *P. aeruginosa* and the LecA homologs from *Photorhabdus* and *Xenorhabdus* species showed that PIIA and LecA homologs from the latter two species possess an extension at their C termini. This extension led to the surprising result that the dimerization of dimers is twisted by 90° in PIIA. In contrast, LecA does not possess the five C-terminal residues. As a result, the LecA tetramer is planar and formed by the tail-to-tail arrangement of two dimers (Fig. 6, C and D). We have no indication as to the biological significance of this arrangement, but we believe that the interactions between the tails of the tetramer partners will lead to a significant stabilization of the tetrameric assembly.

Structural basis of α -galactoside specificity of PIIA

To understand the α -galactoside specificity of PIIA, we determined the crystal structures of several PIIA-carbohydrate complexes in the presence of 3 mM calcium chloride in the crystallization buffer (Fig. 7): PIIA in complex with the monosaccharide methyl α -D-galactoside (12), the trisaccharide raffinose (25), and an α -D-galactoside linked to fluorescein (1).

Photorhabdus lectin A — PIIA

Table 3

Data collection and refinement statistics

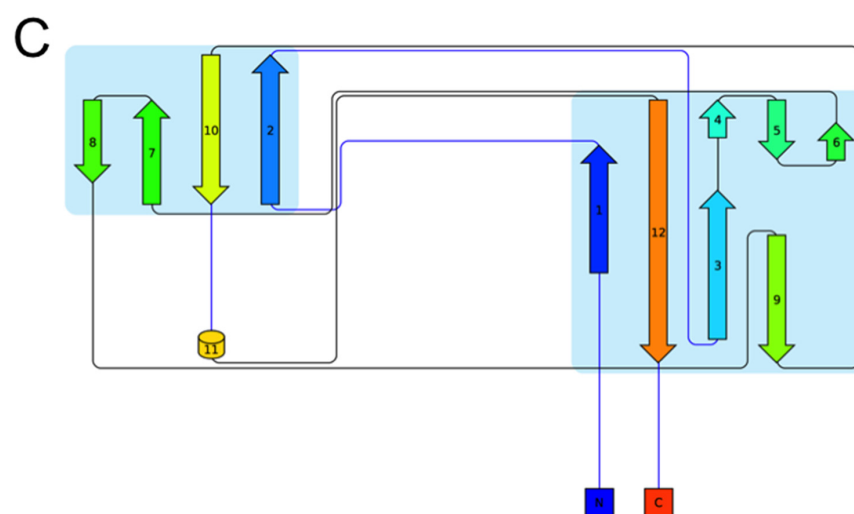
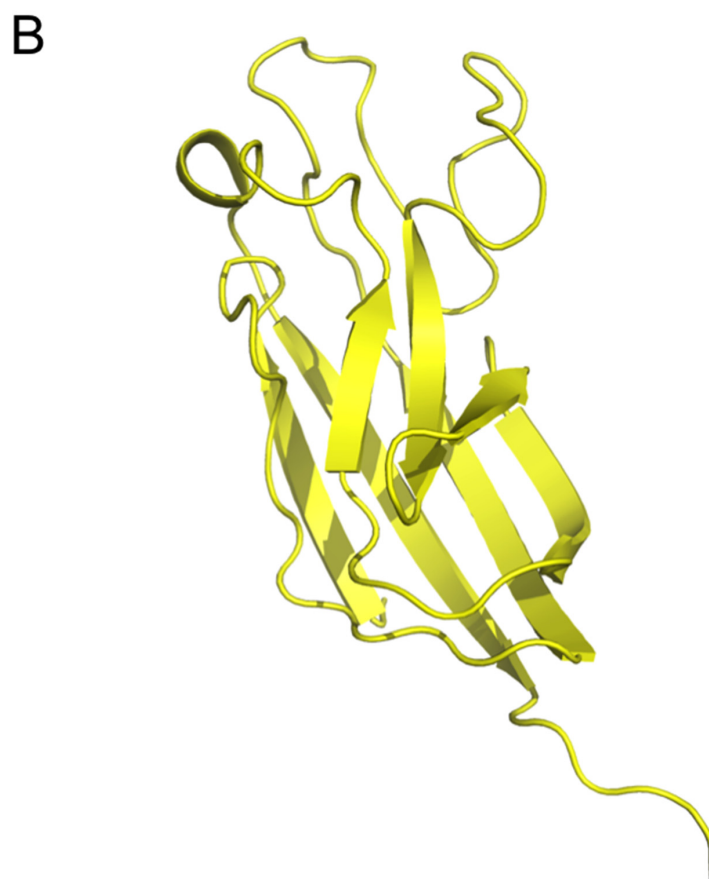
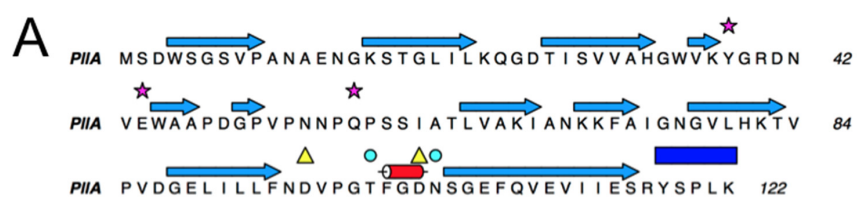
Statistics for the highest-resolution shell are shown in parentheses. r.m.s. is root mean square.

	PIIA, apo, PDB 5OFZ	PIIA, Me- α -Gal (12), PDB 5ODU	PIIA, raffinose (25), PDB 5OFX	PIIA, fluorescent ligand 1, PDB 5OFI
Resolution range	46.05–1.75 (1.81–1.75)	47.2–1.56 (1.62–1.56)	44.09–1.75 (1.81–1.75)	43.76–2.0 (2.07–2.0)
Space group	P 32 2 1	P 1 21 1	P 1	P 21 21 21
Unit cell	92.1 92.1 164.2 90 90 120	62.9 103.3 76.1 90 93.0 90	59.0 63.0 75.9 101.1 112.8 94.4	48.6 134.3 153.0 90 90 90
Total reflections	725,065 (34,414)	597,157 (60,933)	539,432 (54,563)	126,530 (12,830)
Unique reflections	81,583 (7832)	133,175 (13,311)	89,118 (9042)	65,944 (6644)
Multiplicity	8.9 (4.4)	4.5 (4.6)	6.1 (6.0)	1.9 (1.9)
Completeness (%)	99.59 (96.57)	96.18 (95.63)	90.73 (92.05)	95.91 (97.62)
Mean $I/\sigma(I)$	26.62 (3.32)	11.19 (1.22)	9.08 (2.02)	8.23 (2.54)
Wilson B -factor	23.67	14.93	13.78	23.65
R -merge	0.04649 (0.3966)	0.09883 (1.261)	0.1569 (0.7841)	0.05735 (0.2516)
R -meas	0.04921 (0.451)	0.1121 (1.427)	0.1719 (0.8578)	0.08111 (0.3558)
R -pim	0.01592 (0.2106)	0.05232 (0.6619)	0.06949 (0.345)	0.05735 (0.2516)
$CC1/2$	0.999 (0.886)	0.998 (0.358)	0.994 (0.78)	0.996 (0.907)
CC^*	1 (0.969)	1 (0.726)	0.999 (0.936)	0.999 (0.975)
Reflections used in refinement	81,572 (7830)	132,517 (13,152)	89,095 (9038)	65,903 (6639)
Reflections used for R -free	4183 (452)	6491 (608)	4458 (428)	3335 (326)
R -work	0.2006 (0.2858)	0.2050 (0.3530)	0.1849 (0.2669)	0.1864 (0.2446)
R -free	0.2202 (0.3105)	0.2334 (0.3668)	0.2133 (0.2986)	0.2216 (0.3016)
CC (work)	0.943 (0.876)	0.960 (0.626)	0.954 (0.867)	0.957 (0.905)
CC (free)	0.937 (0.823)	0.958 (0.620)	0.940 (0.834)	0.939 (0.820)
No. of non-hydrogen atoms	4138	8639	8749	8306
Macromolecules	3608	7264	7264	7264
Ligands		112	246	180
Solvent	530	1263	1239	862
Protein residues	480	968	968	968
r.m.s. (bonds)	0.009	0.003	0.004	0.004
r.m.s. (angles)	1.00	0.58	0.69	0.61
Ramachandran favored (%)	97.46	98.00	97.69	97.37
Ramachandran allowed (%)	2.54	2.00	2.31	2.63
Ramachandran outliers (%)	0.00	0.00	0.00	0
Rotamer outliers (%)	0.26	0.76	0.51	0.25
Clashscore	3.35	3.92	2.18	1.85
Average B -factor	30.15	22.83	19.00	29.55
Macromolecules	28.81	20.95	17.24	28.84
Ligands		27.65	21.05	29.75
Solvent	39.27	33.22	28.88	35.49
No. of TLS groups	28	50	76	46

Complex crystals of PIIA with **12** were obtained by co-crystallization. The resulting crystals belonged to space group $P2_1$ and were diffracted to 1.56 Å. The overall structure of PIIA does not change upon complex formation ($C\alpha$ r.m.s.d. of 0.12 Å), and we observed unambiguous electron density for Ca^{2+} and the ligand in each of the eight protomers in the asymmetric unit. The canonical Ca^{2+} ion at the sugar-binding site is coordinated by the side chains of Asp-96, Thr-100, Asp-103, and Asn-104 as well as the main-chain carbonyl oxygen atoms of Tyr-38 and Thr-100. The ligand is not involved in crystal contacts and oriented in the same way in each protomer. It sits in a shallow binding pocket and is engaged in a total of 10 hydrogen bonds (protein and the Ca^{2+} ion): the anomeric oxygen (O1) and galactoside C2 hydroxyl with the side chain of Glu-44; sugar C3 hydroxyl with the Ca^{2+} ion, the side chain of Asp-103, and the main chain of Tyr-38; sugar C4 hydroxyl with the Ca^{2+} ion, the side chain of Asp-96, and the main chain of Tyr-38; sugar ring O5 with the side chain of Gln-57; and sugar C6 hydroxyl with the side chain of Gln-57. From this complex structure, it is clear that PIIA is only able to bind to α -galactosides; the side chains of the two amino acids Val-43 and Asn-55 that are absent in LecA form a barrier and any β -linkage would result in a clash with the PIIA surface (Fig. 8). The structure also allowed us to rationalize why D-galactosamine (**10**) is a better binder than D-galactose (**9**), and why N-acetylgalactosamine (**11**) shows no detectable binding. By swapping the C2 hydroxyl group for an amino

group, the sugar can now engage in an additional hydrogen bond with the side chain of Asp-103 (see supplemental Fig. S8). Acetylation of the amino group leads to a clash with the protein and thus abolishes binding.

Complex crystals of PIIA with raffinose were also obtained by co-crystallization. The resulting crystals belonged to space group $P1$ and diffracted to 1.75 Å. As expected, the overall structure of PIIA does not change upon complex formation ($C\alpha$ r.m.s.d. of 0.12 Å). There are eight protomers in the asymmetric unit, and we observed unambiguous electron density for raffinose in all of them. Although some of the raffinose molecules are involved in crystal contacts, the orientation and shape of the trisaccharide is virtually identical in each protomer. The orientation of the galactose moiety does not differ between the monosaccharide and raffinose structures, and the same hydrogen bonds are formed. The α -1,6-linkage leads glucose away from the PIIA surface, but the C4 hydroxyl forms one hydrogen bond with the side chain of Gln-57. Interestingly, the final fructose moiety is pointing back toward the PIIA surface, giving the raffinose an overall horseshoe shape. The fructose C3 and C4 hydroxyls are engaged in a hydrogen bond with the side chain of Glu-44. Glu-44 is also involved in hydrogen bond formation with the galactose C2 hydroxyl, thus linking the two ends of the raffinose horseshoe resulting in an additional intraligand hydrogen bond between fructose C6 hydroxyl with galactose C2 hydroxyl.

Photorhabdus lectin A — PIIA

Photorhabdus lectin A — PIIA

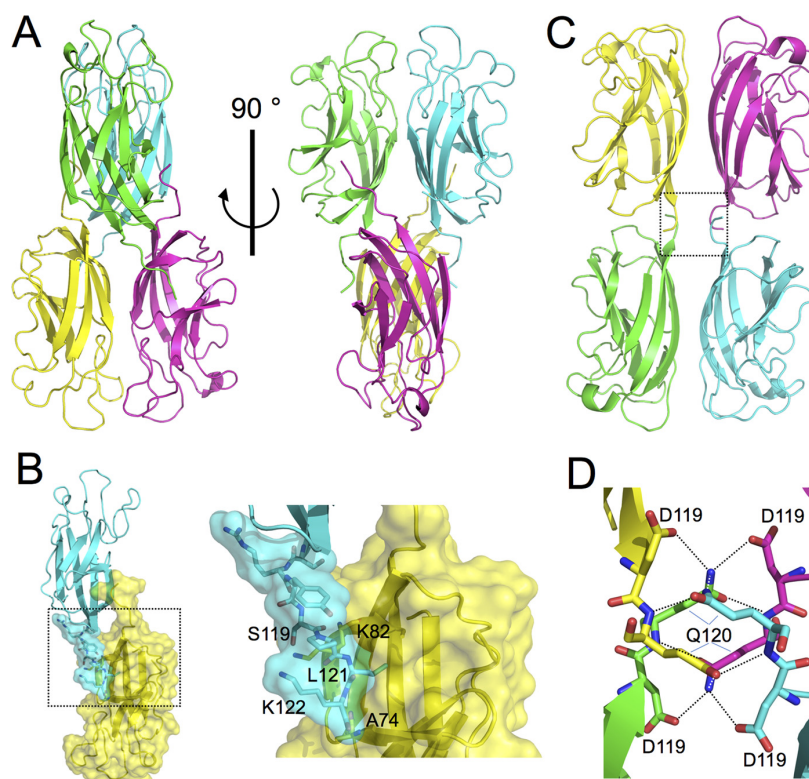


Figure 6. Overall structure of PIIA and comparison to LecA. *A*, schematic representation of the PIIA tetramer. Two parallel dimers (yellow/magenta and green/cyan) form tail-to-tail dimers with a 90° twist. *B*, detailed view of the PIIA tail-to-tail interface. We observe two hydrogen bonds between the side chains of tail Ser-119 (cyan) and Lys-82 (yellow) and the C terminus of the tail and the backbone nitrogen of Ala-74 (yellow). In addition, tail residue Leu-121 is inserted into a hydrophobic pocket of its binding partner. *C*, LecA tetramer is planar, formed by tail-to-tail dimerization of two parallel dimers (yellow/magenta and green/cyan). *D*, much shorter tail of LecA provides several stabilizing hydrogen bonds (dashed lines), but the interactions are not sufficient to cause a twist of the two dimers relative to each other.

Because we used fluorescent probe **1** in our competitive binding assays, we wanted to understand how the probe binds to PIIA. Complex crystals of PIIA with **1** were also obtained by co-crystallization. The resulting crystals belonged to space group $P2_12_12_1$ and diffracted to 2.0 Å. The overall structure of the eight protomers in the asymmetric unit did not differ significantly from the apo structure ($C\alpha$ r.m.s.d. of 0.15 Å), and we observed unambiguous density for **1** in four of the protomers (Fig. 7, *E* and *F*, and supplemental Fig. S10). The interactions of the galactose include all of those observed in the other two structures. Through fortuitous crystal packing, we were able to obtain good electron density for the fluorophore and were able to fit it. The ordered nature of the fluorophore is the result of π -stacking between the tricyclic ring systems of two molecules of **1** bound to symmetry mates.

The strict specificity toward α -galactosides is unique for PIIA when compared with LecA. From the crystal structure of PIIA with **12**, it becomes clear that β -galactosides cannot be recognized without a steric clash with the protein surface of PIIA (Fig. 8*A*). In contrast, LecA opens a shallow cleft close to its anomeric center that allows the accommodation of

large β -linked aglycons, such as in 4-nitrophenyl β -D-galactoside. From a superposition of the binding site amino acid residues of PIIA with LecA, it can be deduced that the additional amino acids Val-43 and Asn-55 present in PIIA are responsible for preventing PIIA from binding β -galactosides (Fig. 8*B*).

Application of PIIA for the detection of the α -Gal epitope

PIIA showed the highest apparent binding on the glycan array to a biantennary *N*-glycan structure carrying the α -Gal epitope on its antenna. This antigen (Gal- α -1,3-Gal- β -1,4-GlcNAc) is a ubiquitous epitope in non-primate mammals and new world monkeys. This carbohydrate structure is the major factor of hyperacute rejection of xenotransplanted organs in humans (29, 41, 42). In pigs, genetic engineering resulted in animals lacking the corresponding galactosyltransferase thus reducing the risk of severe immune responses (31, 43, 44). By using modern techniques such as CRISPR/Cas to engineer animals or animal tissue lacking the α -Gal epitope, quality controls for the complete suppression of the biosynthetic machineries are of crucial importance. Currently, the isolectin GS-IB4

Figure 5. *A*, sequence of PIIA. Secondary structure elements are shown above the sequence (blue arrows, β -strands; red barrel, α -helix). Residues responsible for sugar binding are highlighted with magenta stars, Ca^{2+} -binding residues with cyan circles, and amino acids coordinating both as yellow triangles. Tail residues unique to PIIA and its close homologs are highlighted with a blue box. *B*, schematic representation of a PIIA apo monomer. *C*, fold diagram for the structure shown in *B*.

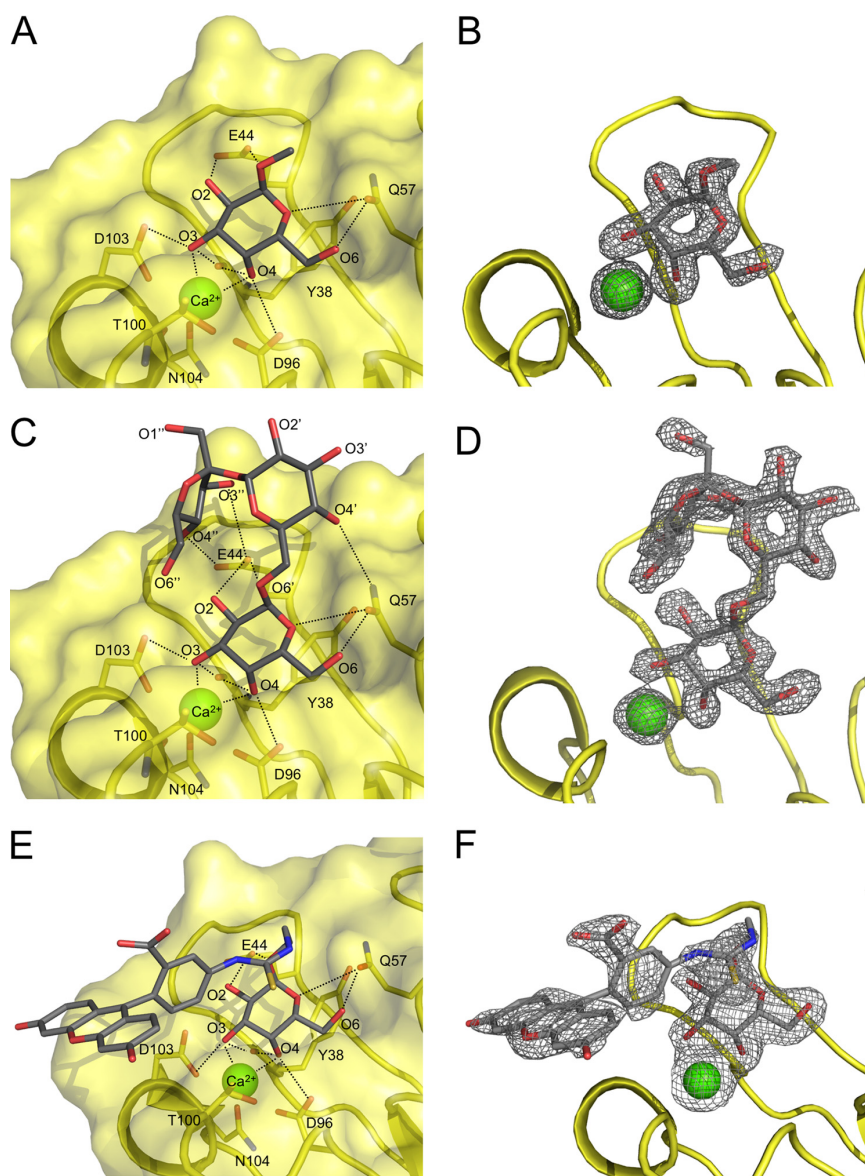
Photorhabdus lectin A — PIIA

Figure 7. PIIA-carbohydrate complex structures. A and B, PIIA bound to methyl α -D-galactoside (**12**). This interaction is stabilized through 10 hydrogen bonds (dashed lines). Eight of them are between the ligand and the protein, and two are provided by the Ca^{2+} ion. C and D, PIIA bound to raffinose (**25**). In addition to the hydrogen bonds observed in A, the glucose moiety forms a hydrogen bond with the side chain of Gln-57, whereas terminal fructofuranoside forms two hydrogen bonds with the side chain of Glu-44, which results in the ligand adopting a horseshoe shape. E and F, PIIA bound to fluorescent tracer **1**. No interactions with the protein are observed beyond the carbohydrate moiety. The fluorescein can only be observed as the result of fortuitous crystal contacts in half of the monomers in the asymmetric unit. PIIA is shown as a yellow schematic/surface representation, ligand as gray sticks, oxygen atoms in red, nitrogen atoms in blue, sulfur atoms in yellow, and Ca^{2+} ions as green spheres. Difference electron density ($F_o - F_c$) contoured to 3σ with phases calculated from a model that was refined in the absence of metal ions is shown as gray isomesh (B, D, and F).

purified from the plant *G. simplicifolia* is used as a tool to identify a wide range of α -galactoside epitopes, among which is the α -Gal epitope (45). Because of the high selectivity of PIIA, this bacterial lectin could be an alternative to the currently used GS-IB4.

The crystal structure of GS-IB4 in complex with the terminal disaccharide Gal- α -1,3-Gal (**20**) as a methyl glycoside shows extensive interactions between the terminal galactose residue and the protein but no contacts with the reducing-end galac-

tose moiety (46). To compare the recognition features of both proteins to this epitope, we have docked the methyl glycoside of **20** into the carbohydrate-binding site of PIIA (supplemental Fig. S9). In this computed structure, the terminal saccharide moiety forms extensive contacts with the lectin receptor. In contrast to GS-IB4, the reducing-end galactose established two more hydrogen bonds with Glu-44 and Asn-55 of PIIA, which may serve as an explanation for the high specificity of PIIA for the Gal- α -1,3-Gal epitope.

Photorhabdus lectin A — PIIA

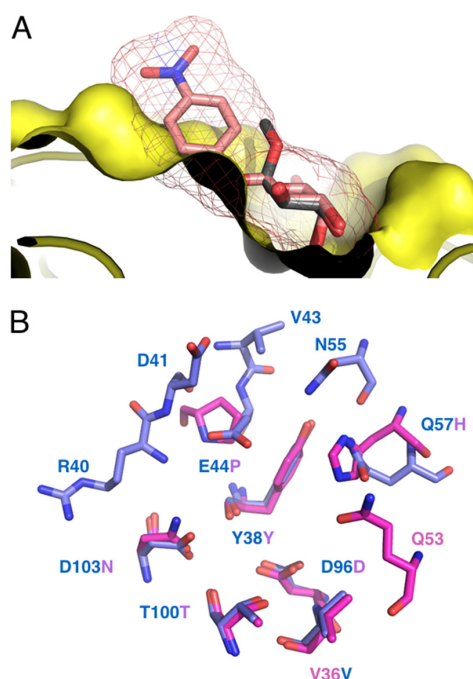


Figure 8. Rationalizing PIIA α -galactoside specificity. *A*, representation of the PIIA (yellow)-binding pocket with methyl α -D-galactoside (**12**, gray sticks). 4-Nitrophenyl β -D-galactoside (salmon sticks and isomesh, taken from PDB 3ZYF) was superposed onto α -D-galactoside. Because of the restricted ligand-binding site of PIIA only α -substituted ligands, leading away from the surface, can be accommodated, whereas β -substituted ligands clash. *B*, superposition of the binding site amino acid residues of PIIA (blue) with LecA (magenta), oxygen atoms, red; nitrogen atoms, blue. Residue numbers correspond to PIIA.

We thus tested the suitability of PIIA to detect the α -Gal epitope in wild-type primary pig kidney cells and cells derived from the corresponding α -1,3-galactosyltransferase knock-out (GTKO) animals (Fig. 9). Both PIIA and the current standard lectin GS-IB4 visualized the α -Gal antigen in wild-type porcine cells similarly. Because the α -Gal antigen is also present on glycolipids in red blood cells (41), we performed hemagglutination experiments with red blood cells (RBC) from wild-type and GTKO pigs. PIIA agglutinated wild-type porcine red blood cells but was unable to agglutinate RBCs from the GTKO pig (Fig. 10, *A* and *B*). In addition, we could further show that this agglutination was galactose-dependent and could be inhibited by the presence of raffinose (Fig. 10C).

Conclusion

The opportunistic pathogen *P. aeruginosa* utilizes the two soluble lectins LecA and LecB for infection of the host and biofilm formation. Although numerous LecB-like proteins have been characterized, LecA orthologs are scarce. Here, we show that various orthologs of LecA are present in the insect pathogenic bacteria from the *Photorhabdus* and *Xenorhabdus* species as well as in the human gut bacterium and pathogen *Enterobacter* spp. A high degree of similarity was observed among those orthologs with LecA having a sequence insert and lacking an otherwise conserved C-terminal tail.

The gene *plu2096* from the entomopathogenic bacterium *P. luminescens* was cloned and recombinantly produced in high

production yields. It encodes the galactose-binding lectin PIIA with 37% identity to LecA. The carbohydrate-binding specificity of PIIA was assessed on a glycan array containing over 600 different carbohydrate epitopes. Interestingly, PIIA showed very strict specificity toward α -galactosides with high apparent binding to the α -Gal epitope as well as to Gal- α -1,4-GlcNAc and Gal- α -1,3-GalNAc.

To date, the biological role of the Gal- α -1,4-GlcNAc epitope remains unclear, and natural sources have not been identified despite the fact that anti-Gal- α -1,4-GlcNAc antibodies are present in human serum (47). In contrast, Gal- α -1,3-GalNAc epitopes are present in nematodes and have, for example, been described in glycolipids from the worms *Ascaris suum* and *Caenorhabditis elegans* (48). Furthermore, Gal- α -1,3-GalNAc is a ubiquitous epitope present on glycoproteins of the nematode *Hemonchus contortus*, and vaccination of lambs with glycoproteins of the sheep parasite *H. contortus* specifically elicited anti-Gal- α -1,3-GalNAc IgG antibodies (49). In addition, α -linked galactosyl residues have been identified in *C. elegans* N-glycans attached to mannose residues (50, 51) or attached to core fucose residues (52). Importantly, the nematodes *C. elegans* and *H. contortus* are both phylogenetically closely related to *Heterorhabditis*, whereas *A. suum* is more distantly related (53). It is thus reasonable to speculate that the Gal- α -1,3-GalNAc epitope recognized by the bacterial lectin PIIA is also present in the nematode *Heterorhabditis* and plays a role in bacterial attachment or symbiosis of *Photorhabdus* species with their native nematode hosts. Moreover, this epitope has been described as one terminal constituent of glycosphingolipids of the insect *Calliphora vicina* pupae (54) and members of the order of diptera, *i.e.* flies, are generally susceptible to infection with *Heterorhabditis* and *P. luminescens*. Therefore, it is possible that Gal- α -1,3-GalNAc is one natural ligand bound by PIIA both in the nematode symbiont and in infected insects.

Based on the carbohydrate specificity of PIIA as determined by the glycan array, PIIA was tested in a porcine cell culture staining experiment for the detection of the α -Gal epitope, the prime reason for hyperacute organ rejection in xenobiotic transplants. PIIA proved to be a suitable detection tool and specifically detected the α -Gal epitope in porcine tissue and on red blood cells. This fact qualifies recombinantly produced PIIA for the efficacy assessment of methods to genetically manipulate cells, such as CRISPR/Cas, for the production of alternative animal cells, tissue, or organisms lacking the α -Gal epitope as donors for xenotransplantation.

We are currently analyzing the biological role of PIIA in *P. luminescens* for its life cycle in nematodes and insects. Furthermore, it will be of interest to analyze the role of PIIA orthologs in the human pathogens *P. asymbiotica* and the *Enterobacter* spp., a group of bacteria that are part of the normal human gut flora with pathogenic potential.

Materials and methods

Chemicals

Methyl α -L-fucoside (**6**), methyl α -D-mannoside (**7**), and D-galactose (**9**) were purchased from Dextra Laboratories (Reading, UK); D-galactosamine (**10**), methyl α -D-galactoside

Phororhabdus lectin A — PIIA

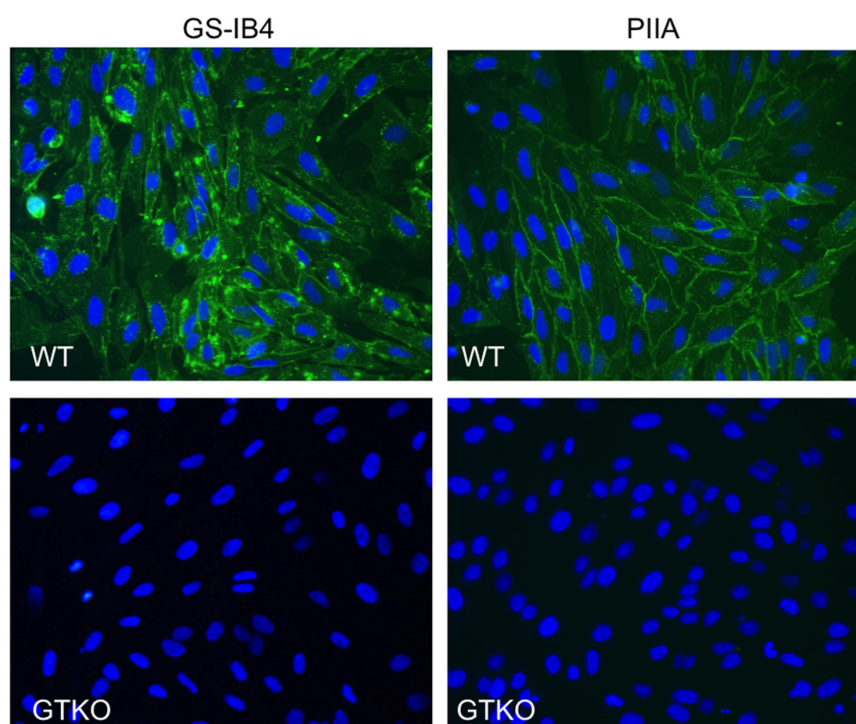


Figure 9. Staining of primary porcine kidney cells from wild-type pigs (WT) and *GGTA1* KO (GTKO) animals unable to produce the α -Gal antigen. Fluorescein-tagged PIIA or GS-IB4 were used as probes and detected the α -Gal antigen in WT cells. Lectin concentration: PIIA, 50 μ g/ml; GS-IB4, 500 μ g/ml, 400 \times magnification.

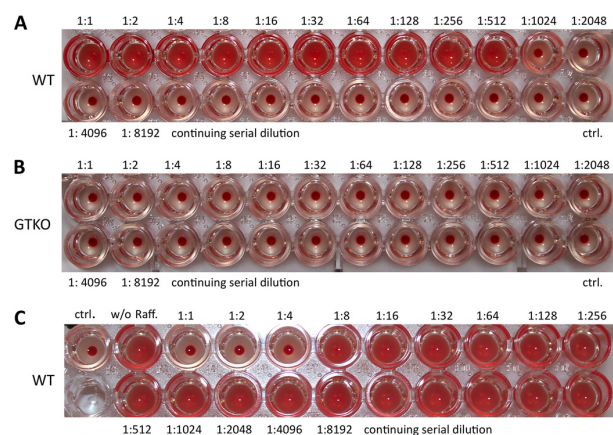


Figure 10. Hemagglutination of porcine red blood cells by PIIA. A, wild-type pig RBCs. B, GTKO pig RBCs. C, inhibition of PIIA-mediated agglutination of wild-type pig RBCs with raffinose.

(12), *p*-nitrophenyl α -D-galactoside (16), 4-methylumbelliferyl α -D-galactoside (17), 5-bromo-4-chloro-3-indolyl α -D-galactoside (18), isopropyl β -D-1-thiogalactoside (IPTG) were from Carbosynth Ltd. (UK); methyl β -D-arabinoside (8) was from Tokyo Chemical Industry (Japan); methyl α -D-glucoside (5), *N*-acetyl-D-galactosamine (11), and stachyose (26) were from Sigma (Germany); melibiose (22) was from MP Biomedicals Llc. (France); raffinose (25) was from Th. Geyer Laboratories (Germany); Gal- α -1,3-Gal (20), Gal- α -1,4-Gal (21), Xeno antigen (27), P1 antigen (28), and blood group B antigens (29, 30)

were from Elicityl OligoTech (France); Gal- α -SP-biotin (13), Gal- α -1,3-GalNAc- α -SP-biotin (23), and Gal- α -1,4-GlcNAc- β -SP-biotin (24) were from Lectinity (Russia); and Gal- α -1,2-Gal- β -1-OMe (19) was from Carbohydrate Synthesis (Oxford, UK). Fluorescent ligands 1–4 were synthesized as described (27).

Allyl α -D-galactopyranoside (14) was synthesized from galactose in a Fischer-type glycosylation with allyl alcohol in presence of Amberlite IR120/H⁺ (supplemental Scheme 1). The title compound was obtained by recrystallization. ¹H NMR (400 MHz, MeOH-*d*₄) δ 5.98 (dddd, *J* = 17.2, 10.4, 6.1, 5.2 Hz, 1H, CH₂CHCH₂O-), 5.33 (dq, *J* = 17.2, 1.7 Hz, 1H, CH₂CHCH₂O-), 5.17 (dq, *J* = 10.4, 1.4 Hz, 1H, CH₂CHCH₂O-), 4.87 (d, *J* = 3.0 Hz, 1H, H1), 4.23 (ddt, *J* = 13.0, 5.3, 1.5 Hz, 1H, CH₂CHCH₂O-), 4.04 (ddt, *J* = 13.0, 6.1, 1.4 Hz, 1H, CH₂CHCH₂O-), 3.93–3.89 (m, 1H, H4), 3.85–3.78 (m, 1H, H5), 3.78–3.76 (m, 2H, H2, H3), 3.73–3.69 (m, 2H, H6). ¹³C NMR (101 MHz, MeOH-*d*₄) δ 135.65 (CH₂CHCH₂O-), 117.48 (CH₂CHCH₂O-), 99.46 (C1), 72.37 (C5), 71.51 (C2/3), 71.16 (C4), 70.21 (C2/3), 69.39 (CH₂CHCH₂O-), 62.78 (C6). Transcripts of NMR spectra are shown in supplemental Figs. 4 and 5).

For allyl 3-*O*-methyl- α -D-galactopyranoside (15), a microwave vial was filled with allyl galactoside 14 (57 mg, 0.26 mmol) and dibutyltin oxide (71 mg, 0.29 mmol), and the reagents were dried *in vacuo*. Dry PhMe/MeCN (5:1, 660 μ l) was added, and the suspension in the sealed tube was exposed to microwave irradiation for 20 min at 150 $^{\circ}$ C. The clear solution was allowed to cool to 50 $^{\circ}$ C, and to the resulting suspension was added MeI (405 μ l, 6.5 mmol) dropwise. The reaction was stirred for 48 h at

Photorhabdus lectin A — PIIA

50 °C, after removal of the volatiles *in vacuo* and purification of the crude product by MPLC, the title compound was obtained as a pure product (40 mg, 65%). ¹H NMR (400 MHz, MeOH-*d*₄) δ 6.08–5.89 (m, 1H, CH₂CHCH₂O-), 5.34 (dd, *J* = 17.2, 1.8 Hz, 1H, CH₂CHCH₂O-), 5.17 (dd, *J* = 10.4, 1.6 Hz, 1H, CH₂CHCH₂O-), 4.85 (d, *J* = 4.0 Hz, 1H, H1), 4.23 (ddt, *J* = 13.0, 5.3, 1.6 Hz, 1H, 1H, CH₂CHCH₂O-), 4.13 (dd, *J* = 3.3, 1.2 Hz, 1H, H4), 4.04 (ddt, *J* = 13.0, 6.1, 1.4 Hz, 1H, CH₂CHCH₂O-), 3.85 (dd, *J* = 10.1, 3.9 Hz, 1H, H2), 3.82–3.77 (m, 1H, H5), 3.76–3.63 (m, 2H, H6), 3.46 (s, 3H, CH₃), 3.42 (dd, *J* = 10.1, 3.2 Hz, 1H, H3). ¹³C NMR (101 MHz, MeOH-*d*₄) δ 135.65 (CH₂CHCH₂O-), 117.50 (CH₂CHCH₂O-), 99.37 (C1), 81.15 (C3), 72.35 (C5), 69.38 (CH₂CHCH₂O-), 69.22 (C2), 66.91 (C4), 62.74 (C6), 57.24 (CH₃). Transcripts of NMR spectra are shown in supplemental Figs. 6 and 7).

Bioinformatics

A BLAST search (blastp) was done using the amino acid sequences of LecA from *P. aeruginosa* as query (accession number Q05097). The search was carried out choosing non-redundant protein sequence database with exclusion of *P. aeruginosa* (taxid: 287). The best 100 matches were chosen for an alignment using the COBALT tool (55). The aligned sequences were clustered using the SECATOR algorithm (56), which relies on BIONJ (57) to build the phylogenetic tree. The best LecA-like sequences (with lowest E-value) from each *Xenorhabdus* and *Photorhabdus* species were aligned with LecA using COBALT, and the conserved sequence was colored using Color Align Conservation (58). The amino acid sequence of hypothetical LecA homologs (with lowest E-value in *Xenorhabdus* and *Photorhabdus* species) were WP_011146351.1 (*P. luminescens*), WP_046975865.1 (*P. temperata*), WP_065824676.1 (*P. asymbiotica*), WP_054480913.1 (*P. heterorhabditis*), WP_038256436.1 (*Xenorhabdus bovienii*), WP_013184196.1 (*Xenorhabdus nematophila*), WP_047963870.1 (*Xenorhabdus khoisanensis*), WP_074019816.1 (*Xenorhabdus thuongxuanensis*), WP_038237499.1 (*Xenorhabdus szentirmaii*), and GenBankTM number SFO04414.1 (*Xenorhabdus japonica*), and SFJ01328.1 (*Xenorhabdus mauleonii*).

Cloning, expression, and purification of recombinant PIIA

Genomic DNA was isolated from *P. luminescens* subsp. *laumondii* TTO1 using GenElute Bacterial Genomic DNA Kit (Sigma). The *plu2096* gene sequence was amplified by PCR with Phusion polymerase (New England Biolabs, UK) and primers introducing NdeI (5'-GGAATTCCATATGTCT-GATTGGTCAGGAAG-3') and BamHI (5'-CGGGATCCT-TATTTTAAAGGGGAGTATCGAG-3') restriction sites. After digestion of the expression vector pET22b(+) (Novagen, Germany) and the PCR product with NdeI and BamHI (New England Biolabs, UK), ligation of the insert was performed with T4 DNA ligase (New England Biolabs, UK) resulting in plasmid pET22b-*plIA*. The sequence was confirmed by sequencing (GATC Biotech, Germany) with primers T7 promotor (5'-TAATACGACTCACTATAGG-3') and T7 terminator (5'-GCTAGTTATTGCTCAGCGG-3').

For expression, pET22b-*plIA* was transformed into chemically competent *E. coli* BL21(DE3), and the expression strain was selected on LB agar supplemented with ampicillin (100 μg

ml⁻¹). 2 liters of LB supplemented with ampicillin (100 μg ml⁻¹) were inoculated with a preculture and grown at 37 °C and 180 rpm to an A₆₀₀ of 0.5–0.6. Expression was induced with addition of IPTG (0.5 mM final concentration), and bacteria were then further cultured for 6 h at 30 °C and 180 rpm. The cells were harvested by centrifugation (3000 × *g*, 10 min), and the pellet was washed with TBS/Ca (20 mM Tris, 137 mM NaCl, 2.6 mM KCl, pH 7.4, supplemented with 100 μM CaCl₂). The cells were resuspended in 25 ml of TBS/Ca with PMSF (1 mM) and lysozyme (0.4 mg ml⁻¹) and subsequently disrupted by five cycles in a microfluidics homogenizer (Microfluidics Corp.). Cell debris was removed by centrifugation (10,000 × *g*, 60 min), and the supernatant was loaded onto a column containing galactosylated (59) or later melibiose-coupled Sepharose CL-6B. The column was washed with TBS/Ca, and PIIA was eluted by addition of 100 mM galactose or 100 mM raffinose to the buffer. The eluted fractions were extensively dialyzed against distilled water and then TBS/Ca buffer. The concentration was determined by UV absorbance at 280 nm using a calculated molar extinction coefficient of 19,480 M⁻¹ cm⁻¹. The yield of purified PIIA was 6 mg (galactose-column) or 19 mg (melibiose-column) per liter of culture volume.

Gel filtration

A HiLoad 16/600 Superdex 200 pg (GE Healthcare) was equilibrated with TBS/Ca buffer (20 mM Tris, 137 mM NaCl, 2.6 mM KCl, pH 7.4, supplemented with 1 mM CaCl₂) with a flow rate of 1 ml/min. A calibration curve for molecular size estimation was generated by loading 10 μM of mixture of standard proteins (lysozyme, DNase I, ovalbumin, and BSA). Thereafter, 10 μM PIIA was loaded on the column and analyzed with the same flow rate.

Dynamic light scattering (DLS) measurements

DLS measurements were performed on a Zetasizer Nano-ZS (Malvern Instruments, UK). Stock solutions were filtered with a syringe filter before measurements. 50 μl of PIIA or LecA (100 mM) in TBS/Ca (20 mM Tris, 137 mM NaCl, 2.6 mM KCl, pH 7.4, supplemented with 1 mM CaCl₂) was measured at 25 °C.

Fluorescent labeling of PIIA and glycan array analysis

PIIA (700 μl, 58 μM in Na₂CO₃ buffer, pH 9.3) was incubated at room temperature under shaking (500 rpm) with fluorescein isothiocyanate (FITC, 33 μl, 3 mg ml⁻¹, in sodium carbonate buffer, pH 9.3) for 1 h. Purification of the labeled protein was performed as described above for unlabeled PIIA; the protein concentration was determined as described previously for LecB-PA14 (19) using an extinction coefficient of 19,480 M⁻¹ cm⁻¹ for PIIA.

FITC-labeled PIIA was tested on the Consortium for Functional Glycomics (CFG) mammalian glycan array (Core H) version 5.3 containing 600 printed glycans in replicates of 6. Standard procedures of Core H (details see <http://www.functionalglycomics.org/glycomics/publicdata/selectedScreens.jsp>)⁴ were run at 5 and 50 μg ml⁻¹ protein based on the protocol

⁴ Please note that the JBC is not responsible for the long-term archiving and maintenance of this site or any other third party hosted site.

Photorhabdus lectin A — PIIA

by Blixt *et al.* (60). Raw data of the PIIA binding experiments are available as [supplemental Tables S1 and S2](#) as an XLS spreadsheet.

Direct binding of fluorescent ligands 1–4 to PIIA

10 μ l of a serial dilution of PIIA in TBS/Ca (618–0.30 μ M) was added in triplicate to a 384-well plate (Greiner Bio-One, Germany, catalog no. 781900). Then, 10 μ l of fluorescent ligand 1–4 dissolved in TBS/Ca were added to PIIA to a final concentration of 10 nM. After incubation for 1 h at room temperature, blank corrected fluorescence intensity was recorded using a PheraStar FS microplate reader (BMG Labtech GmbH, Germany) with excitation filters at 485 nm and emission filters at 535 nm, and fluorescence polarization was calculated. The data were analyzed using a four-parameter fit of the MARS Data Analysis Software (BMG Labtech GmbH, Germany). A minimum of three independent experiments on three plates was performed for each fluorescent ligand.

Competitive binding assay for PIIA

10 μ l of a serial dilution of each tested compounds in TBS/Ca (20 to 0.01 mM) were added in triplicate to a 384-well plate (Greiner Bio-One, Germany, catalog no. 781900). Afterward, 10 μ l of PIIA and **1** were added to each well at final concentrations of 55 μ M and 10 nM, respectively. After incubation for 1 h at room temperature, fluorescence polarization was determined using a microplate reader as described above. The data were analyzed using a four-parameter fit of the MARS Data Analysis Software (BMG Labtech GmbH, Germany). A minimum of three independent experiments on three plates was performed for each compound.

X-ray crystallography

Crystals of apo-PIIA were obtained in 1.6 M sodium citrate tribasic dihydrate, pH 6.5. To solve the PIIA–ligand complex structures, PIIA was co-crystallized in the presence of 10 mM ligand and 3 mM calcium chloride. Optimized crystals of PIIA-**12**, PIIA-**25**, and PIIA-**1** were grown under conditions of 0.2 M ammonium acetate, 0.1 M BisTris buffer, pH 5.5, and 25% PEG 3350; 0.2 M magnesium acetate and 20% PEG 3350; and 0.15 M DL-malic acid and 20% PEG 3350, respectively. Diffraction data for all proteins was collected from single crystals at 100 K. Data for apo-PIIA and PIIA-**12** were obtained at beamline ID23-2 (ESRF) at a wavelength of 0.873 Å, whereas data for the PIIA-**25** and PIIA-**1** were collected at beamline ID30-B (ESRF) at a wavelength of 0.967 Å. Data were processed using Xia2 (61) or XDS (62), and the structures were solved using PHASER (63) molecular replacement with LecA (PDB code 1L7L) as a search model. The models were manually rebuilt with COOT (64) and refined using PHENIX (65) and Refmac5 (66). The structures were validated using MolProbity, and all images were created using PyMOL (67).

Molecular modeling

Docking was performed using PLANTS version 1.1 (68). The calculation of charge and energy minimization of the protein and ligand was performed with Molecular Operating Environment (MOE) version 2014.09 (Chemical Computing Group

Inc., Montreal, Quebec, Canada). Then, the standard docking procedure was used to dock D-galactosamine (**10**) and the methyl glycoside of **20** into the binding pocket of the apo-PIIA crystal structure. The docking site was limited to a 13 Å radius sphere centered in the mass center (coordination: $X = -8.624$, $Y = 15.131$, and $Z = 45.115$) of the crystallized protein. Asp-103, Asp-96, Gln-57, and Glu-44 were set as flexible residues in the input file.

Generation of primary GTKO cells

Pigs lacking the GTKO were generated by disrupting the causative galactosyltransferase gene *GGTA1*, according to the procedure described in Klymiuk *et al.* (69). First, a bacterial artificial chromosome (BAC) containing the target region of the porcine genome, CH242-21F3, was modified by bacterial recombineering in a way that it contained a STOP box right after the START codon of *GGTA1*, resulting in the termination of protein translation as well as RNA transcription of the gene, and a floxed resistance cassette for neomycin selection. Then, this modified BAC was nucleofected into pig primary cells according to Richter *et al.* (70), and single-cell clones were generated under antibiotic selection and propagated to yield cells for DNA isolation and somatic cell nuclear transfer (SCNT). Single-cell clones were screened for homologous recombination by a quantitative PCR-based loss-of-wild-type allele approach, and cell clones that indicated a heterozygous modification of the *GGTA1* allele were used for SCNT to generate heterozygous knock-out pigs. After birth, one of the animals was sacrificed, and primary cells were cultivated and nucleofected with a plasmid encoding Cre recombinase. Again, single-cell clones were generated and now screened for the removal of the neomycin selection cassette. Another round of SCNT was performed to generate heterozygous KO animals lacking the neomycin selection cassette. Pigs were then maintained and bred to achieve homozygous GTKO pigs after two generations. Primary cells from such GTKO animals were isolated according to the procedure described by Richter *et al.* (70), and these cells were used for evaluating the specificity and sensitivity of the PIIA lectin.

Lectin staining of porcine cells

For lectin staining, 1×10^4 cells were seeded in 6-channel slides (IBIDI, Martinsried, Germany), coated with collagen type 1 (Serva Electrophoresis, Heidelberg, Germany), and cultivated under conventional conditions (70). When reaching a confluence of 80–100%, cells were stained for 15 min with 5 μ g/ml Hoechst 33342 and subsequently with FITC-labeled isolectin B4 (GS-IB4, Sigma, 500 μ g/ml) or FITC-labeled PIIA (50 μ g/ml) for 1 h at room temperature. After washing with PBS, cells were visualized in a fluorescence microscope (Axiovert 200, Zeiss).

Hemagglutination of porcine red blood cells

Hemagglutination was done in analogy to a previously published protocol (34). Lithium-heparinized pig blood was centrifuged at $1000 \times g$ for 5 min. Plasma was removed, and the pRBCs were washed with 45 ml of PBS three times. A 10% pRBC solution was prepared by diluting 1 ml of pRBCs with 9 ml of

Photorhabdus lectin A — PIIA

PBS ($A_{600} = 7$). Then, 50 μ l of PBS was added to each well of a 96-well plate. Thereafter, 50 μ l of PIIA (2.5 mg/ml) were added to the first well and mixed, and 50 μ l of this mixture was transferred to the second well. Serial dilution of PIIA was continued until 23 dilutions were obtained. 50 μ l of 10% pRBCs from WT or GTKO pig were added to each well, and the plate was incubated for 2 h at room temperature. Inhibition of PIIA-mediated WT pRBC agglutination was then tested with raffinose. A serial dilution of raffinose (20 mM) was mixed with the lowest lectin concentration showing agglutination (2.4 μ g/ml). After incubation for 30 min at room temperature, pRBCs were added. The plate was incubated for 2 h at room temperature.

Author contributions—A. T. conceived and coordinated the study. G. B., J. K., and A. T. wrote the paper. G. B. and A. T. designed, performed, and analyzed the experiments shown in Figs. 1–4 and Tables 1 and 2. G. B. performed docking experiments. D. H. performed chemical synthesis of compounds. S. W. designed and performed cloning of PIIA expression vector with assistance of G. B., A. S., and J. K. designed, performed, and analyzed the experiments shown in Figs. 5–8 and Table 3 with assistance of G. B., E. M. J., N. K., and E. W. designed, performed, and analyzed the experiments shown in Figs. 9 and 10. All authors reviewed the results and approved the final version of the manuscript.

Acknowledgments—We are grateful to Prof. Rolf Müller (HIPS Saarbrücken) for providing the *P. luminescens* strain used in this study and to the Consortium for Functional Glycomics (Core H, Protein–Glycan Interaction Resource of the Consortium for Functional Glycomics and National Institutes of Health Supporting Grant R24 GM098791) for the glycan array analysis of PIIA. We acknowledge use of the ESRF synchrotron (beamlines ID23-2 and ID30-B). GTKO pigs were produced with funding from Deutsche Forschungsgemeinschaft Grant TRR 127 “Biology of xenogeneic cell, tissue, and organ transplantation—from bench to bedside.”

References

- Poinar, G. O., Thomas, G. M., and Hess, R. (1977) Characteristics of the specific bacterium associated with *Heterorhabditis bacteriophora* (Heterorhabditidae: Rhabditida). *Nematologica* **23**, 97–102
- Thomas, G. M., and Poinar, J. R. (1979) *Xenorhabdus* gen. nov., a genus of entomopathogenic, nematophilic bacteria of the family Enterobacteriaceae. *Int. J. Syst. Evol. Microbiol.* **29**, 352–360
- Boemare, N., Akhurst, R., and Mourant, R. (1993) DNA relatedness between *Xenorhabdus* spp. (Enterobacteriaceae), symbiotic bacteria of entomopathogenic nematodes, and a proposal to transfer *Xenorhabdus luminescens* to a new genus, *Photorhabdus* gen. nov. *Int. J. Syst. Evol. Microbiol.* **43**, 249–255
- Forst, S., and Neilson, K. (1996) Molecular biology of the symbiotic-pathogenic bacteria *Xenorhabdus* spp., and *Photorhabdus* spp. *Microbiol. Rev.* **60**, 21–43
- Fischer-Le Saux, M., Viillard, V., Brunel, B., Normand, P., and Boemare, N. E. (1999) Polyphasic classification of the genus *Photorhabdus* and proposal of new taxa: *P. luminescens* subsp. *luminescens* subsp. nov., *P. luminescens* subsp. *akhurstii* subsp. nov., *P. luminescens* subsp. *laumondii* subsp. nov., *P. temperata* sp. nov., *P. temperata* subsp. *temperata* subsp. nov., and *P. asymbiotica* sp. nov. *Int. J. Syst. Bacteriol.* **49**, 1645–1656
- Ferreira, T., van Reenen, C. A., Endo, A., Tailliez, P., Pagès, S., Spröer, C., Malan, A. P., and Dicks, L. M. (2014) *Photorhabdus heterorhabditis* sp. nov., a symbiont of the entomopathogenic nematode *Heterorhabditis zealandica*. *Int. J. Syst. Evol. Microbiol.* **64**, 1540–1545
- Hapeshi, A., and Waterfield, N. R. (2017) *Photorhabdus asymbiotica* as an insect and human pathogen. *Curr. Top. Microbiol. Immunol.* **402**, 159–177
- Akhurst, R., and Boemare, N. (1990) in *Entomopathogenic Nematodes in Biological Control* (Gaugler, R., and Kaya, H. K., eds) pp. 75–90, CRC Press Inc., Boca Raton, FL
- Akhurst, R., and Dunphy, G. (1993) in *Parasites and Pathogens of Insects* (Beckage, N. E., Thompson, S. A., and Federici, B. A., eds) Vol. 2, pp. 1–23, Academic Press, New York
- Duchaud, E., Rusniok, C., Frangeul, L., Buchrieser, C., Givaudan, A., Taourit, S., Bocs, S., Boursaux-Eude, C., Chandler, M., Charles, J.-F., Dassa, E., Derose, R., Derzelle, S., Freyssinet, G., Gaudriault, S., et al. (2003) The genome sequence of the entomopathogenic bacterium *Photorhabdus luminescens*. *Nat. Biotechnol.* **21**, 1307–1313
- Bowen, D., Rocheleau, T. A., Blackburn, M., Andreev, O., Golubeva, E., Bhartia, R., and French-Constant, R. H. (1998) Insecticidal toxins from the bacterium *Photorhabdus luminescens*. *Science* **280**, 2129–2132
- Guo, L., Fatig, R. O., 3rd., Orr, G. L., Schafer, B. W., Strickland, J. A., Sukhapinda, K., Woodsworth, A. T., and Petell, J. K. (1999) *Photorhabdus luminescens* W-14 insecticidal activity consists of at least two similar but distinct proteins. Purification and characterization of toxin A and toxin B. *J. Biol. Chem.* **274**, 9836–9842
- Kumar, A., Šýkorová, P., Demo, G., Dobeš, P., Hyršl, P., and Wimmerová, M. (2016) A novel fucose-binding lectin from *Photorhabdus luminescens* (PLL) with an unusual heptablated β -propeller tetrameric structure. *J. Biol. Chem.* **291**, 25032–25049
- Wagner, S., Sommer, R., Hinsberger, S., Lu, C., Hartmann, R. W., Empting, M., and Titz, A. (2016) Novel strategies for the treatment of *Pseudomonas aeruginosa* infections. *J. Med. Chem.* **59**, 5929–5969
- Diggle, S. P., Stacey, R. E., Dodd, C., Cámara, M., Williams, P., and Winzer, K. (2006) The galactophilic lectin, LecA, contributes to biofilm development in *Pseudomonas aeruginosa*. *Environ. Microbiol.* **8**, 1095–1104
- Tielker, D., Hacker, S., Loris, R., Strathmann, M., Wingender, J., Wilhelm, S., Rosenau, F., and Jaeger, K.-E. (2005) *Pseudomonas aeruginosa* lectin LecB is located in the outer membrane and is involved in biofilm formation. *Microbiology* **151**, 1313–1323
- Garber, N. (1997) Specific Adherence Mechanisms in Microbiology and Immunology. *Nova Acta Leopoldina* 1997, 75
- Mitchell, E., Houles, C., Sudakevitz, D., Wimmerova, M., Gautier, C., Pérez, S., Wu, A. M., Gilboa-Garber, N., and Imberty, A. (2002) Structural basis for oligosaccharide-mediated adhesion of *Pseudomonas aeruginosa* in the lungs of cystic fibrosis patients. *Nat. Struct. Biol.* **9**, 918–921
- Sommer, R., Wagner, S., Varrot, A., Nycholat, C. M., Khaledi, A., Häussler, S., Paulson, J. C., Imberty, A., and Titz, A. (2016) The virulence factor LecB varies in clinical isolates: consequences for ligand binding and drug discovery. *Chem. Sci.* **7**, 4990–5001
- Sudakevitz, D., Kostlánová, N., Blatman-Jan, G., Mitchell, E. P., Lerrer, B., Wimmerová, M., Katcoff, D. J., Imberty, A., and Gilboa-Garber, N. (2004) A new *Ralstonia solanacearum* high-affinity mannose-binding lectin RS-III structurally resembling the *Pseudomonas aeruginosa* fucose-specific lectin PA-III. *Mol. Microbiol.* **52**, 691–700
- Beshir, G., Sommer, R., Hauck, D., Siebert, D. C. B., Hofmann, A., Imberty, A., and Titz, A. (2016) Development of a competitive binding assay for the *Burkholderia cenocepacia* lectin BC2L-A and structure activity relationship of natural and synthetic inhibitors. *Med. Chem. Commun.* **7**, 519–530
- Lameignere, E., Shiao, T. C., Roy, R., Wimmerova, M., Dubreuil, F., Varrot, A., and Imberty, A. (2010) Structural basis of the affinity for oligomannosides and analogs displayed by BC2L-A, a *Burkholderia cenocepacia* soluble lectin. *Glycobiology* **20**, 87–98
- Marchetti, R., Malinowska, L., Lameignere, E., Adamova, L., de Castro, C., Cioci, G., Stanetty, C., Kosma, P., Molinaro, A., Wimmerova, M., Imberty, A., and Silipo, A. (2012) *Burkholderia cenocepacia* lectin A binding to heptoses from the bacterial lipopolysaccharide. *Glycobiology* **22**, 1387–1398
- Zinger-Yosovich, K., Sudakevitz, D., Imberty, A., Garber, N. C., and Gilboa-Garber, N. (2006) Production and properties of the native *Chromobacterium violaceum* fucose-binding lectin (CV-III) compared to homo-

Photorhabdus lectin A — PIIA

- logous lectins of *Pseudomonas aeruginosa* (PA-III) and *Ralstonia solanacearum* (RS-III). *Microbiology* **152**, 457–463
25. Imberty, A., Wimmerová, M., Mitchell, E. P., and Gilboa-Garber, N. (2004) Structures of the lectins from *Pseudomonas aeruginosa*: insight into the molecular basis for host glycan recognition. *Microbes Infect.* **6**, 221–228
 26. McMahon, K. (2009) Structural and Functional Characterisation of Lectins from the PA-IL Superfamily. Ph.D. thesis, Dublin City University, Dublin, Ireland
 27. Joachim, I., Rikker, S., Hauck, D., Ponader, D., Boden, S., Sommer, R., Hartmann, L., and Titz, A. (2016) Development and optimization of a competitive binding assay for the galactophilic low affinity lectin LecA from *Pseudomonas aeruginosa*. *Org. Biomol. Chem.* **14**, 7933–7948
 28. Cioci, G., Mitchell, E. P., Gautier, C., Wimmerová, M., Sudakevitz, D., Pérez, S., Gilboa-Garber, N., and Imberty, A. (2003) Structural basis of calcium and galactose recognition by the lectin PA-IL of *Pseudomonas aeruginosa*. *FEBS Lett.* **555**, 297–301
 29. Galili, U. (2005) The α -Gal epitope and the anti-Gal antibody in xenotransplantation and in cancer immunotherapy. *Immunol. Cell Biol.* **83**, 674–686
 30. Duffy, M. S., Morris, H. R., Dell, A., Appleton, J. A., and Haslam, S. M. (2006) Protein glycosylation in *Parelaphostrongylus tenuis*—first description of the Gal α 1–3Gal sequence in a nematode. *Glycobiology* **16**, 854–862
 31. Ekser, B., and Cooper, D. K. (2010) Overcoming the barriers to xenotransplantation: prospects for the future. *Expert Rev. Clin. Immunol.* **6**, 219–230
 32. Blanchard, B., Nuriso, A., Hollville, E., Tétaud, C., Wiels, J., Pokorná, M., Wimmerová, M., Varrot, A., and Imberty, A. (2008) Structural basis of the preferential binding for globo-series glycosphingolipids displayed by *Pseudomonas aeruginosa* lectin I. *J. Mol. Biol.* **383**, 837–853
 33. Eierhoff, T., Bastian, B., Thuenauer, R., Madl, J., Audfray, A., Aigal, S., Juillot, S., Rydell, G. E., Müller, S., de Bentzmann, S., Imberty, A., Fleck, C., and Römer, W. (2014) A lipid zipper triggers bacterial invasion. *Proc. Natl. Acad. Sci. U.S.A.* **111**, 12895–12900
 34. Hauck, D., Joachim, I., Frommeyer, B., Varrot, A., Philipp, B., Möller, H. M., Imberty, A., Exner, T. E., and Titz, A. (2013) Discovery of two classes of potent glycomimetic inhibitors of *Pseudomonas aeruginosa* LecB with distinct binding modes. *ACS Chem. Biol.* **8**, 1775–1784
 35. Wohlschlager, T., Buttschi, A., Grassi, P., Sutov, G., Gauss, R., Hauck, D., Schmieder, S. S., Knobel, M., Titz, A., Dell, A., Haslam, S. M., Hengartner, M. O., Aebi, M., and Künzler, M. (2014) Methylated glycans as conserved targets of animal and fungal innate defense. *Proc. Natl. Acad. Sci. U.S.A.* **111**, E2787–E2796
 36. Sommer, R., Hauck, D., Varrot, A., Imberty, A., Künzler, M., and Titz, A. (2016) O-Alkylated heavy atom carbohydrate probes for protein X-ray crystallography: Studies towards the synthesis of methyl 2-O-methyl-L-selenofucopyranoside. *Beilstein J. Org. Chem.* **12**, 2828–2833
 37. Chen, C. P., Song, S. C., Gilboa-Garber, N., Chang, K. S., and Wu, A. M. (1998) Studies on the binding site of the galactose-specific agglutinin PA-IL from *Pseudomonas aeruginosa*. *Glycobiology* **8**, 7–16
 38. Kim, H.-S., Cha, E., Kim, Y., Jeon, Y. H., Olson, B. H., Byun, Y., and Park, H.-D. (2016) Raffinose, a plant galactoside, inhibits *Pseudomonas aeruginosa* biofilm formation via binding to LecA and decreasing cellular cyclic diguanylate levels. *Sci. Rep.* **6**, 25318
 39. Landsteiner, K., and Levine, P. (1927) Further observations on individual differences of human blood. *Exp. Biol. Med.* **24**, 941–942
 40. Khan, F., Khan, R. H., Sherwani, A., Mohmood, S., and Azfer, M. A. (2002) Lectins as markers for blood grouping. *Med. Sci. Monit.* **8**, RA293–RA300
 41. Macher, B. A., and Galili, U. (2008) The Gal α 1,3Gal β 1,4GlcNAc-R (α -Gal) epitope: a carbohydrate of unique evolution and clinical relevance. *Biochim. Biophys. Acta* **1780**, 75–88
 42. Li, S., Waer, M., and Billiau, A. D. (2009) Xenotransplantation: role of natural immunity. *Transpl. Immunol.* **21**, 70–74
 43. Yamada, K., Yazawa, K., Shimizu, A., Iwanaga, T., Hisashi, Y., Nuhn, M., O'Malley, P., Nobori, S., Vagefi, P. A., Patience, C., Fishman, J., Cooper, D. K., Hawley, R. J., Greenstein, J., Schuurman, H.-J., et al. (2005) Marked prolongation of porcine renal xenograft survival in baboons through the use of α 1,3-galactosyltransferase gene-knockout donors and the cotransplantation of vascularized thymic tissue. *Nat. Med.* **11**, 32–34
 44. Klymiuk, N., Aigner, B., Brem, G., and Wolf, E. (2010) Genetic modification of pigs as organ donors for xenotransplantation. *Mol. Reprod. Dev.* **77**, 209–221
 45. Puga Yung, G. L., Li, Y., Borsig, L., Millard, A.-L., Karpova, M. B., Zhou, D., and Seebach, J. D. (2012) Complete absence of the α Gal xenoantigen and isoglobotrihexosylceramide in α 1,3galactosyltransferase knock-out pigs. *Xenotransplantation* **19**, 196–206
 46. Tempel, W., Tschampel, S., and Woods, R. J. (2002) The xenograft antigen bound to *Griffonia simplicifolia* lectin 1-B(4). X-ray crystal structure of the complex and molecular dynamics characterization of the binding site. *J. Biol. Chem.* **277**, 6615–6621
 47. Obukhova, P., Rieben, R., and Bovin, N. (2007) Normal human serum contains high levels of anti-Gal α 1–4GlcNAc antibodies. *Xenotransplantation* **14**, 627–635
 48. Gerdt, S., Dennis, R. D., Borgonie, G., Schnabel, R., and Geyer, R. (1999) Isolation, characterization and immunolocalization of phosphorylcholine-substituted glycolipids in developmental stages of *Caenorhabditis elegans*. *Eur. J. Biochem.* **266**, 952–963
 49. van Stijn, C. M., van den Broek, M., Vervelde, L., Alvarez, R. A., Cummings, R. D., Tefsen, B., and van Die, I. (2010) Vaccination-induced IgG response to Gal α 1–3GalNAc glycan epitopes in lambs protected against *Haemonchus contortus* challenge infection. *Int. J. Parasitol.* **40**, 215–222
 50. Yan, S., Jin, C., Wilson, I. B., and Paschinger, K. (2015) Comparisons of *Caenorhabditis* fucosyltransferase mutants reveal a multiplicity of isomeric N-glycan structures. *J. Proteome Res.* **14**, 5291–5305
 51. Yan, S., Brecker, L., Jin, C., Titz, A., Dragosits, M., Karlsson, N. G., Jantsch, V., Wilson, I. B., and Paschinger, K. (2015) Bisecting galactose as a feature of N-glycans of wild-type and mutant *Caenorhabditis elegans*. *Mol. Cell. Proteomics* **14**, 2111–2125
 52. Yan, S., Bleuler-Martinez, S., Plaza, D. F., Künzler, M., Aebi, M., Joachim, A., Razzazi-Fazeli, E., Jantsch, V., Geyer, R., Wilson, I. B., and Paschinger, K. (2012) Galactosylated fucose epitopes in nematodes: increased expression in a *Caenorhabditis* mutant associated with altered lectin sensitivity and occurrence in parasitic species. *J. Biol. Chem.* **287**, 28276–28290
 53. Meldal, B. H., Debenham, N. J., De Ley, P., De Ley, I. T., Vanfleteren, J. R., Vierstraete, A. R., Bert, W., Borgonie, G., Moens, T., Tyler, P. A., Austen, M. C., Blaxter, M. L., Rogers, A. D., and Lamshead, P. J. (2007) An improved molecular phylogeny of the Nematoda with special emphasis on marine taxa. *Mol. Phylogenet. Evol.* **42**, 622–636
 54. Dennis, R. D., Geyer, R., Egge, H., Menges, H., Stirn, S., and Wiegandt, H. (1985) Glycosphingolipids in insects. Chemical structures of ceramide monosaccharide, disaccharide, and trisaccharide from pupae of *Calliphora vicina* (Insecta: Diptera). *Eur. J. Biochem.* **146**, 51–58
 55. Papadopoulos, J. S., and Agarwala, R. (2007) COBALT: constraint-based alignment tool for multiple protein sequences. *Bioinformatics* **23**, 1073–1079
 56. Wicker, N., Perrin, G. R., Thierry, J. C., and Poch, O. (2001) Secator: a program for inferring protein subfamilies from phylogenetic trees. *Mol. Biol. Evol.* **18**, 1435–1441
 57. Gascuel, O. (1997) BIONJ: an improved version of the NJ algorithm based on a simple model of sequence data. *Mol. Biol. Evol.* **14**, 685–695
 58. Stothard, P. (2000) The sequence manipulation suite: JavaScript programs for analyzing and formatting protein and DNA sequences. *BioTechniques* **28**, 1102
 59. Fornstedt, N., and Porath, J. (1975) Characterization studies on a new lectin found in seeds of *Vicia ervilia*. *FEBS Lett.* **57**, 187–191
 60. Blixt, O., Head, S., Mondala, T., Scanlan, C., Huflejt, M. E., Alvarez, R., Bryan, M. C., Fazio, F., Calarese, D., Stevens, J., Razi, N., Stevens, D. J., Skehel, J. J., van Die, I., Burton, D. R., Wilson, I. A., Cummings, R., Bovin, N., Wong, C.-H., and Paulson, J. C. (2004) Printed covalent glycan array for ligand profiling of diverse glycan binding proteins. *Proc. Natl. Acad. Sci. U.S.A.* **101**, 17033–17038
 61. Winter, G. (2010) xia2: an expert system for macromolecular crystallography data reduction. *J. Appl. Crystallogr.* **43**, 186–190
 62. Kabsch, W. (2010) XDS. *Acta Crystallogr. D Biol. Crystallogr.* **66**, 125–132

Photorhabdus lectin A — PIIA

63. McCoy, A. J., Grosse-Kunstleve, R. W., Adams, P. D., Winn, M. D., Storoni, L. C., and Read, R. J. (2007) Phaser crystallographic software. *J. Appl. Crystallogr.* **40**, 658–674
64. Emsley, P., Lohkamp, B., Scott, W. G., and Cowtan, K. (2010) Features and development of Coot. *Acta Crystallogr D Biol. Crystallogr.* **66**, 486–501
65. Adams, P. D., Afonine, P. V., Bunkóczi, G., Chen, V. B., Davis, I. W., Echols, N., Headd, J. J., Hung, L.-W., Kapral, G. J., Grosse-Kunstleve, R. W., McCoy, A. J., Moriarty, N. W., Oeffner, R., Read, R. J., Richardson, D. C., *et al.* (2010) PHENIX: a comprehensive Python-based system for macromolecular structure solution. *Acta Crystallogr D Biol. Crystallogr.* **66**, 213–221
66. Murshudov, G. N., Skubák, P., Lebedev, A. A., Pannu, N. S., Steiner, R. A., Nicholls, R. A., Winn, M. D., Long, F., and Vagin, A. A. (2011) REFMAC5 for the refinement of macromolecular crystal structures. *Acta Crystallogr D Biol. Crystallogr.* **67**, 355–366
67. Schrödinger L. (2015) *The PyMOL Molecular Graphics System*, Version 1.8, New York
68. Korb, O., Stützle, T., and Exner, T. E. (2006) PLANTS: application of ant colony optimization to structure-based drug design. *Lecture Notes in Computer Science* **4150**, 247–258
69. Klymiuk, N., Mundhenk, L., Kraeche, K., Wuensch, A., Plog, S., Emrich, D., Langenmayer, M. C., Stehr, M., Holzinger, A., Kröner, C., Richter, A., Kessler, B., Kurome, M., Eddicks, M., Nagashima, H., *et al.* (2012) Sequential targeting of CFTR by BAC vectors generates a novel pig model of cystic fibrosis. *J. Mol. Med.* **90**, 597–608
70. Richter, A., Kurome, M., Kessler, B., Zakhartchenko, V., Klymiuk, N., Nagashima, H., Wolf, E., and Wuensch, A. (2012) Potential of primary kidney cells for somatic cell nuclear transfer mediated transgenesis in pig. *BMC Biotechnol.* **12**, 84

3.5. STRUCTURE-GUIDED ENGINEERING OF PLLA CARBOHYDRATE BINDING SPECIFICITY

Ghamdan Beshr, Anika Liu, and Alexander Titz

Introduction

The role of lectins in glycomics and the need to characterize more lectins were previously mentioned in subchapter 1.3. An alternative approach to improve lectin-based glycome profiling is engineering of the existing lectins, thereby gaining more lectins with different specificities.¹ Structure-based site-directed mutagenesis is the most widely used method to alter lectin specificity, enhance the binding affinity of lectins to their ligand, or understand the basis of the interactions between lectins and their binding partners.²⁻⁸ In subchapter 3.4, we characterized a new lectin (called PIIA) in entomopathogenic *Photorhabdus luminescens* bacterium, which has a sharp specificity toward α -galactoside epitopes.

In this study, we have aimed to extend the scope of the application of PIIA through structure-based, site-directed mutagenesis. Here, we tried to modify PIIA's binding specificity through a structural comparison with its ortholog LecA from *P. aeruginosa*, which binds D-galactosides (Gal), and N-acetylgalactosamine (GalNAc) without anomeric specificity. Based on our detailed knowledge of the PIIA structure, we modified the CRD of PIIA with the aim to get two novel recombinant PIIA mutants: one with a relaxed α -/ β -Gal specificity and another with α -Gal and α -GalNAc specificity. This would extend the available lectin repertoire and provide useful insights, also for comparable approaches to other lectins in the future.

Experimental details

Homology model

The homology models of the PIIA-V43G/N55G were generated via the Phyre² web portal using PIIA-wild type crystal structure (PDB code 5OUD) as the template.⁹

Site-directed mutagenesis

All mutants were generated by a QuickChange site-directed mutagenesis¹⁰ using plasmid pET22b-*pIIA* as the template and phusion polymerase (New England Biolabs, UK). The PCR primers (MWG-Biotech AG, Ebersberg, Germany) were designed to introduce point mutation at the desired positions (Table 1A). The reaction for either a forward or a reverse primer was separately performed in a 25 μ L volume using a PCR thermocycler (TProfessional thermocycler, analytic jena, Germany) (Table 1B). Thereafter, the separately amplified DNA strands were combined and reannealed, as in Table 1C. The parent template was afterwards digested by Dnpi restriction enzymes (New England Biolabs, UK) (> 1 h at 37 °C) and then 10 μ L of reaction was transformed (electroporation, 1800 V, 25 μ F, 200 Ω , 5.2 ms) into *E. coli* XL-blue cells and plated onto LB agar supplemented with 0.1 mg/mL ampicillin. After overnight incubation at 37 °C, 3 colonies for each mutant were randomly selected and isolated their plasmids (GenEluteTM Plasmid miniprep Kit, SIGMA, Germany). Finally, the isolated plasmids were sequenced at GATC (Konstanz, Germany) to confirm the correct generation of the desired mutations.

Table 1. Designing and generating of PIIA mutants. **A)** DNA Oligonucleotides used in PCR to generate PIIA mutants. For: forward primer; Rev: reverse primer. **B)** PCR conditions for Quickchange site-directed mutagenesis. **C)** Reannealing conditions of separately amplified DNA stands.

A

Primer name	oligonucleotides
V43G-For	5'-GTGATAATGGTGAATGGGCAGCACCTG-3'
V43G-Rev	5'-CCATTCAACCATTATCACGGCCATATTTAC-3'
N55G-For	5'-CCAATGGTCCACAACCGTCATCAATAGC-3'
N55G-Rev	5'-GTTGTGGACCATTTGGGTACAGGACCATC-3'
R40G-For	5'-GAAATATGGCGGTGATAATGTTGAATGGGC-3'
R40G-Rev	5'-CATTATCACCGCCATATTTACCCATCC-3'
R40P-For	5'-GAAATATGGCCCGGATAATGTTGAATGGGC-3'
R40P-Rev	5'-CATTATCCGGGCCATATTTACCCATCC-3'
D103N-For	5'-CTTTTGGTAATAATTCAAGTCAAGTCG-3'
D103N-Rev	5'-CTGAATTATTACCAAAAGTACCCGGTACG-3'

B

Temperature [°C]	Time [min]
98	1:00
98	0:30
60	0:50
72	2:48
72	10:00
4	Holding

C

Temperature [°C]	Time [min]
95	5:00
90	1:00
80	1:00
70	0:30
60	0:30
50	0:30
40	0:30
37	Holding

Expression and purification of PIIA mutants

PIIA mutants were expressed and purified according to the previously published protocol.¹¹ In short, pET22b-*pIIA* with the desired mutation was transformed into a chemically competent *E. coli* BL21(DE3) and the expression strain was selected on LB agar, supplemented with ampicillin (100 µg mL⁻¹). 1 L of LB supplemented with ampicillin (100 µg mL⁻¹) was inoculated

with a preculture and grown at 37 °C and 180 rpm to an OD600 of 0.5-0.6. Expression was induced with the addition of IPTG (0.5 mM final concentration) and the bacteria were then further cultured for 6h at 30 °C and 180 rpm. The cells were harvested by centrifugation (9000 x g, 10 min) and the pellet was washed with TBS/Ca (20 mM Tris, 137 mM NaCl, 2.6 mM KCl at pH 7.4, supplemented with 100 µM CaCl₂). The cells were resuspended in 25 mL TBS/Ca with PMSF (1 mM) and lysozyme (0.4 mg mL⁻¹) and subsequently disrupted by 5 cycles in a microfluidics homogenizer (Microfluidics Corp., USA). Cell debris was removed by centrifugation (19'000 x g, 60 min) and the supernatant was loaded onto a column containing galactosylated or melibiose-coupled sepharose CL-6B.² The column was washed with TBS/Ca and PIIA mutants were eluted by the addition of 100 mM galactose to the buffer. The eluted fractions were extensively dialyzed against distilled water and then a TBS/Ca buffer. The concentration was determined by UV absorbance at 280 nm using the calculated molar extinction coefficient (19480 M⁻¹ cm⁻¹).

Competitive binding assay for PIIA

10 µL of a serial dilution of each of the tested compounds in TBS/Ca (20 - 0.01 mM) were added in triplicates to a 384-well plate (Greiner Bio-One, Germany, cat no 781900). Afterwards, 10 µL of PIIA and fluorescent ligand **1** (subchapter 3.4) were added to each well at final concentrations of 55 µM and 10 nM, respectively. After incubation for 1 h at r.t., the blank corrected fluorescence intensity was recorded, using a PheraStar FS microplate reader (BMG Labtech GmbH, Germany) with excitation filters at 485 nm and emission filters at 535 nm, and the fluorescence polarization was calculated. The data were analyzed using a four-parameter fit of the MARS Data Analysis Software (BMG Labtech GmbH, Germany).

Results and discussion

The two CRDs of PIIA and LecA were superposed and, as previously reported in subchapter 3.4, the side-chains of the amino-acids V43 and N55 build a close cleft, which narrows the binding pocket for any β -Gal (Figure 1A). In order to widen the binding pocket, we first generated a homology model of a PIIA mutant, where V43 and N55 are mutated into glycine (PIIA-V43G/N55G). As depicted in figure 1B, an open cleft was created, which might allow β -substituents at D-galactosides to be accommodated. Thus, the *in-vitro* mutations of V43 and N55 were carried out in a stepwise manner, using site-directed mutagenesis.

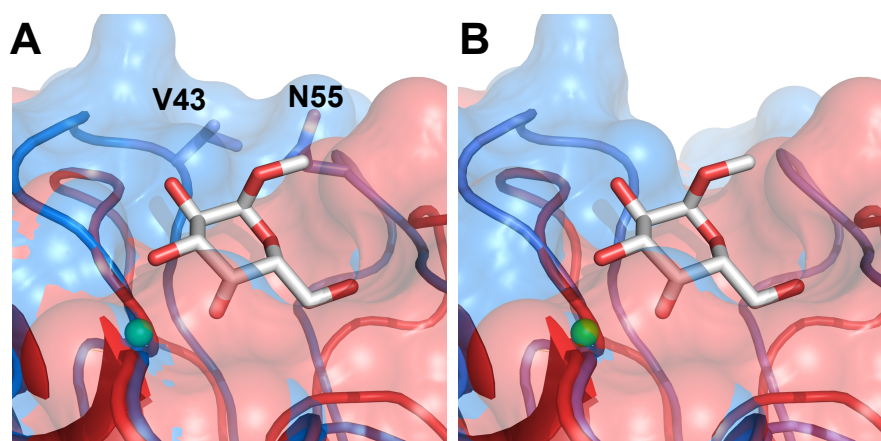
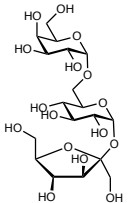
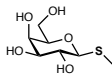
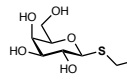
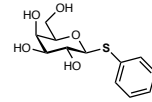
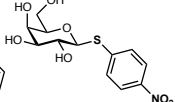
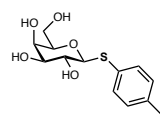
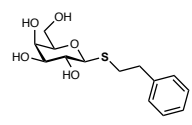
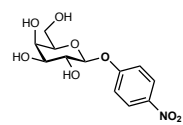
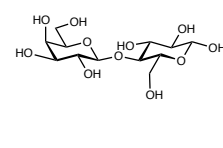


Figure 1. Assignment of the mutated PIIA residues to gain PIIA with α - β -Gal specificity. **A)** Overlay of crystal structures of *P. aeruginosa* LecA (Red, PDB code 1OKO) and *P. luminescens* PIIA (marine, PDB code 5OUD). **B)** Overlay of crystal structures of *P. aeruginosa* LecA (Red, PDB code 1OKO) and the homology model of PIIA-V43G/N55G. The homology model was generated based on the PIIA crystal structure (PDB code 5OUD) using a Phyre² web portal.⁹ Methyl α -D-galactose is depicted as sticks coloured by elements (O: red, C: grey) and PIIA residues (O: red, C: grey, N: blue). Ca^{2+} ion in the binding site is shown as a green sphere. Residue numbers correspond to PIIA.

Both PIIA-V43G and PIIA-V43G/N55G were separately generated, expressed, purified and evaluated, using the established fluorescence polarization assay, which was used for the PIIA wild-type (PIIA-wt) (subchapter 3.4).

Table 2. Biochemical evaluation of β -D-galactosides for PIIA-V43G and PIIA-wt. The IC_{50} values were determined using a competitive binding assay, based on fluorescence polarization, and the standard deviations represent at least two independent experiments. n.i.: no inhibition up to 10 mM.

Compound					
PIIA-V43G IC_{50} [mM]	0.11 ± 0.06	35 ± 5 % inhib. @ 10 mM	45 ± 1 % inhib. @ 10 mM	2.58 ± 0.09	4.06 ± 0.05
PIIA-wt IC_{50} [mM]	0.128	n.i	n.i	51 % inhib. @ 10 mM	36 % inhib. @ 10 mM

Compound				
PIIA-V43G IC_{50} [mM]	5.00 ± 0.78	41 ± 5 % inhib. @ 10 mM	8.46 ± 0.64	68.5 % inhib. @ 10 mM
PIIA-wt IC_{50} [mM]	n.i	n.i	n.i	n.i

The single point mutation (PIIA-V43G) showed a slight improvement in the binding towards β -Gal, especially with phenyl substituents, compared to the PIIA-wt (Table 2). In contrast to this, PIIA-V43G/N55G could not be purified on D-galactose column, which indicates that the insertion of additional N55G mutation led to a complete loss of binding to the D-galactose (Figure 2A). N55 builds two hydrogen bonds with Y36 and Q57 and upon the N55G mutation, these bonds were disrupted and might lead to a misfolding of the binding pocket (Figure 2B). PIIA-V43G/N55S could be next investigated, since the hydroxyl group of serine could retain bridges to Y36 and Q57. Moreover, serine has shorter side chain than asparagine which might reduce the blocking at the binding pocket.

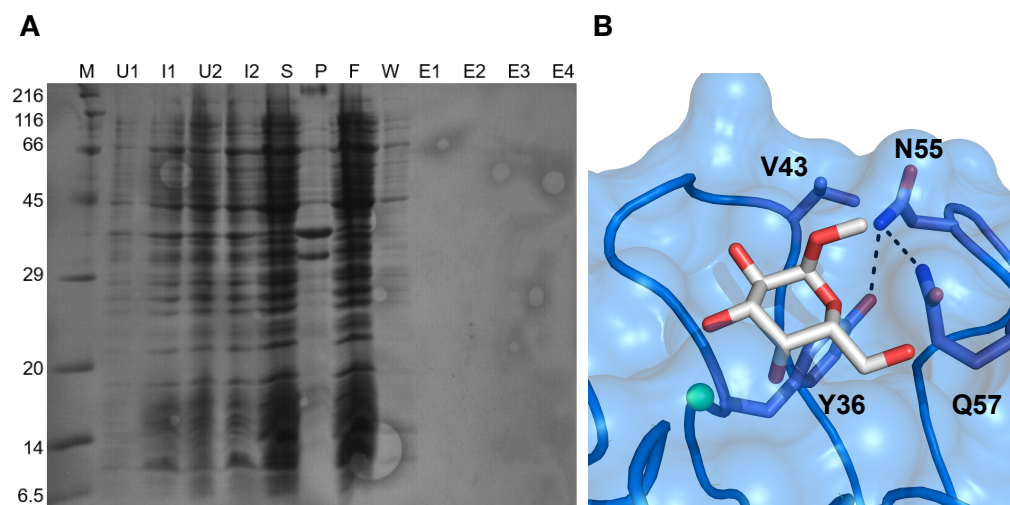


Figure 2. A) 15% SDS page of PIIA-V43G/N55G expression and attempted purification on the D-galactose column. The lanes are as follows: molecular mass marker in kDa (M); Un-induced *E. coli* whole-cell extracts (U); IPTG- induced cultures (I); Supernatant (S); Pellet (P); Flow-through from the D-galactose column (F); Wash (W); Elution with 100 mM of D-galactose (E). The PIIA mutant (13 kDa) did not bind to the column. **B)** CRD of PIIA (PDB code 5ODU) showing the interaction between N55 and Y36 and Q57. Methyl α -D-galactose is depicted as sticks coloured by elements (O: red, C: grey) and PIIA residues (O: red, C: grey, N: blue). Ca^{2+} ion in the binding site is shown as green sphere.

The same approach was followed to design PIIA mutants with extending specificity towards α -GalNAc. The inability of PIIA to bind α -GalNAc is likely to have been caused by a restriction of the binding pocket around the C2 position, where the acetamide group of α -GalNAc is pointed. Structural analysis indicates that the R40 side-chain or the corresponding backbone loop might make a barrier for C2 substituents at α -GalNAc (Figure 3). Reducing blocking at this loop might lead to α -GalNAc binding PIIA, which might potentially function as a tumour probe for Tn antigen (GalNAc α 1-O-Ser/Thr). Tn antigen is expressed in the majority of carcinoma cells and does not appear in normal tissues.¹²

Two point mutations were attempted: the substitution of R40 through glycine, which might eliminate the steric hindrance of the R40 side-chain, and D103 by a neutral residue asparagine, which mimics the charge of the LecA binding pocket close to the acetamide group of GalNAc.

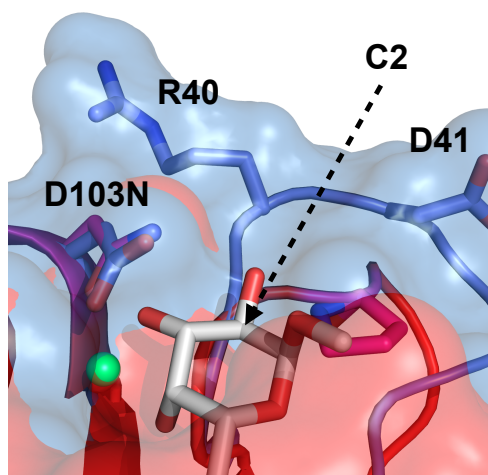
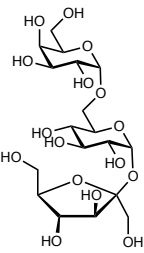
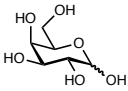
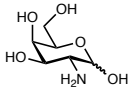
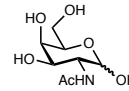


Figure 3. Assignment of the mutated PIIA residues to gain PIIA with an α -Gal and α -GalNAc specificity. **A)** Overlay of the crystal structures of *P. aeruginosa* LecA (Red, PDB code 1OKO) and *P. luminescens* PIIA (marine, PDB code 5ODU). Methyl α -D-galactose is depicted as sticks coloured by elements (O: red, C: grey) and PIIA residues (O: red, C: marine, N: blue). Ca^{2+} ion in the binding site is shown as green sphere. Residue numbers correspond to PIIA and the label starts with PIIA residue and then LecA. The arrow points to the C2 of the carbohydrate ligand where the acetamide group in the GalNAc is extended.

PIIA-R40G/D103N was successfully performed, expressed, purified, and biochemically evaluated. Unfortunately, these mutations did not extend the binding to GalNAc and it is therefore not a successful PIIA mutant (Table 3). D-galactosamine is a compound that binds to the PIIA-wt, and upon changing the charge at the CRD of the PIIA mutant through inserting a neutral residue (N103), it led to complete loss of binding to D-galactosamine. This can be explained by a missing hydrogen bond, which should be formed by D103 in the PIIA-wt (see subchapter 3.4)

Thereafter, an R40 was mutated to proline in addition to D103N to ensure that the proline might bend the loop in a favourable way, thus creating more space to accommodate the substituents at C2 of the D-galactosides. The successfully purified PIIA-R40P/D103N was evaluated with some sugars and, like PIIA-wt, it could not recognize GalNAc (Table 3).

Table 3. IC₅₀ values of GalNAc, D-galactosamine and other sugars for PIIA-R40G/D103N and PIIA-P40G/D103N are compared to IC₅₀ values of PIIA-wt from subchapter 3.4. The IC₅₀ values were determined once in duplicates, using a competitive binding assay based on fluorescence polarization. n.i.: no inhibition up to 10 mM.

Compound				
	Raffinose	D-galactose	D-galactosamine	N-acetyl-D-galactosamine
PIIA-R40G/D103N IC ₅₀ [mM]	0.210	1.12	n.i	n.i
PIIA-R40P/D103N IC ₅₀ [mM]	0.34	1.21	n.i	n.i
PIIA-wt IC ₅₀ [mM]	0.11	1.57	0.68	n.i

In conclusion, the knowledge that we gained from this study highlighted the importance of N55 in PIIA's CRD and the possibility to alter the binding specificity of PIIA towards D-galactosamine by D103 mutation.

References

- (1) Hu, D.; Tateno, H.; Hirabayashi, J. Lectin Engineering, a Molecular Evolutionary Approach to Expanding the Lectin Utilities. *Molecules* **2015**, *20* (5), 7637–7656.
- (2) Mrázková, J.; Malinová, L.; Wimmerová, M. Step-By-Step In Vitro Mutagenesis: Lessons From Fucose-Binding Lectin PA-IIL. In *In Vitro Mutagenesis*; Springer, 2017; pp 399–419.
- (3) Nishiguchi, M.; Yoshida, K.; Sumizono, T.; Tazaki, K. Studies by Site-Directed Mutagenesis of the Carbohydrate-Binding Properties of a Bark Lectin from Robinia pseudoacacia. *FEBS Lett.* **1997**, *403* (3), 294–298.
- (4) Chen, Y.; Lu, K.; Li, J.; Liang, D.; Luo, H.; Wang, X.; Wang, X.; Bao, J. Structure and Function Analysis of Polygonatum cyrtoneura Lectin by Site-Directed Mutagenesis. *Acta Biochim. Biophys. Sin. (Shanghai)*. **2017**, *49* (12), 1099–1111.
- (5) Arango, R.; Rodriguez-Arango, E.; Adar, R.; Belenky, D.; Loontjens, F. G.; Rozenblatt, S.; Sharon, N. Modification by Site-Directed Mutagenesis of the Specificity of Erythrina corallodendron Lectin for Galactose Derivatives with Bulky Substituents at C-2. *FEBS Lett.* **1993**, *330* (2), 133–136.
- (6) Jordan, E. T.; Goldstein, I. J. Site-Directed Mutagenesis Studies on the Lima Bean Lectin. *FEBS J.* **1995**, *230* (3), 958–964.
- (7) Thamotharan, S.; Karthikeyan, T.; Kulkarni, K. A.; Shetty, K. N.; Surolia, A.; Vijayan, M.; Suguna, K. Modification of the Sugar Specificity of a Plant Lectin: Structural Studies on a Point Mutant of Erythrina corallodendron Lectin. *Acta Crystallogr. Sect. D Biol. Crystallogr.* **2011**, *67* (3), 218–227.
- (8) Adhikari, P.; Bachhawat-Sikder, K.; Thomas, C. J.; Ravishankar, R.; Jeyaprakash, A. A.; Sharma, V.; Vijayan, M.; Surolia, A. Mutational Analysis at Asn-41 in Peanut agglutinin A RESIDUE CRITICAL FOR THE BINDING OF THE TUMOR-ASSOCIATED THOMSEN-FRIEDENREICH ANTIGEN. *J. Biol. Chem.* **2001**, *276* (44), 40734–40739.
- (9) Kelley, L. A.; Mezulis, S.; Yates, C. M.; Wass, M. N.; Sternberg, M. J. E. The Phyre2 Web Portal for Protein Modeling, Prediction and Analysis. *Nat. Protoc.* **2015**, *10* (6), 845.
- (10) Zhang, J.-H.; Chung, T. D. Y.; Oldenburg, K. R. A Simple Statistical Parameter for Use in Evaluation and Validation of High Throughput Screening Assays. *J. Biomol. Screen.* **1999**, *4* (2), 67–73.
- (11) Beshr, G.; Sikandar, A.; Jemiller, E.-M.; Klymiuk, N.; Hauck, D.; Wagner, S.; Wolf, E.; Koehnke, J.; Titz, A. Photobacterium luminescens Lectin A (PIIA): A New Probe for Detecting α -Galactoside-Terminating Glycoconjugates. *J. Biol. Chem.* **2017**, *292* (48), 19935–19951.
- (12) Fu, C.; Zhao, H.; Wang, Y.; Cai, H.; Xiao, Y.; Zeng, Y.; Chen, H. Tumor-Associated Antigens: Tn Antigen, sTn Antigen, and T Antigen. *Hla* **2016**, *88* (6), 275–286.

4. CONCLUSION AND OUTLOOK

Bacterial biofilm is a survival strategy which protects bacteria from their outer environments, particularly from antibiotics. Nowadays, many bacteria have developed resistance to most existing antibiotics, and consequently finding a new target or a new class of anti-infective agents is the focus of many research groups. Several strategies, such as the inhibition of quorum sensing, adhesive organelle, cell division, and bacterial lectins as well as the cleavage of peptidoglycan, have been pursued to prevent biofilm formation. The targeting of Gram-negative bacterial lectins is a recent approach to hinder biofilm formation, which eventually led to improve the efficacy of existing antibiotics.^{36,53} Our research group has successfully developed glycomimetic inhibitors for *P. aeruginosa* LecB, using a rational structure-based design approach, and valuable progress has also been made in terms of the potency and the pharmacokinetic properties of inhibitors.⁴³ This work aimed to find new classes of anti-biofilm agents for opportunistic human pathogens, such as *P. aeruginosa* and *B. cenocepacia*, by screening libraries, studying self-assembled photo-switchable multivalent inhibitors, and exploring the recognition of inhibitors of the investigated lectins.

The search for new classes of lectin inhibitors from non-carbohydrate-based compound libraries was a challenge and with a very low hit rate (0.05 %). Lectins are highly specific to their carbohydrate ligands. As reported in subchapters 3.3 and 3.4, masking or changing any of hydroxyl groups at the carbohydrate ligand, which coordinate the calcium ions in the CRD, leads to a complete loss of binding affinity. In this context, the simplest strategy to develop a potent lectin inhibitor is structure-based drug design. Whereas by the screening approach, there is a high cost associated with this process and it has been estimated that approximately 20,000 compounds need to be tested in order to find one that become a marketable drug.⁵⁴ However, for any future screening work for lectin inhibitors, there are several points that should be taken into consideration.

First, the search should be focused on libraries that contain carbohydrate-based compounds, where the sugar recognizes the lectin's CRD and the aglycon part additionally interacts with the protein surface to enhance the binding affinity. Second, the finding of non-carbohydrate LecB or LecA inhibitors remains a challenge. Third, for any future investigation of bacterial extracts against lectins we should be aware of the false positive signals that might come from sugars in the cell-cultivating media.

Glycans generally have a weak binding affinity to their lectins; in nature, they overcome this problem by multivalency.³⁶ Thus, several multivalent inhibitors have been designed and synthesized for bacterial lectins, such as *P. aeruginosa* LecA and LecB, which display a higher potency compared to their monovalent ligands. Most of the multivalent inhibitors are based on calixarene, pentaerythritol, glyconanoparticle or peptide dendrimer scaffolds and their presentation is sometime limited due to scaffold rigidity and furthermore their synthesis and purification are complicated.^{38,55} In contrast to the conventional multivalent LecA and LecB inhibitors, it was demonstrated in this work the simple preparation of self-assembled photo-switchable multivalent inhibitors using glycoamphiphiles, which can be easily synthesized and the ligand valency of which can be controlled through the appropriate molecular design. Moreover, the glycoamphiphiles were seen to have moderate-to-potent inhibition of both *P. aeruginosa* lectins. This system is new and still needs further optimization but may be applied in the future as a targeted delivery vehicle with photo-triggered release properties.

Exploring *P. aeruginosa* lectin homologs from other pathogenic bacteria and characterizing them was the second objective of this work. Here, a SAR study to understand the recognition of carbohydrates in newly discovered *B. cenocepacia* BC2L-A was carried out. Using our knowledge of its homolog from *P. aeruginosa* (LecB), we could develop the first set of glycomimetic BC2L-A inhibitors.⁴⁸ In addition to this, this SAR study on *B. cenocepacia* BC2L-A lectin highlighted the possibility of developing a broad-spectrum anti-biofilm agent that could inhibit the biofilm formation in both human pathogens (i.e. *P. aeruginosa* and *B. cenocepacia*) by targeting their

mannose-binding lectins (i.e. LecB and BC2L-A), as they infect patients simultaneously and a mixed biofilm from both bacteria has been identified in CF isolates.⁵⁶ Therefore, mannoheptose with a (6S)-configuration is a potential candidate and requires further optimization, since it showed moderate binding to LecB and BC2L-A in the IC₅₀ range of 82 - 217 μ M and 13 - 116 μ M, respectively.^{48,57}

LecA homologs were identified for the first time in this work in several *Photorhabdus*, *Xenorhabdus*, and *Enterobacter* species; this is a new area of exploration in the search for more pathogenic bacterial lectins (see subchapter 3.4). The characterization of the *P. luminescens* PIIA lectin was a successful contribution to glycomics, particularly for lectin microarray technology and biomedical research. In addition to using PIIA as a probe in xenotransplantation, PIIA could be also utilized to detect α -Gal terminals in other biomedical research, such as in malaria and tuberculosis control, the agglutination of blood group B, the differentiation of endothelial cells, and the tracing of central and peripheral neuronal pathways.⁵⁸⁻⁶¹ We therefore have to continue characterizing more new lectins and exploring their carbohydrate specificity to improve glycome profiling as well as to understand their biological roles.

In subchapter 3.4, we identified several LecA homologs in *Enterobacter spp.* These bacteria are Gram-negative bacilli and belong to the Enterobacteriaceae family. They are taken on a clinical significance over the last decade and the National Healthcare Safety Network (2008) reported that approximately 5 % of nosocomial bacteremia cases originated from *Enterobacter spp.*⁶²⁻⁶⁴ The characterization of LecA homologs in *Enterobacter spp.* is therefore a project of high importance, which I am currently supervising a master thesis on this work to reveal the role of LecA homologs in *Enterobacter* pathogenicity and might become a new target for new anti-infectives.

10. References

- (1) Varki, A.; Cummings, R.; Esko, J.; Freeze, H.; Hart, G.; Marth, J. Essentials of Glycobiology Cold Spring Harbor Laboratory Press. New York **1999**, 66–84.
- (2) Ghazarian, H.; Idoni, B.; Oppenheimer, S. B. A Glycobiology Review: Carbohydrates, Lectins and Implications in Cancer Therapeutics. *Acta Histochem.* **2011**, *113* (3), 236–247.
- (3) Krishnamoorthy, L.; Mahal, L. K. Glycomic Analysis: An Array of Technologies. *ACS Chem. Biol.* **2009**, *4* (9), 715–732.
- (4) Dell, A.; Galadari, A.; Sastre, F.; Hitchen, P. Similarities and Differences in the Glycosylation Mechanisms in Prokaryotes and Eukaryotes. *International Journal of Microbiology*. 2010.
- (5) Robert, K. Y.; Nakatani, Y.; Yanagisawa, M. The Role of Glycosphingolipid Metabolism in the Developing Brain. *J. Lipid Res.* **2009**, *50* (Supplement), S440–S445.
- (6) Hannun, Y. A.; Obeid, L. M. Principles of Bioactive Lipid Signalling: Lessons from Sphingolipids. *Nat. Rev. Mol. cell Biol.* **2008**, *9* (2), 139.
- (7) Lodish, H.; Berk, A.; Zipursky, S. L.; Matsudaira, P.; Baltimore, D.; Darnell, J. Molecular Cell Biology 4th Edition. *Natl. Cent. Biotechnol. Information, Bookshelf* **2000**.
- (8) Bertozzi, C. R.; Sasisekharan, R. Glycomics, Essentials of Glycobiology. Cold Spring Harbor (NY): Cold Spring Harbor Laboratory Press 2009.
- (9) Macher, B. A.; Galili, U. The Gal α 1,3Gal β 1,4GlcNAc-R (α -Gal) Epitope: A Carbohydrate of Unique Evolution and Clinical Relevance. *Biochimica et Biophysica Acta - General Subjects*. 2008, pp 75–88.
- (10) Brockhausen, I.; Schutzbach, J.; Kuhns, W. Glycoproteins and Their Relationship to Human Disease. *Cells Tissues Organs* **1998**, *161* (1–4), 36–78.
- (11) Turner, G. A. N-Glycosylation of Serum Proteins in Disease and Its Investigation Using Lectins. *Clin. Chim. acta* **1992**, *208* (3), 149–171.
- (12) Furukawa, K.; Kobata, A. IgG Galactosylation-Its Biological Significance and Pathology. *Mol Immunol* **1991**, *28* (12), 1333–1340.
- (13) Orntoft, T. F.; Meldgaard, P.; Pedersen, B.; Wolf, H. The Blood Group ABO Gene Transcript Is down-Regulated in Human Bladder Tumors and Growth-Stimulated Urothelial Cell Lines. *Cancer Res.* **1996**, *56* (5), 1031–1036.
- (14) Janković, M. Glycans as Biomarkers: Status and Perspectives. *J. Med. Biochem.* **2011**, *30* (3), 213–223.
- (15) Goldstein, I. J. What Should Be Called a Lectin? *Nature* **1980**, *285*, 66.
- (16) Hirabayashi, J.; Yamada, M.; Kuno, A.; Tateno, H. Lectin Microarrays: Concept, Principle and Applications. *Chem. Soc. Rev.* **2013**, *42* (10), 4443–4458.
- (17) Ito, H.; Kuno, A.; Sawaki, H.; Sogabe, M.; Ozaki, H.; Tanaka, Y.; Mizokami, M.; Shoda, J.; Angata, T.; Sato, T.; et al. Strategy for Glycoproteomics: Identification of Glyco-Alteration Using Multiple Glycan Profiling Tools. *J. Proteome Res.* **2009**, *8* (3), 1358–1367.

- (18) Narimatsu, H.; Sawaki, H.; Kuno, A.; Kaji, H.; Ito, H.; Ikehara, Y. A Strategy for Discovery of Cancer Glyco-Biomarkers in Serum Using Newly Developed Technologies for Glycoproteomics. *FEBS J.* **2010**, 277 (1), 95–105.
- (19) Hu, D.; Tateno, H.; Hirabayashi, J. Lectin Engineering, a Molecular Evolutionary Approach to Expanding the Lectin Utilities. *Molecules* **2015**, 20 (5), 7637–7656.
- (20) Esko, J. D.; Sharon, N. Microbial Lectins: Hemagglutinins, Adhesins, and Toxins. *Essentials of Glycobiology* **2009**, 3rd ed.
- (21) Diggle, S. P.; Stacey, R. E.; Dodd, C.; Cámara, M.; Williams, P.; Winzer, K. The Galactophilic Lectin, LecA, Contributes to Biofilm Development in *Pseudomonas aeruginosa*. *Environ. Microbiol.* **2006**, 8 (6), 1095–1104.
- (22) Tielker, D.; Hacker, S.; Loris, R.; Strathmann, M.; Wingender, J.; Wilhelm, S.; Rosenau, F.; Jaeger, K.-E. *Pseudomonas aeruginosa* Lectin LecB Is Located in the Outer Membrane and Is Involved in Biofilm Formation. *Microbiology* **2005**, 151 (Pt 5), 1313–1323.
- (23) Inhülsen, S.; Aguilar, C.; Schmid, N.; Suppiger, A.; Riedel, K.; Eberl, L. Identification of Functions Linking Quorum Sensing with Biofilm Formation in *Burkholderia cenocepacia* H111. *Microbiologyopen* **2012**, 1 (2), 225–242.
- (24) Wagner, S.; Sommer, R.; Hinsberger, S.; Lu, C.; Hartmann, R. W.; Empting, M.; Titz, A. Novel Strategies for the Treatment of *Pseudomonas aeruginosa* Infections. *J. Med. Chem.* **2016**, 59 (13), 5929–5969.
- (25) Santajit, S.; Indrawattana, N. Mechanisms of Antimicrobial Resistance in ESKAPE Pathogens. *Biomed Res. Int.* **2016**, 2016.
- (26) Flemming, H. C.; Wingender, J. The Biofilm Matrix. *Nat Rev Microbiol* 8: 623–633. **2010**.
- (27) Eierhoff, T.; Bastian, B.; Thuenauer, R.; Madl, J.; Audfray, A.; Aigal, S.; Juillot, S.; Rydell, G. E.; Müller, S.; de Bentzmann, S.; et al. A Lipid Zipper Triggers Bacterial Invasion. *Proc Natl Acad Sci U S A* **2014**, 111 (35), 12895–12900.
- (28) Kadam, R. U.; Bergmann, M.; Hurley, M.; Garg, D.; Cacciarini, M.; Swiderska, M. A.; Nativi, C.; Sattler, M.; Smyth, A. R.; Williams, P.; et al. A Glycopeptide Dendrimer Inhibitor of the Galactose-Specific Lectin LecA and of *Pseudomonas aeruginosa* Biofilms. *Angew. Chemie Int. Ed.* **2011**, 50 (45), 10631–10635.
- (29) Rodrigue, J.; Ganne, G.; Blanchard, B.; Saucier, C.; Giguère, D.; Shiao, T. C.; Varrot, A.; Imberty, A.; Roy, R. Aromatic Thioglycoside Inhibitors against the Virulence Factor LecA from *Pseudomonas aeruginosa*. *Org. Biomol. Chem.* **2013**, 11 (40), 6906.
- (30) Visini, R.; Jin, X.; Bergmann, M.; Michaud, G.; Pertici, F.; Fu, O.; Pukin, A.; Branson, T. R.; Thies-Weesie, D. M. E.; Kemmink, J.; et al. Structural Insight into Multivalent Galactoside Binding to *Pseudomonas aeruginosa* Lectin LecA. *ACS Chem. Biol.* **2015**, 10 (11), 2455–2462.
- (31) Duchaud, E.; Rusniok, C.; Frangeul, L.; Buchrieser, C.; Givaudan, A.; Taourit, S.; Bocs, S.; Boursaux-Eude, C.; Chandler, M.; Charles, J.-F.; et al. The Genome Sequence of the Entomopathogenic Bacterium *Photobacterium luminescens*. *Nat. Biotechnol.* **2003**, 21 (11), 1307.
- (32) McMahon, K. (2009) Structural and Functional Characterisation of Lectins from the PA-IL

- Superfamily, Ph.D. thesis, Dublin City University, Dublin, Ireland.
- (33) Imberty, A.; Wimmerová, M.; Mitchell, E. P.; Gilboa-Garber, N. Structures of the Lectins from *Pseudomonas aeruginosa*: Insights into the Molecular Basis for Host Glycan Recognition. *Microbes Infect.* **2004**, *6* (2), 221–228.
 - (34) Bartels, K. M.; Funken, H.; Knapp, A.; Brocker, M.; Bott, M.; Wilhelm, S.; Jaeger, K. E.; Rosenau, F. Glycosylation Is Required for Outer Membrane Localization of the Lectin LecB in *Pseudomonas aeruginosa*. *J. Bacteriol.* **2011**, *193* (5), 1107–1113.
 - (35) Sommer, R.; Wagner, S.; Varrot, A.; Nycholat, C. M.; Khaledi, A.; Häussler, S.; Paulson, J. C.; Imberty, A.; Titz, A. The Virulence Factor LecB Varies in Clinical Isolates: Consequences for Ligand Binding and Drug Discovery. *Chem. Sci.* **2016**, *7* (8), 4990–5001.
 - (36) Sommer, R.; Joachim, I.; Wagner, S.; Titz, A. New Approaches to Control Infections: Anti-Biofilm Strategies against Gram-Negative Bacteria. *Chim. Int. J. Chem.* **2013**, *67* (4), 286–290.
 - (37) Johansson, E. M. V.; Crusz, S. A.; Kolomiets, E.; Buts, L.; Kadam, R. U.; Cacciarini, M.; Bartels, K.-M.; Diggle, S. P.; Cámara, M.; Williams, P.; et al. Inhibition and Dispersion of *Pseudomonas aeruginosa* Biofilms by Glycopeptide Dendrimers Targeting the Fucose-Specific Lectin LecB. *Chem Biol* **2008**, *15* (12), 1249–1257.
 - (38) Bernardi, A.; Jiménez-Barbero, J.; Casnati, A.; De Castro, C.; Darbre, T.; Fieschi, F.; Finne, J.; Funken, H.; Jaeger, K.-E.; Lahmann, M.; et al. Multivalent Glycoconjugates as Anti-Pathogenic Agents. *Chem Soc Rev* **2013**, *42* (11), 4709–4727.
 - (39) Marotte, K.; Sabin, C.; Prévile, C.; Moumé-Pymbock, M.; Wimmerová, M.; Mitchell, E. P.; Imberty, A.; Roy, R. X-Ray Structures and Thermodynamics of the Interaction of PA-IIL from *Pseudomonas aeruginosa* with Disaccharide Derivatives. *ChemMedChem* **2007**, *2* (9), 1328–1338.
 - (40) Andreini, M.; Anderluh, M.; Audfray, A.; Bernardi, A.; Imberty, A. Monovalent and Bivalent N-Fucosyl Amides as High Affinity Ligands for *Pseudomonas aeruginosa* PA-IIL Lectin. *Carbohydr. Res.* **2010**, *345* (10), 1400–1407.
 - (41) Hauck, D.; Joachim, I.; Frommeyer, B.; Varrot, A.; Philipp, B.; Möller, H. M.; Imberty, A.; Exner, T. E.; Titz, A. Discovery of Two Classes of Potent Glycomimetic Inhibitors of *Pseudomonas aeruginosa* LecB with Distinct Binding Modes. *ACS Chem Biol* **2013**, *8* (8), 1775–1784.
 - (42) Sommer, R.; Exner, T. E.; Titz, A. A Biophysical Study with Carbohydrate Derivatives Explains the Molecular Basis of Monosaccharide Selectivity of the *Pseudomonas aeruginosa* Lectin LecB. *PLoS One* **2014**, *9* (11), e112822.
 - (43) Sommer, R.; Wagner, S.; Rox, K.; Varrot, A.; Hauck, D.; Wamhoff, E.-C.; Schreiber, J.; Ryckmans, T.; Brunner, T.; Rademacher, C.; et al. Glycomimetic, Orally Bioavailable LecB Inhibitors Block Biofilm Formation of *Pseudomonas aeruginosa*. *J. Am. Chem. Soc.* **2017**, *140* (7), 2537–2545.
 - (44) Zinger-Yosovich, K.; Sudakevitz, D.; Imberty, A.; Garber, N. C.; Gilboa-Garber, N. Production and Properties of the Native Chromobacterium violaceum Fucose-Binding Lectin (CV-IIL) Compared to Homologous Lectins of *Pseudomonas Aeruginosa* (PA-IIL) and *Ralstonia solanacearum* (RS-IIL). *Microbiology* **2006**, *152* (2), 457–463.

-
- (45) Lameignere, E.; Malinovská, L.; Sláviková, M.; Duchaud, E.; Mitchell, E. P.; Varrot, A.; Sedo, O.; Imberty, A.; Wimmerová, M. Structural Basis for Mannose Recognition by a Lectin from Opportunistic Bacteria *Burkholderia cenocepacia*. *Biochem J* **2008**, *411* (2), 307–318.
- (46) Šulák, O.; Cioci, G.; Delia, M.; Lahmann, M.; Varrot, A.; Imberty, A.; Wimmerová, M. A TNF-like Trimeric Lectin Domain from *Burkholderia cenocepacia* with Specificity for Fucosylated Human Histo-Blood Group Antigens. *Structure* **2010**, *18* (1), 59–72.
- (47) Sudakevitz, D.; Imberty, A.; Gilboa-Garber, N. Production, Properties and Specificity of a New Bacterial L-Fucose-and D-Arabinose-Binding Lectin of the Plant Aggressive Pathogen *Ralstonia solanacearum*, and Its Comparison to Related Plant and Microbial Lectins. *J. Biochem.* **2002**, *132* (2), 353–358.
- (48) Beshr, G.; Sommer, R.; Hauck, D.; Siebert, D. C. B.; Hofmann, A.; Imberty, A.; Titz, A. Development of a Competitive Binding Assay for the *Burkholderia cenocepacia* Lectin BC2L-A and Structure Activity Relationship of Natural and Synthetic Inhibitors. *Medchemcomm* **2016**, *7* (3), 519–530.
- (49) Pifferi, C.; Goyard, D.; Gillon, E.; Imberty, A.; Renaudet, O. Synthesis of Mannosylated Glycodendrimers and Evaluation against BC2L-A Lectin from *Burkholderia cenocepacia*. *Chempluschem* **2017**, *82* (3), 390–398.
- (50) Csávás, M.; Malinovská, L.; Perret, F.; Gyurkó, M.; Illyés, Z. T.; Wimmerová, M.; Borbás, A. Tri-and Tetravalent Mannoclusters Cross-Link and Aggregate BC2L-A Lectin from *Burkholderia cenocepacia*. *Carbohydr. Res.* **2017**, *437*, 1–8.
- (51) Šulák, O.; Cioci, G.; Lameignère, E.; Balloy, V.; Round, A.; Gutsche, I.; Malinovská, L.; Chignard, M.; Kosma, P.; Aubert, D. F.; et al. *Burkholderia cenocepacia* BC2L-C Is a Super Lectin with Dual Specificity and Proinflammatory Activity. *PLoS Pathog.* **2011**, *7* (9), e1002238.
- (52) *The Bacterial Challenge: Time to React*; 2009.
- (53) Roy, R.; Tiwari, M.; Donelli, G.; Tiwari, V. Strategies for Combating Bacterial Biofilms: A Focus on Anti-Biofilm Agents and Their Mechanisms of Action. *Virulence* **2017**, No. just-accepted, 0.
- (54) Reddy, M. R.; Parrill, A. L. Overview of Rational Drug Design; ACS Publications, 1999.
- (55) Barnard, A.; Smith, D. K. Self-Assembled Multivalency: Dynamic Ligand Arrays for High-Affinity Binding. *Angew. Chemie Int. Ed.* **2012**, *51* (27), 6572–6581.
- (56) Tomlin, K. L.; Coll, O. P.; Ceri, H. Interspecies Biofilms of *Pseudomonas aeruginosa* and *Burkholderia cepacia*. *Can. J. Microbiol.* **2001**, *47* (10), 949–954.
- (57) Hofmann, A.; Sommer, R.; Hauck, D.; Stifel, J.; Göttker-Schnetmann, I.; Titz, A. Synthesis of Mannoheptose Derivatives and Their Evaluation as Inhibitors of the Lectin LecB from the Opportunistic Pathogen *Pseudomonas aeruginosa*. *Carbohydr Res* **2015**, *412*, 34–42.
- (58) Cabezas-Cruz, A.; De La Fuente, J. Immunity to α -Gal: The Opportunity for Malaria and Tuberculosis Control. *Front. Immunol.* **2017**, *8*, 1733.
- (59) Sahagun, G.; Moore, S. A.; Fabry, Z.; Schelper, R. L.; Hart, M. N. Purification of Murine Endothelial Cell Cultures by Flow Cytometry Using Fluorescein-Labeled *Griffonia simplicifolia* Agglutinin. *Am. J. Pathol.* **1989**, *134* (6), 1227.

- (60) Li, H.; Nomura, S.; Mizuno, N. Binding of the Isolectin I-B4 from Griffonia simplicifolia to the General Visceral Afferents in the Vagus Nerve: A Light-and Electron-Microscope Study in the Rat. *Neurosci. Lett.* **1997**, 222 (1), 53–56.
- (61) Bendelac, A.; Zhou, D.; Teyton, L.; Savage, P. Methods of Activating NKT Cells. *U.S. Patent* 7,998,739. 16 Aug. **2011**.
- (62) Sanders, W. E.; Sanders, C. C. Enterobacter Spp.: Pathogens Poised to Flourish at the Turn of the Century. *Clin. Microbiol. Rev.* **1997**, 10 (2), 220–241.
- (63) Streit, J. M.; Jones, R. N.; Sader, H. S.; Fritsche, T. R. Assessment of Pathogen Occurrences and Resistance Profiles among Infected Patients in the Intensive Care Unit: Report from the SENTRY Antimicrobial Surveillance Program (North America, 2001). *Int. J. Antimicrob. Agents* **2004**, 24 (2), 111–118.
- (64) Hidron, A. I.; Edwards, J. R.; Patel, J.; Horan, T. C.; Sievert, D. M.; Pollock, D. A.; Fridkin, S. K.; others. Antimicrobial-Resistant Pathogens Associated with Healthcare-Associated Infections: Annual Summary of Data Reported to the National Healthcare Safety Network at the Centers for Disease Control and Prevention, 2006–2007. *Infect. Control Hosp. Epidemiol.* **2008**, 29 (11), 996–1011.

5. SUPPORTING INFORMATION

5.1. SUPPORTING INFORMATION FOR SUBCHAPTER 3.1

Table S1. Testing of LecB stability at different concentration of DMSO by determine the IC₅₀ value of compound 2 at different DMSO concentration. This experiment was performed once,

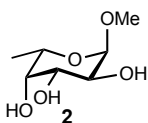
	LecB IC ₅₀ [μM]			
	0 % DMSO	1 % DMSO	2 % DMSO	5 % DMSO
	0.79	0.92	0.51	0.57

Table S2. List of compounds of test plate with their DMSO stocks. n.p. : the concentration of compound was not provided.

	Compound	Concentration in DMSO stock		Compound	Concentration in DMSO stock
1	Actinomycin D	1 mM	25	Quercetin	3 mg/ml
2	Acyclovir	0.5 mg/ml	26	Rapamycin	11 μM
3	Amphotericin B	0.2 mg/mL	27	Resveratrol	0.1 mg/ml
4	Ampicillin	1 mg/ml	28	Rifampicin	1 mg/ml
5	Anisomycin	45 μM	29	Staurosporine	0.05 mg/ml
6	Antimycin A	0.1 mg/ml	30	Sulfamethazin	0.1 mg/ml
7	Bay 11-7085	1 mg/mL	31	Sulfamethoxazol	2 mg/ml
8	Brefeldin A	1100 μM	32	Tetrazyklin	0.1 mg/ml
9	Cisplatin	0.5 mg/ml	33	Trichostatin	1 mM
10	Colchicine	10 mM	34	Zanamivir	0.5 mg/ml
11	Cycloheximide	n.p.	35	WTE (A-A-D-H-A-A-C)	2mM
12	Cytochalasin D	500 μM	36	WTE (A-A-D-E-A-A-C)	2 mM
13	Dexamethasone	1 mM	37	WTE (A-A-H-F-A-A-C)	2 mM
14	Doxorubicin	1100 μM	38	WTE (A-A-I-T-A-A-C)	2 mM
15	Erythromycin	0.1 mg/ml	39	WTE (A-A-K-W-A-A-C)	2 mM
16	Etoposide	1 mM	40	WTE (A-A-R-Q-A-A-C)	2 mM
17	Fluconazol	0.2 mg/ml	41	WTE (A-A-W-E-A-A-C)	2 mM
18	Fludioxonil	1 mg/ml	42	WTE (A-A-W-R-A-A-C)	2 mM
19	Hydroxyurea	5 mg/ml	43	WTE (A-A-N-K-A-A-C)	2 mM
20	Mevastatin	1200 μM	44	PD98059	10 mM
21	Okadaic acid	80 μM	45	SB203580	1 mg/ml
22	Oligomycin	5 mM	46	Simvastatin	0.8 mM
23	PDTC	0.1 mg/ml	47	Chloramphenicol	2 mg/ml
24	Purvalanol A	n.p.	48	Luciferase inhibitor	5 mg/ml

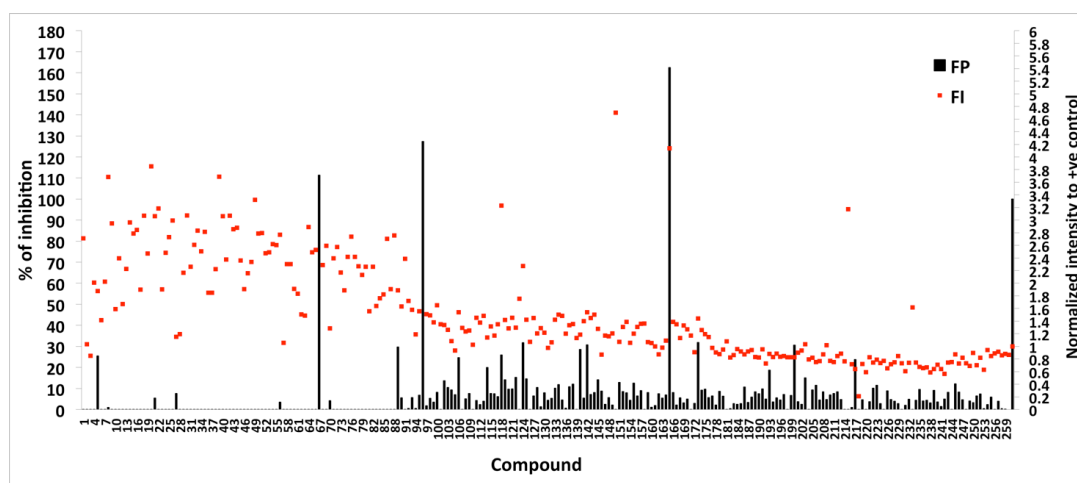


Figure S1. Screening of pure myxobacteria secondary metabolites at 500 μM using a competitive binding assay based on fluorescence polarization. Black columns represent the calculated percentage of inhibition; red squares represent the normalized fluorescence intensity signals to the signal of positive control. The acceptable fluorescence intensity data should have $0.8 < \text{fluorescence intensity} < 1.2$. Each column and square represent the average of results from three different wells. +ve control is L-fucose; -ve control is LecB with tracer **1** and without inhibitors.

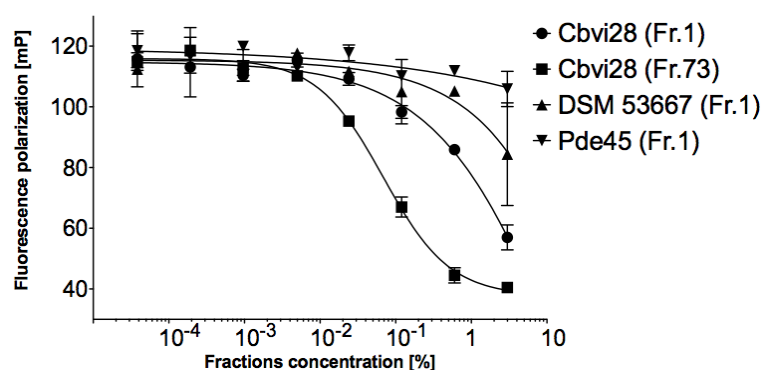


Figure S2. Validation of inhibitory effect of active fractions in myxobacterial extracts to LecB from initial screen by generating their concentration-dependent inhibition curves. Standard deviations were obtained from triplicates on one plate. Fr: fraction.

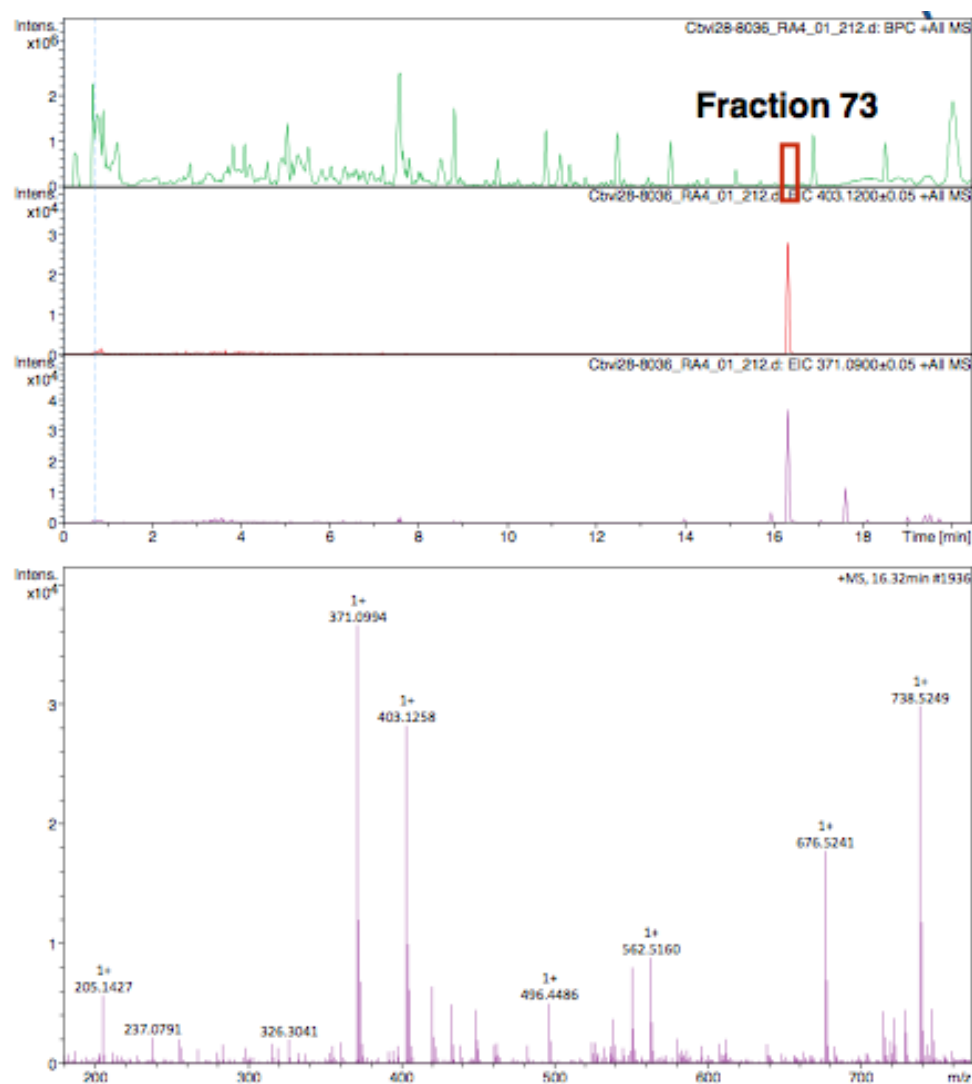


Figure S3. LC-MS spectrum at fraction 73 in fractionation of strain **B** extract.

Table S3. Media and their ingredients which were used in strain **B** cultivation.

		Media				
		CLF	CYH	P	POL	TS
Ingredients		0.4 % Fructose	CY:	0.2 % Peptone	0.3 % Starch	0.4 % Starch
		0.6 % Glucose		0.8 % Starch	0.3 % Probion	1 % Trypton
		1 % Skim milk	0.3 % Casiton	0.4 % Probion	0.05 % CaCl ₂	0.2 % MgSO ₄
		0.2 % Yeast extract	0.1 % Yeast extract	0.2 % Yeast extract	0.2 % MgSO ₄	100 mM
		0.1 % CaCl ₂	0.1 % CaCl ₂	0.1 % CaCl ₂	50 mM HEPES	HEPES
		0.1 % MgSO ₄	50 mM HEPES	0.1 % MgSO ₄		
		50 mM HEPES		100 mM HEPES	pH = 7.2	pH = 7.2
		8 mg/L EDTA-iron	H :	8 mg/L EDTA-iron		
			0.2 % Soy flour	pH = 7.5		
	pH = 7		0.2 % Glucose			
			0.8 % Starch			
			0.2 % Yeast extract			
			0.1 % CaCl ₂			
			0.1 % MgSO ₄			
			50 mM HEPES			
			8 mg/L EDTA-iron			
			pH = 7			

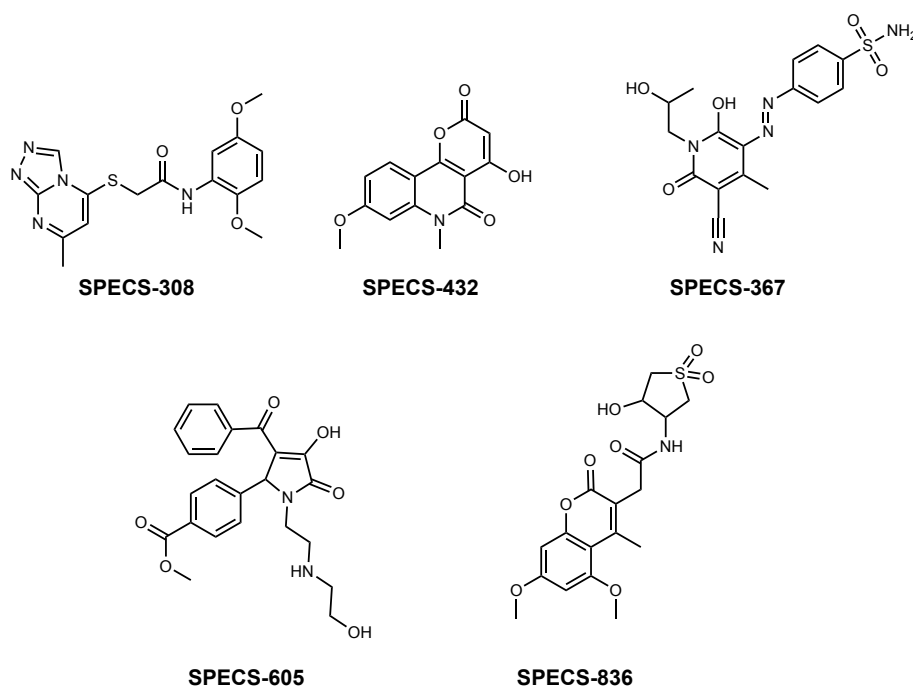


Figure S4. LecB hits from SPECS library, which were identified by screening at 500 μM .

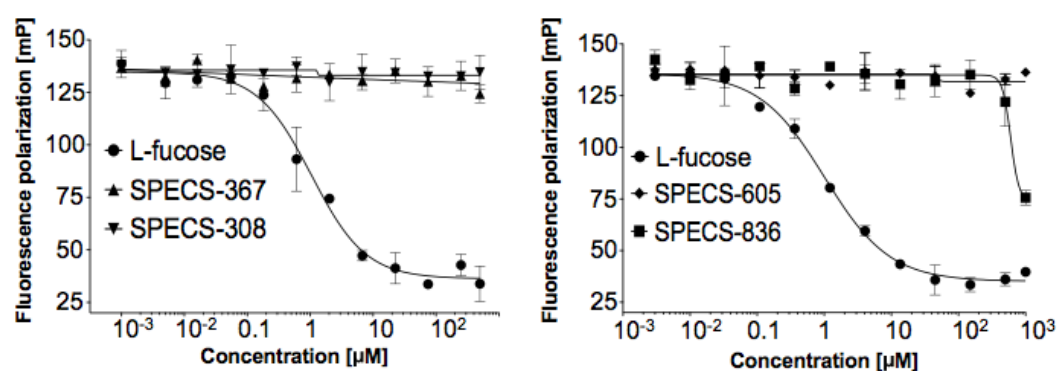
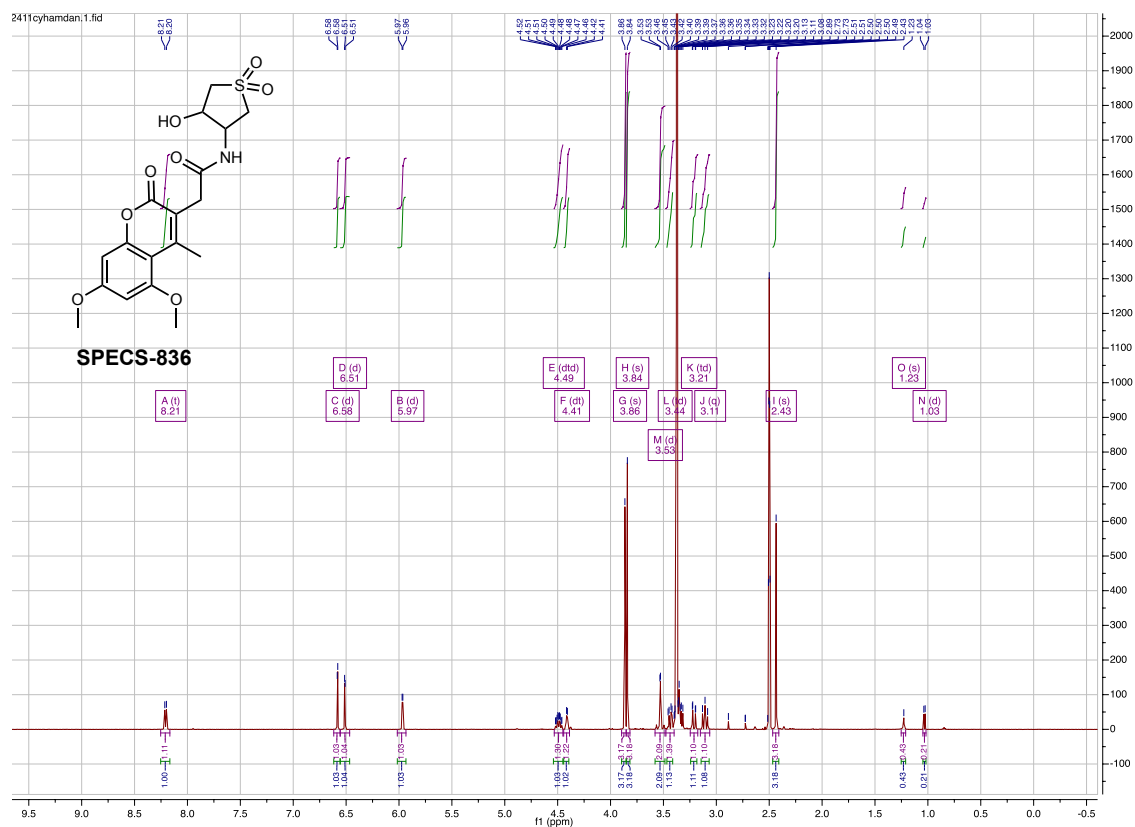


Figure S5. Competitive inhibition of the binding of **1** to LecB with SPECS hits. **Left:** concentration-dependent inhibition curves of **SPECS-367** and **-308** (max conc. is 500 μM). **Right:** concentration-dependent inhibition curves of **SPECS-605** and **-836** (max conc. is 1000 μM). Standard deviations were obtained from triplicates on one plate.

Figure S6. ¹H NMR of SPECS836

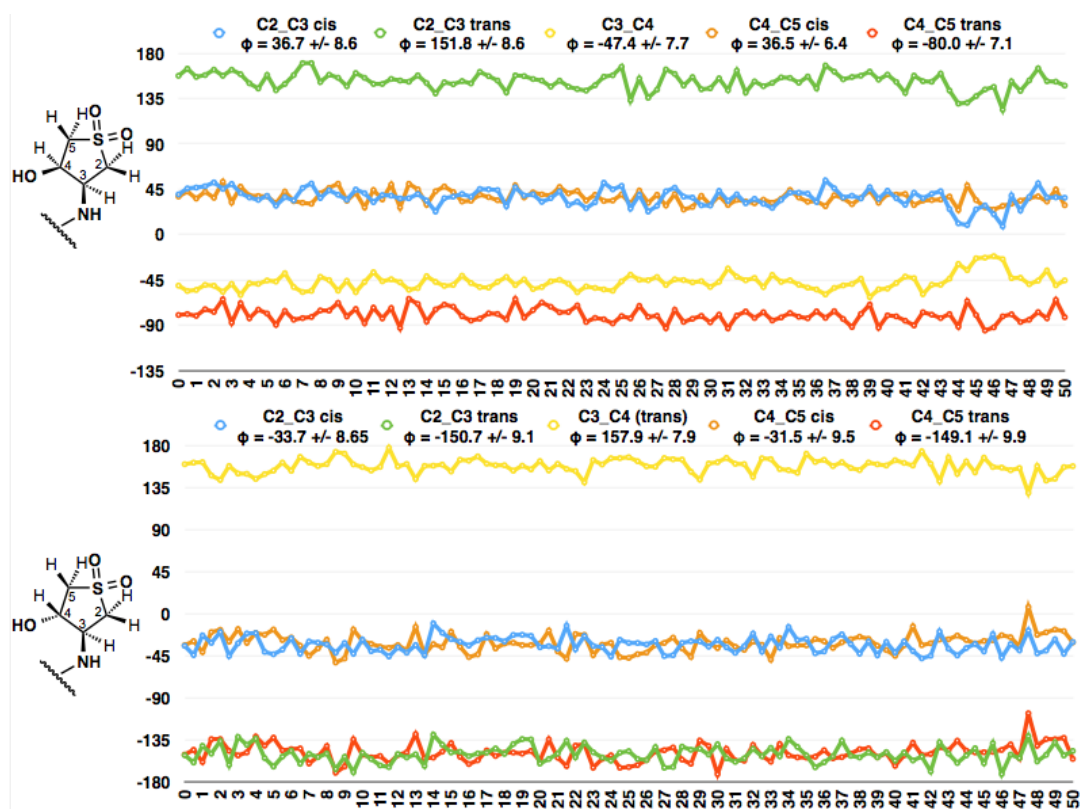


Figure S7. Molecular dynamics study of **SPECS-836** in DMSO. The dihedral angles at the tetrahydrothiophene ring of **SPECS-836** were recorded each 0.5 sec for 50 sec .

Display Report

Analysis Info

Analysis Name D:\Data\CBCH\Ghamdan\170123_GB_OTAVA_116_BA3_01_5447.d

Method 5447.m

Sample Name 170123_GB_OTAVA_116

Comment

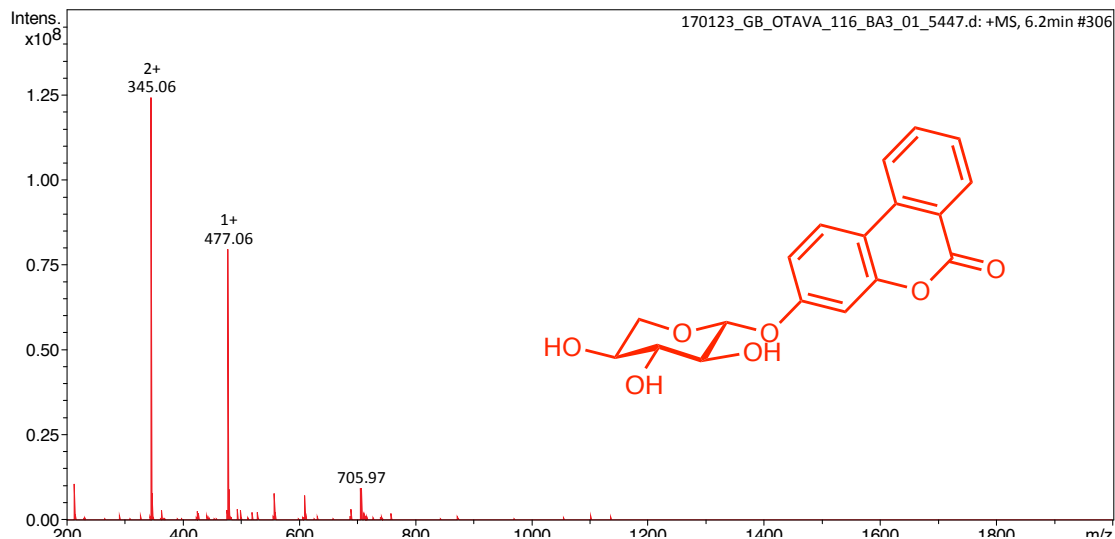
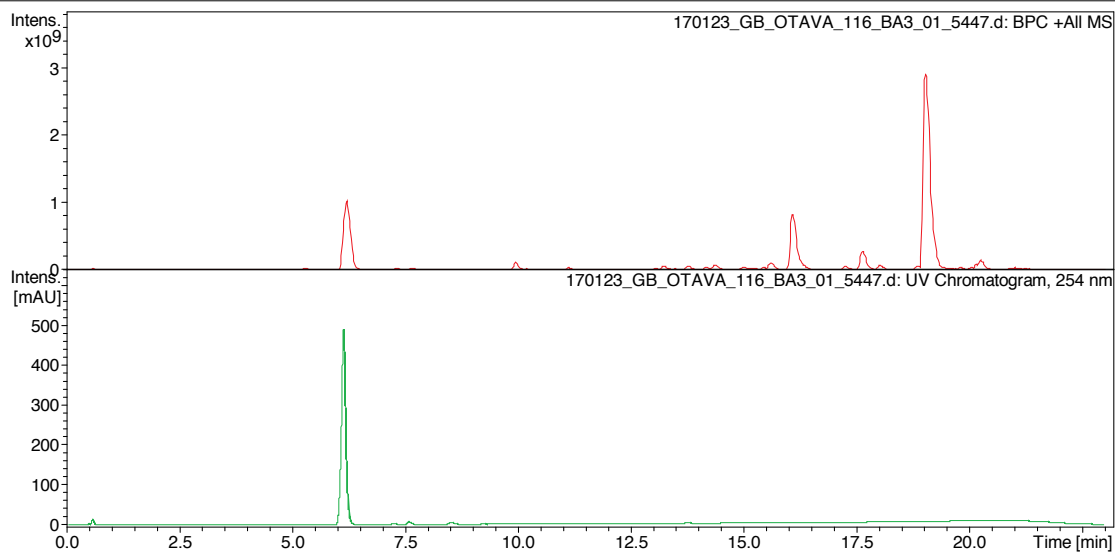
Acquisition Date 1/23/2017 5:06:21 PM

Operator cbch

Instrument amaZon SL

Acquisition Parameter

Ion Source Type	ESI	Ion Polarity	Positive	Alternating Ion Polarity	off
Mass Range Mode	Enhanced Resolution	Scan Begin	200 m/z	Scan End	2000 m/z
Accumulation Time	7088 μ s	RF Level	63 %	Trap Drive	51.4
SPS Target Mass	400 m/z	Averages	5 Spectra	n/a	n/a



Bruker Compass DataAnalysis 4.2

printed: 1/24/2017 9:34:25 AM

by: cbch

Page 1 of 1

Figure S8. LC-MS spectrum of compound OTAVA-116.

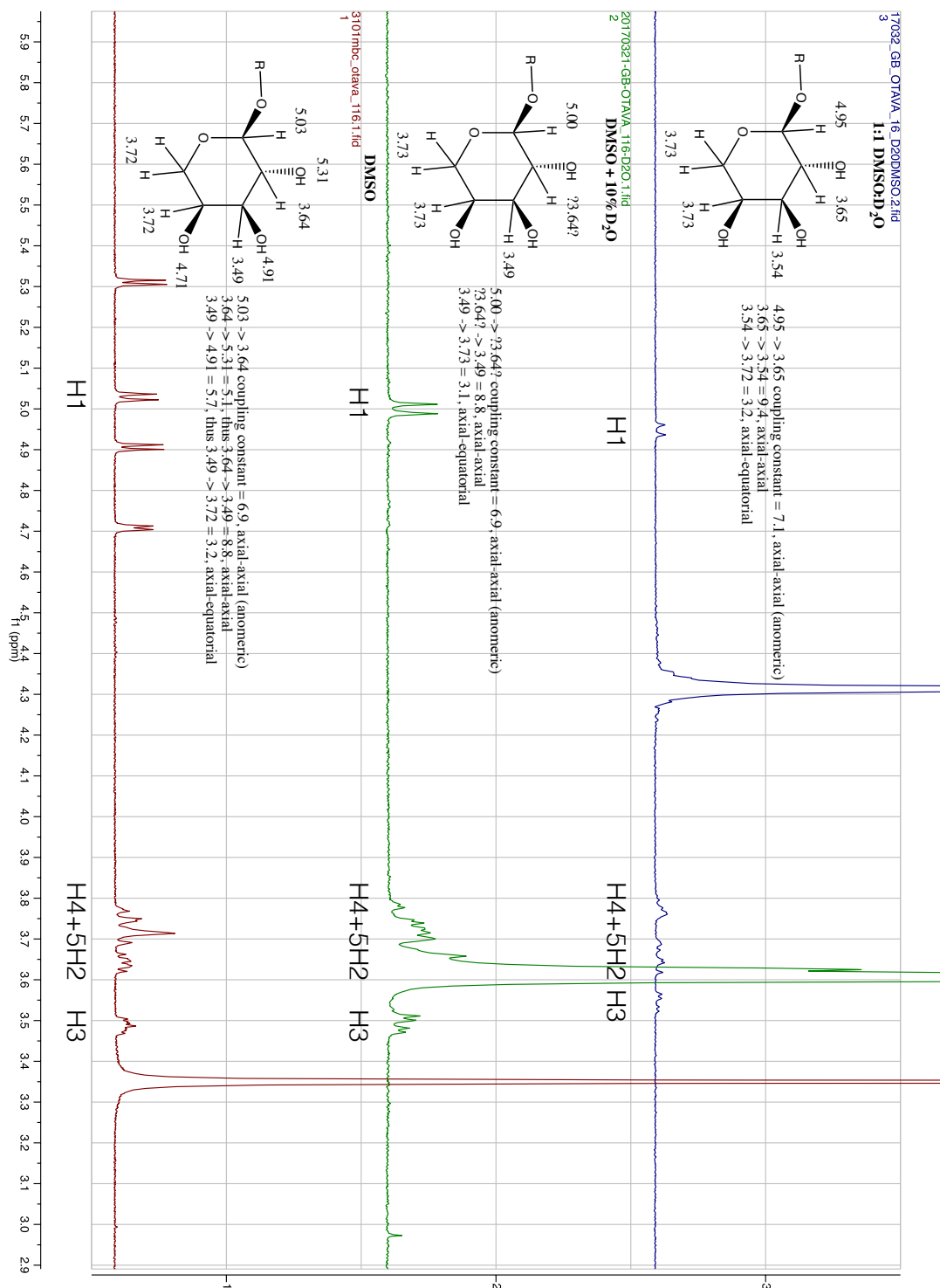
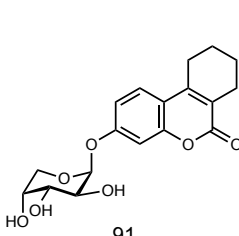
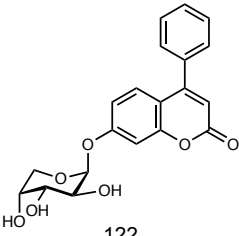
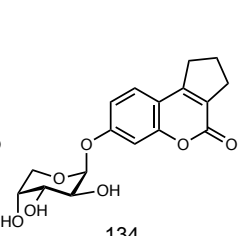
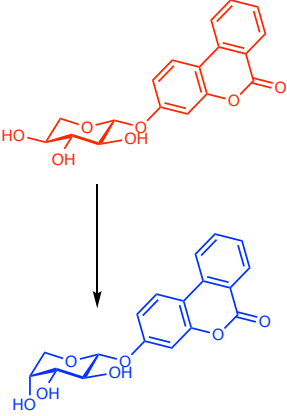
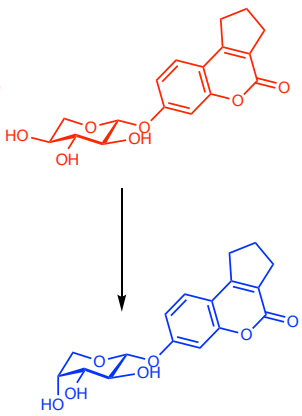
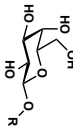
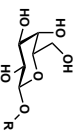
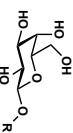
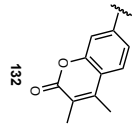
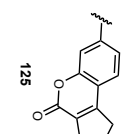
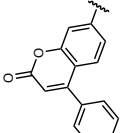
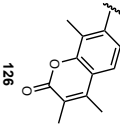
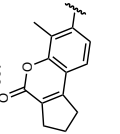
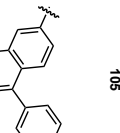
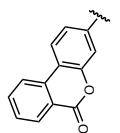
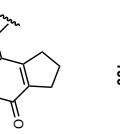
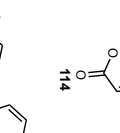
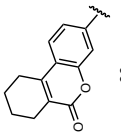
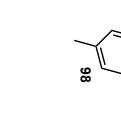
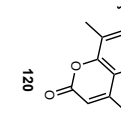
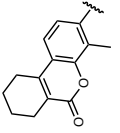
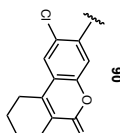
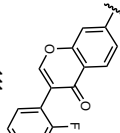


Figure S9. ¹H NMR measurements of compound **OTAVA-116** in different solvents (1:1 DMSO:D₂O, DMSO + 10 % D₂O, DMSO). The analysis was done by Dr. Calvert.

Table S4. Competitive binding assay of identified OTAVA hits with LecB in the initial screen. The red coloured compounds are based on D-xylose which their structures were characterized and showed compounds based on L-arabinose.

	 91	 122	 134
LecB IC ₅₀ [μM]	6.7	9.4	11.3
<hr/>			
	 116	 112	
LecB IC ₅₀ [μM]	7.7	7.4	

A

		<i>Leca</i> IC ₅₀ [μM]	Rel. potency to Me-a-D-gal			<i>Leca</i> IC ₅₀ [μM]	Rel. potency to Me-a-D-gal			<i>Leca</i> IC ₅₀ [μM]	Rel. potency to Me-a-D-gal
	20.3	5.2		25.7	4.1		28.6	3.7			
	45.8	2.2		42.6	2.5		34.5	3.0			
	149.5	0.7		n.d.	n.d.		15.7	6.7			
	20.9	5.0		190.5	0.6		22.5	4.7			
	27.7	3.8									
	37.1	2.8					423.9	0.2			

B

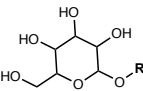
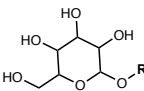
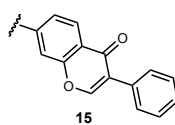
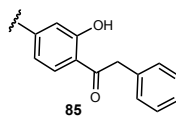
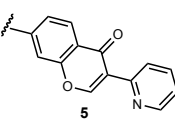
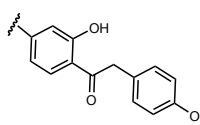
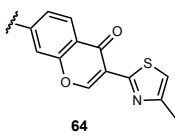
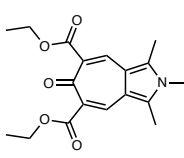
	LecA IC ₅₀ [μM]	Rel. potency to Me α-D-gal		LecA IC ₅₀ [μM]	Rel. potency to Me α-D-gal
 15	30.6	3.4	 85	30.0	3.5
 5	21.7	4.8	 52	29.0	3.6
 64	37.6	2.8	<div>Compound</div>  51	<div>LecA IC₅₀ [μM]</div> n.b	

Table S6. List of tested compounds in glycomimetic-focused library (OTAVA) and their chemical names.

cpd#	Chemical name
1	3,7-bis(methoxycarbonyl)-2,6-dioxobicyclo[3.3.1]nonane-1,5-dicarboxylic acid
2	1-[(3aR,5R,6S,6aR)-6-[(4-ethoxyphenyl)methoxy]-2,2-dimethyl-tetrahydro-2H-furo[2,3-d][1,3]dioxol-5-yl]ethane-1,2-diol
3	(2R)-7-{[(2S,3R,4S,5S,6R)-4,5-dihydroxy-6-(hydroxymethyl)-3-[(2S,3R,4R,5R,6S)-3,4,5-trihydroxy-6-methyloxan-2-yl]oxy}oxan-2-yl]oxy}-5-hydroxy-2-(4-hydroxyphenyl)-3,4-dihydro-2H-1-benzopyran-4-one
4	3-{[2-(dimethylamino)ethyl]amino}-4-hydroxy-1λ-thiolane-1,1-dione hydrochloride
5	3-(pyridin-2-yl)-7-{[3,4,5-trihydroxy-6-(hydroxymethyl)oxan-2-yl]oxy}-4H-chromen-4-one
6	N-{3,4,5,14-tetramethoxy-13-oxotricyclo[9.5.0.0?]?]hexadeca-1(16),2,4,6,11,14-hexaen-10-yl}acetamide
7	3,6-dimethyl 4-[(3-{[3-acetamido-4,5-dihydroxy-6-(hydroxymethyl)oxan-2-yl]oxy}phenyl)amino]quinoline-3,6-dicarboxylate
8	3-(4-chlorophenyl)-7-{[3,4,5-trihydroxy-6-(hydroxymethyl)oxan-2-yl]oxy}-4H-chromen-4-one
9	3-(7,8-dimethoxy-2-methyl-4-oxo-3,4-dihydro-2H-1-benzopyran-2-yl)propanoic acid
10	1-(3-{4-[3-(4-carbamoylpiperidin-1-yl)-2-hydroxypropoxy]phenoxy}-2-hydroxypropyl)piperidine-4-carboxamide
11	(2S)-2-[(4-{[(1S)-1-carboxy-2-phenylethyl]carbamoyl}piperazine-1-carbonyl)amino]-3-phenylpropanoic acid
12	3-hydroxy-4-[(2-methoxyethyl)amino]-1λ-thiolane-1,1-dione
13	3-{[2-(furan-2-yl)ethyl]amino}-4-hydroxy-1λ-thiolane-1,1-dione
14	2-(4,5-dimethoxy-3-oxo-1,3-dihydro-2-benzofuran-1-yl)acetic acid
15	3-phenyl-7-{[3,4,5-trihydroxy-6-(hydroxymethyl)oxan-2-yl]oxy}-4H-chromen-4-one
16	2-[(5Z)-5-[(4-methoxyphenyl)methylidene]-4-oxo-2-sulfanylidene-1,3-thiazolidin-3-yl]-N-[2,4,5-trihydroxy-6-(hydroxymethyl)oxan-3-yl]acetamide
17	3-{[3-(dimethylamino)propyl]amino}-4-hydroxy-1λ-thiolane-1,1-dione
18	3,6-dimethyl 4-[(4-{[3-acetamido-4,5-dihydroxy-6-(hydroxymethyl)oxan-2-yl]oxy}phenyl)amino]quinoline-3,6-dicarboxylate
19	2-methyl-3-(pyridin-2-yl)-7-{[3,4,5-trihydroxy-6-(hydroxymethyl)oxan-2-yl]oxy}-4H-chromen-4-one
20	1-(3,5-dimethoxybenzoyl)piperidine-3-carboxylic acid
21	2-(4-carbamoylpiperidin-1-yl)-2-oxoacetic acid
22	tert-butyl 4-[(3-methoxy-3-oxopropyl)carbamoyl]piperazine-1-carboxylate
23	1-[(tert-butoxy)carbonyl]piperidine-4-carboxylic acid
24	3-hydroxy-4-[4-(2-hydroxyethyl)piperazin-1-yl]-1λ-thiolane-1,1-dione
25	2-(hydroxymethyl)-6-(naphthalen-2-yloxy)oxane-3,4,5-triol
26	3-(1,1-dioxo-1λ-thiolan-3-yl)-1-methyl-1-(3-methyl-1,1-dioxo-1λ-thiolan-3-yl)urea
27	2-(3,4,5-trihydroxyoxan-2-yl)-2,3,4,5-tetrahydro-1,2,4-triazine-3,5-dione
28	3-{[2-(dimethylamino)ethyl]amino}-4-hydroxy-1λ-thiolane-1,1-dione
29	N-[2-(4-{[2-(4-chlorophenyl)quinazolin-4-yl]amino}phenoxy)-4,5-dihydroxy-6-(hydroxymethyl)oxan-3-yl]acetamide
30	5-hydroxy-7-(octyloxy)-3-(4-{[3,4,5-trihydroxy-6-(hydroxymethyl)oxan-2-yl]oxy}phenyl)-4H-chromen-4-one

31	4-amino-7-methoxy-2,3,4,5-tetrahydro-1-benzoxepin-5-ol hydrochloride
32	ethyl 2-(4-carbamoylpiperidin-1-yl)acetate
33	4-(3-Methoxy-propylamino)-1,1-dioxo-tetrahydro-1lambda*6*-thiophen-3-ol
34	2-{1-[(tert-butoxy)carbonyl]-4-hydroxypiperidin-4-yl}acetic acid
35	3-hydroxy-4-{[3-(morpholin-4-yl)propyl]amino}-1lambda-thiolane-1,1-dione hydrochloride
36	5,7-dihydroxy-3-(4-{[(2S,3R,4S,5S,6R)-3,4,5-trihydroxy-6-(hydroxymethyl)oxan-2-yl]oxy}phenyl)-4H-chromen-4-one
37	3-hydroxy-4-[(3-methoxypropyl)amino]-1lambda-thiolane-1,1-dione hydrochloride
38	9-[3,4-dihydroxy-5-(hydroxymethyl)oxolan-2-yl]-8-(methylamino)-6,9-dihydro-1H-purin-6-one
39	3-(2-fluorophenyl)-7-{[3,4,5-trihydroxy-6-(hydroxymethyl)oxan-2-yl]oxy}-4H-chromen-4-one
40	methyl 7,8-dichloro-4-[(4-{[3-acetamido-4,5-dihydroxy-6-(hydroxymethyl)oxan-2-yl]oxy}phenyl)amino]quinoline-3-carboxylate
41	3-(4-fluorophenyl)-7-{[3,4,5-trihydroxy-6-(hydroxymethyl)oxan-2-yl]oxy}-4H-chromen-4-one
42	1-(2-hydroxy-4-{[3,4,5-trihydroxy-6-(hydroxymethyl)oxan-2-yl]oxy}phenyl)-2-(1,3-thiazol-4-yl)ethan-1-one
43	(4R,6R)-3-amino-6-(hydroxymethyl)oxane-2,4,5-triol hydrochloride
44	3-[5-amino-4-(4-methyl-1,3-thiazol-2-yl)-3-oxo-2,3-dihydro-1H-pyrrol-1-yl]-4-hydroxy-1lambda-thiolane-1,1-dione
45	5,5-dimethyl 2,2-dimethyl-1,3-dioxane-5,5-dicarboxylate
46	(1S,2R)-2-(4-[(1R,2S)-2-carboxycyclohexaneamido]phenyl)carbamoylcyclohexane-1-carboxylic acid
47	3-hydroxy-4-{[2-(morpholin-4-yl)ethyl]amino}-1lambda-thiolane-1,1-dione
48	4-[N-(4-methoxyphenyl)acetamido]-1,1-dioxo-1lambda-thiolan-3-yl acetate
49	3-(2,3-dihydro-1,4-benzodioxin-6-yl)-7-{[2,3,4-trihydroxy-5-(hydroxymethyl)cyclohexyl]oxy}-4H-chromen-4-one
50	3-(4-ethylbenzenesulfonyl)-4-[(2-methoxyethyl)amino]-1lambda-thiolane-1,1-dione
51	5,7-diethyl 1,2,3-trimethyl-6-oxo-2H,6H-cyclohepta[c]pyrrole-5,7-dicarboxylate
52	1-(2-hydroxy-4-{[3,4,5-trihydroxy-6-(hydroxymethyl)oxan-2-yl]oxy}phenyl)-2-(4-methoxyphenyl)ethan-1-one
53	3-(2-methyl-1,3-thiazol-4-yl)-7-{[3,4,5-trihydroxy-6-(hydroxymethyl)oxan-2-yl]oxy}-4H-chromen-4-one
54	6,7-dimethoxy-5-oxo-2H,3H,5H,9bH-[1,3]thiazolo[2,3-a]isoindole-3-carboxylic acid
55	1,3-diethyl 2-(1,1-dioxo-1lambda-thiolan-3-yl)propanedioate
56	1-tert-butyl 3-methyl 4-oxopyrrolidine-1,3-dicarboxylate
57	1-[(6-methyl-2,4-dioxo-1,2,3,4-tetrahydropyrimidin-5-yl)sulfonyl]piperidine-3-carboxylic acid
58	3-hydroxy-4-[(3-hydroxypropyl)amino]-1lambda-thiolane-1,1-dione
59	4-[N-(4-chlorophenyl)acetamido]-1,1-dioxo-1lambda-thiolan-3-yl acetate
60	2-amino-8-bromo-9-[3,4-dihydroxy-5-(hydroxymethyl)oxolan-2-yl]-6,9-dihydro-1H-purin-6-one
61	4-(2-{[(3S,4R)-4-(4-ethylbenzenesulfonyl)-1,1-dioxo-1lambda-thiolan-3-yl]amino}ethyl)benzene-1-sulfonamide
62	3-[(6-tert-butyl-3-carbamoyl-4,5,6,7-tetrahydro-1-benzothiophen-2-yl)carbamoyl]propanoic acid
63	3-(4-bromophenyl)-7-{[3,4,5-trihydroxy-6-(hydroxymethyl)oxan-2-yl]oxy}-4H-chromen-4-one

64	3-(4-methyl-1,3-thiazol-2-yl)-7-{[3,4,5-trihydroxy-6-(hydroxymethyl)oxan-2-yl]oxy}-4H-chromen-4-one
65	methyl (2R,3S)-2-[(4-{[(2S,3R)-1-methoxy-3-methyl-1-oxopentan-2-yl]carbamoyl}piperazine-1-carbonyl)amino]-3-methylpentanoate
66	2-(1,1-dioxo-1λ-thiolan-3-yl)-N,N'-bis(2-hydroxyethyl)propanediamide
67	1-tert-butyl 4-ethyl 3-oxopiperidine-1,4-dicarboxylate
68	5-hydroxy-2-(4-methoxyphenyl)-8-(3-methylbut-2-en-1-yl)-7-{[(2S,3R,4S,5S,6R)-3,4,5-trihydroxy-6-(hydroxymethyl)oxan-2-yl]oxy}-3-{[(2S,3R,4R,5R,6S)-3,4,5-trihydroxy-6-methyloxan-2-yl]oxy}-4H-chromen-4-one
69	N-[6-(2-chlorophenoxy)-2-(furan-2-yl)-8-hydroxy-hexahydro-2H-pyrano[3,2-d][1,3]dioxin-7-yl]acetamide
70	3-[(3-acetylphenyl)amino]-4-hydroxy-1λ-thiolane-1,1-dione
71	8-bromo-9-[3,4-dihydroxy-5-(hydroxymethyl)oxolan-2-yl]-6,9-dihydro-1H-purin-6-one
72	methyl 7,8-dichloro-4-[(3-{[3-acetamido-4,5-dihydroxy-6-(hydroxymethyl)oxan-2-yl]oxy}phenyl)amino]quinoline-3-carboxylate
73	2-methyl-4-(3,4,5-trimethoxybenzoyl)morpholine
74	5-hydroxy-7-methoxy-3-(4-{[3,4,5-trihydroxy-6-(hydroxymethyl)oxan-2-yl]oxy}phenyl)-4H-chromen-4-one
75	3-(4-methoxyphenoxy)-7-{[3,4,5-trihydroxy-6-(hydroxymethyl)oxan-2-yl]oxy}-4H-chromen-4-one
76	(2S)-2-[(4-{[(1S)-1-carboxy-2-methylpropyl]carbamoyl}piperazine-1-carbonyl)amino]-3-methylbutanoic acid
77	3-[4-(4-chlorophenyl)-4-hydroxypiperidin-1-yl]-4-hydroxy-1λ-thiolane-1,1-dione
78	2-{1-[(3,5-dimethoxyphenyl)methyl]-3-oxopiperazin-2-yl}acetic acid
79	(2S)-5-hydroxy-2-(3-hydroxy-4-methoxyphenyl)-7-[(3,4,5-trihydroxy-6-{[(3,4,5-trihydroxy-6-methyloxan-2-yl)oxy]methyl}oxan-2-yl)oxy]-3,4-dihydro-2H-1-benzopyran-4-one
80	3-hydroxy-4-[(2-methoxyethyl)amino]-1λ-thiolane-1,1-dione hydrochloride
81	3,4-dimethyl 2-(2-methoxyacetamido)-4H,5H,6H-cyclopenta[b]thiophene-3,4-dicarboxylate
82	3-(2,3-dihydro-1,4-benzodioxin-6-yl)-7-{[3,4,5-trihydroxy-6-(hydroxymethyl)oxan-2-yl]oxy}-4H-chromen-4-one
83	N-[4,5-dihydroxy-6-(hydroxymethyl)-2-(3-{[2-(4-methylphenyl)quinazolin-4-yl]amino}phenoxy)oxan-3-yl]acetamide
84	N-[2-(4-acetylphenoxy)-4,5-dihydroxy-6-(hydroxymethyl)oxan-3-yl]acetamide
85	1-(2-hydroxy-4-{[3,4,5-trihydroxy-6-(hydroxymethyl)oxan-2-yl]oxy}phenyl)-2-phenylethan-1-one
86	1-{4-[(3,4,5-trihydroxyoxan-2-yl)amino]phenyl}ethan-1-one
87	(2S)-2-[(4-{[(1S)-1-carboxy-2-methylbutyl]carbamoyl}piperazine-1-carbonyl)amino]-3-methylpentanoic acid
88	3-{[(2S,3R,4S,5S,6R)-3,4,5-trihydroxy-6-(hydroxymethyl)oxan-2-yl]oxy}-6H-benzo[c]chromen-6-one
89	4-methyl-3-{[(2S,3R,4S,5S,6R)-3,4,5-trihydroxy-6-(hydroxymethyl)oxan-2-yl]oxy}-6H,7H,8H,9H,10H,11H-cyclohepta[c]chromen-6-one
90	4-methyl-3-{[(2S,3R,4S,5R,6R)-3,4,5-trihydroxy-6-(hydroxymethyl)oxan-2-yl]oxy}-6H,7H,8H,9H,10H-cyclohexa[c]chromen-6-one
91	3-{[(2S,3S,4R,5R)-3,4,5-trihydroxyoxan-2-yl]oxy}-6H,7H,8H,9H,10H-cyclohexa[c]chromen-6-one
92	4-(4-methoxyphenyl)-7-{[(2S,3R,4S,5S,6R)-3,4,5-trihydroxy-6-(hydroxymethyl)oxan-2-yl]oxy}-2H-chromen-2-one

93	4-ethyl-7-methyl-5-{[(2S,3R,4S,5S,6R)-3,4,5-trihydroxy-6-(hydroxymethyl)oxan-2-yl]oxy}-2H-chromen-2-one
94	7-{[(2S,3R,4S,5S,6R)-3,4,5-trihydroxy-6-(hydroxymethyl)oxan-2-yl]oxy}-1H,2H,3H,4H-cyclopenta[c]chromen-4-one
95	3-{[(2S,3R,4S,5S,6R)-3,4,5-trihydroxy-6-(hydroxymethyl)oxan-2-yl]oxy}-6H,7H,8H,9H,10H-cyclohexa[c]chromen-6-one
96	3-{[(2S,3R,4S,5R,6R)-3,4,5-trihydroxy-6-(hydroxymethyl)oxan-2-yl]oxy}-6H-benzo[c]chromen-6-one
97	3,4,7-trimethyl-5-{[(2S,3R,4S,5S,6R)-3,4,5-trihydroxy-6-(hydroxymethyl)oxan-2-yl]oxy}-2H-chromen-2-one
98	7-methyl-9-{[(2S,3R,4S,5R,6R)-3,4,5-trihydroxy-6-(hydroxymethyl)oxan-2-yl]oxy}-1H,2H,3H,4H-cyclopenta[c]chromen-4-one
99	6-chloro-4-ethyl-7-{[(2S,3R,4S,5S,6R)-3,4,5-trihydroxy-6-(hydroxymethyl)oxan-2-yl]oxy}-2H-chromen-2-one
100	6-methyl-7-{[(2S,3R,4S,5R,6R)-3,4,5-trihydroxy-6-(hydroxymethyl)oxan-2-yl]oxy}-1H,2H,3H,4H-cyclopenta[c]chromen-4-one
101	4-methyl-3-{[(2S,3R,4S,5S,6R)-3,4,5-trihydroxy-6-(hydroxymethyl)oxan-2-yl]oxy}-6H,7H,8H,9H,10H-cyclohexa[c]chromen-6-one
102	2-chloro-3-{[(2S,3R,4S,5R,6R)-3,4,5-trihydroxy-6-(hydroxymethyl)oxan-2-yl]oxy}-6H,7H,8H,9H,10H-cyclohexa[c]chromen-6-one
103	3,4,8-trimethyl-7-{[(2S,3R,4S,5S,6R)-3,4,5-trihydroxy-6-(hydroxymethyl)oxan-2-yl]oxy}-2H-chromen-2-one
104	6-methyl-7-{[(2S,3R,4S,5R)-3,4,5-trihydroxyoxan-2-yl]oxy}-1H,2H,3H,4H-cyclopenta[c]chromen-4-one
105	4-phenyl-7-{[(2S,3R,4S,5R,6R)-3,4,5-trihydroxy-6-(hydroxymethyl)oxan-2-yl]oxy}-2H-chromen-2-one
106	3-{[(2S,3R,4S,5R)-3,4,5-trihydroxyoxan-2-yl]oxy}-6H,7H,8H,9H,10H-cyclohexa[c]chromen-6-one
107	2-chloro-3-{[(2S,3R,4S,5S,6R)-3,4,5-trihydroxy-6-(hydroxymethyl)oxan-2-yl]oxy}-6H,7H,8H,9H,10H-cyclohexa[c]chromen-6-one
108	4-(4-methoxyphenyl)-8-methyl-7-{[(2S,3R,4S,5R,6R)-3,4,5-trihydroxy-6-(hydroxymethyl)oxan-2-yl]oxy}-2H-chromen-2-one
109	4-ethyl-8-methyl-7-{[(2S,3R,4S,5S,6R)-3,4,5-trihydroxy-6-(hydroxymethyl)oxan-2-yl]oxy}-2H-chromen-2-one
110	4-phenyl-7-{[(2S,3R,4S,5R)-3,4,5-trihydroxyoxan-2-yl]oxy}-2H-chromen-2-one
111	3-methyl-1-{[(2S,3R,4S,5R,6R)-3,4,5-trihydroxy-6-(hydroxymethyl)oxan-2-yl]oxy}-6H,7H,8H,9H,10H-cyclohexa[c]chromen-6-one
112	7-{[(2S,3R,4S,5R)-3,4,5-trihydroxyoxan-2-yl]oxy}-1H,2H,3H,4H-cyclopenta[c]chromen-4-one
113	4-methyl-3-{[(2S,3R,4S,5S,6R)-3,4,5-trihydroxy-6-(hydroxymethyl)oxan-2-yl]oxy}-6H-benzo[c]chromen-6-one
114	4-(4-methoxyphenyl)-7-{[(2S,3R,4S,5R,6R)-3,4,5-trihydroxy-6-(hydroxymethyl)oxan-2-yl]oxy}-2H-chromen-2-one
115	4-ethyl-7-{[(2S,3R,4S,5S,6R)-3,4,5-trihydroxy-6-(hydroxymethyl)oxan-2-yl]oxy}-2H-chromen-2-one
116	3-{[(2S,3R,4S,5R)-3,4,5-trihydroxyoxan-2-yl]oxy}-6H-benzo[c]chromen-6-one
117	2,2-dimethyl-12-{[(2S,3R,4S,5S,6R)-3,4,5-trihydroxy-6-(hydroxymethyl)oxan-2-yl]oxy}-2,3,4,6,7,8,9,10-octahydro-1,11-dioxatetraphen-10-one
118	7-methyl-9-{[(2S,3R,4S,5S,6R)-3,4,5-trihydroxy-6-(hydroxymethyl)oxan-2-yl]oxy}-1H,2H,3H,4H-cyclopenta[c]chromen-4-one

119	6-methyl-7-{[(2S,3R,4S,5S,6R)-3,4,5-trihydroxy-6-(hydroxymethyl)oxan-2-yl]oxy}-1H,2H,3H,4H-cyclopenta[c]chromen-4-one
120	8-methyl-4-phenyl-7-{[(2S,3R,4S,5R,6R)-3,4,5-trihydroxy-6-(hydroxymethyl)oxan-2-yl]oxy}-2H-chromen-2-one
121	8-methyl-4-propyl-7-{[(2S,3R,4S,5S,6R)-3,4,5-trihydroxy-6-(hydroxymethyl)oxan-2-yl]oxy}-2H-chromen-2-one
122	4-phenyl-7-{[(2S,3S,4R,5R)-3,4,5-trihydroxyoxan-2-yl]oxy}-2H-chromen-2-one
123	2,2-dimethyl-12-{[(2S,3R,4S,5R,6R)-3,4,5-trihydroxy-6-(hydroxymethyl)oxan-2-yl]oxy}-2,3,4,6,7,8,9,10-octahydro-1,11-dioxatetraphen-10-one
124	3-methyl-1-{[(2S,3R,4S,5S,6R)-3,4,5-trihydroxy-6-(hydroxymethyl)oxan-2-yl]oxy}-6H,7H,8H,9H,10H-cyclohexa[c]chromen-6-one
125	7-{[(2S,3R,4S,5R,6R)-3,4,5-trihydroxy-6-(hydroxymethyl)oxan-2-yl]oxy}-1H,2H,3H,4H-cyclopenta[c]chromen-4-one
126	3,4,8-trimethyl-7-{[(2S,3R,4S,5R,6R)-3,4,5-trihydroxy-6-(hydroxymethyl)oxan-2-yl]oxy}-2H-chromen-2-one
127	8-methyl-4-phenyl-7-{[(2S,3R,4S,5S,6R)-3,4,5-trihydroxy-6-(hydroxymethyl)oxan-2-yl]oxy}-2H-chromen-2-one
128	3-{[(2S,3S,4R,5R)-3,4,5-trihydroxyoxan-2-yl]oxy}-6H-benzo[c]chromen-6-one
129	2,2-dimethyl-12-{[(2S,3S,4S,5S,6R)-3,4,5-trihydroxy-6-(hydroxymethyl)oxan-2-yl]oxy}-2,3,4,6,7,8,9,10-octahydro-1,11-dioxatetraphen-10-one
130	3-{[(2S,3R,4S,5S,6R)-3,4,5-trihydroxy-6-(hydroxymethyl)oxan-2-yl]oxy}-6H,7H,8H,9H,10H,11H-cyclohepta[c]chromen-6-one
131	3-{[(2S,3R,4S,5R,6R)-3,4,5-trihydroxy-6-(hydroxymethyl)oxan-2-yl]oxy}-6H,7H,8H,9H,10H-cyclohexa[c]chromen-6-one
132	3,4-dimethyl-7-{[(2S,3R,4S,5R,6R)-3,4,5-trihydroxy-6-(hydroxymethyl)oxan-2-yl]oxy}-2H-chromen-2-one
133	4-phenyl-7-{[(2S,3R,4S,5S,6R)-3,4,5-trihydroxy-6-(hydroxymethyl)oxan-2-yl]oxy}-2H-chromen-2-one
134	7-{[(2S,3S,4R,5R)-3,4,5-trihydroxyoxan-2-yl]oxy}-1H,2H,3H,4H-cyclopenta[c]chromen-4-one
135	4-propyl-7-{[(2S,3R,4S,5S,6R)-3,4,5-trihydroxy-6-(hydroxymethyl)oxan-2-yl]oxy}-2H-chromen-2-one

5.2. SUPPORTING INFORMATION FOR SUBCHAPTER 3.2**Photoswitchable Janus Glycodendrimer Micelles as Multivalent Inhibitors of LecA and LecB from *Pseudomonas aeruginosa***

Yingxue Hu,^a Ghamdan Beshr,^b Christopher J. Garvey,^c Alexander Titz,^b Rico F. Tabor^a and Brendan L. Wilkinson.*^d

- a) School of Chemistry, Monash University, Victoria 3800, Australia.
- b) Chemical Biology of Carbohydrates, Helmholtz Institute for Pharmaceutical Research Saarland (HIPS), D-66123 Saarbrücken, Germany, and Deutsches Zentrum für Infektionsforschung, Standort Hannover-Braunschweig.
- c) Australian Centre for Neutron Scattering, ANSTO, Lucas Heights, New South Wales 2234, Australia.
- d) School of Science and Technology, The University of New England, New South Wales 2351, Australia.

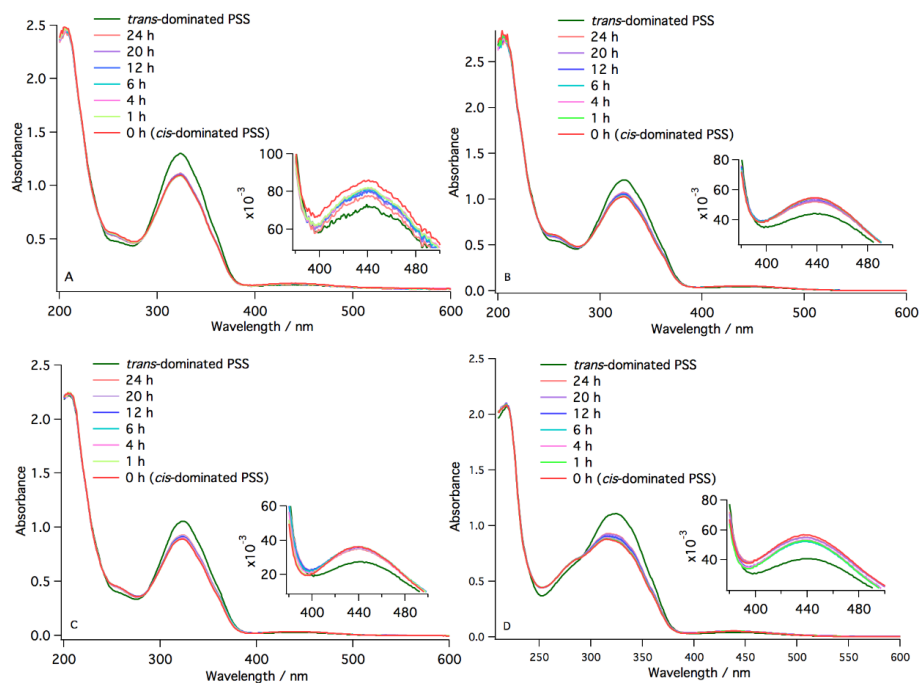


Figure S1. Thermal *cis-trans* relaxation of glycodendrimers A) Man(3,5)8 **1**, B) Man(3,5)2Et8 **2**, C) Man(3,5)12 **3** and D) Man(3,4,5)2Et8 **4** (0.05 mM in Milli-Q water) at 20°C.

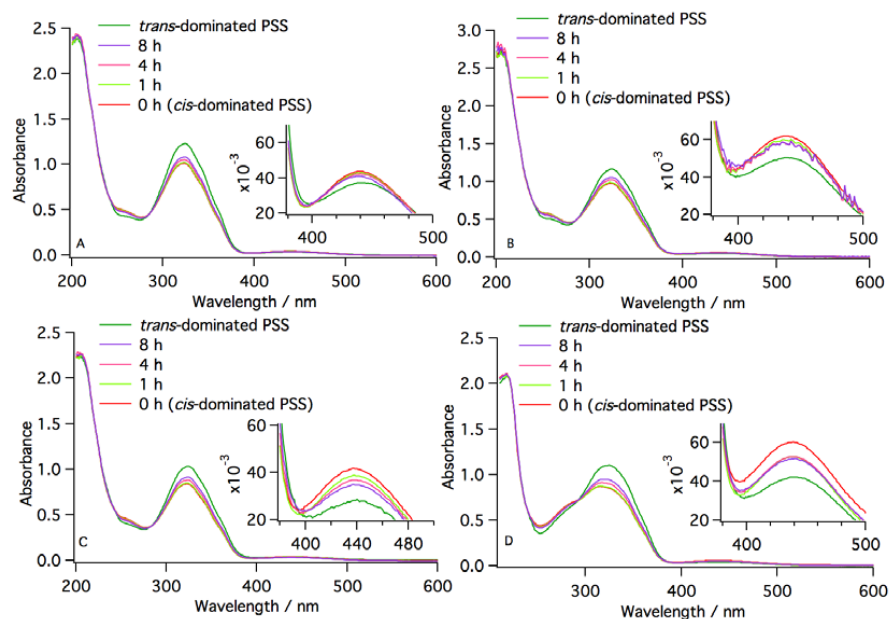


Figure S2. Thermal *cis-trans* relaxation of glycodendrimers A) Man(3,5)8 **1**, B) Man(3,5)2Et8 **2**, C) Man(3,5)12 **3** and D) Man(3,4,5)2Et8 **4** (0.05 mM in Milli-Q water) at 37°C.

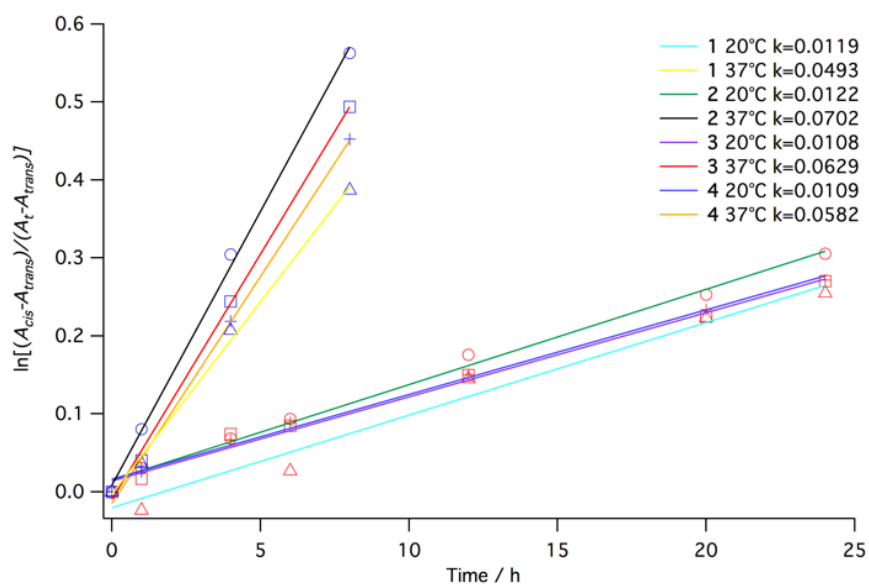


Figure S3. Time dependence of the absorbance changes at 325 nm for thermal *cis-to-trans* isomerization of glycodendrimers **1–4** in the dark in Milli-Q water at 20°C and 37°C.

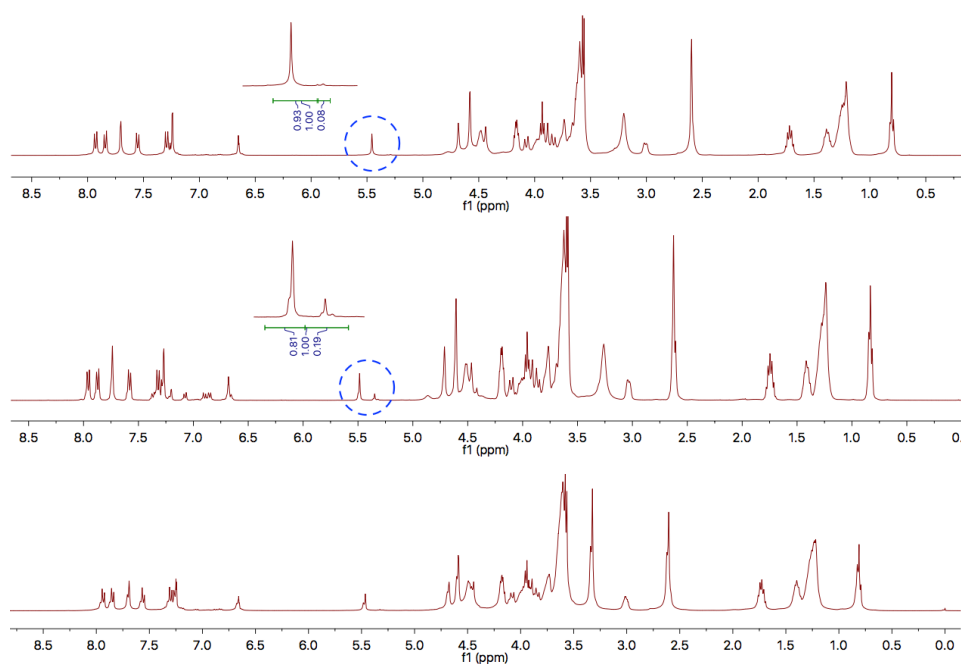


Figure S4. ^1H NMR spectra of Man(3,5)8 **1** before UV photoirradiation (top), after UV photoirradiation (middle), and after blue light photoirradiation (bottom).

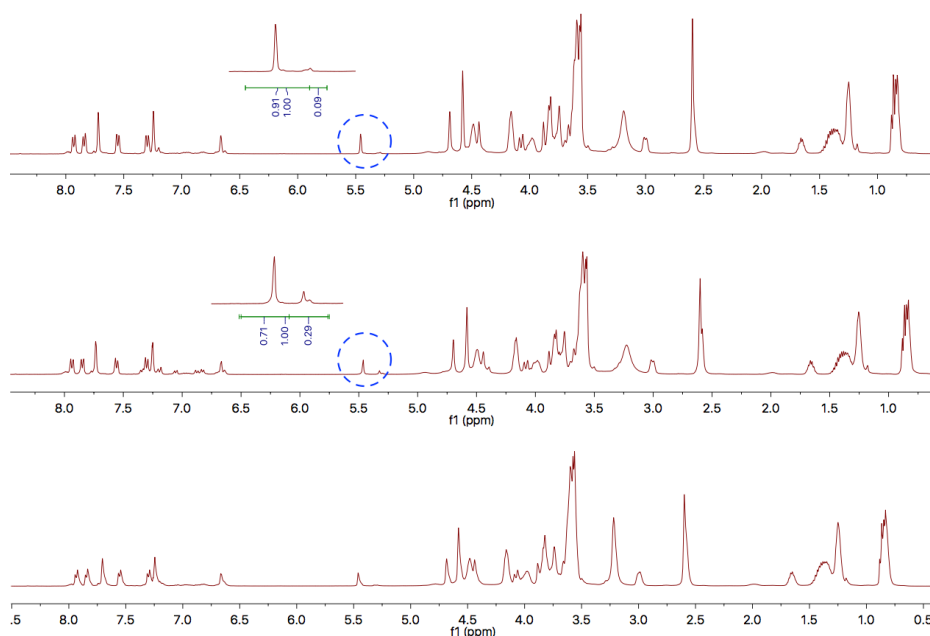


Figure S5. ^1H NMR spectra of Man(3,5)2Et8 **2** before UV photoirradiation (top), after UV photoirradiation (middle), and after blue light photoirradiation (bottom).

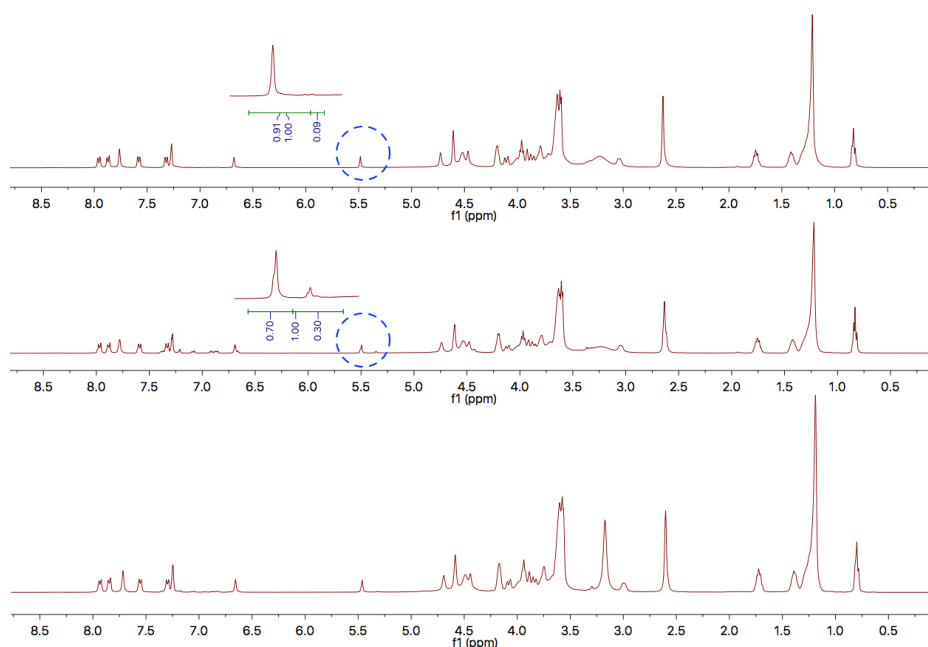


Figure S6. ^1H NMR spectra of Man(3,5)12 **3** before UV photoirradiation (top), after UV photoirradiation (middle), and after blue light photoirradiation (bottom).

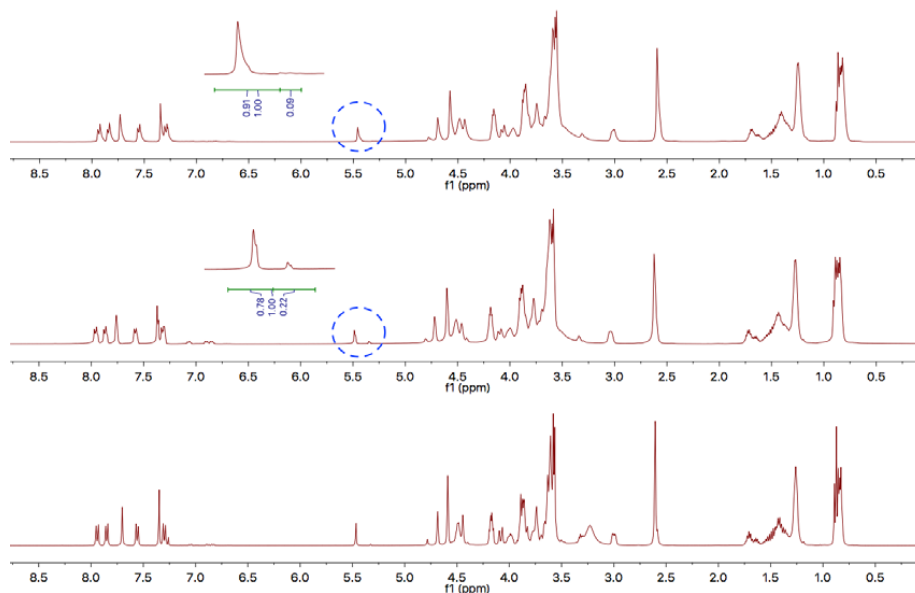


Figure S7. ^1H NMR spectra of Man(3,4,5)2Et8 **4** before UV photoirradiation (top), after UV photoirradiation (middle), and after blue light photoirradiation (bottom).

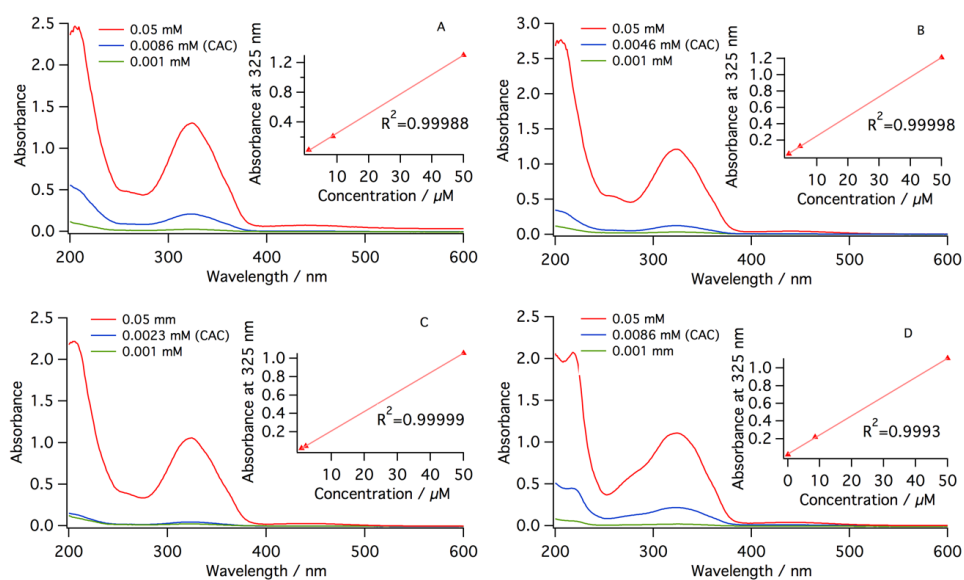


Figure S8. UV-vis absorbance of A) Man(3,5)8 **1**, B) Man(3,5)2Et8 **2**, C) Man(3,5)12 **3** and D) Man(3,4,5)2Et8 **4** in Milli-Q water at 20°C under different concentrations. (Insets) Plots of the UV-vis absorbance measured at 325 nm as a function of concentration.

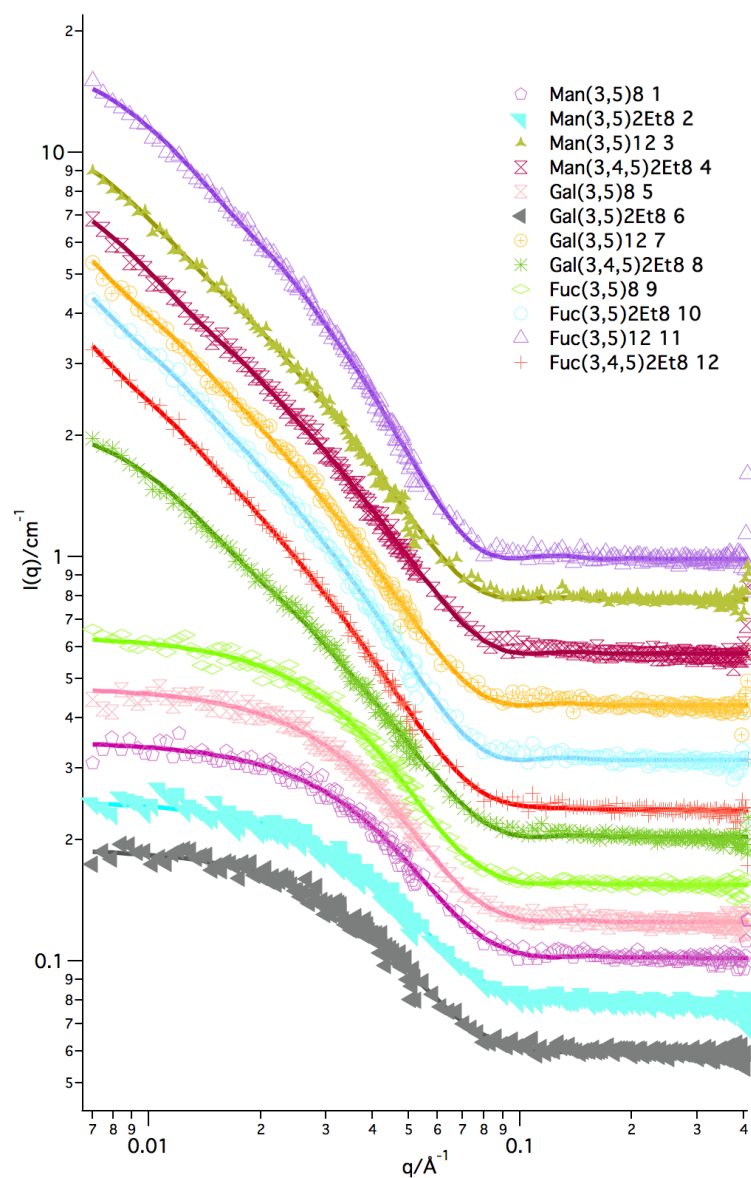


Figure S9. SANS data (symbols) and model fits (lines) for glycodendrimers **1–12** in the *trans*-dominated PSS at a concentration of 0.1 mM in D₂O.

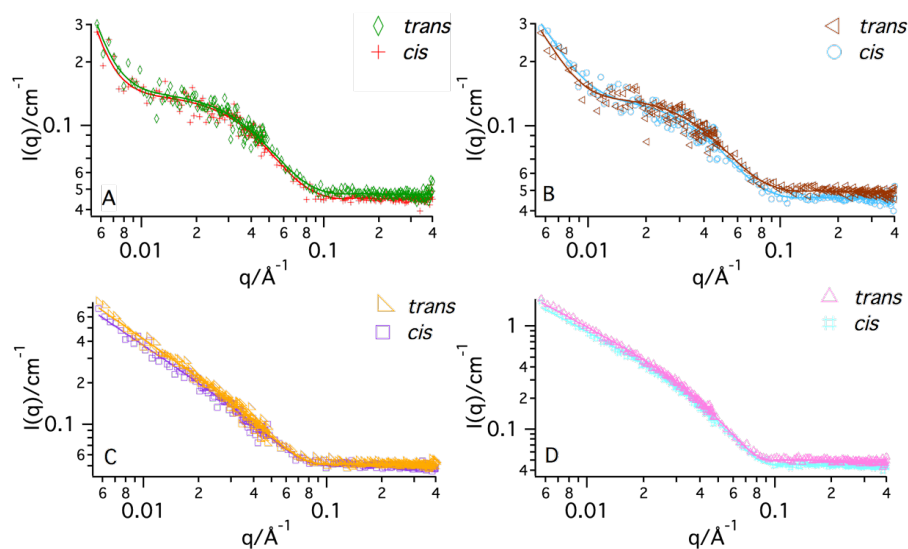


Figure S10. SANS data (symbols) and model fits (lines) for glycodendrimer A) Man(3,5)8 **1**, B) Man(3,5)2Et8 **2**, C) Man(3,5)12 **3** and D) Man(3,4,5)2Et8 **4** in the *trans* PSS and *cis* PSS at a concentration of 0.1 mM in D₂O.

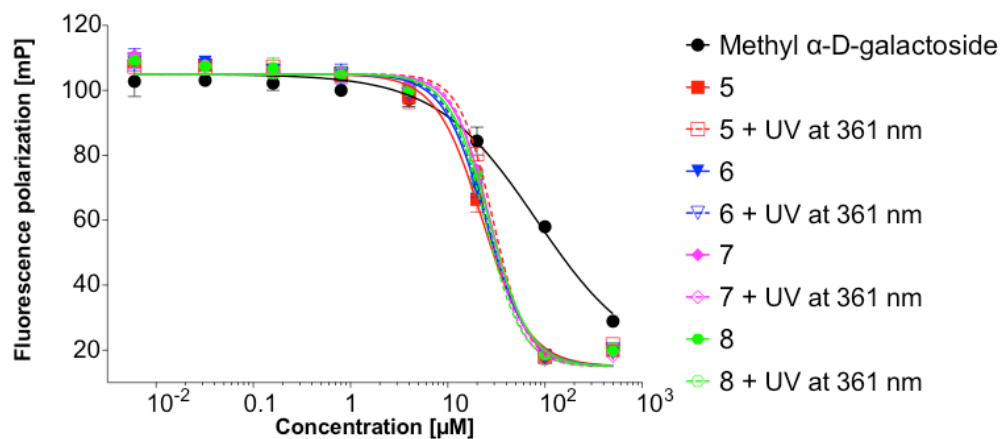


Figure S11. Representative example of the fluorescence polarization-based competitive binding assay of LecA with compounds **5**–**8** or methyl α -D-galactoside.

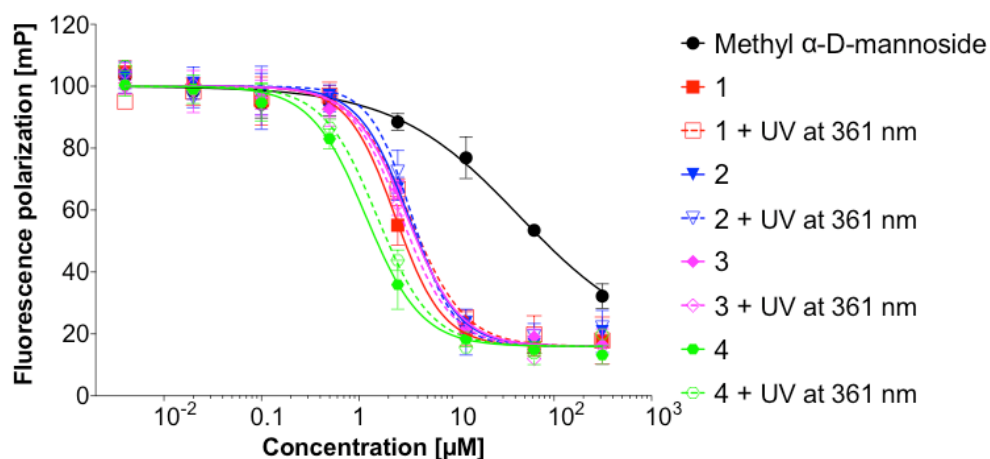


Figure S12. Representative example of the fluorescence polarization-based competitive binding assay of LecB with compounds **1–4** or methyl α-D-mannoside.

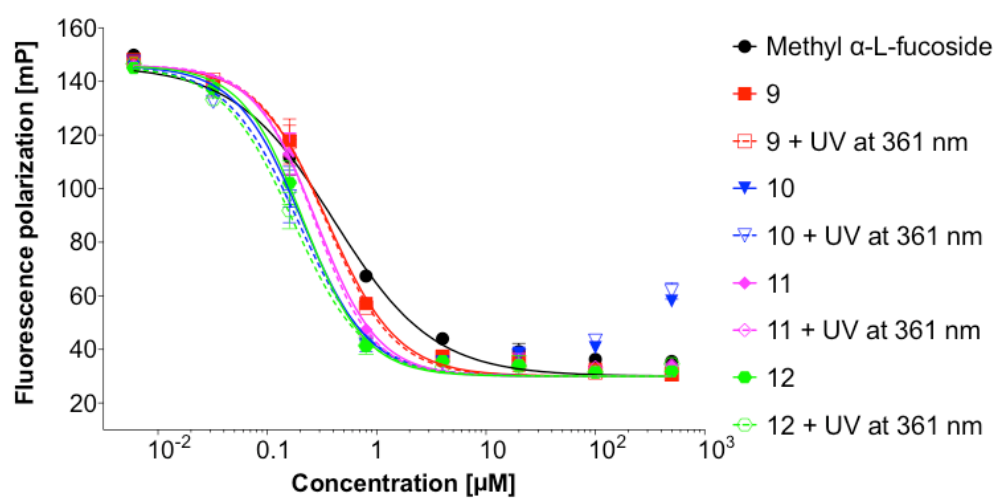


Figure S13. Representative example of the fluorescence polarization-based competitive binding assay of LecB with compounds **9–12** or methyl α-L-fucoside.

Table S1. CAC values, DLS results, SANS fitting parameters and lectin binding results of glycodendrimer **1–12**.

Name	CAC/mM ^a	N _{agg} ^b	A _{hg} ^c /nm ²	Eff. Diam./nm (PDI) ^d		SANS ^e	
				Before UV	After UV	Radius/Å	Length/Å
1	0.0086	138	1.07	112(0.21)	199(0.17)	34	104
2	0.0046	128	1.07	149 (0.23)	226 (0.15)	32	104
3	0.0023	918	0.79	109 (0.24)	109 (0.39)	39	550
4	0.0086	795	0.87	105 (0.25)	111 (0.24)	36	574
5	0.0085	162	0.98	110 (0.20)	138 (0.18)	35	109
6	0.0092	149	1.01	138 (0.26)	147 (0.20)	33	112
7	0.0080	1424	0.79	114 (0.23)	102 (0.18)	38	903
8	0.0100	536	0.90	102 (0.23)	91 (0.19)	35	406
9	0.0200	182	0.97	110 (0.29)	159 (0.24)	37	115
10	0.0085	1603	0.71	183 (0.21)	119 (0.25)	38	921
11	0.0048	799	0.78	123 (0.17)	129 (0.18)	41	441
12	0.0054	996	0.96	134 (0.17)	138 (0.19)	32	915

^a Measured in ultrapure water at 20°C; ^b N_{agg} = aggregation number; ^c A_{hg} = area per headgroup;

^d DLS samples were prepared at 0.1 mM; ^e SANS samples were dissolved in D₂O at 0.1 mM, and were all fitted to cylindrical shaped structure.

Analytical data

Man(3,5)8 1: This compound was prepared from **27** and **31** according to general procedure 3 and isolated as an orange solid (Yield: 45%). Mp = 212.4°C; [α]_D²⁰ 111.6 (c, 0.06 in CH₃OH); FT-IR: ν_{\max} /cm⁻¹ 3413, 2922, 1735, 1593, 1348, 1092, 840, 674; ¹H NMR (400 MHz, 10% CD₃OD in CDCl₃) δ 7.93 (d, *J* = 8.85 Hz, 2H, 2×ArH), 7.84 (d, *J* = 8.42 Hz, 2H, 2×ArH), 7.71–7.70 (m, 2H, 2×ArH), 7.55 (d, *J* = 8.55 Hz, 2H, 2×ArH), 7.30–7.24 (m, 4H, 2×ArH, 2×CH (triazole)), 6.65 (t, *J* = 2.23 Hz, 1H, ArH), 5.46 (s, 1H, CH), 4.78–4.44 (m, 14H), 4.18–3.56 (m, 54H), 3.02–2.99 (m, 2H), 2.59 (s, 8H, 4×CH₂), 1.75–1.68 (m, 4H, 2×CH₂), 1.40–1.21 (m, 20H, 10×CH₂), 0.80 (t, *J* = 6.72 Hz, 6H, 2×CH₃); ¹³C NMR (100 MHz, 10% CD₃OD in CDCl₃) δ 172.4, 172.1, 160.3, 144.8, 126.9, 124.1, 122.7, 122.4, 108.2, 99.9, 72.8, 71.1, 70.3, 69.6, 69.4,

68.9, 68.4, 65.4, 64.2, 63.9, 49.9, 49.1, 48.9, 37.2, 31.7, 29.2, 29.1, 28.9, 28.8, 25.9, 22.6, 13.9; ESI-HRMS (m/z) calculated for $C_{83}H_{122}N_8O_{32} = 1765.8057 [M + Na]^+$, found 1765.8063 $[M + Na]^+$.

Man(3,5)2Et8 2: This compound was prepared from **28** and **31** according to general procedure 3 and isolated as an orange solid (Yield: 42%). Mp = 203.7°C; $[\alpha]_D^{20}$ 103.0 (c , 0.065 in CH_3OH); FT-IR: ν_{max}/cm^{-1} 3395, 2925, 1735, 1595, 1347, 1030, 841, 673; 1H NMR (400 MHz, 10% CD_3OD in $CDCl_3$) δ 7.93 (d, $J = 7.53$ Hz, 2H, $2 \times ArH$), 7.84 (d, $J = 7.41$ Hz, 2H, $2 \times ArH$), 7.72 (s, 2H, $2 \times ArH$), 7.55 (d, $J = 7.56$ Hz, 2H, $2 \times ArH$), 7.31–7.24 (m, 4H, $2 \times ArH$, $2 \times CH$ (triazole)), 6.66 (s, 1H, ArH), 5.46 (s, 1H, CH), 4.69–4.44 (m, 14H), 4.16–3.49 (m, 54H), 3.01–2.99 (m, 2H), 2.59 (s, 8H, $4 \times CH_2$), 1.68–1.63 (m, 2H, $2 \times CH$), 1.49–1.25 (m, 16H, $8 \times CH_2$), 0.88–0.83 (m, 12H, $4 \times CH_3$); ^{13}C NMR (100 MHz, 10% CD_3OD in $CDCl_3$) δ 172.4, 172.1, 160.5, 144.7, 126.9, 124.2, 124.1, 122.7, 122.4, 108.2, 99.8, 72.7, 70.8, 70.3, 69.6, 69.4, 68.9, 65.4, 64.2, 63.9, 60.9, 49.9, 49.3, 49.1, 48.9, 48.7, 39.3, 37.2, 30.4, 29.0, 28.8, 23.8, 22.9, 13.9, 11.0; ESI-HRMS (m/z) calculated for $C_{83}H_{122}N_8O_{32} = 1765.8057 [M + Na]^+$, found m/z 894.3980 $[M + 2Na]^+$.

Man(3,5)12 3: This compound was prepared from **29** and **31** according to general procedure 3 and isolated as an orange solid (Yield: 49%). Mp = 189.9°C; $[\alpha]_D^{20}$ 105.4 (c , 0.055 in CH_3OH); FT-IR: ν_{max}/cm^{-1} 3396, 2921, 1736, 1591, 1351, 1094, 841; 1H NMR (400 MHz, 10% CD_3OD in $CDCl_3$) δ 7.96 (d, $J = 8.28$ Hz, 2H, $2 \times ArH$), 7.87 (d, $J = 8.01$ Hz, 2H, $2 \times ArH$), 7.76 (s, 2H, $2 \times ArH$), 7.58 (d, $J = 8.01$ Hz, 2H, $2 \times ArH$), 7.33–7.20 (m, 4H, $2 \times ArH$, $2 \times CH$ (triazole)), 6.68 (s, 1H, ArH), 5.48 (s, 1H, CH), 4.73–4.47 (m, 14H), 4.19–3.59 (m, 54H), 3.05–3.03 (m, 2H), 2.62 (s, 8H, $4 \times CH_2$), 1.76–1.71 (m, 4H, $2 \times CH_2$), 1.42–1.21 (m, 32H, $16 \times CH_2$), 0.84–0.81 (m, 6H, $2 \times CH_3$); ^{13}C NMR (100 MHz, 10% CD_3OD in $CDCl_3$) δ 172.4, 172.1, 160.3, 144.7, 126.9, 124.1, 122.7, 122.4, 108.2, 99.8, 70.3, 69.6, 68.9, 68.4, 65.4, 64.1, 63.8, 49.9, 49.3, 49.1, 48.9, 37.2, 31.8, 29.5, 29.3, 29.1, 28.9, 28.8, 25.9, 22.6, 13.9; ESI-HRMS (m/z) calculated for $C_{91}H_{138}N_8O_{32} = 1877.9309 [M + Na]^+$, found m/z 950.9617 $[M + 2Na]^+$.

Man(3,4,5)2Et8 4: This compound was prepared from **30** and **31** according to general procedure 3 and isolated as an orange solid (Yield: 51%). Mp = 233.8°C; $[\alpha]_D^{20}$ 80.0 (c , 0.08 in CH_3OH); FT-IR: ν_{max}/cm^{-1} 3395, 2928, 1735, 1331, 1094, 837; 1H NMR (400 MHz, 10% CD_3OD in $CDCl_3$) δ 7.93 (d, $J = 8.68$ Hz, 2H, $2 \times ArH$), 7.84 (d, $J = 8.21$ Hz, 2H, $2 \times ArH$), 7.73 (s, 2H, $2 \times ArH$), 7.55 (d, $J = 8.21$ Hz, 2H, $2 \times ArH$), 7.34–7.27 (m, 4H, $2 \times ArH$, $2 \times CH$ (triazole)), 5.46

(s, 1H, *CH*), 4.78–4.43 (m, 14H), 4.17–3.56 (m, 56H), 3.02–3.00 (m, 2H), 2.59 (s, 8H, 4×*CH*₂), 1.71–1.25 (m, 27H, 3×*CH*, 12×*CH*₂), 0.88–0.82 (m, 18H, 6×*CH*₃); ¹³C NMR (100 MHz, 10% CD₃OD in CDCl₃) δ 172.4, 172.1, 153.1, 150.1, 144.7, 143.1, 126.9, 124.2, 124.1, 123.3, 122.7, 122.5, 108.0, 99.8, 71.3, 71.0, 70.3, 69.6, 69.4, 68.9, 66.5, 65.4, 64.1, 63.8, 60.9, 49.9, 49.2, 49.0, 48.8, 48.6, 40.6, 39.5, 37.2, 30.4, 30.3, 29.2, 29.0, 28.9, 28.8, 23.8, 23.6, 23.0, 22.9, 13.9, 11.0; ESI-HRMS (*m/z*) calculated for C₉₁H₁₃₈N₈O₃₃ = 1893.9259 [*M* + Na]⁺, found 1893.9246 [*M* + Na]⁺.

Gal(3,5)8 **5**: This compound was prepared from **27** and **32** according to general procedure 3 and isolated as an orange solid (Yield: 44%). Mp = 205.3°C; [α]_D²⁰ 148.6 (c, 0.055 in CH₃OH); FT-IR: ν_{max} /cm⁻¹ 3395, 2923, 1734, 1893, 1350, 1038, 840; ¹H NMR (400 MHz, 10% CD₃OD in CDCl₃) δ 7.96–7.83 (m, 6H, 4×*ArH*, 2×*CH* (triazole)), 7.58–7.55 (m, 2H, 2×*ArH*), 7.35–7.25 (m, 4H, 4×*ArH*), 6.68–6.63 (m, 1H, *ArH*), 5.48–5.46 (m, 1H, *CH*), 4.58–4.44 (m, 10H), 4.17–4.06 (m, 10H), 3.97–3.84 (m, 10H), 3.69–3.29 (m, 40H), 2.61–2.59 (m, 8H, 4×*CH*₂), 1.76–1.69 (m, 4H, 2×*CH*₂), 1.41–1.22 (m, 20H, 10×*CH*₂), 0.82–0.79 (m, 6H, 2×*CH*₃); ¹³C NMR (100 MHz, 10% CD₃OD in CDCl₃) δ 172.4, 160.3, 144.5, 126.9, 124.6, 124.1, 122.7, 122.4, 108.2, 103.4, 74.7, 73.3, 70.9, 70.3, 69.5, 68.9, 68.4, 67.8, 64.2, 63.8, 61.2, 50.3, 49.3, 49.1, 48.9, 31.7, 29.2, 29.1, 28.9, 28.8, 25.9, 22.5, 13.9; ESI-HRMS (*m/z*) calculated for C₈₃H₁₂₂N₈O₃₂ = 1765.8057 [*M* + Na]⁺, found *m/z* 894.3968 [*M* + 2Na]⁺.

Gal(3,5)2Et8 **6**: This compound was prepared from **28** and **32** according to general procedure 3 and isolated as an orange solid (Yield: 54%). Mp = 201.1°C; [α]_D²⁰ 175.7 (c, 0.05 in CH₃OH); FT-IR: ν_{max} /cm⁻¹ 3395, 2928, 1734, 1595, 1347, 1035, 843, 756; ¹H NMR (400 MHz, 10% CD₃OD in CDCl₃) δ 8.16 (d, *J* = 8.75 Hz, 2H, 2×*ArH*), 8.10–8.07 (m, 4H, 2×*ArH*, 2×*CH* (triazole)), 7.78 (d, *J* = 8.29 Hz, 2H, 2×*ArH*), 7.53 (d, *J* = 8.54 Hz, 2H, 2×*ArH*), 7.48 (s, 2H, 2×*ArH*), 6.89 (s, 1H, *ArH*), 5.69 (s, 1H, *CH*), 4.79–4.67 (m, 10H), 4.39–4.29 (m, 10H), 4.11–4.03 (m, 12H), 3.90–3.66 (m, 34H), 2.83 (s, 8H, 4×*CH*₂), 1.91–1.88 (m, 2H, 2×*CH*), 1.68–1.48 (m, 16H, 8×*CH*₂), 1.11–1.06 (m, 12H, 4×*CH*₃); ¹³C NMR (100 MHz, 10% CD₃OD in CDCl₃) δ 172.5, 172.1, 160.5, 153.1, 144.5, 126.9, 124.6, 124.2, 122.7, 122.4, 108.2, 70.8, 70.3, 69.5, 68.9, 64.2, 63.8, 49.6, 49.4, 49.2, 48.9, 39.3, 37.2, 30.5, 29.0, 28.8, 23.8, 22.9, 13.9, 11.0. ESI-HRMS (*m/z*) calculated for C₈₃H₁₂₂N₈O₃₂ = 1765.8057 [*M* + Na]⁺, found *m/z* 894.3987 [*M* + 2Na]⁺.

Gal(3,5)12 **7**: This compound was prepared from **29** and **32** according to general procedure 3 and isolated as an orange solid (Yield: 42%). Mp = 187.5°C; $[\alpha]_{\text{D}}^{20}$ 156.7 (*c*, 0.065 in CH₃OH); FT-IR: $\nu_{\text{max}}/\text{cm}^{-1}$ 3395, 2921, 1732, 1592, 1350, 1037, 840, 754; ¹H NMR (400 MHz, 10% CD₃OD in CDCl₃) δ 8.21 (d, *J* = 8.70 Hz, 2H, 2×ArH), 8.15–8.12 (m, 4H, 2×ArH, 2×CH (triazole)), 7.84 (d, *J* = 8.44 Hz, 2H, 2×ArH), 7.76 (s, 2H, 2×ArH), 7.58 (d, *J* = 8.82 Hz, 2H, 2×ArH), 7.53–7.52 (m, 4H, 2×ArH), 6.94 (s, 1H, ArH), 5.74 (s, 1H, CH), 4.85–4.72 (m, 10H), 4.45–4.35 (m, 10H), 4.23–4.09 (m, 12H), 3.95–3.69 (m, 34H), 2.88 (s, 8H, 4×CH₂), 2.02–1.97 (m, 4H, 2×CH₂), 1.69–1.64 (m, 4H, 2×CH₂), 1.47 (s, 28H, 14×CH₂), 1.09–1.06 (m, 6H, 2×CH₃); ¹³C NMR (100 MHz, 10% CD₃OD in CDCl₃) δ 160.3, 144.5, 126.9, 124.6, 124.2, 122.7, 122.4, 108.3, 74.7, 70.3, 69.6, 68.9, 68.4, 64.2, 63.8, 49.4, 49.2, 48.9, 31.8, 29.6, 29.5, 29.3, 29.1, 28.9, 25.9, 22.6, 13.9. ESI-HRMS (*m/z*) calculated for C₉₁H₁₃₈N₈O₃₂ = 1877.9309 [*M* + Na]⁺, found 1877.9312 [*M* + Na]⁺.

Gal(3,4,5)2Et8 **8**: This compound was prepared from **30** and **32** according to general procedure 3 and isolated as an orange solid (Yield: 40%). Mp = 223.7°C; $[\alpha]_{\text{D}}^{20}$ 62.6 (*c*, 0.075 in CH₃OH); FT-IR: $\nu_{\text{max}}/\text{cm}^{-1}$ 3400, 2922, 1731, 1585, 1331, 1093, 839, 751; ¹H NMR (400 MHz, 10% CD₃OD in CDCl₃) δ 8.16–8.14 (m, 2H, 2×ArH), 8.09–8.05 (m, 4H, 2×ArH, 2×CH (triazole)), 7.78–7.76 (m, 2H, 2×ArH), 7.56–7.47 (m, 4H, 4×ArH), 5.68 (s, 1H, CH), 4.78–4.66 (m, 10H), 4.38–4.28 (m, 10H), 4.14–4.04 (m, 12H), 3.89–3.65 (m, 34H), 2.81 (s, 8H, 4×CH₂), 1.94–1.47 (m, 27H, 3×CH, 12×CH₂), 1.10–1.04 (m, 18H, 6×CH₃); ¹³C NMR (100 MHz, 10% CD₃OD in CDCl₃) δ 172.5, 172.2, 164.9, 153.1, 144.5, 126.9, 124.1, 122.7, 122.5, 108.0, 103.4, 74.6, 71.3, 70.3, 69.5, 68.9, 67.8, 64.2, 63.9, 50.3, 49.3, 49.2, 48.9, 40.6, 39.5, 37.2, 30.5, 30.3, 29.2, 29.0, 28.9, 23.8, 23.6, 23.0, 22.9, 14.0, 13.9, 11.0. ESI-HRMS (*m/z*) calculated for C₉₁H₁₃₈N₈O₃₃ = 1893.9259 [*M* + Na]⁺, found *m/z* 958.9582 [*M* + 2Na]⁺.

Fuc(3,5)8 **9**: This compound was prepared from **27** and **33** according to general procedure 3 and isolated as an orange solid (Yield: 46%). Mp = 153.8°C; $[\alpha]_{\text{D}}^{20}$ 66.6 (*c*, 0.085 in CH₃OH); FT-IR: $\nu_{\text{max}}/\text{cm}^{-1}$ 3409, 2921, 1735, 1595, 1348, 1032, 841, 754; ¹H NMR (400 MHz, 10% CD₃OD in CDCl₃) δ 7.94–7.74 (m, 6H, 4×ArH, 2×CH (triazole)), 7.56–7.54 (m, 2H, 2×ArH), 7.33–7.17 (m, 4H, 4×ArH), 6.65–6.64 (m, 1H, ArH), 5.46 (m, 1H, CH), 4.71–4.43 (m, 12H), 4.16–4.06 (m, 8H), 3.95–3.83 (m, 10H), 3.66–3.41 (m, 34H), 2.60 (s, 8H, 4×CH₂), 1.72–1.70 (m, 4H, 2×CH₂), 1.39–1.37 (m, 4H, 2×CH₂), 1.21 (s, 18H, 6×CH₂, 2×CH₃), 1.09–0.79 (m, 4H, 2×CH₂), 0.80–0.79 (m, 6H, 2×CH₃); ¹³C NMR (100 MHz, 10% CD₃OD in CDCl₃) δ 172.4, 172.0, 160.3, 153.0, 152.8, 126.9, 124.1, 122.7, 122.3, 108.2, 101.4, 98.9, 71.7, 70.3, 69.5, 69.3,

68.9, 68.5, 68.4, 66.3, 65.8, 63.8, 49.4, 49.2, 48.9, 48.7, 48.5, 37.2, 31.7, 29.2, 29.1, 29.0, 28.9, 28.7, 25.9, 22.5, 15.9, 13.9. ESI-HRMS (m/z) calculated for $C_{83}H_{122}N_8O_{30} = 1733.8159$ [$M + Na$] $^+$, found 1733.8152 [$M + Na$] $^+$.

Fuc(3,5)2Et8 **10**: This compound was prepared from **28** and **33** according to general procedure 3 and isolated as an orange wax (Yield: 34%). $[\alpha]_D^{20}$ 78.7 (c , 0.07 in CH_3OH); FT-IR: ν_{max}/cm^{-1} 3438, 2925, 1735, 1592, 1350, 1092, 843, 754; 1H NMR (400 MHz, 10% CD_3OD in $CDCl_3$) δ 7.94 (d, $J = 8.68$ Hz, 2H, $2 \times ArH$), 7.86–7.83 (m, 4H, $2 \times ArH$, $2 \times CH$ (triazole)), 7.56 (d, $J = 8.37$ Hz, 2H, $2 \times ArH$), 7.30 (d, $J = 8.68$ Hz, 2H, $2 \times ArH$), 7.25–7.24 (m, 2H, $2 \times ArH$), 6.67–6.66 (m, 1H, ArH), 5.46–5.44 (s, 1H, CH), 4.72–4.36 (m, 12H), 4.18–4.06 (m, 10H), 3.89–3.79 (m, 14H), 3.62–3.41 (m, 28H), 2.60 (s, 8H, $4 \times CH_2$), 1.69–1.62 (m, 2H, $2 \times CH$), 1.39–1.25 (m, 14H, $7 \times CH_2$), 1.10–1.08 (m, 2H, CH_2), 0.88–0.81 (m, 18H, $6 \times CH_3$); ^{13}C NMR (100 MHz, 10% CD_3OD in $CDCl_3$) δ 172.4, 164.9, 160.5, 126.9, 124.1, 122.7, 122.4, 108.2, 70.8, 70.4, 69.6, 69.4, 68.9, 66.3, 65.9, 64.3, 63.8, 49.9, 49.5, 49.2, 49.0, 48.8, 39.3, 37.2, 30.4, 28.9, 28.8, 23.8, 22.9, 15.9, 13.9, 10.9. ESI-HRMS (m/z) calculated for $C_{83}H_{122}N_8O_{30} = 1733.8159$ [$M + Na$] $^+$, found m/z 878.4021 [$M + 2Na$] $^+$.

Fuc(3,5)12 **11**: This compound was prepared from **29** and **33** according to general procedure 3 and isolated as an orange solid (Yield: 47%). $Mp = 146.4^\circ C$; $[\alpha]_D^{20}$ 76.5 (c , 0.065 in CH_3OH); FT-IR: ν_{max}/cm^{-1} 3413, 2923, 1735, 1592, 1348, 1091, 842, 754; 1H NMR (400 MHz, 10% CD_3OD in $CDCl_3$) δ 7.94–7.84 (m, 6H, $4 \times ArH$, $2 \times CH$ (triazole)), 7.57–7.55 (m, 2H, $2 \times ArH$), 7.31–7.17 (m, 4H, $4 \times ArH$), 6.66–6.65 (m, 1H, ArH), 5.46 (s, 1H, CH), 4.72–4.39 (m, 12H), 4.17–4.06 (m, 8H), 3.97–3.83 (m, 12H), 3.65–3.36 (m, 32H), 2.60 (s, 8H, $4 \times CH_2$), 1.72–1.71 (m, 4H, $2 \times CH_2$), 1.39–1.38 (m, 4H, $2 \times CH_2$), 1.19 (s, 30H, $2 \times CH_3$, $12 \times CH_2$), 1.09–1.08 (m, 4H, $2 \times CH_2$), 0.81–0.78 (m, 6H, $2 \times CH_3$); ^{13}C NMR (100 MHz, 10% CD_3OD in $CDCl_3$) δ 172.4, 160.3, 126.9, 124.4, 124.1, 122.7, 122.3, 108.2, 98.9, 71.7, 70.3, 69.5, 69.4, 68.9, 68.5, 68.4, 66.3, 65.9, 64.3, 63.8, 49.9, 49.4, 49.2, 49.0, 48.8, 37.2, 31.8, 29.5, 29.2, 29.0, 28.8, 25.9, 22.6, 15.9, 13.9. ESI-HRMS (m/z) calculated for $C_{91}H_{138}N_8O_{30} = 1845.9411$ [$M + Na$] $^+$, found m/z 934.9670 [$M + 2Na$] $^+$.

Fuc(3,4,5)2Et8 **12**: This compound was prepared from **30** and **33** according to general procedure 3 and isolated as an orange wax (Yield: 37%). $[\alpha]_D^{20}$ 130.0 (c , 0.03 in CH_3OH); FT-IR: ν_{max}/cm^{-1} 3407, 2922, 1731, 1331, 1093, 840; 1H NMR (400 MHz, 10% CD_3OD in $CDCl_3$) δ 7.95–7.93 (m, 2H, $2 \times ArH$), 7.86–7.84 (m, 2H, $2 \times ArH$), 7.57–7.55 (m, 2H, $2 \times ArH$), 7.35–

7.27 (m, 4H, 4×ArH), 5.47 (s, 1H, CH), 4.83–4.44 (m, 10H), 4.18–4.06 (m, 10H), 3.89–3.34 (m, 46H), 2.61 (s, 8H, 4×CH₂), 1.71–1.64 (m, 3H, 3×CH), 1.52–1.09 (m, 30H, 2×CH₃, 12×CH₂), 0.89–0.83 (m, 18H, 6×CH₃); ¹³C NMR (100 MHz, 10% CD₃OD in CDCl₃) δ 172.4, 172.1, 172.0, 164.9, 153.2, 153.1, 152.8, 150.1, 143.1, 140.1, 126.9, 124.1, 123.3, 122.7, 122.5, 108.0, 101.4, 71.3, 70.3, 69.4, 68.9, 63.8, 63.4, 62.7, 40.6, 39.5, 37.2, 30.5, 30.3, 29.2, 29.0, 28.9, 28.8, 23.8, 23.6, 23.0, 22.9, 16.0, 13.9, 11.0. ESI-HRMS (*m/z*) calculated for C₉₁H₁₃₈N₈O₃₁ = 1861.9360 [*M* + Na]⁺, found *m/z* 942.9638 [*M* + 2Na]⁺.

3,5-dialkyloxybenzoic acid **13**: This compound was prepared from methyl 3,5-dihydroxybenzoate and 1-bromooctane according to general procedure 4, and was isolated as white solid (quantitative yield). Mp = 58.0°C; FT-IR: ν_{max}/cm⁻¹ 2917, 1559, 1388, 1264, 1154, 1015, 855, 720; ¹H NMR (400 MHz, CDCl₃) δ 7.23 (d, *J* = 2.32 Hz, 2H, 2×ArH), 6.69 (t, *J* = 2.37 Hz, 1H, ArH), 3.98 (t, *J* = 6.59 Hz, 4H, 2×CH₂), 1.80–1.75 (m, 4H, 2×CH₂), 1.48–1.28 (m, 20H, 10×CH₂), 0.91–0.87 (m, 6H, 2×CH₃); ¹³C NMR (100 MHz, CDCl₃) δ 171.9, 160.2, 130.9, 108.2, 107.5, 68.4, 31.8, 29.3, 29.2, 26.0, 22.7, 14.1; ESI-HRMS (*m/z*) calculated for C₂₃H₃₈O₄ = 377.2697 [*M* - H]⁻, found 377.2697 [*M* - H]⁻.

3,5-bis((2-ethylhexyl)oxy)benzoic acid **14**: This compound was prepared from methyl 3,5-dihydroxybenzoate and 2-ethylhexyl bromide according to general procedure 4, and was isolated as colorless liquid (quantitative yield). FT-IR: ν_{max}/cm⁻¹ 2926, 1689, 1592, 1444, 1296, 1166, 1053, 735; ¹H NMR (400MHz, CDCl₃) 7.23 (2H, d, *J* = 2.36 Hz), 6.69 (1H, t, *J* = 2.26 Hz), 3.91–3.84 (4H, m), 1.77–1.68 (2H, m), 1.56–1.26 (16H, m), 0.96–0.88 (12H, m); ¹³C NMR (100 MHz, CDCl₃) δ 172.2, 160.5, 131.0, 108.1, 107.5, 70.8, 39.4, 30.5, 29.1, 23.9, 23.3, 23.1, 14.1, 11.1; ESI-HRMS (*m/z*) calculated for C₂₃H₃₈O₄ = 377.2697 [*M* - H]⁻, found 377.2697 [*M* - H]⁻.

3,5-bis(dodecayloxy)benzoic acid **15**: This compound was prepared from methyl 3,5-dihydroxybenzoate and 1-bromododecane according to general procedure 4, and was isolated as white solid (quantitative yield). Mp = 67.6°C; FT-IR: ν_{max}/cm⁻¹ 2916, 1686, 1596, 1394, 1316, 1161, 1058, 857, 669; ¹H NMR (400 MHz, CDCl₃) δ 7.23 (d, *J* = 2.33 Hz, 2H, 2×ArH), 6.69 (t, *J* = 2.31 Hz, 1H, ArH), 3.98 (t, *J* = 6.50 Hz, 4H, 2×CH₂), 1.80–1.77 (m, 4H, 2×CH₂), 1.47–1.44 (m, 4H, 2×CH₂), 1.36–1.28 (m, 32H, 16×CH₂), 0.88 (t, *J* = 7.06 Hz, 6H, 2×CH₃); ¹³C NMR (100 MHz, CDCl₃) δ 171.7, 160.2, 130.9, 108.2, 107.5, 68.4, 31.9, 29.7, 29.6, 29.4,

29.2, 26.0, 22.7, 14.1; ESI-HRMS (m/z) calculated for $C_{31}H_{54}O_4=489.3949$ $[M - H]^-$, found 489.3945 $[M - H]^-$.

3,4,5-tris((2-ethylhexyl)oxy)benzoic acid **16**: This compound was prepared from methyl 3,4,5-dihydrobenzoate and 2-ethylhexyl bromide according to general procedure 4, and was isolated as colorless liquid (quantitative yield). FT-IR: $\nu_{\max}/\text{cm}^{-1}$ 2914, 1685, 1590, 1395, 1317, 1163, 1059, 858, 669; ^1H NMR (400 MHz, CDCl_3) δ 7.33 (s, 2H, $2\times\text{ArH}$), 3.96–3.87 (m, 6H, $3\times\text{CH}_2$), 1.80–1.26 (m, 27H, $3\times\text{CH}$, $12\times\text{CH}_2$), 0.96–0.89 (m, 18H, $4\times\text{CH}_3$); ^{13}C NMR (100 MHz, CDCl_3) δ 171.7, 153.1, 143.2, 123.4, 108.1, 71.4, 40.6, 39.6, 30.5, 30.4, 29.3, 29.1, 23.8, 23.7, 23.1, 14.1, 11.2, 11.1; ESI-HRMS (m/z) calculated for $C_{31}H_{54}O_5=505.3898$ $[M - H]^-$, found 505.3892 $[M - H]^-$.

4-hydroxy-4'-formylazobenzene **17**¹: A suspension of 2 g 4-aminobenzaldehyde was prepared at 0°C in 11 mL water. At the same temperature was separately dissolved 1.1 g sodium nitrite in 8 mL water. To the suspension of 4-aminobenzaldehyde was simultaneously added at vigorous stirring the solution of sodium nitrite and 8 mL of 24% HCl solution. After 1 hour, a cooled to 0°C solution of 1.6 g phenol in 10 mL 6% NaOH solution was added to the reaction mixture. The end of the azo coupling was checked by TLC and the precipitate was filtered off to afford the final compound as brown-red solid (1.2g, 32%). Mp = 210°C; FT-IR: $\nu_{\max}/\text{cm}^{-1}$ 3308, 1670, 1584, 1281, 1128, 834; ^1H NMR (400MHz, $\text{C}_6\text{D}_6\text{O}$) 10.07 (1H, s), 8.01 (2H, d, $J = 8.53$ Hz), 7.92 (2H, d, $J = 8.53$ Hz), 7.79 (2H, d, $J = 8.91$ Hz), 6.79 (2H, d, $J = 8.88$ Hz); ^{13}C NMR (100 MHz, $(\text{CD}_3)_2\text{SO}$) δ 192.4, 177.7, 158.1, 140.7, 134.2, 131.2, 121.5, 120.6; ESI-HRMS (m/z) calculated for $\text{C}_{13}\text{H}_{10}\text{N}_2\text{O}_2=225.0669$ $[M - H]^-$, found 225.0670 $[M - H]^-$.

Compound **18**: This compound was prepared from **13** and **17** according to general procedure 1 and was isolated as an orange solid (Yield: 60%). Mp = 44.1°C; FT-IR: $\nu_{\max}/\text{cm}^{-1}$ 2917, 1702, 1594, 1444, 1295, 1161, 1053, 839, 752; ^1H NMR (400 MHz, CDCl_3) δ 10.10 (s, 1H, CHO), 8.06–8.03 (m, 6H, $6\times\text{ArH}$), 7.40 (d, $J = 8.89$ Hz, 2H, $2\times\text{ArH}$), 7.33 (d, $J = 2.35$ Hz, 2H, $2\times\text{ArH}$), 6.73 (t, $J = 2.33$ Hz, 1H, ArH), 4.01 (t, $J = 6.60$ Hz, 4H, $2\times\text{CH}_2$), 1.84–1.77 (m, 4H, $2\times\text{CH}_2$), 1.49–1.44 (m, 4H, $2\times\text{CH}_2$), 1.38–1.29 (m, 16H, $8\times\text{CH}_2$), 0.89 (t, $J = 6.95$ Hz, 6H, $2\times\text{CH}_3$). ^{13}C NMR (100 MHz, CDCl_3) δ 191.6 (CHO), 164.7 (C=O), 160.4, 155.8, 153.8, 150.2, 137.5, 130.7, 124.6, 123.4, 122.6, 108.3, 107.4, 68.5 (CH_2), 31.8 (CH_2), 29.4 (CH_2), 29.3 (CH_2), 29.2 (CH_2), 26.0 (CH_2), 22.7 (CH_2), 14.1 (CH_3). ESI-HRMS (m/z) calculated for $\text{C}_{36}\text{H}_{46}\text{N}_2\text{O}_5=586.7730$ $[M + H]^+$, found 586.4662 $[M + H]^+$.

Compound **19**: This compound was prepared from **14** and **17** according to general procedure 1 and was isolated as an orange wax (Yield: 56%). FT-IR: $\nu_{\max}/\text{cm}^{-1}$ 2925, 1701, 1444, 1189, 1034, 754; ^1H NMR (400 MHz, CDCl_3) δ 10.01 (s, 1H, CHO), 7.98–7.95 (m, 6H, 6 \times ArH), 7.32 (d, J = 8.84 Hz, 2H, 2 \times ArH), 7.25 (d, J = 2.36 Hz, 2H, 2 \times ArH), 6.66 (t, J = 2.29 Hz, 1H, ArH), 3.83–3.80 (m, 4H, 2 \times CH₂), 1.67–1.64 (m, 4H, 2 \times CH), 1.46–1.23 (m, 16H, 8 \times CH₂), 0.88–0.81 (m, 12H, 4 \times CH₃); ^{13}C NMR (100 MHz, CDCl_3) δ 191.6 (CHO), 164.8 (C=O), 160.6, 155.8, 153.8, 150.2, 137.5, 130.7, 124.6, 123.4, 122.6, 108.3, 107.3, 70.8, 70.7, 39.4, 30.6, 29.1, 23.9, 23.1, 14.1, 11.2 (CH₃). ESI-HRMS (m/z) calculated for $\text{C}_{36}\text{H}_{46}\text{N}_2\text{O}_5$ =587.3479 [M + H]⁺, found 587.3477 [M + H]⁺.

Compound **20**: This compound was prepared from **15** and **17** according to general procedure 1 and was isolated as an orange solid (Yield: 51%). Mp = 58.5°C; FT-IR: $\nu_{\max}/\text{cm}^{-1}$ 2917, 1702, 1594, 1347, 1165, 1046, 838, 752; ^1H NMR (400 MHz, CDCl_3) δ 10.01 (s, 1H, CHO), 7.97–7.95 (m, 6H, 6 \times ArH), 7.31 (d, J = 8.73 Hz, 2H, 2 \times ArH), 7.24 (d, J = 2.04 Hz, 2H, 2 \times ArH), 6.64 (s, 1H, ArH), 3.92 (t, J = 6.74 Hz, 4H, 2 \times CH₂), 1.73–1.68 (m, 4H, 2 \times CH₂), 1.39–1.35 (m, 4H, 2 \times CH₂), 1.18 (br s, 32H, 16 \times CH₂), 0.79 (t, J = 6.49 Hz, 6H, 2 \times CH₃); ^{13}C NMR (100 MHz, CDCl_3) δ 191.5 (CHO), 164.7 (C=O), 160.4, 155.8, 153.8, 150.2, 137.5, 130.7, 124.6, 123.4, 122.6, 108.3, 107.4, 68.4, 31.9, 29.7, 29.6, 29.4, 29.2, 26.1, 22.7. ESI-HRMS (m/z) calculated for $\text{C}_{44}\text{H}_{62}\text{N}_2\text{O}_5$ =697.4585 [M - H]⁻, found 697.5886 [M - H]⁻.

Compound **21**: This compound was prepared from **16** and **17** according to general procedure 1 and was isolated as an orange wax (Yield: 61%). FT-IR: $\nu_{\max}/\text{cm}^{-1}$ 2929, 1701, 1428, 1330, 1180, 937, 752; ^1H NMR (400 MHz, CDCl_3) δ 10.14 (s, 1H, CHO), 8.10–8.08 (m, 6H, 6 \times ArH), 7.46–7.43 (m, 4H, 4 \times ArH), 4.01–3.94 (m, 6H, 3 \times CH₂), 1.83–1.36 (m, 27H, 3 \times CH, 12 \times CH₂), 0.99–0.94 (m, 18H, 6 \times CH₃); ^{13}C NMR (100 MHz, CDCl_3) δ 191.6 (CHO), 164.8 (C=O), 155.8, 153.9, 153.2, 150.2, 143.3, 137.5, 130.7, 124.6, 123.3, 122.7, 108.1, 71.4, 40.7, 39.6, 30.6, 29.1, 23.9, 23.1, 14.1, 11.2. ESI-HRMS (m/z) calculated for $\text{C}_{44}\text{H}_{62}\text{N}_2\text{O}_6$ =714.4602, found 714.5860.

Compound **22**: This compound was prepared from **18** according to general procedure 2 and was isolated as an orange solid (Yield: 61%). Mp = 139.4°C; FT-IR: $\nu_{\max}/\text{cm}^{-1}$ 2923, 1739, 1590, 1297, 1161, 1034, 754; ^1H NMR (400 MHz, CDCl_3) δ 7.93 (d, J = 8.81 Hz, 2H, 2 \times ArH), 7.85 (d, J = 8.27 Hz, 2H, 2 \times ArH), 7.55 (d, J = 8.36 Hz, 2H, 2 \times ArH), 7.29–7.25 (m, 4H, 4 \times ArH), 6.65 (s, 1H, ArH), 5.41 (s, 1H, CH), 4.13–4.05 (m, 4H), 3.93 (t, J = 6.53 Hz, 4H, 2 \times CH₂), 3.70

(d, $J = 11.6$ Hz, 2H), 3.46 (s, 2H), 1.76–1.69 (m, 4H, $2 \times CH_2$), 1.39–1.35 (m, 4H, $2 \times CH_2$), 1.25–1.18 (m, 16H, $8 \times CH_2$), 0.83–0.79 (m, 6H, $2 \times CH_3$); ^{13}C NMR (100 MHz, CDCl_3) δ 164.8 (C=O), 160.4, 153.1, 152.8, 150.3, 140.6, 130.8, 126.9, 124.2, 122.9, 122.4, 108.3, 107.4, 101.4, 70.1, 68.5, 65.4, 63.9, 38.9, 31.8, 29.4, 29.3, 29.2, 26.0, 14.1. ESI-HRMS (m/z) calculated for $\text{C}_{41}\text{H}_{56}\text{N}_2\text{O}_8 = 705.4109$ $[M + \text{H}]^+$ 727.3928 $[M + \text{Na}]^+$, found 705.4114 $[M + \text{H}]^+$, 727.3935 $[M + \text{Na}]^+$.

Compound 23: This compound was prepared from **19** according to general procedure 2 and was isolated as an orange solid (Yield: 53%). Mp = 123.6°C; FT-IR: $\nu_{\text{max}}/\text{cm}^{-1}$ 2927, 1743, 1592, 1298, 1168, 1037, 752; ^1H NMR (400 MHz, CDCl_3) δ 8.01 (d, $J = 8.90$ Hz, 2H, $2 \times \text{ArH}$), 7.93 (d, $J = 8.68$ Hz, 2H, $2 \times \text{ArH}$), 7.63 (d, $J = 8.41$ Hz, 2H, $2 \times \text{ArH}$), 7.37 (d, $J = 8.84$ Hz, 2H, $2 \times \text{ArH}$), 7.34 (d, $J = 2.44$ Hz, 2H, $2 \times \text{ArH}$), 6.74 (t, $J = 2.30$ Hz, 1H, ArH), 5.49 (s, 1H, CH), 4.18 (d, $J = 11.76$ Hz, 2H), 4.12 (s, 2H), 3.93–3.89 (m, 4H), 3.78 (d, $J = 12.05$ Hz, 2H), 3.54 (s, 2H), 1.76–1.71 (m, 2H, $2 \times \text{CH}$), 1.55–1.29 (m, 16H, $8 \times CH_2$), 0.97–0.89 (m, 12H, $4 \times CH_3$); ^{13}C NMR (100 MHz, CDCl_3) δ 164.9 (C=O), 160.6, 153.1, 152.8, 150.3, 140.6, 130.8, 126.9, 124.2, 122.9, 122.4, 108.2, 107.3, 101.4, 70.9, 70.0, 65.4, 63.9, 39.4, 38.9, 30.5, 29.1, 23.9, 23.1, 14.1, 11.2. ESI-HRMS (m/z) calculated for $\text{C}_{41}\text{H}_{56}\text{N}_2\text{O}_8 = 705.4109$ $[M + \text{H}]^+$ 727.3928 $[M + \text{Na}]^+$, found 705.4113 $[M + \text{H}]^+$, 727.3930 $[M + \text{Na}]^+$.

Compound 24: This compound was prepared from **20** according to general procedure 2 and was isolated as an orange solid (Yield: 57%). Mp = 132.0°C; FT-IR: $\nu_{\text{max}}/\text{cm}^{-1}$ 2919, 1747, 1595, 1446, 1296, 1167, 1037, 754; ^1H NMR (400 MHz, CDCl_3) δ 8.01 (d, $J = 8.83$ Hz, 2H, $2 \times \text{ArH}$), 7.93 (d, $J = 8.66$ Hz, 2H, $2 \times \text{ArH}$), 7.63 (d, $J = 8.41$ Hz, 2H, $2 \times \text{ArH}$), 7.37 (d, $J = 8.90$ Hz, 2H, $2 \times \text{ArH}$), 7.33 (d, $J = 2.33$ Hz, 2H, $2 \times \text{ArH}$), 6.73 (t, $J = 2.33$ Hz, 1H, ArH), 5.49 (s, 1H, CH), 4.19 (d, $J = 11.87$ Hz, 2H), 4.12 (s, 2H), 4.01 (t, $J = 6.50$ Hz, 4H), 3.78 (d, $J = 11.87$ Hz, 2H), 3.53 (s, 2H), 1.82–1.78 (m, 4H, $2 \times CH_2$), 1.49–1.45 (m, 4H, $2 \times CH_2$), 1.37–1.27 (m, 32H, $16 \times CH_2$), 0.88 (t, $J = 6.65$ Hz, 6H, $2 \times CH_3$); ^{13}C NMR (100 MHz, CDCl_3) δ 164.8 (C=O), 160.4, 153.1, 152.8, 150.3, 140.6, 130.8, 126.9, 124.2, 122.9, 122.4, 108.3, 107.4, 101.4, 70.0, 68.5, 65.4, 63.9, 38.9, 31.9, 29.7, 29.6, 29.4, 29.2, 26.0, 22.7, 14.1. ESI-HRMS (m/z) calculated for $\text{C}_{49}\text{H}_{72}\text{N}_2\text{O}_8 = 817.5361$ $[M + \text{H}]^+$ 839.5180 $[M + \text{Na}]^+$, found 817.5365 $[M + \text{H}]^+$, 839.5185 $[M + \text{Na}]^+$.

Compound 25: This compound was prepared from **21** according to general procedure 2 and was isolated as an orange solid (Yield: 46%). Mp = 92.5°C; FT-IR: $\nu_{\text{max}}/\text{cm}^{-1}$ 2925, 1735, 1584,

1428, 1332, 1182, 1093, 1008, 753; ^1H NMR (400 MHz, CDCl_3) δ 8.02 (d, J = 8.84 Hz, 2H, $2\times\text{ArH}$), 7.93 (d, J = 8.54 Hz, 2H, $2\times\text{ArH}$), 7.63 (d, J = 8.46 Hz, 2H, $2\times\text{ArH}$), 7.43 (s, 2H, $2\times\text{ArH}$), 7.37 (d, J = 8.89 Hz, 2H, $2\times\text{ArH}$), 5.49 (s, 1H, CH), 4.20–4.12 (m, 4H), 3.98–3.93 (m, 6H), 3.78 (d, J = 12.06 Hz, 2H), 3.53 (s, 2H), 2.64–2.61 (m, 2H), 1.80–1.32 (m, 27H, $3\times\text{CH}$, $12\times\text{CH}_2$), 0.98–0.89 (m, 18H, $6\times\text{CH}_3$); ^{13}C NMR (100 MHz, CDCl_3) δ 164.9 (C=O), 153.2, 152.8, 150.3, 143.2, 140.7, 126.9, 124.2, 123.4, 122.8, 122.6, 108.1, 101.4, 76.1, 71.4, 70.0, 65.4, 63.9, 40.7, 39.6, 38.9, 30.6, 29.1, 23.9, 23.2, 14.1, 11.2. ESI-HRMS (m/z) calculated for $\text{C}_{49}\text{H}_{72}\text{N}_2\text{O}_9$ =833.5810 $[M + \text{H}]^+$ 855.5130 $[M + \text{Na}]^+$, found 833.5314 $[M + \text{H}]^+$, 855.5127 $[M + \text{Na}]^+$.

14-oxo-4,7,10,13-tetraoxaheptadec-1-yn-17-oic acid **26**: This compound was prepared according to literature procedure over two steps.² Sodium hydride (2.6g, 65 mmol, 65 equiv. 60% disperse in mineral oil) was slowly added to a solution of triethyleneglycol (15.02g, 100 mmol, 100 equiv.) in dry THF (75 mL) and the mixture stirred for 30 min at 0°C under N_2 . Propargyl bromide (5.4 mL, 50 mmol, 50 equiv.) was slowly injected to the reaction mixture, followed by stirring at 0°C for 2 hours and at room temperature for 20 hours. The mixture was poured into water, extracted with DCM, dried over Na_2SO_4 and purified by flash chromatography using EtOAc:hexane (3:2) as the eluent to afford the intermediate as pale yellow oil (3.95g, 43%). FT-IR: $\nu_{\text{max}}/\text{cm}^{-1}$ 2921, 2852, 1736, 1457, 1069; ^1H NMR (400MHz, CDCl_3) δ 5.15 (s, 1H, OH), 4.29–4.09 (m, 4H, $2\times\text{CH}_2$), 3.68–3.54 (m, 10H, $5\times\text{CH}_2$), 2.43–2.42 (m, 1H, CH); ^{13}C NMR (100 MHz, CDCl_3) δ 79.5, 74.9, 72.4, 70.3, 70.2, 68.8, 61.2, 58.1; LCMS (m/z) calculated for $\text{C}_9\text{H}_{16}\text{O}_4$ =189.1 $[M + \text{H}]^+$, found 189.1 $[M + \text{H}]^+$. The synthetic intermediate (2 g, 10.6 mmol, 1 equiv.) and succinic anhydride (1.28 g, 12.8 mmol, 1.2 equiv.) were dissolved in anhydrous DCM (10 mL) under N_2 . To this reaction mixture, triethylamine (1.48 mL, 10.6 mmol, 1 equiv.) was added dropwise. The reaction mixture was then stirred at room temperature for 24 hours under N_2 , before poured into water (60 mL) and neutralized with 1N HCl. The organic layer was then washed with brine, dried over Na_2SO_4 , concentrated under reduced pressure and purified by flash chromatography to afford the final product as pale yellow oil (2.02g, 68.3%). FT-IR: $\nu_{\text{max}}/\text{cm}^{-1}$ 1728, 1349, 1088, 834, 635; ^1H NMR (400 MHz, CDCl_3) δ 4.25–4.23 (m, 2H, CH_2), 4.18 (d, J = 2.40 Hz, 2H, CH_2), 3.69–3.64 (m, 11H, $5\times\text{CH}_2$, CH), 2.64 (s, 4H, CH_2); ^{13}C NMR (100 MHz, CDCl_3) δ 176.2, 172.1, 79.6, 79.5, 74.9, 70.3, 70.2, 70.1, 68.8, 63.7, 58.1, 28.8, 28.7; ESI-HRMS (m/z) calculated for $\text{C}_{13}\text{H}_{20}\text{O}_7$ =287.1136 $[M - \text{H}]^-$, found 287.1133 $[M - \text{H}]^-$.

Compound **27**: This compound was prepared from **22** and **26** according to general procedure 1 and was isolated as an orange wax (Yield: 67%). FT-IR: $\nu_{\text{max}}/\text{cm}^{-1}$ 2923, 1735, 1592, 1348, 1095, 843, 755; ^1H NMR (400 MHz, CDCl_3) δ 7.99 (d, $J = 8.92$ Hz, 2H, $2\times\text{ArH}$), 7.91 (d, $J = 8.49$ Hz, 2H, $2\times\text{ArH}$), 7.61 (d, $J = 8.58$ Hz, 2H, $2\times\text{ArH}$), 7.35 (d, $J = 8.87$ Hz, 2H, $2\times\text{ArH}$), 7.31 (d, $J = 2.24$ Hz, 2H, $2\times\text{ArH}$), 6.70 (t, $J = 2.27$ Hz, 1H, ArH), 5.50 (s, 1H, CH), 4.51 (s, 2H), 4.26–4.12 (m, 10H), 4.00–3.95 (m, 6H), 3.89–3.86 (m, 2H), 3.69–3.63 (m, 20H), 2.66 (s, 8H, $4\times\text{CH}_2$), 2.44–2.42 (m, 2H, $2\times\text{CH}$), 1.81–1.74 (m, 4H, $2\times\text{CH}_2$), 1.47–1.41 (m, 4H, $2\times\text{CH}_2$), 1.36–1.27 (m, 16H, $8\times\text{CH}_2$), 0.89–0.85 (m, 6H, $2\times\text{CH}_3$); ^{13}C NMR (100 MHz, CDCl_3) δ 172.2, 171.9, 164.7, 160.3, 153.1, 152.9, 150.2, 140.2, 130.9, 127.0, 124.2, 122.8, 122.4, 108.2, 101.5, 79.7, 74.6, 70.6, 70.4, 69.5, 69.1, 69.0, 68.4, 63.9, 63.4, 62.7, 58.4, 37.3, 31.8, 29.3, 29.2, 29.1, 29.0, 28.9, 26.0, 22.7, 14.1; ESI-HRMS (m/z) calculated for $\text{C}_{67}\text{H}_{92}\text{N}_2\text{O}_{20}=1245.6316$ [$M + \text{H}$] $^+$ 1267.6135 [$M + \text{Na}$] $^+$, found 1245.6305 [$M + \text{H}$] $^+$, 1267.6129 [$M + \text{Na}$] $^+$.

Compound **28**: This compound was prepared from **23** and **26** according to general procedure 1 and was isolated as an orange wax (Yield: 63%). FT-IR: $\nu_{\text{max}}/\text{cm}^{-1}$ 2929, 1734, 1592, 1347, 1096, 841; ^1H NMR (400 MHz, CDCl_3) δ 8.01 (d, $J = 8.88$ Hz, 2H, $2\times\text{ArH}$), 7.92 (d, $J = 8.44$ Hz, 2H, $2\times\text{ArH}$), 7.63 (d, $J = 8.49$ Hz, 2H, $2\times\text{ArH}$), 7.37 (d, $J = 8.84$ Hz, 2H, $2\times\text{ArH}$), 7.32 (d, $J = 2.33$ Hz, 2H, $2\times\text{ArH}$), 6.73 (t, $J = 2.30$ Hz, 1H, ArH), 5.52 (s, 1H, CH), 4.52 (s, 2H), 4.27–4.13 (m, 10H), 3.97–3.88 (m, 8H), 3.72–3.63 (m, 20H), 2.68 (s, 8H, $4\times\text{CH}_2$), 2.44–2.42 (m, 2H, $2\times\text{CH}$), 1.75–1.72 (m, 2H, $2\times\text{CH}$), 1.52–1.25 (m, 16H, $8\times\text{CH}_2$), 0.95–0.89 (m, 12H, $4\times\text{CH}_3$); ^{13}C NMR (100 MHz, CDCl_3) δ 172.2, 171.1, 164.8, 160.6, 153.1, 152.9, 150.3, 140.2, 130.8, 127.0, 124.4, 122.8, 122.4, 108.2, 101.5, 79.7, 74.6, 70.8, 70.6, 70.4, 69.5, 69.1, 63.9, 63.4, 58.4, 39.4, 37.3, 33.9, 30.5, 29.1, 29.0, 28.9, 24.9, 23.9, 23.0, 14.1, 11.1; ESI-HRMS (m/z) calculated for $\text{C}_{67}\text{H}_{92}\text{N}_2\text{O}_{20}=1245.6316$ [$M + \text{H}$] $^+$ 1267.6135 [$M + \text{Na}$] $^+$, found 1245.6294 [$M + \text{H}$] $^+$, 1267.6130 [$M + \text{Na}$] $^+$.

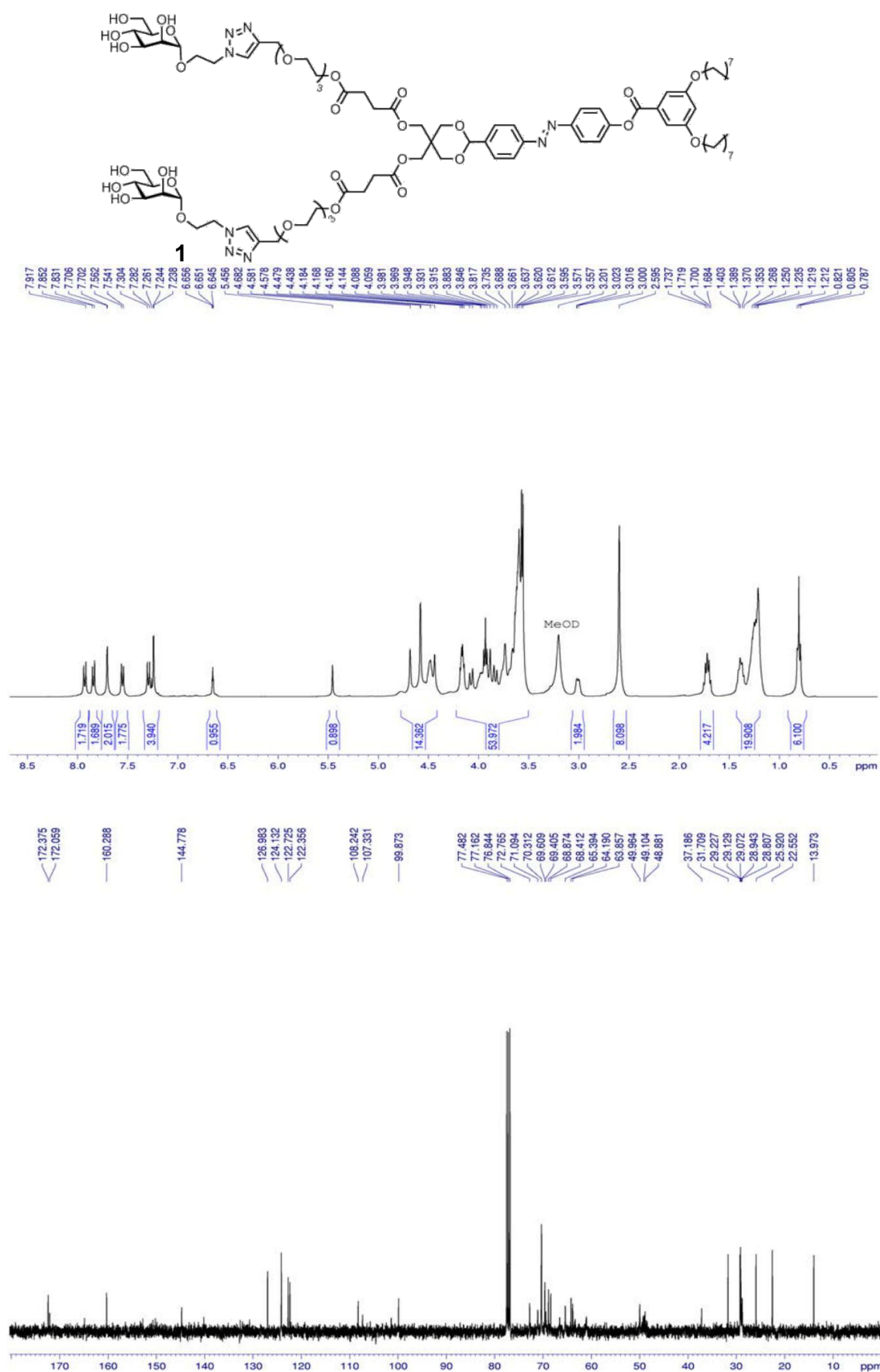
Compound **29**: This compound was prepared from **24** and **26** according to general procedure 1 and was isolated as an orange wax (Yield: 57%). FT-IR: $\nu_{\text{max}}/\text{cm}^{-1}$ 2926, 1735, 1593, 1348, 1097, 841; ^1H NMR (400 MHz, CDCl_3) δ 7.99 (d, $J = 8.73$ Hz, 2H, $2\times\text{ArH}$), 7.91 (d, $J = 8.34$ Hz, 2H, $2\times\text{ArH}$), 7.62 (d, $J = 8.35$ Hz, 2H, $2\times\text{ArH}$), 7.37–7.31 (m, 4H, $4\times\text{ArH}$), 6.71 (s, 1H, ArH), 5.51 (s, 1H, CH), 4.51 (s, 2H), 4.27–4.13 (m, 10H), 4.01–3.87 (m, 8H), 3.71–3.63 (m, 20H), 2.67 (s, 8H, $4\times\text{CH}_2$), 2.44–2.42 (m, 2H, $2\times\text{CH}$), 1.86–1.75 (m, 4H, $4\times\text{CH}_2$), 1.45–1.42 (m, 4H, $2\times\text{CH}_2$), 1.33–1.25 (m, 32H, $16\times\text{CH}_2$), 0.88–0.85 (m, 6H, $2\times\text{CH}_3$); ^{13}C NMR (100 MHz, CDCl_3) δ 172.2, 171.9, 164.7, 160.4, 153.1, 152.9, 150.3, 140.2, 130.9, 127.0, 124.2,

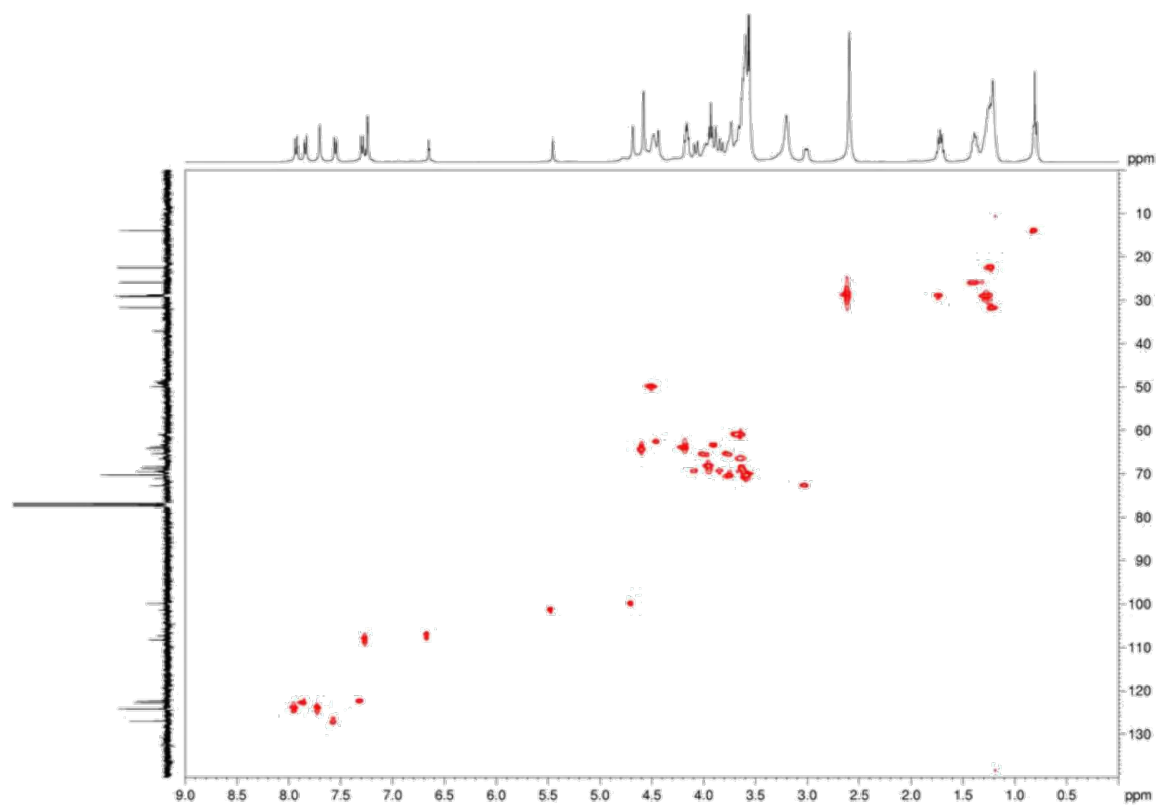
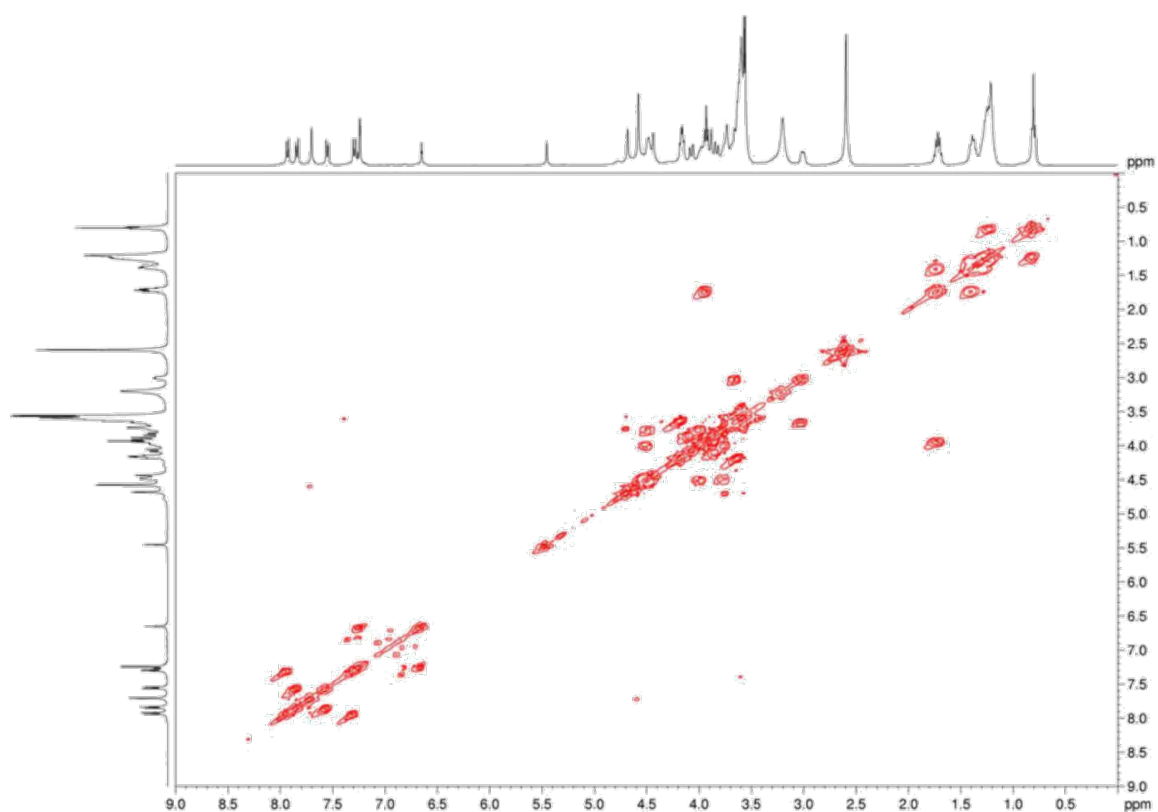
122.8, 122.4, 108.2, 107.3, 101.5, 79.7, 74.6, 70.6, 70.5, 69.5, 69.1, 69.0, 68.4, 63.9, 63.4, 62.7, 58.4, 37.3, 31.9, 29.7, 29.6, 29.4, 29.2, 29.0, 28.9, 26.0, 22.7, 14.1; ESI-HRMS (m/z) calculated for $C_{75}H_{108}N_2O_{20}$ = 1357.7568 $[M + H]^+$ 1379.7387 $[M + Na]^+$, found 1357.7605 $[M + H]^+$, 1379.7400 $[M + Na]^+$.

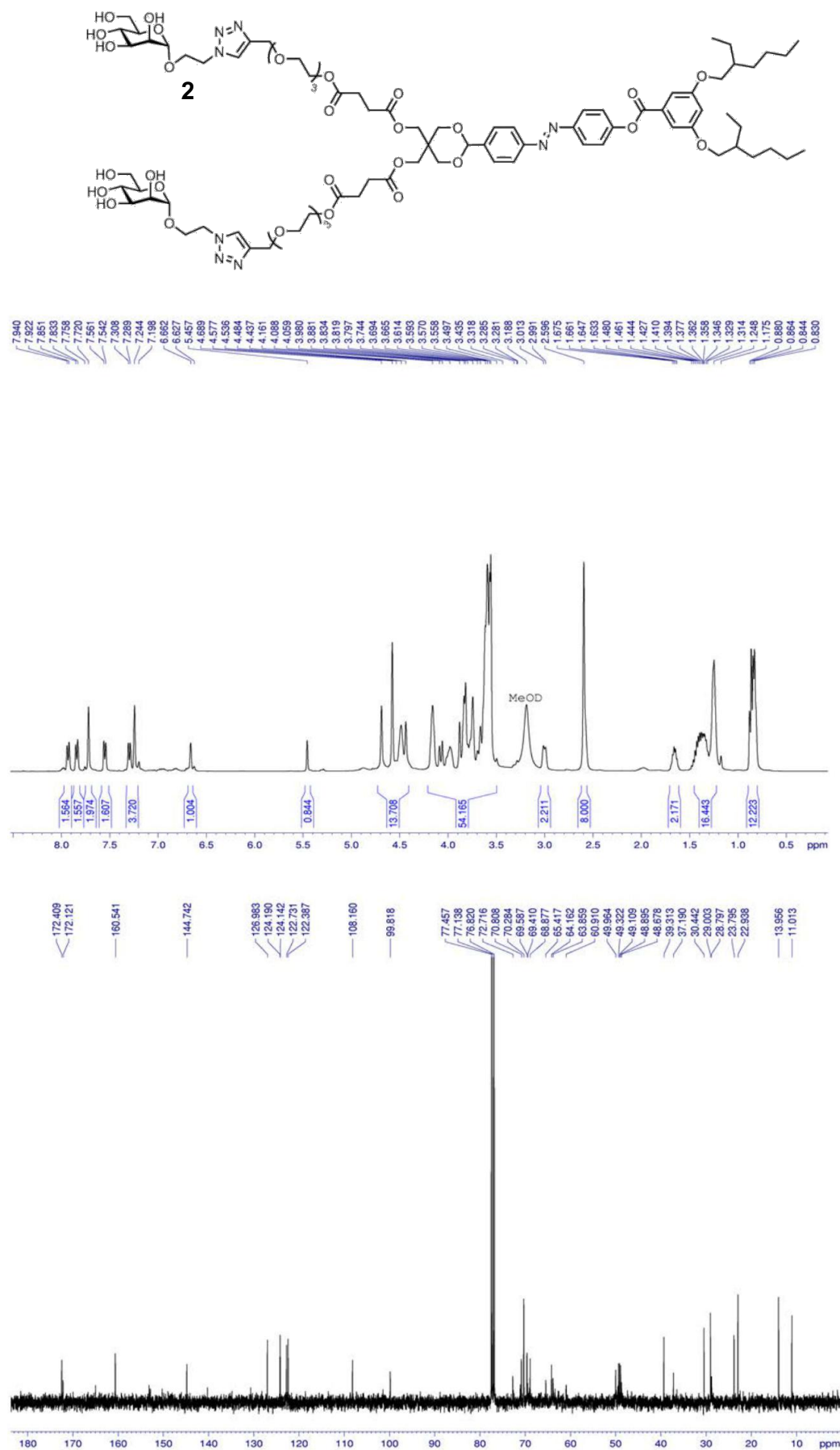
Compound 30: This compound was prepared from **25** and **26** according to general procedure 1 and was isolated as an orange wax (Yield: 46%). FT-IR: $\nu_{\max}/\text{cm}^{-1}$ 2932, 1731, 1333, 1183, 1095, 1009, 938, 840, 755; ^1H NMR (400 MHz, CDCl_3) δ 8.00 (d, $J = 8.90$ Hz, 2H, $2\times\text{ArH}$), 7.92 (d, $J = 8.44$ Hz, 2H, $2\times\text{ArH}$), 7.62 (d, $J = 8.48$ Hz, 2H, $2\times\text{ArH}$), 7.41 (s, 2H, $2\times\text{ArH}$), 7.36 (d, $J = 8.93$ Hz, 2H, $2\times\text{ArH}$), 5.51 (s, 1H, CH), 4.51 (s, 2H), 4.27–4.13 (m, 10H), 3.96–3.87 (m, 8H), 3.71–3.63 (m, 20H), 2.67 (s, 8H, $4\times\text{CH}_2$), 2.44–2.42 (m, 2H, $2\times\text{CH}$), 1.88–1.30 (m, 27H, $3\times\text{CH}$, $12\times\text{CH}_2$), 0.95–0.87 (m, 18H, $6\times\text{CH}_3$); ^{13}C NMR (100 MHz, CDCl_3) δ 172.2, 171.9, 164.8, 153.3, 153.2, 152.9, 150.2, 143.1, 140.2, 127.0, 124.2, 123.4, 122.8, 122.5, 108.1, 101.5, 79.7, 74.6, 71.4, 70.6, 70.4, 69.5, 69.1, 69.0, 63.9, 63.4, 62.7, 58.4, 40.7, 39.6, 37.3, 30.5, 30.4, 29.3, 29.1, 29.0, 28.9, 23.9, 23.7, 23.1, 14.2, 14.1, 11.2; ESI-HRMS (m/z) calculated for $C_{75}H_{108}N_2O_{21}$ = 1373.7517 $[M + H]^+$ 1395.7336 $[M + Na]^+$, found 1373.7531 $[M + H]^+$, 1395.7316 $[M + Na]^+$.

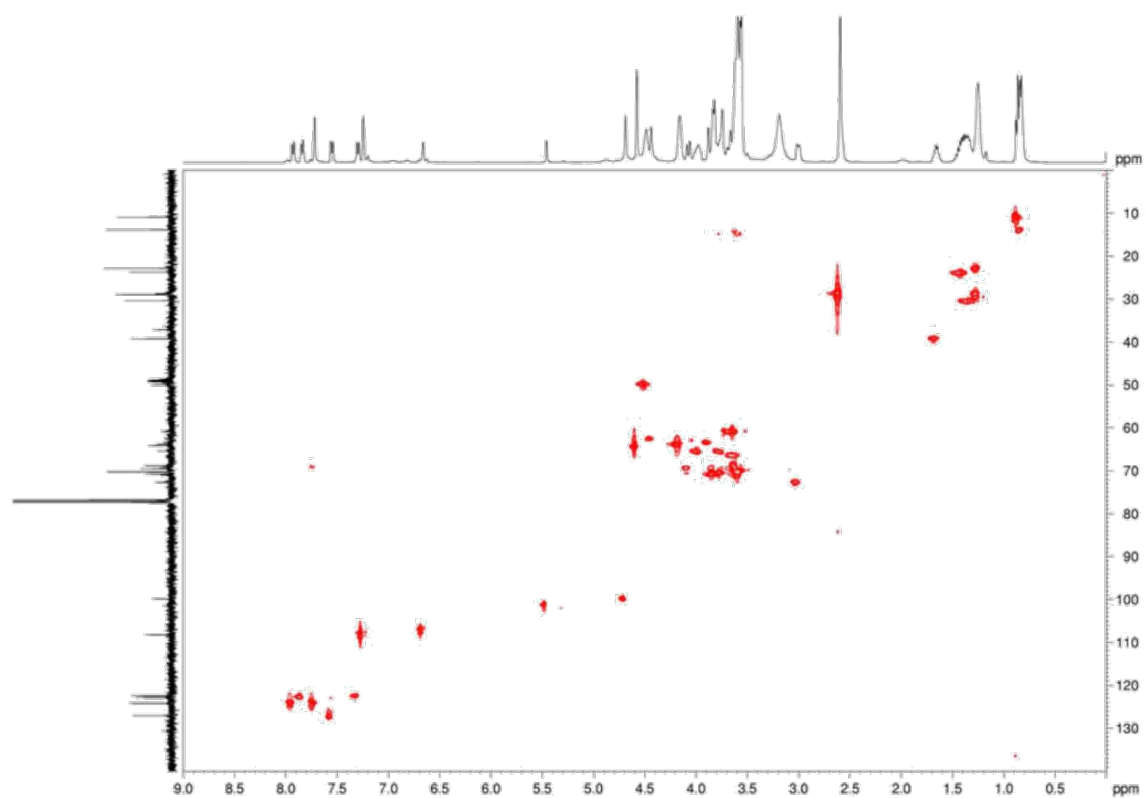
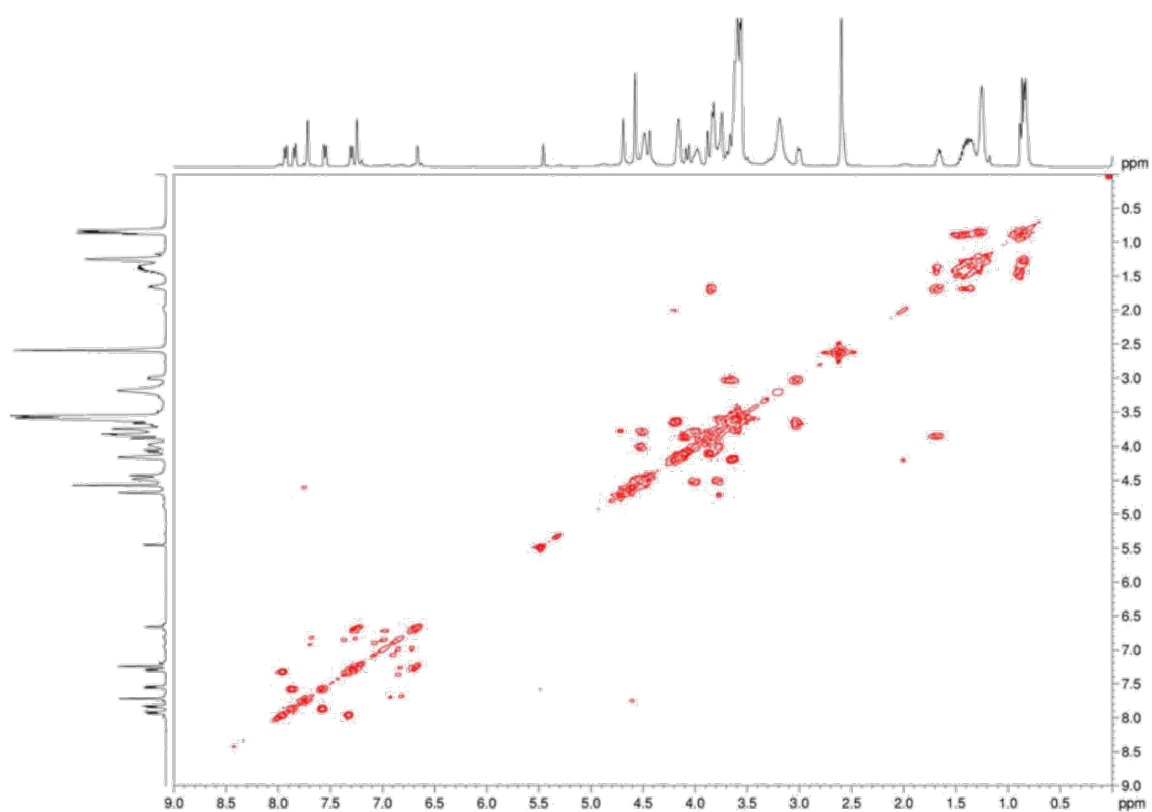
2-azidoethyl α -D-mannopyranoside 31: This compound was prepared from α -D-mannose pentaacetate according to general procedure 5 and was isolated as white solid (Yield: 74%). Mp = 132.8°C; $[\alpha]_D^{20}$ 125.0 (c , 0.06 in CH_3OH); FT-IR: $\nu_{\max}/\text{cm}^{-1}$ 2922, 2100, 1559, 1406, 1287, 1056, 648; ^1H NMR (400 MHz, CD_3OD) δ 4.85 (d, $J = 1.48$ Hz, 1H, $H-1$), 3.96–3.84 (m, 3H, $H-2$, $H-3$, $H-4$), 3.78–3.73 (m, 2H, $H-6$), 3.69–3.57 (m, 3H, $H-5$, $\text{CH}_2\text{CH}_2\text{N}_3$), 3.45–3.42 (m, 2H, CH_2N_3); ^{13}C NMR (100 MHz, CD_3OD) δ 100.4, 73.4, 71.0, 70.6, 67.1, 66.3, 61.3, 50.4; LCMS: m/z calculated for $\text{C}_8\text{H}_{15}\text{N}_3\text{O}_6$ = 272.1 $[M + Na]^+$, found 272.1 $[M + Na]^+$.

2-azidoethyl β -D-galactopyranoside 32: This compound was prepared from β -D-galactose pentaacetate according to general procedure 5 and was isolated as colorless wax (Yield: 77%). $[\alpha]_D^{20}$ 18.9 (c , 0.19 in CH_3OH); FT-IR: $\nu_{\max}/\text{cm}^{-1}$ 2102, 1580, 1369, 1047; ^1H NMR (400 MHz, CD_3OD) δ 4.30 (d, $J = 7.36$ Hz, 1H, $H-1$), 4.07–4.01 (m, 1H, OCH), 3.89–3.88 (m, 1H, $H-4$), 3.79–3.74 (m, 3H, $H-2$, $H-3$, OCH), 3.59–3.49 (m, 5H, $H-5$, $\text{CH}_2\text{CH}_2\text{N}_3$, CH_2N_3); ^{13}C NMR (100 MHz, CD_3OD) δ 103.7, 75.3, 73.5, 71.1, 68.9, 67.8, 61.0, 50.7; LCMS (m/z) calculated for $\text{C}_8\text{H}_{15}\text{N}_3\text{O}_6$ = 272.1 $[M + Na]^+$, found 272.1 $[M + Na]^+$.

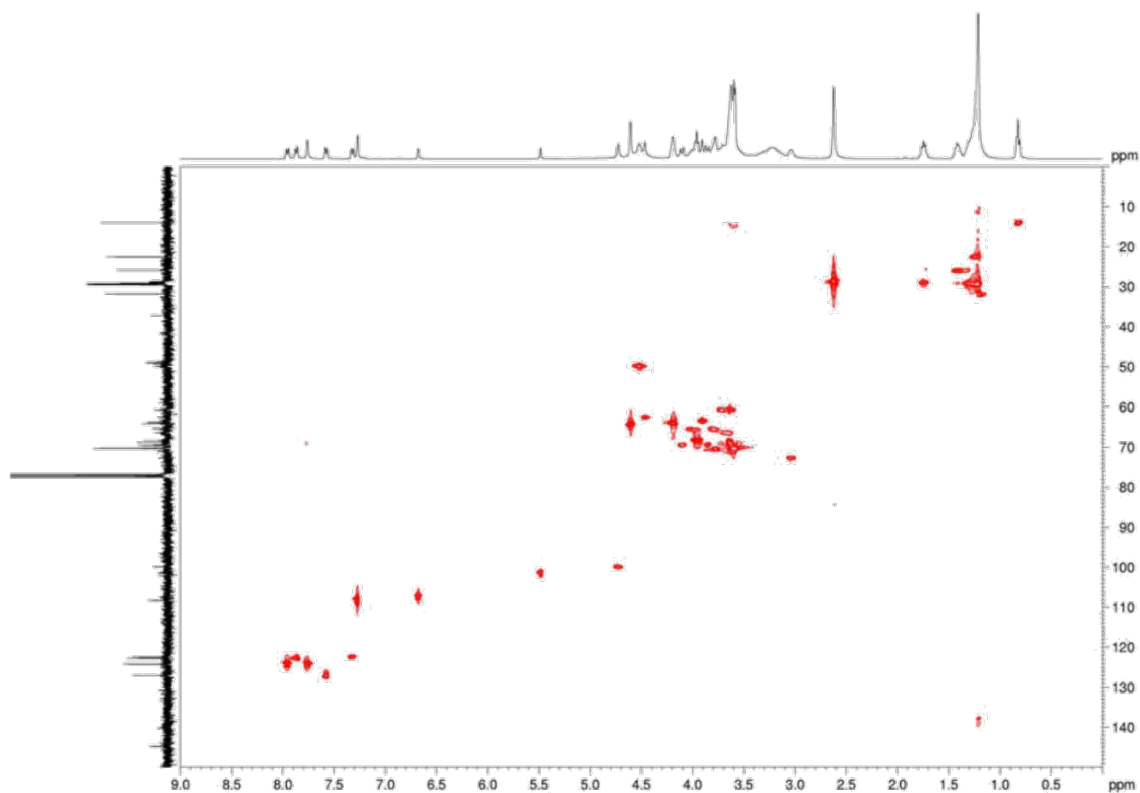
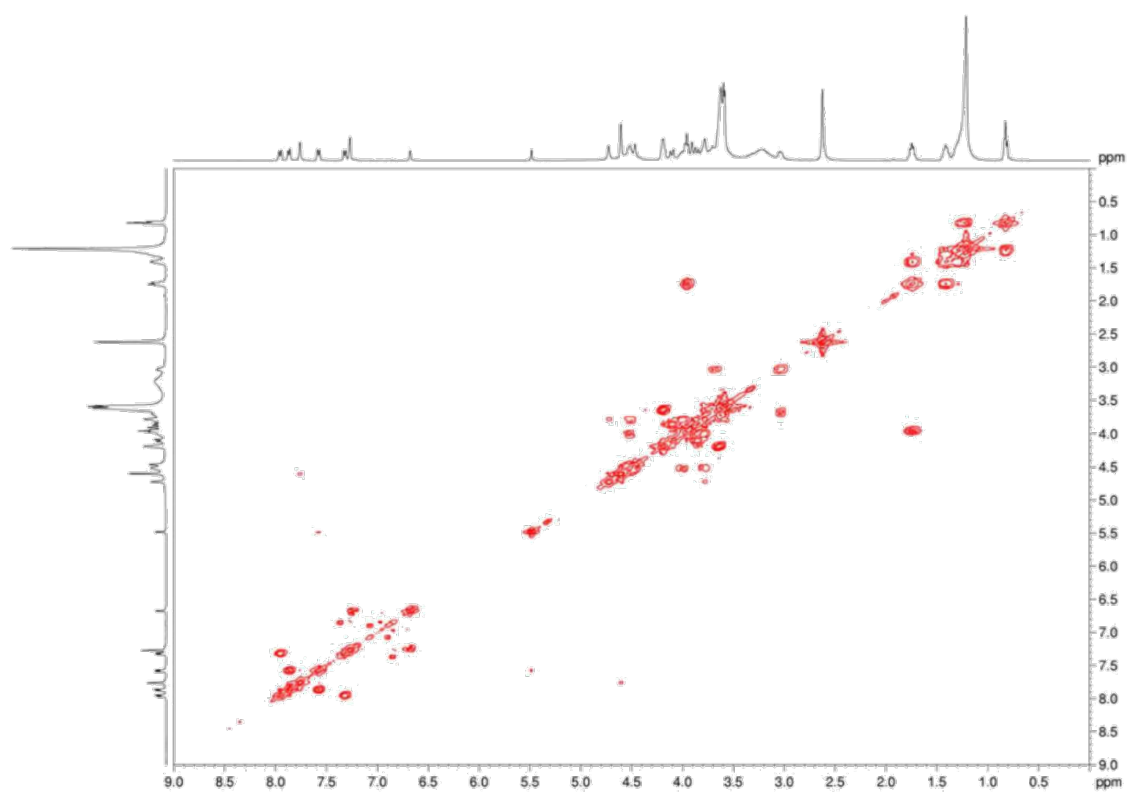


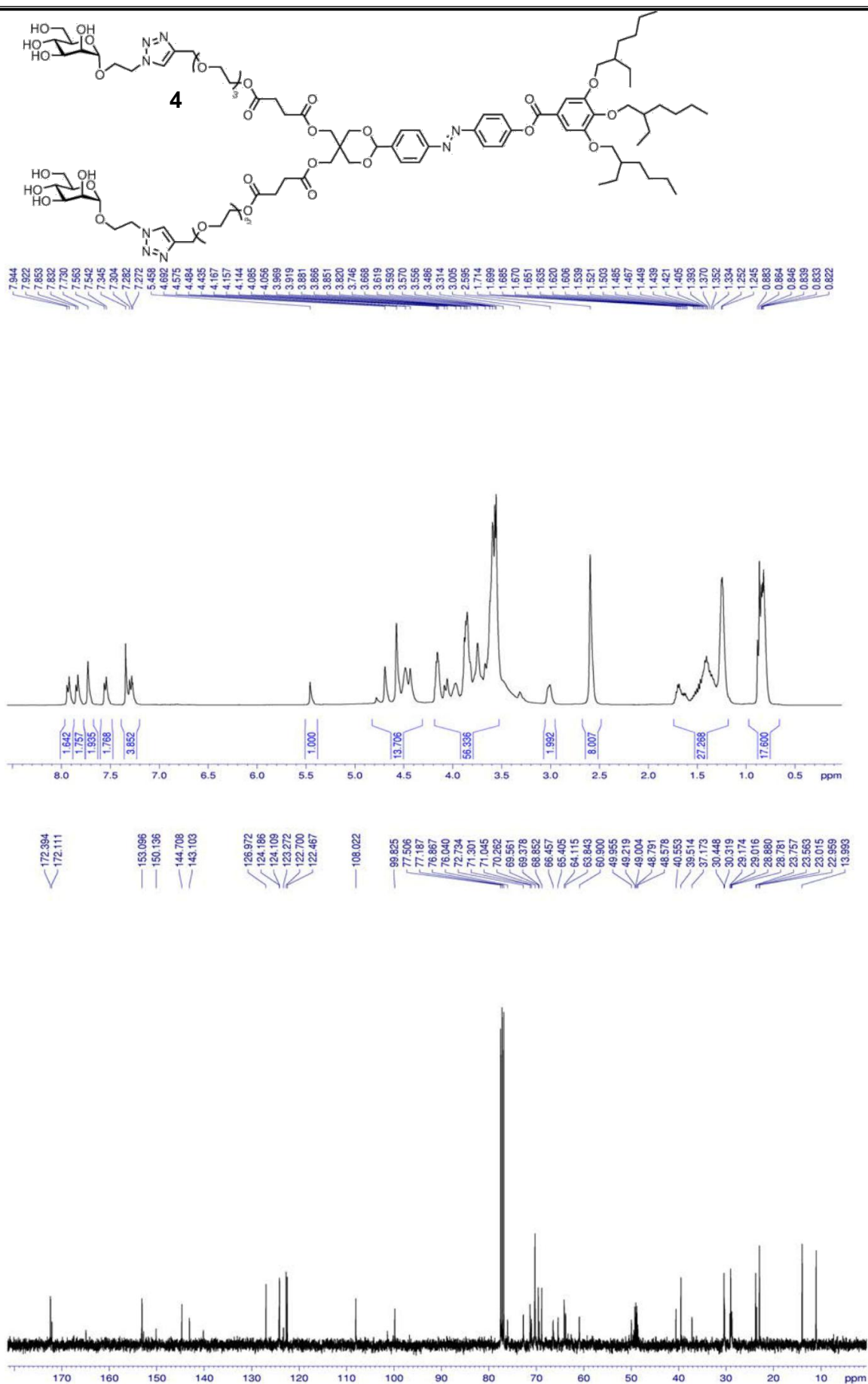


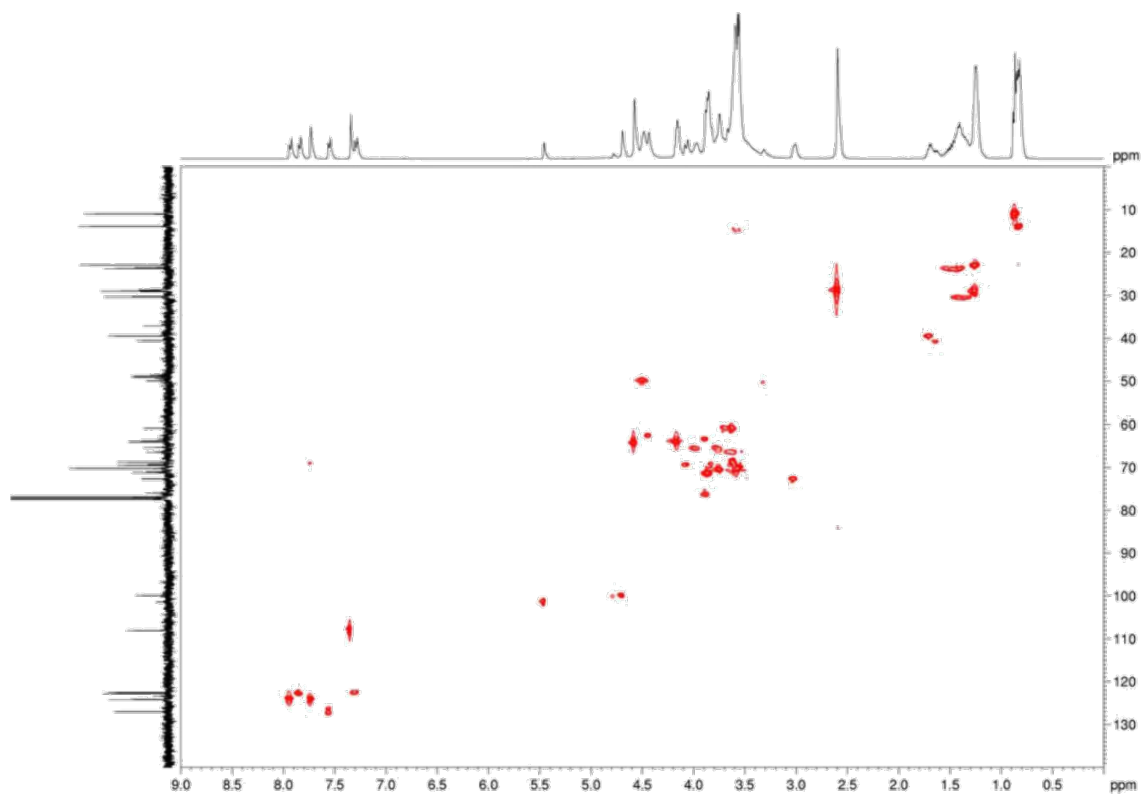
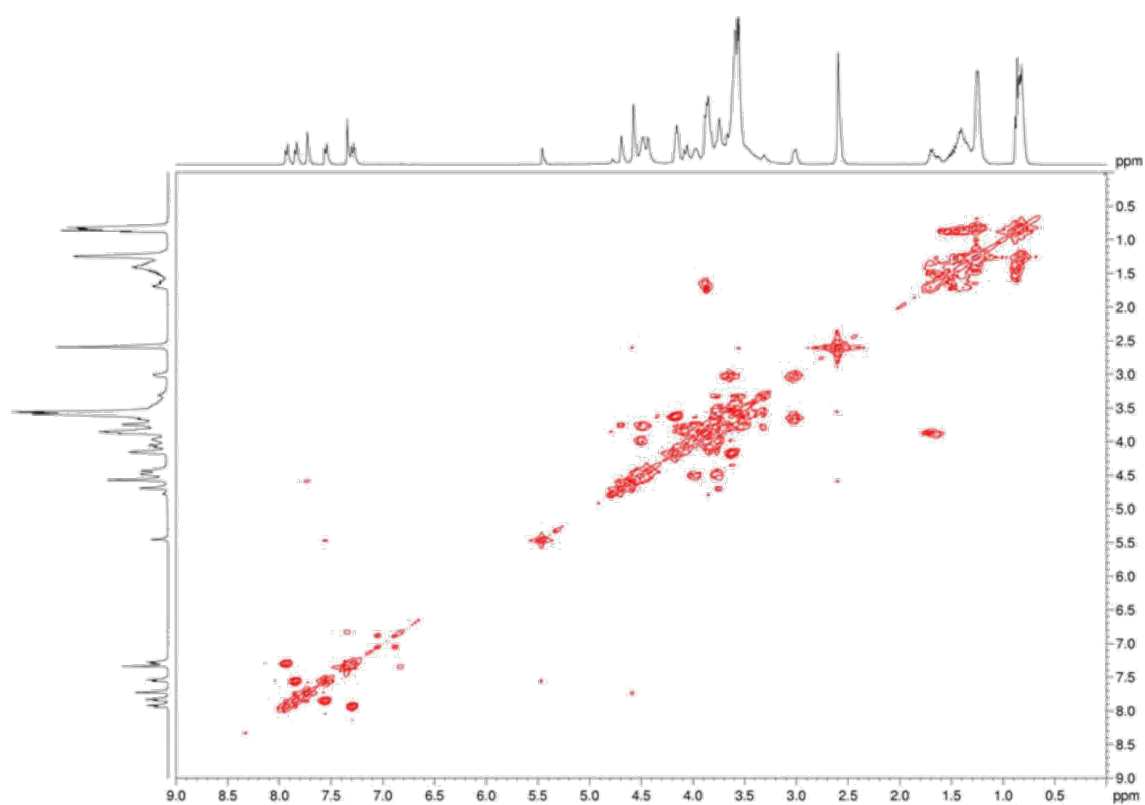


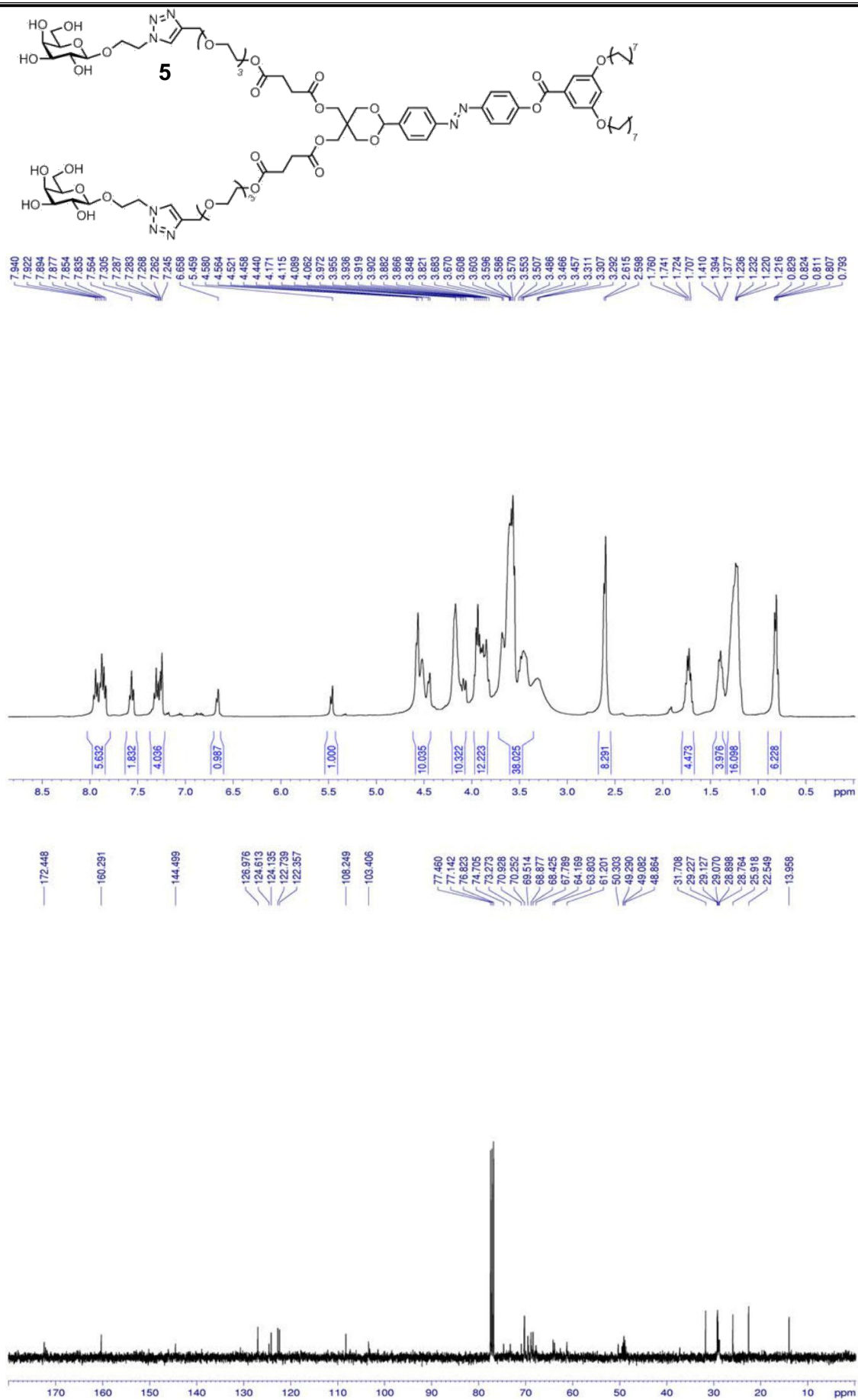


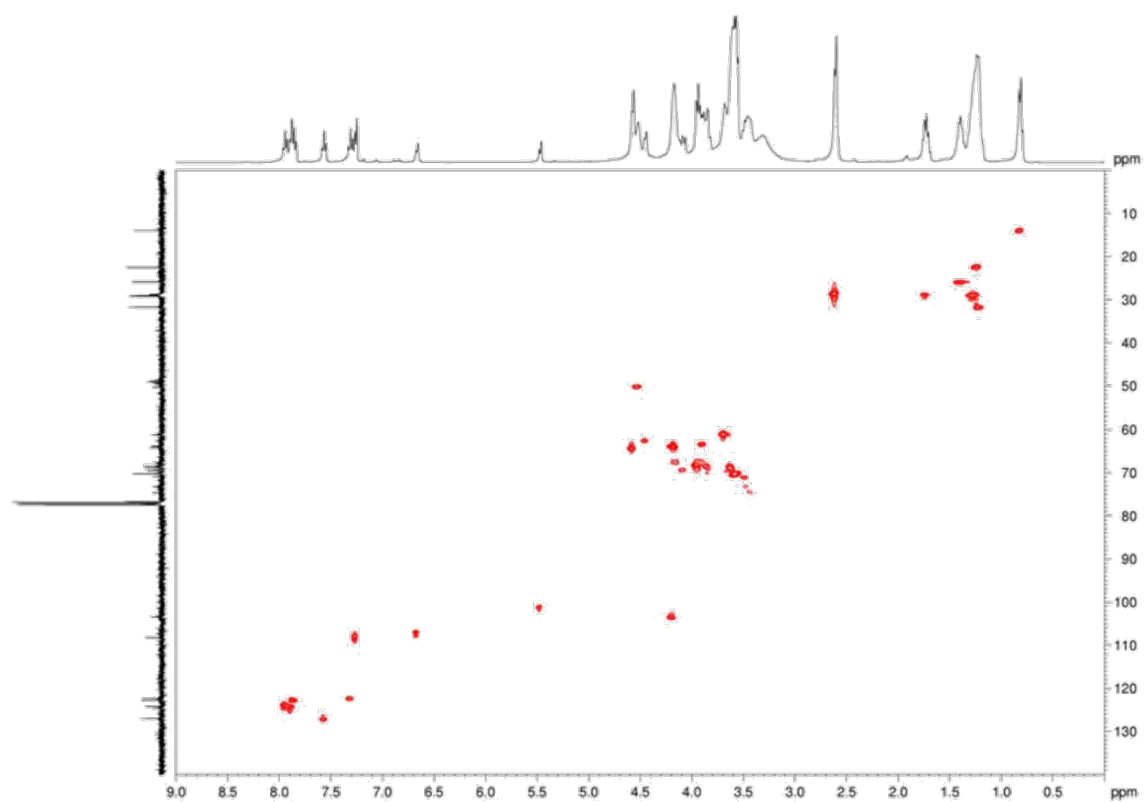
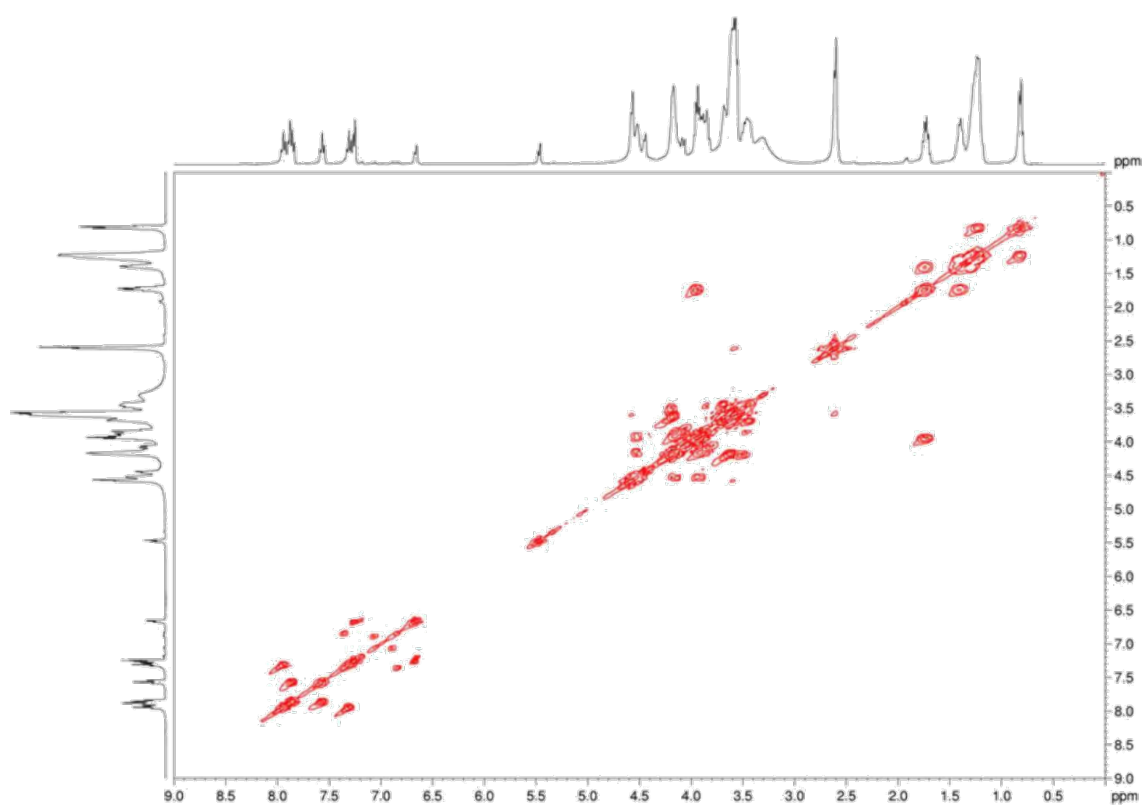


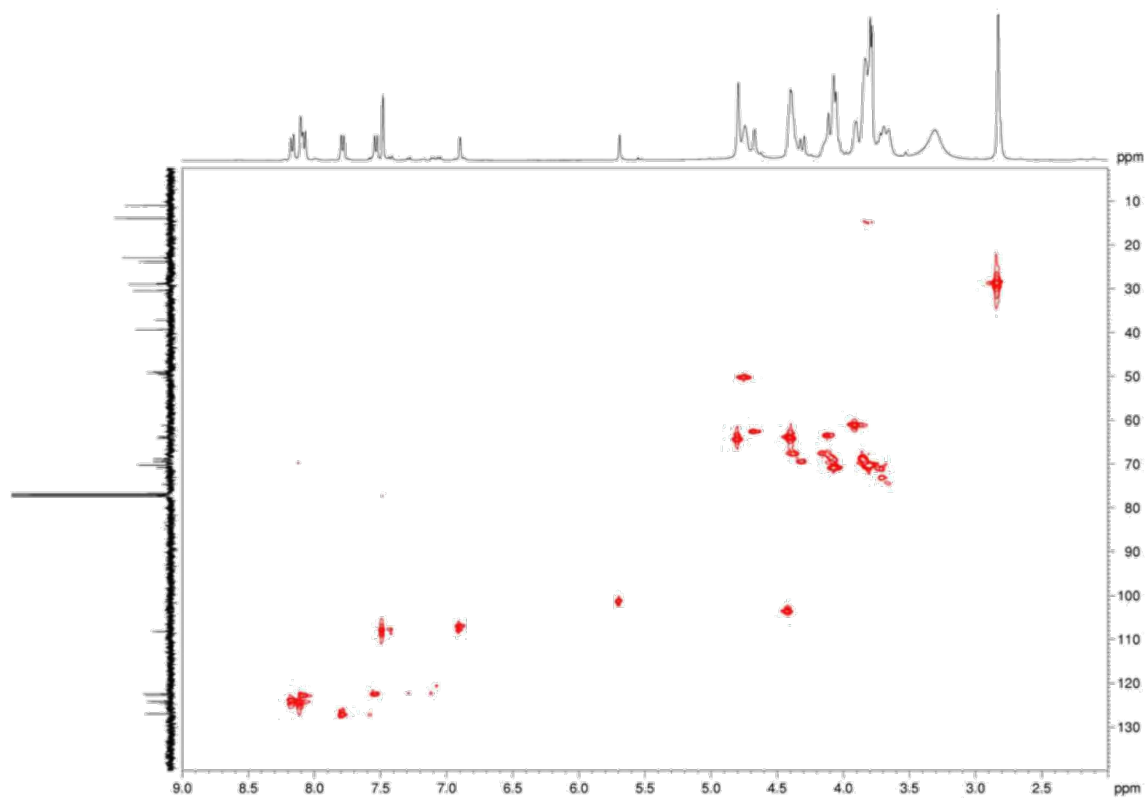
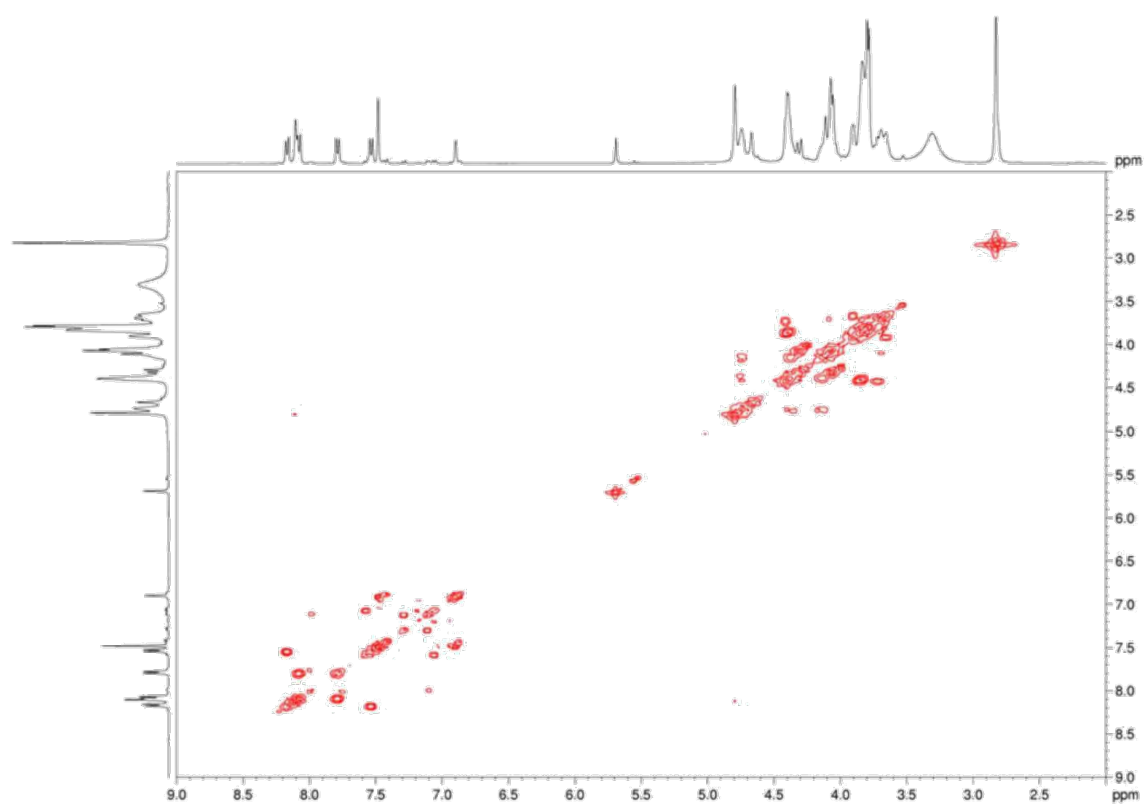


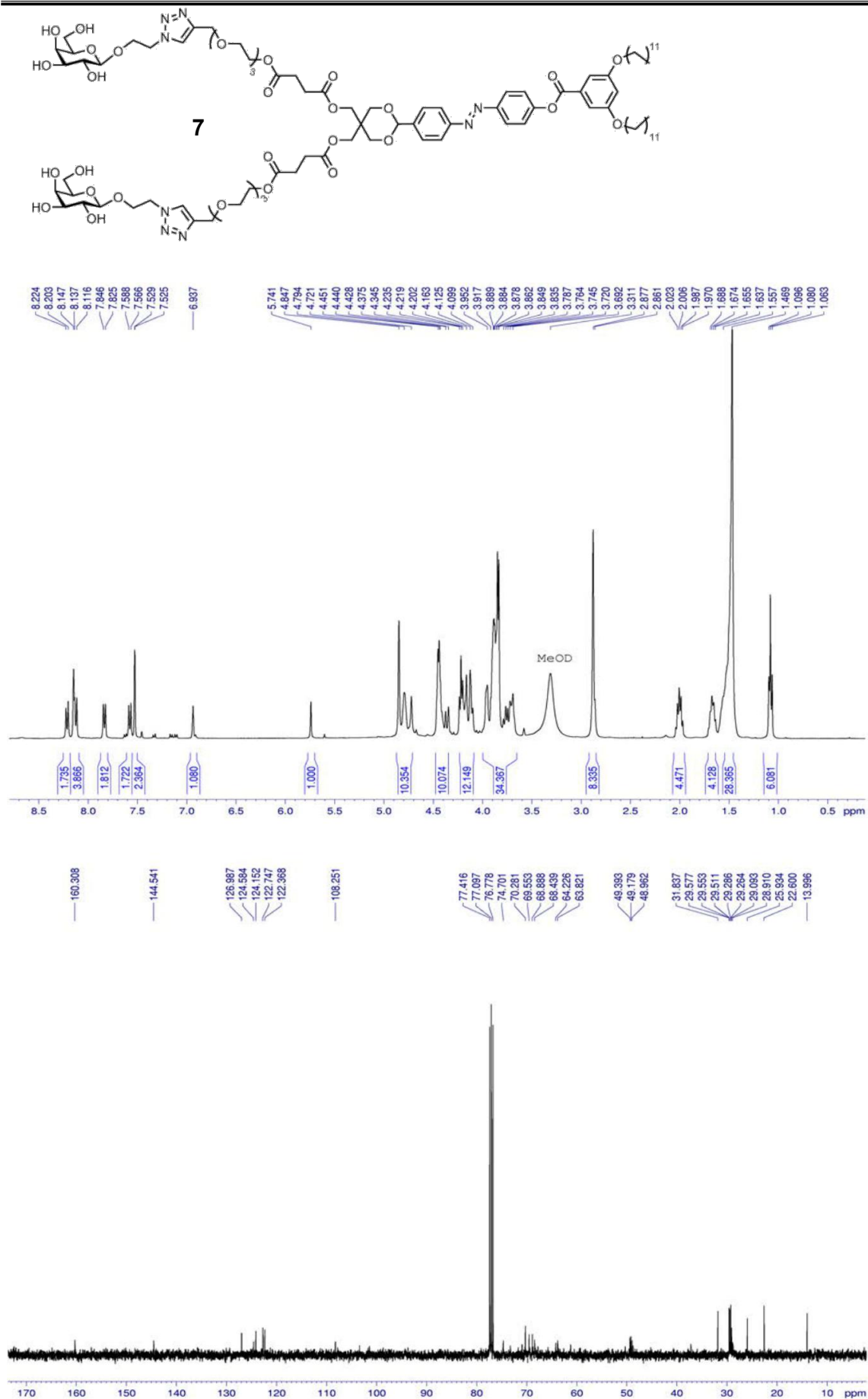


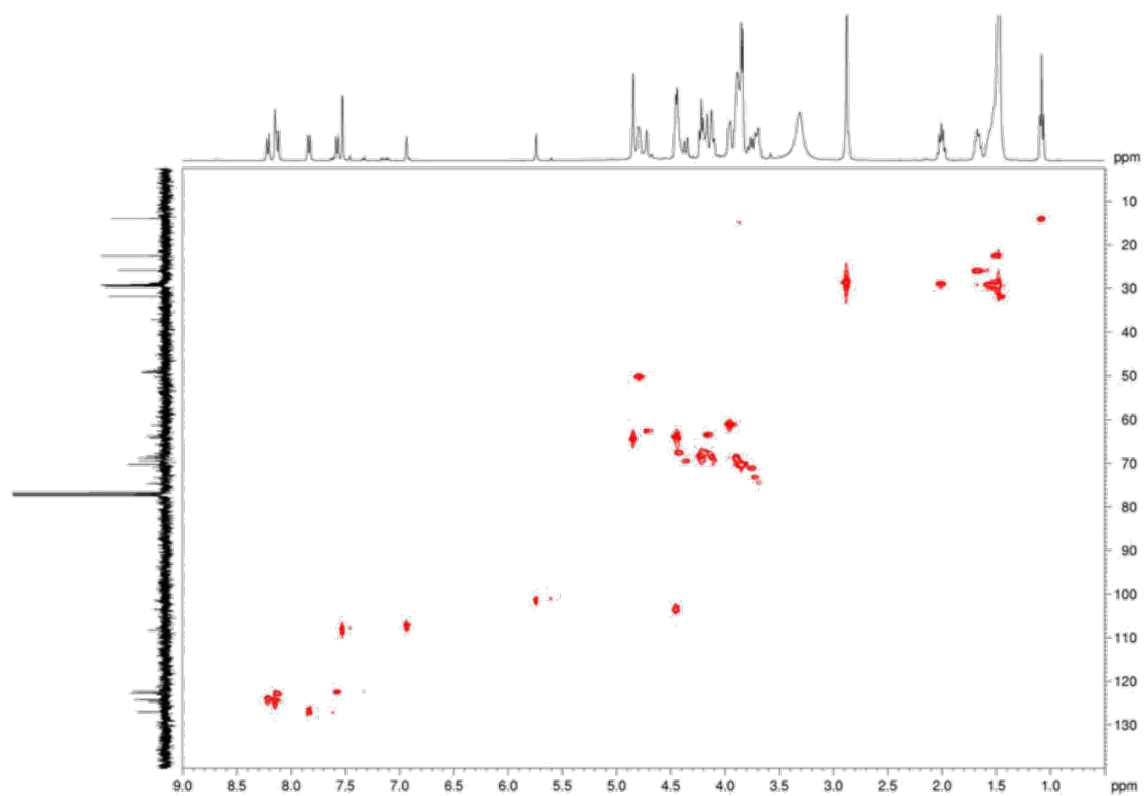
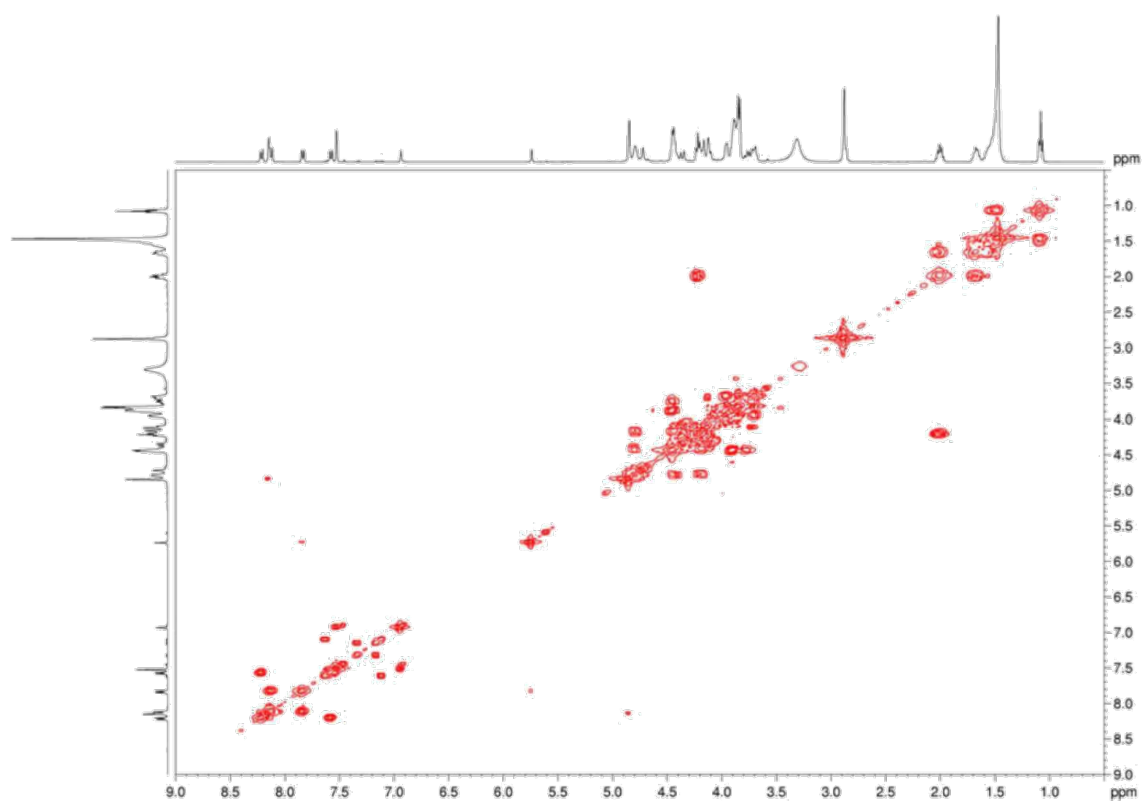




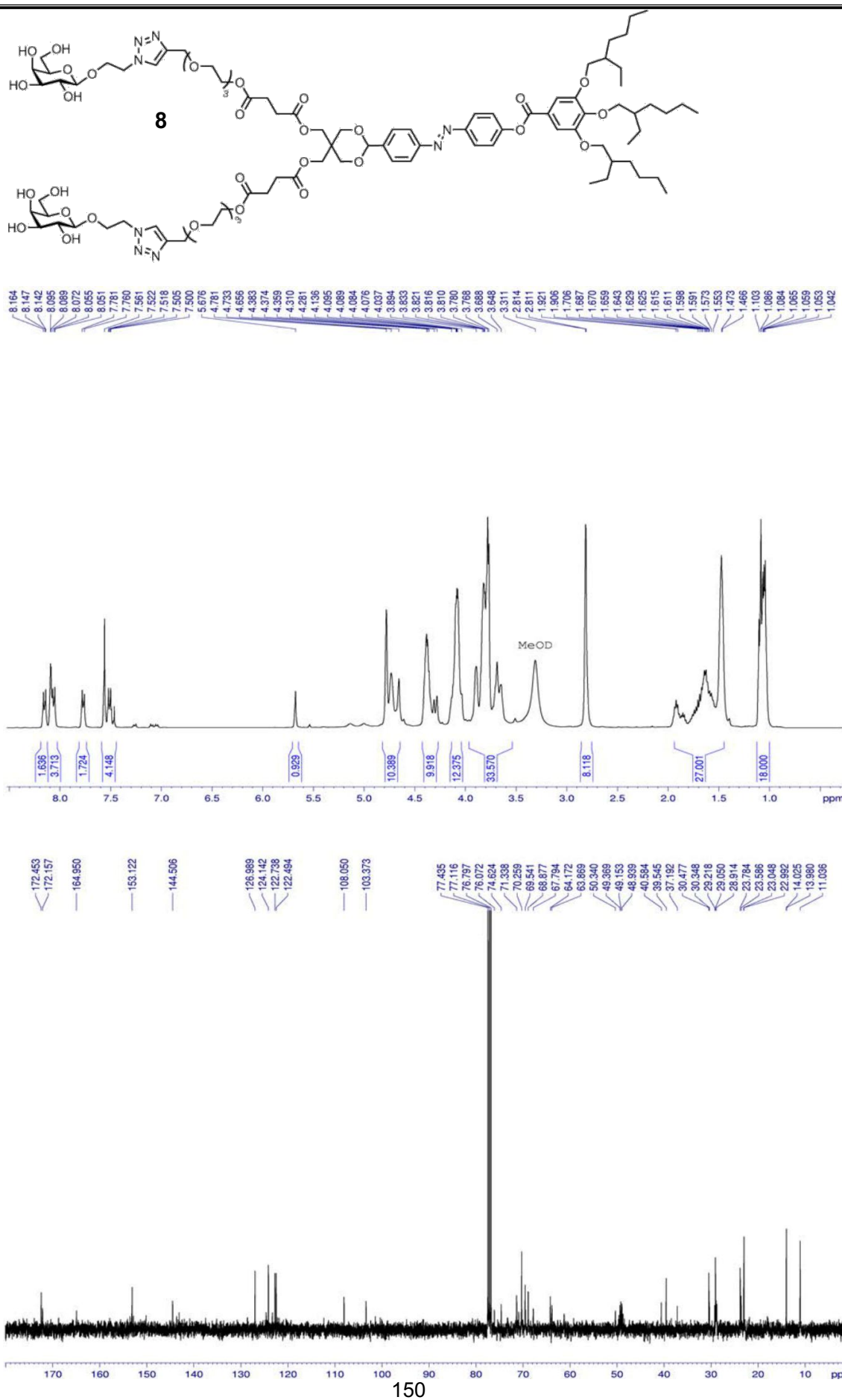


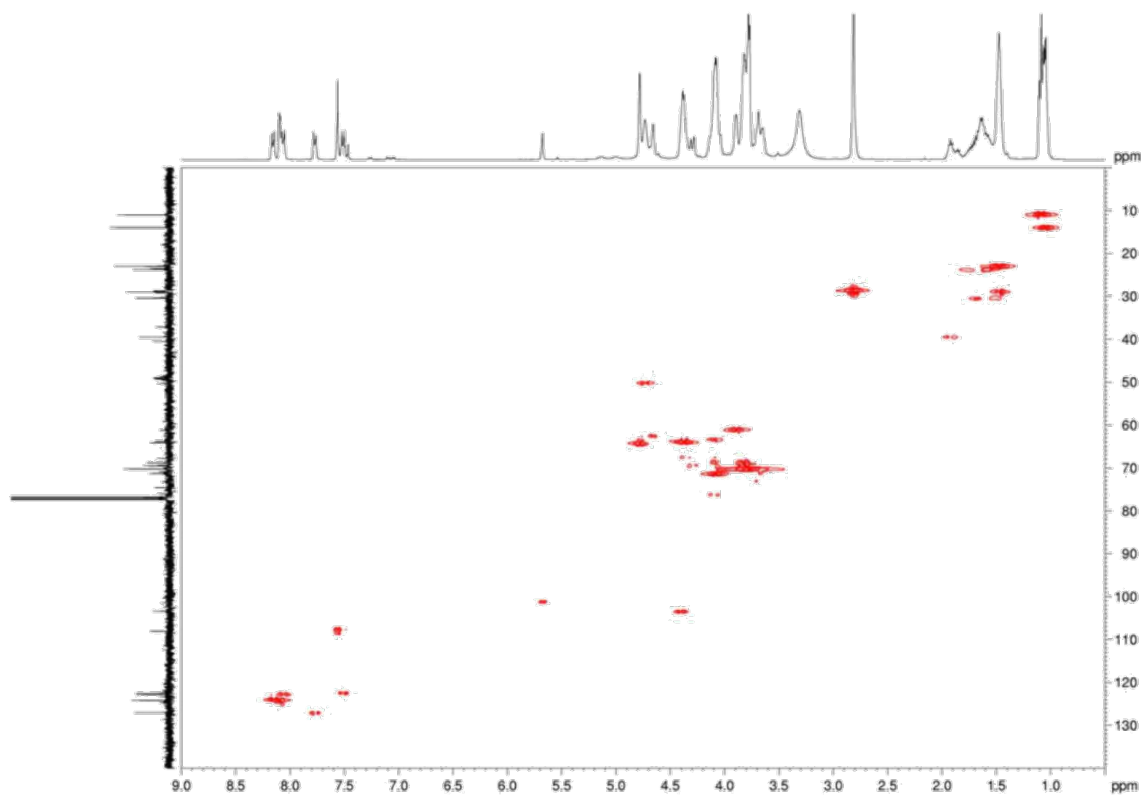
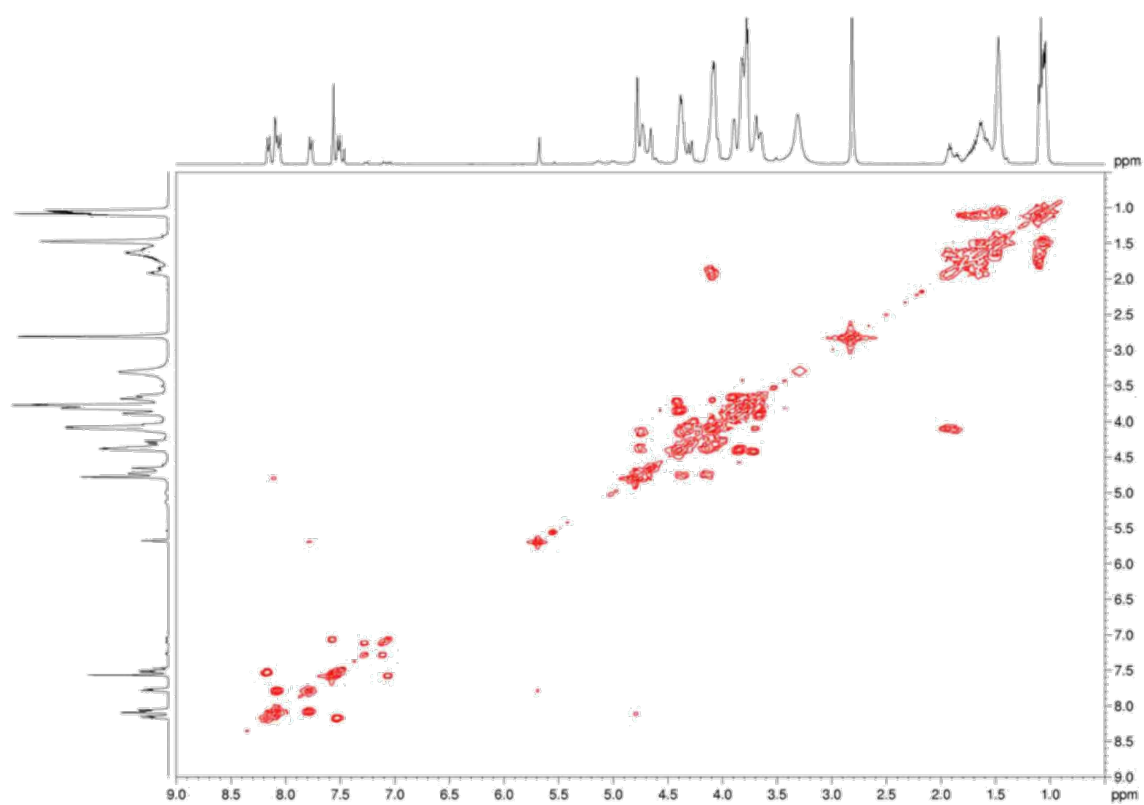


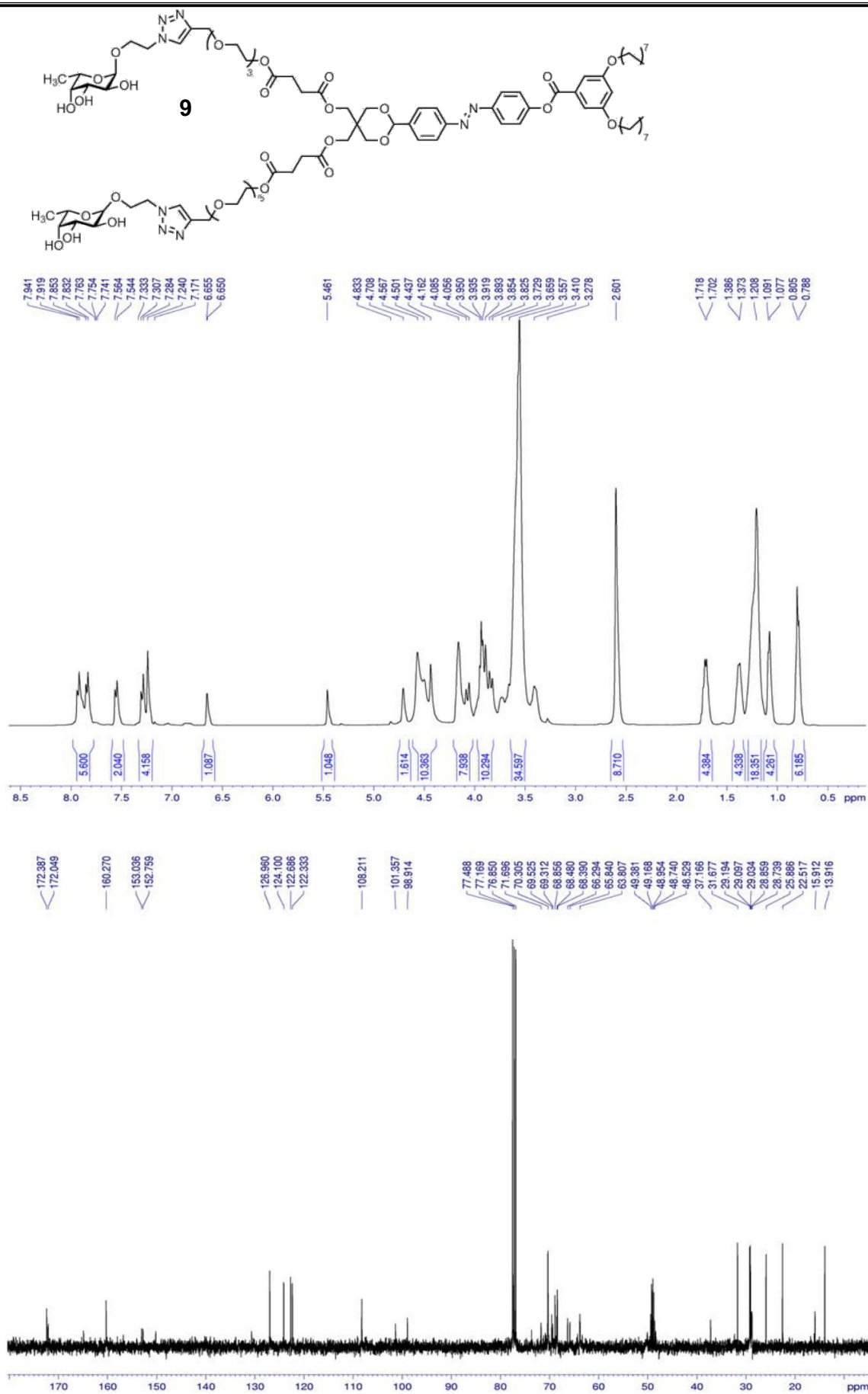


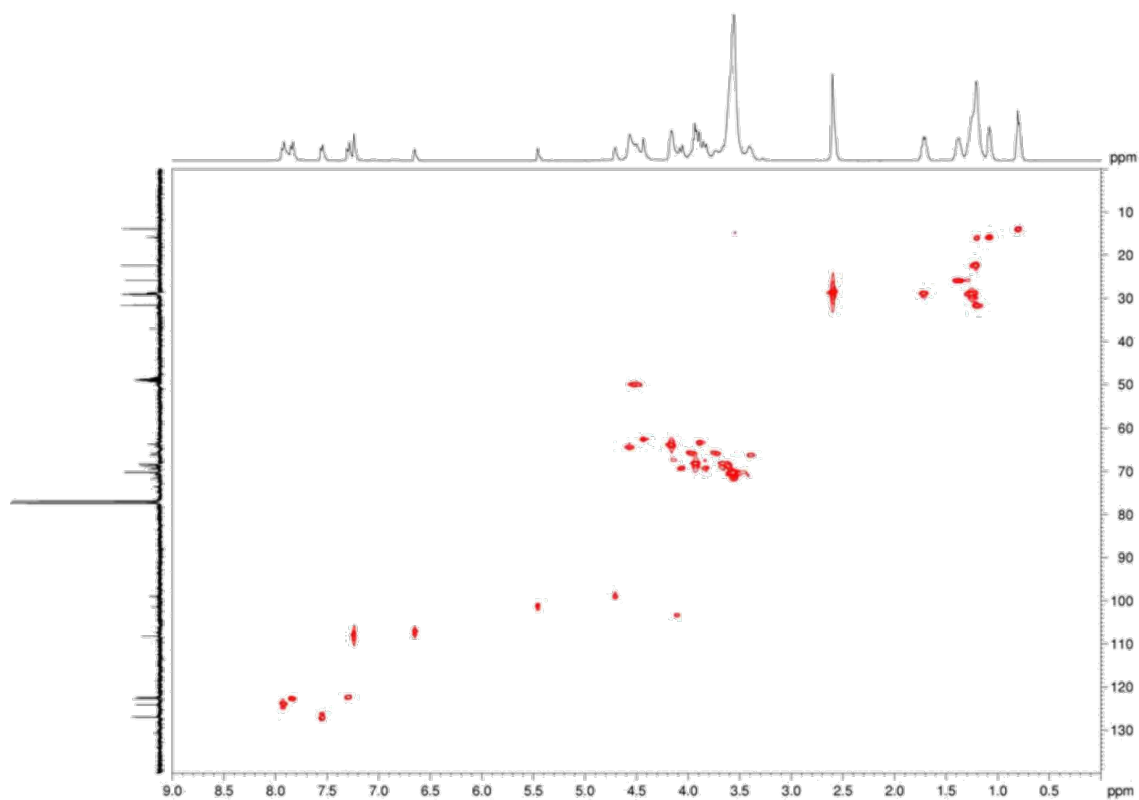
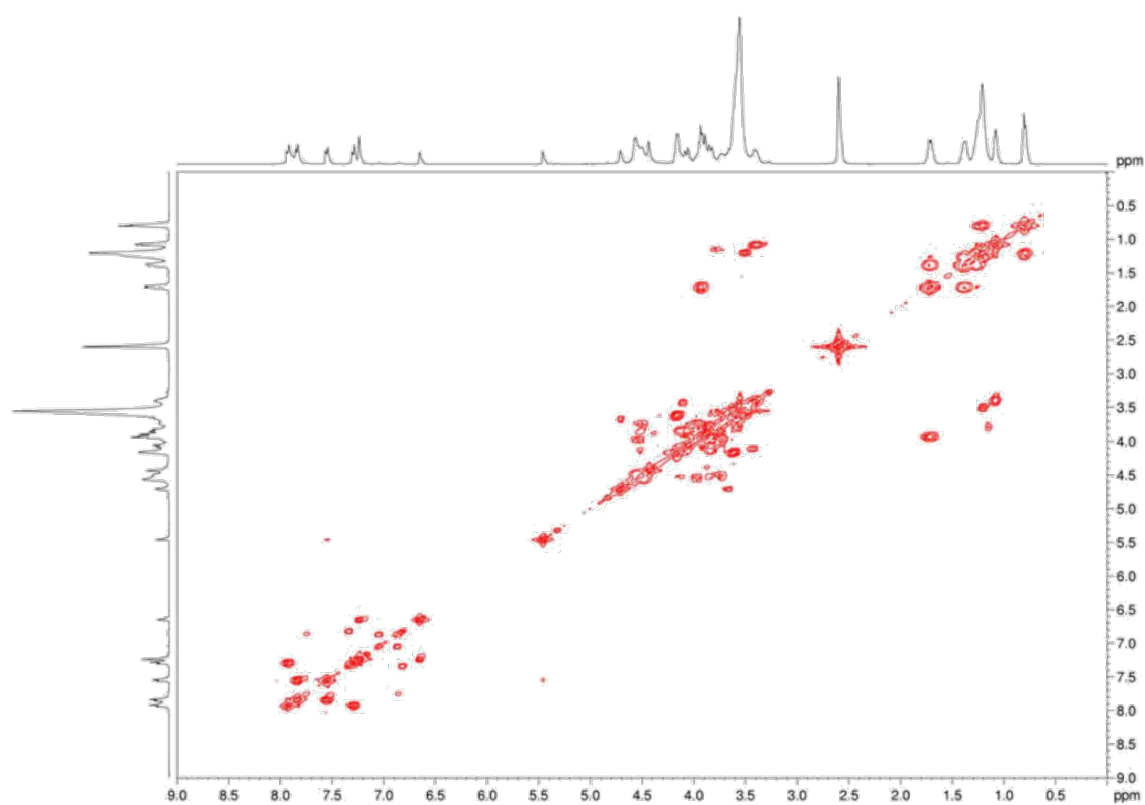


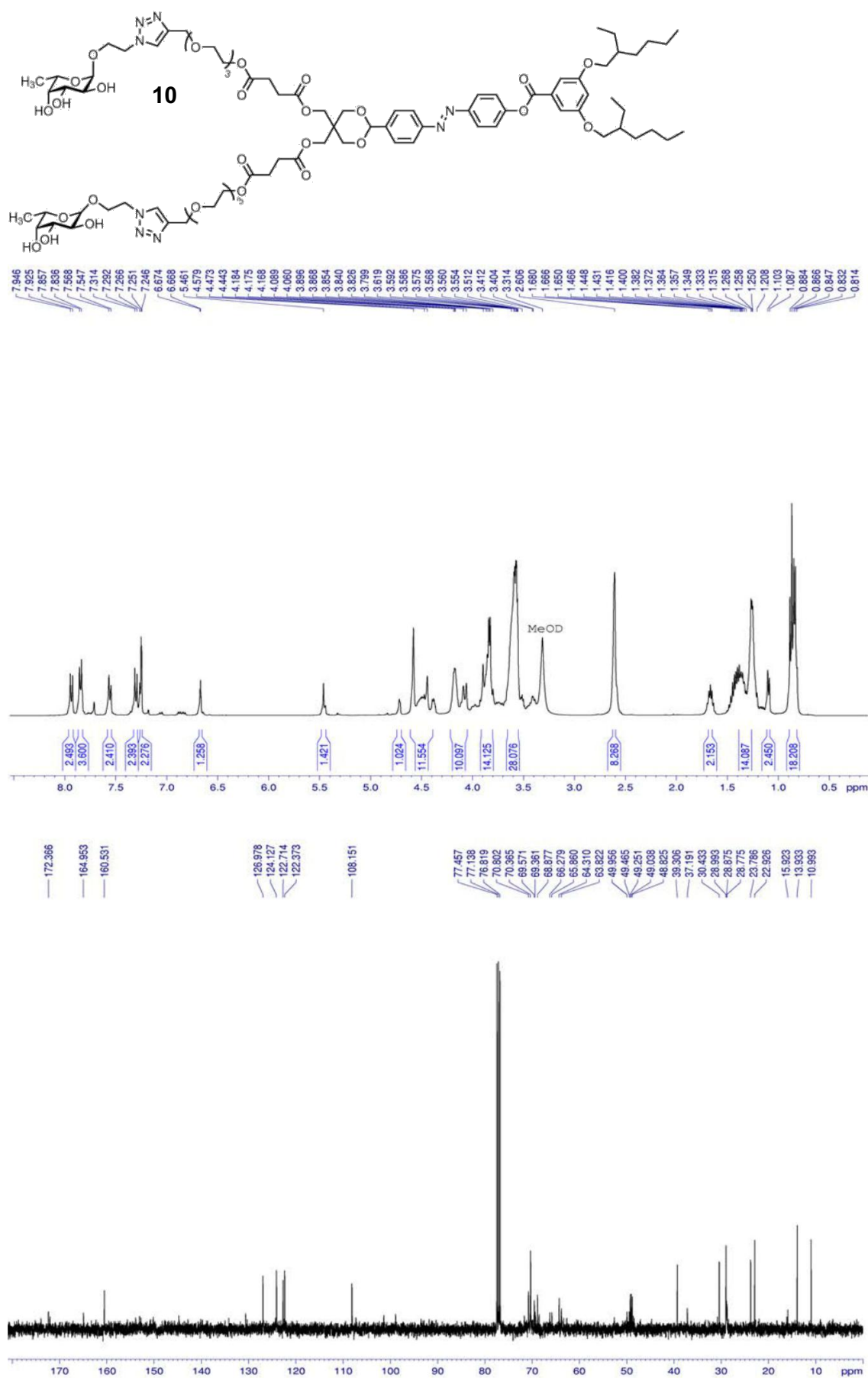
SUPPORTING INFORMATION

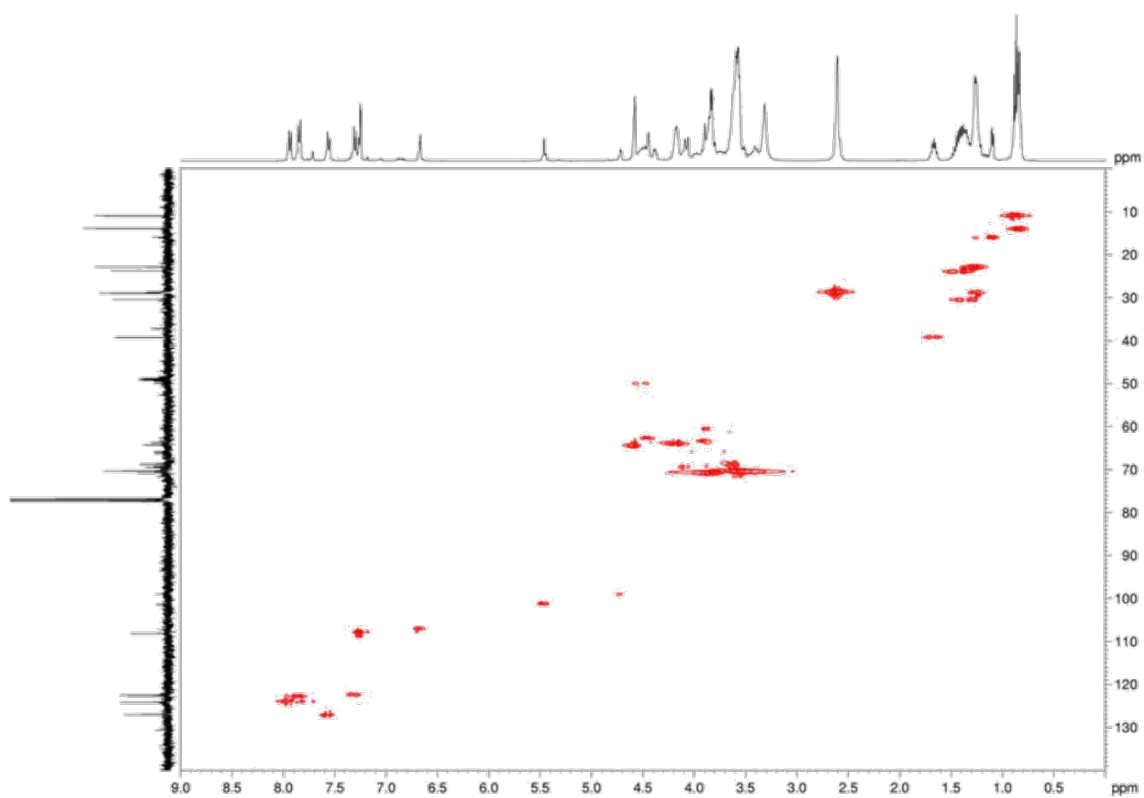
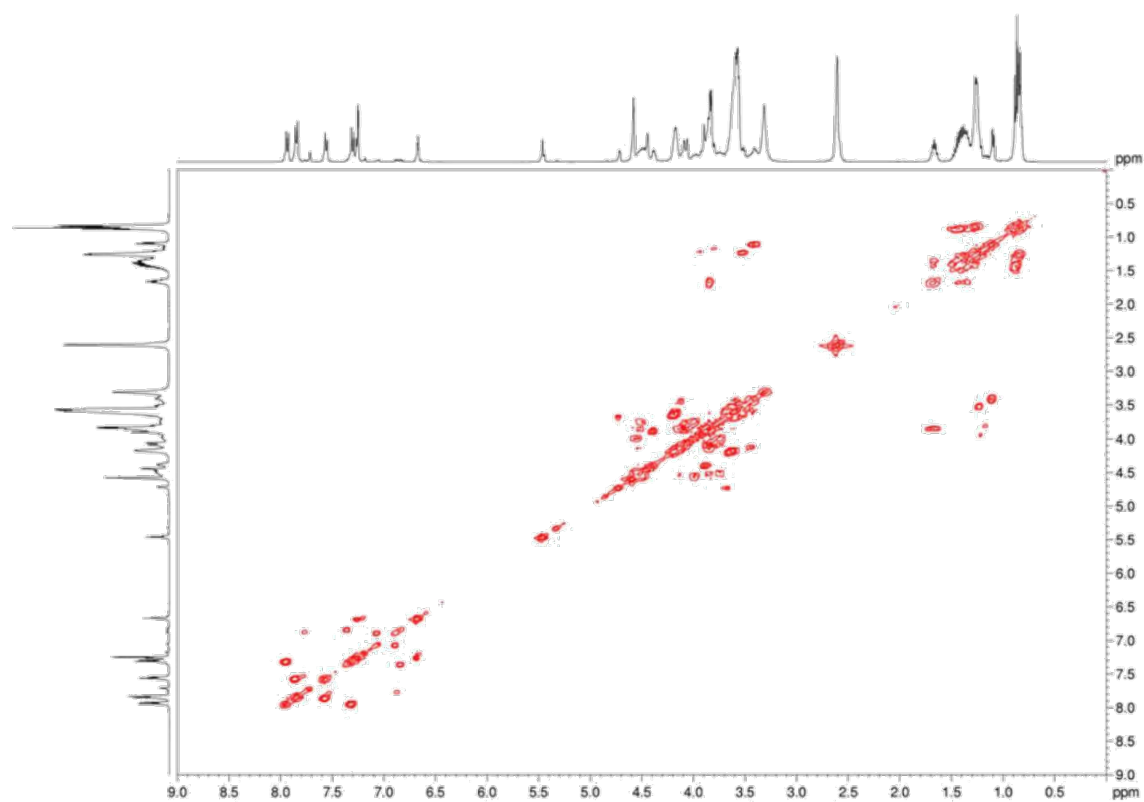


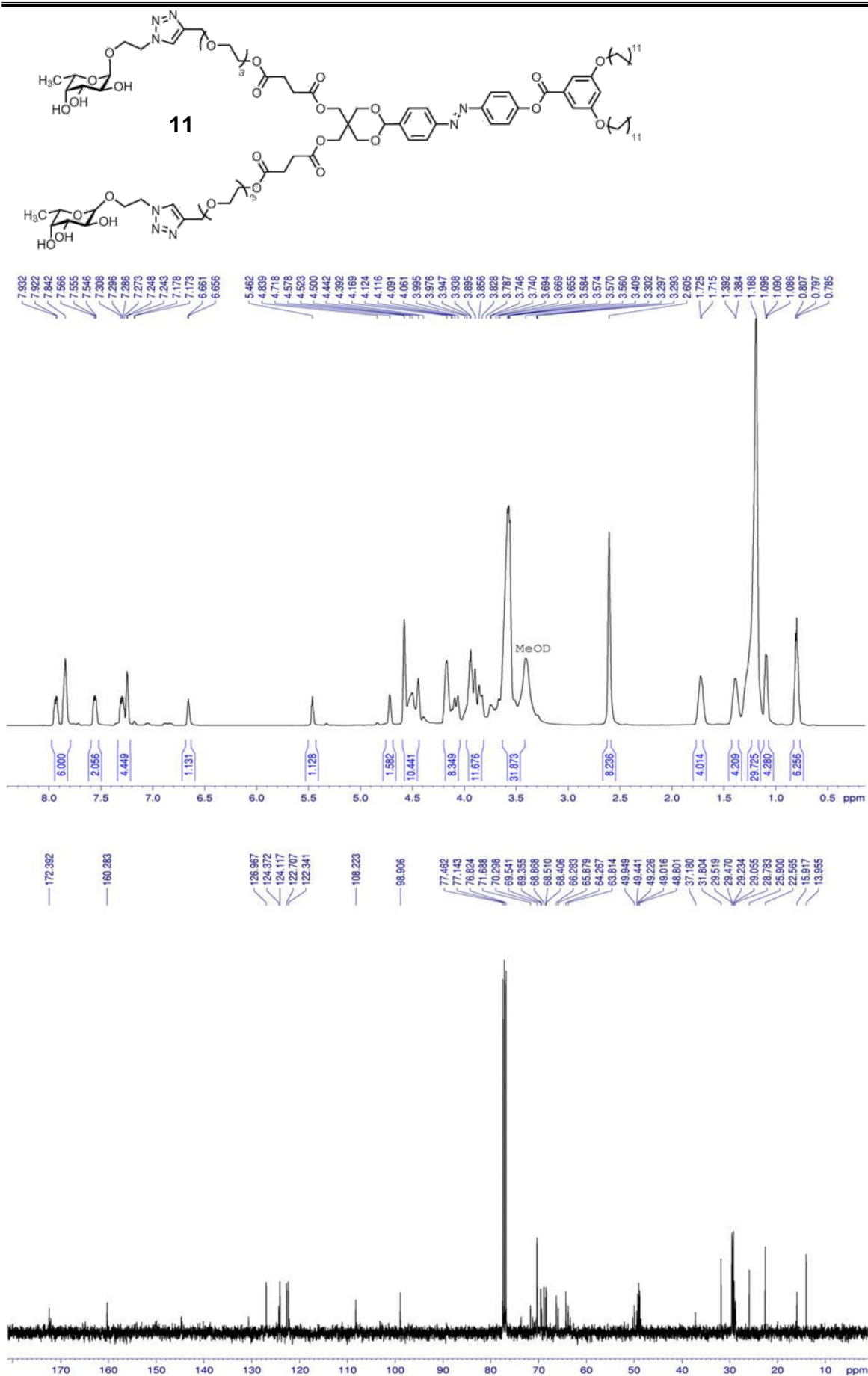


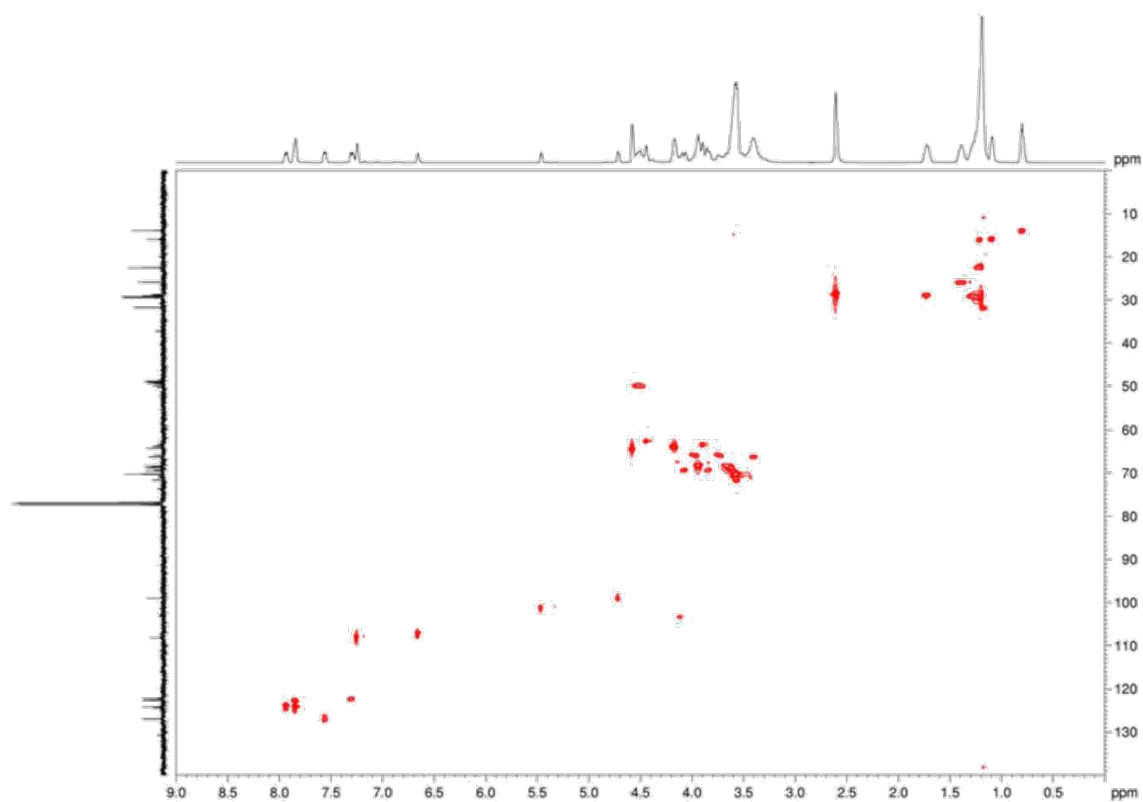
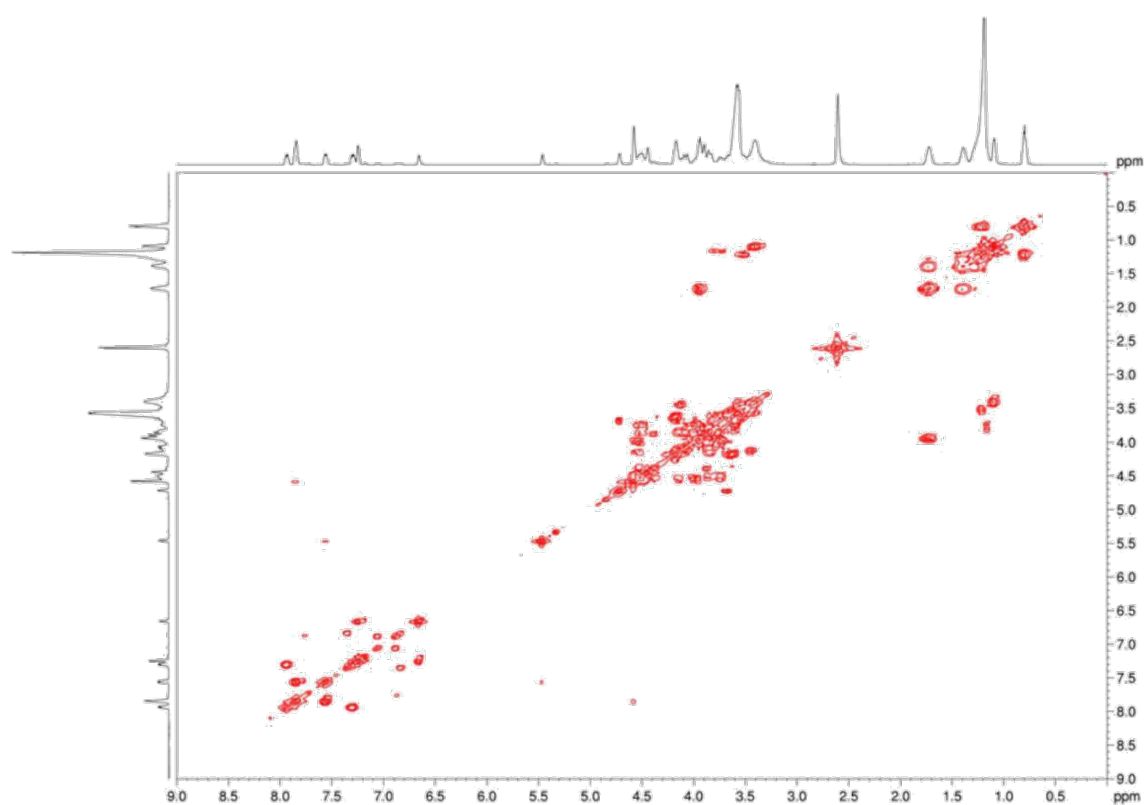


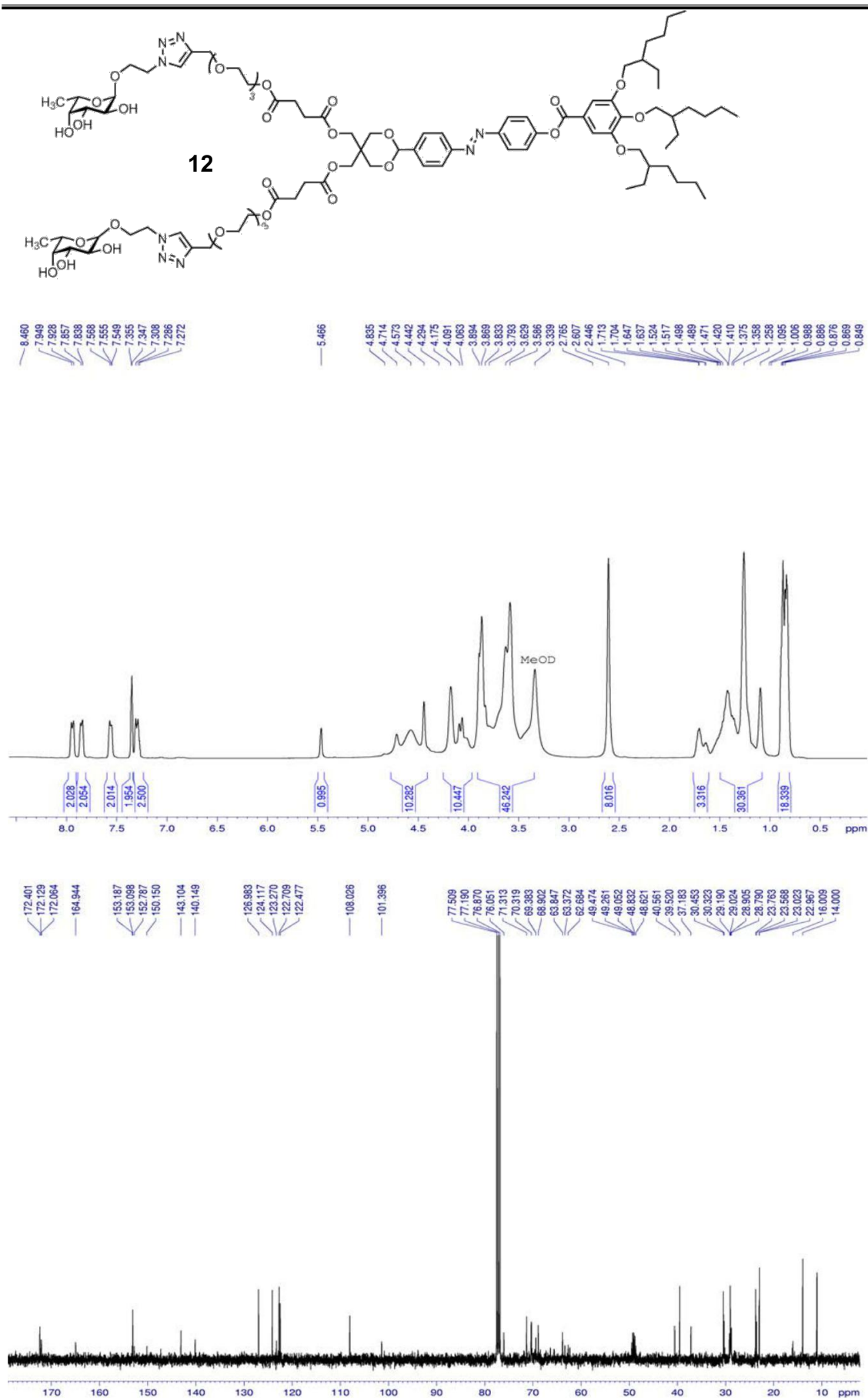


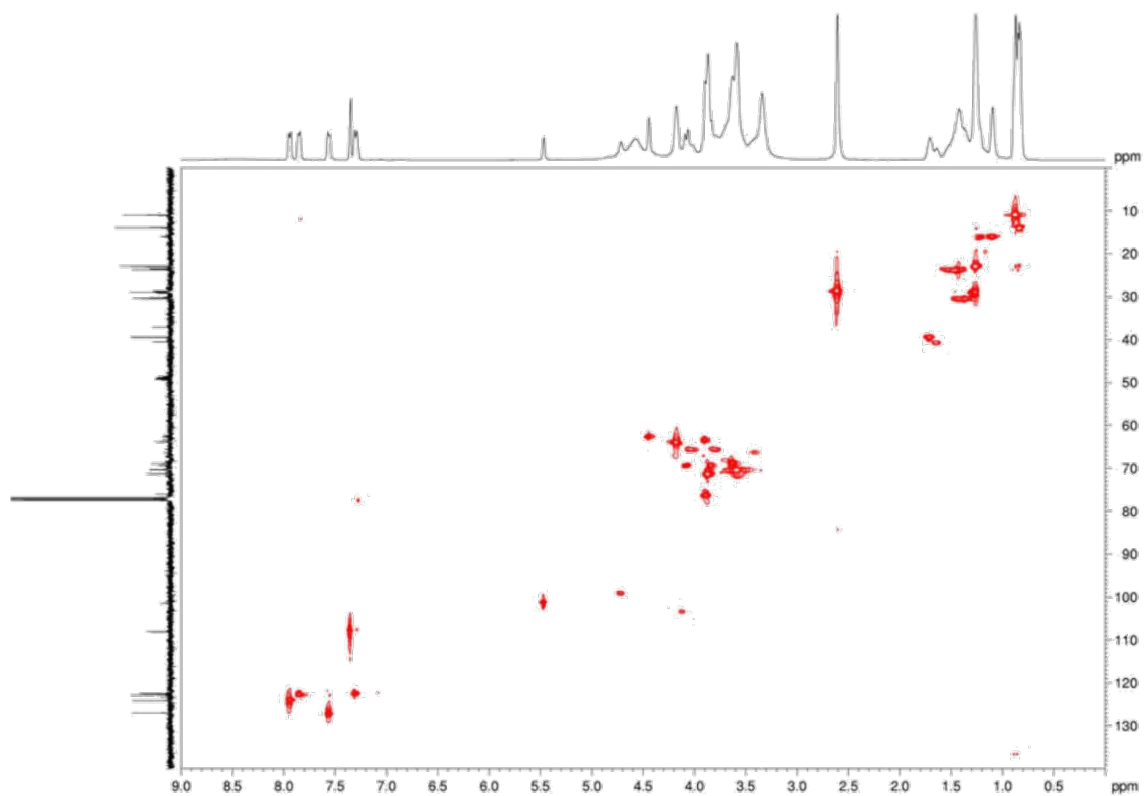
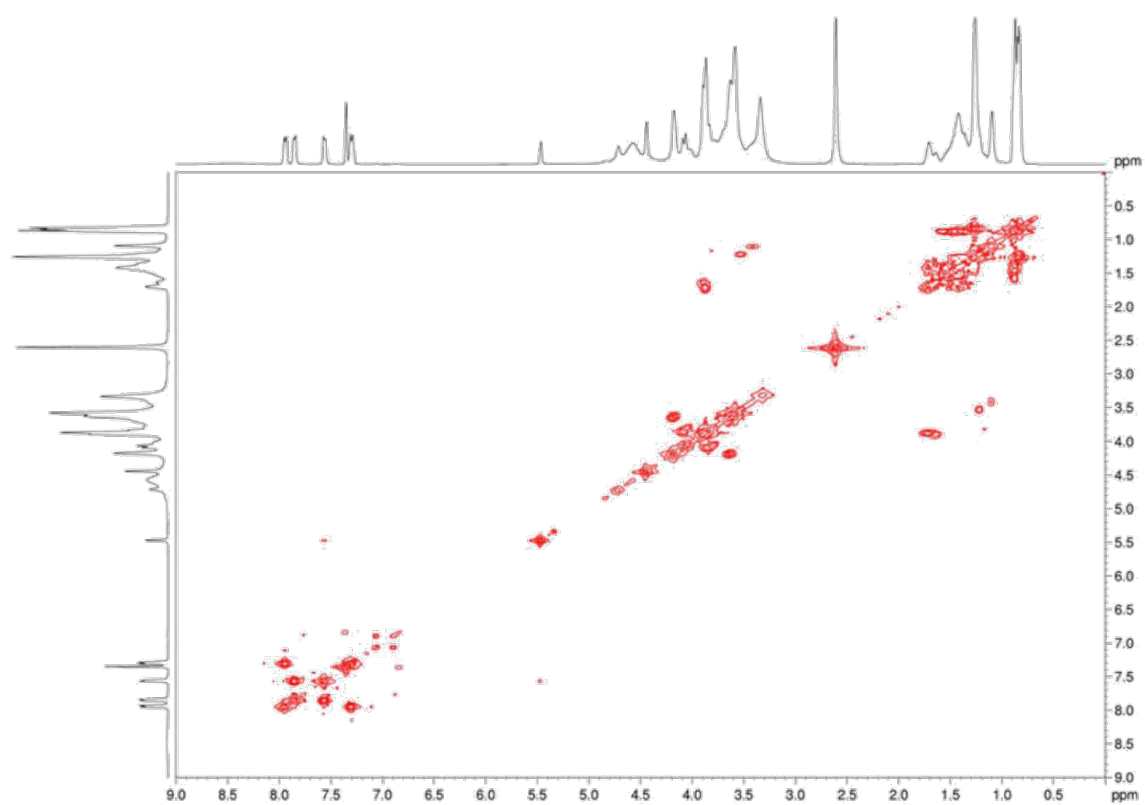


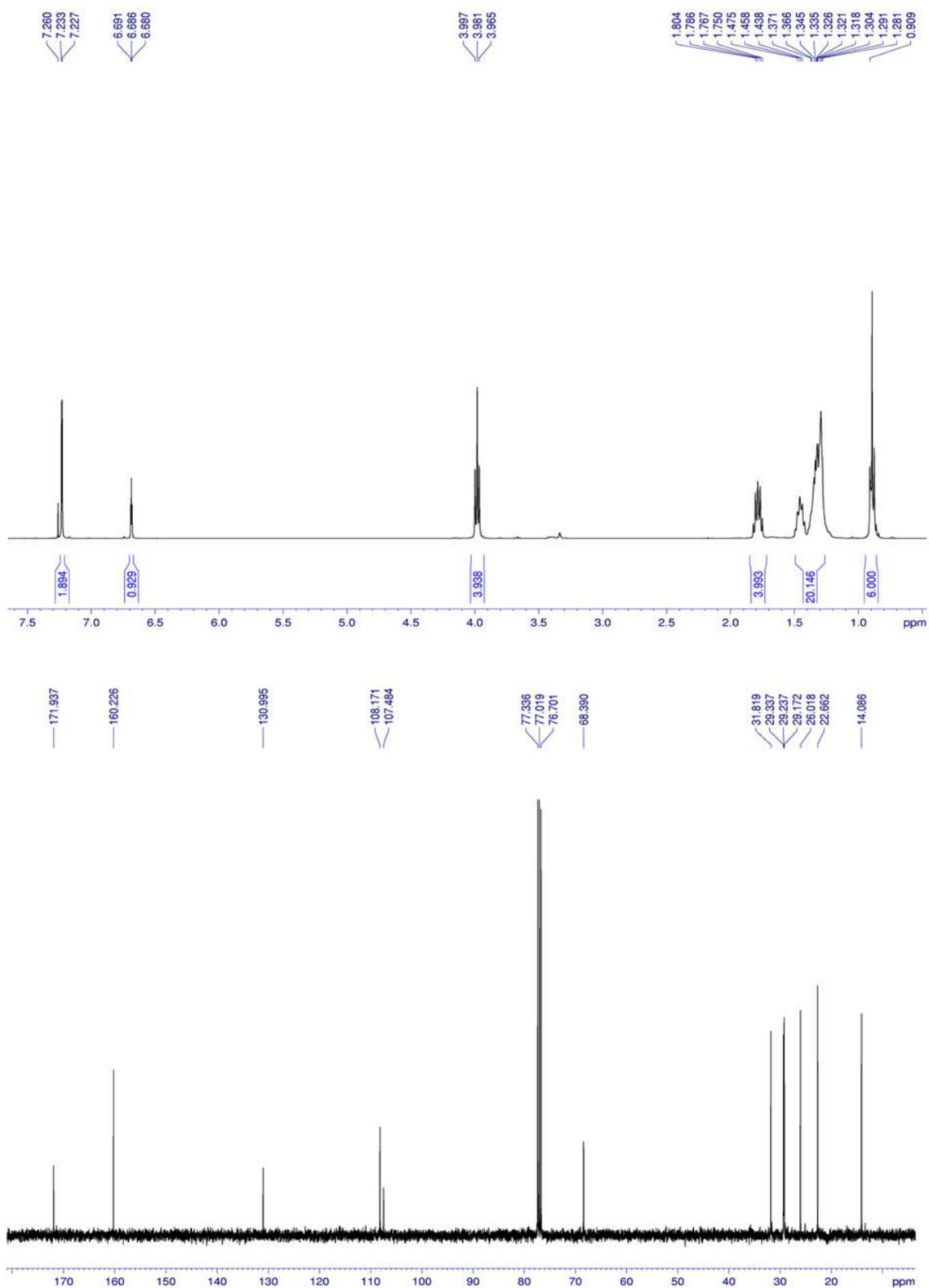
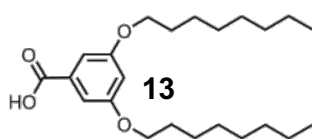


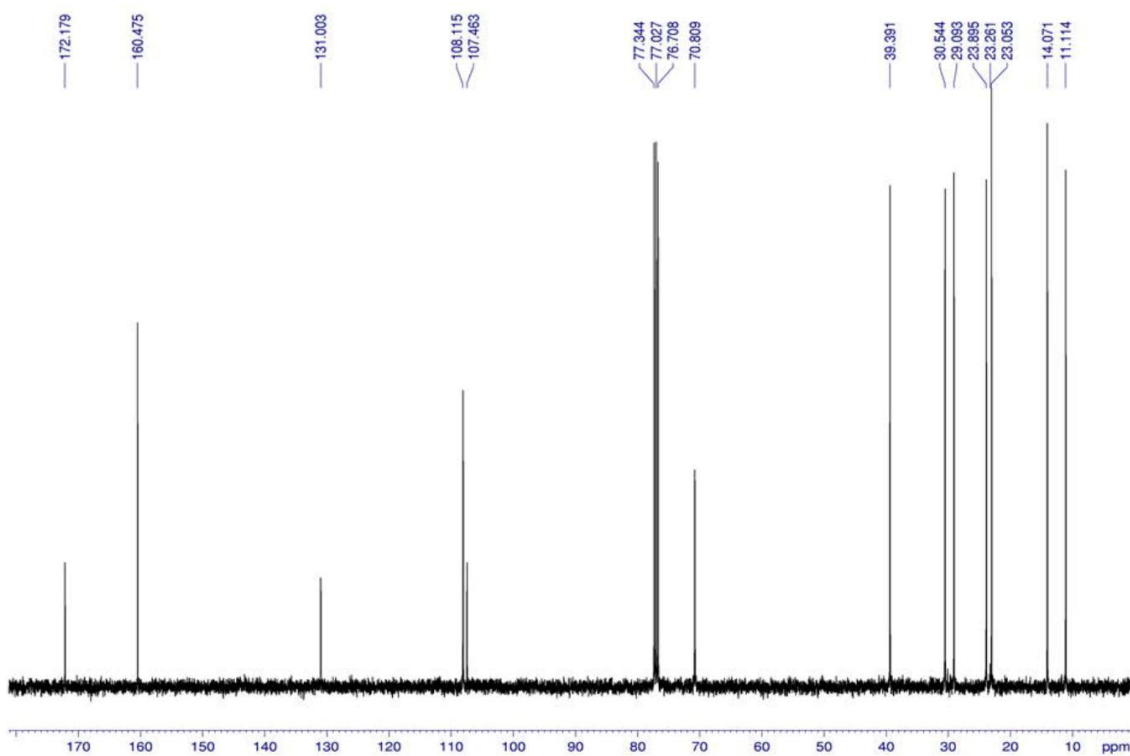
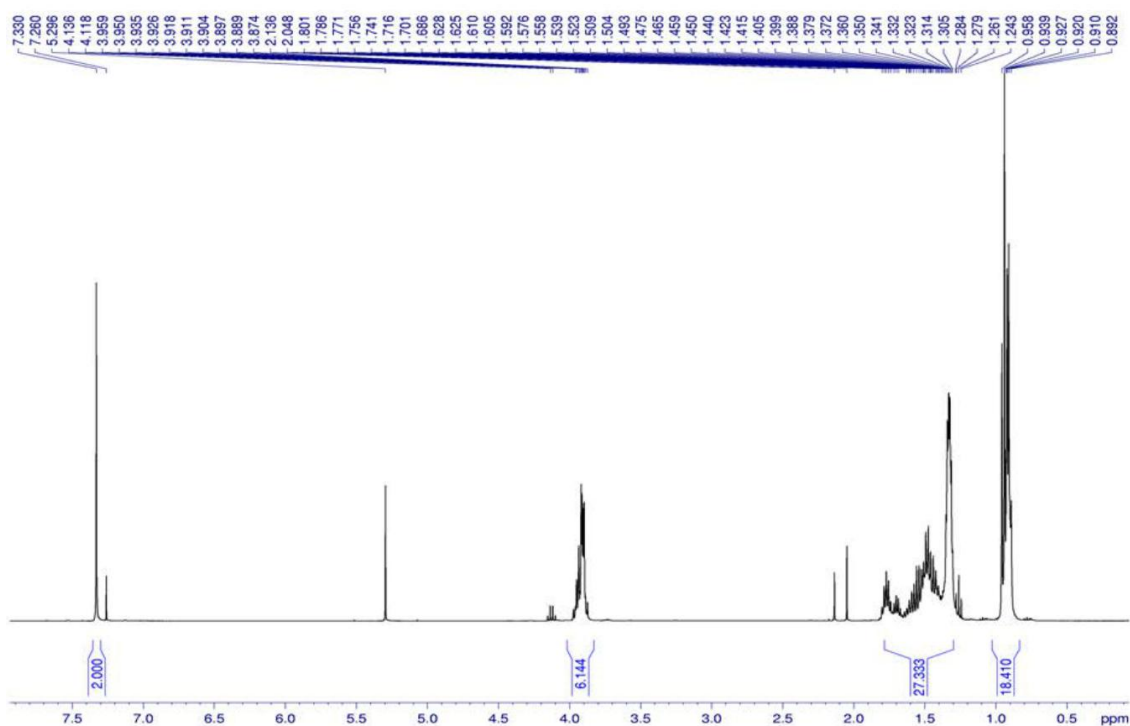
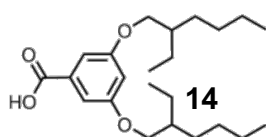


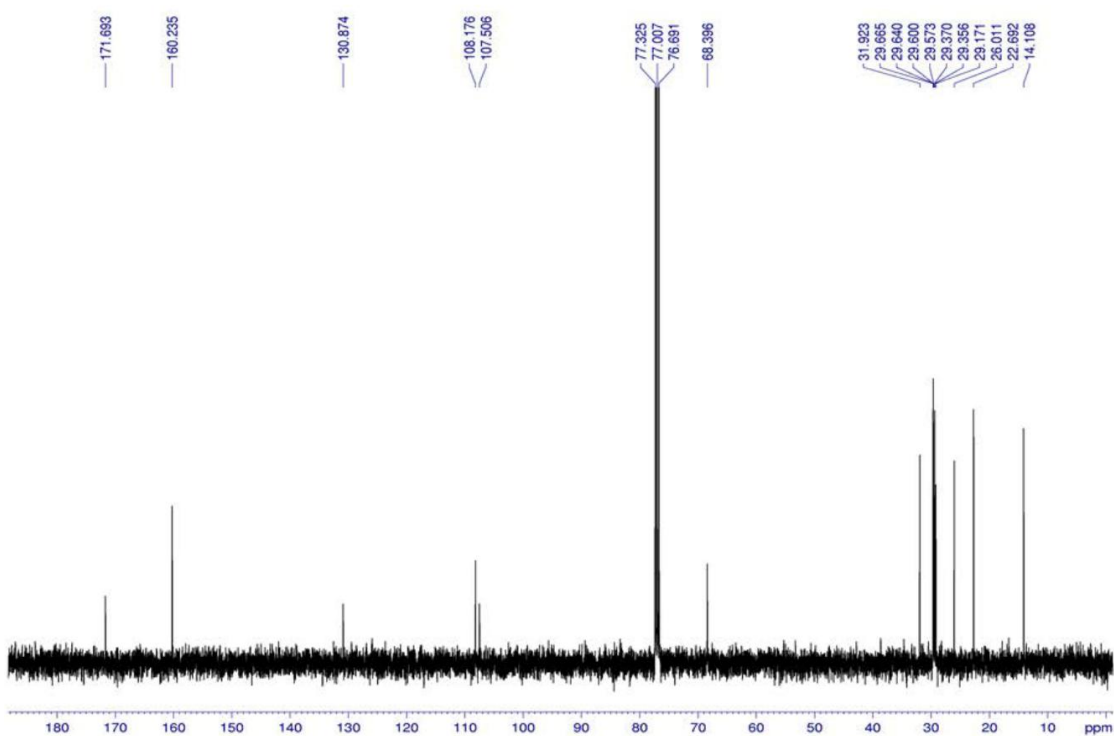
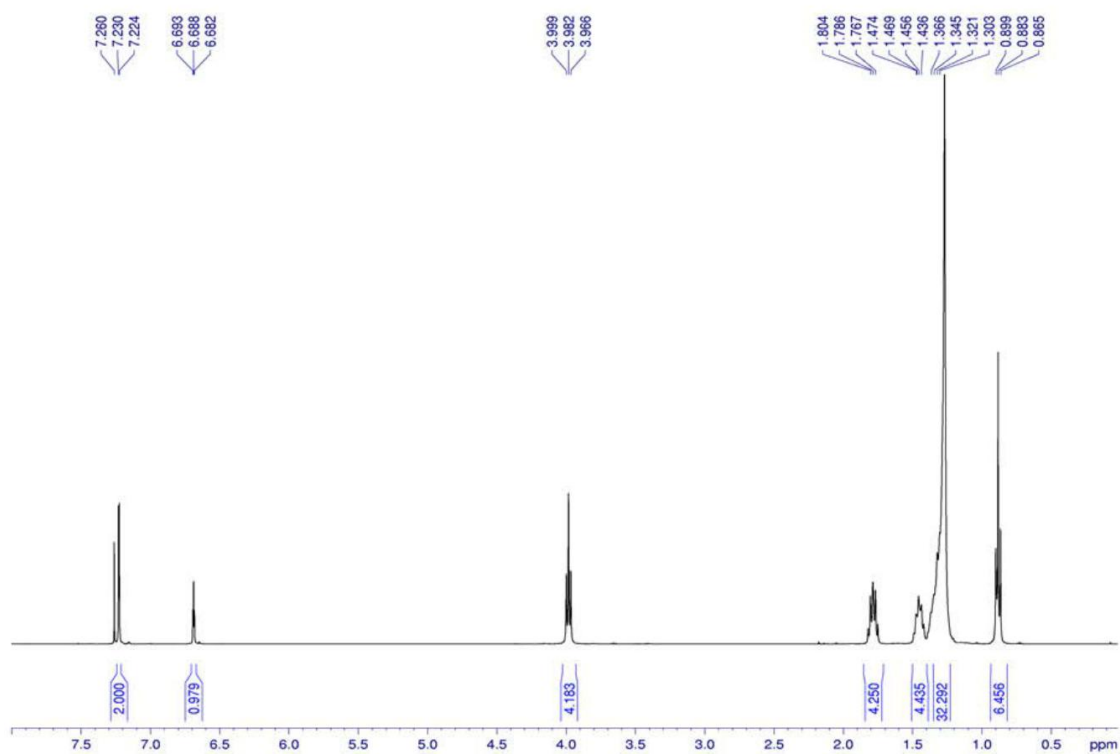
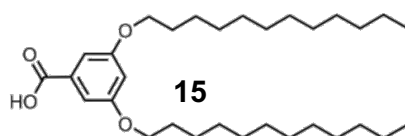


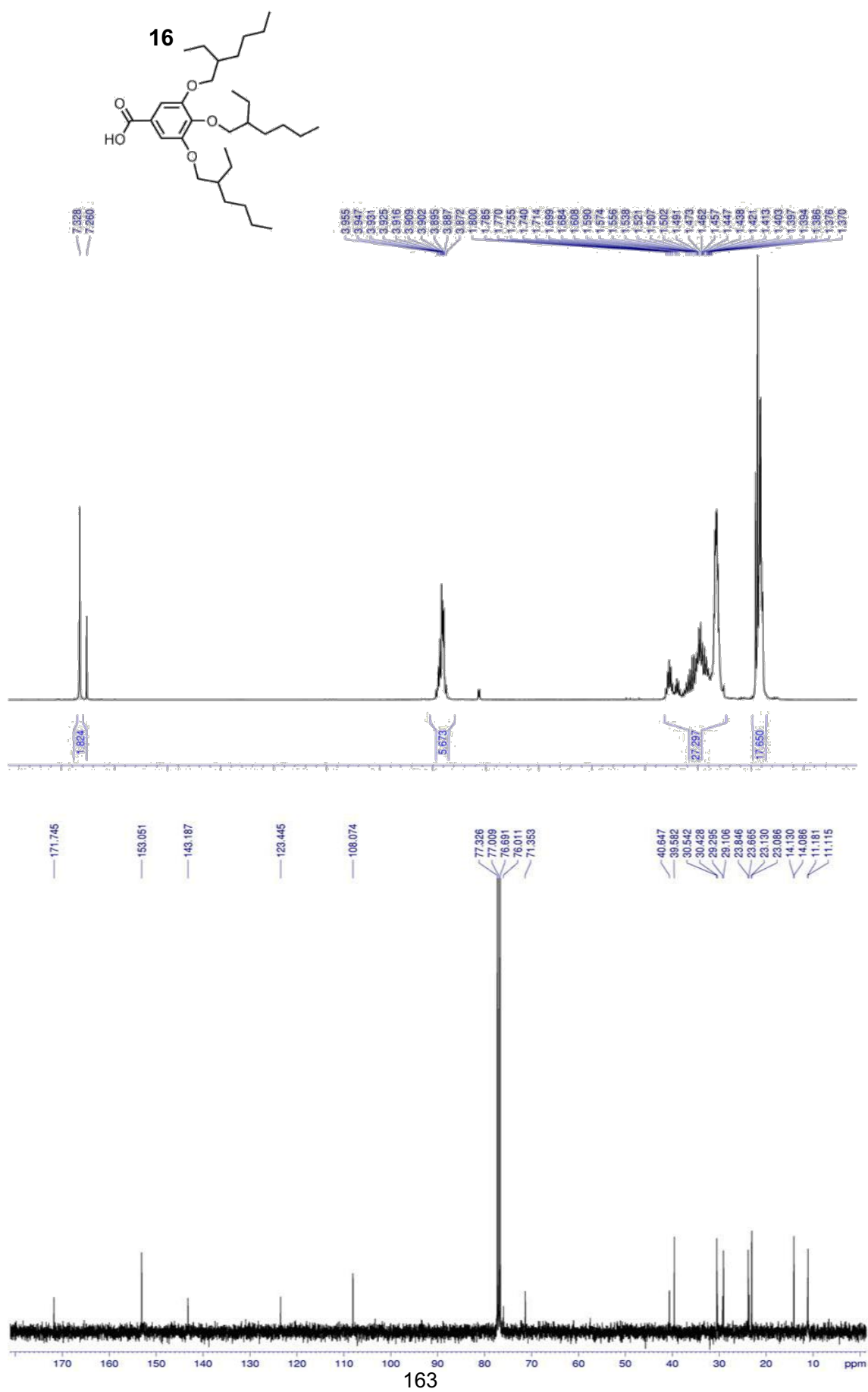


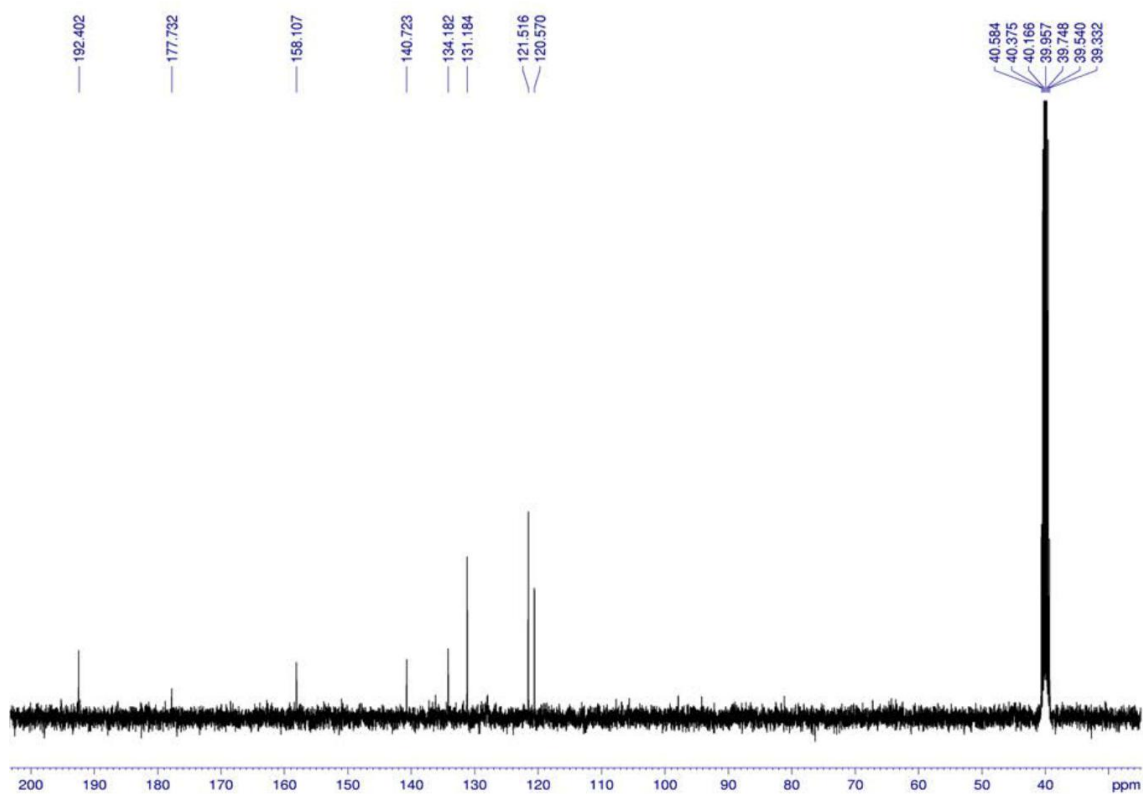
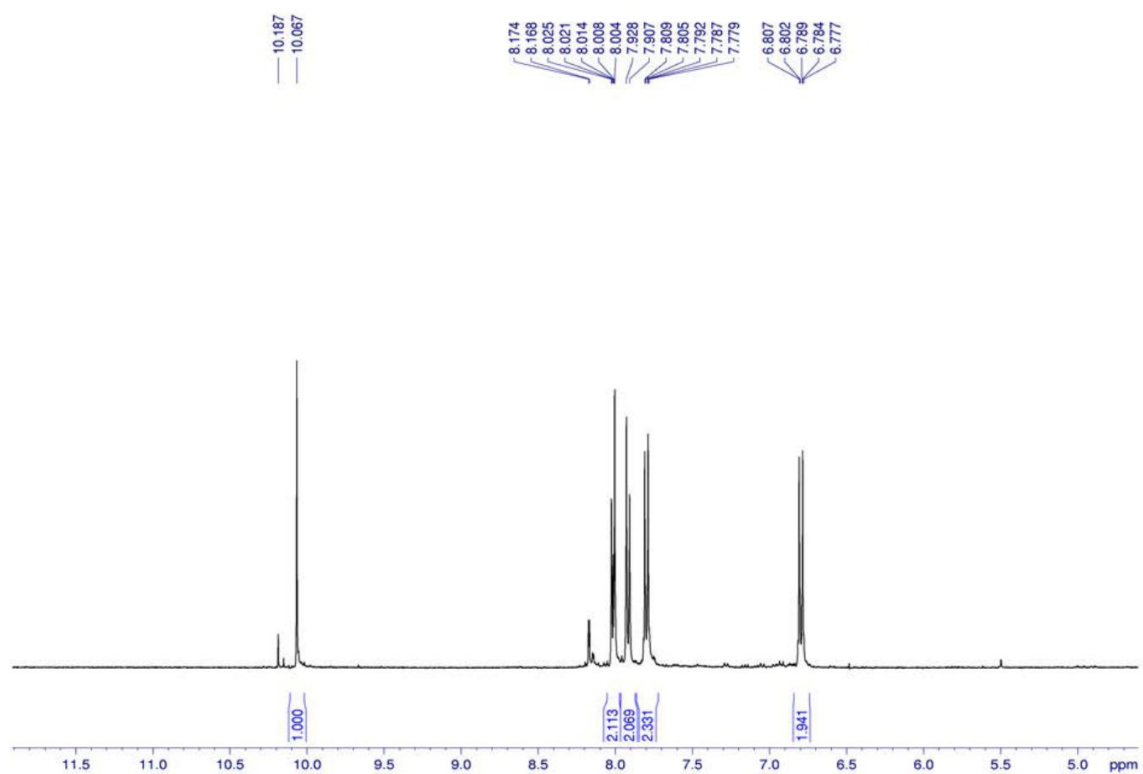
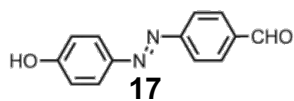


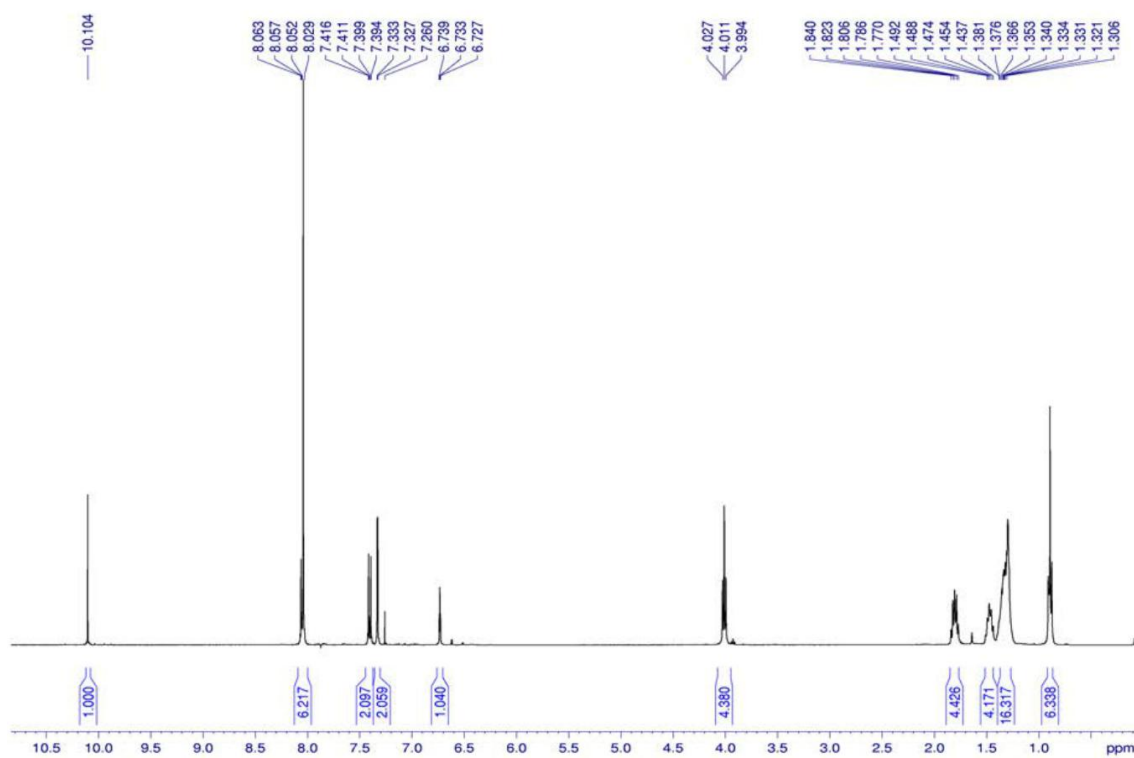
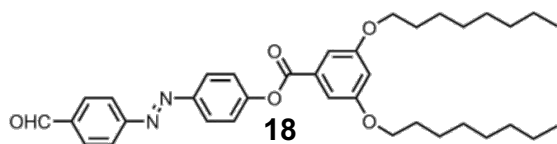


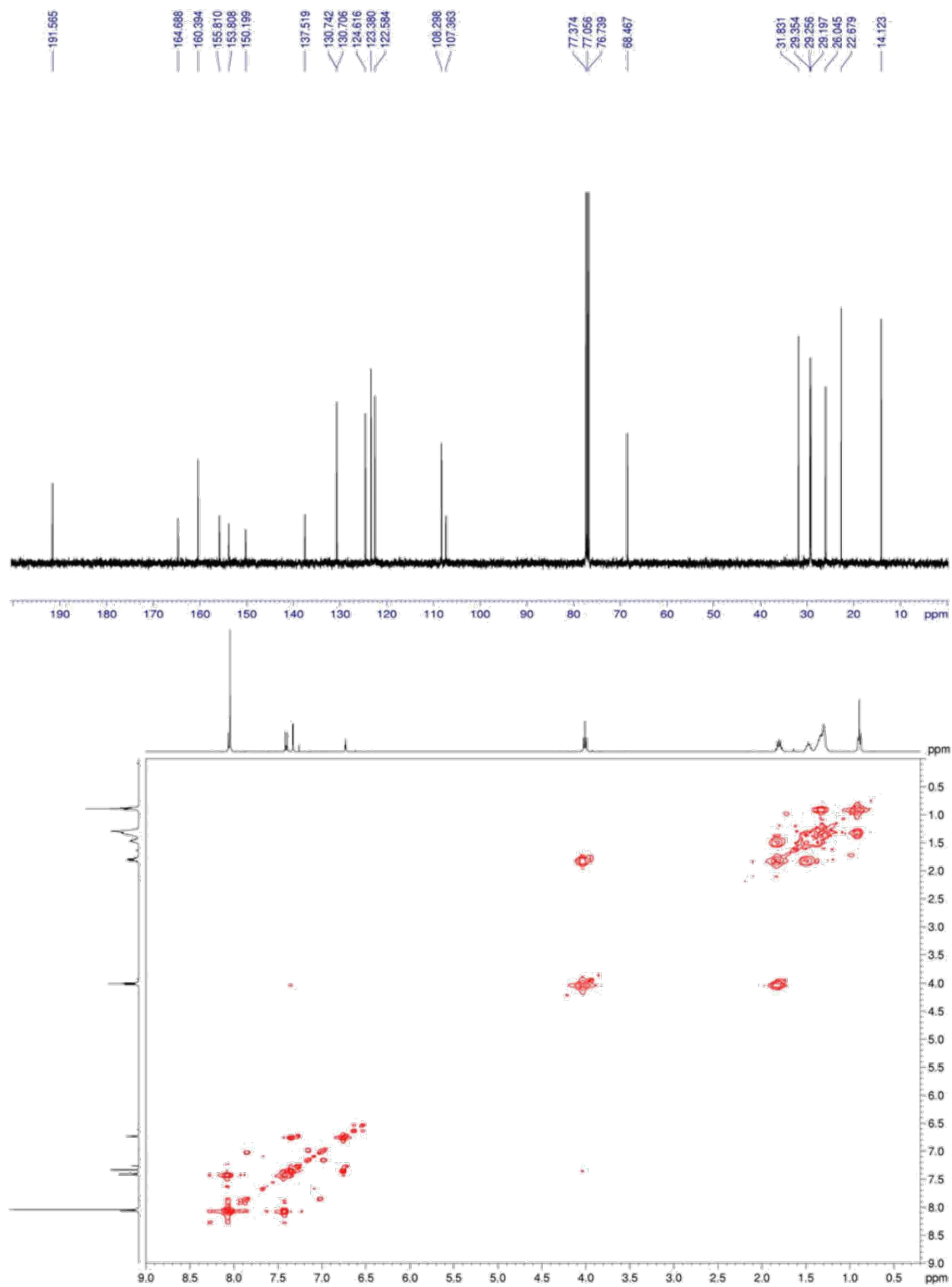


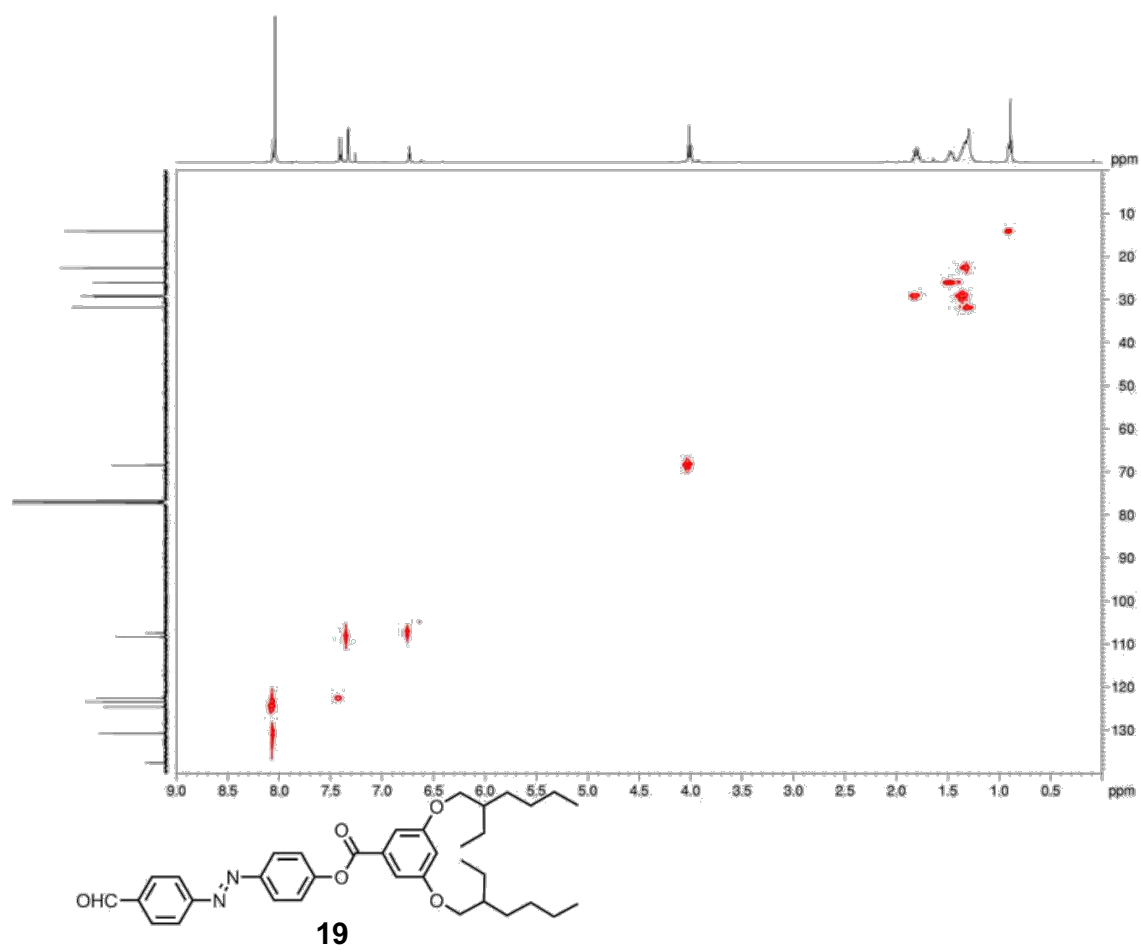


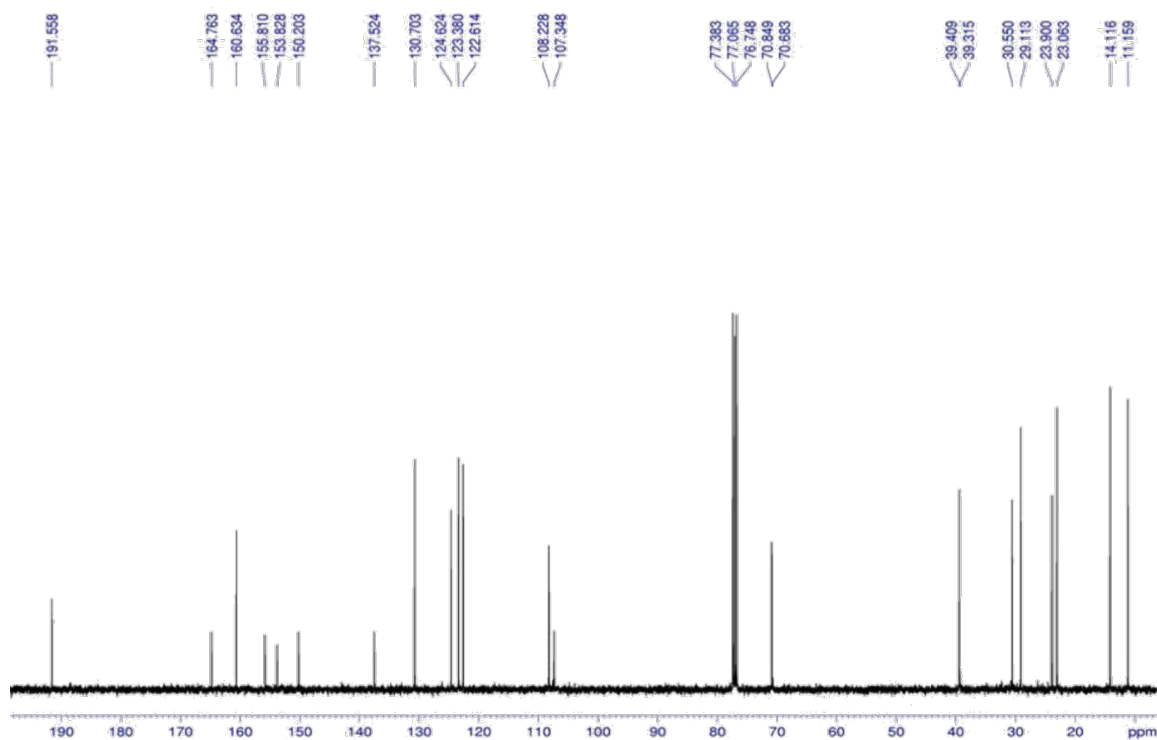
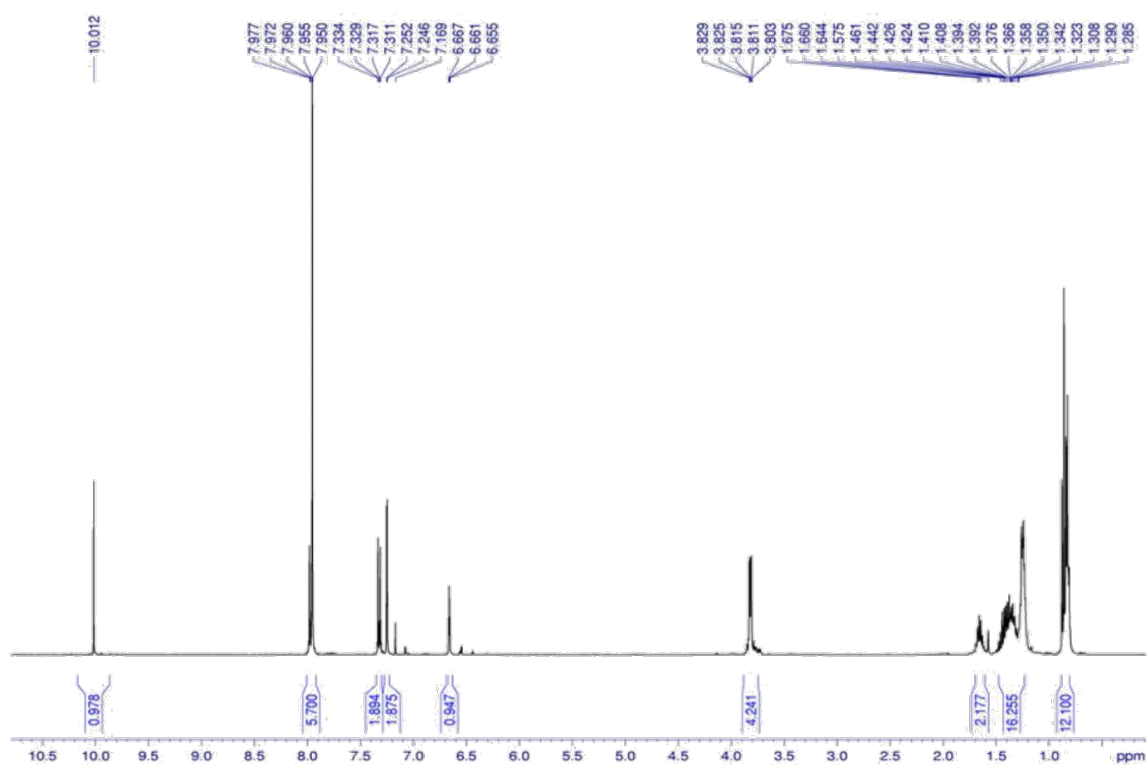


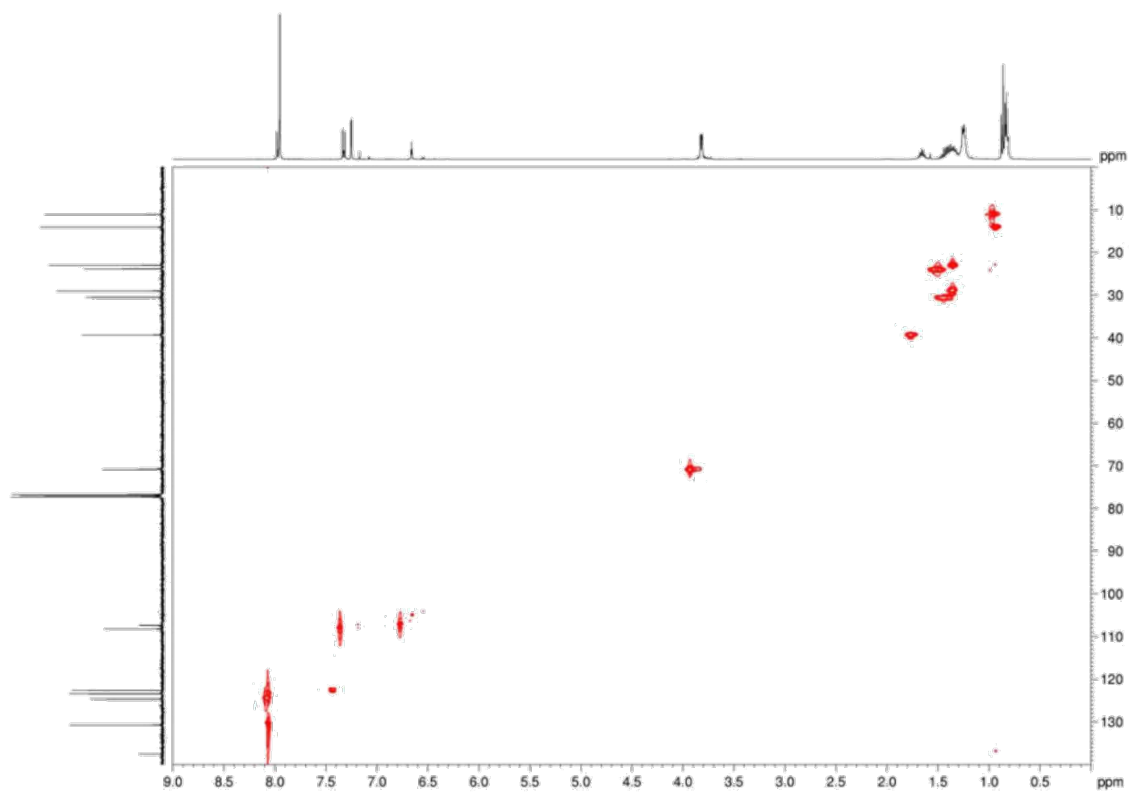
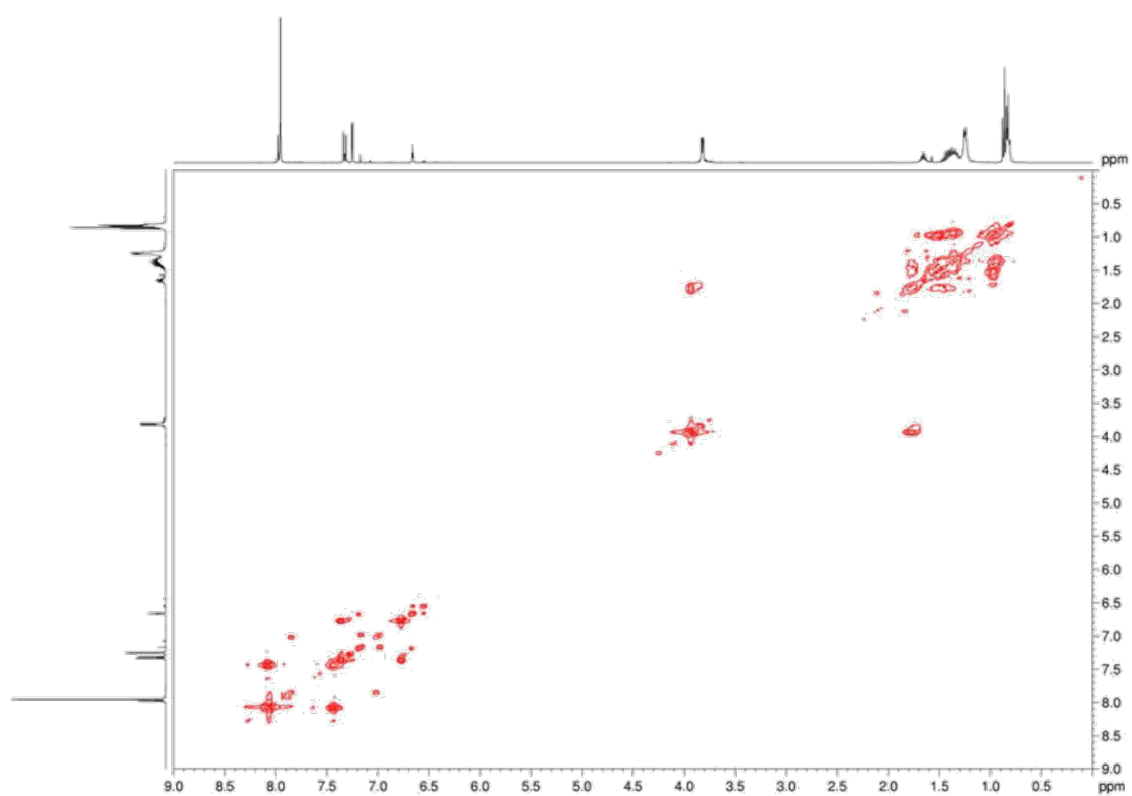


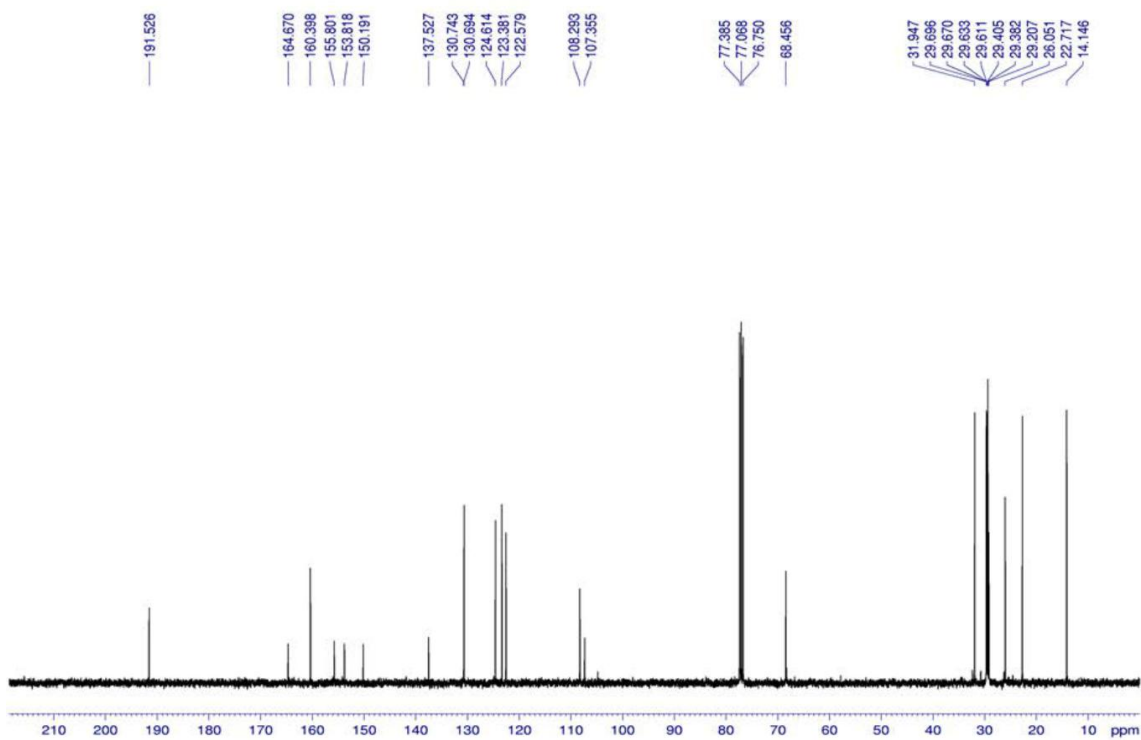
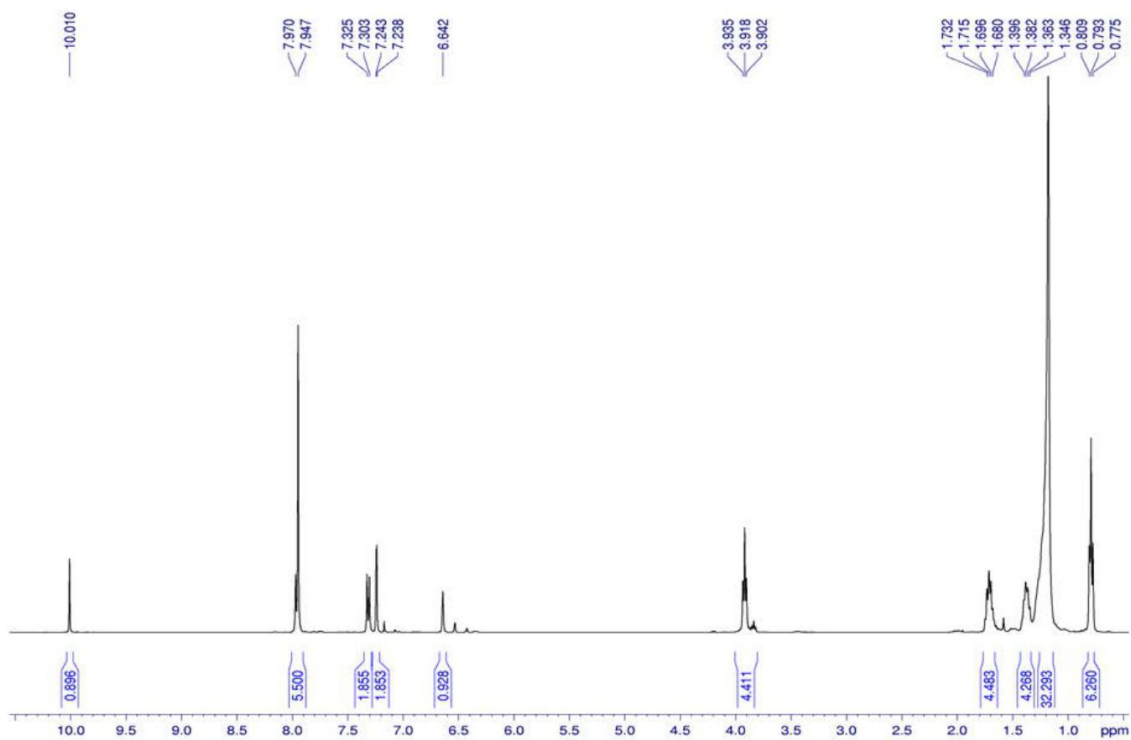
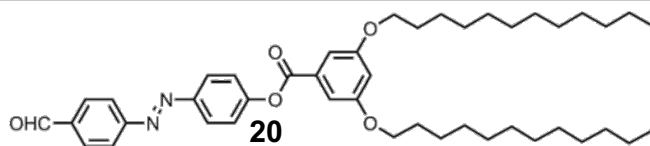


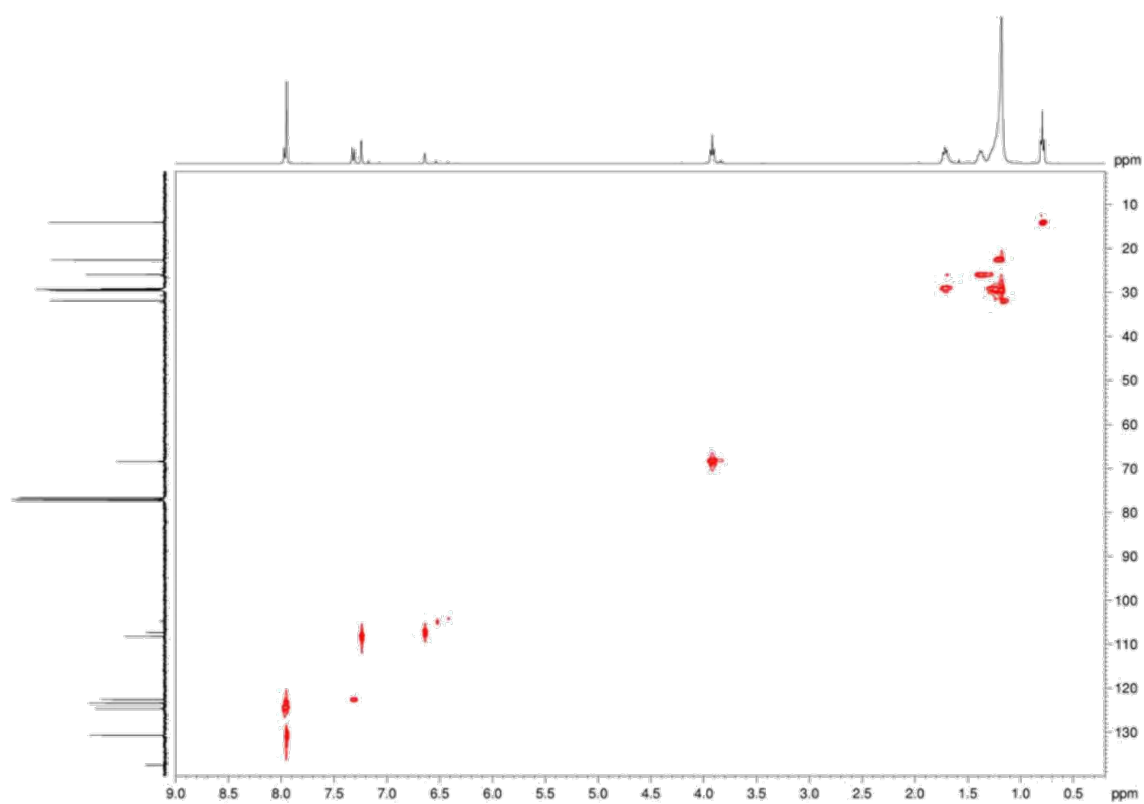
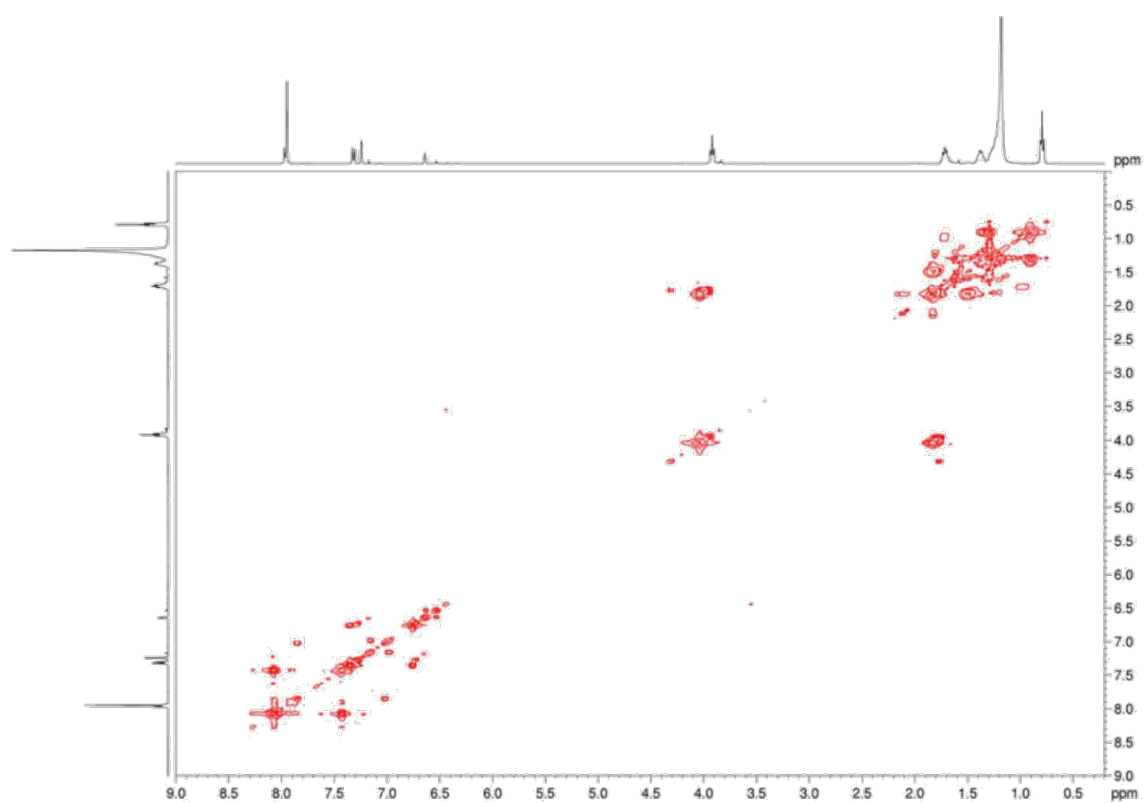


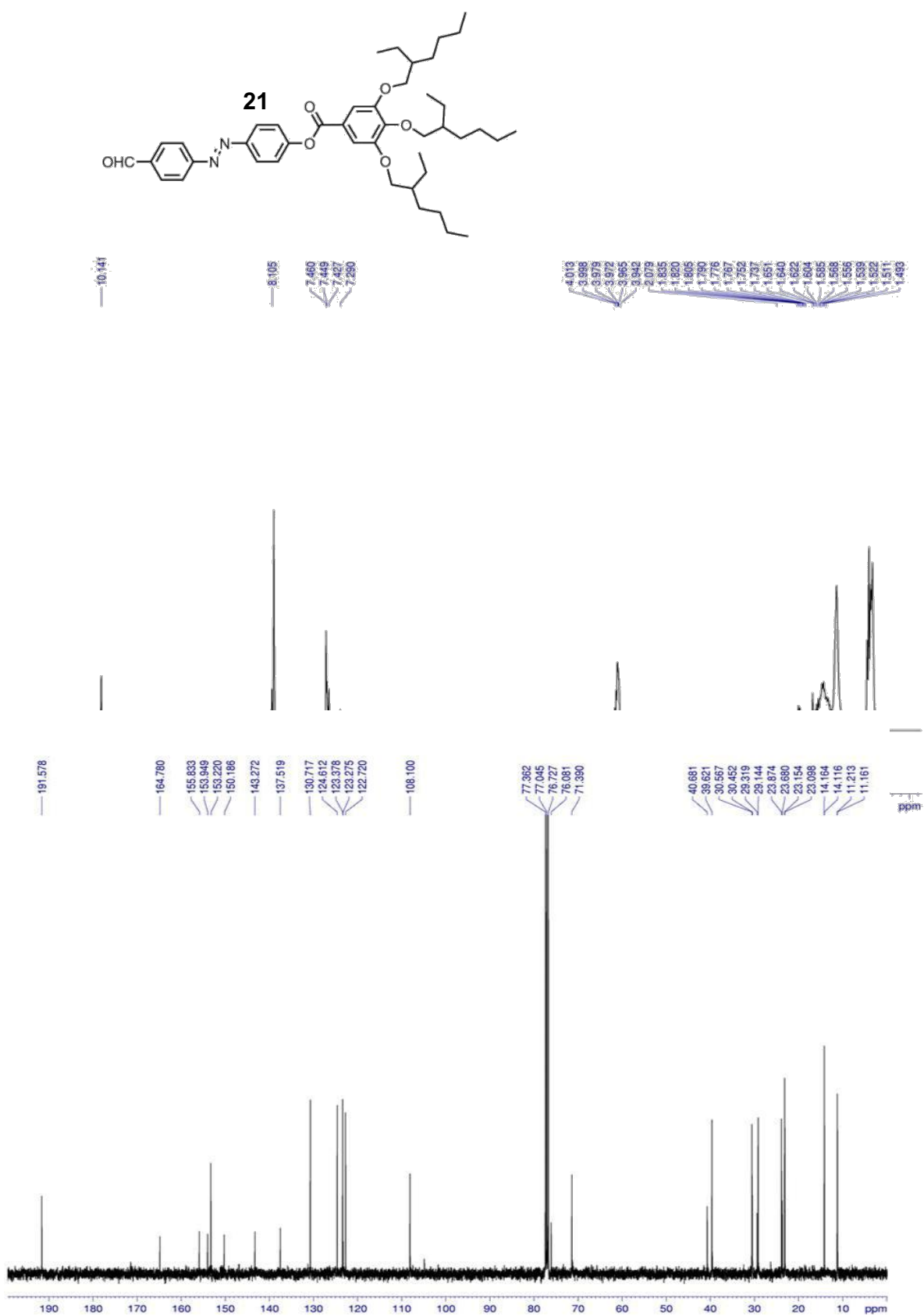


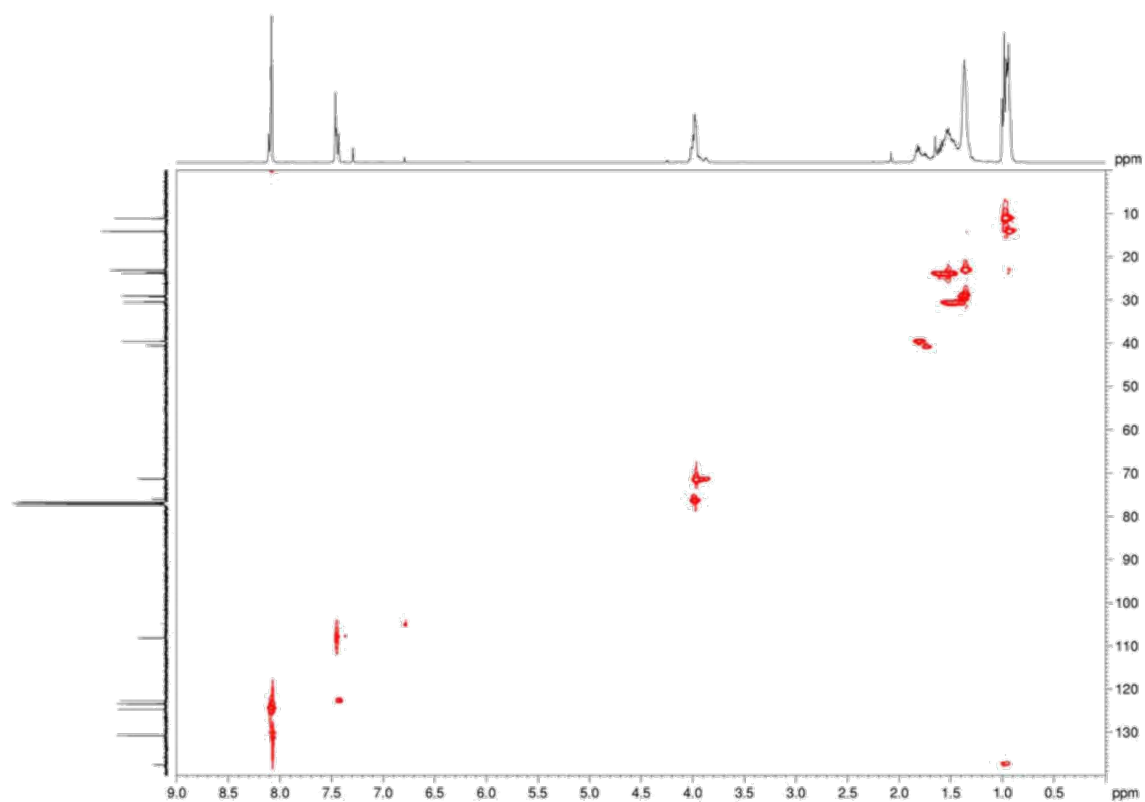
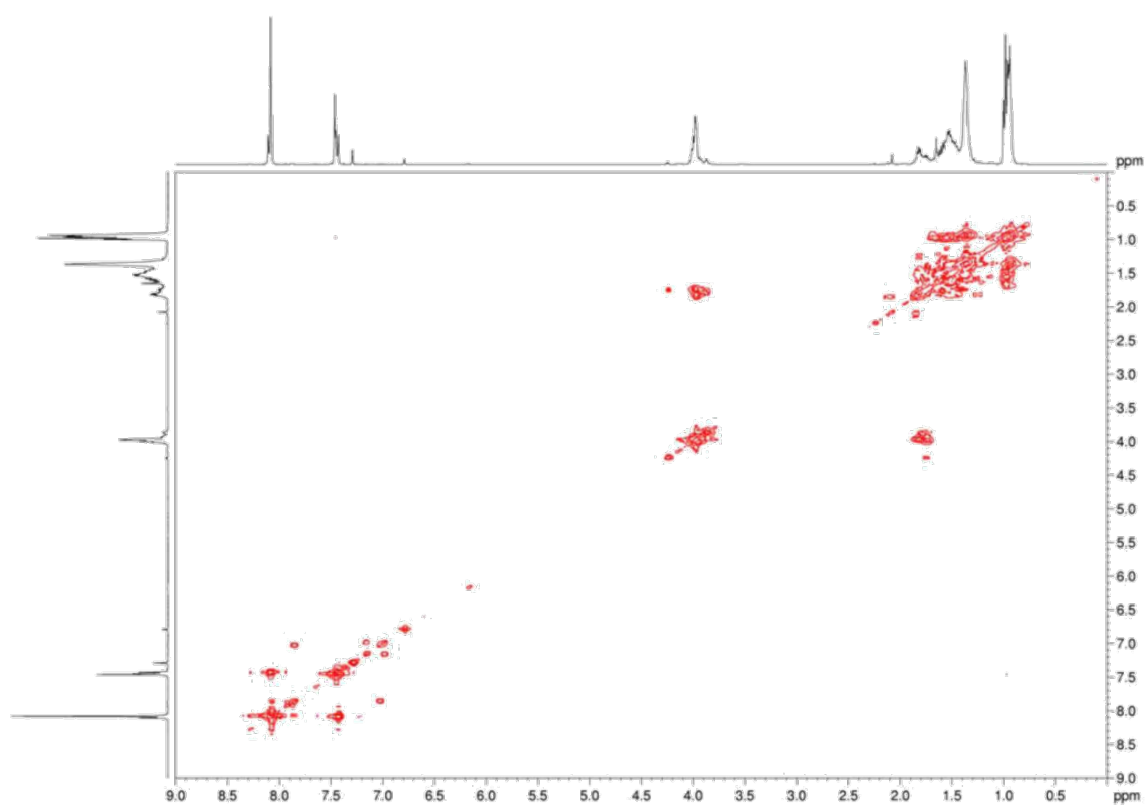


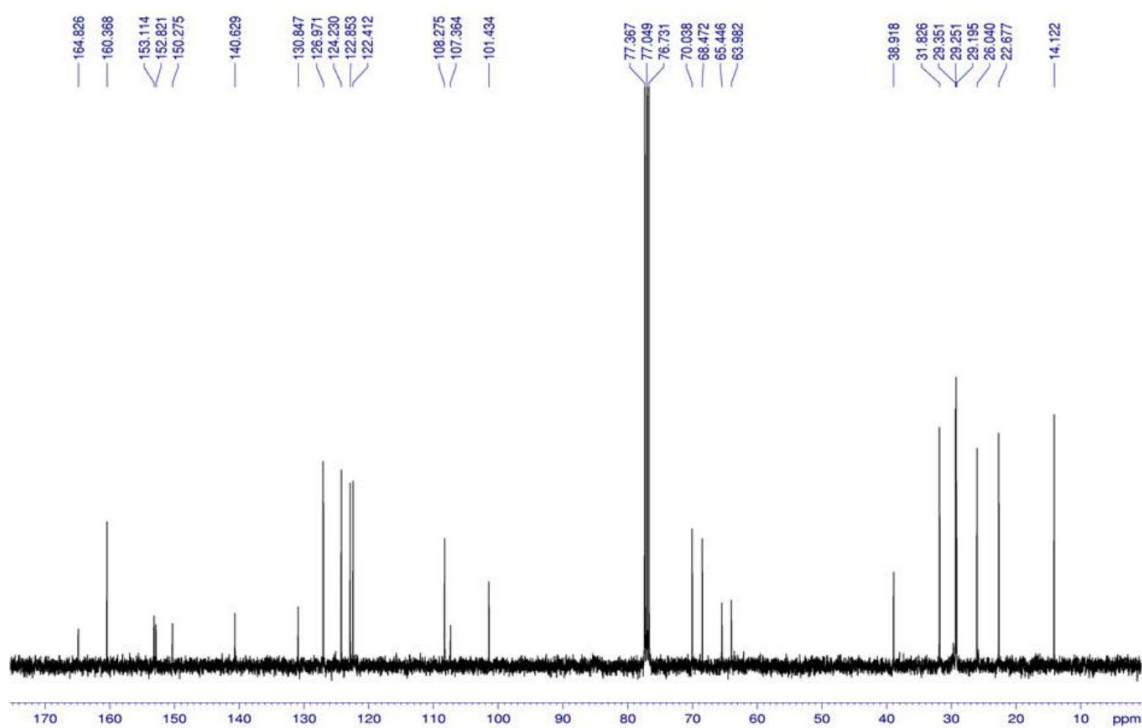
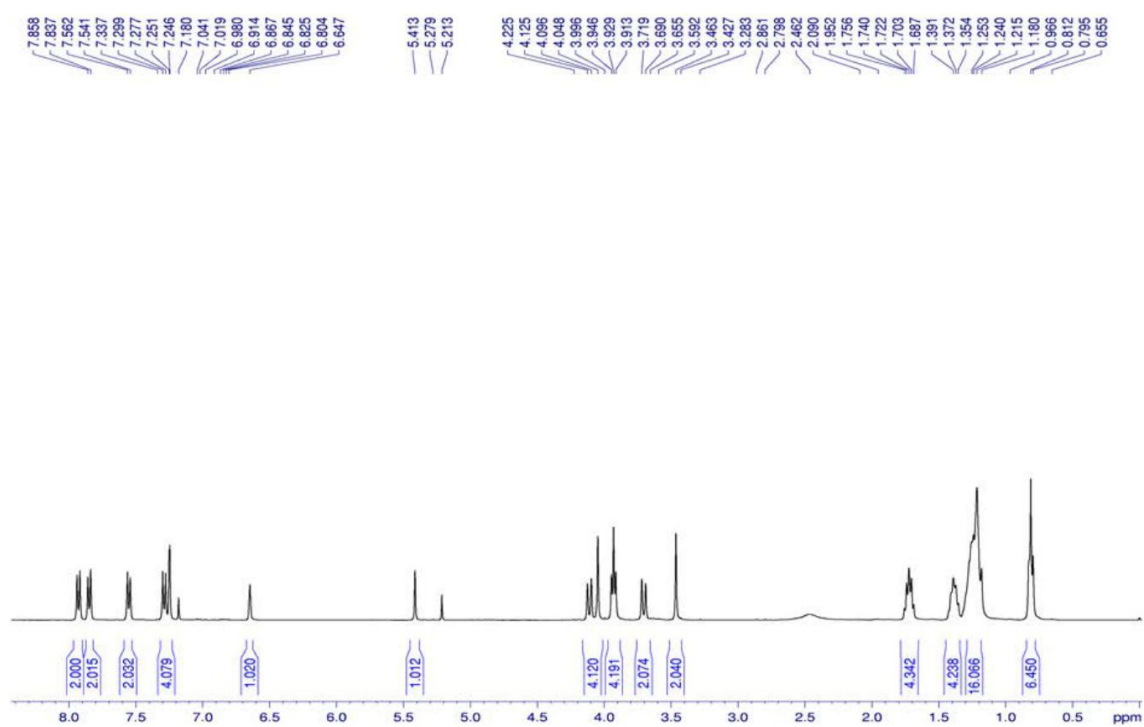
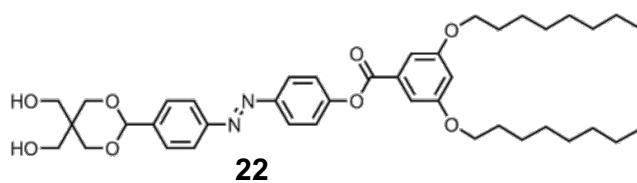


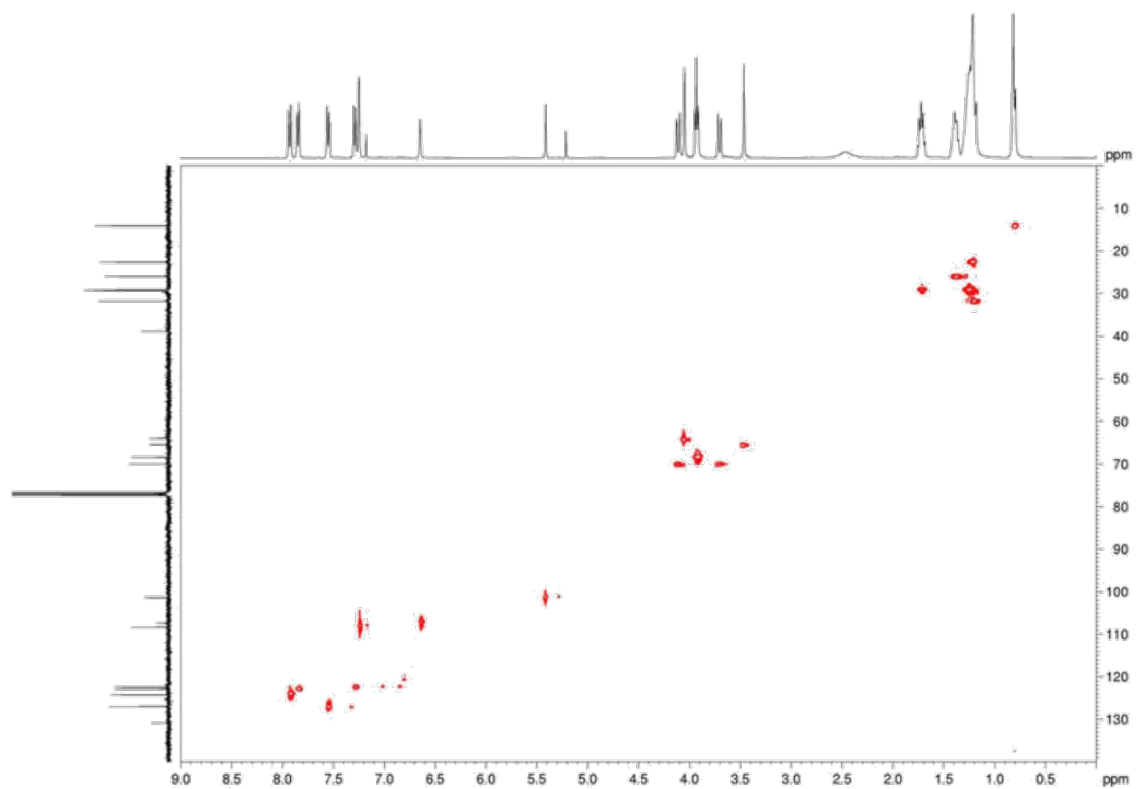
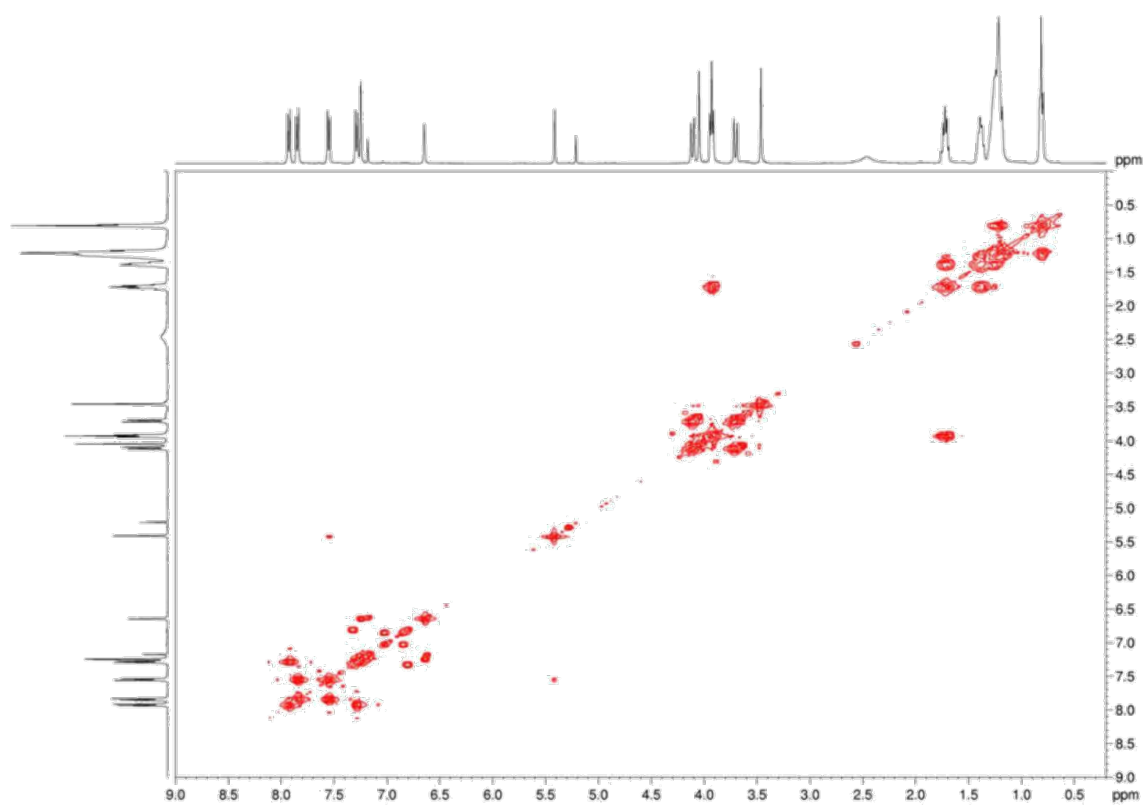


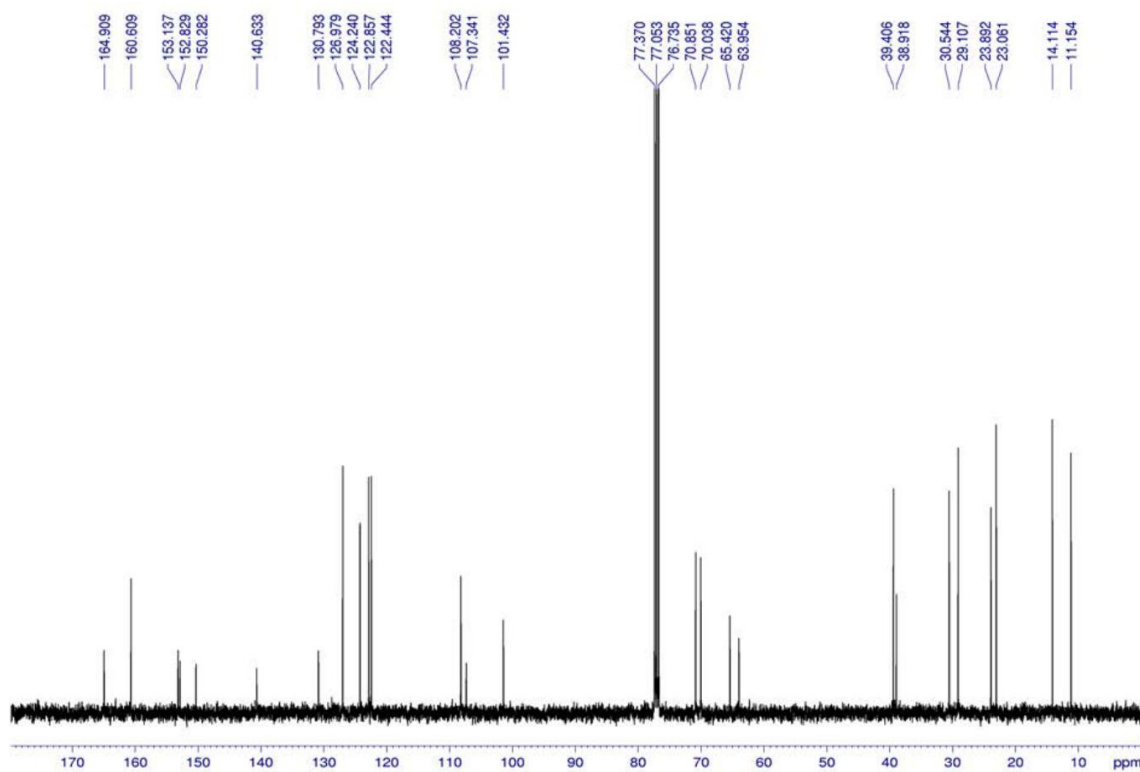
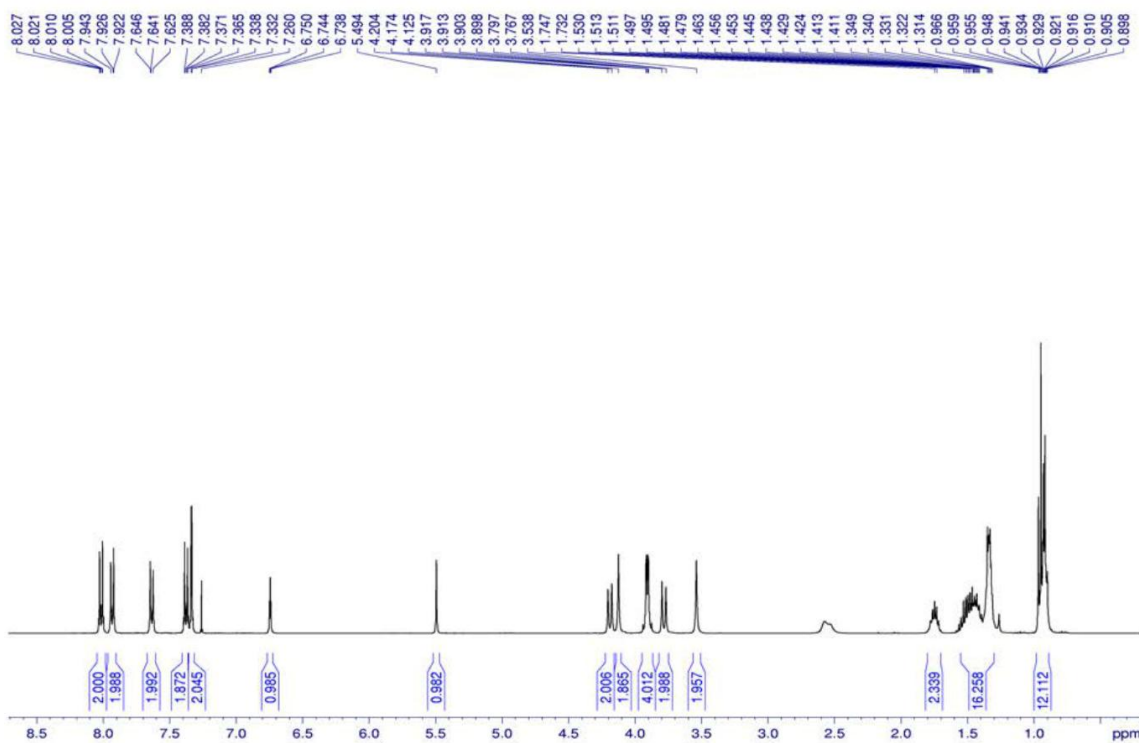
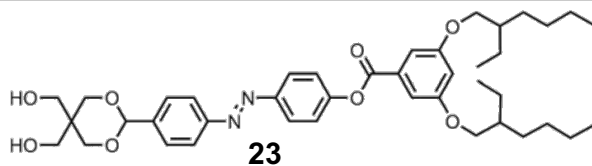


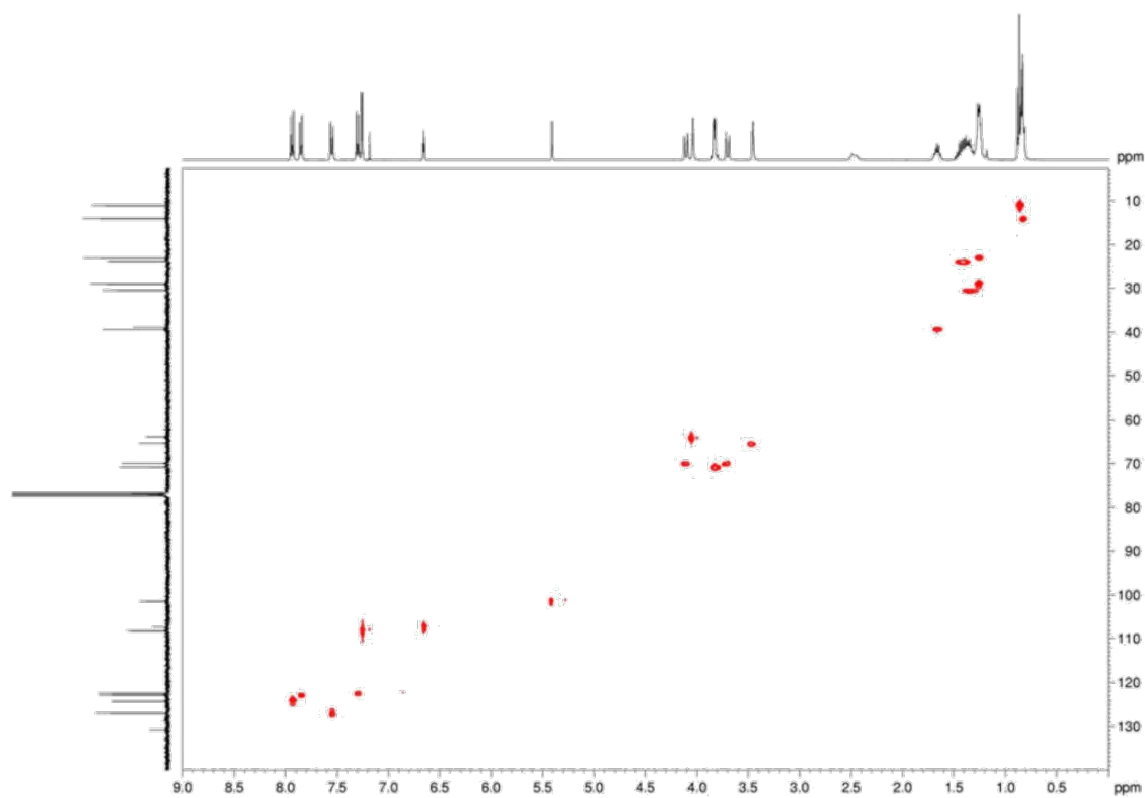
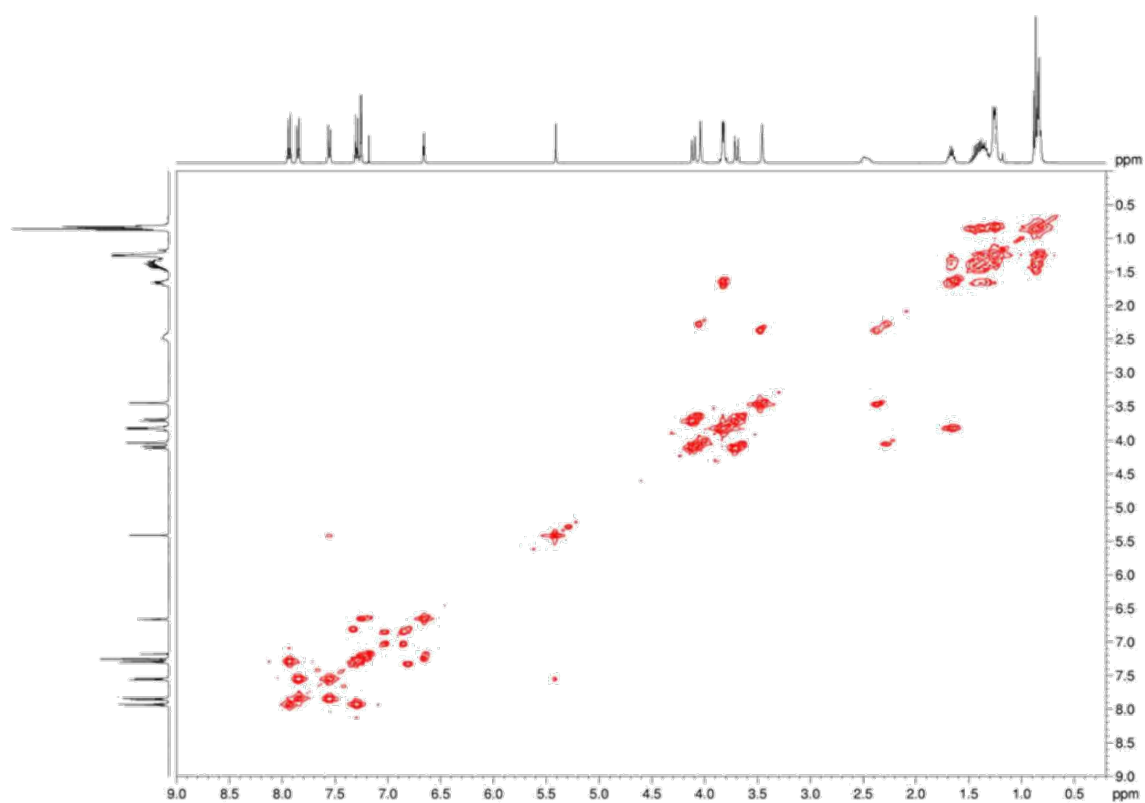


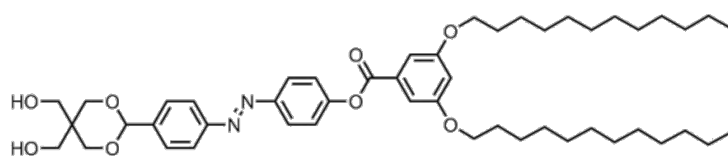
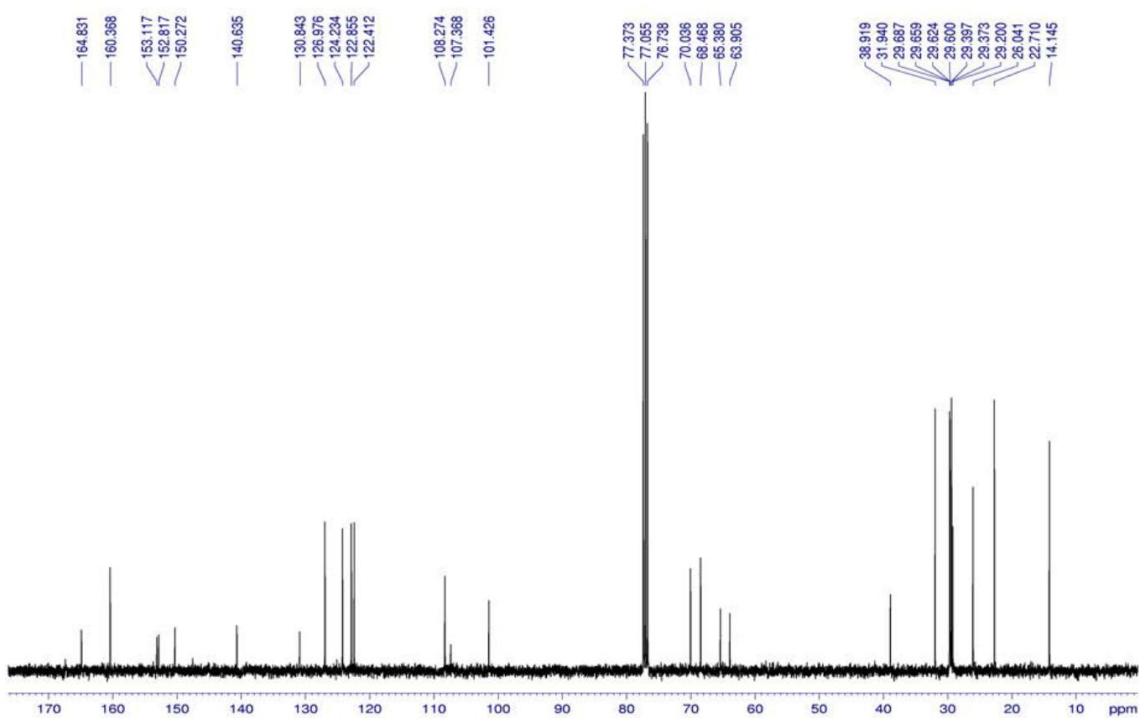
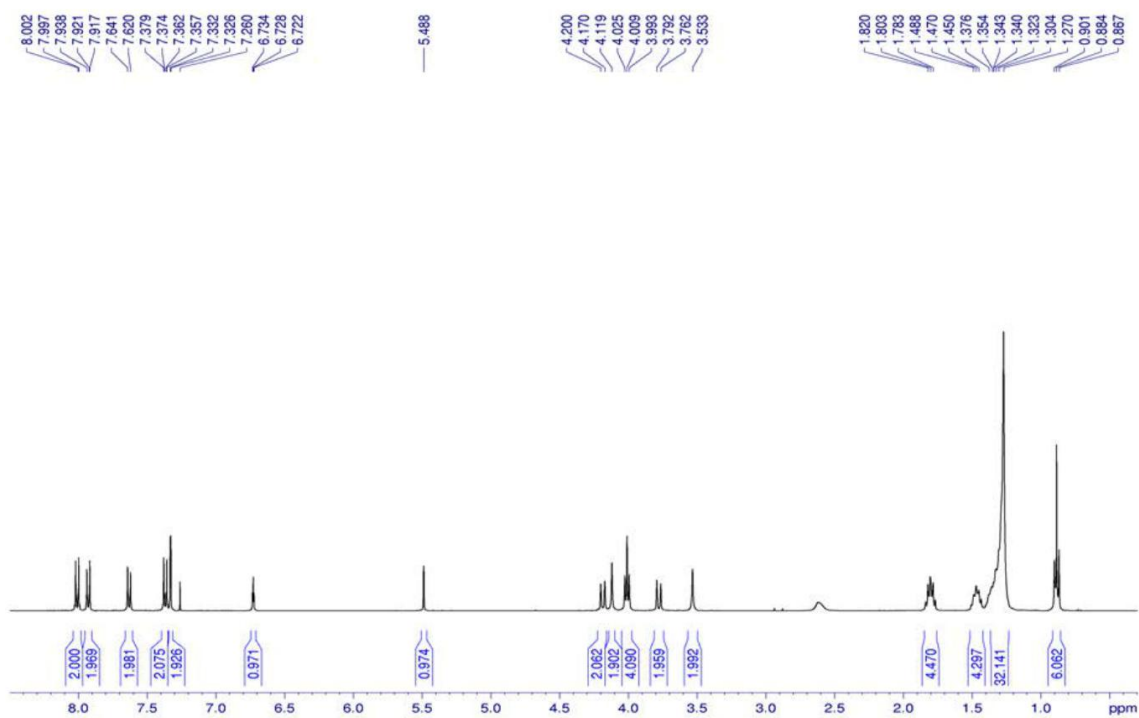


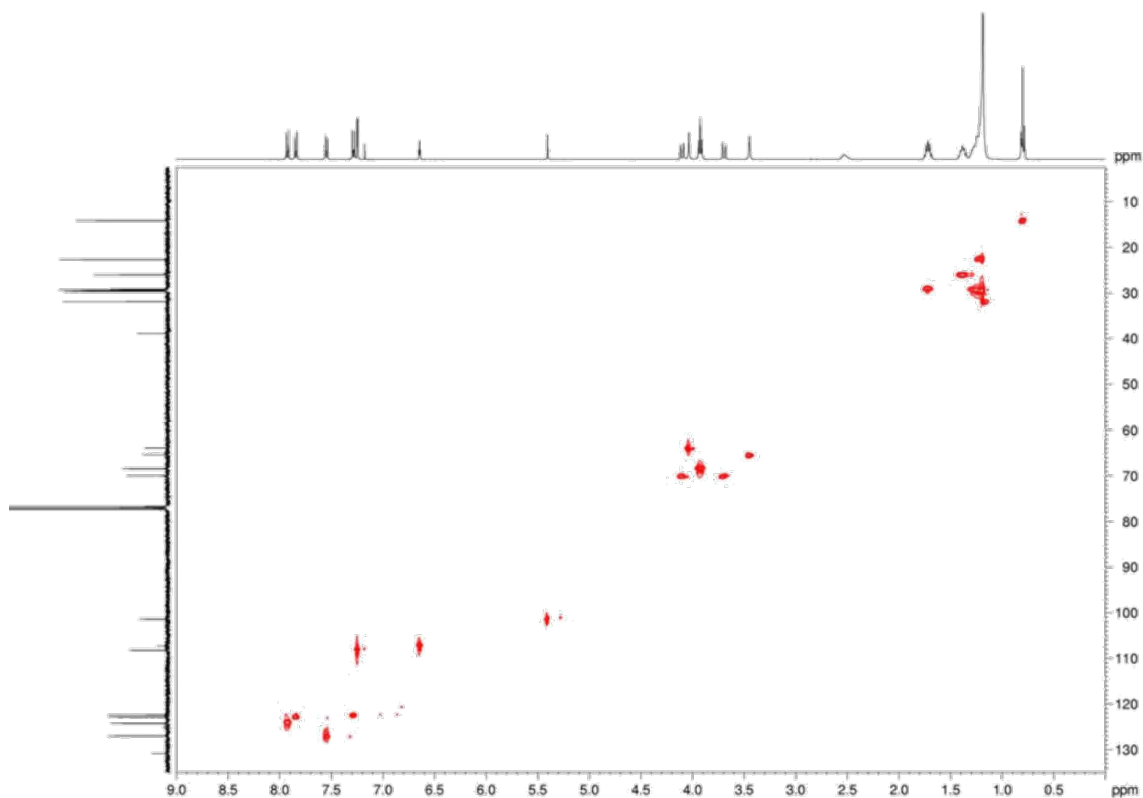
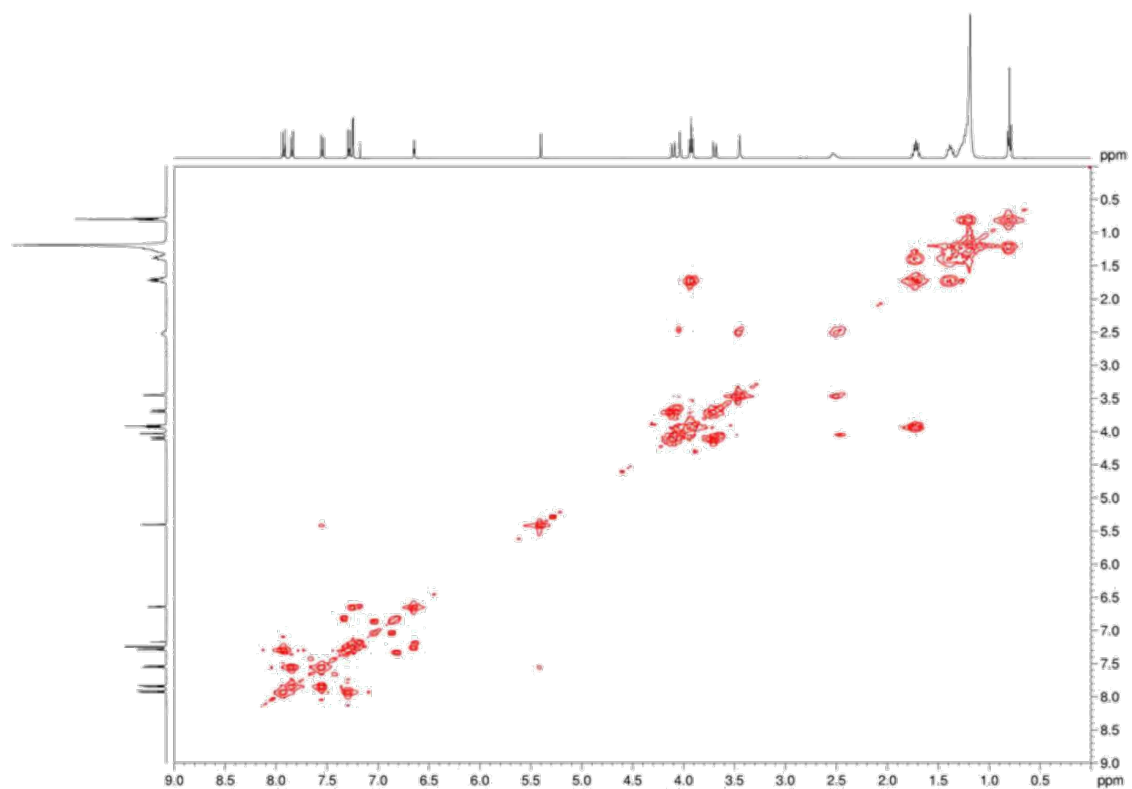


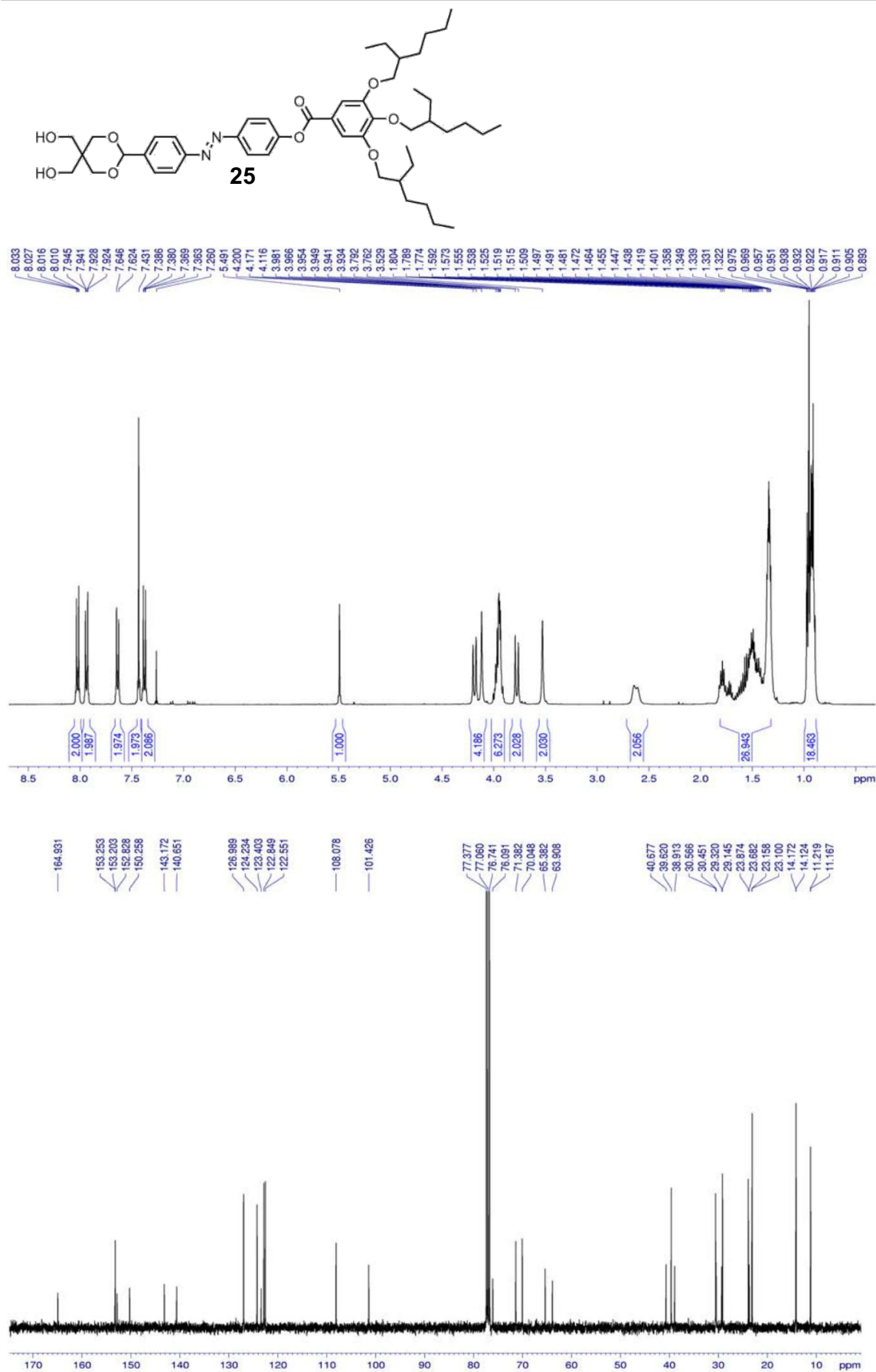


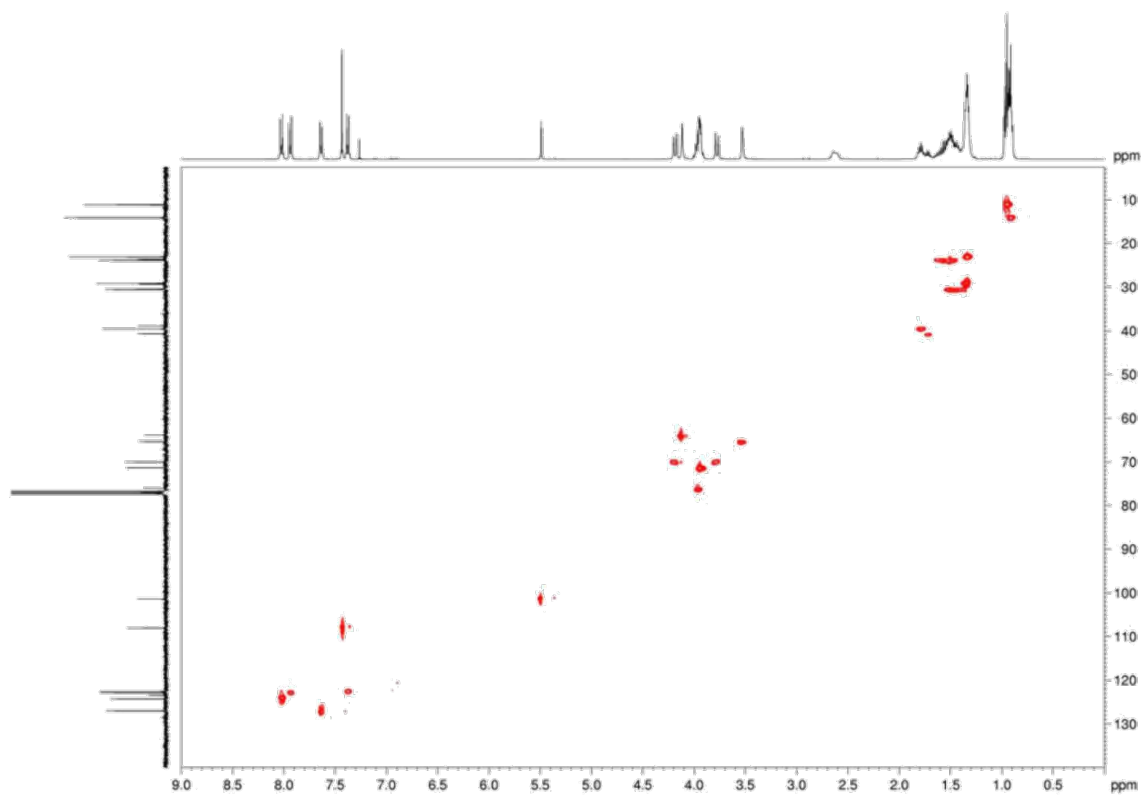
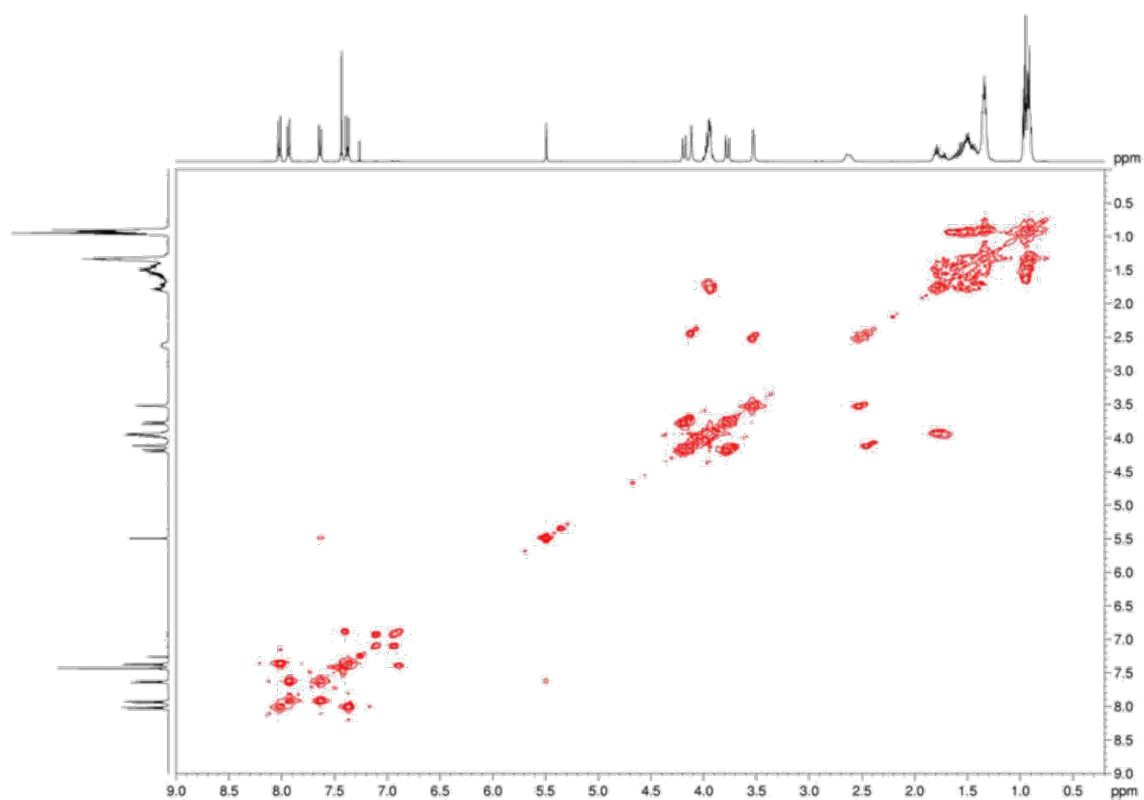


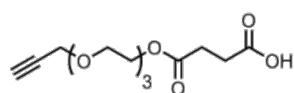
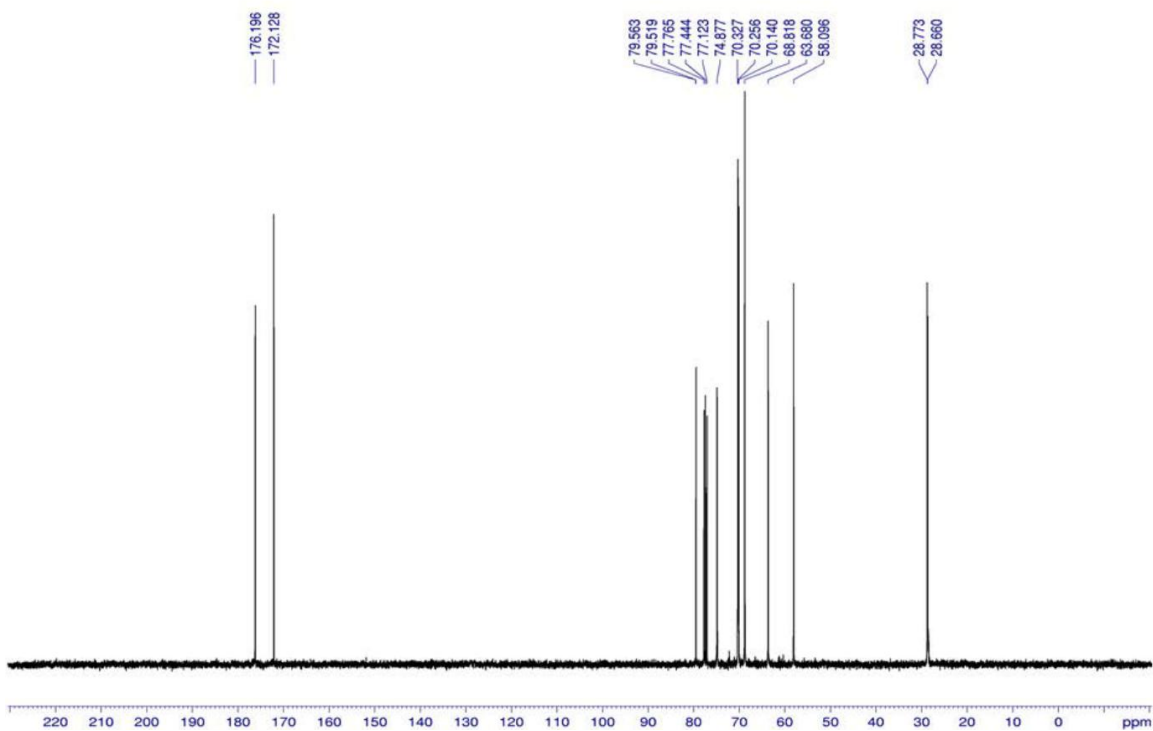
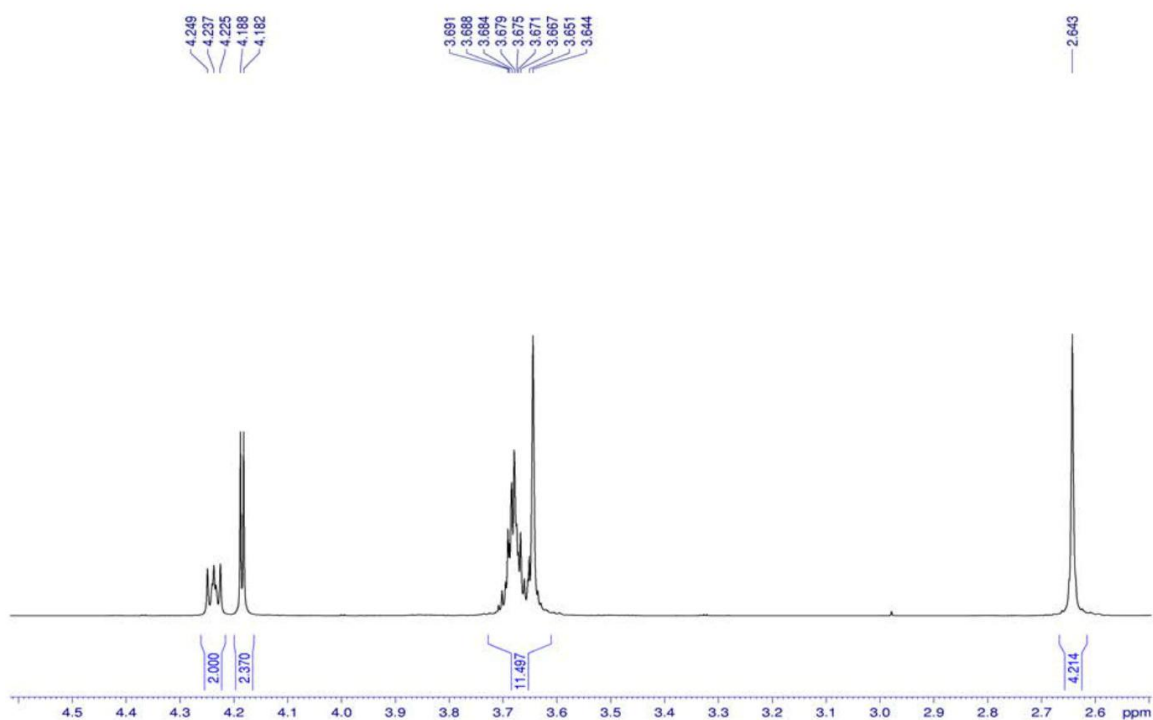


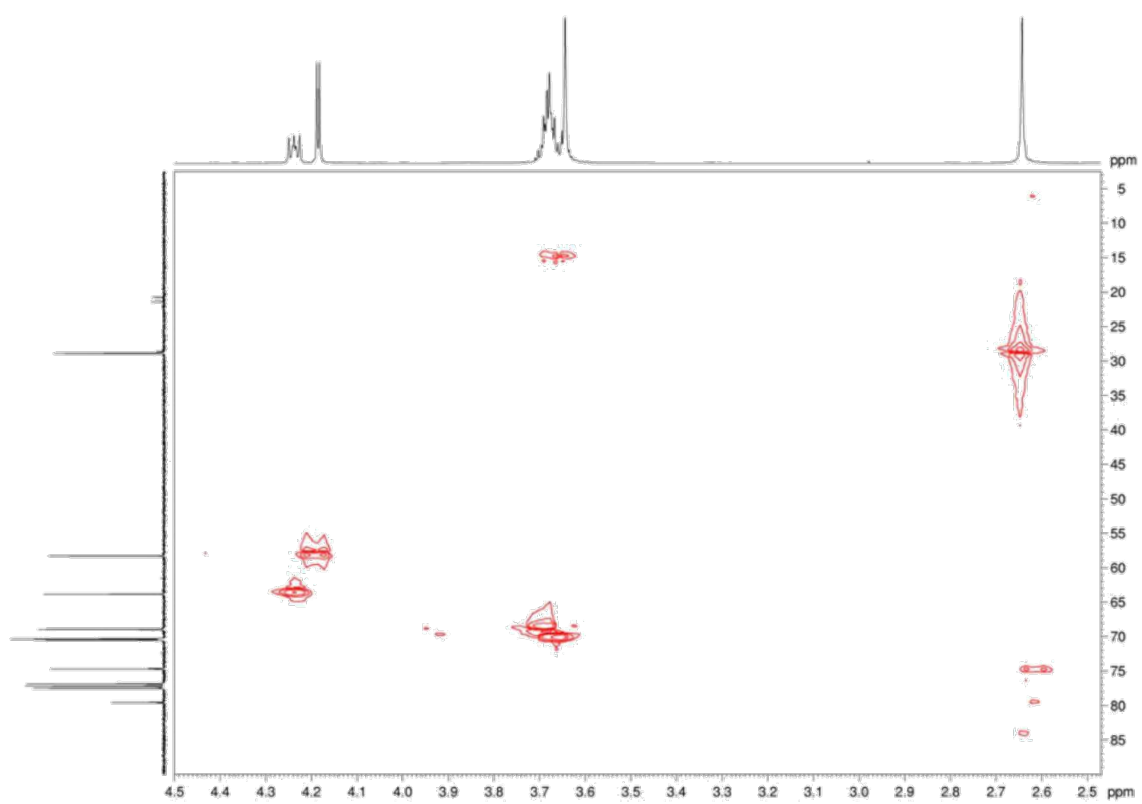
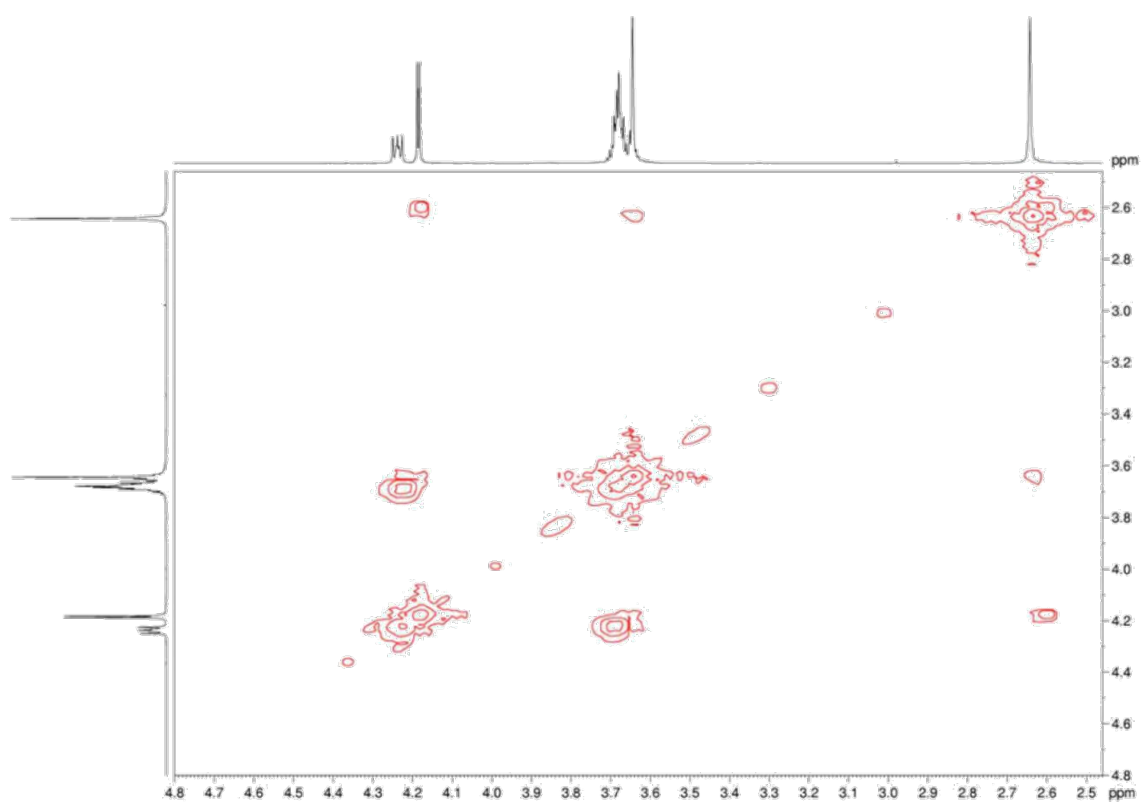
**24**

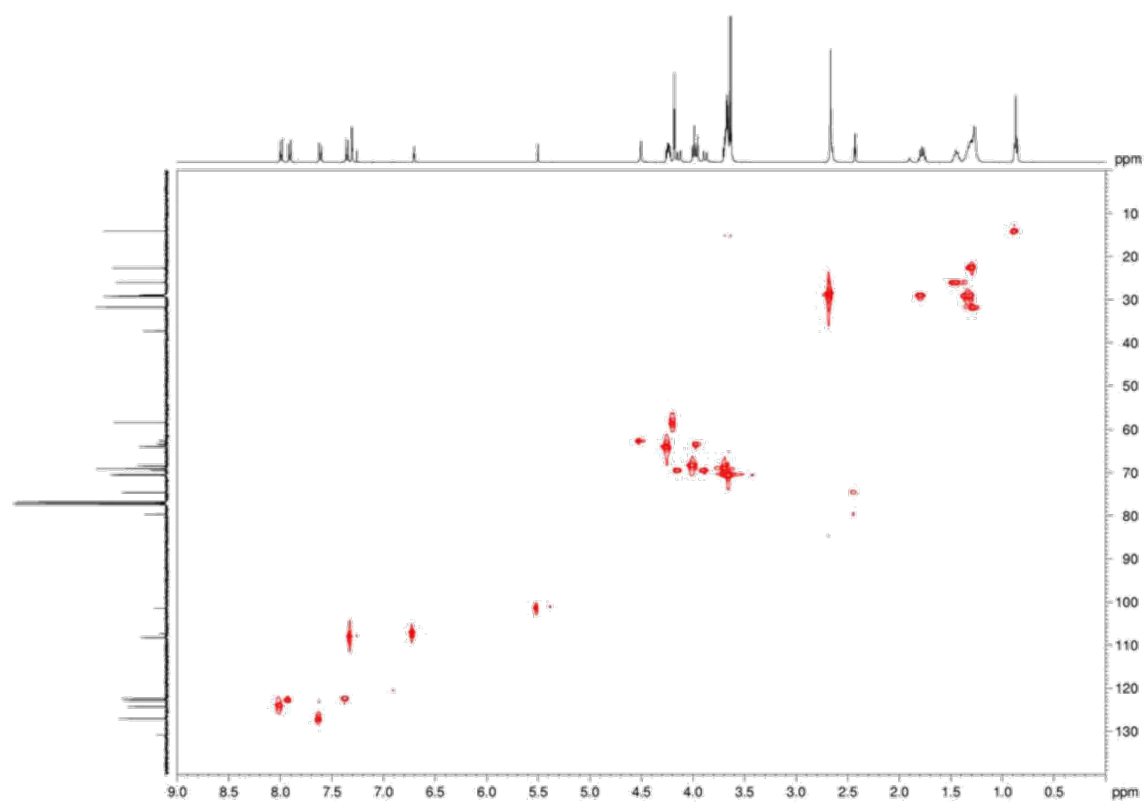
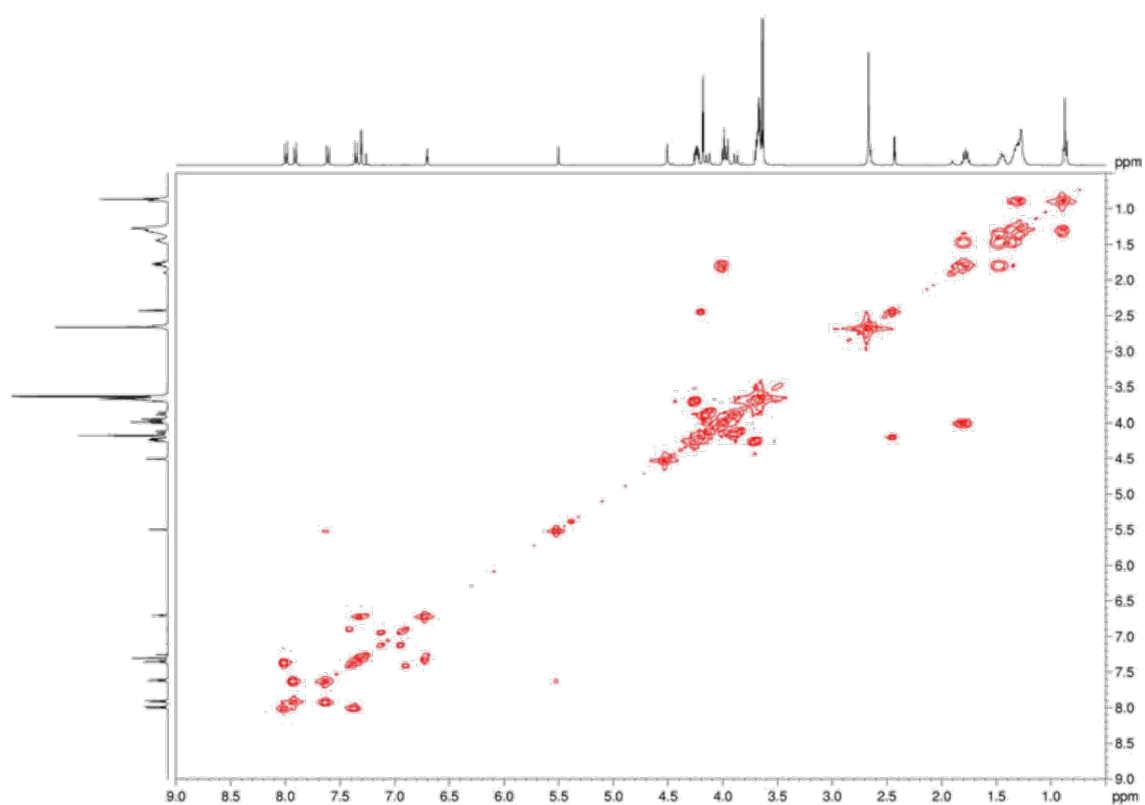


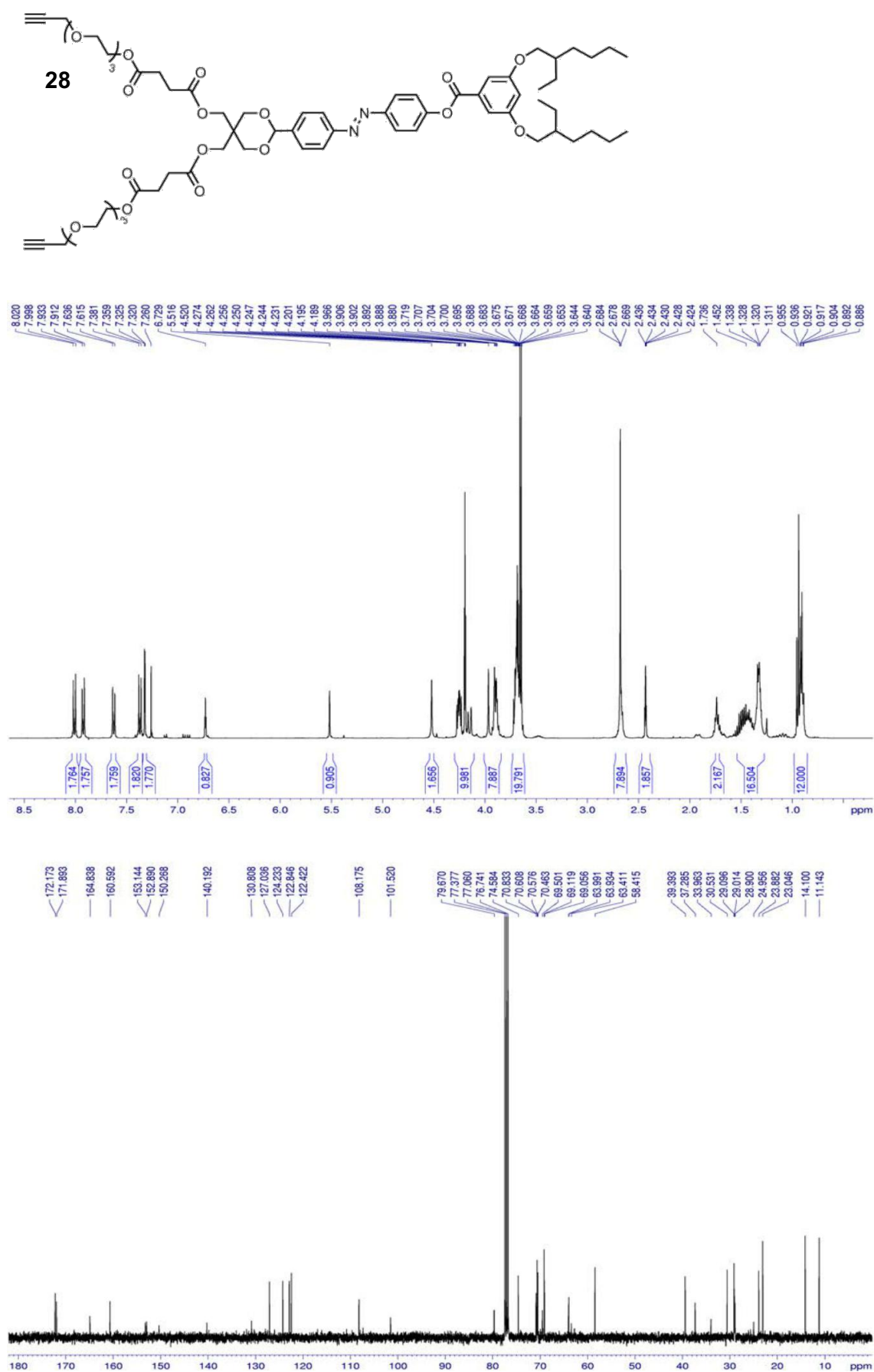


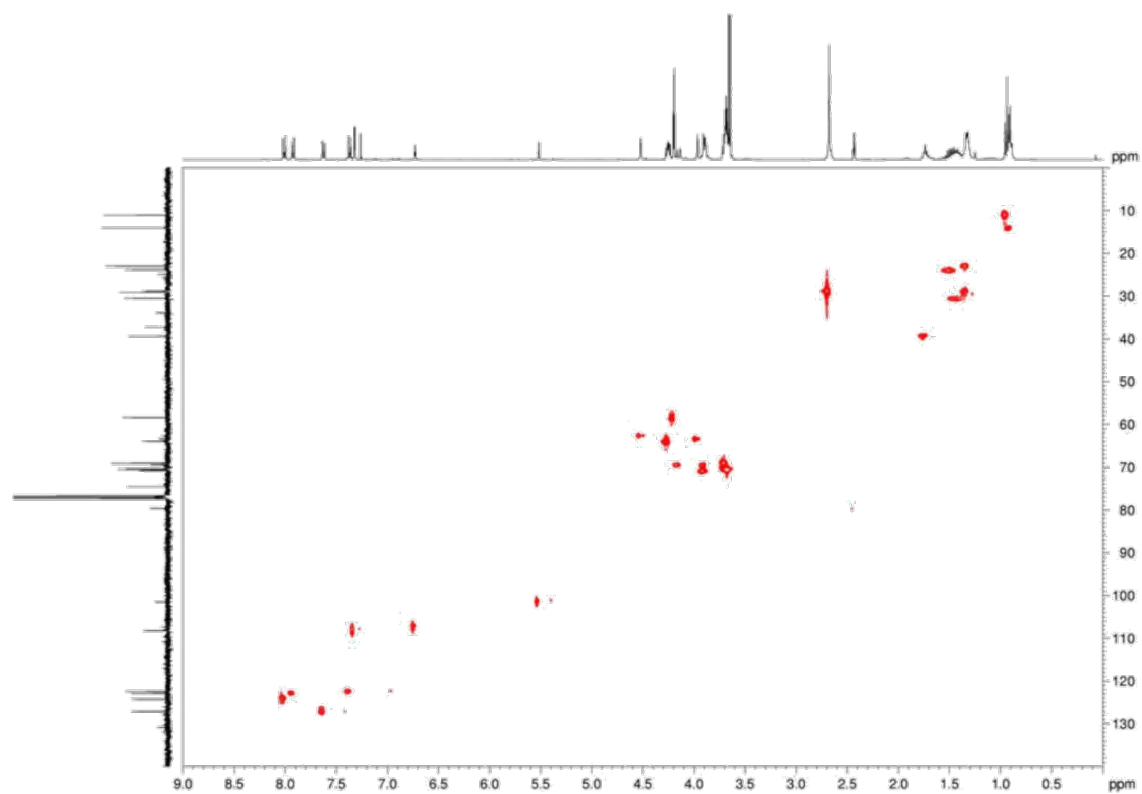
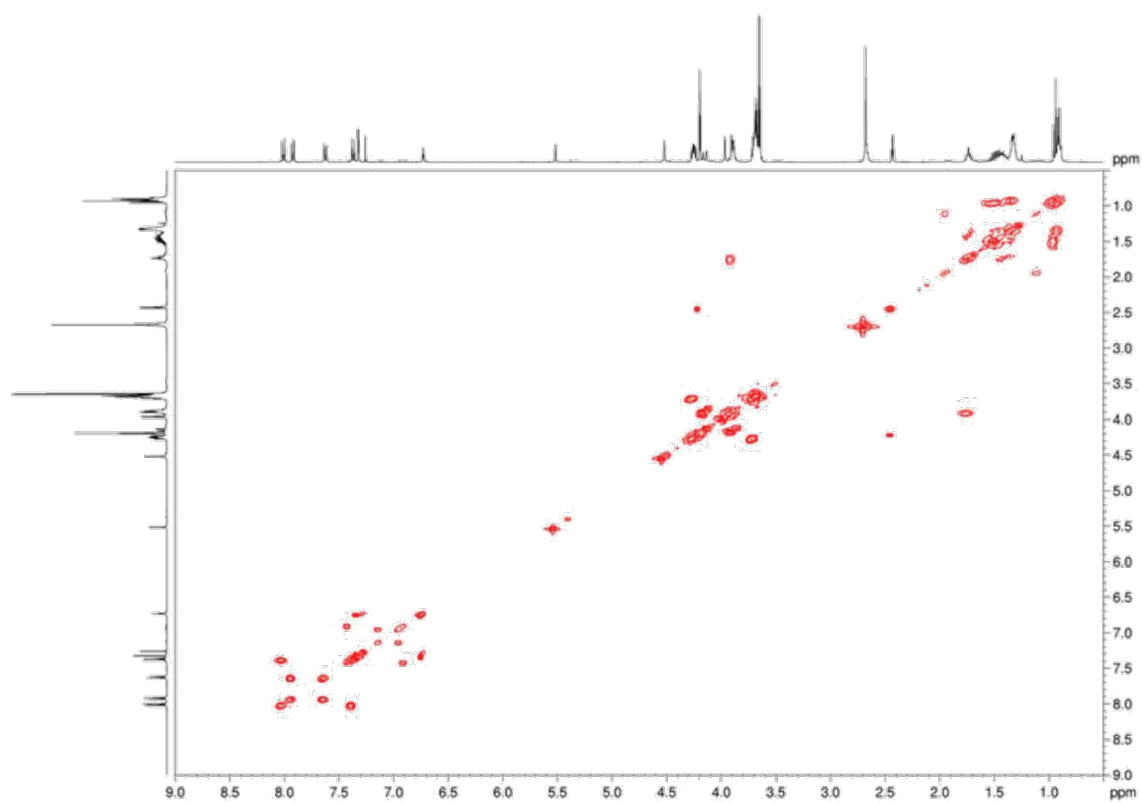


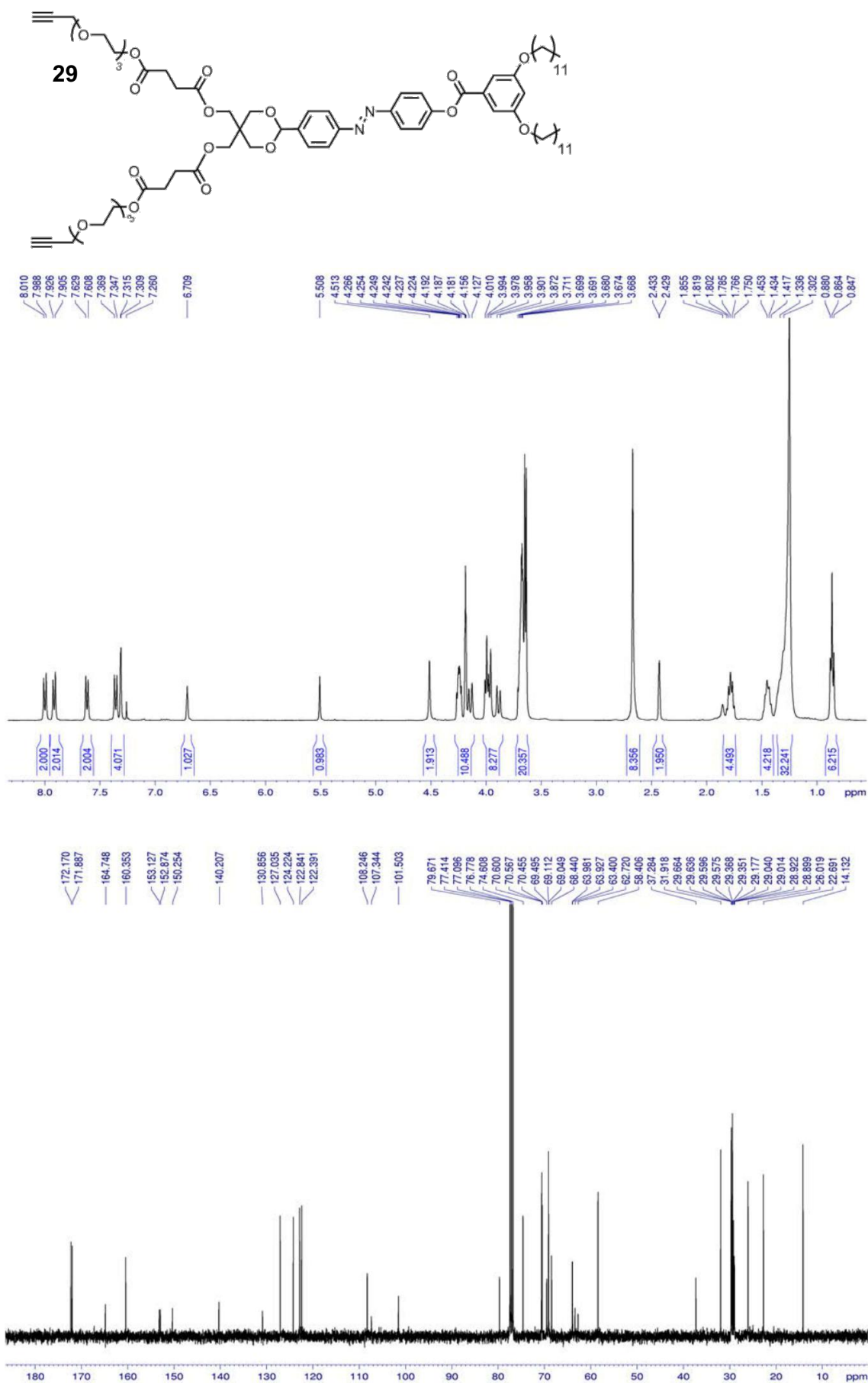
**26**

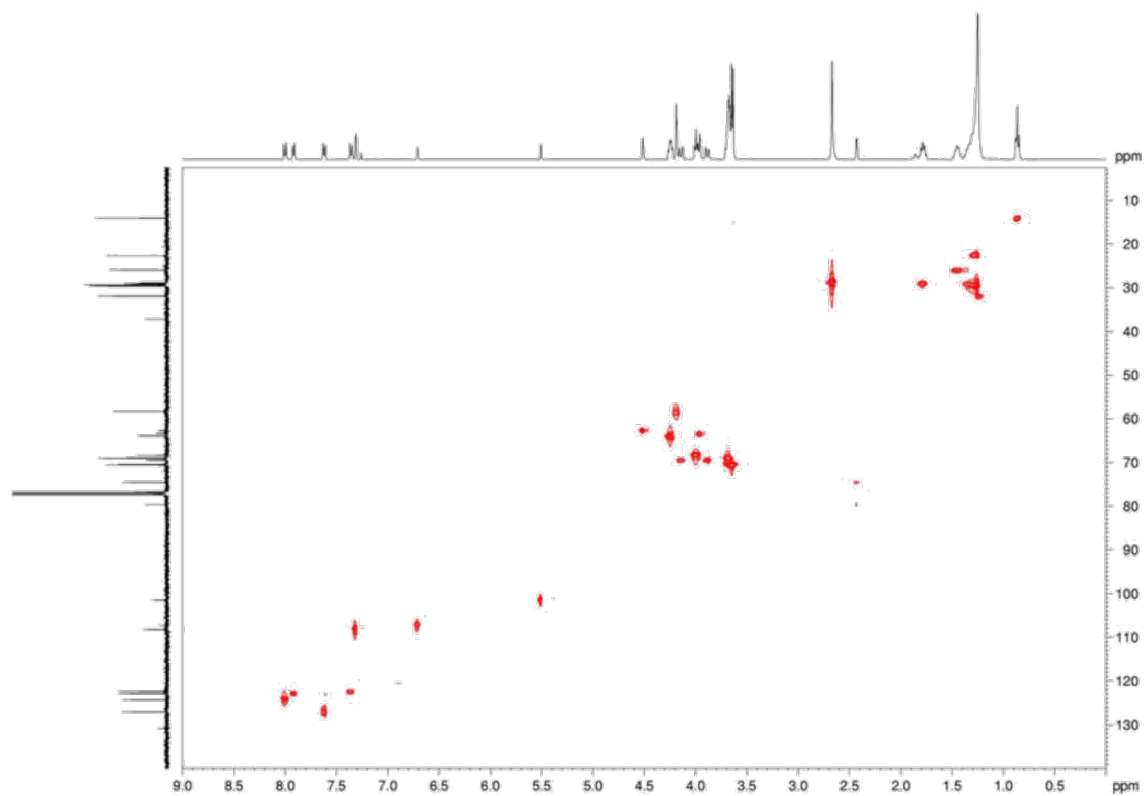
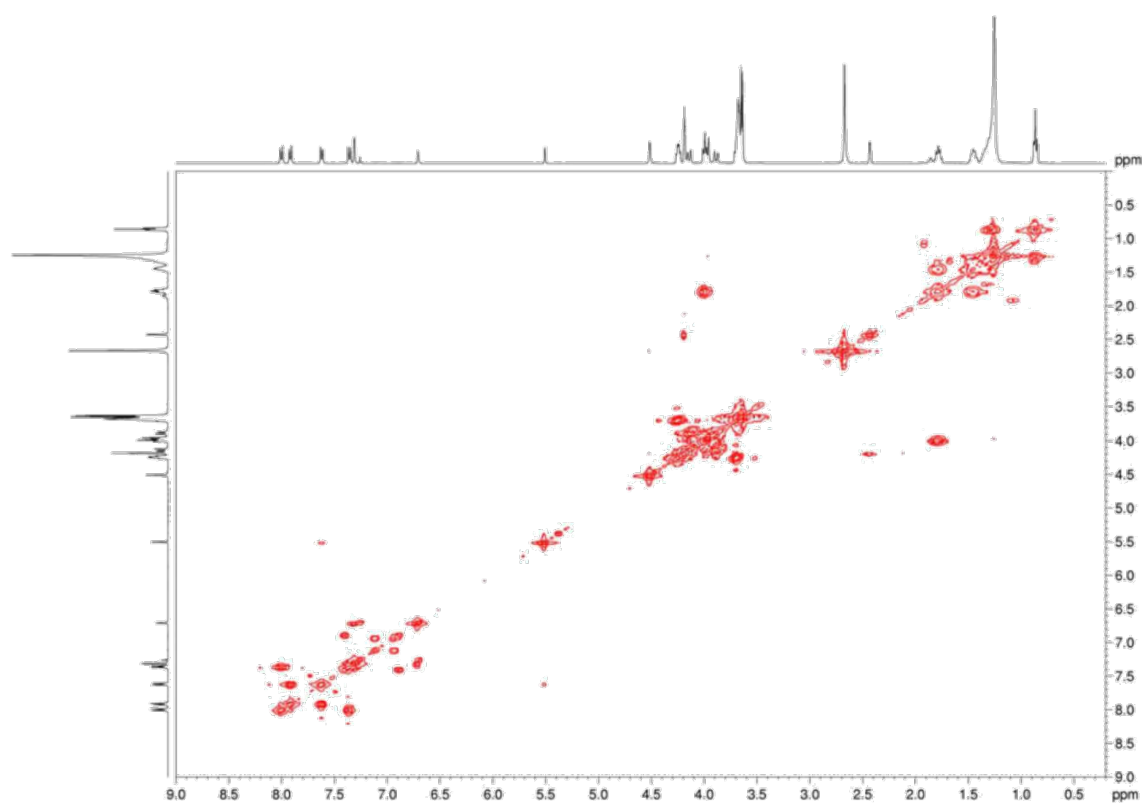


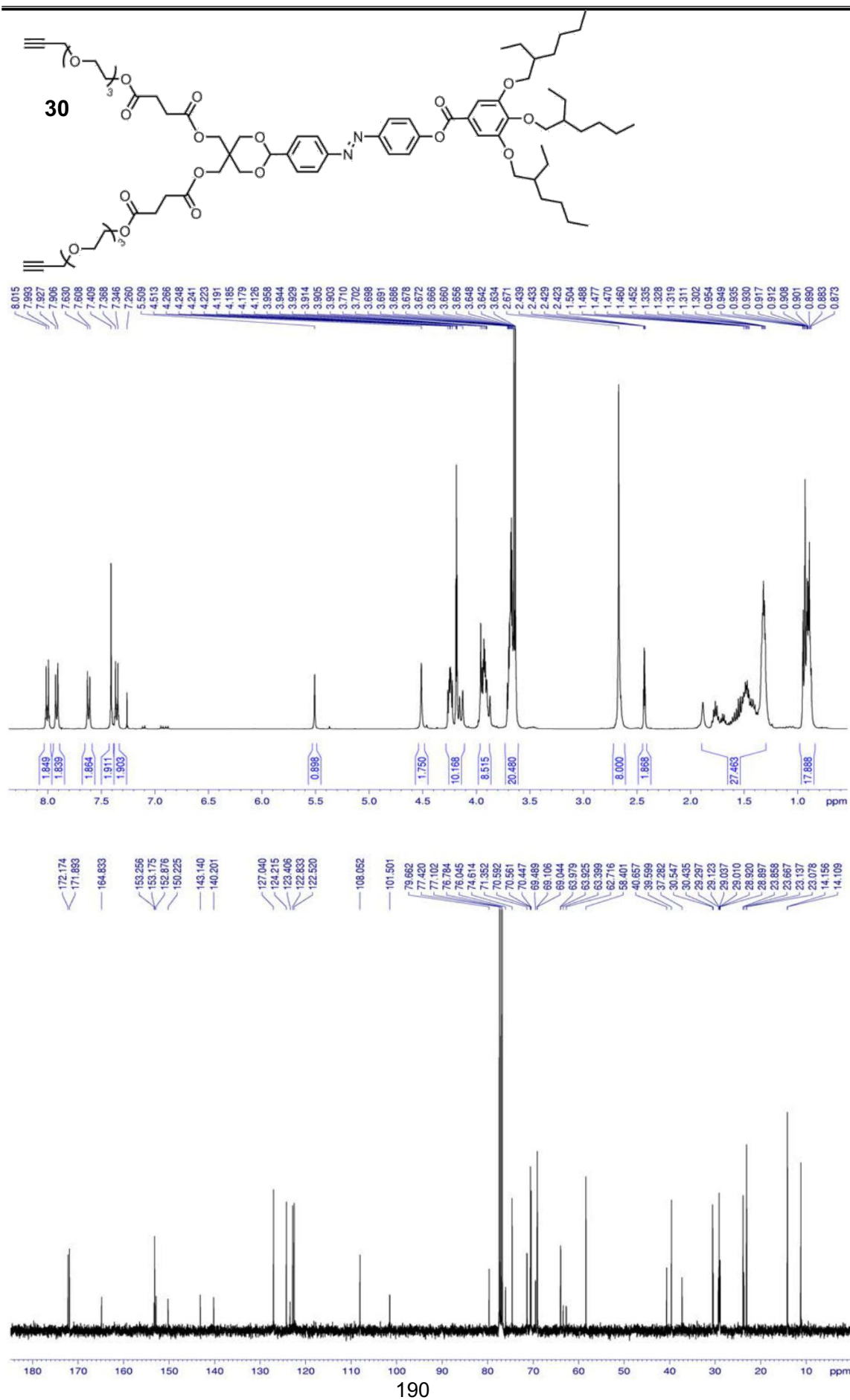


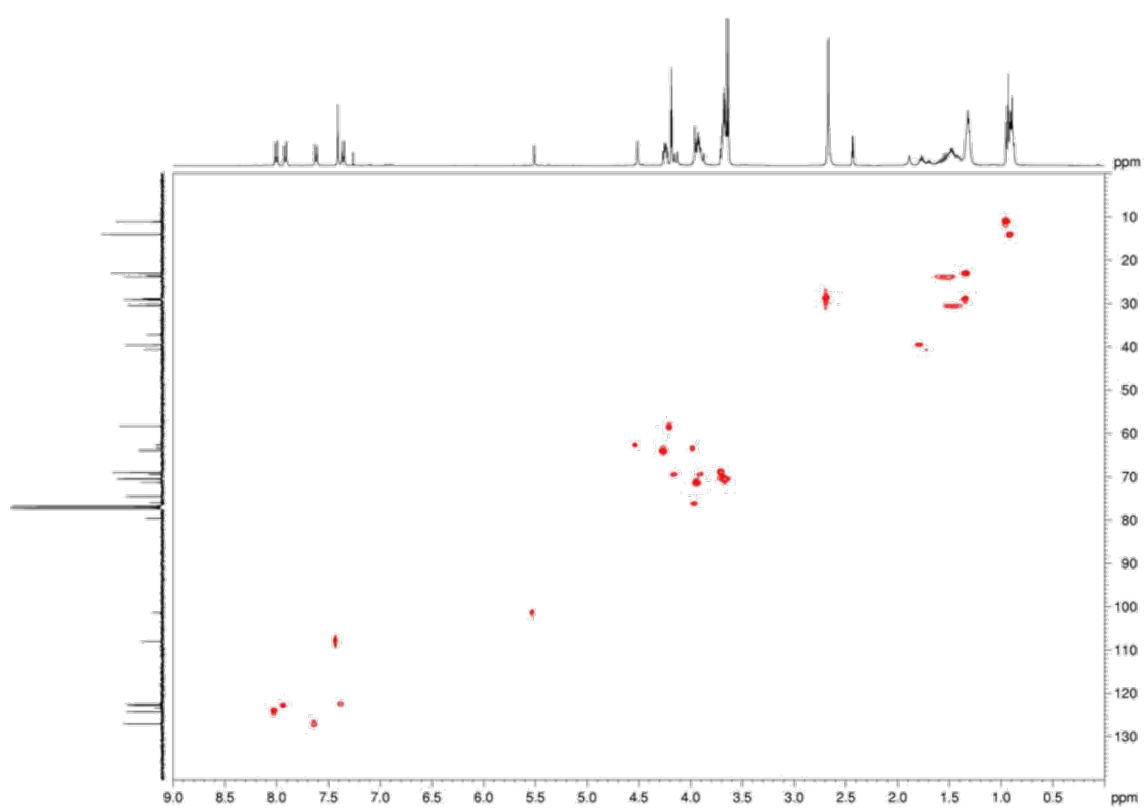
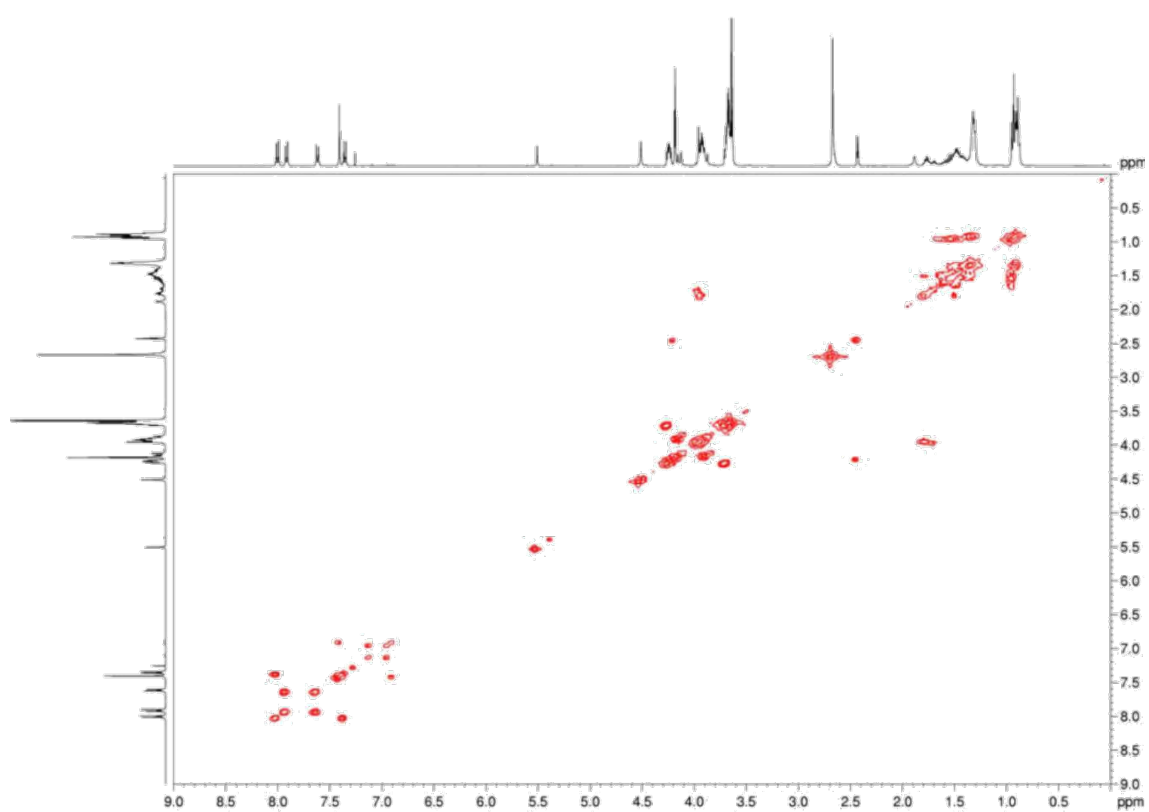


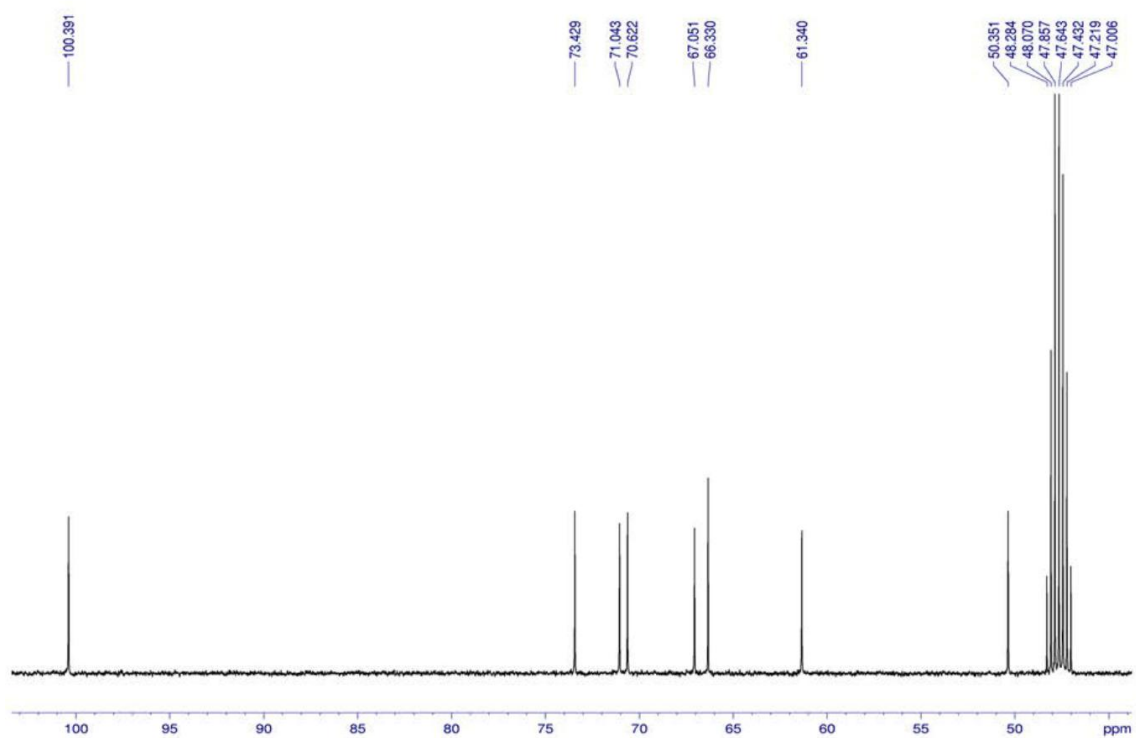
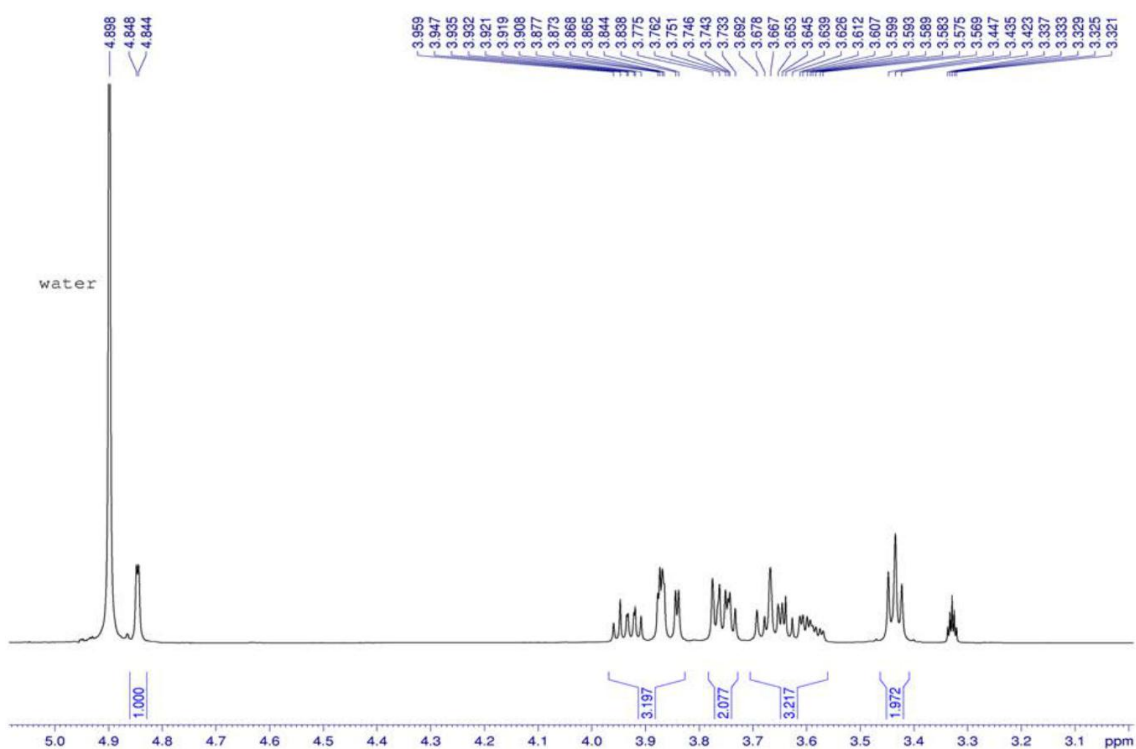
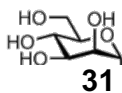


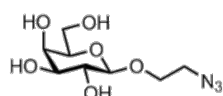
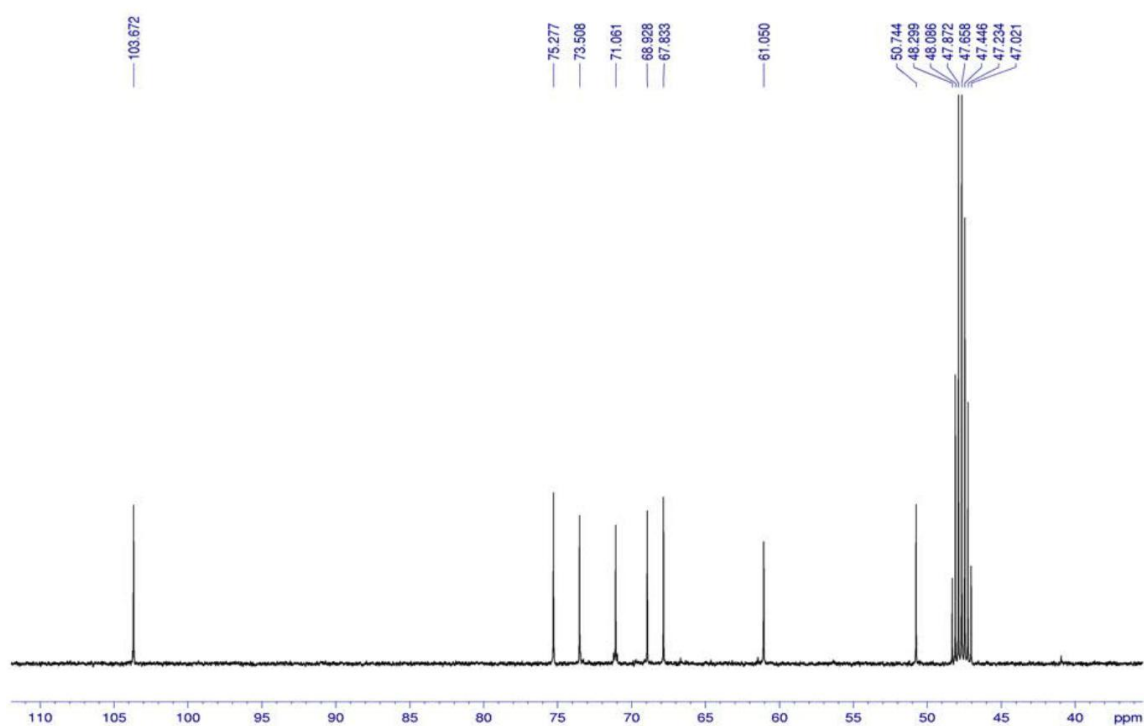
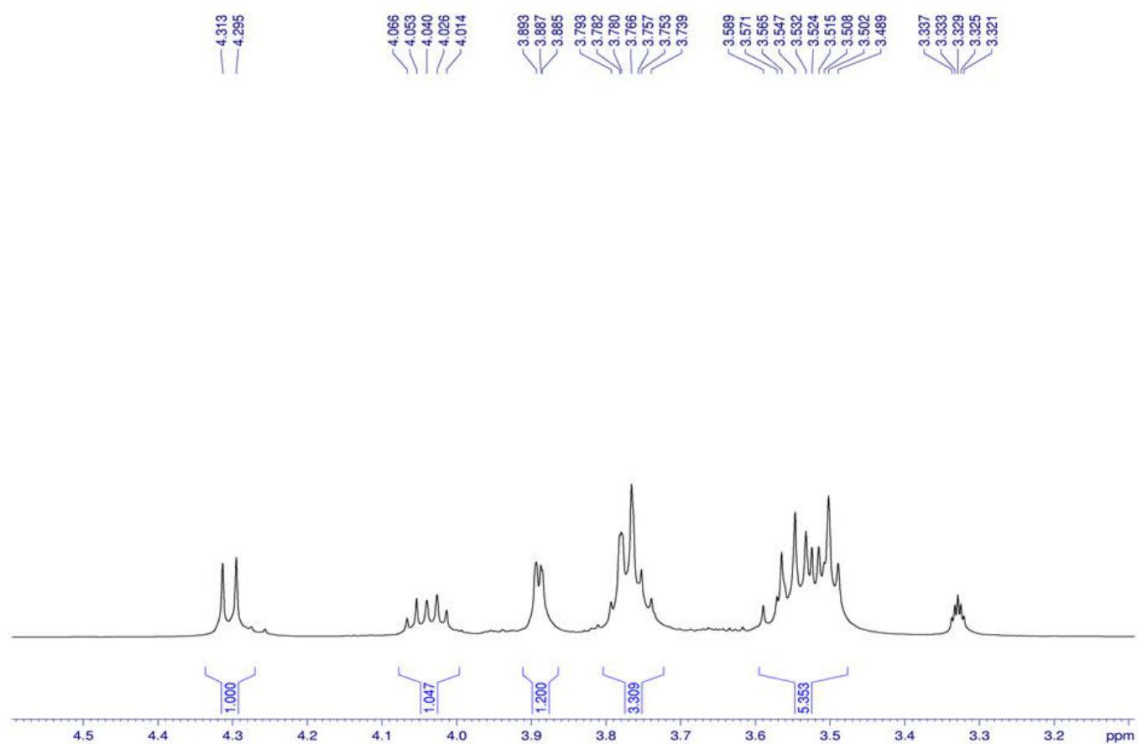




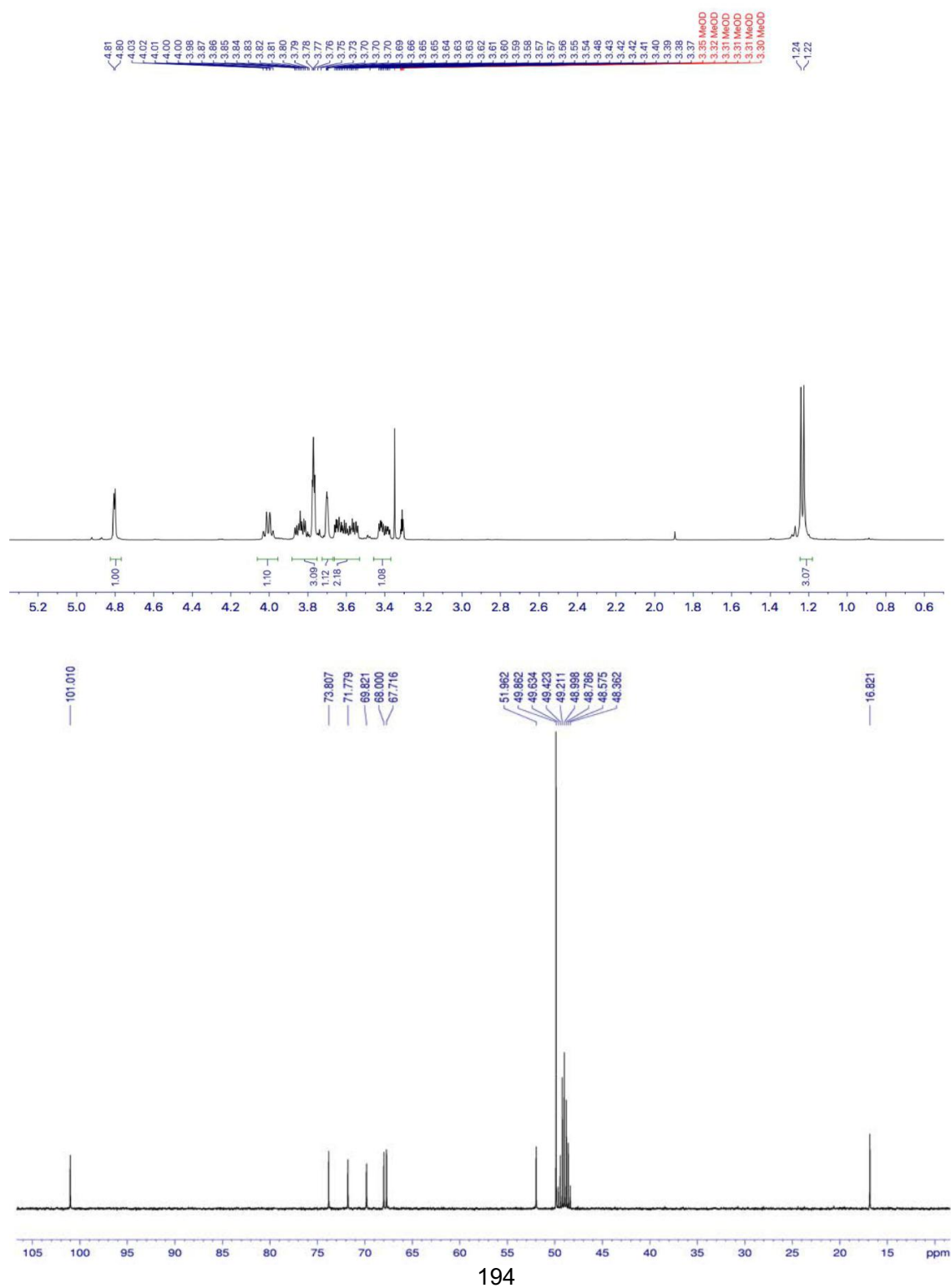
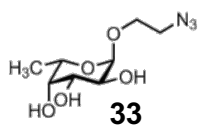






**32**

SUPPORTING INFORMATION



5.3. SUPPORTING INFORMATION FOR SUBCHAPTER 3.3

Supporting Information to

**Development of a competitive binding assay for the *Burkholderia cenocepacia*
lectin BC2L-A and structure activity relationship of natural and synthetic
inhibitors**

Ghamdan Beshra^{a,b#}, Roman Sommer^{a,b,c#}, Dirk Hauck^{a,b,c}, David Chan Bodin Siebert^{a,b,c,†}, Anna
Hofmann^{c,‡}, Anne Imberty^d and Alexander Titz^{a,b,c*}

^aChemical Biology of Carbohydrates, Helmholtz Institute for Pharmaceutical Research Saarland (HIPS), D-66123 Saarbrücken, Germany

^bDeutsches Zentrum für Infektionsforschung (DZIF), Standort Hannover-Braunschweig, Germany

^cDepartment of Chemistry and Graduate School Chemical Biology, University of Konstanz, D-78457 Konstanz, Germany

^dCentre de Recherches sur les Macromolécules Végétales (CERMAV)-CNRS and Université Grenoble Alpes, F-38041 Grenoble, France

*Corresponding author

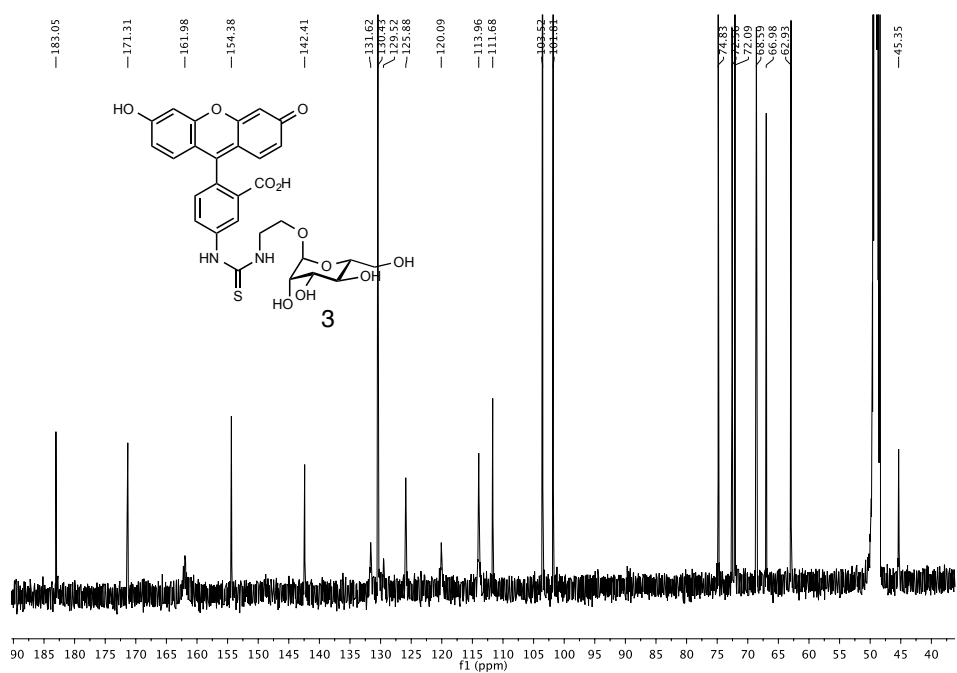
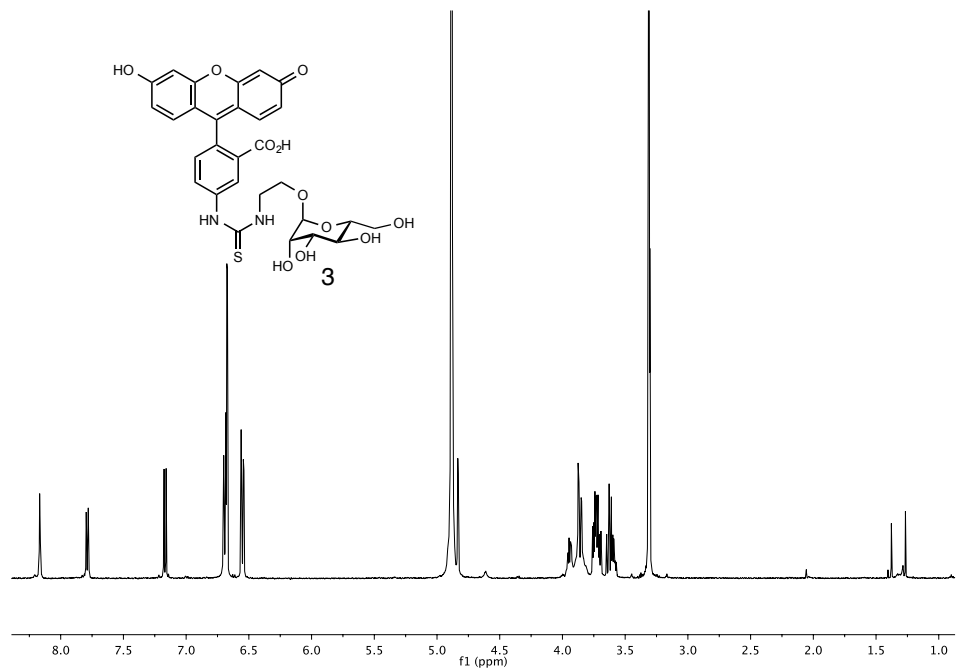
Chemical Biology of Carbohydrates, Helmholtz Institute for Pharmaceutical Research Saarland
D-66123 Saarbrücken, email: alexander.titz@helmholtz-hzi.de

Both authors contributed equally.

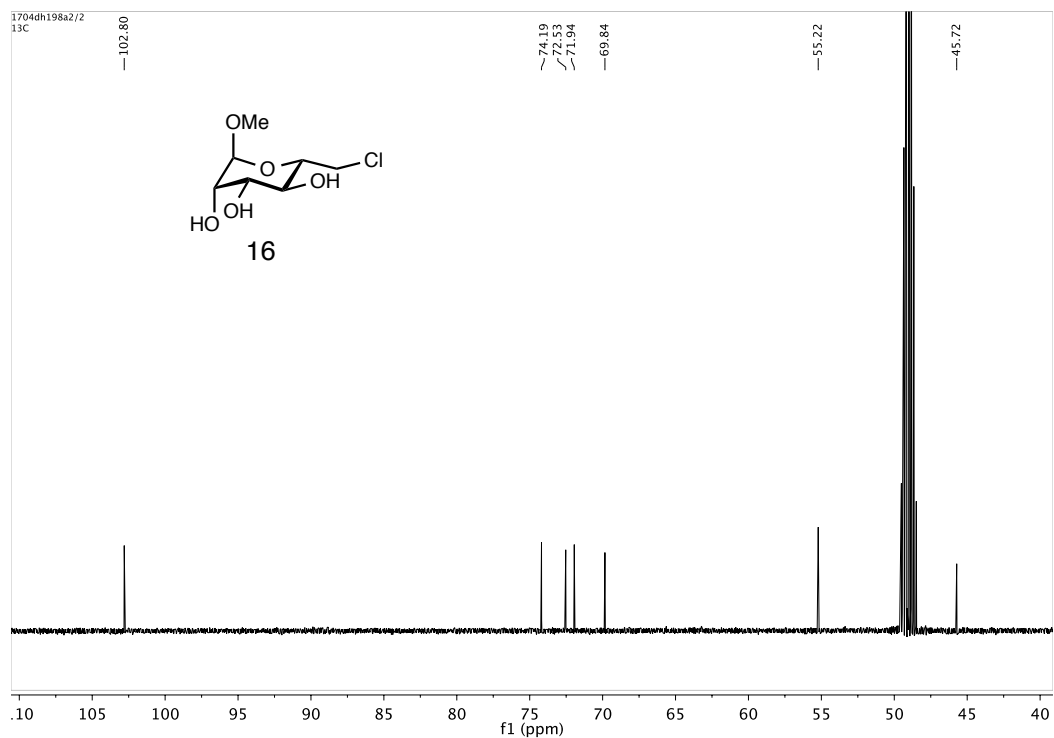
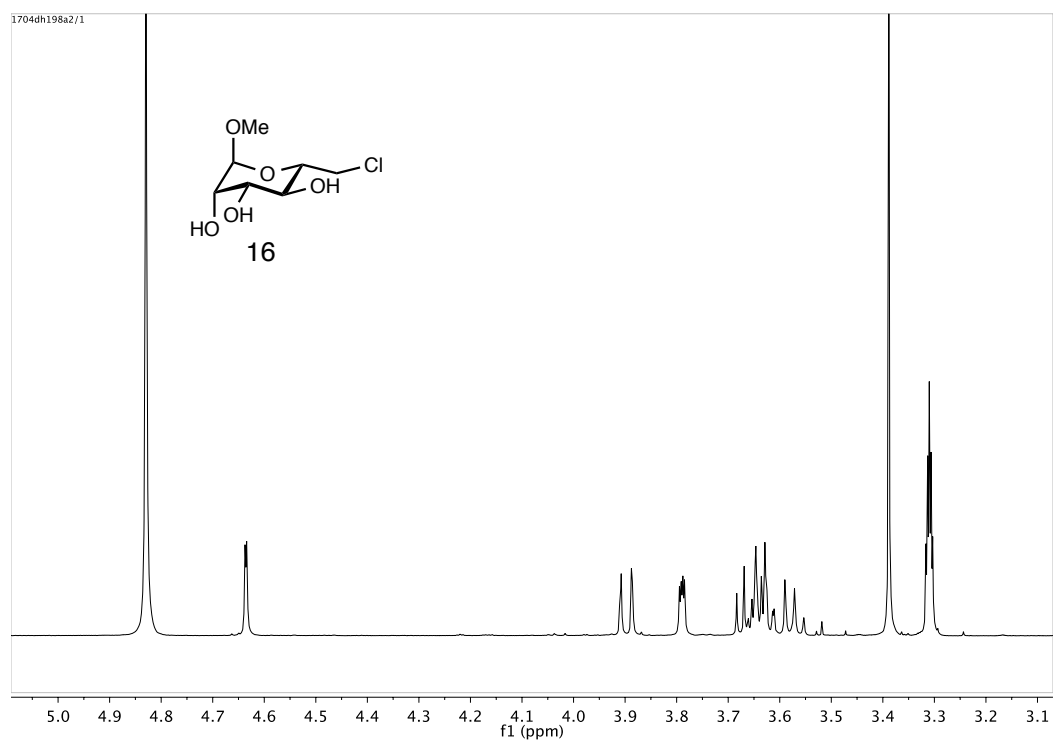
†Current address: Institute for Applied Synthetic Chemistry, TU Wien, Getreidemarkt 9, A-1060 Vienna, Austria

‡Current address: Institute of Pharmacy and Food Chemistry, University of Würzburg, D-97074 Würzburg, Germany.

^1H -NMR, ^{13}C -NMR and ^{19}F -NMR traces of synthesized compounds

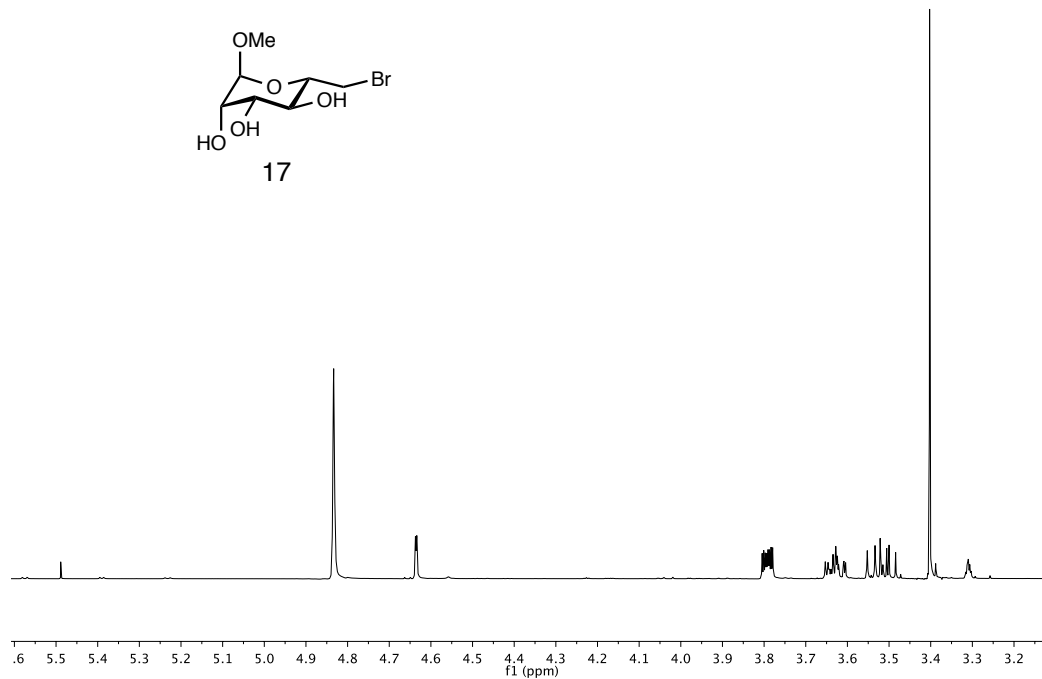
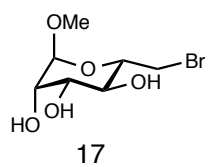


SUPPORTING INFORMATION

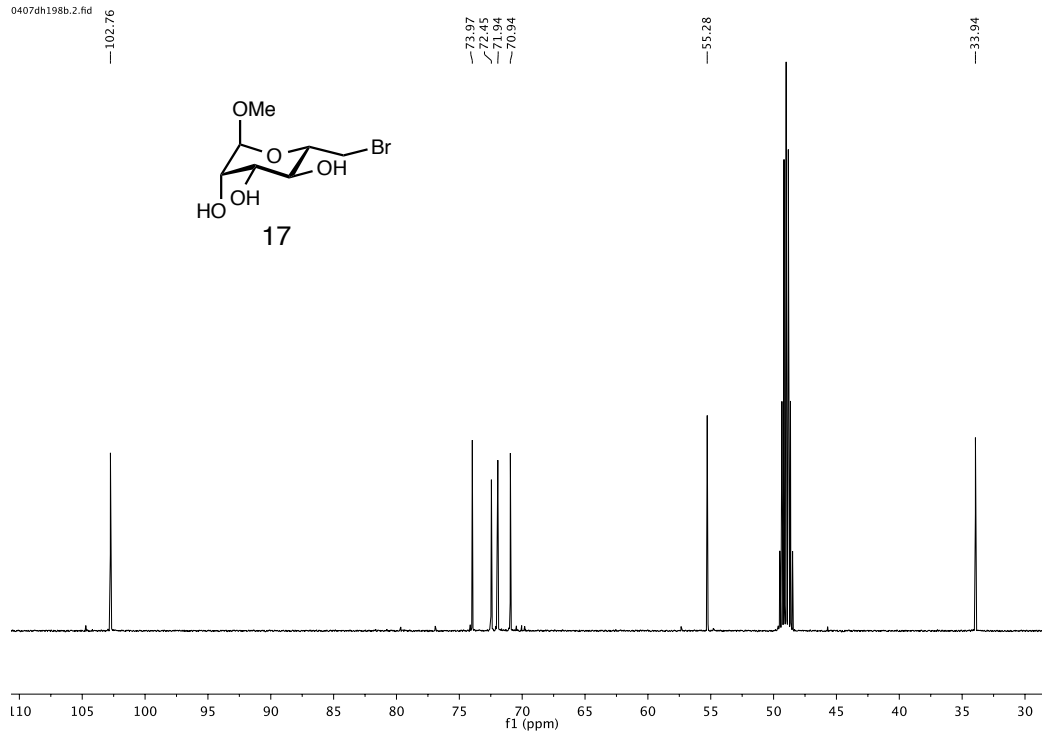
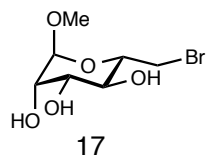


SUPPORTING INFORMATION

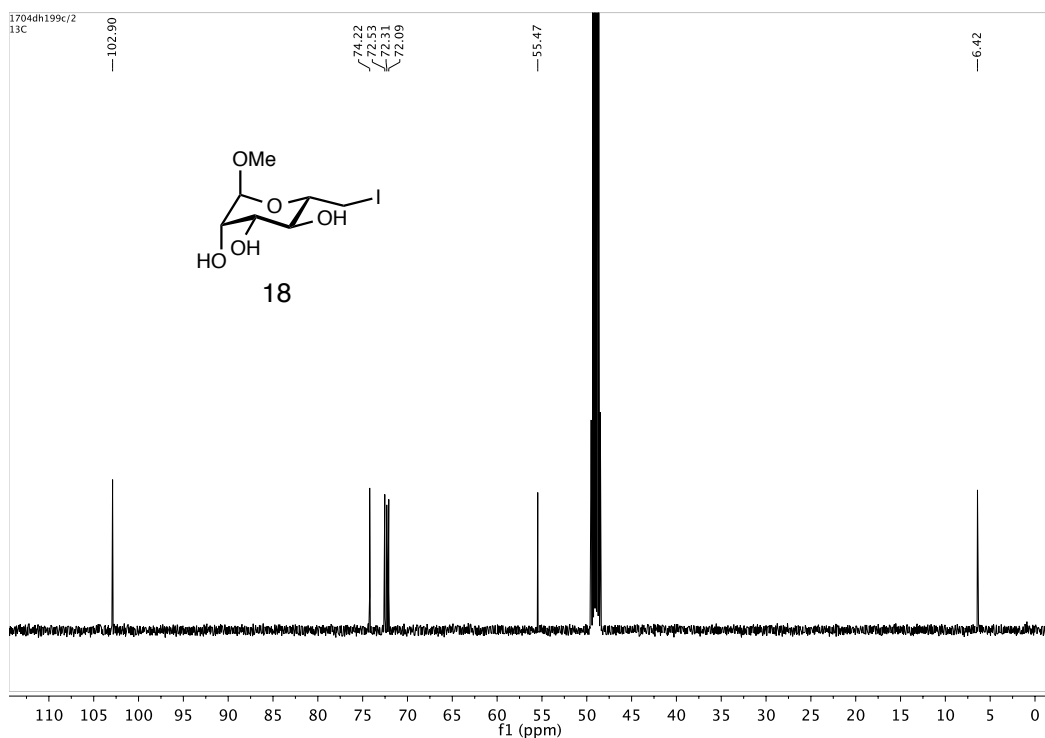
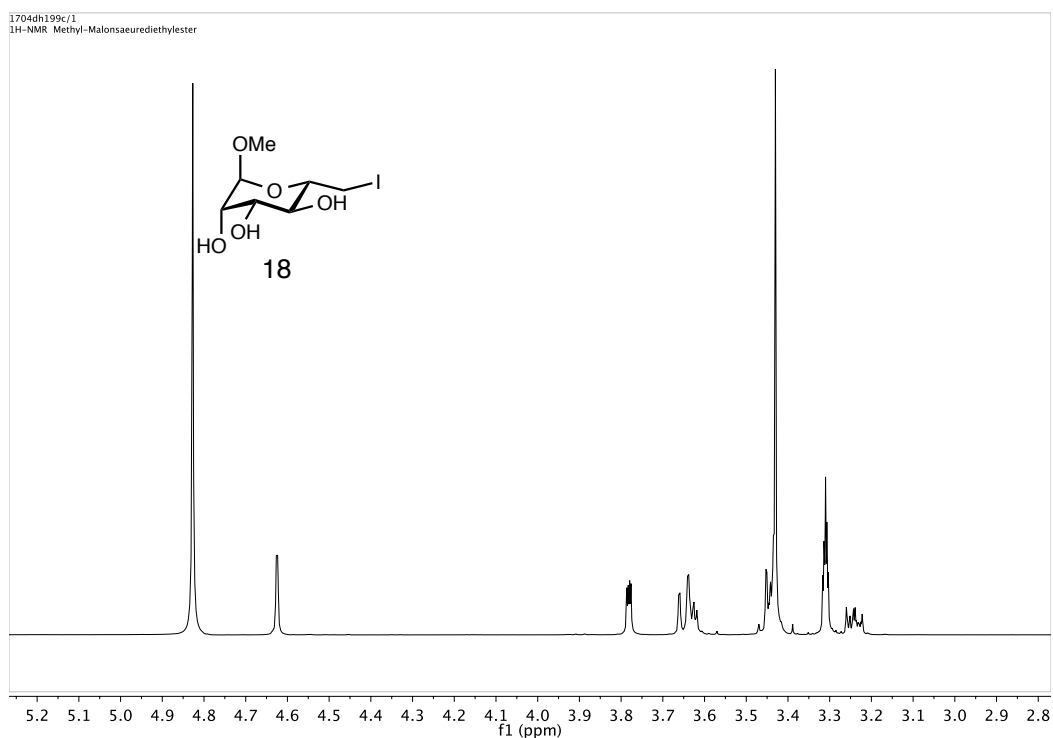
0407dh198b.1.fid



0407dh198b.2.fid

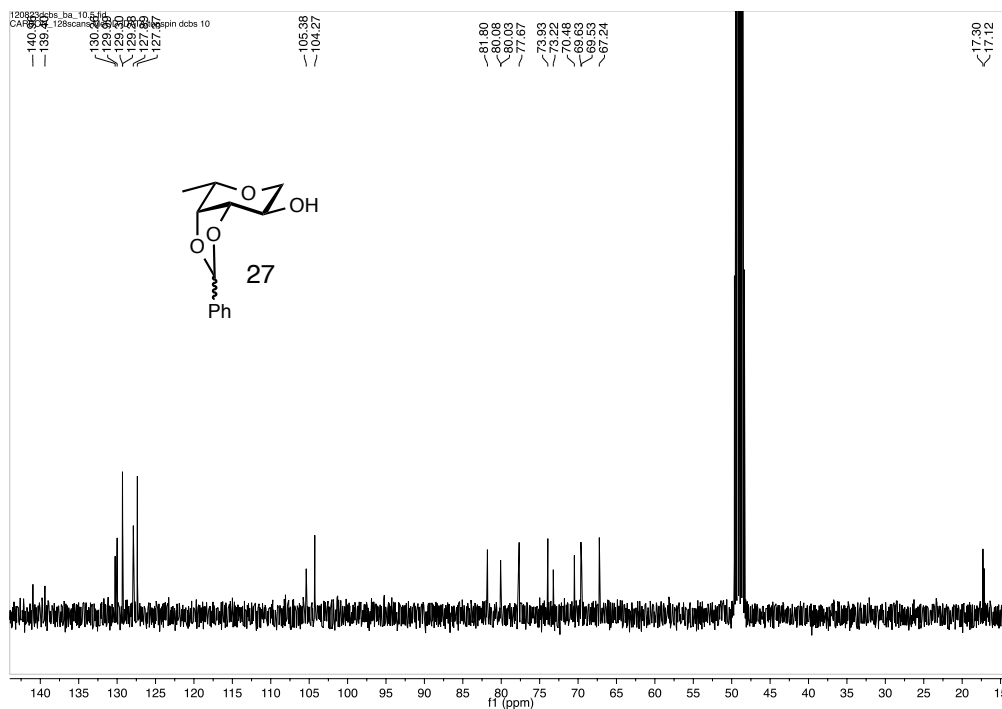
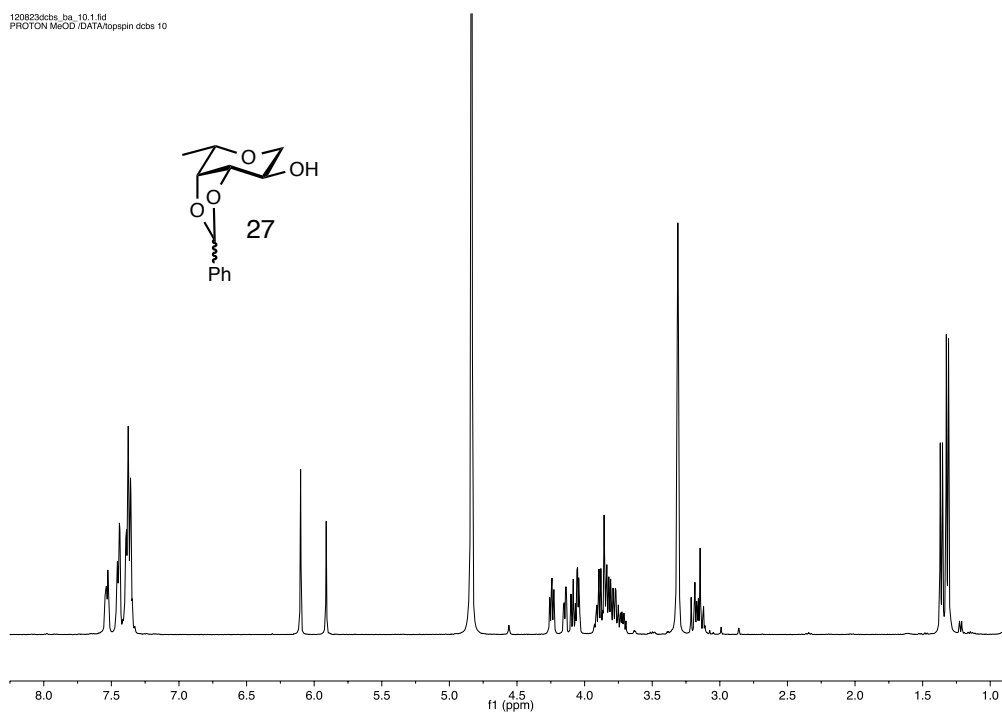


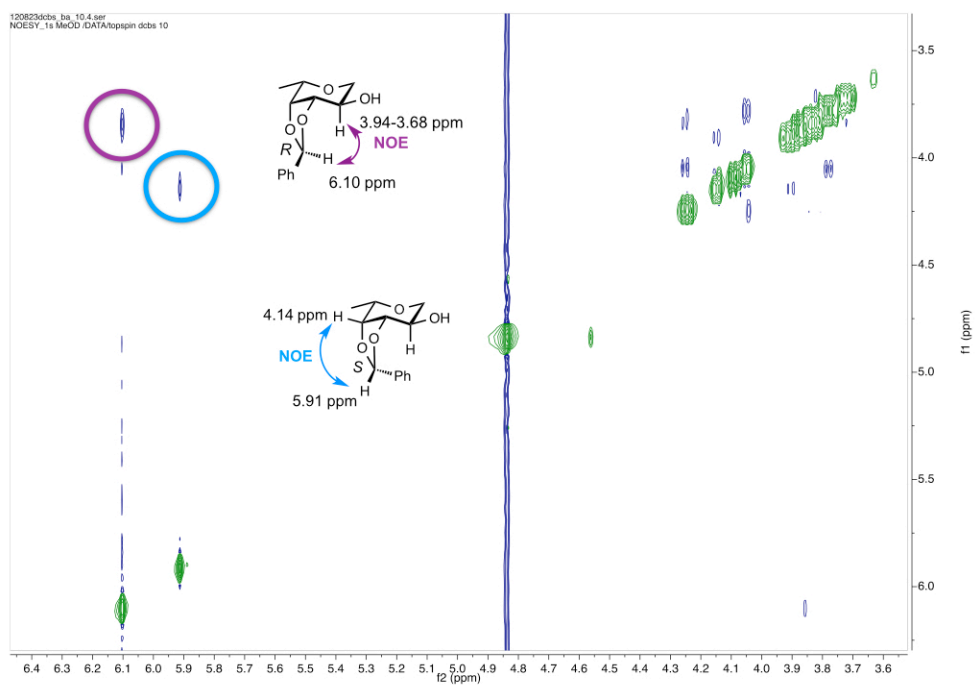
SUPPORTING INFORMATION



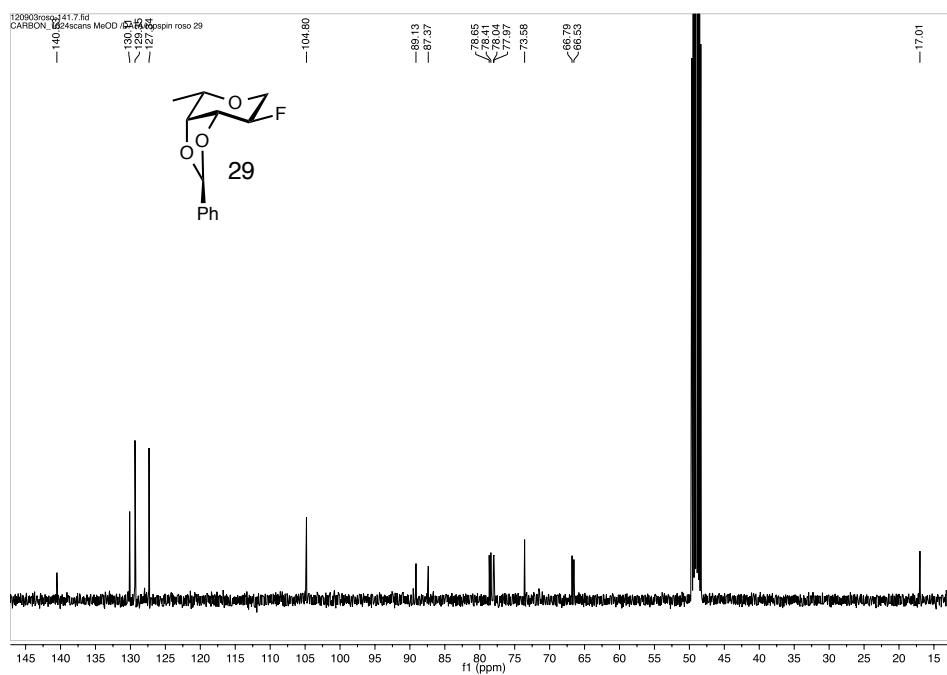
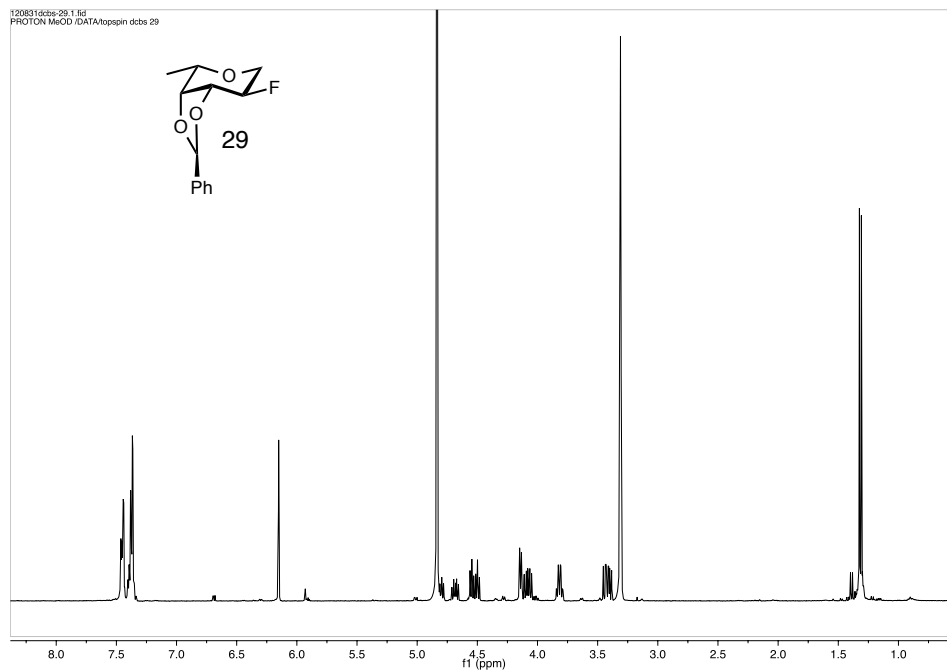
SUPPORTING INFORMATION

120823dcbs_ba_10.1.fid
PROTON MeOD /DATA/topspin dcbs 10

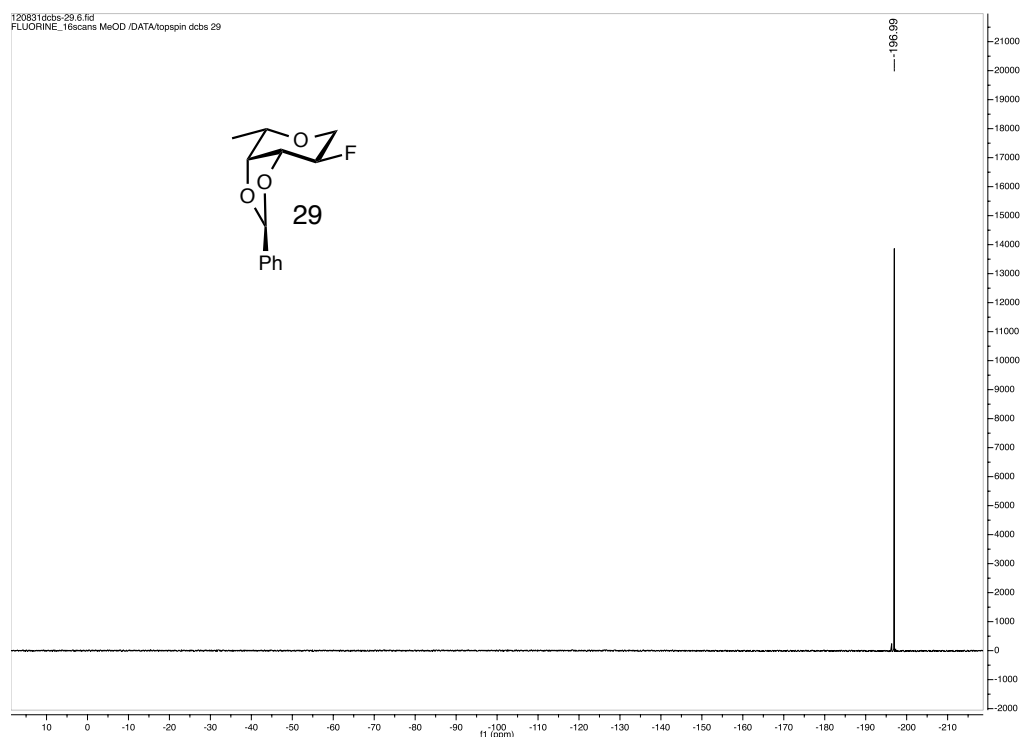




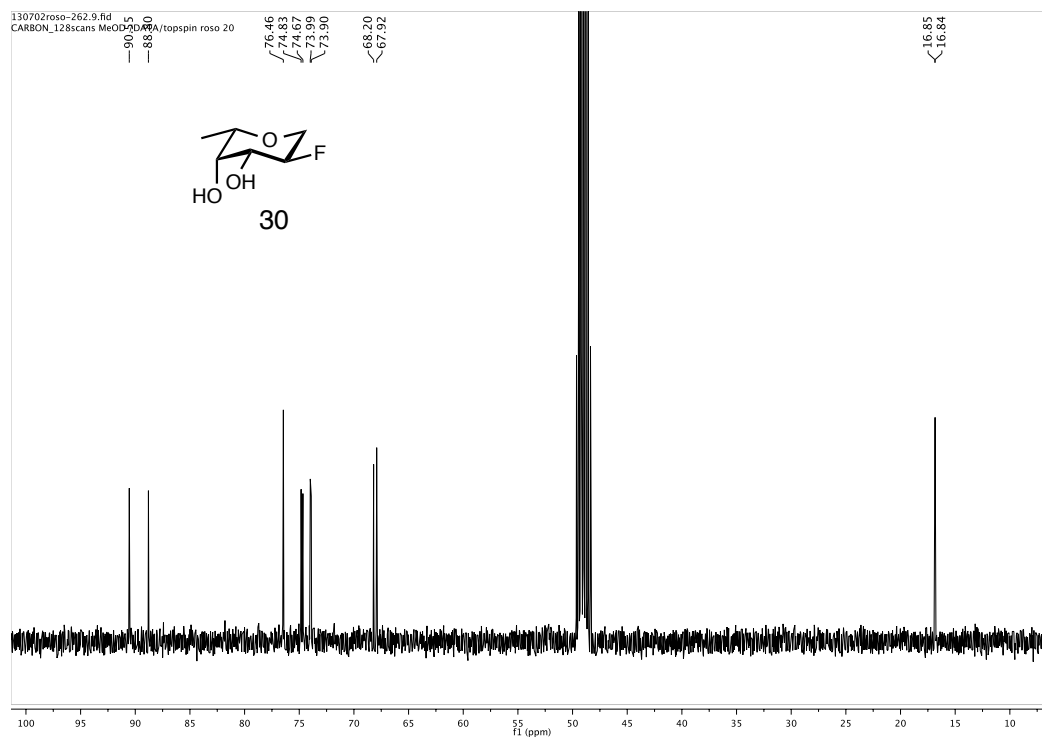
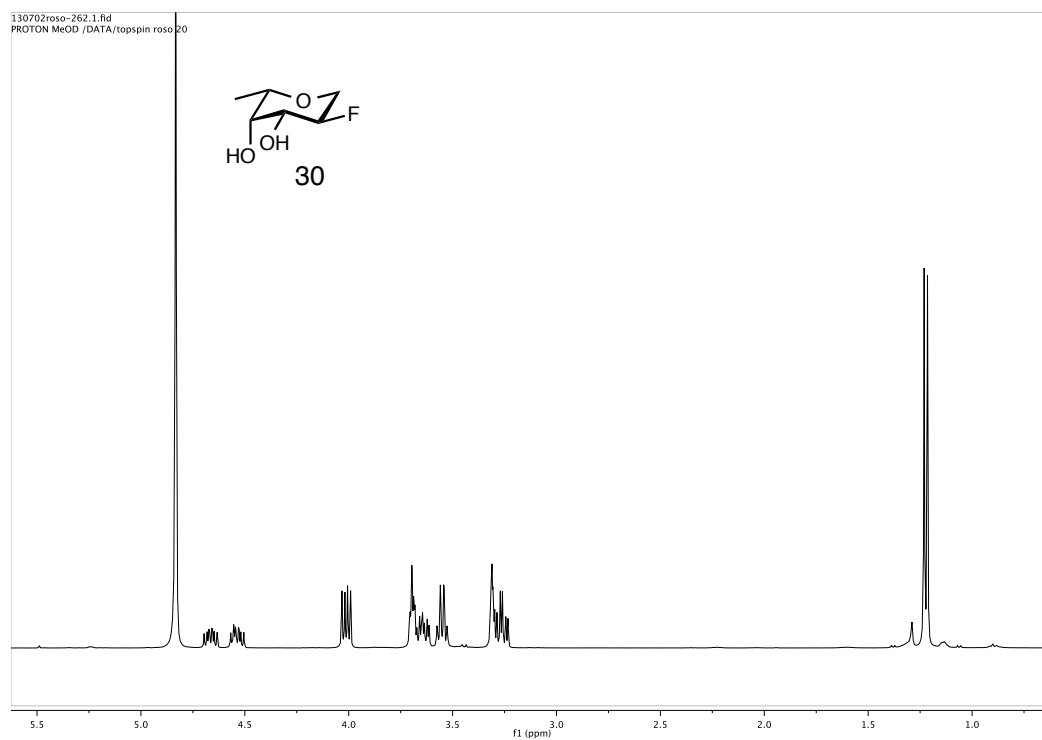
SUPPORTING INFORMATION



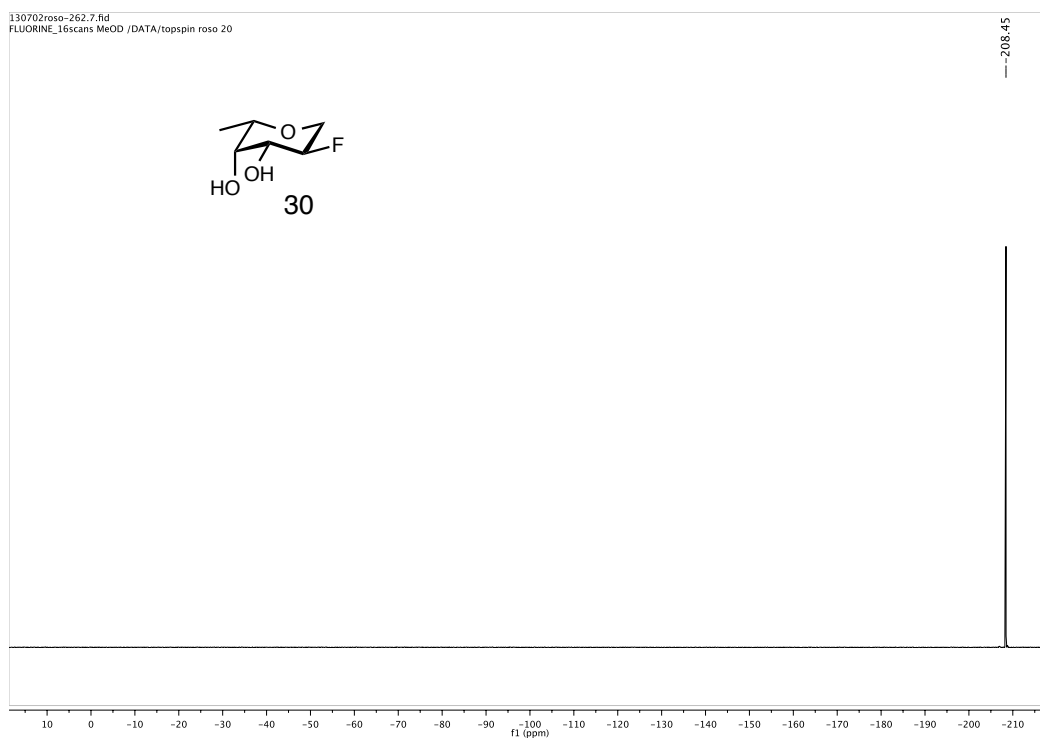
SUPPORTING INFORMATION



SUPPORTING INFORMATION

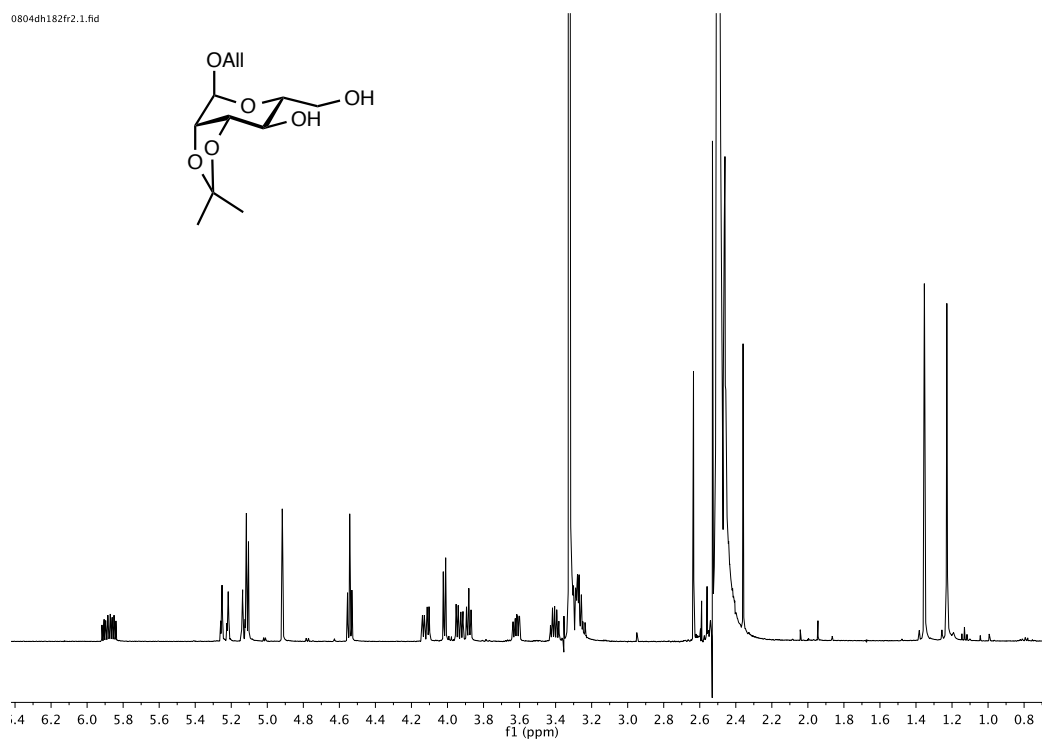


SUPPORTING INFORMATION

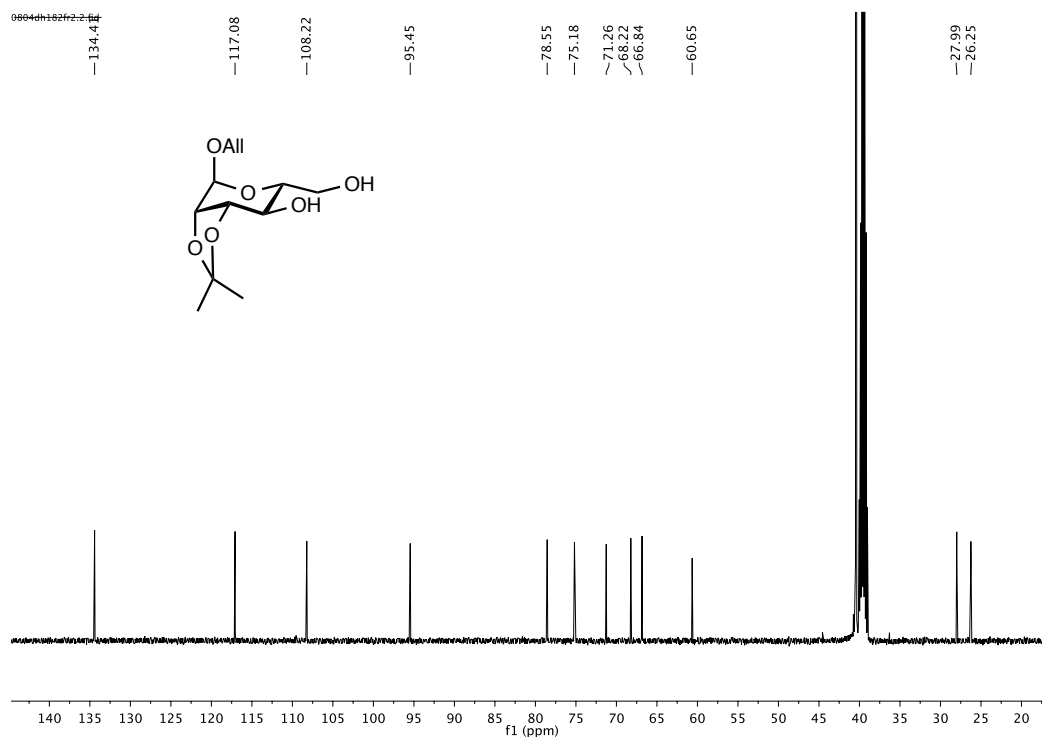


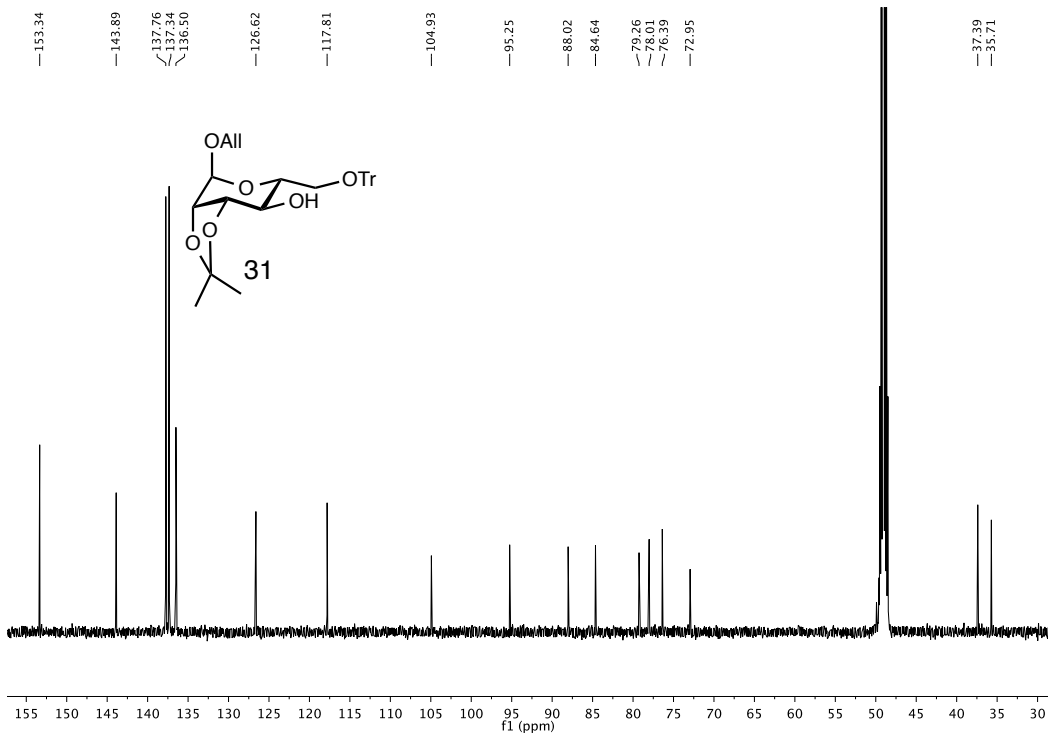
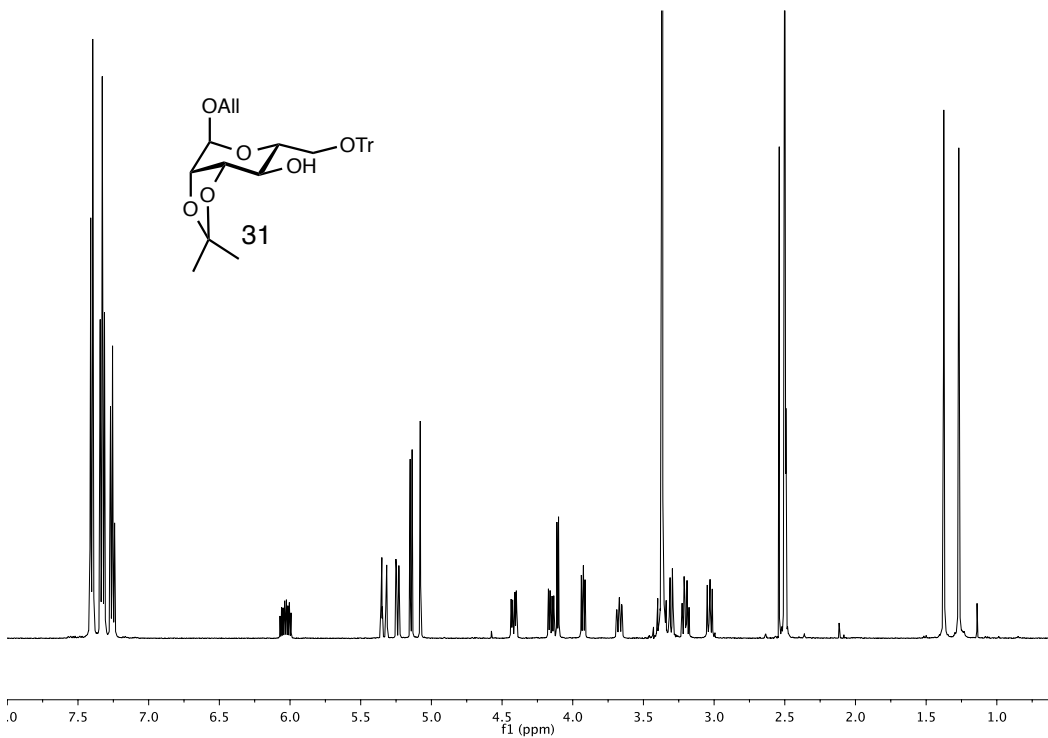
SUPPORTING INFORMATION

0804dh182fr2.1.fid



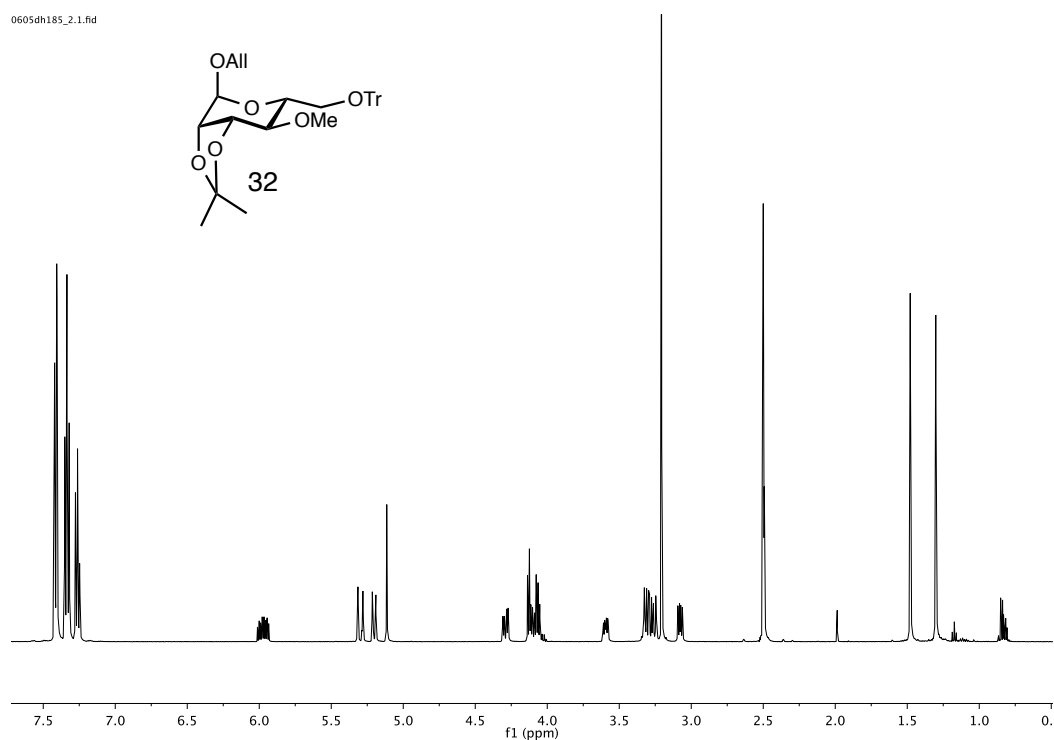
0804dh182fr2.2.fid



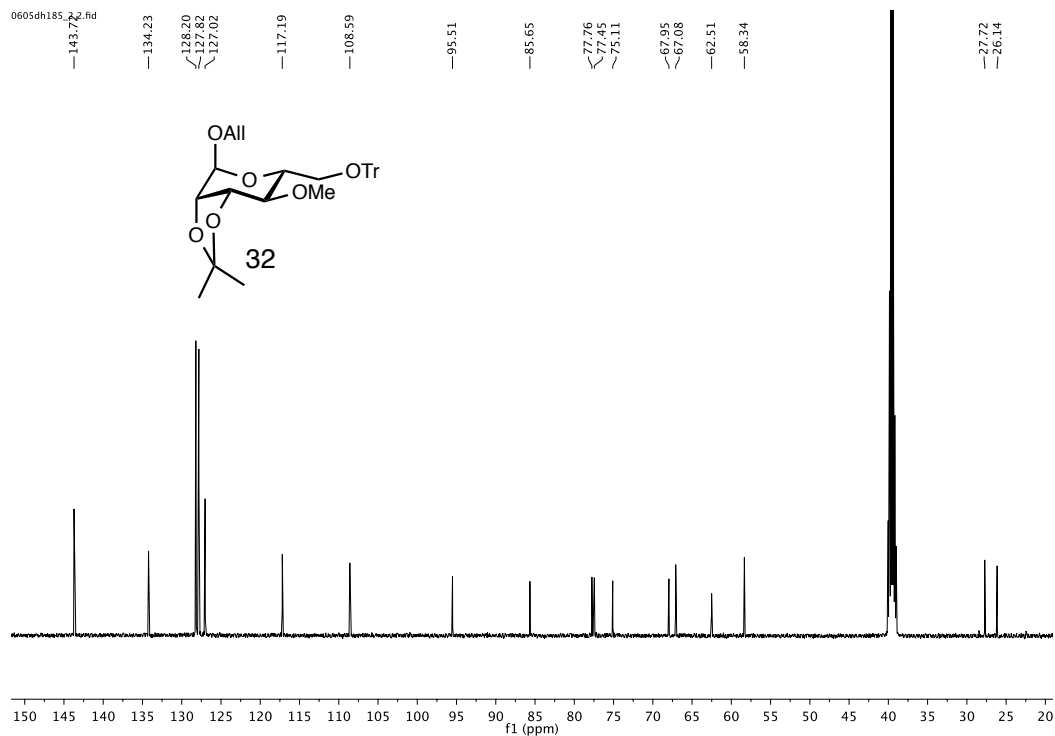


SUPPORTING INFORMATION

0605dh185_2.1.fid



0605dh185_2.2.fid



SUPPORTING INFORMATION

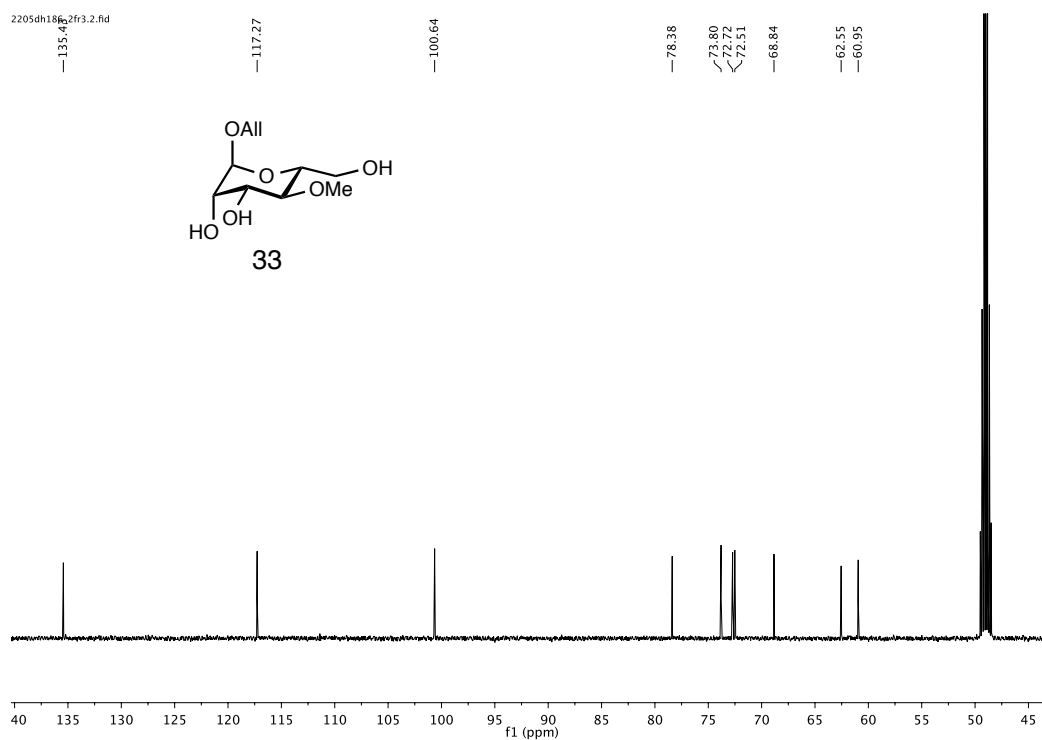
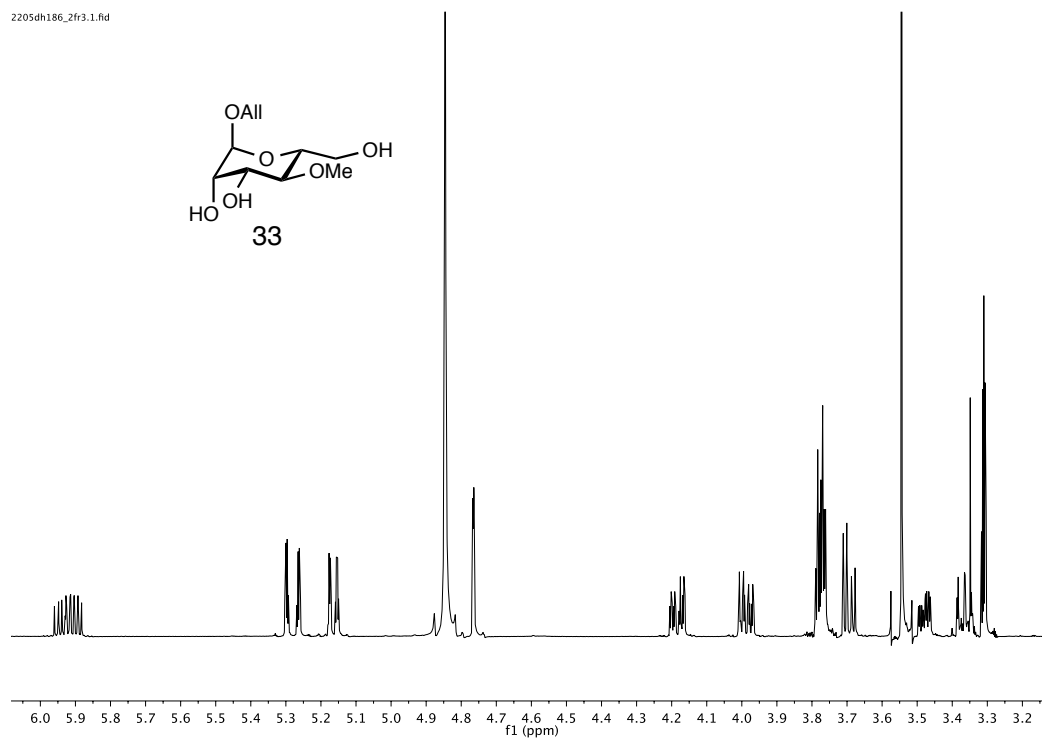
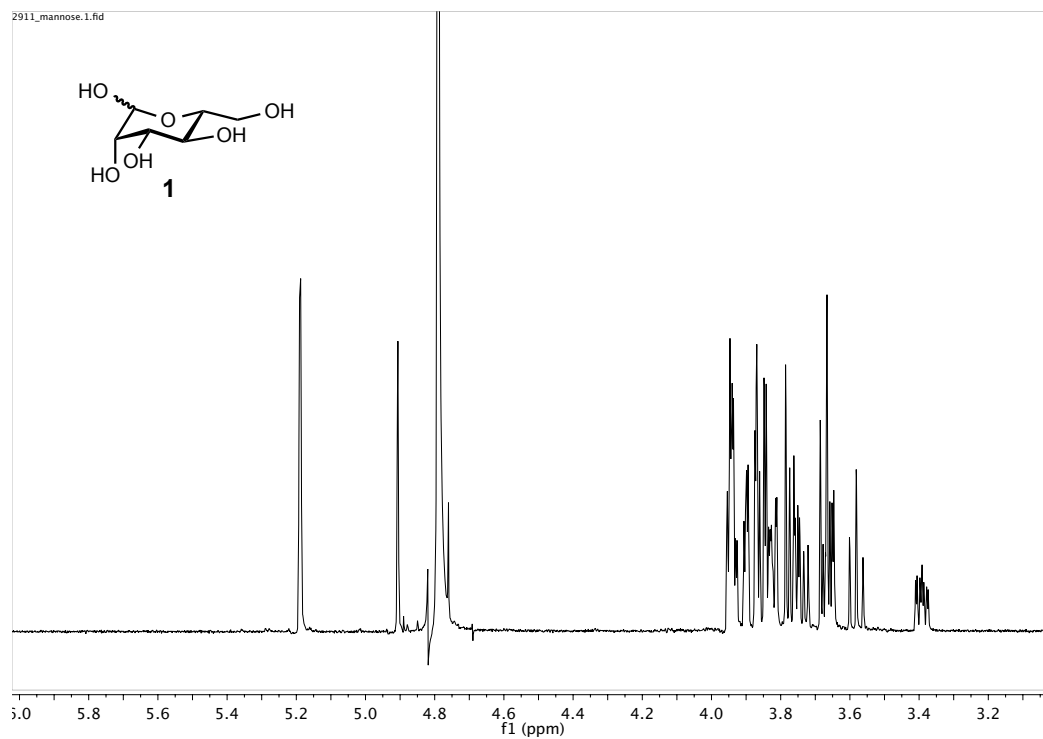
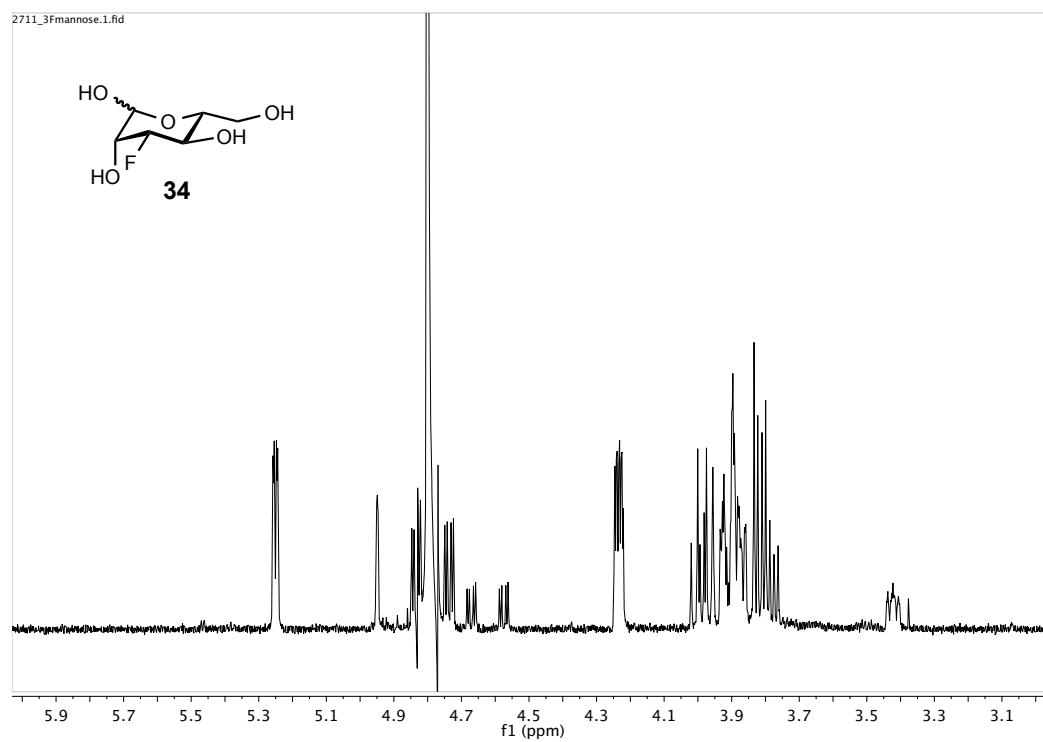
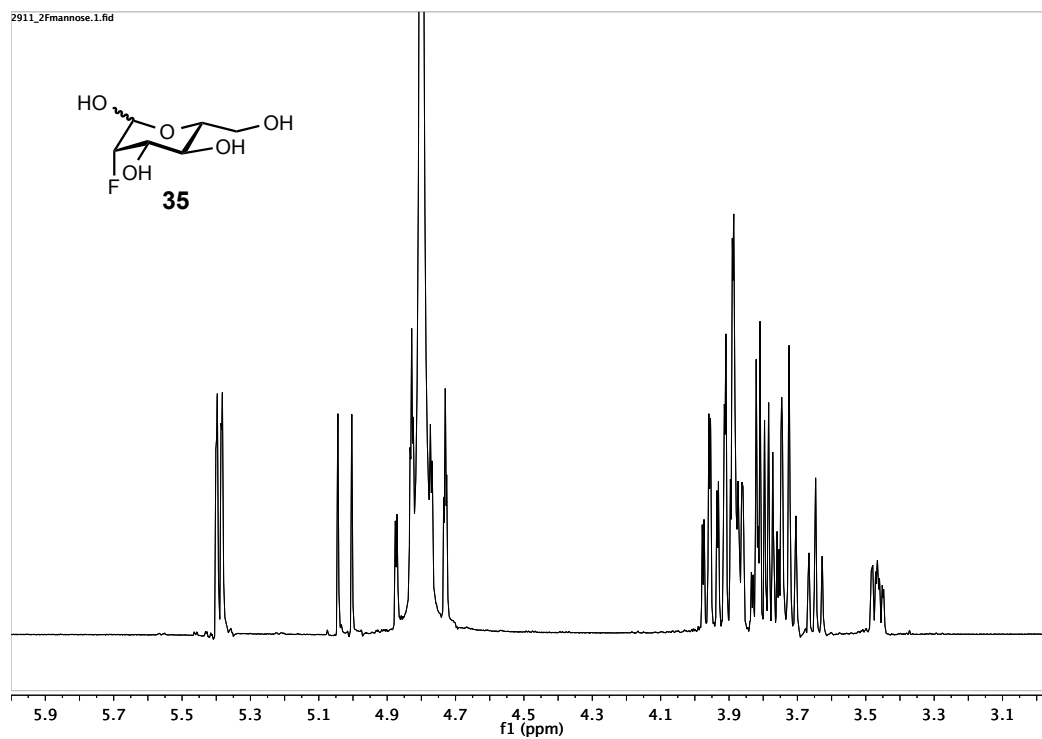


Table S1: Calculation of inhibition constants (K_i) from IC_{50} values

K_d (tracer 3) [μM]	3.1	
concentration of 3 [μM]	0.01	
compound	IC_{50} [μM]	K_i [μM]
1	10.8	10.8
5	498	496.4
10	13	13.0
11	2.9	2.9
12	7.0	7.0
14	14.5	14.5
15	7.4	7.4
20	116	115.6
21	104	103.7
22	64	63.8
25	19	18.9
26	13.8	13.8

Calculation performed using the Cheng-Prusoff equation initially developed for competitive inhibition of enzymes (Cheng, Y.C. and Prusoff, W.H. *Biochem. Pharm.*, 1973, 22:3099-108).

¹H-NMR trace of **1**¹H-NMR trace of **34**

¹H-NMR trace of **35**

5.4. SUPPORTING INFORMATION FOR SUBCHAPTER 3.4

Supporting Information to

***Photorhabdus luminescens* lectin A (PllA) - a new probe for detecting α -galactoside-terminating glycoconjugates**

Ghamdan Beshr^{a,b}, Asfandiyar Sikandar^c, Eva-Maria Jemiller^d, Nikolai Klymiuk^d, Dirk Hauck^{a,b},

Stefanie Wagner^{a,b}, Eckhard Wolf^d, Jesko Koehnke^{c*}, and Alexander Titz^{a,b*}

^a Chemical Biology of Carbohydrates, Helmholtz Institute for Pharmaceutical Research Saarland (HIPS),
D-66123 Saarbrücken, Germany

^b Deutsches Zentrum für Infektionsforschung (DZIF), Standort Hannover-Braunschweig, Germany

^c Structural Biology of Biosynthetic Enzymes, Helmholtz Institute for Pharmaceutical Research Saarland
(HIPS), D-66123 Saarbrücken, Germany

^d Chair for Molecular Animal Breeding and Biotechnology, Gene Center and Department of Veterinary
Sciences, LMU Munich, 81377 Munich, Germany

SUPPORTING INFORMATION

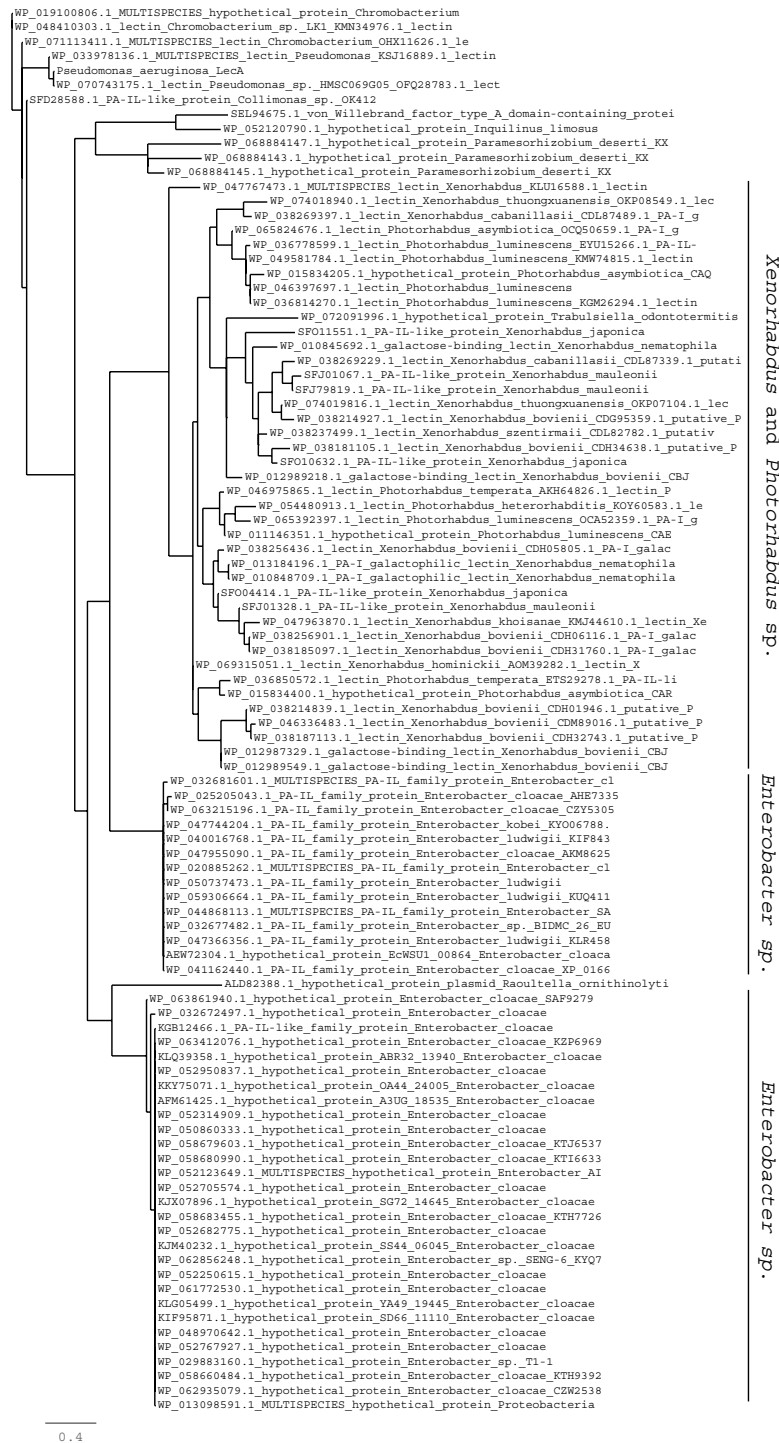


Figure S1. LecA heterologs found in a BLAST search using protein blast BLASTP 2.6.0+ and the sequence of LecA from *P. aeruginosa* PAO1 (GenBank AAG05958.1) against the non redundant nucleotide collection while excluding the genus *Pseudomonas*.

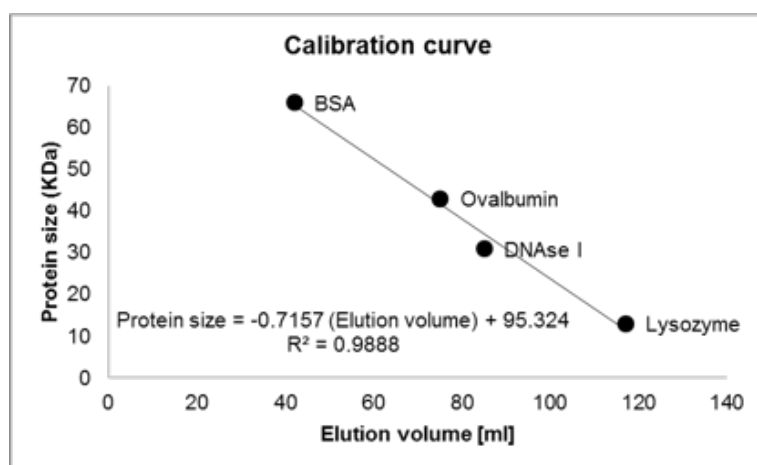


Figure S2. Calibration of the size-exclusion chromatography column using 4 known proteins as molecular mass standards. The elution volume of PLLA was 95 mL (see Figure 2).

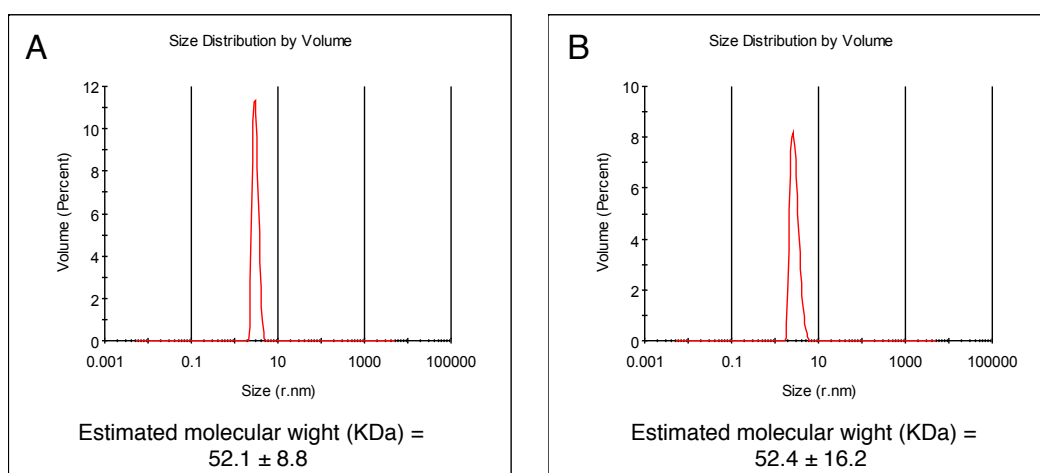
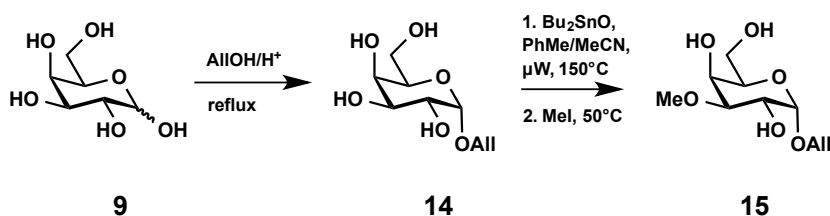


Figure S3. Dynamic light scattering of (A) PLLA and (B) LecA a suggested tetramer formation of both lectins in aqueous solution.



Scheme S1: Synthesis of allyl α -D-galactoside and methylation in position 3.

SUPPORTING INFORMATION

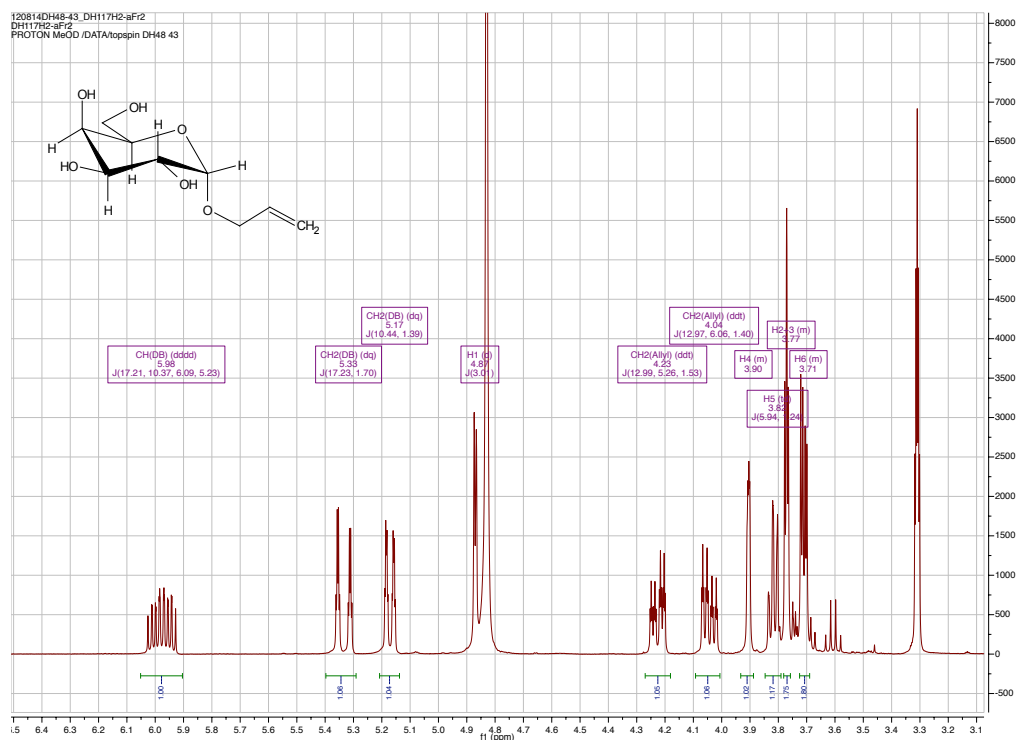


Figure S4. ^1H NMR of **14**

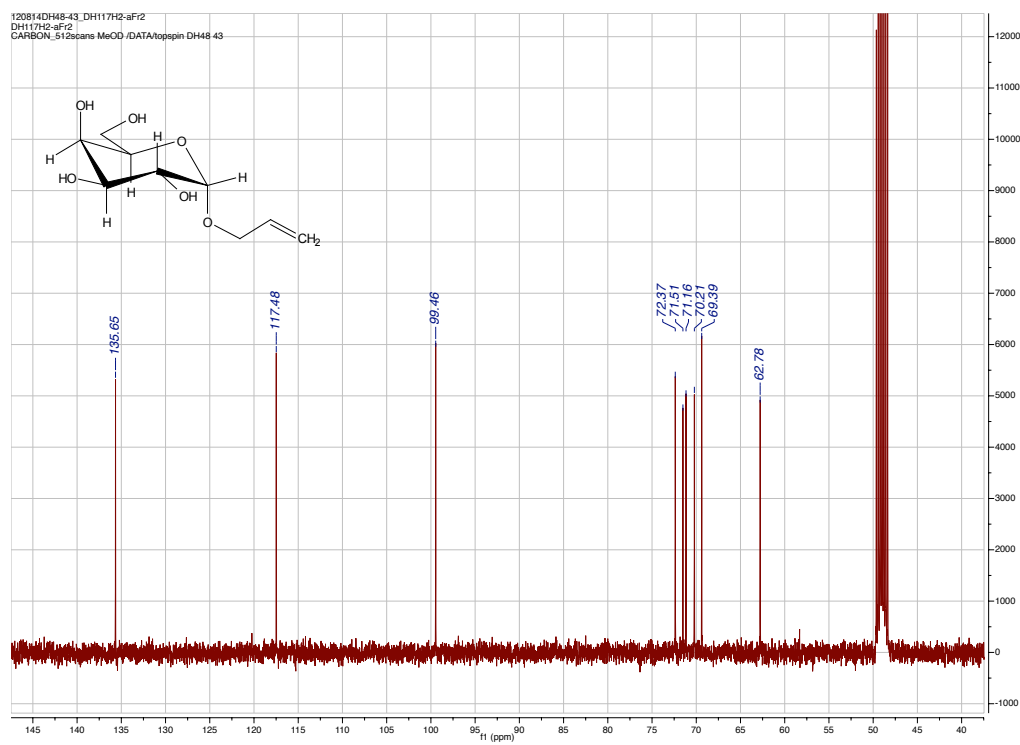
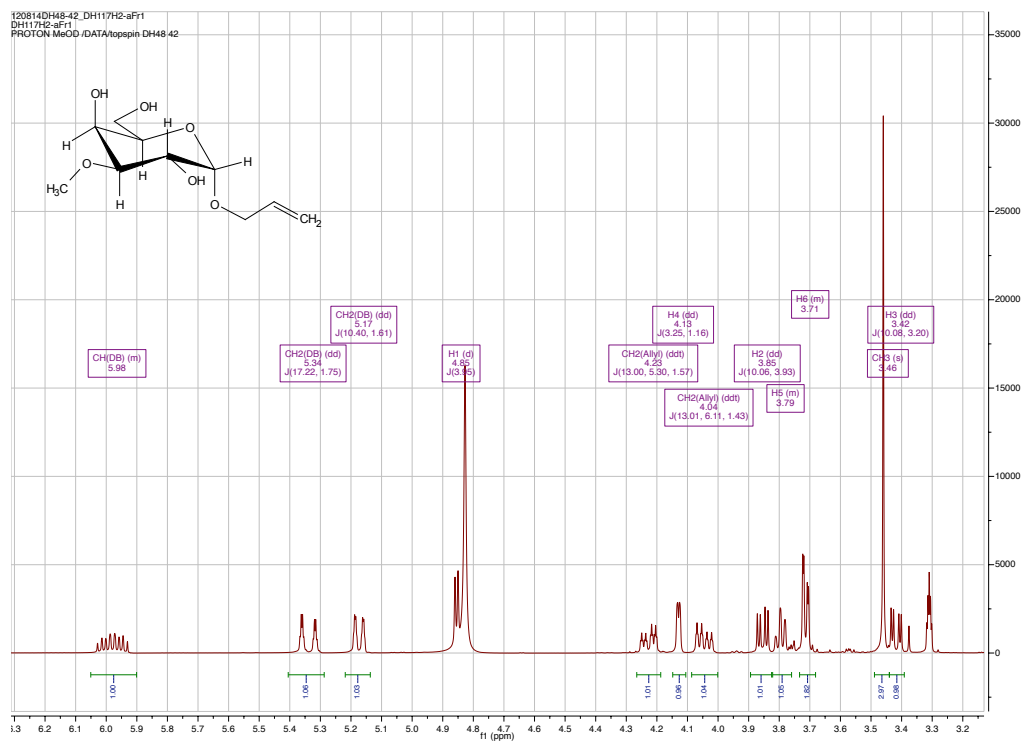
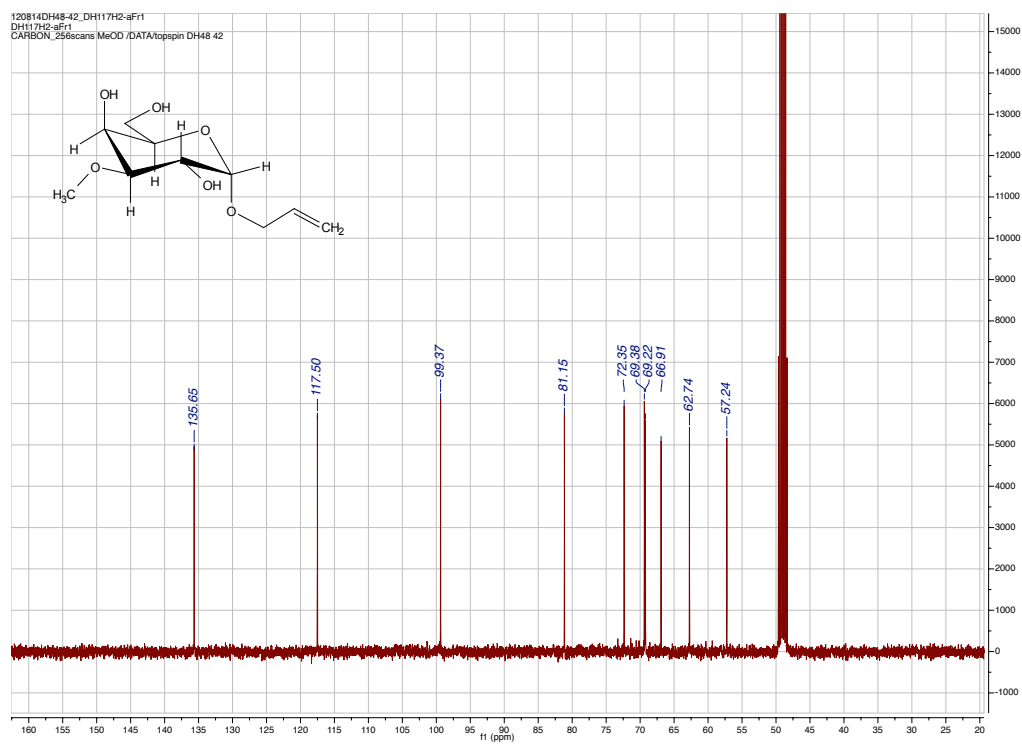


Figure S5. ¹³C NMR of 14

Figure S6. ¹H NMR of 15Figure S7. ¹³C NMR of 15

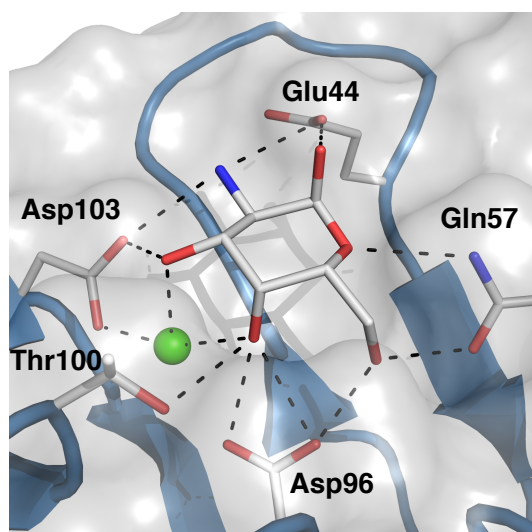


Figure S8. Molecular docking of D-galactosamine (**10**) in the PIIA binding pocket. Interactions between ligand and protein or protein-bound calcium are indicated as dashed lines. The carbohydrate recognition domain of PIIA is presented as cartoon with transparent surface. Ligand and amino acids forming interaction with the ligand are depicted as sticks colored by elements (N: blue, O: red, C: grey). The Ca^{2+} -ion is shown as green sphere.

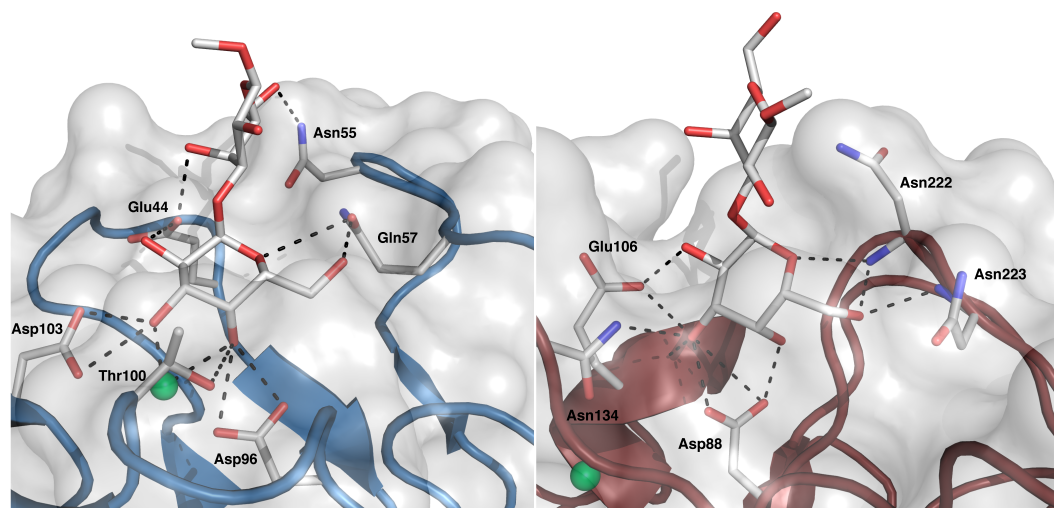


Figure S9. (left) Molecular docking of methyl glycoside of Gal- α -1,3-Gal (**20**) in the PIIA binding pocket. **(right)** Crystal structure of GS-IB4 in complex with methyl glycoside of **20** (pdb code: 1HQL); Interactions between ligand and protein or protein-bound calcium are indicated as dashed lines. The carbohydrate recognition domain of PIIA or GS-IB4 is presented as cartoon with transparent surface. Ligand and amino acids forming interaction with the ligand are depicted as sticks colored by elements (N: blue, O: red, C: grey). The Ca^{2+} -ion is shown as green sphere.

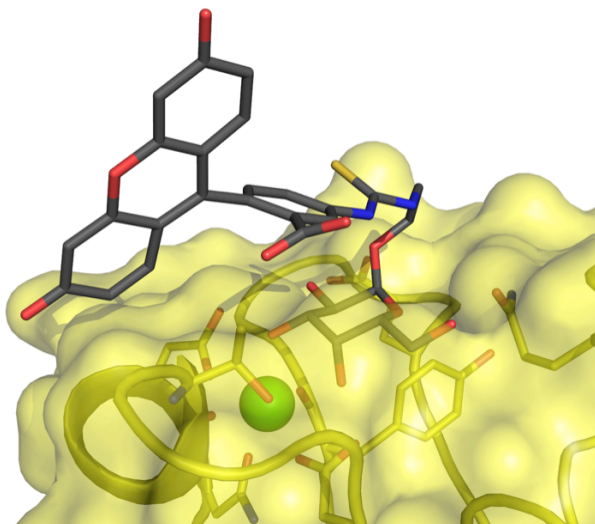


Figure S10. PIIA bound to **1**, additional angle of view. No interactions with the protein are observed beyond the carbohydrate moiety. The fluorescein can only be observed as the result of fortuitous crystal contacts in half of the monomers in the asymmetric unit. PIIA is shown as a yellow cartoon/surface representation, ligand as grey sticks and the Ca²⁺ ion as green spheres.



Figure S11. Superposition of PIIA (yellow) and LecA (PDB ID 4LKD, orange). Ca²⁺ ions are coloured to match proteins.

CONFERENCE CONTRIBUTIONS

Poster Presentations

Ghamdan Beshr, Roman Sommer, Dirk Hauck, Anne Imberty and Alexander Titz. Structure activity relationship study of inhibitors for *Burkholderia cenocepacia* lectin BC2L-A. European UGM & Conference (MOE), May 2016, Vienna, Austria.

Ghamdan Beshr, Roman Sommer, Dirk Hauck, Anne Imberty and Alexander Titz. Development of a competitive binding assay for the *Burkholderia cenocepacia* lectin BC2L-A and structure activity relationship of natural and synthetic inhibitors. 6th HIPS Symposium Recent Developments in Infection Research, June 2016, Saarbrücken, Germany.

Ghamdan Beshr, Asfandiyar Sikandar, Eva-Maria Jemiller, Nikolai Klymiuk, Dirk Hauck, Stefanie Wagner, Eckhard Wolf, Jesko Koehnke, and Alexander Titz. Characterization of a new highly α -galactose specific lectin of bacterial origin. 19th EUROCARB Conference, July 2017, Barcelona, Spain.

Oral Presentation

Ghamdan Beshr, Roman Sommer, Dirk Hauck, Anne Imberty and Alexander Titz. Structure activity relationship study of inhibitors for *Burkholderia cenocepacia* lectin BC2L-A. DPhG-Doktorandentagung, March 2016, Aachen, Germany

CURRICULUM VITAE

Personal Information

Name: Ghamdan Beshr
E-Mail: ghamdanb@gmail.com
Date/Place of Birth: 30.08.1985 Taiz, Yemen
Nationality: Yemeni/German

Education

09/2014.- To Date **Dr. rer. nat. (Ph.D.)**
Helmholtz Institute for Pharmaceutical Research Saarland &
Saarland University, Saarbrücken, Germany.
Supervisor: Dr. Alexander Titz.

10/2010 - 11/2013 **Master of Science in Biotechnology**
Saarland University – Germany.
Supervisor: Prof. Dr. Elmar Heinzle

10/2004 - 2/2009 **Bachelor of Science in Pharmacy**
Jordan University of Science and Technology – Jordan

9/2001 - 7/2003 **General high school certificate**
Alamjad High School - Yemen

Work Experience

09.2014- to Date **Research Associate** – Helmholtz Institute for Pharmaceutical
Research Saarland. Saarbrücken, Germany

Awards and Scholarships

2010 - 2013 Full scholarship covering the study towards master's degree in
biotechnology at Saarland University - Germany.

2004 - 2009 Full scholarship covering the study towards bachelor's degree in
pharmacy at Jordan University of Science and Technology –
Jordan.

Languages

- Arabic - German - English

ACKNOWLEDGEMENT

First and foremost, I would like to thank Dr. Alexander Titz for giving me the unique opportunity to be part of such a prestigious team at his research group at the Helmholtz Institute for Pharmaceutical Research Saarland (HIPS). I will be forever appreciative of his excellent mentoring and of his being an ever-shining example of an admirable scientist and a kind and humane supervisor.

I am also grateful to my second supervisor, Prof. Dr. Rolf W. Hartmann, for accepting me as one of his students and being my second supervisor for the last four years.

I would also like to express my deepest appreciation to Dr. Roman Sommer, Dr. Matthew Calvert, Dr. Stefanie Wagner, Dirk Hauck, and Ines Joachim for their immeasurable efforts and consistent help throughout my studies.

I am very thankful to Prof. Dr. Uli Kazmaier for my admission to the Interdisciplinary Graduate School of Natural Product Research and for financing my participation in various conferences.

Great thanks to all my former and current colleagues in the Chemical Biology of Carbohydrates and Drug Design and Optimization Departments in the HIPS for creating such a cooperative atmosphere during the whole time I was working on my PhD.

Thank you to all my friends, especially Ammar, Shadi, Musaab, Yaser, Natalia, Haitham, Ahmed, Mohammed, Nashrawan, Lisa, Esther, Verena, and Amina for their support and for everything.

Finally, I would like to offer my heartfelt thanks to my family for supporting me all the time.